Flood dynamics, hazard and risks in an active alluvial fan system threatening Ciudad Juárez Chihuahua, Mexico.

PhD thesis

by

David Zúñiga de León

December 2012

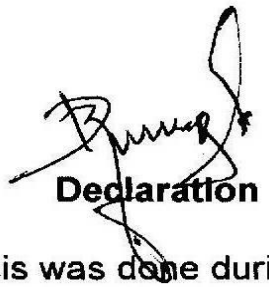

Declaration

The work contained in this thesis was done during the years 2008-2012 at Brunel University. This thesis was prepared independently and has not been submitted for any other degree.

ABSTRACT

The aim of this research is to assess hazards and risks associated with flooding in the city of Juárez, northern México, where there is a flood threat from active alluvial fans from mountains to the southwest and from the Rio Grande (Bravo River) to the northwest forming the northeast border of the city. Aims of this Ph.D were addressed processing a digital elevation model (DEM) of the study area in a GIS platform to define the several alluvial fans, and thus to examine their history and palaeohydrology. Three OSL dates in the youngest parts of the fans show ages ranging from 74 - 31 ka. However, the fans were subsequently incised, broadly correlating with later Pleistocene to Holocene processes upstream, published in literature, in New México. These changes are not obviously linked to glacial-interglacial cycles, and there is indication of local controls of interplay of climate and topography, for which this work is a preliminary study.

The flood threat to Juárez was addressed by using a classification of the uneven topography of the eroded alluvial fans, plus the Bravo River flood plain, into basins and sub-basins. Field and laboratory work was used to define litho-facies of soils and rocks, location of structures such as, topographic and hydrologic apex and drainage system in the fans. The data were then used in association with published information on the parameters of the basins and sub-basins provided in published documents from the Mexican authorities to make flood models of the area, using standard models of HEC-HMS and HEC-RAS methods widely applied in semi-arid regions. The result was estimation of the ability of existing flood defences to resist high-flow floods that may be expected in upcoming decades. The modelling predicts that only a small number of the existing defences will hold in a catastrophic 1:100-year flood, and that substantial parts of the city are in considerable danger. Such results are important in relation to the expanded and dense population in Juárez, which is concentrated mostly on the most active part of the flooding system, the Colorado Fan, which is the subject of a focussed secondary study of vulnerability mapping. The map reveals that areas of the city of low socio-economic development are under the greatest threat. Therefore there is a need for reconsideration of the city's flood planning, and remediation, plus the application of enforcements of areas which should not be built on, because of the threats.

LIST OF CONTENTS

Title.....i

Declaration.....ii

Abstract.....iii

List of contents.....iv

Appendices.....x

List of Figures.....xi

		CHAPTER 1	
1.1		AIMS OF THIS STUDY	1
1.2		BACKGROUND TO THIS STUDY	2
1.2.1		The nature of the problems	2
1.2.2		Justification of this research	3
1.3		LOCATION AND DEMOGRAPHIC FEATURES OF THE STUDY AREA	3
1.4		CLIMATIC SETTING	7
1.4.1		General situation.	7
1.4.2		El Niño Southern Oscillation (ENSO)	8
1.5		HISTORICAL PERSPECTIVE..	11
1.5.1		Chamizal and the Cordova island problems	12
1.6		THESIS OUTLINE	15
		CHAPTER 2	
2.1		INTRODUCTION	17
2.1.1		Cretaceous, Tertiary and Quaternary tectonic settings of the study area	17
2.1.2		Alluvial fans concepts	21
2.1.3		Regional Pleistocene to Holocene fluvial and alluvial sedimentary structures	29

2.1.4		Santa Fe formation|	31
2.1. 5		Cabeza de Vaca lake barreal lake and playa lake of anapra port|	32
2.1.6		Pleistocene-Holocene soils imbricated in camp rice and Fort Hancock formation	41
2.1. 7		Glacial-interglacial Pleistocene-Holocene aeolian sediments reworked	42
2.1.8		Lacustrine and playa lake deposits inset in Fort-Hancock and Camp Rice formations	43
2.1.9		Climate and global change.	44
2.1.10		Fluvial Bravo river system evolution during Pleistocene-Holocene tim	44
2.2		CLIMATIC OVERVIEW AND STATISTICAL METEROLOGICAL APPROACHES.	47
2.2.1		Introduction	47
2.2.2		Climate overview	48
2.2.3		El Niño Southern Oscilation (ENSO)	51
2.2.4		(ENSO) analysis in El Paso Texas USA area	53
2.2.5		La Niña analysis at El Paso Texas	54
2.2.6		Meteorological and Hydrological datasets	56
2.2.6.1		NOAA (2009).	56
2.2.6.2		Frequency/magnitude atlas for the south-central United States	56
2.2.6.3		Statistical approaches	56
2.2.6.4		Concentration time parameter	57
2.2.6.5		Kiprich Formulae	58
2.2.6.6		Boreholes Litology	59
		CHAPTER 3	
3.1		INTRODUCTION	60
3.2		FIELD AND DESK WORK TO ASSESS ALLUVIAL AND FLUVIAL STRUCTURES	66
3.2.1		Introduction	70
3.2.2		Soils classification|	70
3.2.3		Alluvial and fluvial soils lithology using osl dating method	70
3.3		MODELLING TECHNIQUES TO PERFORM FLOODING AND RISKS	77
3.3.1		Flooding hazard in one dimension using hec hms computer program	77
3.3.2		Geometric data extraction streams network from (dem) using arc-view 3.2	80
3.3.3		Hydrology Engineering Centre-River Analysis System (HEC-RAS).	83
3.3.4		Exportation of HEC-RAS file into (arc-view 3.2, 2002)	84
3.3.5		Import the hec-ras file and map of flooding using (arc-view 3.2, 2002)	84
3.3.6		Flooding hazard in flat valley areas	85

3.3.7		Flooding hazard and flooding risk models	85
3.3.8		Complementary information regarded to computer modeling programs	86
		CHAPTER 4	
4.1		INTRODUCTION	90
4.2		GEOLOGICAL SETTINGS OF ALLUVIAL FANS|	90
4.2.1		Results of Geological features	90
4.2.2		OSL dating results of Colorado alluvial fans	91
4.2.3		Borehole lithologies in alluvial fills and fluvial soils	92
4.2.4		Dynamic of fluvial and alluvial sedimentary structures	101
4.3		RESULTS OF ACTIVE ALLUVIAL FAN DYNAMICS	102
4.3.1		Geographic location; boundary extension and general description	102
4.3.2		Main components and boundary extension of northwest fans (sector 1)	106
4.3.3		Anapra alluvial fan sector 1 description	108
4.3.4		Palo chino and Jarudo alluvial fan photo inventory and evolution	116
4.3.5		Photo description and evolution of Snake and Colorado fans sector	125
4.3.6		Summary	128
		CHAPTER 5	
5.1		INTRODUCTION FLOOD ASSESSMENT USING MODELS	129
5.2		HEC-HMS COMPUTER PROGRAM FOR FLOOD MODELING AND HYDROGRAPHS	130
5.2.1		Rainfall data collection	130
5.2.2		Statistical approaches to assess the design hyetograph for 24 hmr	130
5.2.2.1		Gumbel EV1 Probability Distribution Function (PDF)	130
5.2.2.2		Log Pearson Type iii Probability Distribution Function	132
5.2.2.3		Design storm for the study area using Cheng-Lung-Chen approach	135
5.2.2.4		Hyetograph for the study area	135
5.3		HYDROGRAPH DEVELOPMENT USING THE CN METHOD OF SCS (1986)	136
5.3.1		(CN) method description	137
5.3.2		Basin and sub-basins location and CN parameters determination	137
5.3.2.1		Jarudo sub-basin location and network distribution description	138
	5.3.2.1.1	*(CN) Curve Number coefficient determination for Jarudo basin*	139

	5.3.2.1.2	*Concentration time and Lag-time evaluation for Jarudo basin*	140
	5.3.2.1.3	*Peak discharge and water storage using HEC-HMS for Jarudo basin*	140
5.3.2.2		Anapra basin network distribution and description	143
	5.3.2.2.1 to 5.3.2.2.19	*Description of Anapra drainage system.*	143-149
5.3.2.3		(CN) curve number coefficient of Anapra basin (see appendix 5.4.2)	150
5.3.2.4		Concentration time and Lag-Time of anapra basin. (see appendix 5.4.2)	150
5.3.2.5		Peak discharge and store water using hec-hms for Anapra basin	150
5.3.2.6		Center Basin network distribution and description	153
	5.3.2.3.1 to 5.3.2.3.18	*Description of Centre basin drainage system.*	154-159
.	5.3.2.3.19	*(CN) Curve Number factor method of Centre basin (Appendix 5.4.3) Information for this is in Appendix 5.4.3.*	159
	5.3.2..3.20	*Centre basin Physiographic and hydrologic values (Appendix 5.4.3) Information for this is in Appendix 5.4.3.*	159
	5.3.2.3.21.	*Peak discharge and store water using HEC-HMS for Centre Basin*	159
5.3.2.4		Barreal Basin network distribution and description	161
	5.3.2.4.1 to5.3.2.4.11	*Description of Barreal basin drainage system*	162-165
	5.3.2.4.12	*(CN) Curve Number coefficient Barreal Basin (Appendix 5.4.4) Information for this is in Appendix 5.4.4.*	165
	5.3.2.4.13	*Physiographic and hydrologic values of Barreal (Appendix 5.4.4) Information for this is in Appendix 5.4.4.*	165
	5.3.2.4.14	*Peak discharge and store water using HEC-HMS for Barreal basin.*	165
5.3.2.5		Airport Basin network distribution and description	166
	5.3.2.5.1to 5.3.2.5.19	*Description of Airport Basin drainage system*	167-172
	5.3.2.5.20	*C.N and Hydrologic parameters of Airport basin (Appendix 5.4.5) Information is provided in Appendix 5.4.5.*	173
	5.3.2.5.21	*Concentration time and Lag-time for Airport basin (Appendix 5.4.5) Information is provided in Appendix 5.4.5.*	173
	5.3.2.5.22	*Peak discharge and storage of water using HEC-HMS for Airport Basin.*	173
5.3.2.6		Bravo River Basin network distribution	174
	5.3.2.6.1 to 5.3.2.6.12	*Description of Bravo River basin drainage system*	175-179
	5.3.2.6.13	*C.N and Hydrologic parameters Bravo River basin (Appendix 5.4.6)*	179

		Information is provided in Appendix 5.4.6.	
	5.3.2.6.14	*Concentration time and Lag-Time for Bravo River Basin (Appendix 5.4.6)*	179
5.3.5.6		Peak discharge and storage of water using hec-hms for Bravo River Basin	179
5.3.2.7		Acequias Basin network distribution and description	180
	5.3.2.7.1 to 5.3.2.7.7	*Description of Acequias Basin drainage system*	180-182
	5.3.2.7.8	*C.N and Hydrologic parameters Acequias basin (Appendix 5.4.7)* *Information is provided in Appendix 5.4.7.*	182
	5.3.2.7.9	*Concentration time and Lag-Time for Acequias basin (Appendix 5.4.7) Information is provided in Appendix 5.4.7.*	182
	5.3.2.7.10	*Peak discharge and store water using HEC-HMS for Acequias Basin.*	182
5.3.2.8		Chamizal Basin network distribution and description	183
	5.3.2.8.1 to5.3.2.8.4	*Chamizal Basin network distribution and description*	184-185
	5.3.2.8.5.	*C.N and Hydrologic parameters Chamizal Basin (Appendix 5.4.8) Information is provided in Appendix 5.4.8.*	185
	5.3.2.8.6	*Concentration time and Lag-time for Chamizal basin (Appendix 5.4.8)* *Information is provided in Appendix 5.4.8.*	185
	5.3.2.8.7.	*Peak discharge and storage of water using HEC-HMS for Acequias Basin.*	185
		CHAPTER 6	
6.1		INTRODUCTION	188
6.2		Overview of design storm in the study area	188
6.2.1		Design Hyetogram to model HEC-HMS Hydrographs	188
6.3		HYDROGRAPH DESIGN	188
6.3.1		Introduction	188
6.3.2		Discharge results (hydrographs) for Anapra and Center sector	193
6.4		FLOODING HAZARD MODEL METHODOLOGY	193
6.4.1		Introduction	193
6.4.2		HEC-RAS transference reaches zones for flow model application.	194
6.4.3		Flooding results using the hec-ras computer program	201
6.4.3.1		Methodology to assess flooding hazard	201
6.4.3.2		Summary of the flooding results using HEC-RAS	201
6.4.4		Arc-view 3.2 and HEC-GEOras post-processor	205
6.4.4.1		Overview main tasks	205
6.4.4.2		Flooding hazard models with 5m and 1m resolution dem	206
	6.4.4.2.1	*Flooding in flat valley areas*	206
	6.4.4.2.2	*Flooding risk model from vulnerability matrix*	213

		CHAPTER 7	
7.1		INTRODUCTION TO DISCUSSION	218
7.2		FAN SYSTEM AND BRAVO RIVER FLUVIAL SYSTEM IN RELATION TO TOPOGRAPHY AND CLIMATE CHANGE IN RECENT HISTORY	219
7.2.1		Fan and river response to local topography	219
7.2.2		Fan and river response to climate change	219
7.3		LOODING FEATURES THREATENING JUÁREZ CITY	
7.3.1		Current and historical flood threats to juárez city	223
7.3.2		Current and historical flood threats to juárez city	225
7.4		EFFECT OF ENGINEERING WORK IN FLOOD MITIGATION	225
7.4.1		Fluvial process of the Bravo River affected by dam construction	229
7.4.2		Engineering works that affect the natural processes of alluvial fans	230
7.4.3		How could these flood-prevention measures be modified to mitigate the flooding	232
		CHAPTER 8	
8.1		MAIN OUTCOMES OF THIS STUDY	233
8.2		RECOMMENDATIONS FOR MITIGATION OF FLOODING PROBLEMS	235
		REFERENCES	236-251

APPENDICES

APPENDIX OF CHAPTER 1 .....1A; 1B & 1C

APPENDIX OF CHAPTER 3.....3A; 3B; 3C; 3D; 3E; 3F & 3G

APPENDIX OF CHAPTER 4.....4A1; 4A2; 4A3; 4A4; 4B & 4C

APPENDIX OF CHAPTER 5.....5.1; 5.2; 5.3; 5.3A; 5.4; 5.4.1 & 5.4.2 to 5.4.8

APPENDIX OF CHAPTER 6.....6A; 6B; 6C & 6D

LIST OF FIGURES

Figure number	Description	Page number
Figure 1.1	Location of major features of the study area	4
Figure1.2A	Study area location and main features	5
Figure 1.2B	View across the Hueco Bolson from the "Wind-Rose" panoramic Viewpoint located in km 15+100 of Camino Real road overlooking Juárez	6
Figure1.2.C	View across the Bravo River from the Franklin Mts in Texas	7
Figure 1.3	Accumulated annual average precipitation of the study area during the period 1957 to 2009	8
Figure 1.4	Monthly average and monthly maximum precipitation on the study area	8
Figure 1.5	Episodic storms of high intensity and short duration registered in the study area during the last 39 years	9
Figure 1.6	Illustration of the effects of the flooding in June 2006	10
Figure 1.7	Landslide in July 2008 in the Camino Real road	11
Figure 1.8	Rio Grande during the period 1852 and 1889. Shows Cordoba and Chamizal islands	14
Figure 1.9	Chamizal case convention of 1911 signed on January 14, 1963 between Mexico and U.S.A.	15
Figure 2.1	Structural and tectonic model showing evolution of Juárez Mountains	18
Figure 2. 2	Cross sections A, B, C, D and E shows the deformation style of Juárez Mountains	19
Figure 2.3	Geological map of the Sierra de Juárez Chihuahua, México	20
Figure 2.4	Plan view line sketches based on topographic maps and aerial photographs of the fans and drainage basins	24
Figure 2.5	Schematic diagrams of the common primary and secondary processes on alluvial fans.	25
Figure 2.6	Two phases in the development of alluvial fans under the influence of tectonic uplift	26
Figure 2.7	Diagram showing development of alluvial fan and shifts in the location of erosion and deposition	27
Figure 2. 8	Formation of alluvial fans under climate operation mode in an equilibrium hypothesis	28
Figure 2.9	Evolution of the ancestral Rio Grande system (Pink colour) during Pliocene and Early Pleistocene time	33

Figure 2.10	Map of the southern Rio Grande rift New México area	34
Figure 2.11	Palaeogeographic map of aggradational phase of the Rio Grande rift	36
Figure 2.12	Palaeogeographic map of aggradational phase of the Rio Grande rift	37
Figure 2.13	Palaeogeographic map of aggradational phase of the Rio Grande rift	38
Figure 2.14	Generalized geologic map and cross sections of Palomas Basin	39
Figure 2.15	Schematic cross section of a Half Graben of Palomas Basin	40
Figure 2.16	Stratigraphic and drill hole sections of Pleistocene fluvial deposits of the ancestral and modern Rio Grande along the Rio Grande valley	46
Figure 2.17	Illustrates the variability in the earth's orbit around the sun at various times scales measured in tens of thousands of years referred to as orbital parameters	49
Figure 2.18	Schematic variations in relative temperature during the last 20000 years and the advance of glaciers from selected regions of the globe	50
Figure 2.19	Numerical simulation of variation in the Precession (Δ e sin φ), Obliquity and Eccentricity (degrees) during the past 800,000 years	51
Figure 2.20	Daily solar irradiance (W/m^2) from 1980 to 2004 and Sunspots	53
Figure 2.21	Commonly autumn precipitation blue colour followed to a decrease in amount of spring precipitation red colour from 1899 to 1983	54
Figure 2.22	The percent of Normal during spring (red colour) predominates over the percent of Normal occurred during winter season	54
Figure 2.23	A) Seasonal Precipitation (in.) for La Niña Years vs. Non-La Niña Years B) difference between La Niña and Non-La Niña events	55
Figure 3.1	Digital Elevation Model (DEM) of the study area built with 5m contour levels	61
Figure 3.2	The graph shows how elevation in the vertical scale is linked to the distance from the origin in the horizontal scale	63
Figure 3.3	Satellite Images formed the entire study area of Juárez City	64
Figure 3.4	Digital Slope Model	65
Figure 3.5	Location sites where samples P1, P2 and P3 were collected for OSL dating alluvial fan	67
Figure 3.5A	OSL sites location of collected sample P1 of Colorado Alluvial fan	68
Figure 3.5B	OSL sites location of collected sample P2 of Colorado Alluvial fan	69
Figure 3.5C	OSL sites location of collected sample P3 of Colorado Alluvial fan	69
Figure 3.6	Sample collection in fine sands bellow the alluvial Colorado Alluvial fan	70
Figure 3.7	location of Gravels, Cobbles, Pebbles and Sands on the Bravo River relict terrace located at the cross intersection of Hortencia and Guadalajara streets, Felipe Angeles Neighbourhood	70
Figure 3.7A	Size distribution of pebbles and sands collected from Bravo River terrace relict located at cross of Hortencia and Guadalajara streets	71
Figure 3.8	Ranges of diameters for coarse particle sizing	72

Figure 3.8A	Requirements for soil to be classified as well graded. (ASTM 1985)	73
Figure 3.9	Casa Grande coup for (L.L) determination of fine soils as clay, silt or silty-clay. (ASTM 1985)	74
Figure 3.10	Plasticity chart applied to fine soils classification	75
Figure 3.11	Typical shapes of bulky or equidemensional grains	75
Figure 3.12	Shows the areas of Juárez Mountains where took place sample collection	76
Figure 3.13	Table 1 Example of SCS runoff curve numbers (CN) for a composite terrain	79
Figure 3.14	Table 2 NRCS parameters needed to assess CN	79
Figure 3.15	Digital Elevation Model (1M) corresponded to the west sector of Juárez city	82
Table 4.1	Quartz OSL data and ages from urban outcrops around Ciudad Juárez México	92
Table 4.2	Boreholes location of cross sections in Figs. 4.1C and 4.1D	93
Figure 4.1A	Anapra alluvial fan Geologic map	95
Figure 4.1B	Colorado Mountain Front alluvial fan Geologic map	96
Figure 4.1C	Center Sector fan Geologic map	97
Figure 4.1D	Southeast alluvial fan Geologic map	98
Figure 4.2	Cross Section Anapra alluvial fan	99
Figure 4.3	Cross Section Colorado alluvial fan	100
Figure 4.4	Topo-hydraulic map of the study area	104
Figure 4.5	Three sectors of alluvial fans	105
Figure 4.6	Location of the Anapra alluvial fan sector	106
Figure 4.7	Main components of Anapra alluvial fan	107
Figure 4.8	Anapra fan features	112
Figure 4.9	Proximal Medial and Distal segments of. Anapra Alluvial fan	113
Figure 4.10	Snake and Colorado alluvial fan main components of central sector	118
Figure 4.11	Symbology for proximal, medial and distal segments of alluvial fans	123
Figure 4.12	Nine sites of sample collection and photoinventory	124
Figure 4.13	Complementary Topo-hydraulic map of the Palo Chino and Jarudo alluvial fan	126
Figure 4.14	Complementary Topo-hydraulic map of the Palo Chino and Jarudo alluvial fan and associated fan model generation	127
Figure 5.1	Historical rainfall of 24HMR for the study area from 1969-2007	129
Figure 5.2	Excedence probability (Pe) derived from the Gumbel Statistical approach	131

Figure 5.3	Shows the results of 24HMR predicted for different return period using the Gumbel Extreme Value type 1 probability distribution function	132
Figure 5.4	Log Pearson III model prediction of 24HMR for different return periods	133
Figure 5.5	Graphic of Log Pearson Type III Probability Distribution Function (PDF)	134
Figure 5.6	Hyetogram for the study area	136
Figure 5.7	General map of study area showing locations of the eight basins	137
Figure 5.8	Shows the distribution of sub-basins within Jarudo Basin	138
Figure 5.9	Peak discharge (PD) and stored water (SW) for sub-basins in the Jarudo basin	141
Figure 5.10	HEC-HMS simulation flooding hazard model for the Jarudo basin	141
Figure 5.11	Twelve structures with storage capacity (S.C.) versus HEC-HMS simulation flooding water volume (M.W.V.) for Jarudo basin.	142
Figure 5.12	Anapra sub basin distribution	143
Figure 5.13	Peak discharge and stored water for sub-basins allocated on the Anapra basin	151
Figure 5.14	HEC-HMS simulation flooding hazard model components for the Jarudo basin	152
Figure 5.15	Structure storage capacity (S.C) versus HEC-HMS simulation flooding water volume for Anapra basin	153
Figure 5.16	Center Basin sub-basin distribution	153
Figure 5.17	Peak discharge and stored water for the 34 sub-basins in the Centre basin	160
Figure 5.18	HEC-HMS simulation flooding hazard model components for Centre basin	160
Figure 5.19	Structure storage capacity (S.C) versus HEC-HMS simulation flooding water volume for Center basin	161
Figure 5.20	Barreal sub-basins location and distribution	162
Figure 5.21	Peak discharge and stored water for sub-basins allocated on the Barreal basin	165
Figure 5.22	HEC-HMS simulation flooding hazard model components for Bareal basin	166
Figure 5.23	Airport sub-basin distribution	167
Figure 5.24	Peak discharge and stored water for sub-basins allocated on the Airport basin	173
Figure 5.25	HEC-HMS simulation flooding hazard model components for Airport basin	174
Figure 5.26	Structure storage capacity (S.C) versus HEC-HMS simulation flooding water volume for Airport basin	174
Figure 5.27	Bravo River sub-basin distribution and location	175
Figure 5.28	Shows the results of the concentration time as well as the Lag-time	179

	for the sub-basin located within the Bravo River basin	
Figure 5.29	HEC-HMS simulation flooding hazard model components for Bravo river basin	180
Figure 5.30	Acequias Basin and sub-basin distribution	180
Figure 5.31	Peak discharge and stored water for sub-basins located in the Acequias basin	183
Figure 5.32	Peak discharge and stored water for sub-basins located in the Acequias basin	183
Figure 5.33	Chamizal sub-basin distribution	184
Figure 5.34	Peak discharge and stored water for sub-basins located in the Chamizal basin	186
Figure 5.35	HEC-HMS simulation flooding hazard model components for Chamizal basin	186
Figure 5.36	Map of locations of sluice gates allowing floodwaters to exit to the Bravo River in the Chamizal Basin area	187
Figure 6.1	Anapra Basin and its sub-basins locations	189
Figure 6.2	Center Basin and its sub-basins locations	190
Figure 6.3	Peak descharge of Anapra basin	191
Figure 6.4	Peak discharge of Center Basin	192
Figure 6.5	Link between the transference reaches zone 1	195
Figure 6.6	Association and organization of HEC-HMS hydrographs plans for flooding hazard plan (PF3 to Tr 100 years) into the HEC-RAS program	196
Figure 6.7	Association and organization of HEC-HMS hydrographs plans for flooding hazard plan (PF3 to Tr 100 years) into the HEC-RAS program	197
Figure 6.8	Association and organization of HEC-HMS hydrographs plans for flooding hazard plan (PF3 to Tr 100 years) into the HEC-RAS program	198
Figure 6.9	Association and organization of HEC-HMS hydrographs plans for flooding hazard plan (PF3 to Tr 100 years) into the HEC-RAS program	199
Figure 6.10	Association and organization of HEC-HMS hydrographs plans for flooding hazard plan (PF3 to Tr 100 years) into the HEC-RAS program	200
Figure 6.11	Water Surface elevation of stream AW1: 10 years (PF1); 50 years (PF2) and 100 years (PF3) return periods: A) Shows a perspective view of the profile	203
Figure 6.12	Flooding Hazard model for the Northwest sector of Juárez City	207
Figure 6.13	Flooding Hazard model for the Center sector of Juárez City	208
Figure 6.14	Flooding Hazard model for the Southeast sector of Juárez City	209
Figure 6.15	Flooding hazard model derived from 1m DEM resolution for the Anapra sector:	210
Figure 6.16	Flooding hazard model derived from 1m DEM resolution for the centre sector	211
Figure 6.17	Flooding hazard model derived from 1m DEM resolution	212

	for the Southeast sector	
Figure 6.18	General Flood Risk map related to the whole study area (Northwest and centre sectors)	214
Figure 6.19	Northwest risk flooding map derived from 1m resolution DEM	215
Figure 6.20	Southeast risk flooding map derived from 1m resolution DEM	216

.....

CHAPTER 1

INTRODUCTION TO THE STUDY AREA

1.1. AIMS OF THIS STUDY

This research investigates an active alluvial fan system in relation to the local geological setting, in Ciudad Juárez, northern Mexico. The overall aim is to assess the dynamics of the fluvial and alluvial fans which influence Ciudad Juárez to understand the dangers to the city's population as a result of flooding from the nearby Juárez Mountains and the Bravo River (also called Rio Grande). The work uses multiple methodologies and data, centred on a Geographic Information System (GIS) platform, which includes: geological fieldwork, historical rainfall and flood information, landform modeling, and assessment of rainfall patterns that cause flooding. Thus the work is an integrated approach to understand the local earth-surface dynamics and apply this in a practical sense, to assist planning of flood mitigation.

The major questions that need to be answered in this thesis are as follows:

1. What is the behavior of the fan system and the Bravo River in relation to local topography and climatic change in recent geological history?
2. What is the flood threat to the city, how has it changed in recent years, and how might it change in future decades?
3. What is the effect of engineering works on the Bravo River and in the area of the city that have modified the natural processes of the rivers and fans; and to what extent are flood protection measures in Ciudad Juárez successful in preventing loss to the city and its inhabitants?

From these aims, there are two expected major outcomes from this research:

1. Understanding of the processes of alluvial fan evolution, and river behaviour, in the study area that includes: the nature of rock formations and their susceptibility to erosion, locations

of the key sources of sediment feeding the streams, capacity of streams and their ability to transport sediment.

2. An analysis of the hazards to the population of Ciudad Juárez that result from the alluvial fan and river processes that include: flood maps using GIS, modelling of flooding, and its effects on the city's population. This may assist hazard mitigation planning in the city.

1.2. BACKGROUND TO THIS STUDY

1.2.1. The nature of the problems

Ciudad Juárez is located in a desert area prone to catastrophic flooding events derived from two principal sources: ***Firstly,*** episodic storms which produce inundations with interruption of the transportation system as well as important damages and losses to people and their homes mostly those who live in areas of active alluvial fans. ***Secondly,*** the Bravo River is the other source of risk for approximately 50% of Juárez population who live near to the valley areas. ***In addition,*** there is threat of landslides in some parts of the city close to the mountains, but this aspect is not included in this thesis, since it is relatively limited in importance, requires a different modelling approach; landslides will be considered in later research. In the following subsections of this background description of the fundamental aspects of the flooding problems are highlighted.

The Bravo River begins in the Rocky Mountains, USA, and during its history has changed its course many times producing disasters and inundations. High intensity short duration episodic storms in the study area between 1969 and 2009 led to severe flooding that caused problems for the hydraulic infrastructure of dykes, and landslides on the Camino Real road (a new highway through the hills west of the city).

In order to illustrate the scale of the problems, a major historical example is outlined later in this chapter and detailed in appendix 1A: the events of 1864 and1897 in the Chamizal area next to the Bravo River that resulted in an International treaty between Mexico and USA governments.

1.2.2. Justification of this research

The disastrous precipitation events causing flooding in the city in recent times clearly demonstrate an urgent need to understand the processes operating and what actions are necessary to implement in order to avoid or mitigate the flooding and landslide problems, which occur in a city built upon active alluvial fan system. On the other hand, urbanization of the city has been extended into areas subject to high risk of damage because of this system. For this reason, and because runoff increases in urbanized areas due to covering of absorptive substrate, it is important to understand the effects on Juárez city, for mitigation and planning. In addition, there is little published research on the processes of the alluvial fans, so a key aspect of this thesis is to develop the knowledge base, so that it can be applied to assist in future planning of Juárez City. Thus, municipal construction specifications should be reviewed in order to build the new homes in areas away from active alluvial fans.

1.3. LOCATION AND DEMOGRAPHIC FEATURES OF THE STUDY AREA.

Ciudad Juárez, Chihuahua State, is located adjacent to the north border of México, next to El Paso, Texas, USA (Latitude 31° 07´ 38" N -31° 48´ 00" N, Longitude 106 ° 98´ 44" W-108 ° 06´ 57" W) and lies between the Bravo River to the north and Juárez Mountains to the South (Figs. 1.1, 1.2A, 1.2B and 1.2C). Juárez dates back to 1659 and has an estimated population of 1, 313,318 in the 2005 census (although now is estimated to be approximately 1,5 million), a territorial area of 4,853.8 km^2, an urbanized area of 225 km^2, a perimeter of 323 km, and a mean sea level elevation of 1150 m above mean sea level (INEGI 2002).

Figure 1.1. A) Location of major features of the study area. BR: Bravo River; Urbanized area; IDF: location of rainfall gauge station in El Paso Texas (which provides the Intensity Duration Frequency dataset); 24HMR: location of rainfall gauge station in Juárez (24 hours Maximum Rainfall). Source: Map of America (Google 2007). And B) Shows Map of America where red point shows location of study area. Source: www.maparchive.org/.../north_america_ref02.jpg.

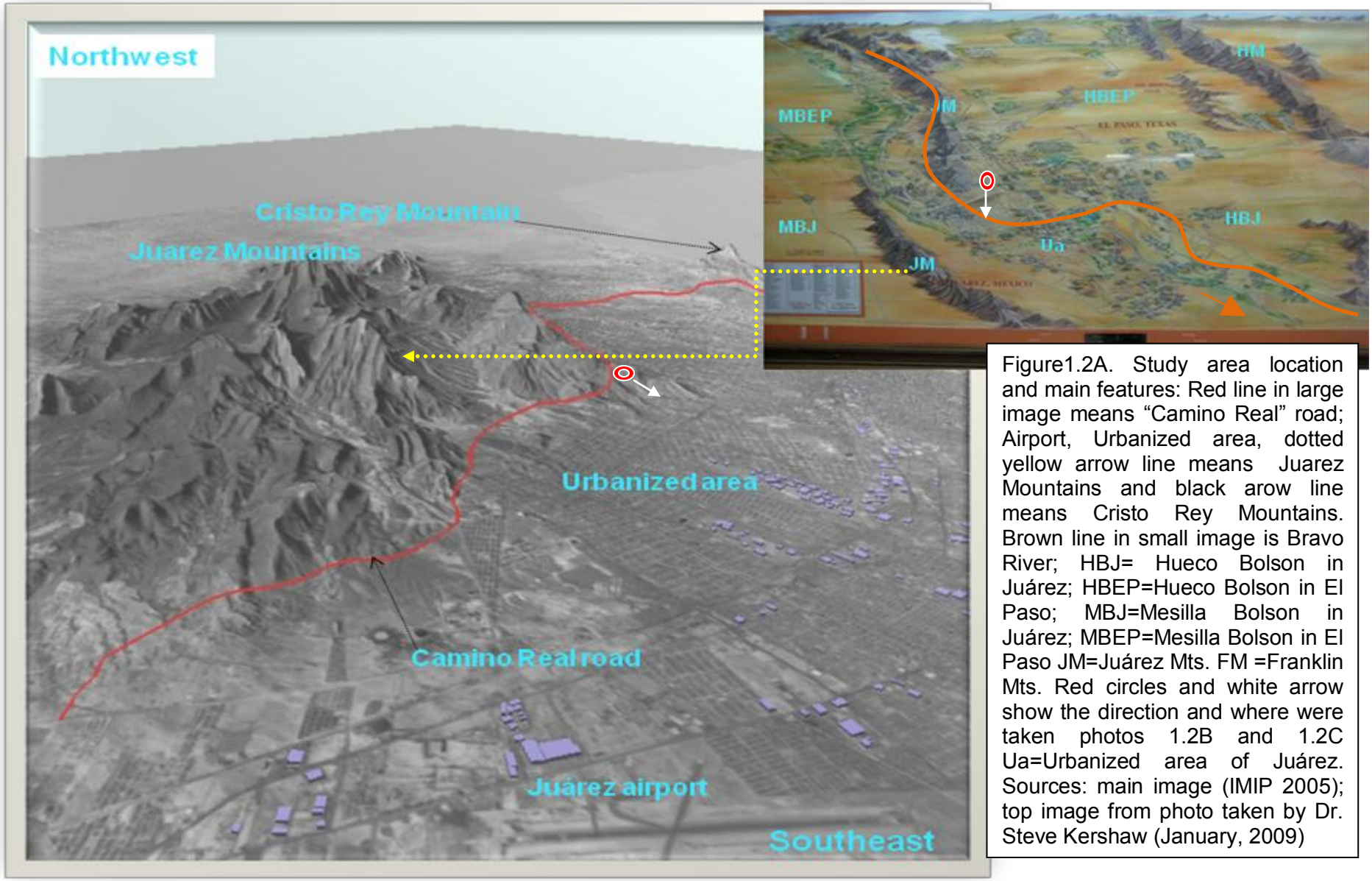

Figure1.2A. Study area location and main features: Red line in large image means "Camino Real" road; Airport, Urbanized area, dotted yellow arrow line means Juarez Mountains and black arow line means Cristo Rey Mountains. Brown line in small image is Bravo River; HBJ= Hueco Bolson in Juárez; HBEP=Hueco Bolson in El Paso; MBJ=Mesilla Bolson in Juárez; MBEP=Mesilla Bolson in El Paso JM=Juárez Mts. FM =Franklin Mts. Red circles and white arrow show the direction and where were taken photos 1.2B and 1.2C Ua=Urbanized area of Juárez. Sources: main image (IMIP 2005); top image from photo taken by Dr. Steve Kershaw (January, 2009)

Figure 1.2B. View across the Hueco Bolson from the "Wind-Rose" panoramic viewpoint located in km 15+100 of Camino Real road overlooking Juárez. The photo illustrates the urbanized areas of Juárez and El Paso Texas; dotted black line shows the Bravo River course, which also represents the political division between México and USA.

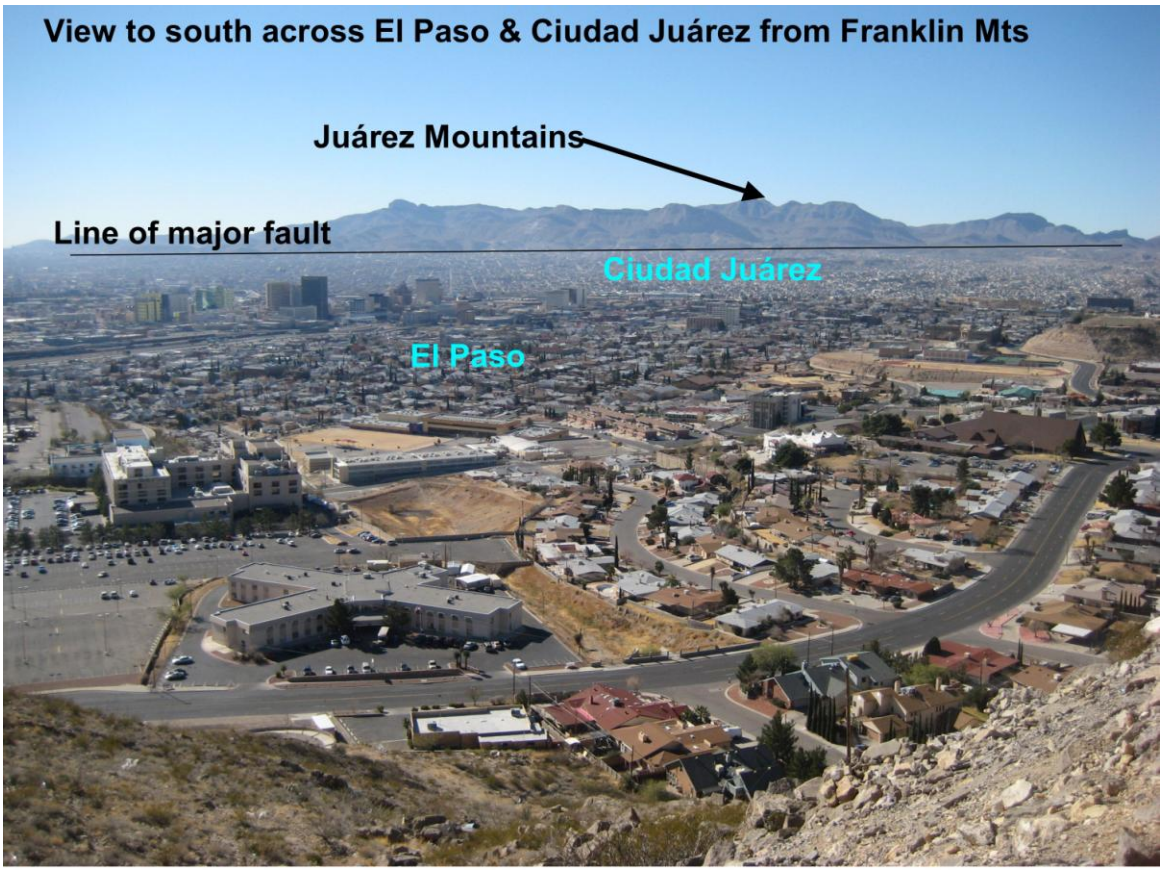

Figure 1.2.C. View across the Bravo River from the Franklin Mts in Texas, showing the Bravo River basin with El Paso in the foreground, Juárez in the background and the Juárez Mts in the distance, with indication of major normal fault across the front of the Juárez Mts.

1.4. CLIMATIC SETTING

1.4.1. General situation

In the study area, climatic information about weather is scarce. Only climatic records from 1957 to 2009 are documented. Therefore these datasets were used to identify two key features: A) Average annual accumulated precipitation of 254 mm that confirms the arid climate in the study area in recent times (See Fig. 1.3). B) Monthly average and monthly maximum precipitation registered during the same period is presented in Fig. 1.4 suggesting that highest rainfall fall in the summer months of July, August and September and little rainfall in the winter season. These are indicators of the desert characteristics of the region. Thus, to include the influence of some atmospheric perturbation, section 1.5.1 considers some features important for the rainfall design model adapted for the study area later in this thesis.

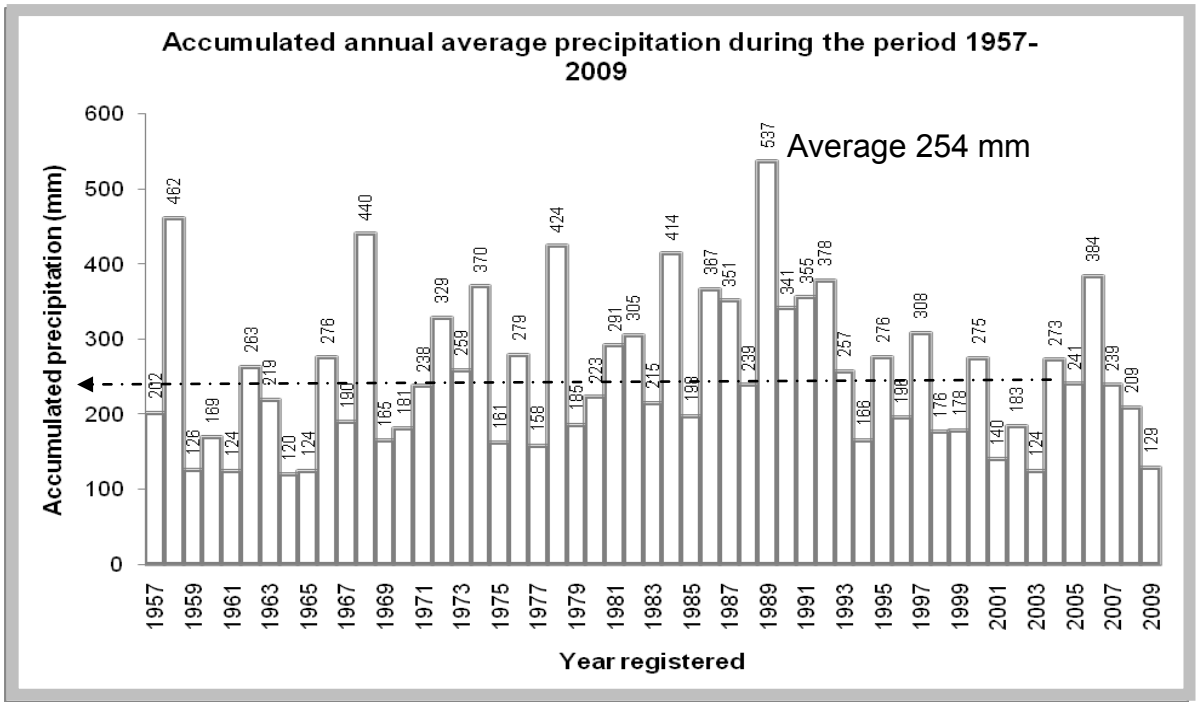

Figure 1.3. Accumulated annual average precipitation of the study area during the period 1957 to 2009. The total average is 254 mm. Source: CNA (2008)

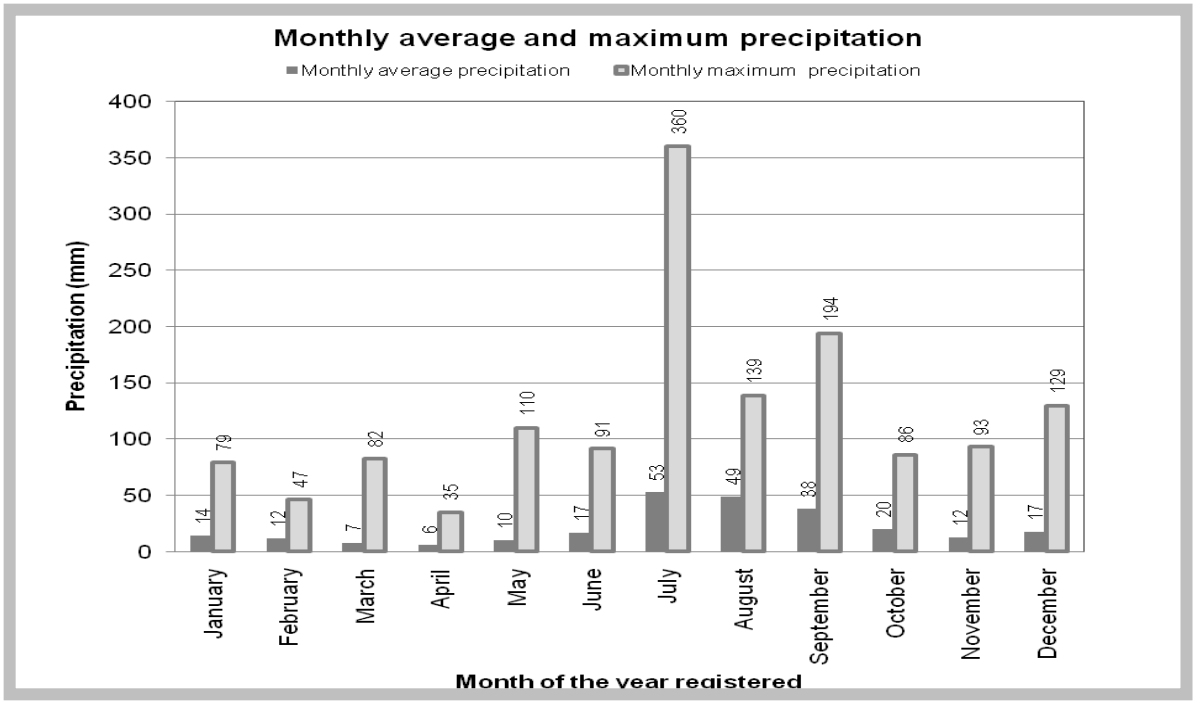

Figure 1.4. Monthly average and monthly maximum precipitation on the study area. Values are lower enough to consider the study area as desert. Source: CNA (2008) period (1957-2009).

1.4.2. El Niño Southern Oscillation (ENSO)

Nowadays Juárez city, as many regions of the world, has been affected by El Niño Southern Oscillation (ENSO) due to changes in atmospheric circulation patterns. These anomalies produced high intensity and short duration storms particularly in the region of this study. For this reason, a brief review of (ENSO) is presented in the literature review (see Chapter 2; sections 2.2.3; 2.2.4 and 2.2.5; Figs. 2.21, 2.22 and 2.23) and (NOAA 2009) which shows the weather from El Paso Texas from 1878 to 2008. Therefore, the design storm for the study area is based on episodic rainfall, derived from storms of high intensity and short duration typical of summer seasons. In addition, total annual accumulated precipitation between 1957 and 2009 (see, Fig. 1.3) and average monthly precipitation for the same period (see, Fig. 1.4) were provided by the National Water Commission of Juárez city (CNA 2008). Thus, between 1969 and 2009, only the maximum daily precipitation for every year (CNA 2008) is available as a continuous dataset (Fig. 1.5). Finally, Fig. 1.6 shows photographs of flood devastation, and Fig. 1.7 illustrates cliff collapse on the Camino Real road.

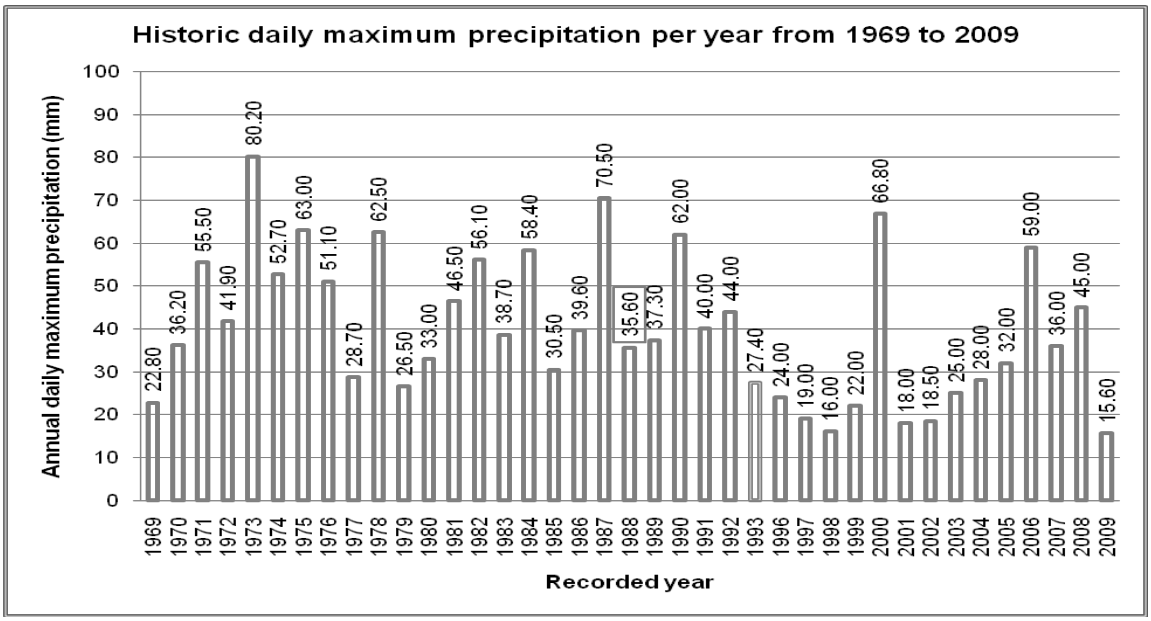

Figure 1.5. Episodic storms of high intensity and short duration registered in the study area during the last 39 years. This histogram shows the largest rainfall event which occurred within a single 24-hour period for each year, also called the 24-hour maximum rainfall (24HMR). The most intense event of 80.2 mm of daily maximum precipitation occurred in 1973, and the least intense was in 2009 Source: CNA (2008) for the period 1969-2006 and UACJ (2010) for 2007-2009. This histogram is part of the dataset used later in this thesis to evaluate extreme event statistics as part of the flood predictions affecting Juárez.

Figure 1.6. Illustration of the effects of the flooding in June 2006. Ojitos dyke and Trituradora reservoir: (A) and Los Ojitos (B) located at the Northeast of Juárez Mountains. In photo (C) is presented the effect of sediments deposited downward of the dyke and trituradora reservoir, one day after the storm event occurred in 09/06/2006. Also, in photo (D) a brigade of Mexican Red Cross helpers, evacuating, and recovering some belongings of people.

Figure 1.7. Landslide in July 2008 in the Camino Real road over a mountainous area of the road at position km 11+700. Note that the recent construction of this highway has led to instability of the surrounding rock mass, directly causing the collapse. The bedrock in this area is composed of metasediments in a nape sequence, and is heavily fractured, assisting collapse. Because of the weakness of the bedrock in the mountains, much debris was delivered into the city by flooding.

1.5. HISTORICAL PERSPECTIVE

This section describes the historical perspective of the study area and its long-term problems of flooding. This information is treated here rather than in Chapter 2 in order to emphasise the importance of these issues to the local Juárez population, and to emphasise the need for this research. In Appendix 1A Fig. 1A.1 is presented an historical summary dating back to 19th Century (1827-2007) including some information given for witnesses.

In addition, this section illustrates how Bravo River channel moved its path by cutting its banks or beds many times due to competence increment. This competence or velocity increment sometimes was strong enough to produce two meanders shifts during a few months like that occurred during the spring of 1865 along the Mesilla Valley. Similar processes have occurred during recent times stimulated by climate changes and producing

shifts that originated the Chamizal and Cordova Islands. Mack and Leeder (1998) explored these hydrological processes mentioning at least three avulsions of the Bravo River along the Mesilla floodplain (see Appendix 1C and Figs. 1C.1; 1.C.2 and 1.C.3). However, with regard to the study area, Chamizal and Cordova islands were formed during 1844 and 1852 in the north-central part of the Hueco basin. The best-documented case of lateral channel erosion occurred from 1852 to 1889 where the position of the river in the Hueco Basin deserved international attention of Mexico and the United states Authorities. During this event the river moved south-southeastward as much as 1km, causing many unconformities of people which disputed its properties the problem was named “The Chamizal case”. Other events occurred during 1865 in the northern part of the basin and finally in 1903 and 1912 in the southern part of the basin. The last avulsion (1912) occurred in only once flood season. The next section briefly explains the problem derived by the controversy surrounding the USA-Mexico border promoted by flooding events (The Chamizal problem). The information is supported by microfilms available in the UTEP (El Paso Texas University Library and are included in Appendix 1A).

1.5.1 Chamizal and the Cordova Island Problems.

1.5.1.1 Background.

The Chamizal and Cordova islands are two important ancestral terrains nowadays located near the Bravo River along the border line which defines Juárez city and El Paso Texas territories. These islands are the facts of historical Bravo River channel changes which are detailed in Appendix 1C (Mack and Leeder, 1998) and Figs. 1.8 and 1.9 of this chapter. As stated by International Boundary Water Commission (IBWC 2006) (México/United States) the limit between these two countries along El Paso Texas until the Gulf of México was defined by a permanent parallel line following the Bravo River channel highest elevation in agreement with the treaties of 1848 and 1853. Therefore, Bravo River changes trajectory occurred not affected the horizontal boundary line which was established and marked in 1852. Shortly, from 1852 to 1864 natural changes in the Bravo River course occurred. Thus, due to gradual erosion of the banks as well deposition along its plains a portion of the Chamizal tract changed and sediments on the surrounding Cordova Island was levelled. Thus, the Bravo River Channel moved from El Paso Texas area to Juárez city

causing migration of the Chamizal area into Texas (see Figs. 1.8 coffee coloured line) After that another flooding occurred in 1897 which provoked the necessity to canalize the Bravo River channel in order to avoid disasters (Fig. 1.9).

The channel migration of the Bravo river was caused by lateral erosion of its banks and further deposition on the surrounding Chamizal area which was occurred during the spring floods from 1864 to 1868 (Mueller, 1975). Thus nearly 2.5 km of land currently located in the El Chamizal area created by lateral erosion over a period of five years legally became USA territory, where it it still is today (Mack and Leeder, 1998). Despite the convention of 1910 were (Chamizal case) resolution took place, the Mexican commissioner argued that in agreement with the ancestral Guadalupe Hidalgo treaty of 1848 the fixed line should be applied with retroactive effect because the lateral banks of the Bravo River never changed its position and therefore the channel never abandoned its bed. Furthermore, after the convention of 1910 many controversial discussions and diplomatic meetings between México and U.S.A were made in order to solve the problem. Finally on January 14, 1963 were emitted the following arbitration recommendations. The agreement awarded to México 366 Acres (1.48 Km^2) of the Chamizal area and 71 Acres (0.29 Km^2) east of the Cordova Island. Additionally no payments were made between the two governments and the USA received compensation from private Bank for 382 structures included in the transfer. The USA received 193 Acres (0.78 Km^2) of Cordova island from México and the two nations agreed to share equally in the cost of rechanneling the River (Wikipedia, 2012, for a general discussion) (See Fig. 1.9).

In summary, this section highlights the importance of the climate change in the hydrologic processes of the Bravo River. These processes named, capacity and competence were erosion and deposition took place formed these two islands and changed the trajectory of the river in such a way that were deserved the political attention of two nations. Nowadays the international bridge named Cordova-Americas has a complete and efficient system of control emigration from México into USA but from USA to Mexico there is no effective border and is located in the same position as the 1852 and 1989 year positions.

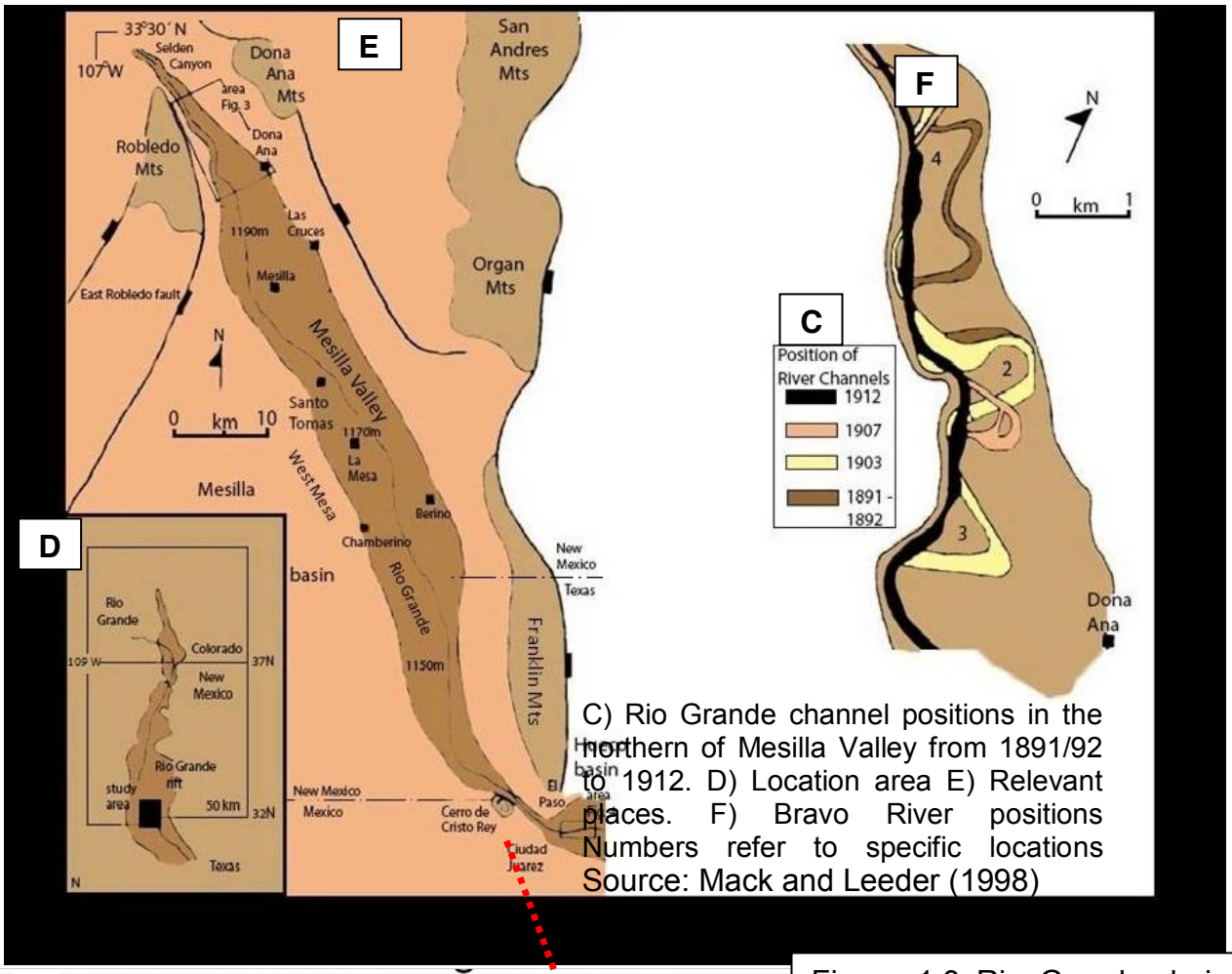

C) Rio Grande channel positions in the northern of Mesilla Valley from 1891/92 to 1912. D) Location area E) Relevant places. F) Bravo River positions Numbers refer to specific locations Source: Mack and Leeder (1998)

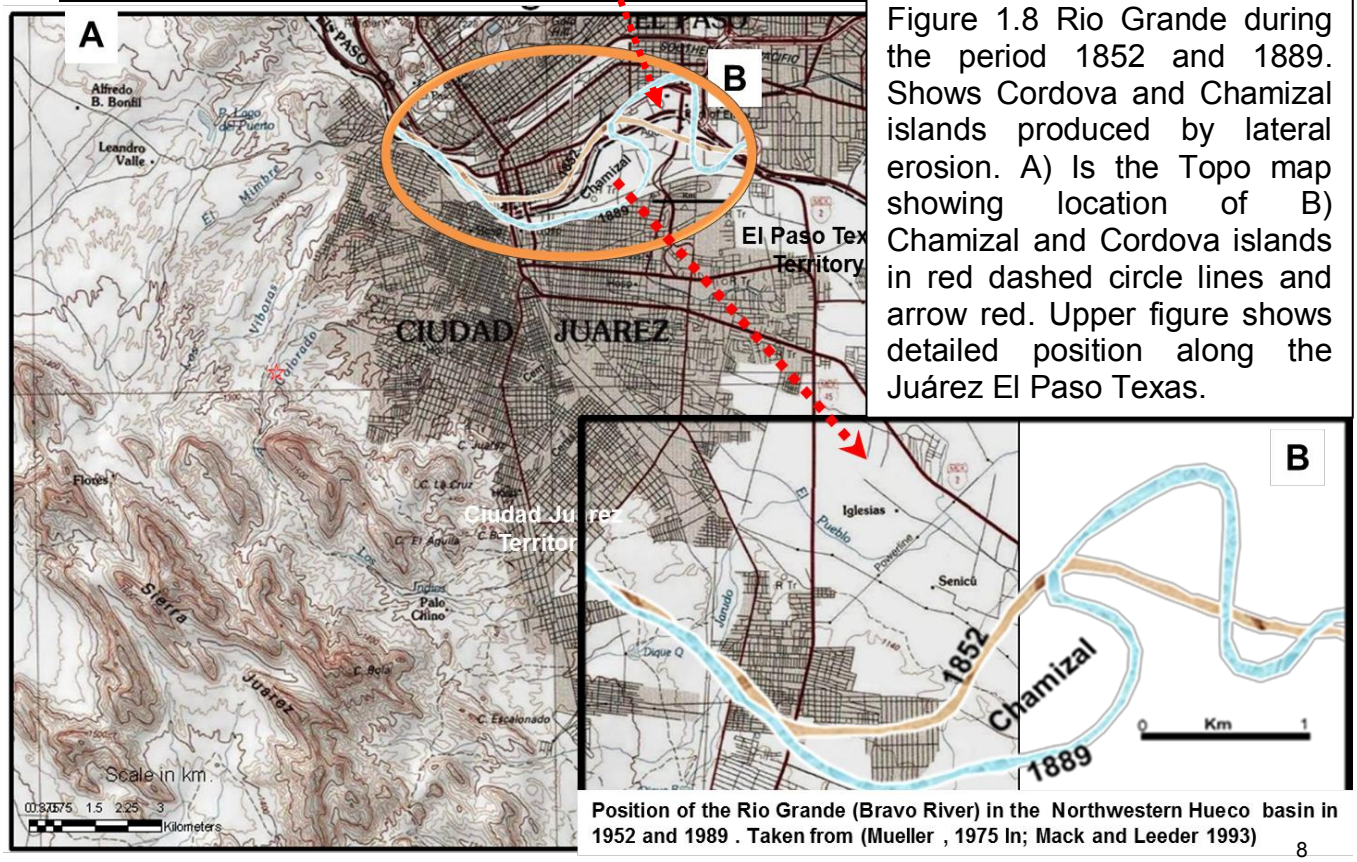

Figure 1.8 Rio Grande during the period 1852 and 1889. Shows Cordova and Chamizal islands produced by lateral erosion. A) Is the Topo map showing location of B) Chamizal and Cordova islands in red dashed circle lines and arrow red. Upper figure shows detailed position along the Juárez El Paso Texas.

Position of the Rio Grande (Bravo River) in the Northwestern Hueco basin in 1952 and 1989 . Taken from (Mueller , 1975 In; Mack and Leeder 1993)

8

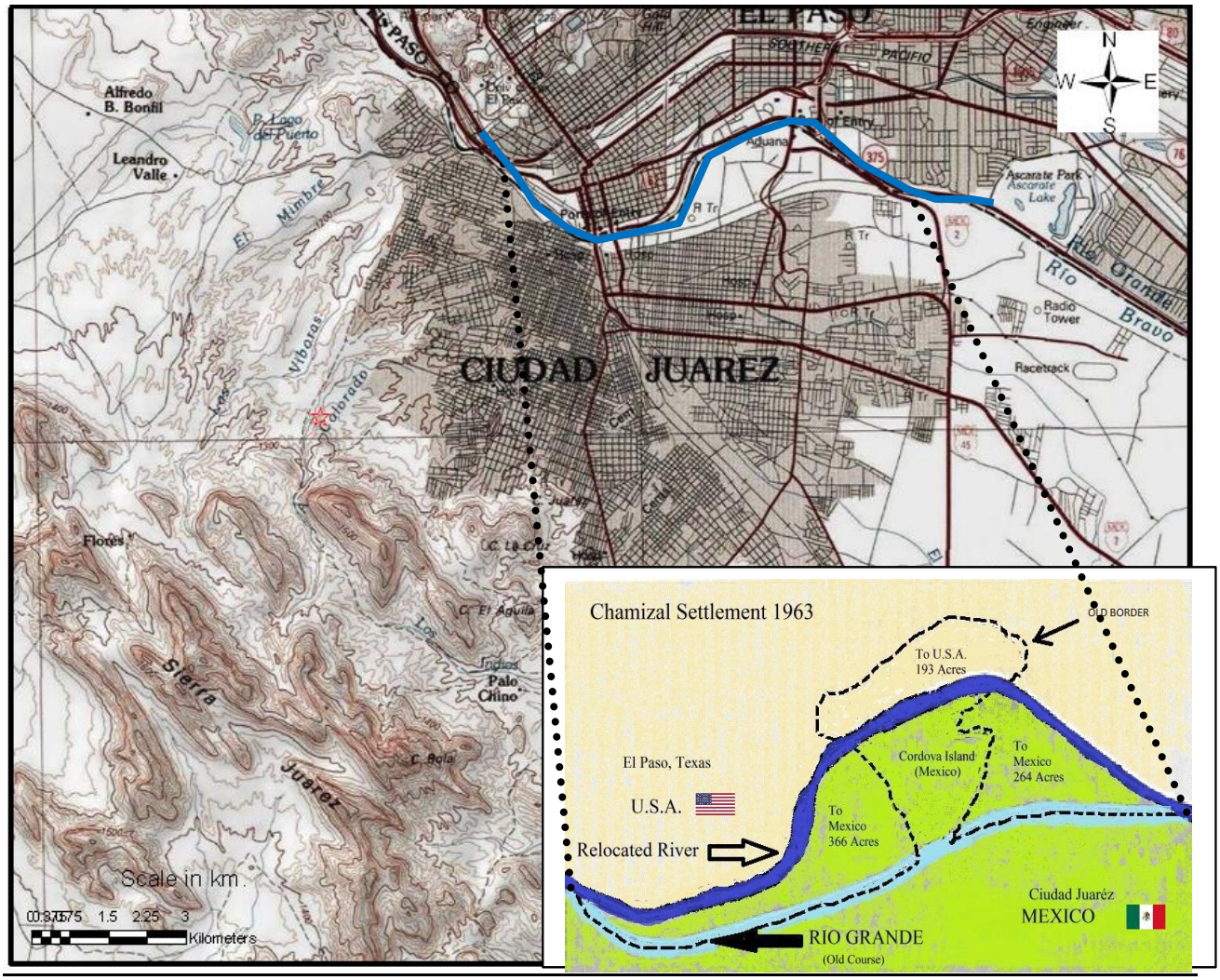

Figure 1.9. Chamizal case convention of 1911 signed on January 14, 1963 between Mexico and U.S.A. **A)** Modern Bravo River path (Blue Line) showing the political Border of Juárez city and El Paso Texas. **B)** Shows areas returned to México property (Chamizal west of Cordova island 366 Acres =1.48 Km^2 and east of Cordova Island 71 Acres = 0.29 Km^2) and areas that should remain to U.S.A (193 Acres=0.78 Km2) Source: Topo-maps (ESRI, 2011) and (Wikipedia, 2012).

1.6 Thesis outline,

The main features of the study area were highlighted in this introduction chapter given special emphasis in some background datasets of Juárez city including flooding events and the big problems derived from them. However, the chapters of the thesis are structured as follows:

Chapter 2 comprises a literature review of the main factors in relation to the thesis divided into five parts: **A)** Faults during Cenozoic and Quaternary time are key features to understand alluvial and fluvial soils behaviour and are treated on the first section of this chapter. **B)** Description of fundamental concepts involved in the alluvial fans production. **C)** Description of Pliocene-Pleistocene geology of Santa Fe Group and Upper Santa Fe Formations are illustrated. **D)** In addition, published works regarded to climate change on the study area and its behavior in the alluvial fans and terrace development are also studied. **E)** Finally, a section on hydrology, meteorology and datasets needed to assess the methods and results chapters are included.

Chapter 3, Methods, explains how digital elevation models were addressed using Arc-GIS platform computer programs. Also, soils classification test and the geophysical method OSL (Optically Stimulated Luminescence dating technique) applied to alluvial fans outcropped the study area were analyzed. Finally, this chapter describes methods to assess the flooding risk models of the three sectors selected for the study area using a GIS multi approach Platform based on digital flooding models.

Alluvial fans derived from Juárez mountains and fluvial Bravo River terraces dynamics were assessed in Chapter 4. Therefore this chapter performs the results of these interbedded Pleistocene to Holocene time sedimentary structures.

With regard to flooding, HEC-HMS computer program gives discharge results of eight basins; Water stored in 52 dykes allocated in the study area and its behaviour. Finally, a description of the stream network system is assessed in chapter 5.

Chapter 6 presents the flooding risk models results for the three sectors located in the study area using a combination of computers programs: Arc-GIS with PreGeoprossessing and Post Geoprossessing modules.

Chapter 7 discuss the results derived in Chapters 4, 5 and 6 in relation to the research aims and main questions presented in Chapter 1. Finally, Chapter 8 gives conclusions and recommendations to improve the civil engineering hydraulic behaviour of dykes and floodgates allocated along alluvial fan sectors as well the Bravo River channel and its floodplain territory.

CHAPTER 2
LITERATURE REVIEW

2.1 INTRODUCTION

This chapter comprises a review of relevant literature documented in the following two sections. Firstly dealing with Cretaceous, Tertiary, Quaternary and Pleistocene-Holocene tectonic regional settings associated with fluvial and alluvial sedimentary structures. Secondly, a climate-focused overview of meteorological, hydrological and statistical approaches for flooding models.

2.1.1 Cretaceous, Tertiary and Quaternary tectonic settings of the study area.

The geology of the study area was examined in some master theses available in El Paso Texas University Library (UTEP): several authors (Swift, 1973; Wacker, 1972 and Nodeland, 1977) described Cenozoic tectonics structural features integrated in the more recent published geological map of the study area (Drewes and Dyer, 1993) (see Fig. 2.2).

The Juárez mountain structure is complex because many tectonic events occurred during Cenozoic time in such way that actually it is difficult to reconstruct it. However, Nodeland (1977), García (1970) and Wacker (1972) are the most relevant publications analyzed in the present research, associated with a unique and realistic deformation model. This model suggests the spatial distribution and arrival time of at least three major thrust sheets occurred along the study area (see Fig. 2.1). Nodeland (1977) stated that Cretaceous rocks located Northeast of Sierra de Juárez began to deform adopting a characteristic Alpine deformation style early in Paleocene time. After that, during Eocene-Oligocene the emplacement of intrusive and extrusive igneous rocks reacted causing an opposite tensive strength and many derived normal faults took place. Then, during Pliocene to Pleistocene time (Basin and Range Province) many bolsons as Hueco and Mesilla Bolsons were formed as a result of the sedimentary filling of depressions. Thus, evidence of Quaternary scarps along Tertiary faults indicates that the Basin and Range Province is currently active in the study area.

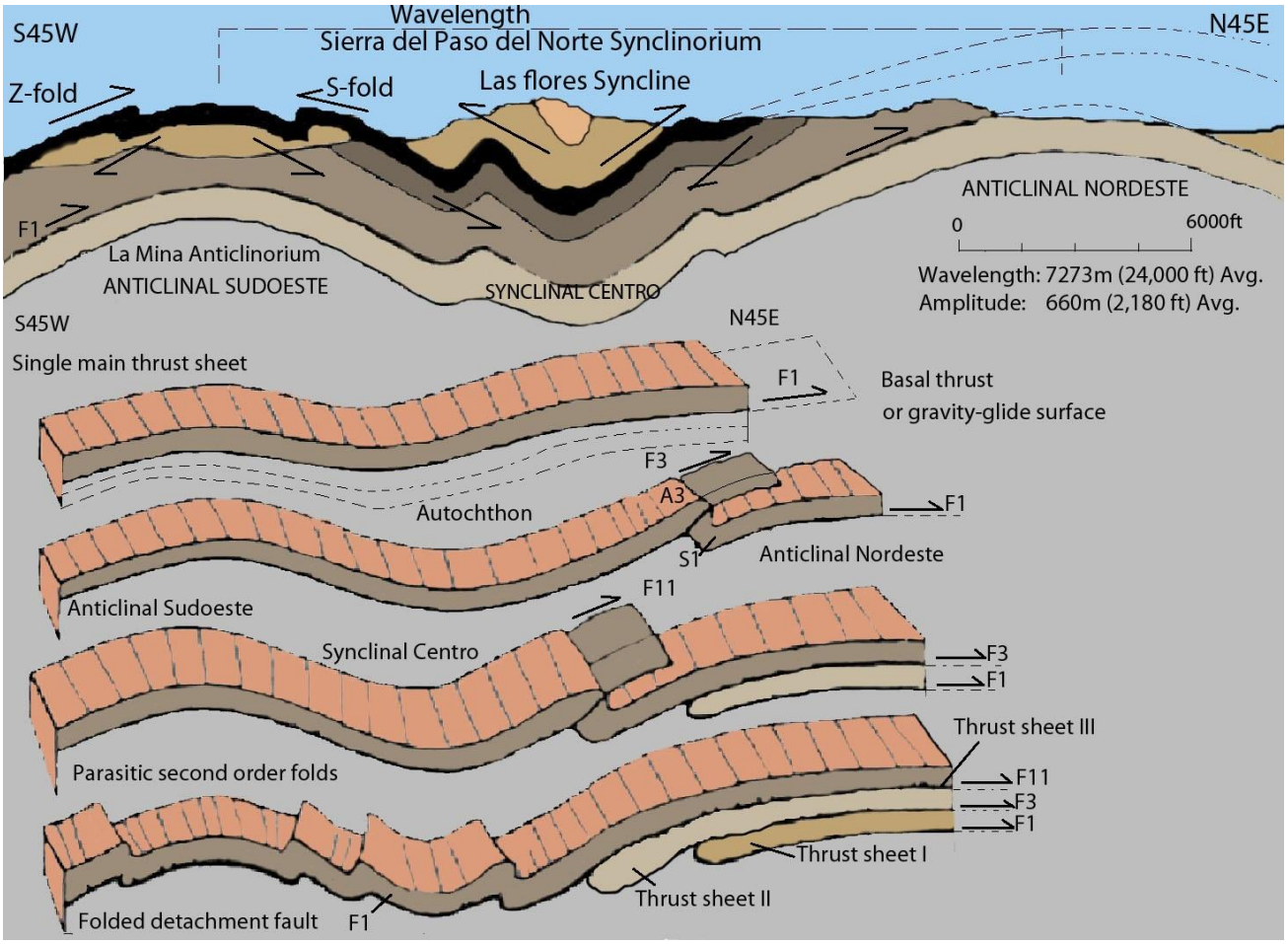

Figure 2.1. Structural and tectonic model showing evolution of Juárez Mountains as well as location of Anticline Northeast, Synclinal Center and Anticline Southeast faults F1, F3 and F11 as well as thrust I, II, and III are related each other. Lower diagrams: structural model which show the sequence arrival order of thrust that affected Cretaceous marine and continental rocks from older to younger (older F1 thrust and F11 younger thrust) text and description were modified and taken from: Nodeland (1977) adapted by David Zuñiga (2012).

Note: F1, F3 and F11 of Nodeland (1977), are equal to: Juárez, La Año and Los Indios thrust faults of Drewes and Dyer (1993) respectively (see Fig. 2.3).

In short a more detailed structural deformation model of Juárez Mountains is shown in cross section given in Fig. 2.2. This section shows how the arrival sheets thrusts are distributed along the study area and are included in the geological map constructed by Drewes and Dyer (1993) (See Fig. 2.3). This map contains all the previous works already published by Nodeland (1977), Wacker (1972), Swift (1973) and García (1970) among others.

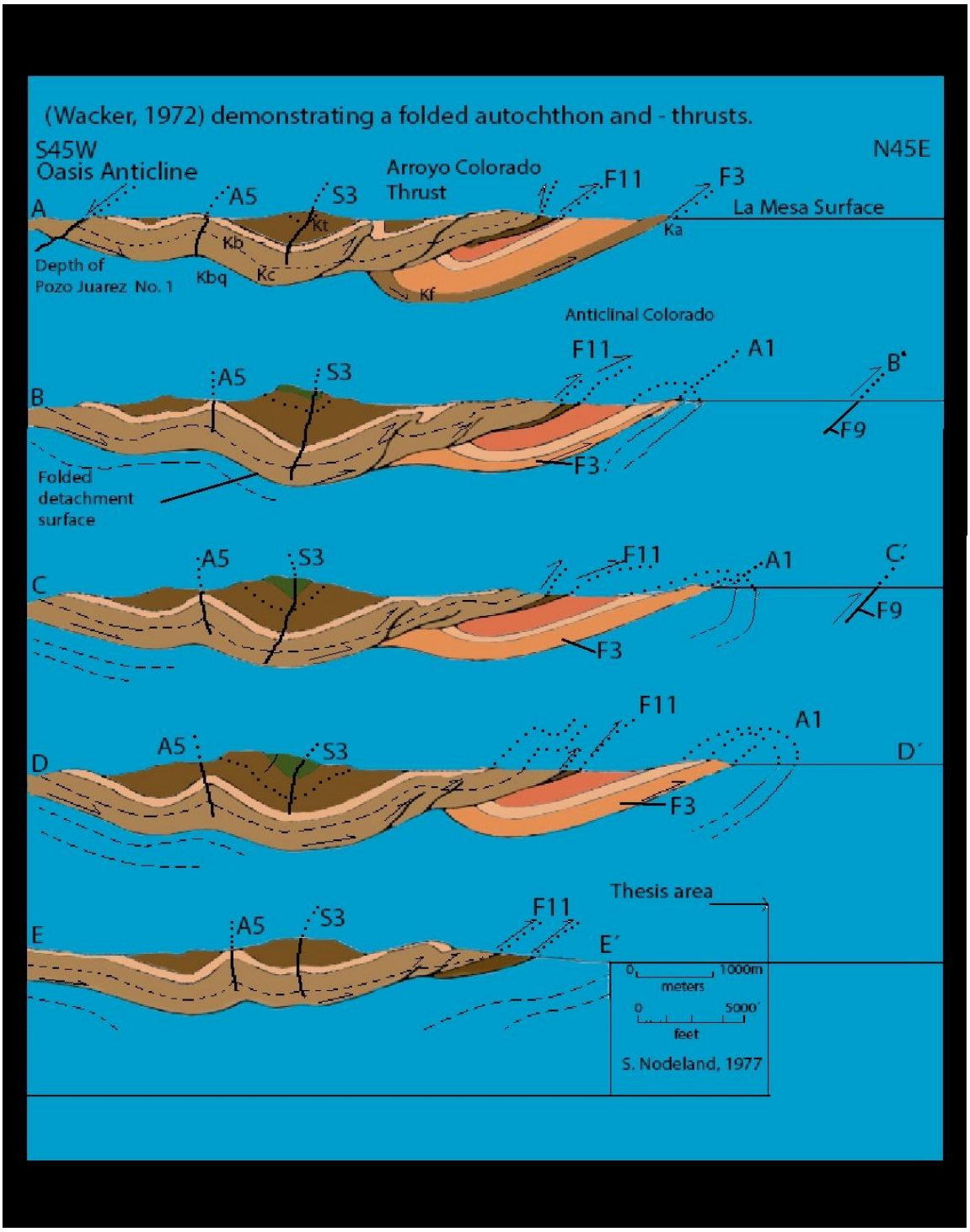

Figure 2.2. Cross sections A, B, C, D and E show the deformation style of Juarez Mountains as well as the complex sets of faults and folds. Note that deformation of Juárez Mountains is more severe at the Center sector where Anticline Colorado is located in contact with older alluvial fans. Source: Wacker (1972) adapted by David Zuñiga (2012).

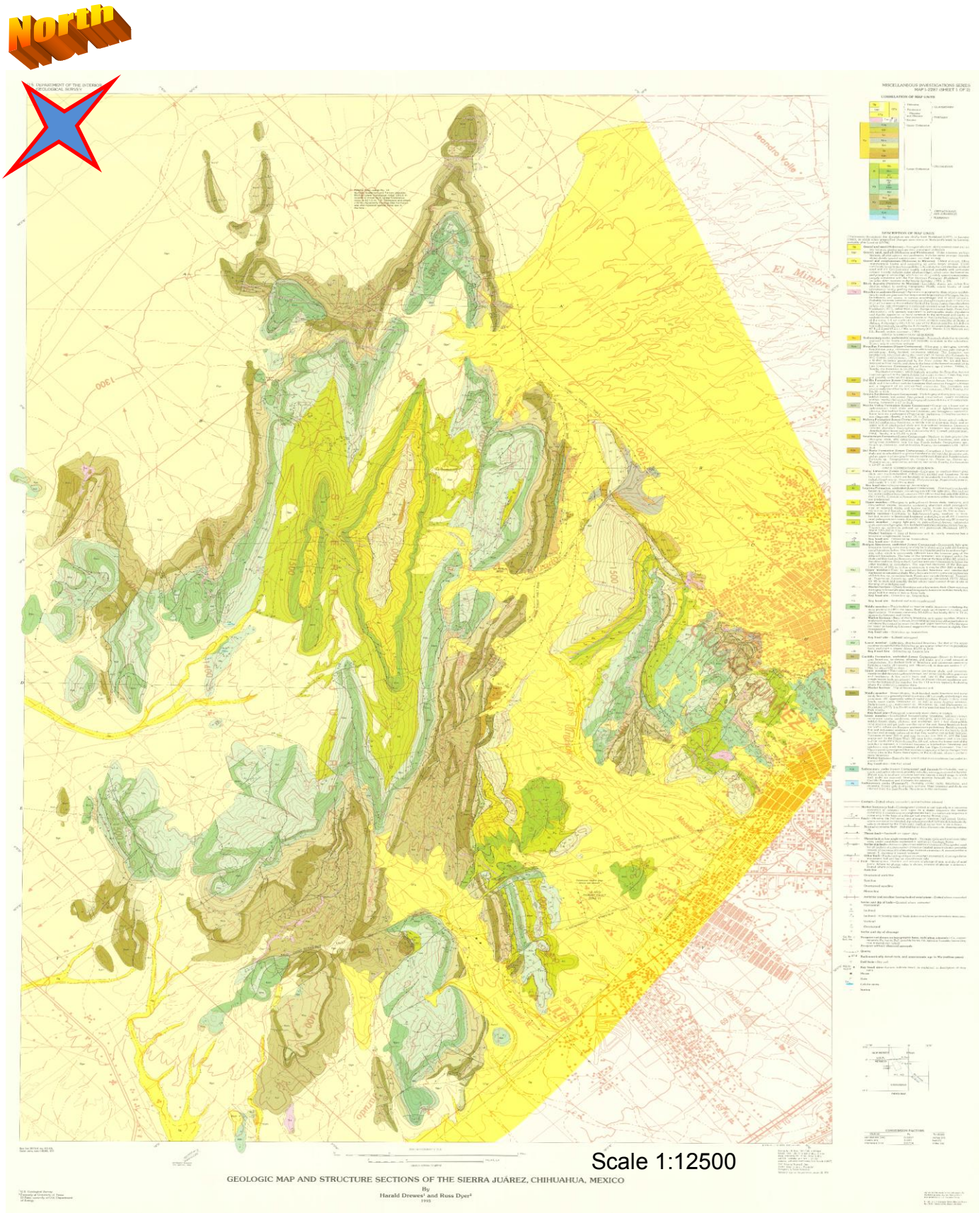

Figure 2.3. Geological map of the Sierra de Juárez Chihuahua, México. Note: map is

rotated and geographic coordinates are indicated along the reference frame. Source: Drewes and Dyer (1993).

Furthermore, García (1970) stated that post-Cretaceous and pre-Pleistocene age andesitic plutons bordered along both edges of the Rio Grande from El Paso, Texas and Juárez City northward to Vado, New Mexico. These andesitic bodies are aligned south to north, and named as: Bola; Juárez; Muleros; Campus; River; Westerner; Colorado; Thunderbird; Three Sisters, and Vado. With regard to the Juárez Mountains, Bola andesite is recognized because some outcrops are located in Cerro Bola in form of thin sills offsetting Cretaceous marine rocks at all places where the Bola andesite is observed. The previous information is relevant to this research because it allows linkage of fault contacts within sedimentary marine as well continental recent deposits also described in results Chapter 4.

In similar research, Uphoff (1968) states that an older thrust named Rio Grande which is marked on the fault scarp of Diablo platform edge in the northern Hueco bolson crops out in the study area, formed during late Cretaceous and Paleocene time. Thus, the ancestral Chihuahua trough was destroyed and its deposits were transported filling the northern Hueco outcropping in the study area. Similarly, Mesilla Bolson, also outcropping in the study area is a typical Basin and Range intermontane basin underlain by Cretaceous and older strata filled with Tertiary and Plio-Pleistocene volcanic clastic deposits. North of the study area, the evidence of north-trending fault dissection along the Bravo River is marked by faults as the Robledo Fault located southeast of the Aden Crater area (Kottlowski, 1958). This information is also relevant for this research because it allows identification of the limit of Hueco and Mesilla bolsons, which are fundamental features of the study area.

2.1.2 Alluvial fans aspects.

Geomorphologic features of sedimentary structures as alluvial fans are explored in this section. Therefore, the processes involved and the geometry adopted for these sedimentary structures involves many important processes and some relevant concepts (see Figs. 2.4 and 2.5). Blair and McPherson (1994) and Bull (1991) stated that primary

sedimentary processes as: landslides, gravity flows and sheet floods or incised channel sheet flows construct and maintain the fan shape. On the contrary, secondary processes comprise so many factors as: (a) water surface action b) wind action, (c) biological turbation, (d) aquifer action, (e) flooding, (f) neotectonic movements and (g) sieve lobes on alluvial fans. The previous processes common during the second fan stage are important because produce diverse and complex sedimentary structures. In this regard, caliche (also called calcrete and calcisoil) is an important stage of soil development relevant to assess alluvial fan dynamics in the study area.

Machete (1985) and Bachman and Machete (1977, Fig. 38 and 39) assembled data from a range of papers published mostly in the early 1970s, and this shows accumulation of calcretes at various times in the latter half of the Quaternary period. Bearing in mind these studies are somewhat older and therefore perhaps less well-constrained than more recent year, of considerable potential significance for this PhD study is the correlation diagram presented by Machete (1985) and Bachman and Machete (1977, Fig. 39). Their compilation shows three areas with a calcrete formed at around 70-75 ka, near Albuquerque, San Acacio and Las Cruces. In the Las Cruces area, the calcrete ages are given for different parts of the sedimentary basin (Machete, 1985; Bachman and Machete, 1977, Fig. 39, right-hand column); thus the border and valley of the area have calcrete dates ranging from 100+/-50 ka to 50 ka, whereas the basin ("bolson") is more tightly constrained to 75 ka. It is perhaps significant that this more tightly constrained calcrete age is from the bolson, which is expected to be wetter for longer since it is expected to be the area where standing water would persist; in the valley and border areas desiccation may have been more easy to achieve, thus periods of drying spread over a longer time period might explain the longer range of dates in those locations. Thus a pervasive episode of aridity around 75 ka might explain the presence of calcrete in the bolson; this is discussed further in Chapter 7 after the details of the new OSL dates are described in this thesis. Machete (1985) and Bachman and Machete (1977, Fig. 38, central graph) compiled slightly different calcrete age data from the Las Cruces area of New Mexico, with ages from ca. 100 - 50 ka and from ca. 20 - 12 ka; thus there is a gap between 50 - 20 ka when no calcrete formed. Therefore there is a little inconsistency between the two compiled datasets presented in Bachman and Machete (1977, Figs. 38 and 39), which is perhaps not surprising since they are presented as tentative, in that paper. Nevertheless, the overall conclusion that can be drawn from this comparison is that around 75 - 70 ka there was an

episode of aridity that affected both the Las Cruces area of New Mexico while younger dates show more localised effects of aridity. The implications of this information for the alluvial fans in the Juárez area are discussed in relation to new OSL dates in Chapter 7.

With regard to morphology Blair and McPherson (1994) state how cutting streams (which usually have defences of 1m to 10 m high and 2 to 150 m wide) could extend from the apex until tens or even hundreds of meters. These main components of alluvial fans could be identified using morphology. Erosive secondary forms, such as gullies perhaps produces features with this scale of relief and maybe develops laterally hundreds of meters. Sand sheet and aeolian sand-dune deposits 1 to 30 m high may moves on to the fan transforming its original structure. Coppice dunes form mounds 1 to 10 m long and 0 to 4 m high. Lateral changes of streams and rivers may result in the erosion of distal fan deposits, leaving cuts of 1 to 10 m high prolonging along the edge of the fan. All these structures already are common along the three alluvial fan systems located in the study area (See chapter 4).

Incised channels, Levees, and lobe boundaries could be identified using satellite images or topographic maps with 1 m interval contour level. The progress of alluvial fans may also be influenced by perennial lakes, marine influence (in much older times), aeolian sand sheets, or rivers that erode or overtop the distal fans. Furthermore, Figs. 2.4 and 2.5 show the different components of alluvial fans such as: main drainage basin, subsidiary drainage basin, beach ridges, debris flow remnants, rank drainage order of the drainage system, topographic apex, hydrologic apex, channel feeder, basin composed of three differents drainage systems, intersection point, active deposition lobe, gully or old channel, and mountain front embayment.

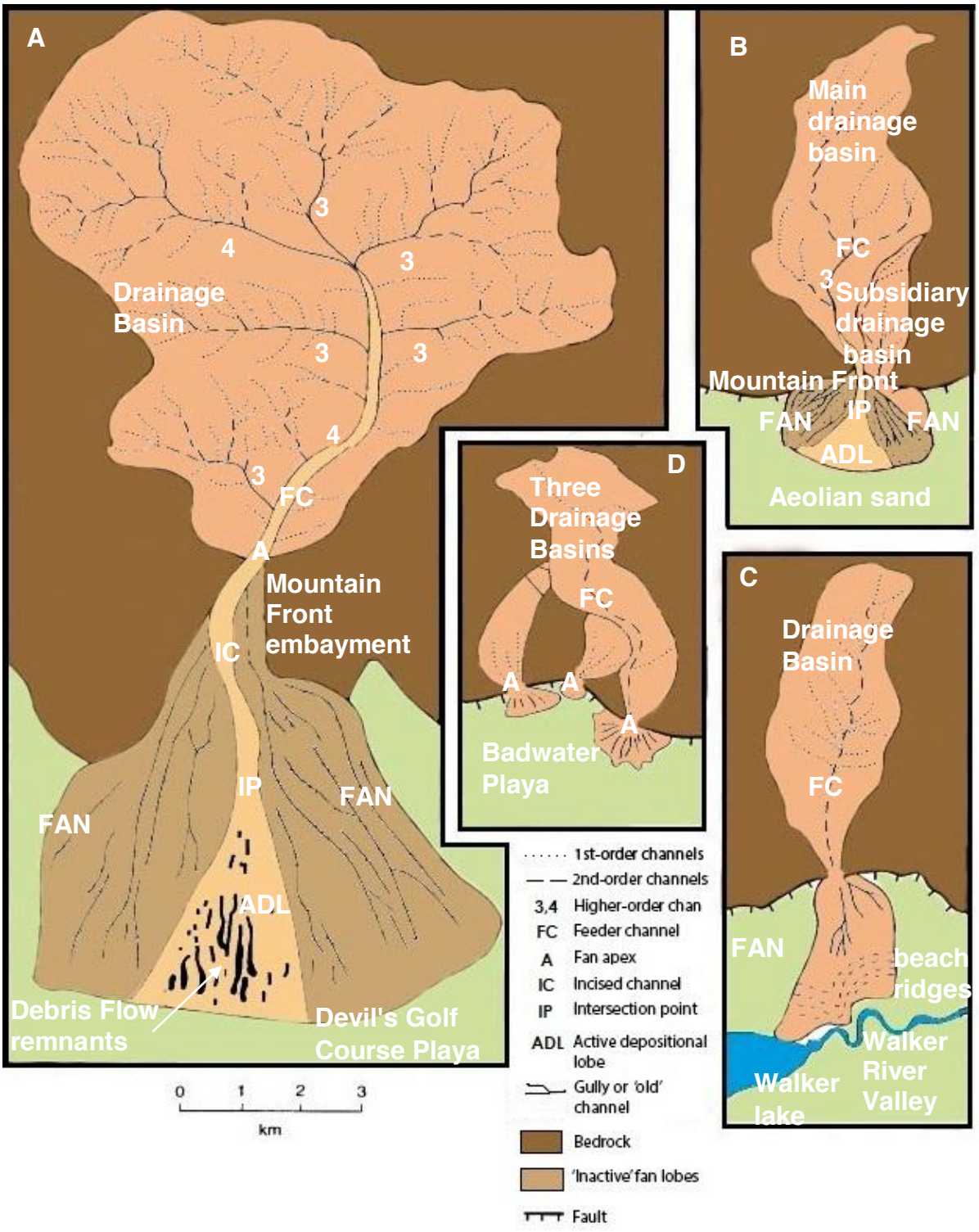

Figure 2.4. Plan view line sketches based on topographic maps and aerial photographs of the fans and drainage basins a) Trail Canyon, (b) Grotto Canyon, (c) Deadman Canyon, and (d) Bad water fans. Note that the stream order given to the drainage network system in Figure (a). Source: Blair and McPherson (1994) adapted by David Zuñiga (2012).

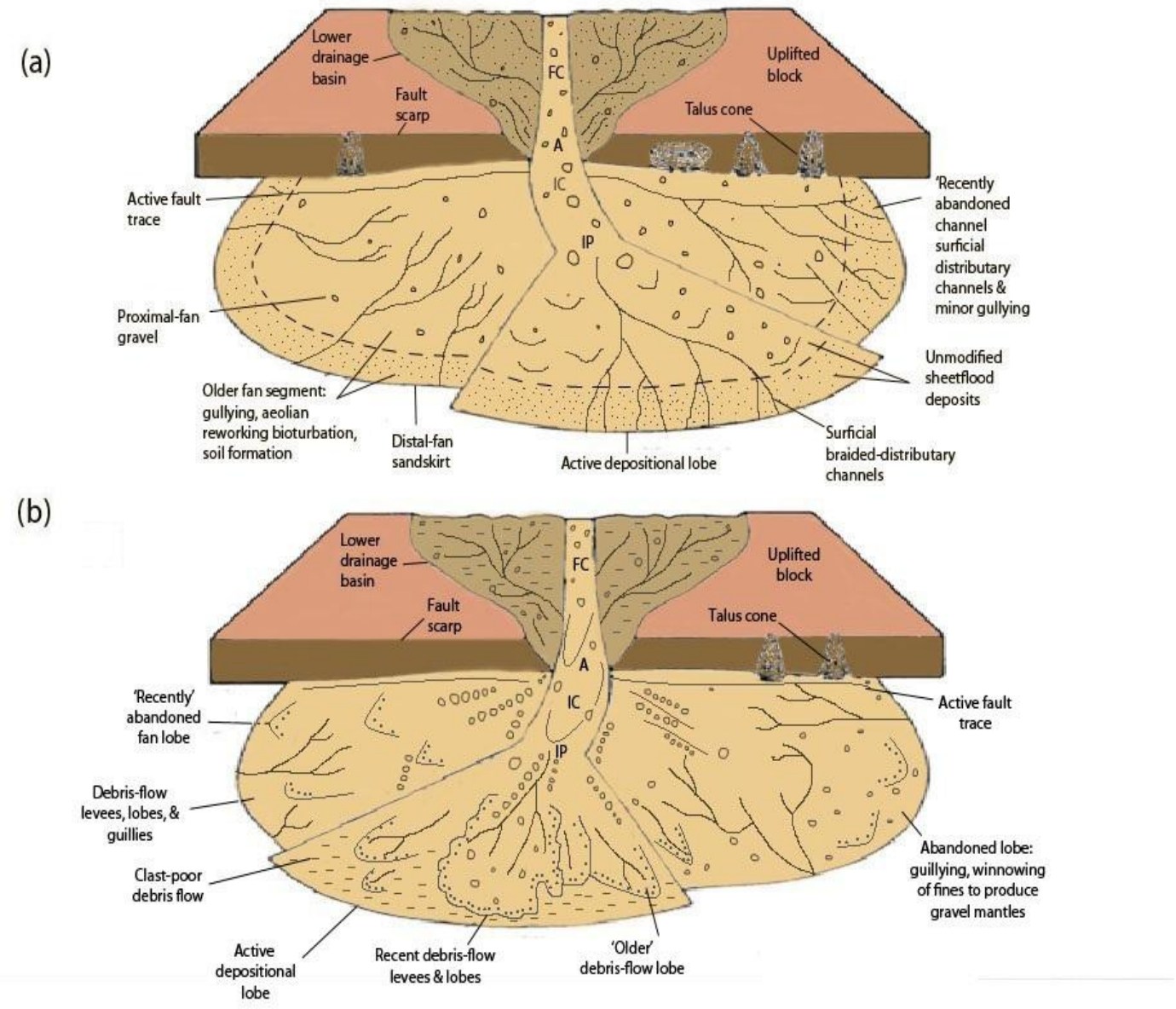

Figure 2.5. Schematic diagrams of the common primary and secondary processes on alluvial fans, including (a) those on fans dominated by water flows, and (b) those on fans dominated by debris flows. These diagrams are based on numerous fans studied by authors. Abbreviations are A= fan apex, FC= Feeder channel, IC= incised channel fan, IP= fan intersection point. Source: Blair and McPherson (1994) adapted by David Zuñiga (2012).

Lecce (1990 in Chapter 3, pages 3 to 24) stated that geomorphology is a threefold subject. Firstly, the significance of process-form relationships with regard to formation of alluvial fans; secondly, the processes responsible for alluvial fans' construction helps to develop understanding of sediment transport in other fluvial or alluvial systems, particularly in semiarid environments (Bull 1968, in Lecce, 1990); thirdly, the geomorphic response of

fan shape to changes in fluvial processes, tectonic activity, climate and drainage basin variables. Fig. 2.6 shows two phases in the development of alluvial fans built under tectonic influence. Showing the depositional area adjacent to the mountain front as well where the deposition is shifted down fan due to stream channel defences. Furthermore, the temporal and dynamic development of alluvial fans derives complex structures that are illustrated in Fig. 2.7. Firstly, the initial stage of formation when a simple front fan is built or when the channel feeder has the freedom to deliver its sediments from the apex until the deposition fan area. Secondly, as a result of aggradation in the area of hydraulic apex the channel feeder is restricted to transport its sediments for the original path splitting its trajectory and producing other channel feeder segment path and a second fan generation is formed. Furthermore, during this stage the secondary processes previously discussed take action producing the reworking of older structures transforming the Landscape and geomorphology of the alluvial fan. Thirdly, it is possible to have another generation of alluvial fans depending of the operation mode tectonic, climatic, or both simultaneously the final structure may be as complex as the interaction of the components involved as well as the regional environment itself. In addition, Lecce (1990) explains how the climate mode operates and how it influence on alluvial fans dynamic.

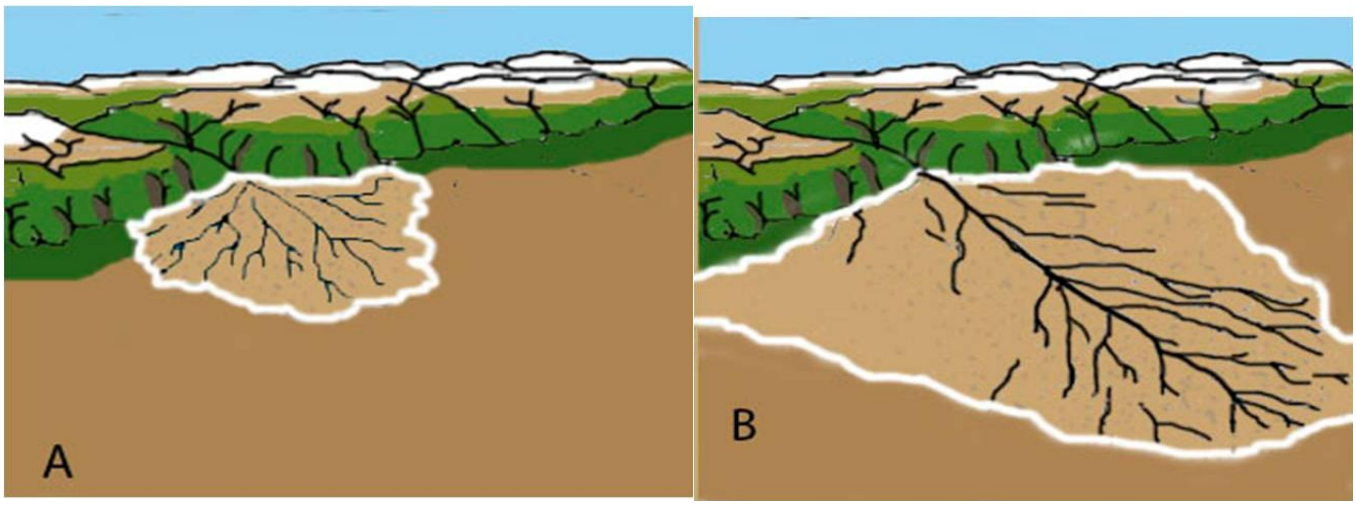

Figure 2.6. Two phases in the development of alluvial fans under the influence of tectonic uplift (A) area of deposition adjacent to the mountain front; (B) Area of deposition shifted dowfan due to stream channel entrenchment. Source: Bull (1968, in Lecce, 1990) adapted by David Zuñiga (2012)

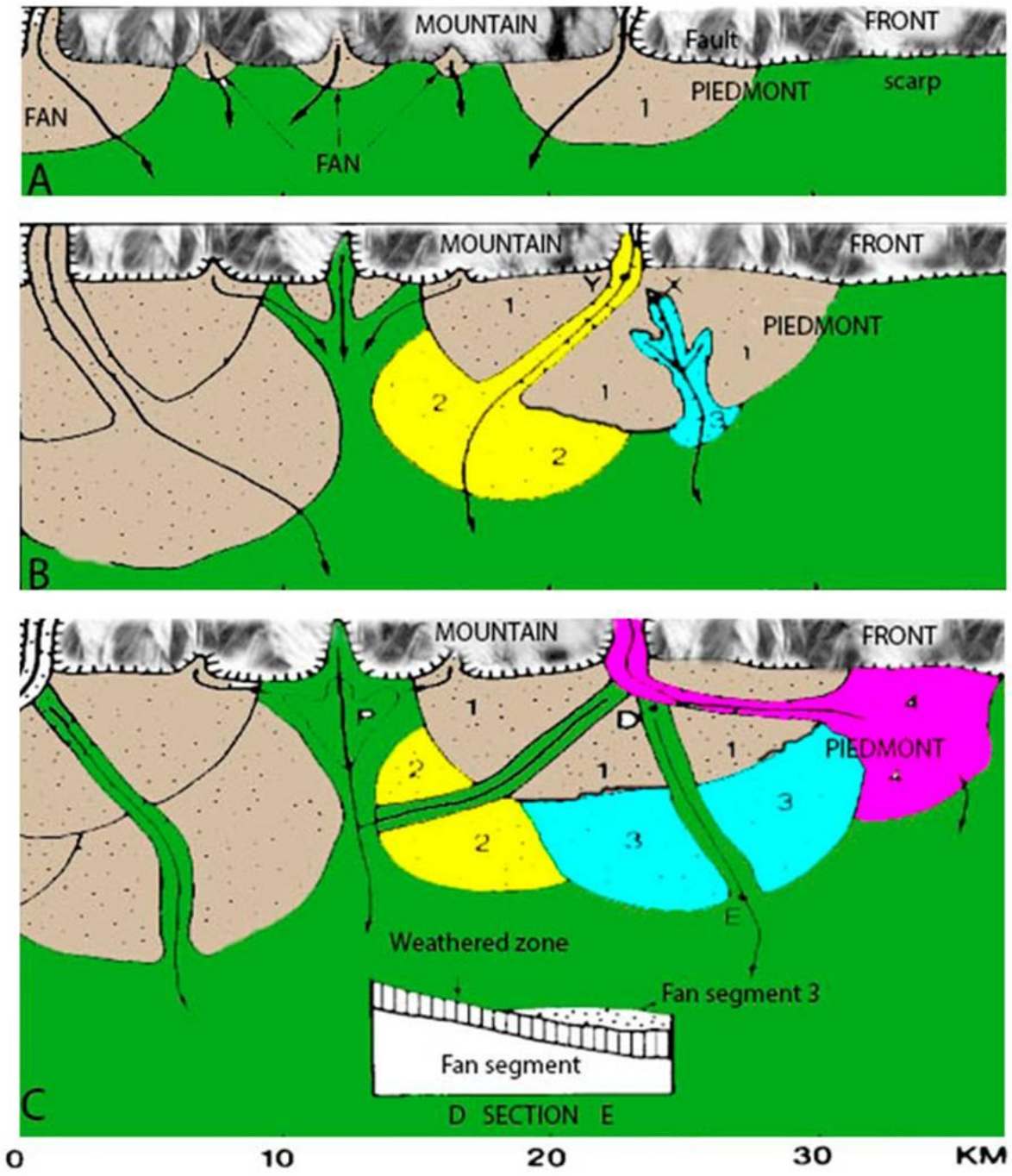

Figure 2.7. Diagram showing development of alluvial fan and shifts in the location of erosion and deposition. (A) Small fans at the base of recently elevated mountain front; (B) Wash has dissected original fan segment (1) and is constructing a new fan segment (2 and 3); (C) Stream piracy has caused the abandonment of segment (2) and (3) and construction of another fan segment (4). Stratigraphic relationships between segment (1) and (3) in Gully D-E. Source: Lecce (1990) adapted by David Zuñiga (2012)

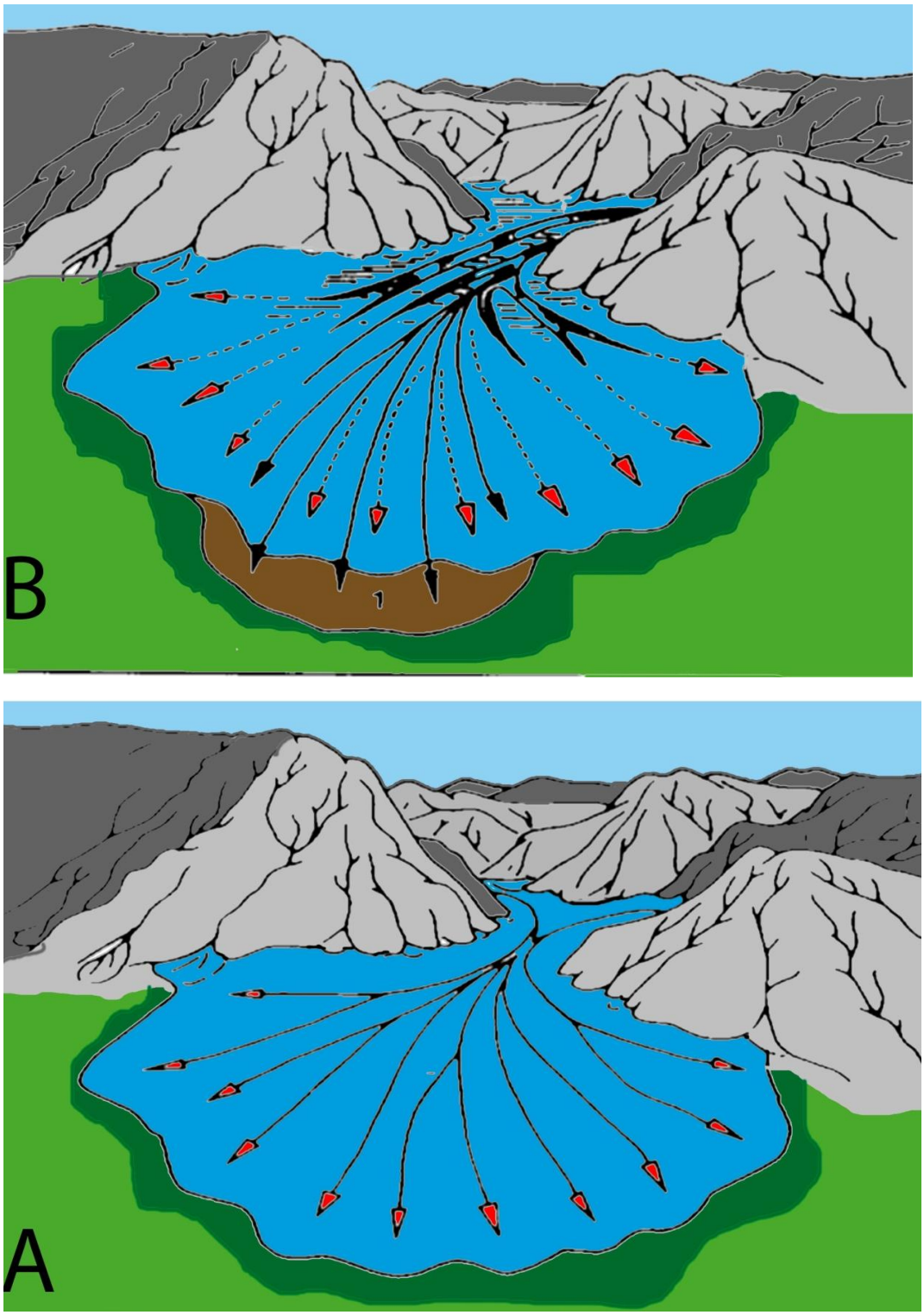

Figure 2.8. Formation of alluvial fans under climate operation mode in an equilibrium hypothesis. (A) Aggradations during more humid or pluvial periods; (B) ditching or incision during a subsequent drier climate period. Intersection point moves down fan and mudflows and other infrequent density flows transport sediment to the owner reaches of the fan,

building it outward into the valley (A). Source: Luisting (1965) adapted by David Zuñiga (2012).

2.1.3 Regional Pleistocene to Holocene fluvial and alluvial sedimentary structures.

Rivers and streams frequently built flat structures named floodplains or valleys. These fill deposits derived from modern rivers or main streams could be named alluvial deposits that occupy extended low gradient terrains or fluvial valley river deposits (Connell and Love, 2001; Connell et al., 1998). Both fluvial and alluvial valley fills are structurally similar and have an eroded base layer overlain by an upper depositional layer. These flat platforms are normally less than 3m thick and are deposited over a flat basement named erosional terraces common in the piedmonts and mountainous reaches of many drainages networks (Pazzaglia and Hawley, 2004). On the other hand, flat deposits more than 3 m thick are common along the medial and lower main streams, mostly where a mountainous drainage passes through the mountain front into a wide valley cutted nearly to the piedmont such as; Aztecas and San Antonio neighbour (ASA), Municipal Cemetery (PC) and Tepeyac Cemetery (TC) deposits allocated along sector Centre 2 on the study area (See map Figs. 4.1B, and 4.1C Chapter 4). Soil thickness, composition along-valley continuity of terraces and alluvial fills depends on the kind of drainage network, but there are some sedimentologic (textural) and geomorphic similarities that suggest a common origin for these deposits (Pazzaglia and Hawley, 2004). Conglomerates composed of well sorted, clast supported, sub angular to rounded gravels and pebbles packed in a medium to coarse sand matrix are the results of channel facies (Connell and Love, 2001; Connell et al., 1998). These structures occasionally preserves bedforms instead, cross stratified finer sandy facies structures commonly does (Pazzaglia and Hawley, 2004). Alluvial deposits and many terraces are filled with aeolian deposits derived from short-term periodic conditions which depends on basin hydrology changes, sediment yield, and/or base-level (tectonics). Finally, when the stream decreases or stops its incision, increase its valley level, and aggraded. After that, another new incision offset the aggraded sediment above the recently formed floodplain, capturing a terrace in the valley margins (Connell and Love, 2001 and Connell et al., 1998). Alluvial gravels are more resistant against fluvial erosion than exposed bedrock not covered with surficial soils. In fact, high porosity of alluvial soils reduces the runoff, producing an effective alluvium protected layer. In the study area, high above of modern base-level river valleys that backfilled with alluvium are now preserved as

interfluves, because the bedrock is more weak and has been everywhere lowered around them (Connell and Love, 2001 and Connell et al., 1998). In Juárez city, the floodplain built by the Bravo River fill more or less continuously with local incised filled valleys through the early Pleistocene and was part of the upper Santa Fe Group (Connell and Love, 2001; Connell et al., 1998). Furthermore, the Bravo River begins to cut just at the end of the early Pleistocene 1 Ma ago. During the glacial-interglacial periods of the past 1 Ma the Bravo River extend its cutting bottom bed creating a wide erosional bench cut above Santa Fe Group, filling the valley and forming a terrace alluvium above these erosional benches (Connell and Love, 2001). Symmetrical terraces are preserved on distal sectors of cross valley and extensive erosional paths which have reduced the Rio Grande valley base level allowing the preservation of younger terraces (Connel and Love, 2001; Connell et al., 1998). Moreover, with regard to the terrace system of the Albuquerque basin, the Edith gravel, deposited during middle Pleistocene (Illinoian or I.S. 6-8 terrace) has now been recently verified by 40Ar-39Ar dating of Llano de Albuquerque basalts at ~160 Ka that inter-fluves with the fine-grained facie of the Edith gravels called the Los Duranes Formation (Connell et al., 1998; Connel and Love, 2001). Furthermore, Wolberg (1980) suggests that the slope of fluvial terraces changes with respect to modern floodplains changes in stream gradient or post-depositional deformation of terraces. One interpretation is given in terms of a changing basin hydrology and the other is in association with active tectonic activity and/or base-level fall. In any interpretation, it is important to note that the Rio Grande as many major perennial rivers, have terraces with more or less parallel slopes to the modern valley. As a result, along the length of the Bravo River its profile keep a uniform incision (Wolberg 1980).

Based on several shallow water borings, the Rio Grande valley is underlain by nearly 25 m of fluvial sediments. These soils fill wide valleys which overlaid the Santa Fe group Formation as well as widely spaced canyon reaches cut in older bedrock units (Hawley et al., 1976). Erosional base deposits below recent alluvial fills are found in the Hueco Bolson northern of Albuquerque Basin close to El Paso, Texas; its longitudinal slope is parallel to the depositional deposits (floodplain). The principal terraces have soils layers filled with (10m to 15 m) related to late Wisconsin (Pinedale) Glaciation of latest Pleistocene age. Above this layer, a thin layer (5-10 m) formed of medium- to fine-grained, laterally and vertically accreted floodplain sediments of Holocene age caps the late Wisconsin an valley-fill sequence. In the future is likely that incision of the Rio Grande would be in a very

dynamic form, creating and destroying terraces due to lateral and vertical incision. This process of lateral incision is valid for ephemeral and perennial rivers systems typical of semi-arid cycle of erosion (Hall 1977). Thus, the rapid vertical incision of rivers and streams in the study area have been formed plain-lowered channels named arroyos or washes. For instance, in the study area big streams as Snakes West, Snakes East and Colorado Streams were formed for this process. The initial stage of entrenchment reduces the stream slope producing incision, which forces them to cutback fast upstream and along the tributaries of the main stream. Therefore, large volume of sediment delivered to the principal incised streams cannot be transported by the reduced slope, and aggradation took place (Wells et al., 1982; Love and Young, 1983).

2.1.4 Santa Fe Formation.

During Oligocene to early Miocene time the Bravo River faced a period of tensive strength (rift) that caused south east river channel migration. Then, the channel shifted to its floodplain center and its flanks were uplifted (Mack et al., 1993). The incision began as a result of the ancient axial-rift of the Bravo River (Kelley et al., 1992; Kelley and Chapin, 1995; Kelley and Chapin, 1997). After that, during Middle to late Miocene the river drainage network moved to incision mode and due to high mechanical erosion coarser and resistant deposits were deposited. These upper layers of soils correspond to lower to middle Santa Fe Formation group (Hawley and Kennedy, 2004). Furthermore, nearly to the end of the middle Miocene fragments of rocks were eroded from neighboring uplifted boundaries and deposited above pre-existing intrabasinal faults blocks. Finally, these debris materials were moved to the point where horsts were filled with lower to middle Santa Fe Group deposits. The new landscape emerged from these sediments followed to aggraded as a single Middle to Upper Santa Fe-age unit during Pliocene and Early Pleistocene (Vanderhill, 1986; Mack et al., 1993; Mack et al., 2006; Hawley and Kennedy, 2004). Then, basin filled ended close to 700,000 years ago.

Juárez City and El Paso, Texas have shared the water derived from the Hueco and Mesilla basins that form part of the Neocene Rio Grande rift tectonic zone.

Summarizing, Fig. 2.9 shows the temporal distribution of Bravo River floodplain deposits occurring during Pliocene to Early Pleistocene. The figure illustrates five main bolsons located near to the study area: Palomas, Jornada, Mimbres, Hueco, Mesilla and de

los Muertos, higligthing fundamental features such as Fillmore Pass where the Bravo River shifted its trajectory from west flank to east flank of Franklin mountains (1 to 3 Ma); Paso del Norte Pass, located between Cristo Rey and Franklin mountains (less than 1 Ma) where the Bravo River incised and shifted its direction. Figure 2.9, also shows the relationship between Bravo River deposits with some important features: Cabeza de Vaca Lake and Bravo River terraces mentioned in the geologic map to the study area (See Figs. 4.1A to 4.1D of results Chapter 4).

2.1. 5 Cabeza de Baca Lake; Barreal Lake and Playa lake of Anapra port.

Fort Hancock and Camp Rice formations previously described are the building blocks that allowed continuous deposition that changed the landscape of the study area. Such structures could be named as piedmonts deposits, alluvial fans, terraces and fluvial valleys.

Furthermore, some features which mark the entry of the ancestral Bravo River to the study area are explained in the next paragraphs. Fig. 2.9 shows how the Bravo River goes from northwest to southeast forming the Cabeza de Vaca Lake which is joined with ephemeral lake deposits and record the entry of the ancestral Rio Grande fluvial network into the southeastern Hueco bolson (Strain, 1966; Hawley et al., 1969; Vanderhill, 1986; Gustavson, 1991; Gile et al., 1981; Mack and Seager, 1990; Leeder et al., 1996a; Mack et al., 1997; Mack et al., 2006).

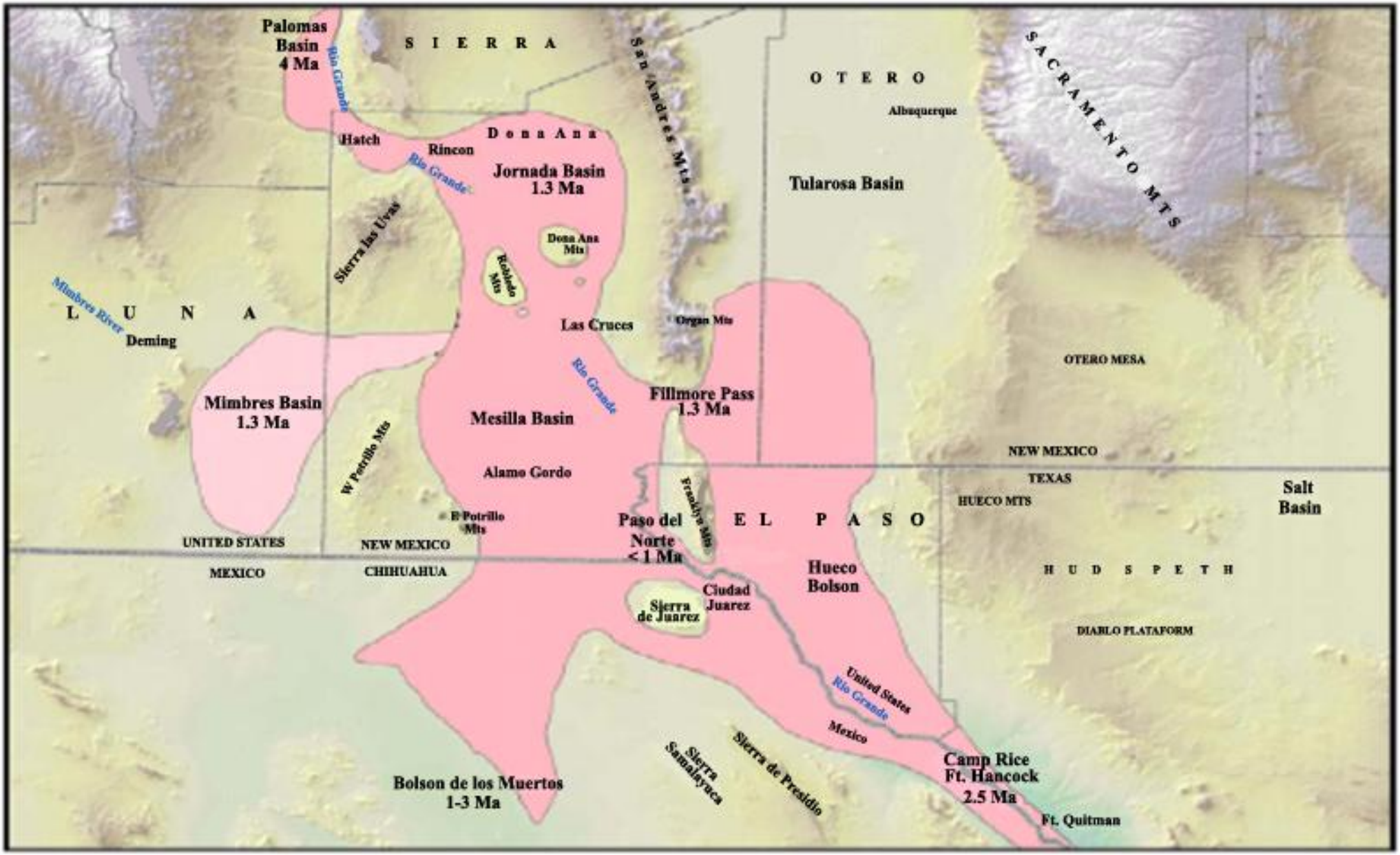

Figure 2.9. Evolution of the ancestral Rio Grande system (Pink colour) during Pliocene and Early Pleistocene time. Source: Hawley and Kennedy (2004)

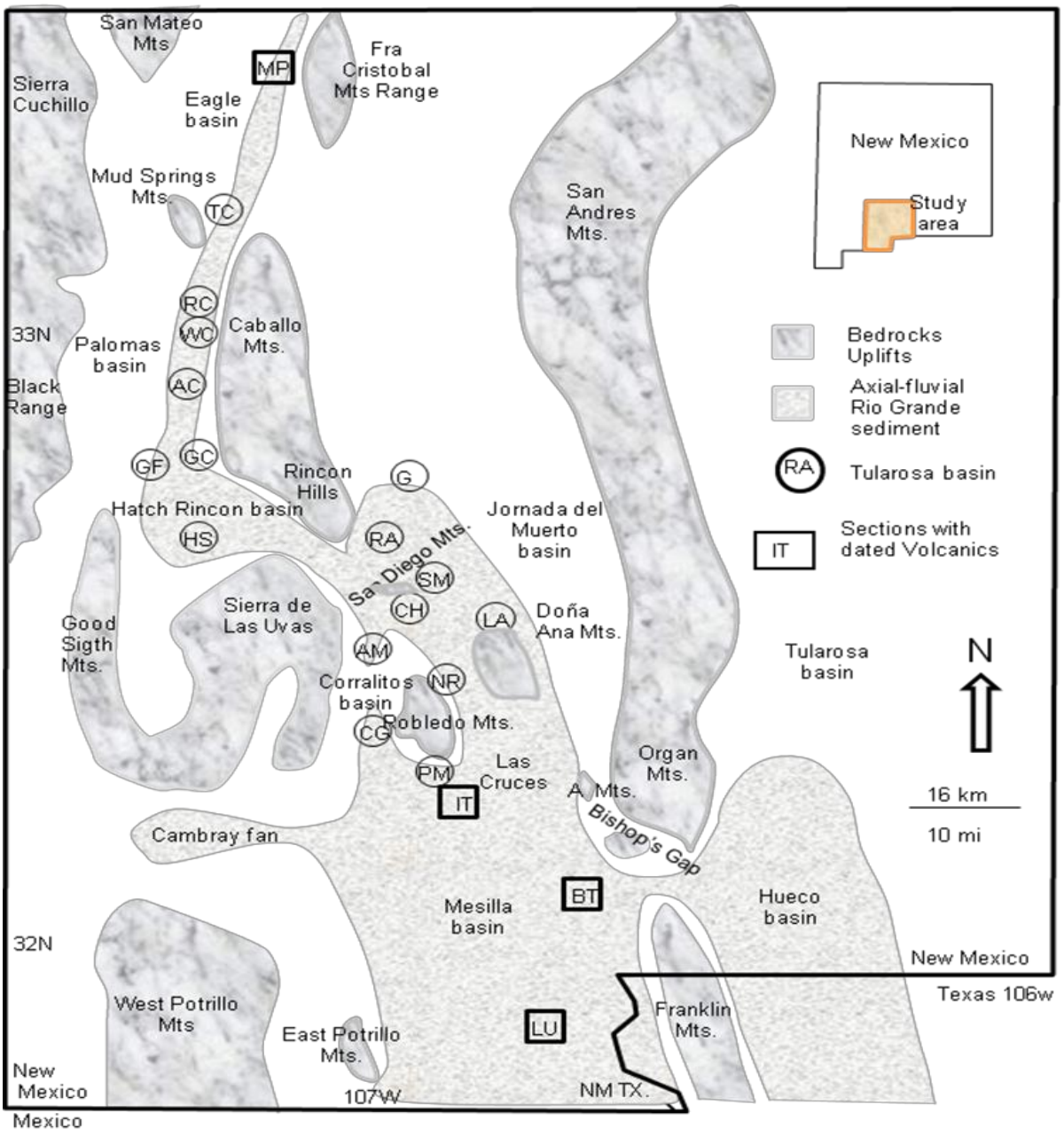

Figure 2.10. map of the southern Rio Grande rift, New Mexico showing location of stratigraphic sections used in this study. MP=Mitchell Point; TC=truth or Consequences; RC=Red Canyon; WC=Wild Horse Canyon; AC=Apache Canyon; GC=Green Canyon; GF=Garfield; HS=Hatch Siphon; RA=Rincon Arroyo; G=Grama; SM=San Diego Mountain; CM=Cedar Hill; AM= Ash Mesa; LA=Lucero Arroyo; NR=Northeast Robledo; CG=Corralitos Graben; PM=Picacho Mountains; IT=Interstate Ten; BT=BerinoRTank; DC=Doña Ana Range Camp; LU=LaUnion. Source: Adapted from Mack et al., 2006

During Pliocene to Early Pleistocene (3 Ma interval) the ancestral Bravo River and their main tributaries, located to the north of the San Juan Latir volcanic fields (southern Rocky Mountains) transported a high volume of debris to the Bravo River rift basin (Gill et al., 2009) these sediments formed the building block of Upper Santa Fe Group Formation in

the Hueco and Mesilla bolsons previously to the integration of the lower Rio Grande with the Gulf of Mexico. The resulted soils of the major fluvial systems as: silty-clay interbeded with sandy-silt, sand and clay were retransported several times filling playa-Lake depressions of a closed Hueco-Tularosa Basin via Fillmore Pass, as well as to the southeast Mimbres basin and Bolson de los Muertos (Strain, 1966; Hawley, 1969; Hawley, 1975; Gile et al., 2009; Seager, 1981; Seager et al., 1987; Mack et al., 1997). This network system is named Cabeza de Baca Lake and underlay the Pleistocene-Holocene Barreal lake located southeast of Juarez city. Another fundamental feature is the Fillmore pass located in the Franklin Mountains north to the study area active during (1-3Ma). The history of the Rio Grande could be divided into four intervals of time, corresponding to the most recent geopolarity chrons: The Camp Rice and Palomas formations that were deposited on an aggradational environment mode subdivided into mid-to late Gilbert Chron (~5 to 3.6 Ma; Figure 2.11), Gauss Chron (3.6 to 2.6 Ma; Fig. 2.12) and Mutuyama Chron (2.6 to 0.78 Ma; Fig. 2.13), while the degradational mode is reserved to the Brunhes Chron (0.78 Ma to present) (Vanderhill, 1986 in: Mack et al., 2006).

Furthermore, Avila (2011) stated that The Eastern Boundary Fault located along the eastern flank of the Franklin Mountains EBFZ, offset the Bravo River. and continues to the south joining with west of Azteca Avenue in Ciudad Juarez (Drewes and Dyer, 1993). This Bravo River rift nowadays is active along Quaternary normal faults, like that rift associated ones in the urbanized areas of El Paso and Ciudad Juarez. Shortly, using gravimetric methods Avila (2011) shows the results in Figs. 5.4 to 5.6, pages 31 to 34 and states his interpretation of the EBFZ using geophysical data. The maps also consider that south of the Franklin Mountains the EBFZ becomes a more complicated structure. One east-west trending structure located south of the U.S border in Juarez is at a point where a associated Laramide thrust fault mapped by Collins and Raney (2000) would converge with the EBFZ. The tilt also suggests a fault located west of the EBFZ that correlates with an arroyo in Juarez called Arroyo de las Vivoras (ADLV) suggesting other faults located perpendicular to the Arroyo fault. Perhaps, the present study of Avila (2011) could be the high probability of a transference fault zone on the northeast of Juárez mountains as stated in Chapter 4 of this thesis. However a more precise faulting study is needed.

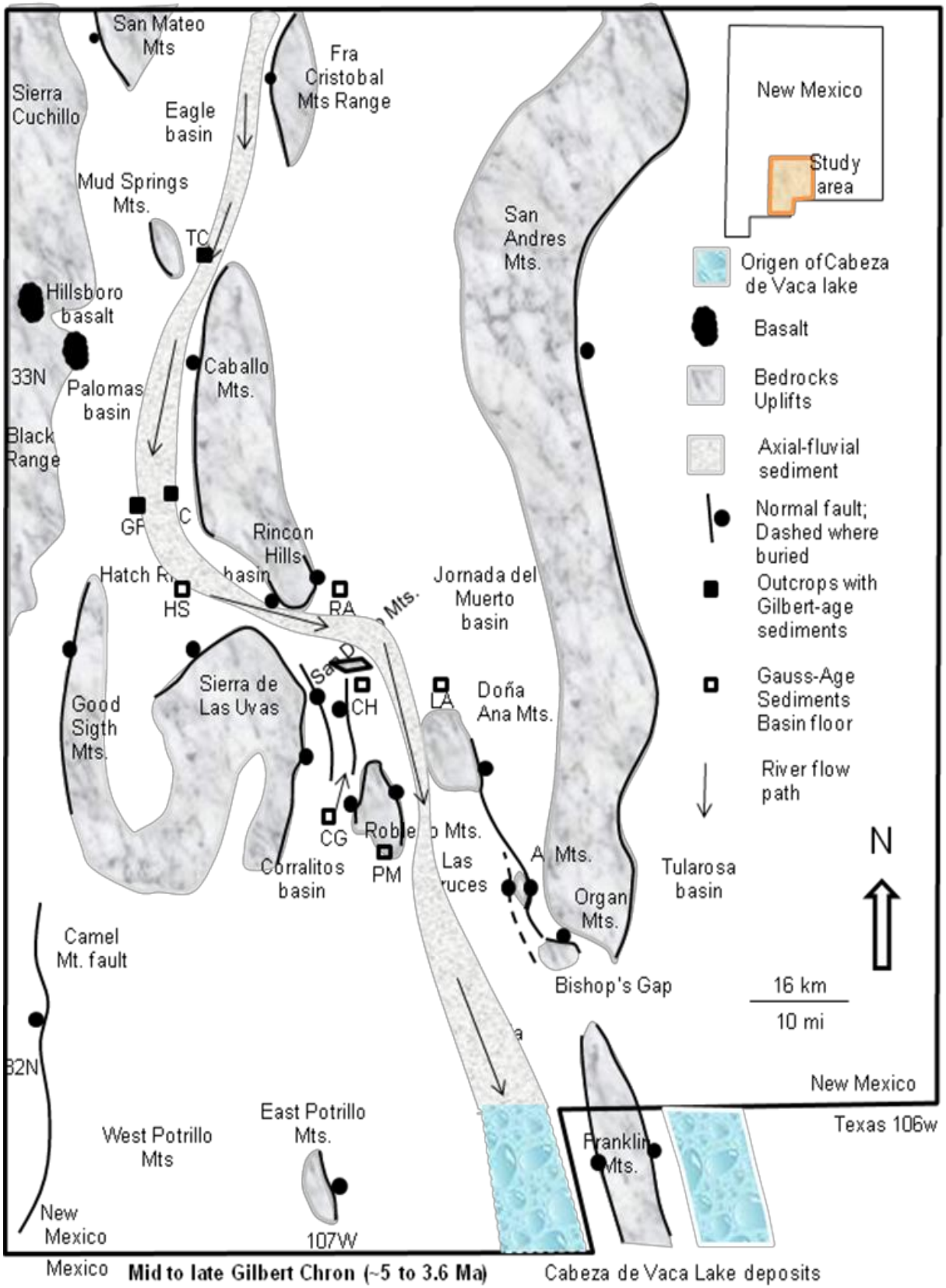

Figure 2.11 Palaeogeographic map of the aggradational phase of the Rio Grande in the Southern Rio Grande rift during the middle lo late Gilbert Chron. Adapted from Mack et al., 2006

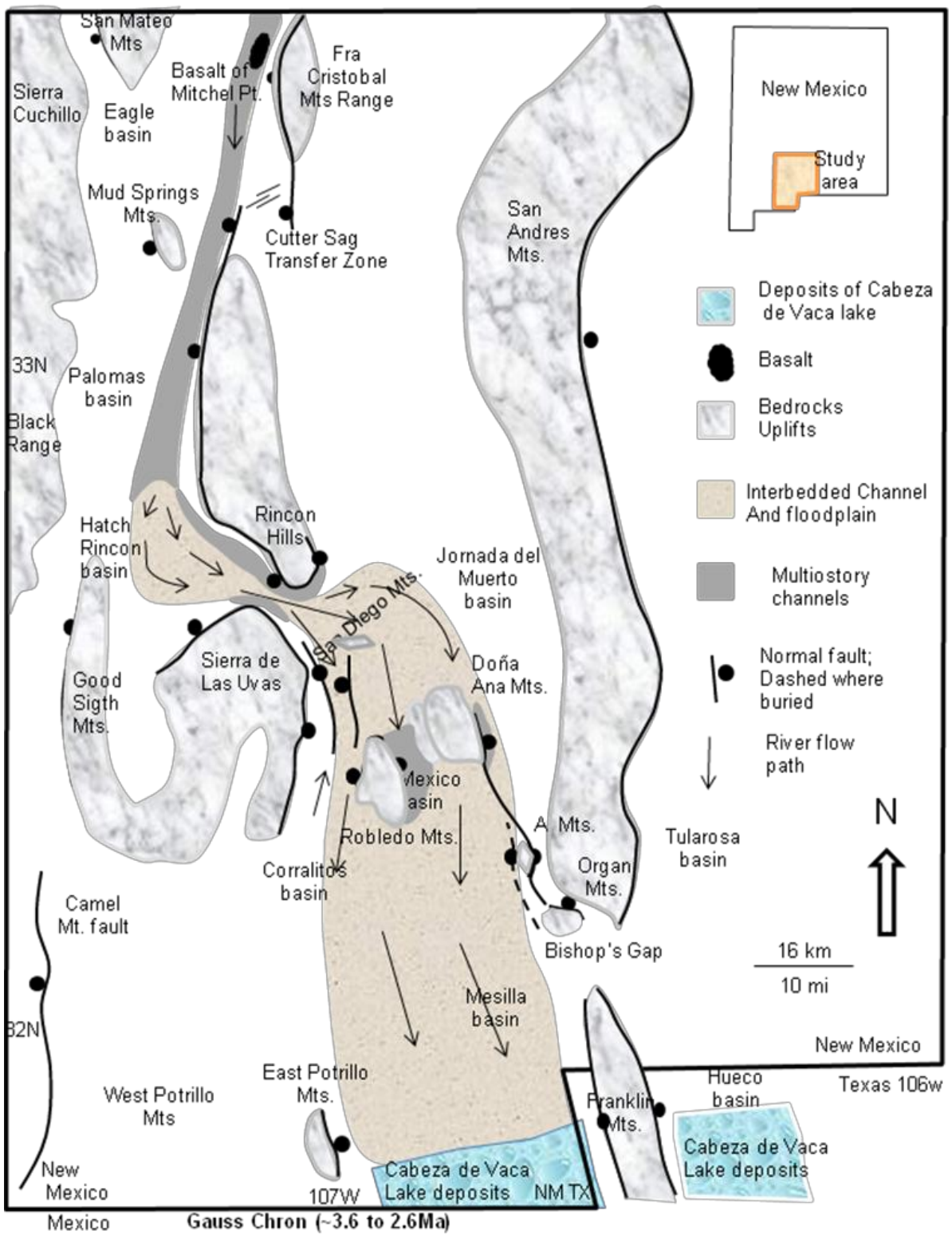

Fig. 2.12 Palaeogeographic map of the aggradational phase of the Rio Grande in the Southern Rio Grande rift during the during the Gauss Chron. Adapted from Mack et al., 2006

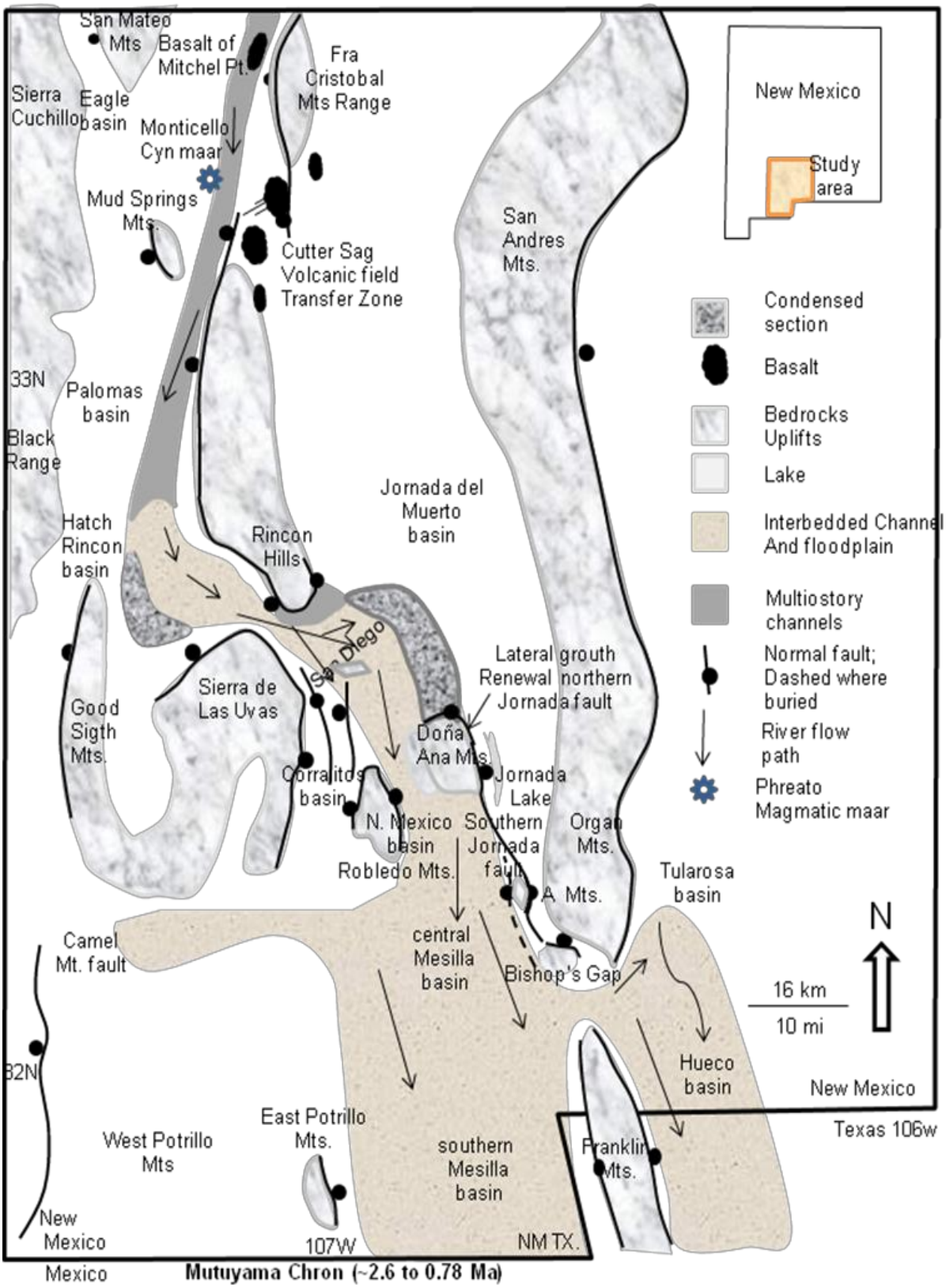

Figure 2.13 Palaeogeographic map of the aggradational phase of the Rio Grande in the Southern Rio Grande rift during the during the Mutuyama Chron Chron. Adapted from Mack et al., 2006

Fig. 2.14 shows the general geologic map and cross sections of the Palomas basin (Camp Rice Formation of the study area). In the following paragraphs some relevant concepts are highlighted regarded to similarities within the study area.

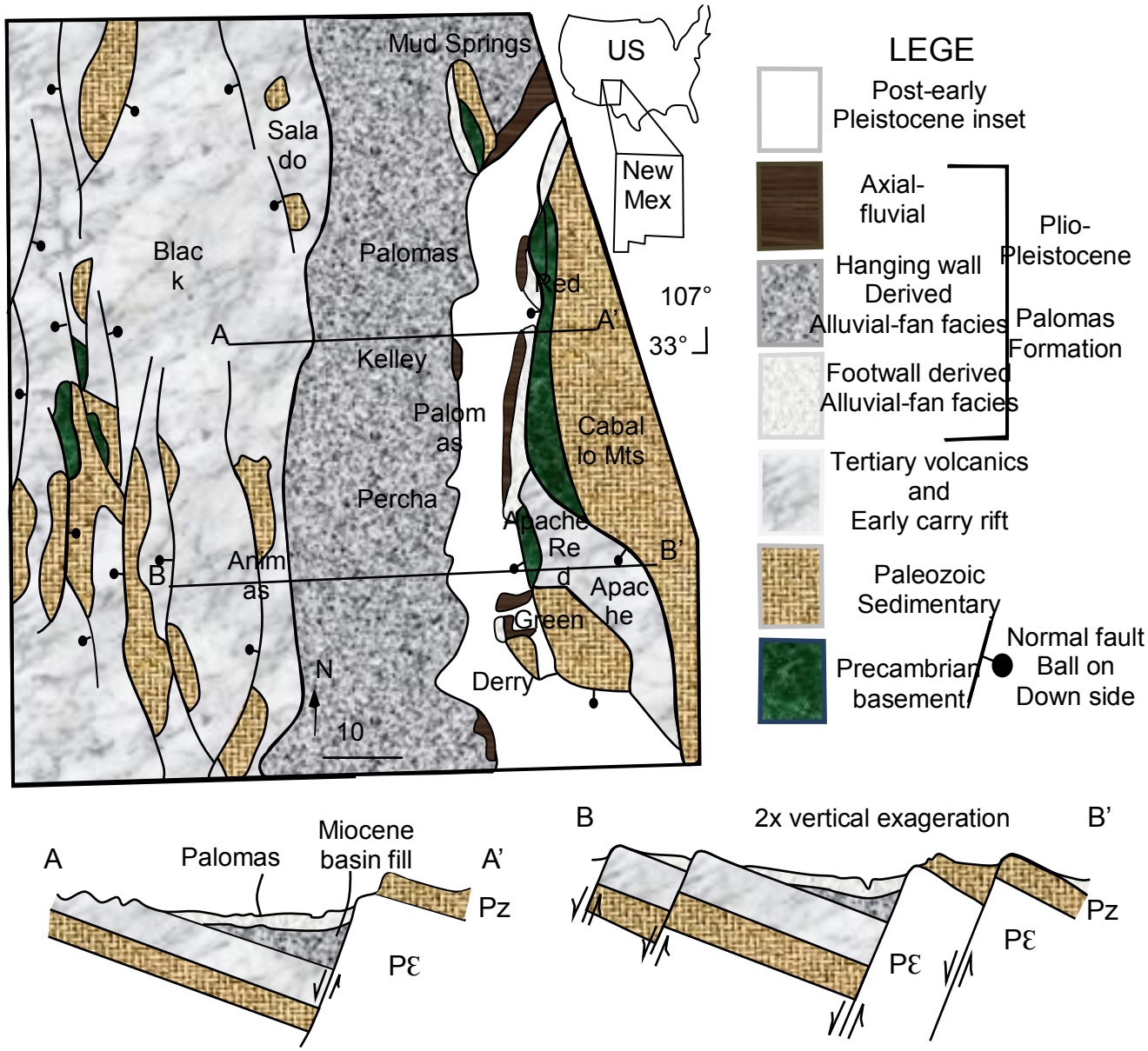

Fig. 2.14 Generalized geologic map and cross sections of the Palomas basin and adjacent mountains in the southerRio Grande rift. Source: Adapted from Seager et al. (1982)

In general, Sections (A-A') and (B-B') of Fig. 2.14 clearly show that orientation, gradient of the hanging wall as well the footwall and their geographic location strongly influenced the behaviour response (Seager et al., 1982). For this reason in relation to the Palomas alluvial fan, little deposition on the footwall is the result of (little radial length<2km, and high gradient (1-4°) (Seager et al., 1982). Also, big discharge of turbulent-flow is undergone, consequently, channel conglomerates and hiperconcentrated flow, mostly composed by pebbly sand are deposited (Seager et al., 1982). On the other hand, fine

sediments like silt and sand are deposited over longer Hanging wall (approximately 15 km), and with gently slopes (0.7-1°) (Seager et al., 1982). In short, sediments with lateral accretion channels and overbank mudstones, are mostly the deposits of medial and distal hanging wall derived fan channels the behaviour of this deposits corresponds to gravel bed streams. Tectonic tilting of the half graven is the probable cause of the fluvial incursions toward the footwall, because toe cutting of the fans is largely restricted to the footwall side of the basin and the number of incursions correlates to distinct segments of the border fault system (Seager et al., 1982).

In short Fig. 2.15 shows three different axial-fluvial channel fan models which are formed by sediments of the Camp-Rice as well Palomas formations north to the study area. Fig. 2. 15A shows an schematic section of half graben structure; Fig. 2.15B shows a full graben and Fig. 2.15C shows Cedar Hills Transference Zone.

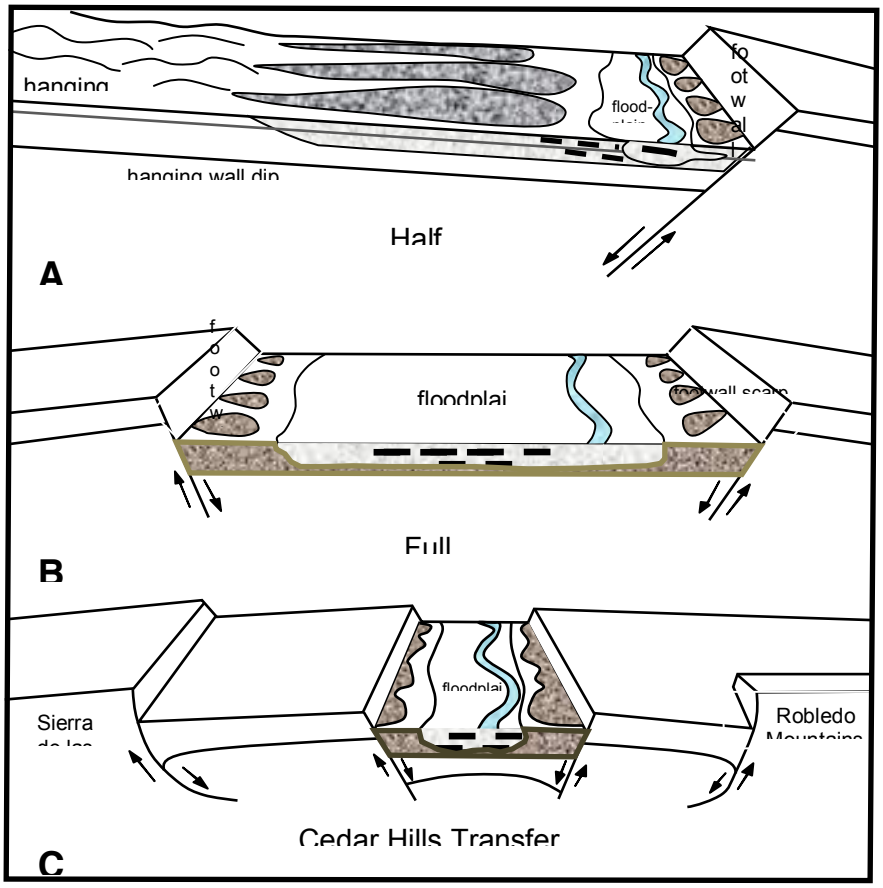

Fig. 2.15 Schematic cross sections of: A. Half graben, B. Full graben, and C. Cedar Hills Transfer Zone, showing distribution of alluvial fan and Axial-fluvial sediment of the Camp Rice and Palomas formations, adapted from Mack and Seagar (1990, 1995), and Mack et al. (2002). Black rectangles in cross-sections represent floodplain and distal alluvial-fans mudstones.

2.1.6 Pleistocene-Holocene soils imbricated in Camp Rice and Fort Hancock formations.

Some fundamental features related to Pleistocene-Holocene deposits associated with Santa Fe group geological formations (Fort Hancock and Camp Rice) are detailed in the following parragraphs. Firstly, the Lava Greek B derived from the Yellowstone-volcanic Ash preserved in a high terrace relict located 75 m above the Bravo River flood plain in the ASARCO-UTEP; and Mesa street suggest the fast, and periodic incision of Paso del Norte and El Paso Juarez valley that would have been under way by 0.64 Ma. That is the Yellowstone-derived volcanic ash (Lava Greek B) (Hawley et al., 1969). The grain size of these sediments depends on the watershed size as well as river channel competence and capacity basically were defined by mixed soils as: gravel, sand, silt, and clay, sometimes loamy sand to sandy loams; pebble gravel and pebble sand which are common structures in the Juárez city study area associated with terraces. Thus, a very important question is how many changes occurred in the Bravo River trajectory along Hueco and Mesilla basins during the upper Santa Fe depositional interval of 2 Ma. Furthermore, the final climatic event occurred during the last glacial cycle, at least (10 ka-25 ka) years ago (Hawley, 1975) may be due to a general trend towards cooler and drier climates. During this time the Bravo River filled with 18-30 m of basal channel (pebble to cobble gravels and sands) as well as braided plain channel (sand and pebble sand); basin floor fluvial plain (sand and pebble gravel; lenses of silty clay); basin floor aeolian sands, lenses of pebble sand and silty clay. Evidence of these terrace deposits was found along the Felipe Angeles neighbourhood in the Juárez city study area (see results Chapter 4)

Secondly, during the glacial-Interglacial of Pleistocene time which marked the final integration of the Rio Grande along the ancestral extend from the Sangre de Cristo mountains through El Paso Texas, and Ciudad Juárez. then the catchment area of the Bravo River increased by nearly 25% Then, during glacial-interglacial of Pleistocene time

(~100 ka) fluvial aggradational cycles as well cycles of incision over great amount of drainage areas were undergone increasing capacity and competence of Bravo River.

Many wells have been drilled in some areas near to the International Border of Chihuahua, Ciudad Juárez, New Mexico and El Paso Texas. The wells located southeast of Juárez Mountains near to the Airport as well Barreal basin contain evidence of older Lacustrine deposits derived from the Fort-Hancock Formation composed by soils of the Lake Cabeza de Vaca deposited early Pleistocene (Kottlowski, 1958; Strain, 1966; Reeves, 1965; Hawley and Kottlowski, 1969) pointed out that during Pliocene-middle Pleistocene the Bravo River flowed from northwest of El Paso Texas to the south into Chihuahua following the Mesilla bolson and terminating in huge lake or lakes. In addition, Kottlowski (1958) and (Gile et al., 1966) stated that Rio Grande integration to the river system was to the north. Incision of the Rio Grande on the Mesilla bolson occurred only after destruction of the temporary base level at El Paso canyon and not by a simple upstream increase in discharge. By early late-Pleistocene time, faults bounding many of the Late Cenozoic mountains had been rejuvenated, many of the bolsons had been filled with thousands of meters of alluvial and lacustrine debris, and the Rio Grande had assumed its present position. It is recognized of course that much of the basin filling also occurred in Late Tertiary time (Hawley et al., 1969). Thus, Lake Cabeza de Vaca had been destroyed and the basin of Lake Palomas created. The large playas presently in the old Lake Palomas basin, which frequently flood during wet years but which have never filled completely to form an integrated lake in Holocene time, are Laguna de Guzman north of Sierra Borregos, Laguna de Palomas south of Palomas, Laguna de Santa Maria south of Sierra de Malpais Laguna, and El Barreal which sur-rounds Sierra Los Muertos; Laguna de Palomas and El Barreal occur along the axis of the floor of a large basin complex, termed Bolson de Los Muertos.

2.1. 7 Glacial-Interglacial Pleistocene-Holocene Aeolian sediments reworked by fluvial and alluvial channels.

Aeolian deposits increases or decreases depending on climatic cycles and source deposits. On the other hand, deposits transportation depends on the availability of fine sand

and silt in fluvial systems (Pazzaglia and Hawley, 2004). Surficial deposits of aeolian origin are common throughout the study area and can be subdivided into three basic categories: (1) sand dunes without vegetative cover, (2) older sand dunes with soil development and little vegetative cover and (3) desert loess which is the dominant soil component in settings ranging from hill-slopes; lower valleys and basalt platforms. Pazzaglia and Hawley (2004) stated that high volumes of sand dunes formation dates from Pleistocene to Holocene climatic transition causing enormous supply of sediments. In addition, clay lunette dunes, are influenced by periodical wet-dry cycles, mostly occurred during the early to middle Holocene climate transition when the path to dryer climates produced a decreasing on the water label and desiccation of emerged late Pleistocene lacustrine beds. Several generations of aeolian deposits, recognizable by laterally extensive and dated paleosols, are evidence for both major and minor climatic changes in New Mexico through the late Pleistocene and Holocene (Wells et al., 1990). For example, the Chaco dune of the San Juan basin (Hack, 1941) has three important aeolian sand deposits, each representing different dune types. Late Pleistocene dunes (Qe1) are primarily widespread sand sheets and modified parabolic dunes whose genesis is consistent with the significant aridification of the southwest following the end of the last glacial maximum.

2.1.8 Lacustrine and playa lake deposits inset in Fort-Hancock and Camp Rice Formations.

Detailed studies of Estancia pluvial lake has improved understanding of climate change on basin hydrology. The sediments of these pluvial lake are exposed in numerous blow-outs in the middle of the Estancia basin, south of I-40 and the town of Moriarity. The blow outs, currently saline playas such as Laguna del Perro, were created in the middle Holocene during a time of increased aridity and lowering of the water table. Aeolian activity desiccated the basin floor creating a window into the lake deposits. A high resolution paleoecological, paleoclimatic, and paleomagnetic record has been extracted from the exposed lake beds (Allen, 1993; Allen and Anderson, 1993; Allen and Anderson, 2000; Allen and Hawley, 1991). Lacustrine stratigraphy is characterized by a massive, bioturbated, blue-gray clay interbedded with thin, white, fine aeolian and water-lain gypsum sand and thin algal-laminated marls thick (~ 1m) beds of blue clay correspond to sustained lake high stands such as those associated with the LGM ~ 20-18 Ka. Zones of intercalated

clay-gypsum/marl characterize the relative low stands such as the post LGM period between 15-14 Ka. Two periodicities of cyclic depositional processes are represented by the increasing and decreasing of clay and marl bed thickness. Decimetre-scale bundles correspond to 1.5 – 2 ky cycles of lake expansion and contraction whereas centimetre-scale bundles correspond to 100-200 year cycles. There are three distinct shorelines associated with different pluvial lakes in the Estancia basin and all are associated with a LGM lake (~18 Ka or younger). The 1890 m shoreline represents the lake at its greatest extent approximately 18 Ka.

A shoreline and prominent spit at 1875 m corresponds to a still stand between ~12 and 14 ka. And a shoreline at 1862 m corresponds to a Younger Dryas lake at ~ 11 ka. The natural sill for the basin lies at 1932 m. An argument has been made that the lake was hydrologically connected across this sill with the Pecos River (Bachhuber, 1989). The argument is based in part on the findings of cutthroat trout (*Oncorhyncus clarki*) in pre-LGM lake beds. Other work (Allen and Hawley, 1991; Allen, 1993; Hawley, 1993a) favours a karstic subterranean drainage system that caused stability of lake level at about 1890 m.

2.1.9 Climate and global change.

Several factors, of base-level, drainage integration, and active tectonics may control fluvial incision. Fluvial terraces indicate that incision is not uniform, instead is interrupted by periods when incision stopped and rivers aggraded. The same processes likely operate on alluvial fan and piedmont deposits and surfaces. The tectonic and base-level setting created the overall landscape geometry into which Quaternary units were deposited, but it was changes in drainage hydrology and sediment yield modulated by climate that produced the observed stratigraphy (Gile et al., 1981; Smith, 1994). New Mexico appears to have been relatively dry through the Neocene and Quaternary. Paleoenvironmental reconstructions for Neocene deposits both inside and outside the rift all favour a semi-arid climate (Tedford, 1981). The same conditions generally persist into the Quaternary with the except that the middle and late Quaternary are characterized by 100-ky glacial-interglacial climatic fluctuations. Glacial climates are generalized as relatively cooler and wetter with a general depression of the tree line, and current low-standing arid to semiarid regions being covered by a more savannah-like vegetative assemblage (Leopold 1951; Spaulding et al.,

1983). As has already been noted, perennial lakes periodically flooded into larger closed basins during Quaternary pluvial intervals; however, it is possible that high and low lake-water levels may not have been synchronous across New Mexico (Allen and Anderson, 2000; Hawley et al., 2000; Hall 1977). Interglacial climates are generally warmer and drier, but water levels are also controlled by precipitation events and seasonal changes related to glacial conditions (Holliday, 1989; Holliday, 2000).

2.1.10 Fluvial Bravo River system evolution during Pleistocene-Holocene time.

Post Santa Fe fluvial deposits of Bravo River in the Albuquerque Basin located central New México. At least five avulsive events of tributaries Bravo River during Pleistocene-Holocene time are here suggested: Firstly, the Lacustrine Cabeza de Vaca Lake of Plio-Pleistocene time (>2.5 Ma) (Strain, 1966; Hawley et al., 1969; Vanderhill, 1986; Gustavson, 1991). Secondly, the ancestral Bravo River trajectory during middle to Late Pleistocene (0.66 Ma to 0.16Ma) (Smith and Kuhle, 1998). Thirdly, the older Bravo River tributaries has built a dissected terrace Late Pleistocene time (0.16 to 0.10 Ma; Connell et al., 1998). Fourthly, another terrace was constructed during approximately Late Pleistocene time (78 to 28 Ka) (Connell et al., 1998). After that, during Holocene time (15 to 22 ka) another climatic change with fluvial terrace deposition took place (Hawley and Kottlowsky, 1969; Hawley et al., 1976; Allen and Anderson, 2000) . Also during this period of time the younger tributaries of the Bravo River were acting. Finally, in recent time 15 ka to the present the last shift of the Bravo River is in progress (Connell et al., 1998).

In order to reinforce the description given on the previous paragraphs a detailed lithological column is given in the following paragraphs. This model considers fluvial deposits between Bravo river and Rio Puerco valleys mostly defined by increasing order of Age: Los Padilla's; Arenal; Los Durane's; Menaul, Edith, and Lomatas Negras Formations (see Fig. 2.16).

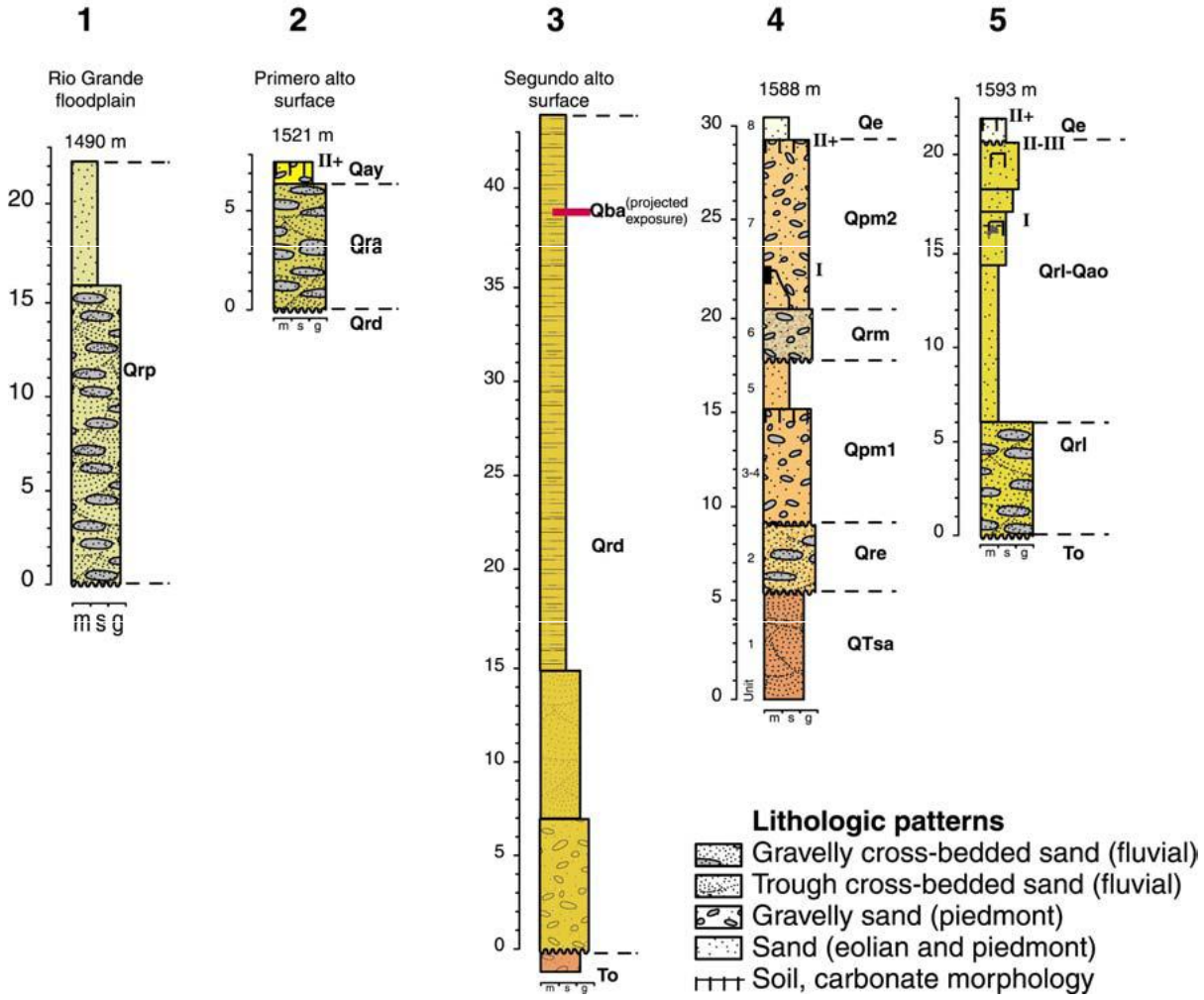

Figure 2.16. Stratigraphic and drill hole sections of Pleistocene fluvial deposits of the ancestral and modern Rio Grande along the Rio Grande valley: 1) Los Padilla's Formation at the Black Mesa-Isleta Drain piezometer nest; 2) Arenal Formation at Efren quarry (modified from Lambert (1968); Machette et al., 1997); 3) Los Duranes Formation at theSierra Vista West piezometer nest. 4) Edith and Menaul formations at SandiaWash (Connell et al., 1998); and 5) Lomatas Negras Formation at Arroyo de las Calabacillas and Arroyo de las LomatasNegras.

Note: Ages of 13 fluvial Quaternary Rio Grande (Bravo River) deposits in the albuquerque area were studied by (Cole and Mahan, 2007). Deposition periods occurred on symmetrical terraces west and east of the River valley and are documented from youngest to oldest in the following paragraphs. Firstly, soils derived from (Primero alto) were built during later Pleistocene due to increasing of river capacity and competence within MIS-3 stage (OSL dates of 47 to 40 ka in Cole and Mahan, 2007). Secondly, fluvial soils terraces of the (Segundo alto) provoked the highest cooling early in MIS-5 stage (90-98ka) based on data basalt flows, In this regard OSL was (63 to 162ka) (Later in this thesis are results in cChapter 4 related to 3 OSL dating of the Colorado alluvial fan, Juarez, very similar to Albuquerque study here described). The third is associated with (Tercero Alto) and (Cuarto

Alto) terraces dated volcanic tephra, tercero alto contains Lava Creek B tephra (639 ka) and cuarto alto contains deposits of Bandelier tuff (1.22 Ma). Shortly, these terraces evidence is preserved in the albuquerque area and are distributed topographically with respect to the local channel of the river in the following position: Cuarto alto, 360 ft; Tercero alto, 300 ft; Segundo alto, 140 ft and finally, Primero alto, 60 ft. The ages recorded by this research are in agreement with the results obtained by the point four of the following summary.

Furthermore, a complementary study of the Nortwest Albuquerque basin named "OSL ages of upper Quaternary eolian sand and paleosols, nortwest Albuquerque Basin, New Mexico" is documented in Stephen et al. (2008). In this research, 12 OSL dating sites along Paseo del volcan corridor Rio Rancho, Sandoval County suggests that at least (0.5 to 1.4 m) of aeolian sand red calcic paleosol carbonate stage I was deposited during the period of 16 to 10 ka early during the Holocene; secondly, underlying an upper Pleistocene sand is an eroded eolian silty sand with a pink calcic paleosoil with stage II carbonate morphology (OSL 130ka).

Summarising the previous information detailed in section 2.1.10, In relation to the study area, there are some important remarks, in the following parragraphs. To address fluvial terraces evolution a depth analysis of Bravo River deposits are needed. The sort of soils actually exhibited in areas of Albuquerque New México have very similar facies and were formed by the Bravo River with the same hydrological and hydraulics principles with similarities in capacity, competence and discharge distribution. The prototype model selected to address fluvial deposits of Bravo River in the study area was the Albuquerque New México fluvial system given in above. Such a model contains fluvial terraces similar to that outcrop in the study area. Then, five formations were found from older to younger: Lomatas Negras (Qrl), Edith (Qe, Qre), Menaul (Qpm1, Qrm, Qpm2), Los Duranes (Qrd), Arenal (Qra, Qay) and finally Los Padillas Formation (Qrp). A brief discussion of fluvial facies inset in the previous five prototype formations are here remarked on, basically because they are the key to understanding their modern spatial and temporal distribution. Therefore, the previous model was adopted like prototype for the study area. However, here are reproduced the previous remarks which suggest at least five avulsive events during Pleistocene Holocene Time: ***First***, the Lacustrine Cabeza de Vaca lake of Plio-

Pleistocene time (>2.5 Ma). **Second**, The ancestral Bravo River trajectory during middle to Late Pleistocene (0.66 Ma to 0.16Ma) was running through the study area and connects the well preserved alluvial terrace named Tepeyac and Municipal Pantheon. ***Third***, the older Bravo River tributaries have built a dissected Alluvial terrace located in their neighborhood that is also marked with blue colour Late Pleistocene time (0.16 to 0.10 Ma). ***Fourth***, another alluvial terrace was constructed during approximately Late Pleistocene time (78 to 28 Ka). ***Fifth***, during Holocene time (15 to 22 Ka) another avulsive shift of Bravo River was occurred and is marked with café color. Also during this period of time the younger tributaries of the Bravo River were acting. ***Finally***, in recent time 15 ka to the present the last shift of the Bravo river occurred to its current path. A complete explanation of fluvial and alluvial soils deposits found during field work is presented in Chapter 4.

2.2 CLIMATE OVERVIEW AND STATISTICAL METEREOLOGIC APPROACHES.

2.2.1 Introduction. *A* Quaternary overview of climate during the last glaciations and Interglaciations are presented first. Then, meteorological, and probabilistic models stated by Ponce (1994) and Cheng (1983) are described. After that, the National Resource Conservation Soils of the United States of America (NRCS of USA) method included within the HEC-HMS Computer Program for simulation of flooding hazard using hydrology concepts and highlighting the Kiprich (1940) formulae to evaluate concentration time is presented.

2.2.2 Climate overview.

Fluvial and alluvial structures are strongly influenced by climate change along others factors which affects the mass availability mostly by mechanical erosion as well as mass transfer via channel feeder. Kevin and Lewis (1997 p. 39) state that during geologic time climate changed several times, therefore, to record these temporal variations and to date these climate fluctuations fossils preserved in soils and rocks are the most precise evidences. There are many subjects that treat to explain the reason that cause climate change and suggest some climatic models behavior. In the next paragraphs some of the causes are explored. Firstly, Milankovitch cyclicity. This astronomer named Milutin Milankovitch evaluated how the solar radiation during summer at latitudes 55^{o}N, 60^{o} N^{o},

and 65^{o} N varied during the past 650,000 years, using several astronomical models that reveal three scales of global climate change produced by temporal variation in the earth's orbit around the sun (Figs. 2.17, 2.18, and 2.19).

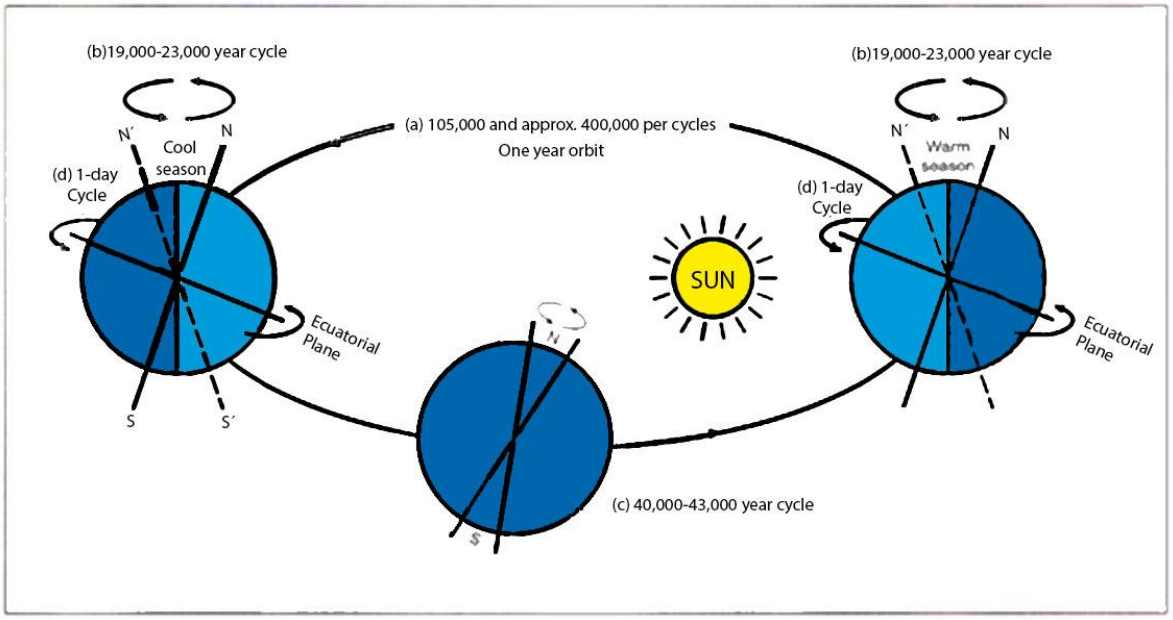

Figure 2.17. Illustrates the variability in the earth's orbit around the sun at various times scales measured in tens of thousands of years referred to as orbital parameters. Long term changes in orbital parameters causes its temporal variation in the amount of solar energy reaching the surface of the earth, which in turn can result in significant changes in global climate, referred to as Milankovitch cyclicity, so named after one of the first people to propose a link between changes in the earth's orbit and the climate change. Source: Opdyke et al. (1966 in Kevin and Lewis, 1997 p.80.)

Fig. 2.17 shows the variability in the earth's orbit around the sun at various times scales measured in tens of thousands of years referred to as orbital parameters which in turn can result in significant changes in global climate, and Fig. 2.18 illustrates a brief history of the last major glaciation that is known by different names through the word. For example the Devensian in Britain, the Wisconsin in North America and the Weichselian in mainland Europe. The Ice age is not a simple event, but a number of spaced cold-period glaciations (glacial) with duration of the order of 100,000 years separated by intervening warmer periods (as opposed to warm intervals within glacial stages, known as interstadials lasting 10,000-20,000 years. In addition, Fig. 2.18 shows the Last Glaciation Maximum (LGM) occurred 18,000 years ago that was a period of extreme cold on earth and in Fig. 2.19 are illustrated the four basics earth movements; Eccentricity, Obliquity, precession and ETM. On the other hand, floral and faunal evidence suggest that there was an abrupt change from warm to cold climate anywhere between 2.25 Ma and 1.65 Ma. Also, the

identification of ice-rapted debris in cores from Antartica depth sea, however, has put the onset of glaciations as far back as 3.5 Ma (Opdyke et al., 1966 in: Kevin and Lewis, 1997, p80).

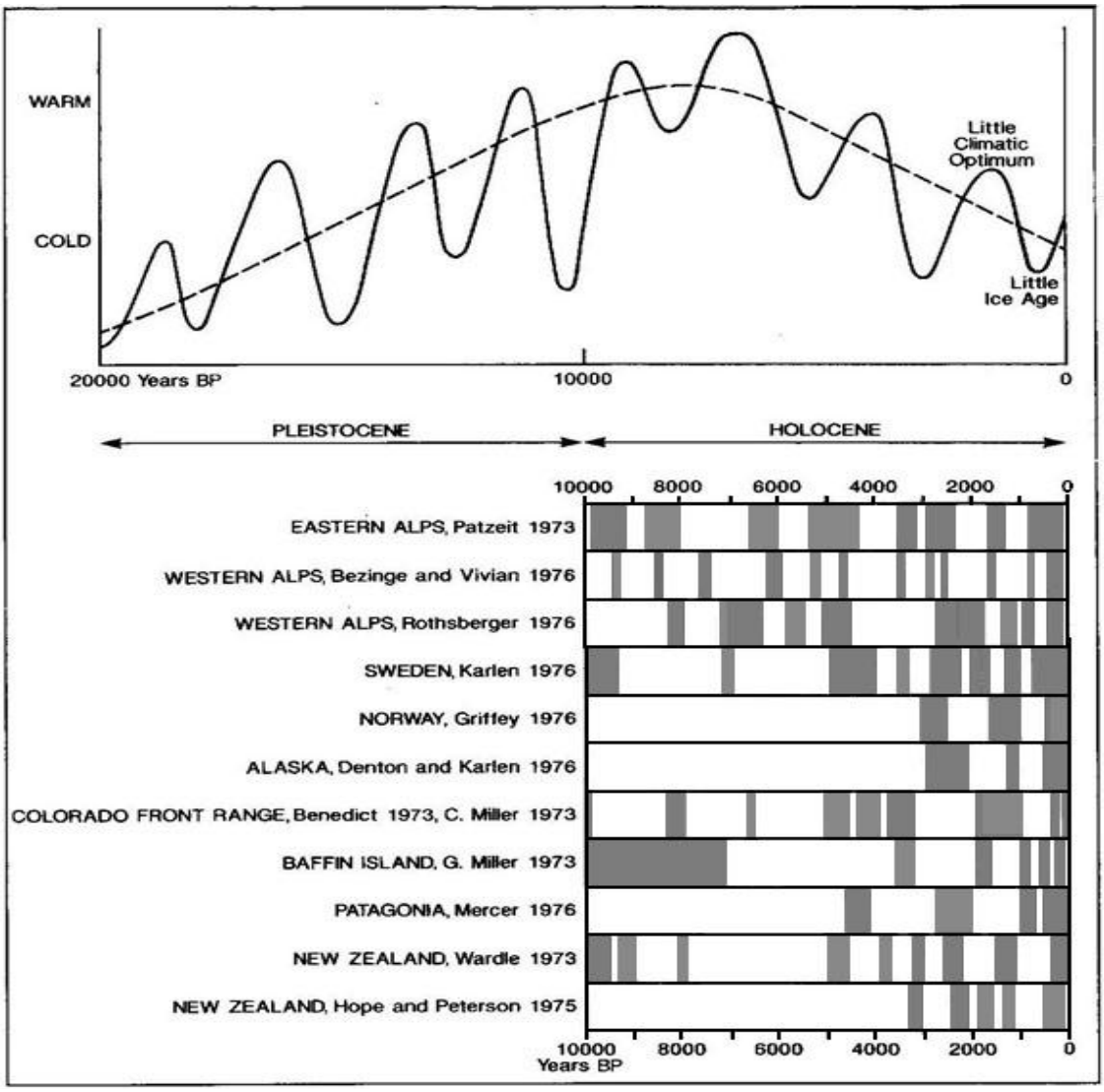

Figure 2.18. Schematic variations in relative temperature during the last 20000 years and the advance of glaciers from selected regions of the globe (shaded). The dashed curve shows how solar radiation varied as a precession-related Milankovitch cycle for a Latitude of 650 N. redrawn and adapted after Pielou (1991) and Grove (1971). Source: Opdyke et al. (1966 in: Kevin and Lewis, 1997, p80).

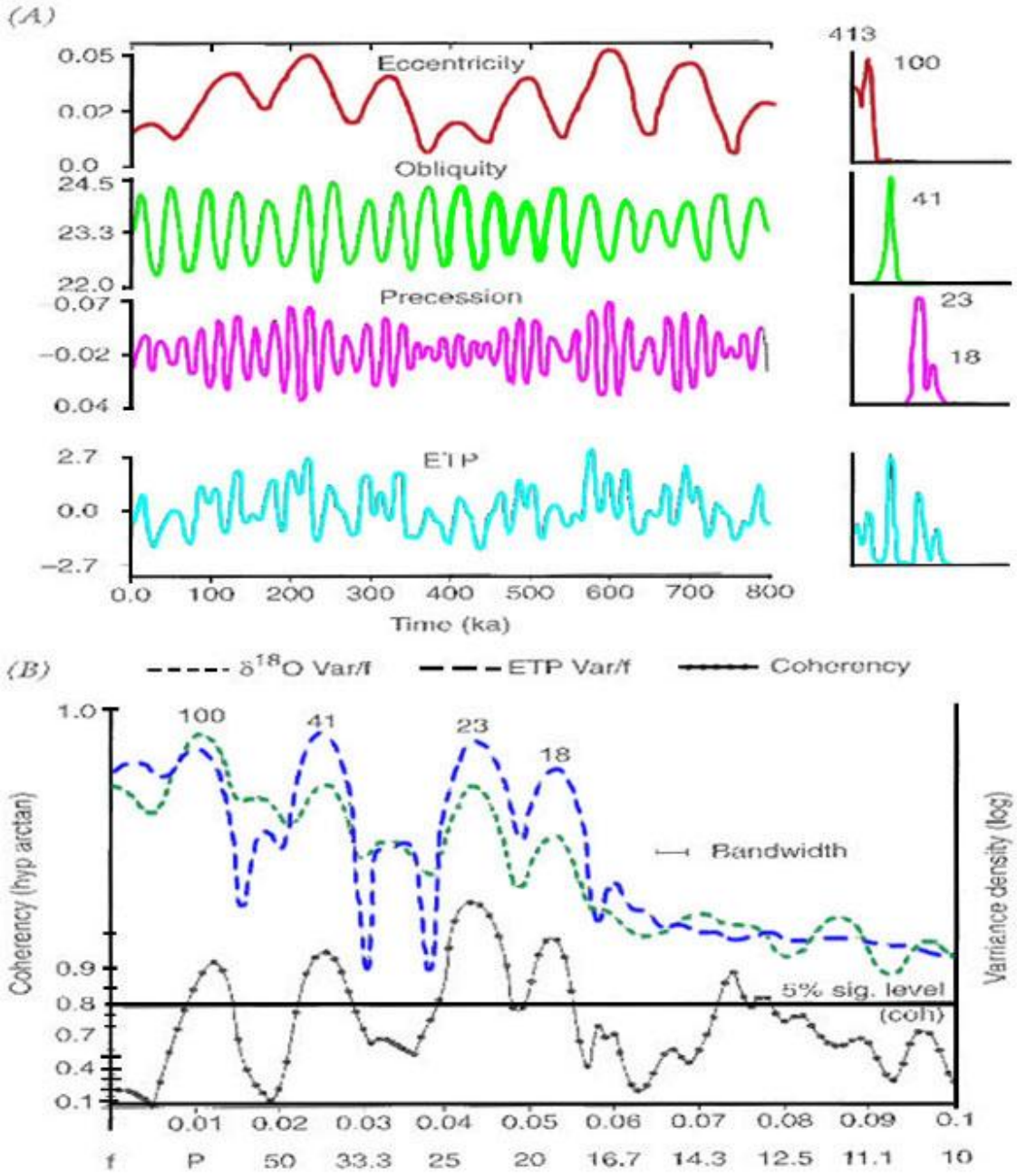

Figure 2.19. (A) Numerical simulation of variation in the Precession (Δ e sin φ), Obliquity and Eccentricity (degrees) during the past 800,000 years. The curve leveled ETP represents a normalized and summed combination of the above quantities. Shown in the right-hand side are the power spectra of each curve with the dominant period in thousands of years indicated. (B) Power spectra comparison between ETP andδ18 O variations for the past 780,000 years, showing good agreements between calculations and the geological record. The lower curve shows the coherency. Source: Opdyke et al. (1966 in: Kevin and Lewis, 1997, p80).

2.2.3 El Niño Southern Oscilation (ENSO)

ENSO which is an atmospheric phenomenon associated with recently climatic changes are described in many scientific papers. In Chapter 1 of the present research were detailed some of the historical features associated to it because the study area has been strongly affected by this phenomenon. El Niño Southern Oscillation is a perturbation of the atmospheric currents that occurs eventually in the Pacific Ocean and came when sea surface temperature (SST) reaches a minimum of 0.5^{o}C above its normal at least during a period of six consecutive months. The El Niño events produce the eastward propagation of a down welling Kelvin wave across the Equatorial Pacific (Kevin and Lewis, 1997, pp 58-59). These waves are confined in a narrow belt by the Coriolis force. Moreover, with respect to climate and specifically to solar radiation there are many theories that treat to explain the problem. Obviously, another important phenomenon regarded to this topic is the sunspot activity that is cover in detail by Kevin and Lewis (1997, pp 60-61). In this, it has been suggested and extremely controversial issue that considers that the sun's core may undergo episodic mixing every few hundred million (2.5 x 10^{8}) years due to a process known to astrophysicists as 'overstability' (Dilke and Gough, 1972 In: Kevin and Lewis, 1997) causing a significant change in solar neutrinos. This process has been invoked as a possible explanation of geological ice ages Mitchell (1976). On shorter time scales, from decades to thousands of years, the sun exhibits sunspots activity. Because the sun is the primary heat source for the Earth-atmosphere system, changes in incoming sunlight can influence climate. Sunspot numbers correlate well with solar irradiance, more sunspots mean a stronger sun while fewer sunspots mean a weaker sun. Fig. 2.20 of Ruddiman (2008) shows this relationship quite well. A sunspot cycle is one in which numbers go from high to low and back to high. This cycle averages about 11 years and is known as the sunspot.

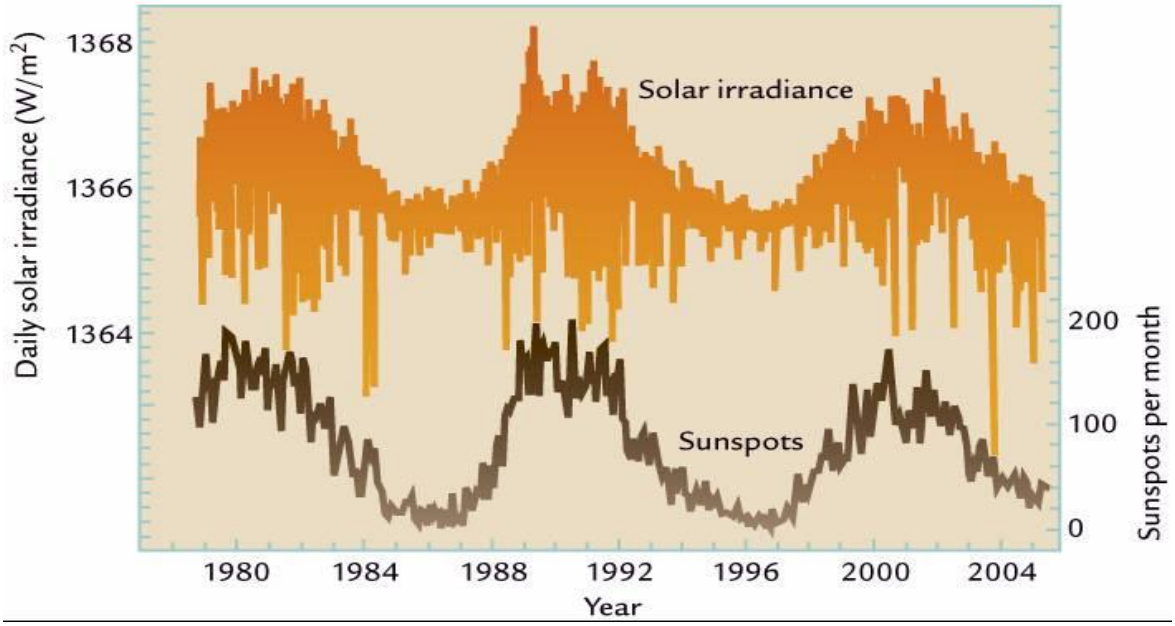

Figure 2.20. Daily solar irradiance (W/m^2) from 1980 to 2004 and Sunspots. Source: Ruddiman (2008)

2.2.4 ENSO Analysis in El Paso Texas USA area.

Many studies as well as data-sets for meteorological features are available near the study area, and will be detailed in the next paragraphs. Andrade and Sellers (1988) and more recently Bradshaw (1993) studied the relationship between ENSO events and their effect on positive impact in the amount of precipitation at El Paso, TX. ENSO events recorded between 1899-1983 (see Fig. 2; appendix 1A). Data-sets were ranked in order of intensity by Rasmusson (1984). A Category 1 event was considered very weak while a Category 4 was considered strong. Only those ENSO events ranked as Category 3 (moderate) or Category 4 (strong) were used in this study (those included 24 events of the 36 originally identified) by Rasmusson (1984) (See Figs. 2 and 3; Appendix 1A). In addition, Andrade and Sellers (1988) found that stronger ENSO events have a direct positive effect (increase) on precipitation received in the southwest United States, especially during the autumn season at the onset of an ENSO event, and also during the following spring. In an effort to evaluate this research for far West Texas, El Paso yearly and seasonal precipitation totals were calculated separately for both ENSO and non-ENSO years of this study and then were compared to average yearly and seasonal precipitation totals between 1899-1983 (see Fig. 3, appendix 1A; and Figs. 2.21 and 2.22). Winter season was defined

as December to February, Spring as March to May, Summer as June to August, and Autumn as September to November. Seasonal comparisons were made from the Autumn of an ENSO onset year to the spring of the year following an ENSO event for a time span of 21 months (see Figs. 2.21 and 2.22). This was done for two reasons: A direct positive effect is seen in El Paso, Texas seasonal precipitation totals during moderate to strong ENSO events, especially during the autumn of an ENSO onset year and the following spring. No relationship was found in regard to a precipitation enhancement relationship during the autumn and spring seasons following a full ENSO event. Only one year in 13 cases indicated greater than normal precipitation during this time.

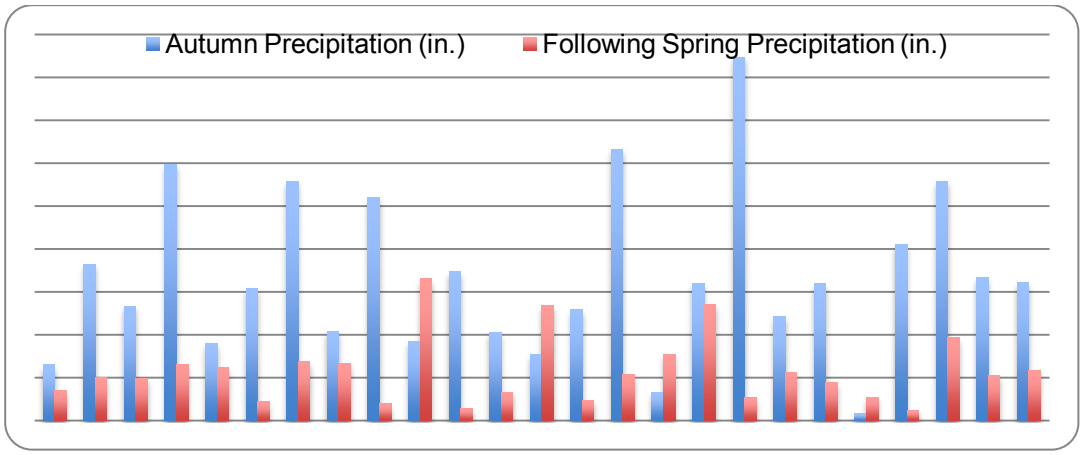

Figure 2.21. Commonly autumn precipitation blue colour followed to a decrease in amount of spring precipitation red colour from 1899 to 1983 period the number in brackets means storm category moderate 3 and strong 4. Source NOAA (2009).

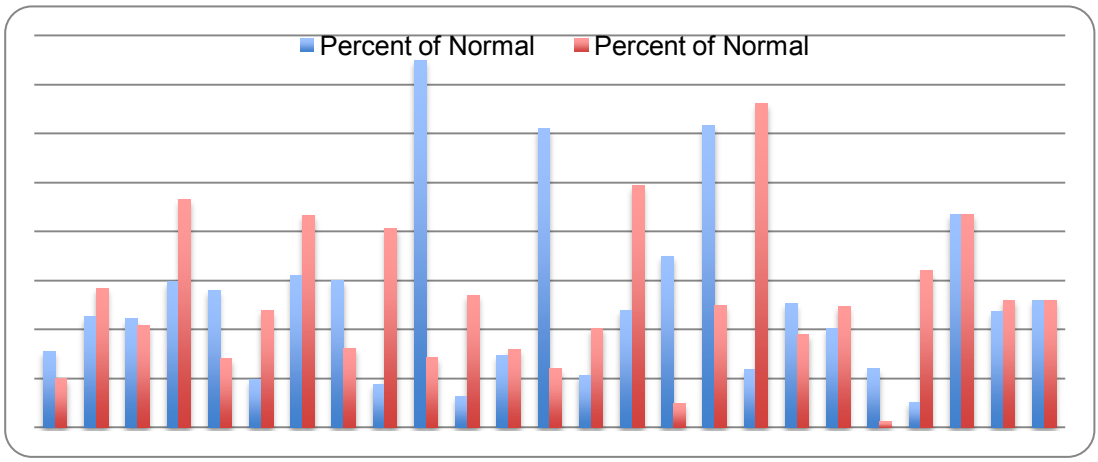

Figure 2.22. The percent of Normal during spring (red colour) predominates over the percent of Normal occurred during winter season (blue colour) with 10 of 25 events during (1899 to 1983) the number in brackets means storm category moderate (3) and strong (4). Source NOAA (2009).

2.2.5 La Niña Analysis at El Paso Texas. La Niña and non-La Niña years together, 20 of the 26 autumns and springs during La Niña years (77%) had below normal precipitation, as did 17 of the 26 winter seasons (65%) (Fig.4; appendix 1A). On average, precipitation received during any one of the three seasons was 61%-76% of normal when normal's computed with all the years inclusive of this study were used. The comparison between average seasonal precipitation totals for La Niña years and average seasonal precipitation totals for the non-La Niña years of this study further demonstrates that La Niña has distinct effects on El Paso, Texas precipitation. For the three seasons, average precipitation during La Niña years ranged from a high of 64% to a low of 53% of the average seasonal precipitation received during non-La Niña years (Fig. 2.23).

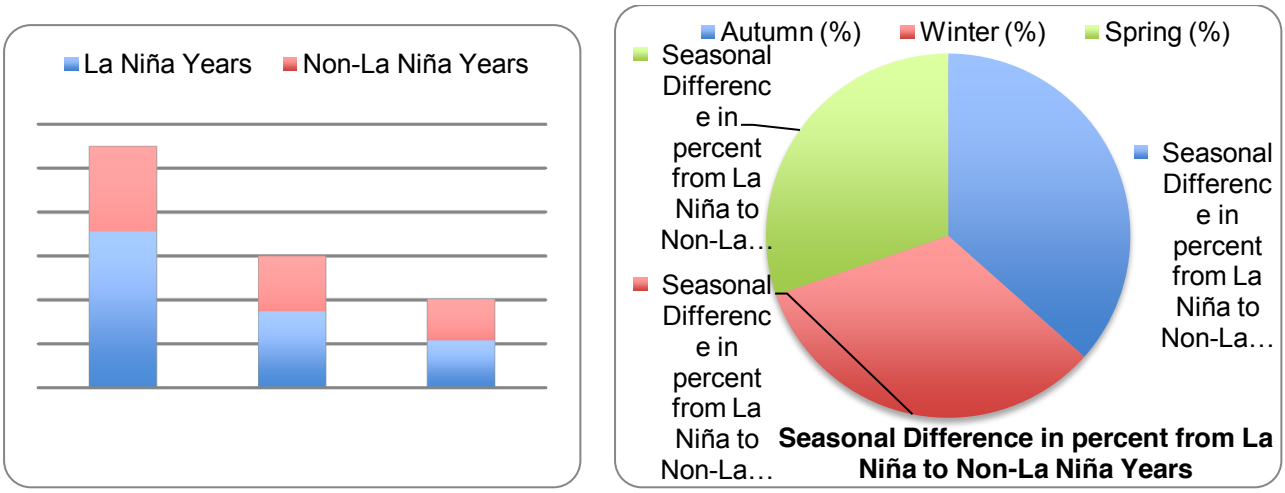

Figure 2.23. A) Seasonal Precipitation (in.) for La Niña Years vs. Non-La Niña Years B) difference between La Niña and Non-La Niña events. Source: NOAA (2009).

Reynolds (1997) Studied the ENSO in El Paso Texas using a similar method to Andrade and Sellers (1988). He found a positive effect on increased precipitation amount, mostly in the autumn of an ENSO onset year and the following spring. 15 of 24 ENSO years events (63%) superated the normal precipitation. In addition, rainfall either in autumn or spring superates 300% of normal four times, but, precipitation for these seasons averaged only 130% of normal for all of the events. On the other hand, considering only 12 events category 4 (strong) the precipitation was greater during Autumn in 7 of the 12 cases (58%) and in 8 of the 12 cases (67%) during the following spring. Finally, considering only the category 4 events, the average percent of normal precipitation for the autumn season of

ENSO onset rose slightly to 132%, while the following spring reached 147%. With regard to the winter season the total precipitation superates the normal in 9 of the 24 cases (38%) instead in 11 of the 24 cases (46%) had above normal summer precipitation. The strong ENSO event of 1914-15 yielded winter precipitation of 5.54 in., which was over 400% of normal, however, seasonal precipitation totals for winter and summer rarely exceeded 200% of normal. This was more common during autumn and spring seasons. When successive ENSO years were not accounted for, greater than normal precipitation was received during the autumn and spring seasons following a full ENSO event in only one of 13 years.

2.2.6 Meteorological and Hydrological datasets

There are four international organizations that publish meteorological and hydrological datasets for locations near the study area as El Paso, Texas. These Institutions are mentioned In the following paragraphs:

2.2.6.1 NOAA (2009). The National Weather Service Forecast Office provided monthly and yearly accumulated precipitation from El Paso, Texas during a period of 130 years (Appendix 1A; Fig. 1).

2.2.6.2 Frequency/Magnitude Atlas for the South-Central United States. (SRCC Technical Report 97-1 Geoscience Publications Department of Geography and Anthropology Louisiana State University Baton Rouge, LA 1997. This technical report gives information about precipitation events in terms of frequency/magnitude which have been taking place in Texas including the El Paso, Texas area. This information is presented in graphic format for different combinations of rainfall/magnitude in hours of the storm duration and its frequency (recurrence interval) in years. So there are graphs for 3, 6, 12 and 24 hours storm duration and 2, 5, 10, 25, 50, and 100 years of recurrence intervals. In short, depending on the storm duration and the recurrence design interval there could be adapted the design rainfall.

2.2.6.3 Statistical approaches. Ponce (1994) Described two probabilistic models that use Probability Distribution Function (PDF) to predict 24Hours Maximum Rainfall (24 HMR) for extreme events and for different return periods, In this chapter are presented two

probabilistic approaches: The Gumbel and Log Pearson III methods. The results of (24HMR) predicted for these models are then extended into a lower duration of the rainfall like 1hour (1HMR). Therefore, the other method is described as Cheng Lung Chen (1983). Finally, the National Resource Conservation Soils of United States of America is further used to simulate the process of rainfall-runoff. These features are fully described in methodology Chapter 3.

2.2.6.4 Concentration time parameter. Kiprich (1940) presented one of the first published works to evaluate Concentration time of a watershed using data from six small basins in Tennessee USA which ranged in area from 0.0051 to 0.5 km^2. He developed a graphical correlation of $((L/(S)^{0.5}))^{0.77}$. Where Tc is the time of concentration in hours, L is the stream length in m and S_s is the stream slope dimensionless.

The application of the HEC-HMS (2002) computer program for flooding hazard modeling requires three steps: Firstly, evaluation of the unit hydrograph of the direct runoff for the different sub-basins. Secondly, Transit of this hydrograph through the different components of the basin and sub-basin models such as reaches, junctions, sinks or dykes to assess the peak discharge for these components. The transit of these hydrographs would be assessed using different methodologies that depends on the hydraulic approach used. The more common methods to transit and evaluate the peak discharge of any hydrograph are six and are described below:

First, The kinematic wave routing, this method is best suited to fairly steep streams and approximates the full unsteady flow equations by ignoring inertial and pressure forces. It excels in urban areas where natural channels have been modified to have regular shapes and slopes. Also, it is assumed that the energy slope is equal to the bed slope. Second, The lag routing method only represents the translation of flood waves without attenuation or diffusion process. Consequently, it is best suited to short stream segments with a predictable travel time that does not vary with flow depth. The only parameter is the lag-time in minutes. Therefore, Inflow to the reach is delayed in time by an amount equal to the specified Lag, and then becomes outflow. Third, Muskingum method. It is used when the watershed basin has multiple sub-basins and it is desired to add hydrographs together from each of the sub-basins to determine the combined hydrographs at critical points. The more

common structure where an inflow hydrograph is needed is a storm water detention basin. This method, models the storage volume of flooding channels by a combination of wedge and prism storage. During the advance of a flood wave, inflow exceeds outflow, producing a wave of storage. During the recession, outflow exceeds inflow, resulting on a negative wave. In addition, there is a prism of storage, which is formed by a volume of constant cross section which is formed along the length of the prismatic channel. Assuming that the cross sectional area of the flood flow is proportional to the discharge of the section, the volume of the prism storage is equal to KQ where K is a proportionality coefficient and the volume of wedge storage is equal to KX(I-Q).

The value of (X) depends on the shape of the modeled wedge storage and varies from 0 for reservoir type storage to 0.5 for a full wedge, when X=0, there is no wedge and then hence no backwater in this case equation (9) results in a linear reservoir model and then S= KQ. The parameter (K) is the time of travel of the flood wave through the channel reach. (K and X) are specified constants throughout the range of flow. Fourth; Modified Plus routing method also called storage routing or level pool routing use conservation of mass and relationship between storage and discharge to route flow through the stream reach. (this method is applied only in areas were gauged station are available within the catchment area). Five, the straddle stagger method uses empirical representation of translation and attenuation processes to route water through a reach. Inflow is delayed a specified amount of time. The delayed flows are average over a specified amount of time to produce the final outflow. The Lag parameter specifies travel time through the reach. Inflow to the reach is delayed in time by an amount equal to the specified lag. The duration parameter specifies the amount of spreading in a flood peak at it travels through the reach. The delayed inflows are averaged over this specified time duration. Six, The constant loss/gain method uses an empirical relationship to calculate channel loss using a fixed flow rate reduction and a ratio of the flow. It does not include any capability to representing gaining streams. A fixed flow rate is subtracted from the routed flow and then the remainder is multiplied by a ratio. The reduced flow becomes the outflow for the reach.

2.2.6.5 Kiprich formulae. Loukas and Quick (1996) performed a “Physically-based estimation of Lag time forested mountainous watersheds”. They mentioned that the Kiprich (1940) equation was one of the first works related to time of concentration of a watershed.

They used six small basins in Tennesse, USA, which varies from 0.0051 to 0.433 km^2 and developed a graphic correlation of $L/S_t^{0.5}$ with the concentration time. Kiprich (1940) suggested that the curves would be applicable to the average small agricultural area ranging in size from 0.003 to 0.5 km^2. Based on these and other data Rowe and Thomas (1942) obtained the following equation: $Tc=0.000325[L/S_S^{0.5}]^{0.77}$ Where; Tc is the time of concentration in hours, L is the length of the stream in meters and S_s is the gradient of the stream dimensionless. Kiprich's equation is widely used both in simulation models and in design for small agricultural as well desert basins.

2.2.6.6 Boreholes lithology. JMAS (2009) Provided lithology of boreholes which are distributed along the hueco aquifer and supply water to the Juárez city population were. These boreholes with depth variable between 250 to 400 m have information of soils lithofacies (see Appendix 4A3 and 4A4) of results Chapter 4 at the end of this thesis.

CHAPTER 3 METHODS

3.1 INTRODUCTION

Many subjects such as: geology; geomorphology; meteorology; hydraulic and hydrology all use computer programs techniques for modeling and map production. In this case these are used to assess alluvial fans and flood risk threatening Juárez city. Therefore, this chapter is divided into three sections: **A)** Computer programs and datasets to address geomorphology and flooding models **B)** Field and desk work to assess alluvial and fluvial deposits and **C)** Modeling techniques to perform flooding hazard and risks.

3.1.1 Computer programs to assess geomorphology and flooding models.

Computer programs to produce models were applied in a routine way. Firstly, Auto-Cad (2009) which is able to work with big files and works within Geographical Information System platform (GIS) was used to update the contour elevation levels that represent topography of the study area and are the main dataset to generate two basic models: Digital Elevation Model (DEM) and Digital Slope Model (DSM). Also, this program was used to perform many tasks such as: Basin and sub-basin delimitation, areas evaluation and slope determination of the streams network system allocated on the study area.

3.1.2 Data sets of topography and urbanized area of the Juárez city.

Fundamental datasets regarded to topography and urbanization of Juárez city were used in order to address further Digital Elevation Model (DEM) and Digital Slope Models (DSM). Thus, two DEM one with contour levels offset every 5 meters (see Fig. 1 Appendix 3A) collected from fieldwork using Geographic Positioning System (GPS). The other based on contour levels every 1m derived using lidar technology provided by UACJ (2011). In addition basic datasets of the study area as: topographic chart (see Fig. 1A appendix 3A); aerial photo (see Fig. 1B Appendix 3A); Digital Elevation Model in raster grid format (see Fig. 1C Appendix 3A) and

finally images derived from Quick Bird sattelite system (see Fig. 1D Appendix 3A) were provided by IMIP (2007) and constitute the support of the tasks mentioned in the following paragraphs.

3.1. 3 Method to perform DEM.

This section briefly explains how to assess the DEM representing the three dimensional terrain elevation of the study area (see Fig. 3.1). This model is explained with more detail in appendix 3B.

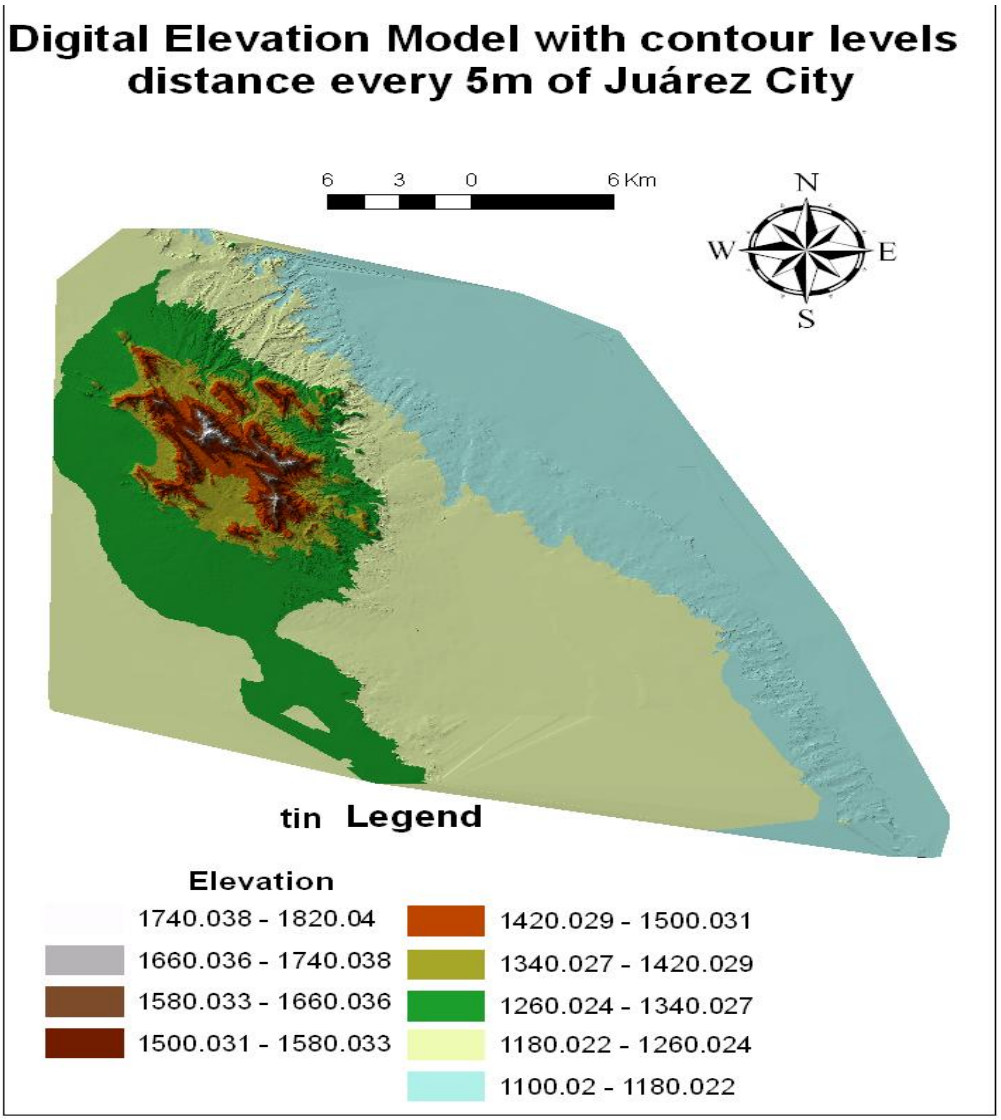

Figure 3.1. Digital Elevation Model (DEM) of the study area built with 5m contour levels: Elevation above the sea level is linked with colours in the tin legend indicated below the figure and the scale is shown above the figure. Created by David Zúñiga

(2009) using (.dxf) extension of Auto Cad file of topographic levels offset every 5m and Arc-Map 9.3 (2009) computer program.

Arc-GIS especially the component called Arc-View 3.2 (2002) was used to perform geomorphologic models and identify the physical mechanisms involved in it. In addition, the digital elevation models of the study area were built through the following steps: 1) Importing the Auto-Cad Civil 2009 dxf file extension which contains the contour levels every 5 m (see Fig. 1 Appendix 3A) into Arc-Map 9.2 (2009) program. This operation is performed using Arc-Catalog program that forms part of the GIS platform or directly within Arc-Map 9.2 program. After that, select the 3D analysis and click create/Modify TIN then select create TIN from features (see Appendix 3B). After that, the source dataset regarded to poly lines (contour levels) should be pointed and indicated the directory where would be saved. The visualization of the Digital Elevation Model would take just a few minutes (see Appendix 3B; steps 1 to 5 of Figs. 1 to 5).

3.1.4 Creating a terrain profile. To perform many cross terrain profiles, the Arc-GIS computer program was used during the present thesis. This program allow to distinguish many hydrogeological tasks such as: a) geological cross sections or define streams gradients anywhere in the upstream and downstream reaches. The process is briefly described here but a detailed explanation is presented in Appendix 3C. Once, activated the TIN feature or DEM, Click the launch Arc-Map program which shows a window. After that, click a new empty map and select the file and directory that contain your dataset. Then, from the menu select the module that contains the three dimension analysis and click 3D analyst. Then, select the file which contains the Triangulated Irregular Network (TIN1) of the Digital Elevation Model (DEM). After that, a window shows the graduated color of the DEM. If the selected colours are appropriated click ok, otherwise, change graduated colours as is required. Then, click TIN layer to do visible and would appeared the different colours with their elevations. After that, click the Interpolate line and draw the line were the cross section is needed over the DEM. Finally, click in create profile graph and the program shows the graphic of the profile which is created (see Fig. 3.2).

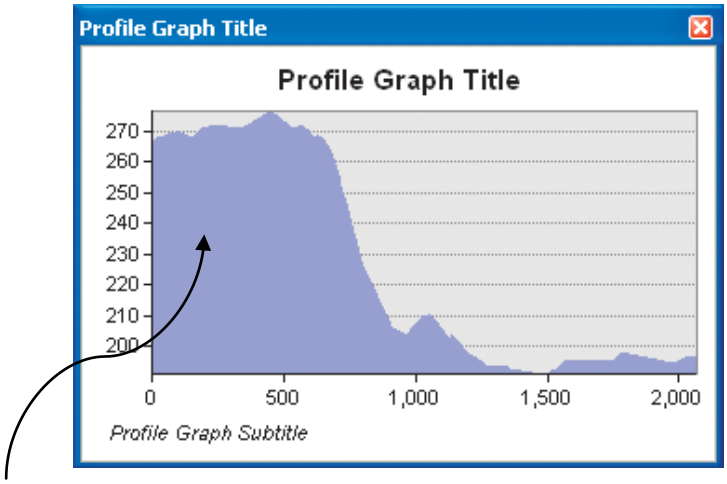

Figure 3.2. The graph shows how elevation in the vertical scale is linked to the distance from the origin in the horizontal scale. Note that the graph could be improved its quality if it is transported into another program as excel in agree with the desired resolution. Source: Arc-Map 9.2 (2009).

3.1.5 Digital Elevation Models with contour levels every 1m.

For practical reasons this subject is explained in section 3.3 (see Figs. 3.15A and 3.15B) of this chapter in order to link the geometric extraction data required for flooding hazard in three dimension defined in the results Chapter 6. The next section explains how to assess the satellite images using the Geographic Information System programs such as: Arc-Map 9.2 (2009) and Arc-Map 9.3 (2009).

3.1.6 Geomorphology analysis and interpretation.

Fundamental tasks performed by the Geographic Information System (GIS) platform are associated with the interpretation and analysis of satellite Images. These datasets were provided by the Geographic Information System laboratory of Ciudad Juárez University and IMIP (2007) (see Fig. 1D appendix 3A) and are integrated by the following images (Rectify a1.tif to a4.tif; Rectify b1.tif to b4.tif; Rectify c1.tif to c5,tif; Rectify d1.tif to d5.tif and Rectify e5.tif to t6.tif). These scanned (.tif files extension) datasets were read using the spatial analyst module of Arc-Map GIS 9.2 and Arc-view GIS 3.2 programs and were georeferenced using the Nad 27 datum and the UTM coordinate system. Shortly, Fig. 3.3 shows the satellite images in raster

format visualized by Arc-View GIS 3.2 (2009) version which is similar to the Arc-Map GIS 9.2.

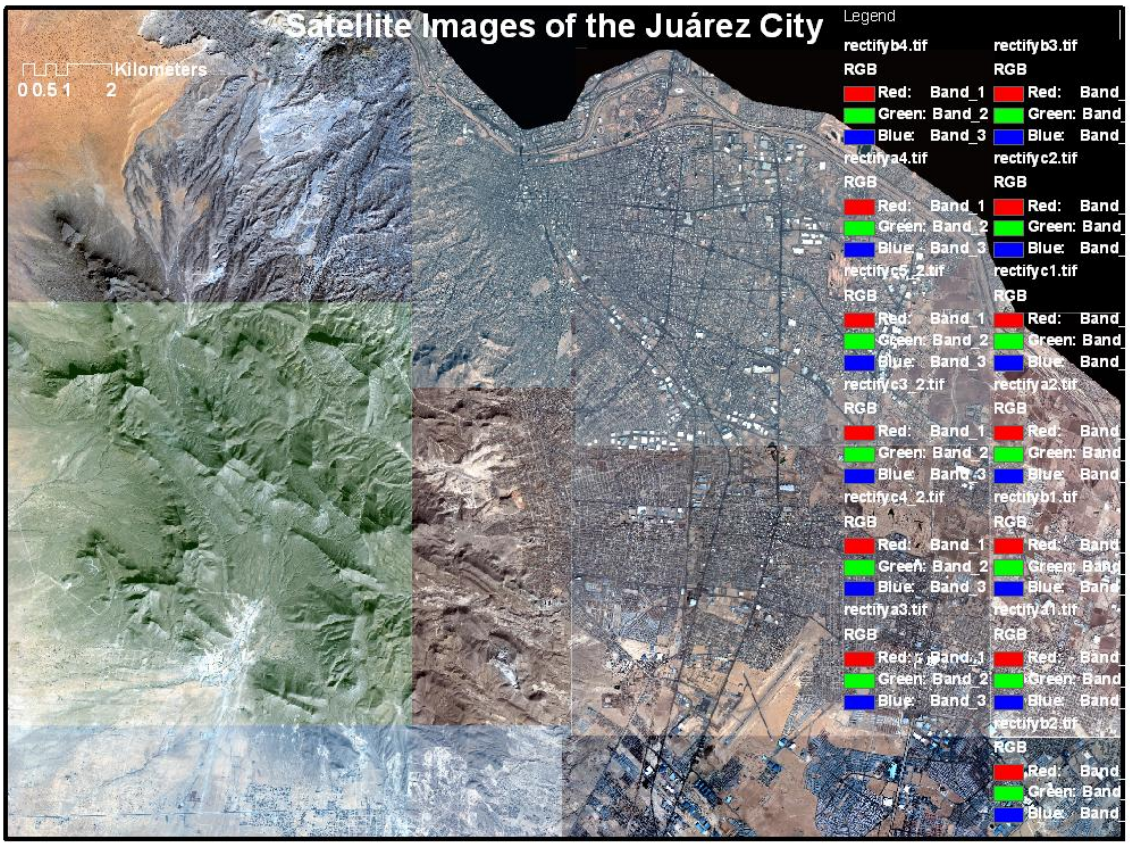

Figure 3.3. Satellite Images formed the entire study area of Juárez City, Legend illustrate the 3 color bands used by the 13 integrated raster images and are shown because it is the resolution used in the electromagnetic field: scale is presented in the upper left corner of the Image: Source: Geographic Information office of Juárez University (IMIP 2007); Coordinate UTM Zone 13N; Datum North American 1927; The process were done using Arc-Map 9.2 (2009)

3.1.7 Digital Slope Model (DSM)

DEM is a fundamental feature used during geomorphology interpretation, structural geology analysis, and alluvial fans dynamic modeling. The method to achieve this model is similar to that used to assess the DEM and also were derived using the contour levels (.dxf) file of Auto-Cad Civil 2009 program dataset. It is also performed using the 3D Analyst module of the Arc-Map 9.2 GIS platform. The DSM of the study area were built through the following steps**: 1)** Importing the (.dxf) Auto-Cad Civil 2009 extension contour levels dataset file into the Arc-Map 9.2 program using Arc-Catalog program that forms part of the GIS platform or directly within Arc-Map 9.2

program. **2)** Select the 3D analyst box and click create/Modify TIN then select derive slope from features. **3)** The source dataset regarded to poly-lines contour level should be pointed and finally indicate the appropriate directory to be saved. **4)** Visualization of the Digital Slope Model would take just a few minutes and the DSM would be displayed. At this part, only one colour for the slope model were drawn. Therefore, to complete the DSM two more steps are needed. **5)** Activate the rendering tab of the TIN feature properties command. **6)** Finally, click a graduated colour and different slope level would be performed. The final file is presented in (Fig. 3.4).

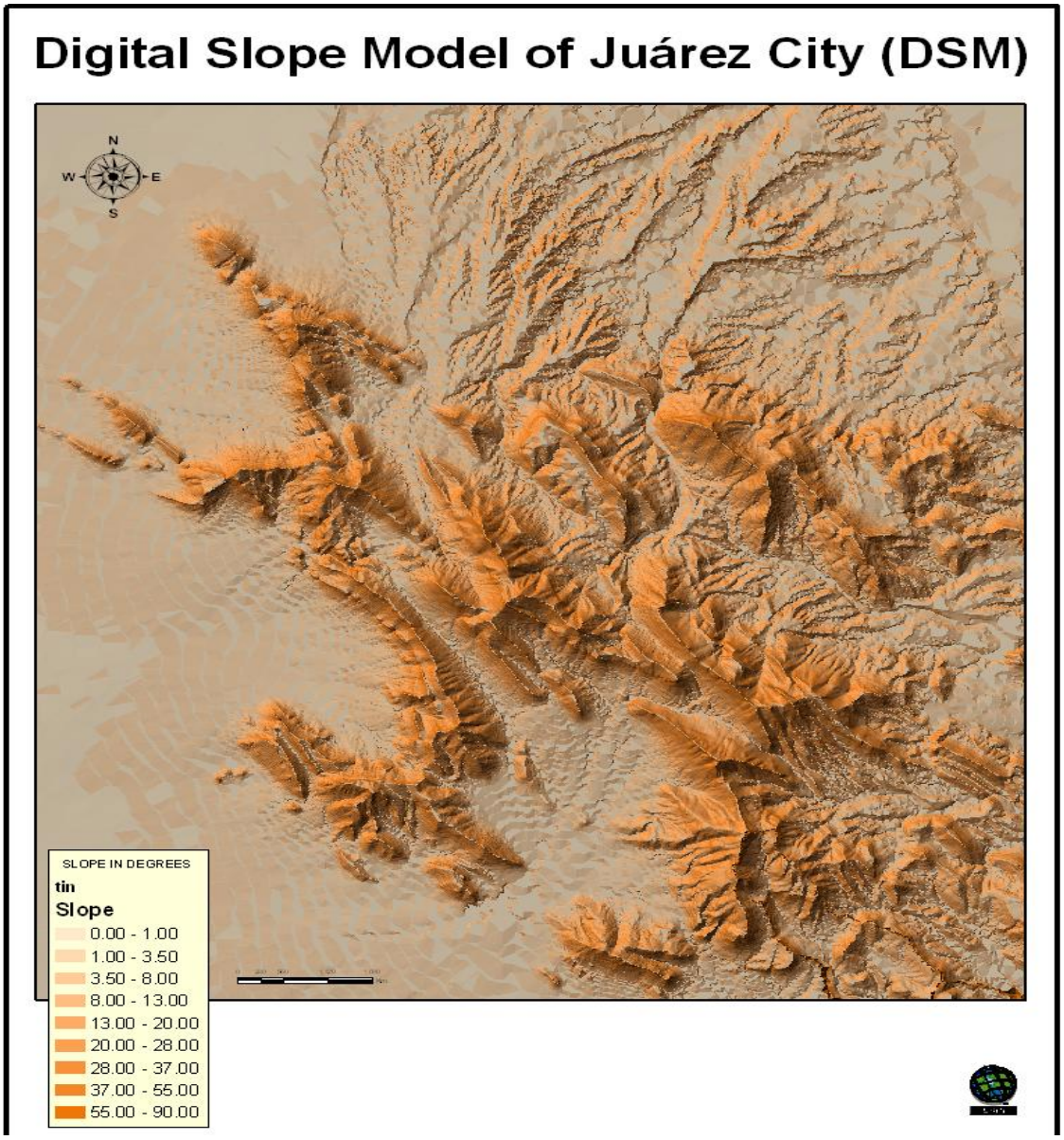

Figure 3.4. Digital Slope Model. Slope is indicated in degrees and bright color bars corresponds to higher values instead paled corresponds to lower slopes. The Model was constructed using the 3D module of the program. Created by David Zúñiga (2009) using Arc-Map 9.2 (2009).

3.2 Field and desk work to assess alluvial and fluvial structures

3.2.1 Introduction.

Field and desk work to assess alluvial fans and fluvial deposits was divided into three subsections: A) Alluvial fans and fluvial soils dynamic using OSL dating, petrography of rocks and boreholes **B)** Coarse and fine soil classification systems and laboratory test; **C**) Fluvial soils derived from the Bravo River and methods to assess geology. The first task performed was to collect surface soils samples, after that, laboratory analysis and soils classification was done. Then, boreholes analysis and facie interpretation. These was fundamental issues to address the alluvial fans as well Bravo River fluvial evolution which are given in the results chapter 4.

3.2.3 Alluvial fans and fluvial soils Lithology using OSL dating method, petrography and boreholes

In order to date alluvial fans and fluvial structures Optical Stimulated Luminescence (OSL) was performed. The samples were collected in 3 specific sites mostly composed of fine quartzite sands (see Figs. 3.5, 3.5A, 3.5B and 3.5C). In addition sample were transported to United States Geological Survey Optically Stimulated Luminescence Lab (USGS OSL Lab) (see Figs. 3.6A and 3.6B). The results of this Geophysical test allow to link the model predicted and the evolution of these sedimentary structures. the procedure involved to the soil dating deserve an special section which is provided in (Appendix 4 of results Chapter 4).

Petrographic classification was another task performed directly in the field along outcrops of alluvial fans and fluvial structures named terraces. Firstly, samples was collected (see sample collection on 3.7A) and transported to UACJ soils laboratory. After that, there was extended in a clean and flat surface and extract a 200 to 400 fragments. Then, fragments were separated with different petrography composition for example: andesitic, felsitic, granite, rhyolite, limestone, sandstone and shale (see Figs. 3.7B and 3.7D). Finally, to represent the total sample into a percent distribution using a pie graphic (see Fig. 3.7B). A complete sample analysis

is presented in Appendix 4A and 4B of results chapter 4. In addition to previous soils analysis performed on the terrain surface also interpretation of soils were done over many boreholes provided by water supply office of Juárez city (JMAS 2009). These boreholes contain lithology and are distributed along the Hueco aquifer which provides water to the Juárez city population. These boreholes with variable depth between 250 m to 400 m have information to soils composition and facie (See Appendixes 4A1 and 4A2 of results chapter 4).

General location of the three collected OSL samples dating to USGS. See UTM coordinates, sample depth and statigrafic details in the next three ilustrations

Fig. 3.5. Location sites were samples P1, P2 and P3 were collected for OSL dating alluvial fan. See Figures 3.5A, 3.5B and 3.5C the location points P1, P2 and P3. Note: Only these three OSL samples were done for two reasons: Firstly, no economic resources were available to perform the 10 samples needed to model of the wall alluvial system. Secondly, these three dating results samples allow to connect with fluvial Bravo River terraces model and assess the more important alluvial fan sector of the study area (Colorado sector). Created by Zúñiga (2012) using GoogleEarth (2009).

In the following page, there is Figure 3.5A. This figure shows the P1 OSL site for sample collection and have two white text labels HOMEAFTER and HOME

BEFORE; these can be ignored since they have no relevance to this sampling.

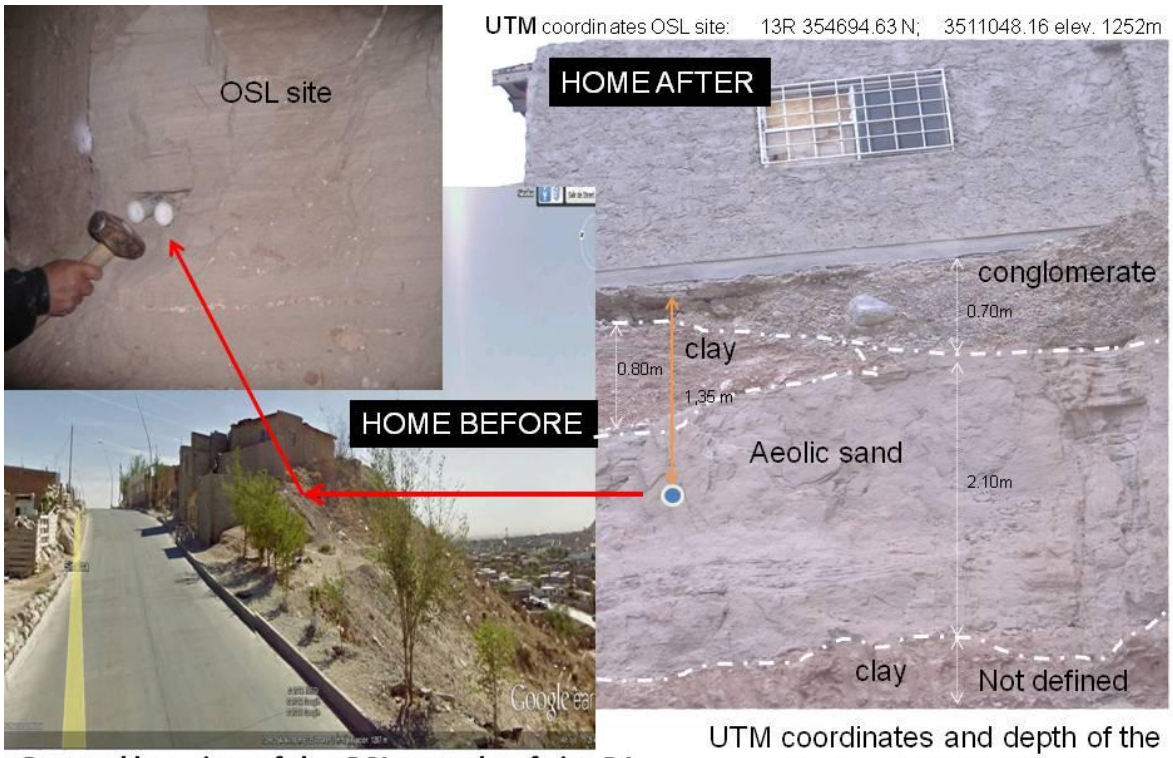

General location of the OSL sample of site P1 (see the home before and after and the

UTM coordinates and depth of the sample site: 13R 354694.63 m E 3511048.16 m elevation 1252 m and the depth = 1.35 m
Collection date: March/18/ 2012

Fig. 3.5A. OSL site location of collected sample (P1) Colorado Alluvial fan

UTM coordinates and depth of the sample site: 13R 356593.59 m E 3511861.18 m elevation 1201m and the depth = 5.55 m
Collection date: March/18/2012

P2

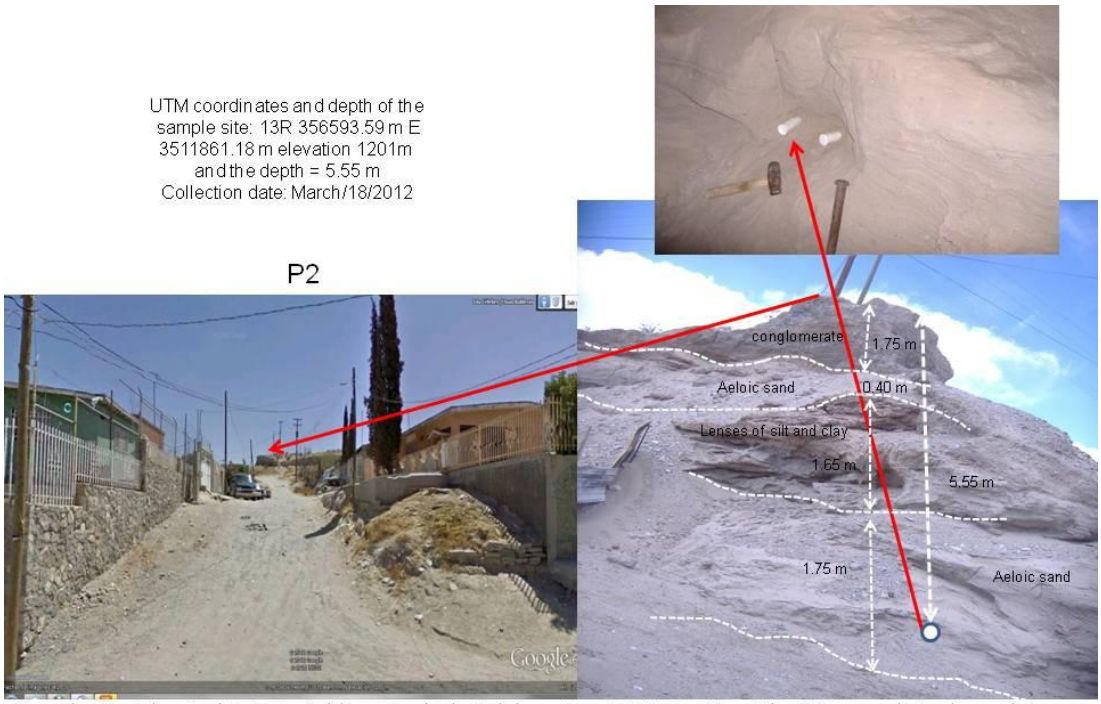

Sample site 2 located in Juan Balderas and Isla Celebes streets intersection. The OSL sample is showed in google picture 2. Note the red arrow showing the road access to the site of sample collection. Also the photo shows the sequence conglomerate (Alluvial fan) and at the base sequence of two layers of windy sand and red clay. Note the picture showing sample collection details.

Fig. 3.5B. OSL site location of collected sample (P2) Colorado Alluvial fan

location of the OSL sample of site P3 showed in picture 3 note the natural terrain showing different layers beginning with conglomerate (Alluvial fan) and at the base sequence of windy sand and red clay.

Fig. 3.5C. OSL site location of collected sample (P3) Colorado Alluvial fan

Figure 3.6. A) Sample collection in fine sands bellow the all uvial Colorado Alluvial fan B) Sample preparation both bulk sample in plastic bags and three plastic pipes 2 in diameter for OSL Geophysical datation tests. Note the sample collection in the field was performed during the night. Created by David Zúñiga (2012)

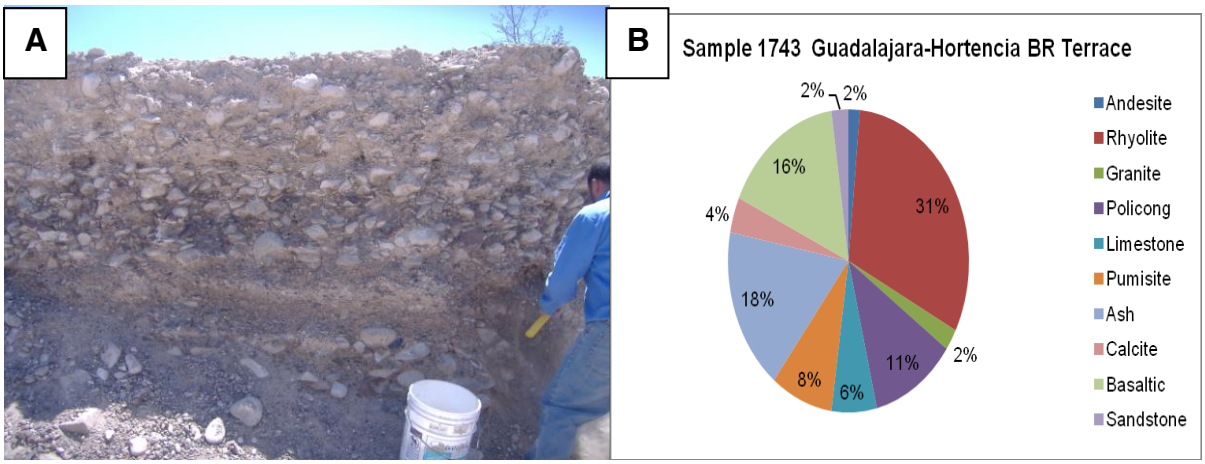

Figure 3.7. location of Gravels, Cobbles, Pebbles and sands on the Bravo River relict terrace located at the cross intersection of Hortencia and Guadalajara streets, Felipe Angeles Neighbour B) results of petrography analysis. Created by David Zúñiga and Juárez University Soils Lab (2012)

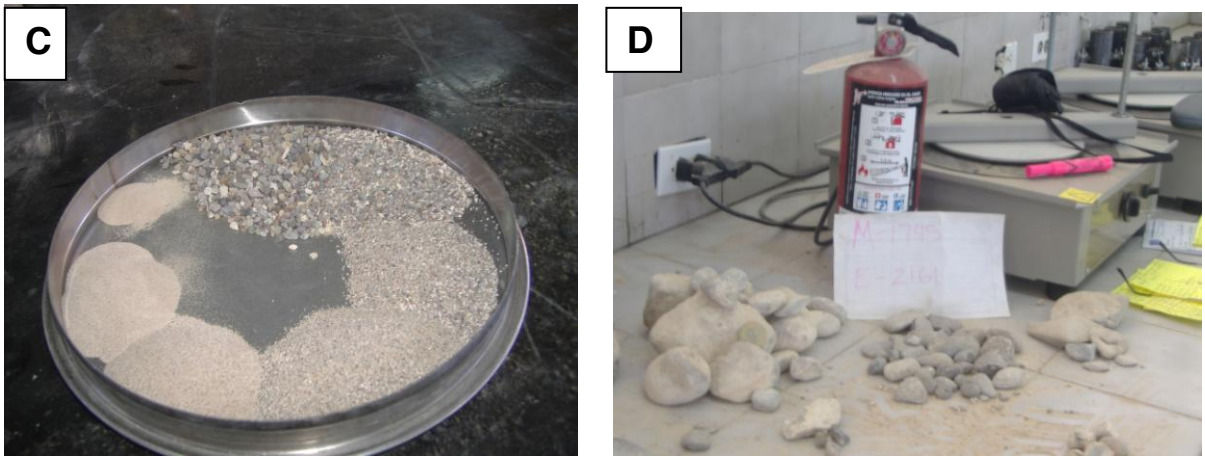

Figure 3.7A C) Size distribution of pebbles and sands collected from Bravo River terrace relict located at cross intersection of Hortencia and Guadalajara streets, 3.7 D) Big gravels of same location of A (1745-2161 sample Lab number). Source: David Zúñiga and Soils Laboratory Juárez University (2012) detailed on appendix 4A1 (See next Picture 3.7 for sample collection location.

3.2.2 Soils classification.

Soils are everywhere covering the landscape with many geometric shapes. These typical soils basically named as: gravel, sand, silt and clay are the building block of all sedimentary structures. However, alluvial fans and fluvial terraces are the concern of this research. Thus, in order to identify these structures and their properly defined facies a traditional classification of soils is needed. Sometimes

aeolian soils, very common on the study area produces silts, fine sands or even coarse sands. Other times, depending of the competence as well capacity of the drainage channel and the source catchment area, mixed soils are deposited. These sedimentary structures are mixed each other forming complex structures such as: conglomerates even with different degree of development derived by their parent rocks (Machete, 1985; Machete et al., 1997; Gile et al., 1966; Bachman and Machete, 1977) (see section 2 of Literature review chapter 2).

The Unified Soil Classification System method was used in this study. This method is widely used to assess soil lithofacies (ASTM 1985). This International Soil classification system is more detailed in appendix 3D and here a brief description is mentioned. Once the representative sample is performed Size distribution of the coarse and fine soil fraction were performed, the system is composed of several sieves of different sizes from number 4 and upper from coarse soils and 4 and less for fine soils. This process is done through the use of an electronic apparatus that produce the vibration of the sample in vertical, horizontal as well as circular movement during a period of approximately 15 minutes. After that, the weight of the fractions of soils retained in the different sieves are recorded and the % that passes the sieve is evaluated. Then, the results are drawn in the (x) axis in logarithmic scale the grain size and in the vertical axis (y) the accumulated (%) by weight that corresponds to the grain size were drawn (See Fig. 3.8). In addition, (Fig. 3.8A) shows expressions to evaluate (Cc) and (Cu) and the further classification as GW or SW in agree with the limits defined for (Cc and Cu) (see Fig. 3.8B).

Soil parameters such as: Liquid Limit (LL); Plastic Limit (PL); size distribution; Curvature coefficient (Cc); Uniformity coefficient (Cu); Linear contraction (LC) are fundamental features to assess lithology. The method is internationally recognized and it is detailed in appendix 3D.

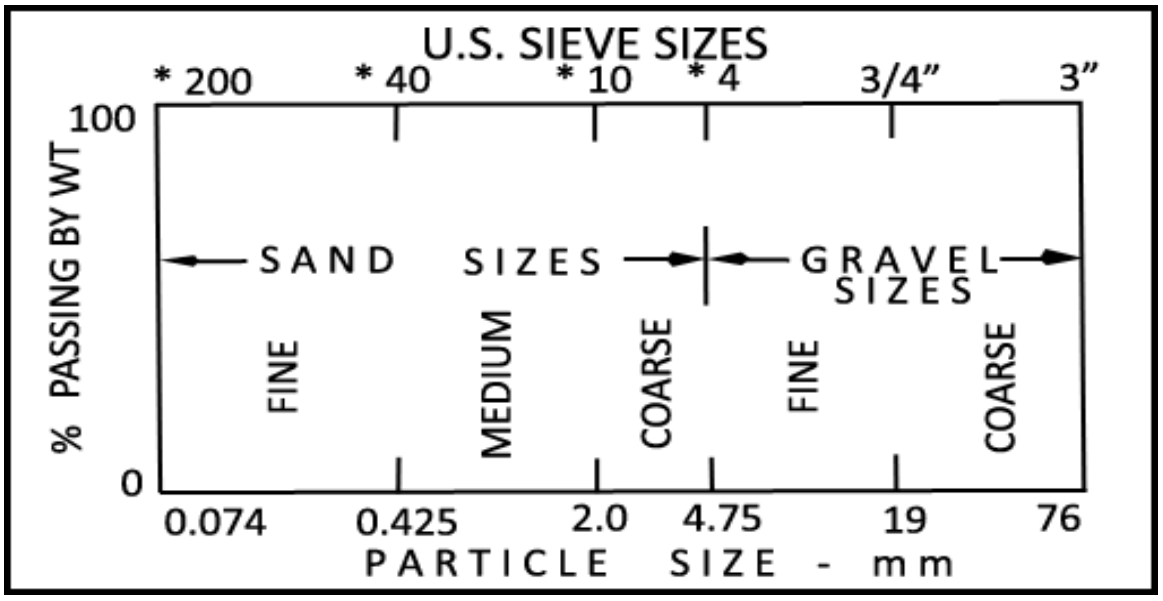

Figure 3.8. Ranges of diameters for coarse particle sizing. The (x) axis shows the size particles in mm and at logarithmic scale and the (y) axis shows the percent of soil passing in weight: Note also the upper axe shows the limits to classify soils as: coarse and fine gravels fine, medium to course sands. Source: ASTM (1985).

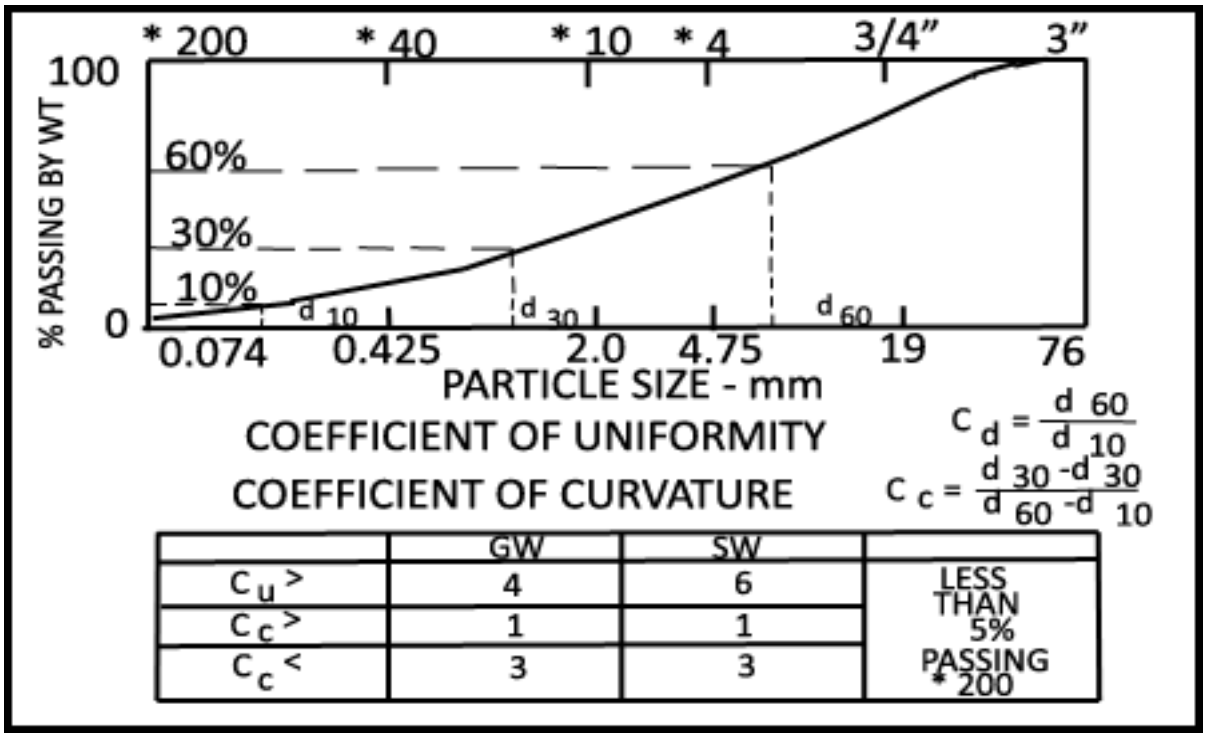

	GW	SW	
$C_u >$	4	6	LESS THAN 5% PASSING * 200
$C_c >$	1	1	
$C_c <$	3	3	

Figure 3.8A. Requirements for soil to be classified as well graded. Cc and Cu in percentage define the soils gradation lower part of the Figure. The upper figure shows the curve distribution in function of size particle (x) and the percent passing the sieve (y) Source: ASTM (1985).

Plastic Limit (P.L.) and Liquid Limit (L.L) were performed simultaneously and were performed over 5 little hand samples of the soil contained several humidity contents that appears to have closely the (L.L) (see Figs. 3.9A and 3.9B). Then, this sample is molded and rolled over a clean glass surface and stop the operation if the sample begin to fissure or break until the roll measure is approximately 9.3 cm long and 3 mm thick then, take a sample weight and put it on the oven during 24 hours at constant temperature of 110° Celsius. After that, determine the weight again and the difference between the initial weight and the final weight divided by the initial weight corresponds to (P.L).This operation is performed to five samples and the final L.P is the average of the LP of the 5 samples (see appendix 3D).

Figure 3.9 A. Casa Grande coup for (L.L) determination of fine soils as clay, silt or silty-clay. Similar to that shown in Figure 3.9 B) Electronic balance to measure weight of the sample before and after of put it into the oven. Note, additional tools to perform LP. Created by David Zúñiga using Soils Laboratory of Juárez University

Soils Classification. This process of classification consist in the use of the plasticity chart using the parameters previously obtained of LL and PL there is evaluated the Plastic Index PI that is the difference between the LL and PL with the PI and the LL and using the Plasticity chart Fig. 3.10 there is possible classify the fine grained soil.

In addition, Fig. 3.11 shows the roundness degree of cobbles and gravels which is an important feature during assessment of the genetic parent rock and its facies relationships of fluvial as well sedimentary structures found along the study area. In this regard, Figs 3.7 A, B, C, and D show how the form origin and degree of

roundness allows to assess the key task of this research and distinguish the fluvial or alluvial sediments origin (see results Chapter 4). Finally, Fig. 3.12 shows how stratigraphy and sedimentary facies are applied in the field to link soils classification with fluvial deposits and alluvial fans soils along the study area.

In short, the previously described methodology was applied to all the soils covered the three alluvial fans sectors of the study area. However, Figure 3.12 shows an example about how the link between the kind of soil derived from the soil classification system was applied to the alluvial fan field identification and a complete description is presented in the results Chapter 4.

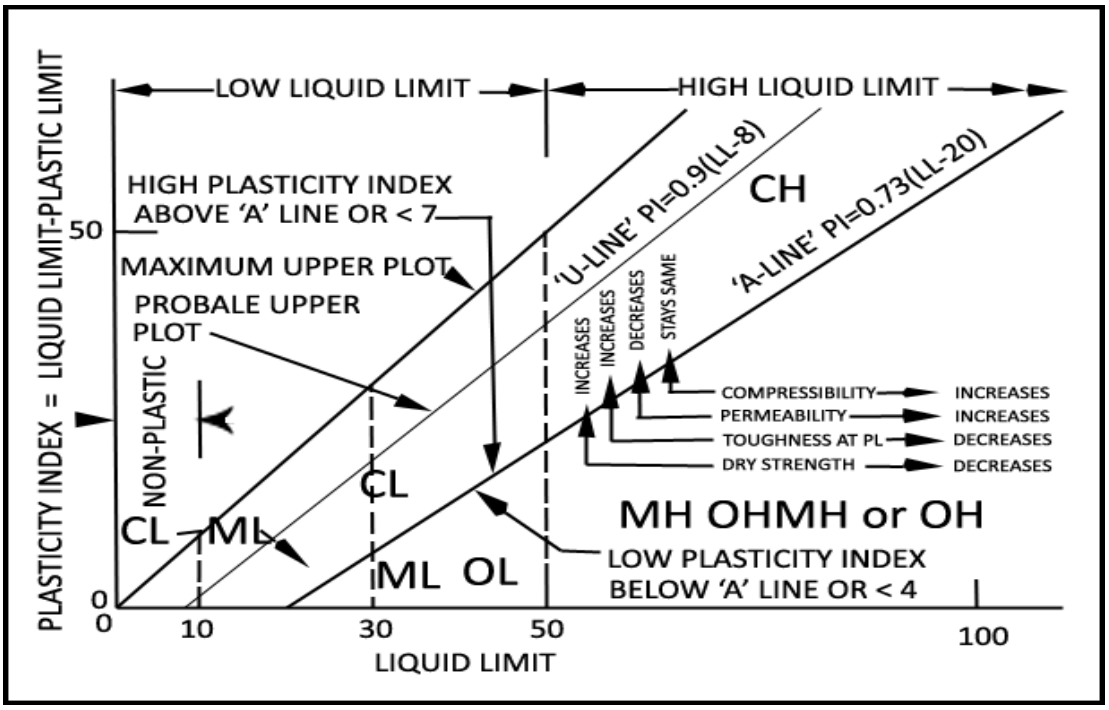

Figure 3.10. Plasticity chart applied to fine soils classification. Figure shows in the X axis scale the liquid limit (LL) in (%) and in the axe (y) the plastic index (PI): Also see different lines that define the border the different kind of soils found. Source: ASTM (1985).

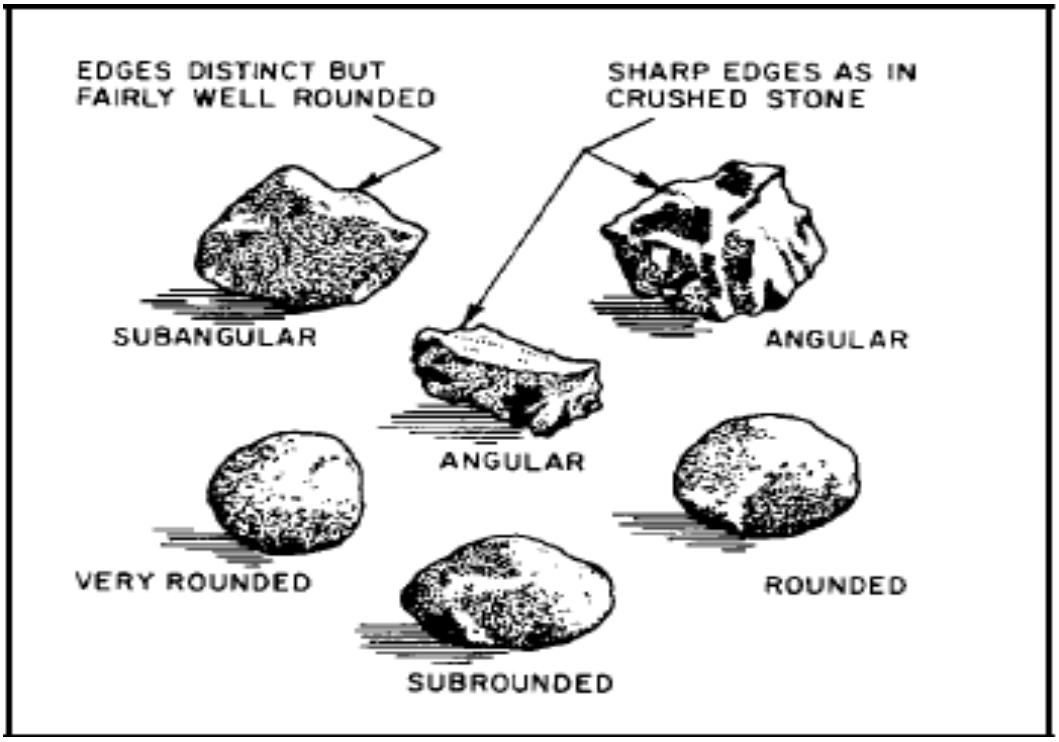

Figure 3.11. Typical shapes of bulky or equidemensional grains. Source: ASTM (1985).

Figure 3.12. Shows the areas of Juarez Mountains where took place sample collection and its further facie interpretation which allow the spatial and temporal distribution of the alluvial fans (a complete sketch is given in results chapter 4)

3.3 Modelling techniques to perform flooding and risks

3.3.1 flooding hazard in one dimension using HEC HMS computer program.

TR-55, SCS (1986) Developped a model approach for flooding hazard. This approach requires basic information such as: Drainage area (A), concentration time (Tc), Curve Number (CN), and design rainfall (hyetogram). Also, requires the spatial rainfall distribution during its duration period and the rainfall losses due to interception in depressive areas. There are several losses of water due to infiltration into rocks and soils during the time of the storm that also are included in this method. In short the NRCS method can be described in three parts: **a**) Rainfall-runoff equation (or Unit Hydrograph) can be defined through the use Curve Number (CN) determination for different landuse and hydrologic soil types that should be represented in the catchment area. **b**) Peak discharge assessment and concentration time (Tc) for the different sub-basins or specific points of the study area and application of the Unit Hydrograph approach in order to evaluate the direct runoff hydrograph of basins and sub-basins considered in the catchment area. **c**) HEC-HMS (2002) version 3.1.0 (Hydrologic Engineering Center-Hydrologic Modeling System). This computer program is specially designed to simulate hydrological problems like flooding hazards. Basically is integrated with three modules: basin model, meteorologic model, and Control Specification Model.

The methodology used in the program is composed of three fundamentals stages: firstly, start creating one new file or open an existing one. Then, introduce the components of the basin model (seven different types of possible components; basin, sub-basin, routing reach, junction, reservoir, source, sink or diversion). Secondly, introduce the meteorologic model which contains the previously evaluated precipitation of design (hyetograph) for the study area. Thirdly, ingress the control specification related to the time duration of the precipitation of design (hyetograph). As a result the program generates the solution of the problem given the peak discharge for different return period of the design storm. The program User's Manual describes how to manage the futures and gives descriptive information on the different mathematical models included. For instance there are models for evaluate

the basin discharge that considers losses such as: SCS, CN; Green and Ampt; Initial and constant; Deficit and constant; Soil Moisture accounting; User specified unit hydrograph; parametric and synthetic unit hydrograph; Snyder unit hydrograph; SCS unit hydrograph model; Clark unit hydrograph; Mod Clark model; Kinematic wave. All the models mentioned are designed to solve specific hydrologic problems and the method selected would be linked with the type of project assessed. In the present research the used model was the SCS unit hydrograph model. This program will be used frequently during the discharge evaluation for different structures such as dykes allocated in the study area.

SCS (1986) proposes a method for midsize catchments analysis named the runoff curve number equation (CN) that has been used by the Soil Conservation Service of the United States SCS (1986) used in this report. This method is assessed through the use of a computer program named HEC-HMS flooding in one dimension. This program is applied in this PhD research for three reasons. Firstly, it permits identification of structures at risk. Secondly, the peak discharge as well the volume of water accumulated in the source and depositional areas of the basins are evaluated. Finally, this method has been applied to simulate dendritic drainage systems in many desert areas of Texas, Arizona, and New México. Therefore, the method is very suitable to simulate flooding on Juárez city which have similar geomorphologic characteristics.

The effective rainfall that produce runoff is a basic feature to support build the hydrographs for the basins and is assessed through the use of a rainfall-runoff equation, commonly named runoff curve number (CN) method mentioned in SCS (1986). The Curve number (CN) parameter was obtained in function of the land-use, impervious surface (I.S.) and the hydrologic soil type for specific sub-basin within the basin considered, (see Fig. 3.13 table 1 and sections 5.3.3.1 to 5.3.3.8 of results chapter 5, Fig. 3.14 and Table 2). Fig. 3.13 Table 1 shows an example for a composite curve number calculation (CN). These parameters are all standard approaches in hydrological modeling.

Land use	% of total land area	Curve Number	Weighted curve Number (% area x CN)
Residential 1/8 –acre soil group B	0.80	0.85	0.68
Meadow good condition soil group C	0.20	0.71	0.14
Total weighted CN = 0.68 + 0.14 = 0.82			

Figure 3.13. Table 1 Example of SCS runoff curve numbers (CN) for a composite terrain. Given a specific land use and hydrologic soil group for two terrains, CN (0.85 and 0.71) were founded (see Fig. 3.14 Table 2). Then using % of total land area (0.80 and 0.20) the total weighted number is evaluated by multiply the two values, therefore factor (CN) is founded. Source: SCS (1986).

Table 2: NRCS runoff curve numbers (CN) for selected urban land use[1]

Cover description		*Curve numbers for hydrologic soil group*			
Cover type and hydrologic condition	**Average impervious area[2]**	**A**	**B**	**C**	**D**
Fully developed urban areas (vegetation established)					
Open space (lawns, parks, golf courses, cemeteries, etc)[3]:					
Poor condition (grass cover <50%)		68	79	86	89
Fair condition (grass cover 50% to 75%)		49	69	79	84
Good condition (grass cover >75%)		39	61	74	80
Impervious areas:					
Paved parking lots, roofs, driveways, etc (excluding ROW)		98	98	98	98
Streets and roads:					
Paved: curbs and storm sewers (excluding ROW)		98	98	98	98
Paved: open ditches (including ROW)		83	89	92	93
Gravel (including ROW)		76	85	89	91
Dirt (including ROW)		72	82	87	89
Western desert urban areas:					
Natural desert landscaping (pervious areas only)[4]		63	77	85	88
Artificial desert landscaping (impervious weed barrier, desert shrub with 1-2 inch sand or gravel mulch and basin borders)		96	96	96	96
Urban districts:					
Commercial and business	85	89	92	94	95
Industrial	72	81	88	91	93
Residential districts by average lot size:					
1/8 acre or less (town houses)	65	77	85	90	92
1/4 acre	38	61	75	83	87
1/3 acre	30	57	72	81	86
1/2 acre	25	54	70	80	85
1 acre	20	51	68	79	84
2 acres	12	46	65	77	82
Developing urban areas					
Newly graded areas (pervious areas only, no vegetation)[5]	77	86	91	94	
Idle lands (CN's are determined using cover types similar to those in Table 3)					

1 Average runoff condition and I_a=0.2S.
2 The average percent impervious area shown was used to develop the composite CN's. Other assumptions are as follows: impervious areas
are directly connected to the drainage system, impervious areas have a CN of 98, and pervious areas are considered equivalent to open space
in good hydrologic condition. CN's for other combinations of conditions pay be computed using Figures 3 or 4.
3 CN's shown are equivalent to those of pasture. Composite CN's may be computed for other combinations of open space cover type.
4 Composite CN's for natural desert landscaping should be computed using Figures 3 or 4, based on the impervious area percentage (CN=98)
and the pervious area CN. The pervious area CN's are assumed equivalent to desert shrub in poor hydrologic condition.
5 Composite CN's to use for the design of temporary measures during grading and construction should be computed using Figures 3 or 4 based
on the degree of development (impervious area percentage) and the CN's for the newly graded pervious areas.

Figure 3.14. Table 2: NRCS parameters needed to assess CN are: Land use and Hydrology soil group are: Curve Number (CN) value used during the application of Service Conservation Soil method using HEC-HMS (2002) flooding model: Source: SCS (1986).

The second stage is the evaluation of features relating to the development of flooding. Such as: the concentration time (defined as the time period between the beginning of runoff and the time that the water reaches the location of interest); and the lag time (defined as the time between the beginning of rainfall and runoff). Various formulae can be used to assess these features, for example the Kirpich (1940) formula, but this is only one that is available, and part of the remaining work of this PhD is to explore other approaches. For small catchments the Kirpich (1940) was used for lag-time evaluation instead of Manning's formulae (Loukas and Quick, 1996) the impervious surface (I.S.) was estimated using satellite images interpretation with Arc-Map program. These initial parameters (Area, CN, I.S., Ia., Tc, and Lag-time). In relation to the results derived from basins and sub-basins allocated on the study area (see Chapter 5, sections 5.3.3.1 to 5.3.3.8 and 5.3.4.1 to 5.3.4.8).

Application of the HEC-HMS computer program in order to model the flooding hazard for the study area. The NRCS hydrologic method introduces the Unit Hydrograph concept and the rainfall-runoff equation derived from values of CN is the basic concept of this method. Also, The method uses the concept of Unit Hydrograph which refers to the representation of the catchment area in terms of a constant runoff layer of (1inch) uniformly covered by an specified storm of certain intensity and duration. For instance, for any storm of the same duration but with different runoff amount (intensity), the hydrograph of direct runoff can be expected to have the same base as the unit hydrograph and ordinates of flow proportional to the runoff volume. Therefore, a storm that produces 2 inches of runoff should have an hydrograph with a flow equal to two times the flow of the unit hydrograph. The process involved is presented in the following paragraphs.

3.3.2 Geometric data extraction for streams network from (DEM) using *Arc-View 3.2 with HEC-GeoRAS.*

Profile centre lines, banks, flow paths and cross sections of the main streams are needed to perform hydraulic and hydrologic calculations. Therefore, the HEC-RAS program is used and the process would be detailed in the following paragraphs: The first step is to open the DEM derived from datasets contained in Figs. 1 and 2 of Appendix 3E of the sector using Arc-View 3.2 (2002) with HEC-GeoRAS; 3D and

spatial extensions updated. Then go to the directory where the DEM of Figs 3.15A or 3.15B are stored and open them. Then minimize the DEM and activate the contour level shape-file in order to work faster. After that, define the stream centreline from upper to lower elevation using the Pre-GeoRAS module and give a reference name to the stream and reach. Then define the left and right banks of streams and reaches always in downstream direction and approximately parallel to the centreline stream. After that, define the flow path from left, centre and right stream centrelines, here it is necessary to edit the data given the corresponded streams and reaches name. Finally, draw the cross sections nearly offset every 50 m or less depending on the terrain topography and this line should be nearly orthogonal to the profile centre. In the present work, manning coefficients were assigned in the HEC-RAS (2002) program. One defined the four basic tasks a definition of three dimension stream centreline and cross sectional for all the streams allocated in the sectors were updated. All these tasks were performed into the module Pre-GeoRAS of Arc-View 3.2 program. Then, export this file into the HEC-RAS (2002) program in order to perform hydrologic and hydraulic calculation. The only task to do is to define the name of the exported (.DSS extension file) and select the output directory for it. Finally, the file exportation into HEC-RAS (2002) program is assessed. In short the graphic illustration performed in these steps is illustrated in Figs. 1, 2 and 3; Appendix 3F. Finally, with this geometric information already assessed then the next step is to assess hydraulic operations and map production using the HEC-RAS computer program which would be explained in section 6.4.1 and 6.4.2 related to HEC-RAS flow model application of the flooding model hazard results Chapter 6.

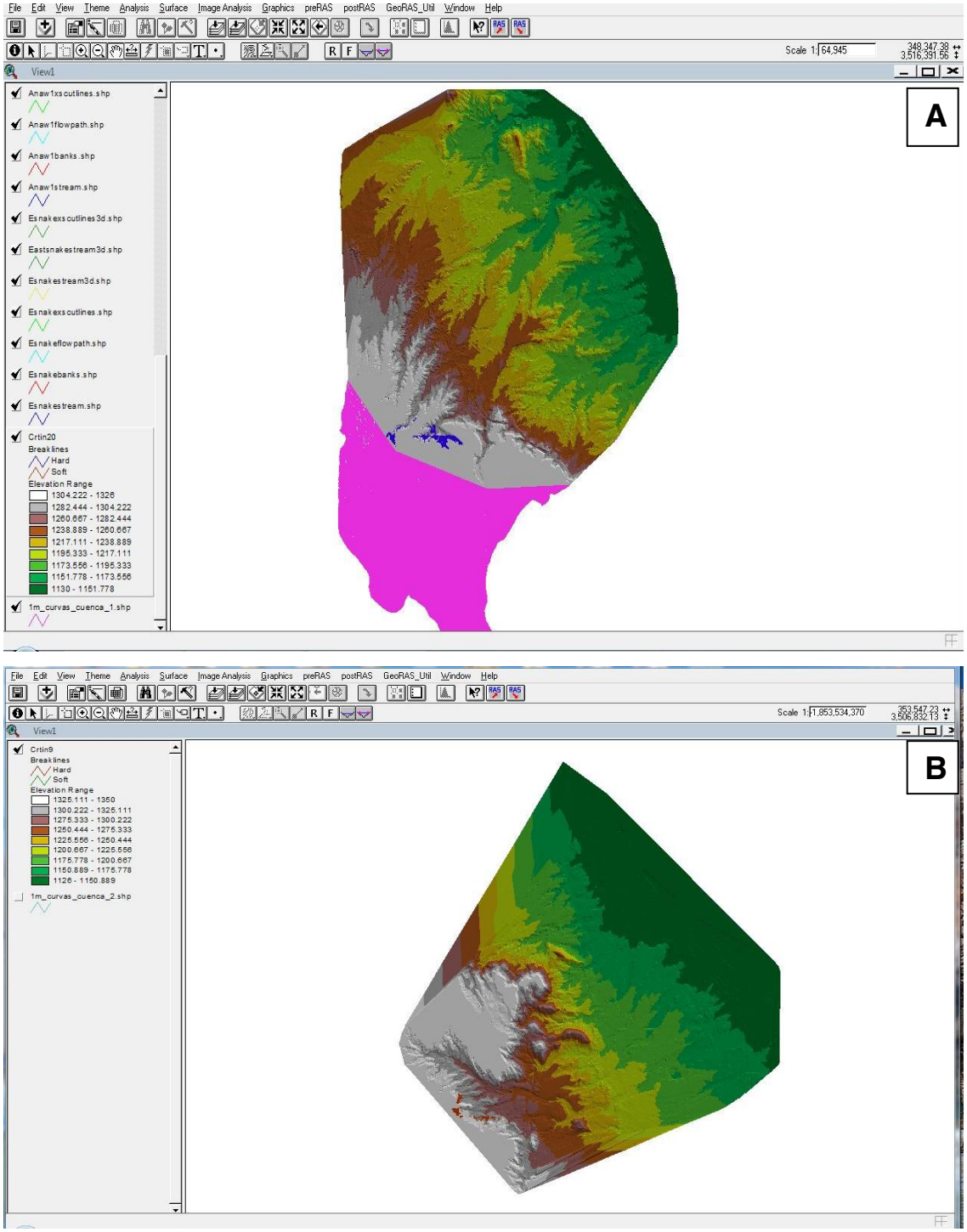

Figure 3.15. Digital Elevation Model corresponded to the west sector of Juárez city based in 1m contour levels Pink colour is sector not included: The bar colour legend is indicated in the left lower of the Map (Crtin 20). Light colours mean higher elevation, instead green colours means lower elevation. Others symbols correspond to the flooding process and are explained in the result chapter 6. B) DEM based on Map (Crtin 9) which corresponds to the central sector Created by David Zúñiga using Geographic Information System Laboratory of Juárez University and Arc-View GIS 3.2 (2002) Program.

3.3.3 Hydrology Engineering Centre-River Analysis System (HEC-RAS) program.

HEC-RAS (2002) Is a program used to solve many hydraulic problems. However, in this research it is applied to extend the hydrographs resulted from HEC-HMS computer program assessed in HEC-HMS (2002) of the results chapter 5. These hydrographs were evaluated for 25, 50 and 100 years return period and were linked to the main basin streams. The transit of these hydrographs along their main streams route allow to define the lateral and vertical extension of the flow. As a result, HEC-RAS (2002) needs stream's geometry explained in section 3.3.2 and 3.3.3 of this chapter and reinforced and assessed in section 6.4.2 of results Chapter 6.

As a result the file exported from Pre-GeoRAS module of Arc-View 3.2shows the profile and sections of Anapra West stream. In short, the following section shows the process to import geometric data described in Section 3.3.4. Firstly, with HEC-RAS (2002) computer program, import the file that contain the geometric data of Anapra west stream and perform some tasks such as: Assign the manning coefficients n. In this regard the program suggest the n values appropriate depending of the soil or rock texture; After that, Adjust the left and right banks (points red to Fig. 1 Appendix 3G); review the flow directions (blue arrow of Fig. 1 Appendix 3G); review data regarded to cross sections using the cross section command (line green of Fig. 1 Appendix 3G); add interpolated cross sections if it is needed; Filter the number of points of all the cross sections (no more than 500 points) and save the cross sections defined in HEC-RAS (2002). Secondly, select steady flow and boundary conditions for each reach or stream. Assign the values derived from HEC-HMS hydrographs for 25; 50 and 100 years return period for all the streams (see table in the right lower part of Fig. 1 Appendix 3G) and save the flow assigned in the HEC-RAS file already using. Finally, running the flow for the desired return period and the response of the program performs the flooding if the data were corrected. On the contrary, if the data are wrong, the program does not work instead would give a mistakes list. For example, a common problem is that the cross sections should contain no more than 500 points. In short, results emerged during hydraulics calculations were performed for all the streams at risk of flooding and the results are

contained in the flooding results chapter 6. This chapter shows only Anapra west 1 stream (see. Fig. 2 Appendix 3G). In the following section the explained exportation of this HEC-RAS file into Arc-View 3.2 (2002) is explained.

3.3.4 Exportation of HEC-RAS file into (Arc-View 3.2, 2002)

To export the HEC-RAS file already assessed which contain the flow model of the stream Anapra west 1 (Figs. 1 and 2 of Appendix 3G) only one task is needed. This task is to save the derived HEC RAS file which contains hydraulic and hydrologic calculation in a (dss extension) format. After that, using the Post processing module of Arc view 3.2 open it.

3.3.5 Import the HEC-RAS file and map of flooding using post GeoRAS Pre-Processing module of Arc-View 3.2 (2002)

In order to achieve the main aim of this research a flow mapping showing the spatial and geographic distribution regarded to 100 years return period of the predicted design storm is needed. For this reason, the three dimension flooding model results would be described for the Anapra west 1 stream and in chapter 6 all the streams at risk of flooding would assessed. First, open the Anapra west 1 stream file located in HEC-RAS program and export it into the Arc-View 3.2 version program. Second, close the HEC-RAS program and go to the Arc-View 3.2 program. Third, open the file that contains DEM and the streams of the sector. Four, open the Post GeoRAS processing module in order to import the Anapra west 1, then the program ask about the input directory where the file is located. Also, the program requires information related the DTM or TIN file name as well the resolution or cell size and the output directory location where the flooding maps would be stored. Obviously, all the shape file geometric components of the Anapra west 1 stream such as: stream centreline; bank stations; flow direction; and cross sections must be active during this process. Finally, the program shows a table with the parameters and the different algebraic operations performed stored in a database file table. When this table appears into the default view of the screen then click accepted and enter. Finally, the program takes some time to display the different three dimension

shape file as: (XS 3D. shp; Banks.shp; xs.shp; SN.shp; BP PF1; Crtin 10; WS PF1; GO PF1; FP PF1. (See Fig. 3.16).

The final Shape files of the flooding model in three dimension are showned in the results chapter 6 and are explained here in the next paragraphs; XS 3D.shp is the shape-file which contain cross sections in three dimension; SN.shp is a shape file that contain stream profile in three dimension; Banks.shp is referred to the shape-file Banks of the stream; xs.shp is the cross sections line given in PreGeoRAS Pre processing module; Crtin 10 is related to the TIN or DEM; WSPF1 is the water surface elevation corresponded to the Flooding plan 1 or 100 years return period; GO PF1 is the shape-file that contain the velocity grid of the flooding hazard to 100 years of return period or Plan number 1; Finally, the more important feature for mapping the Flooding is FP PF1 that is the extension of the flooding plain producing by a design storm corresponding to 100 years return period or the flooding hazard (See Fig. 3.16).

3.3.6 Flooding hazard in flat valley areas.

In relation to Juárez city, there are many flat basins which store water directly during the rainfall storm duration. These isolated depressive basins are very flat (in the order of 10 cm to 100 cm water table) and impossible to detect with the models performed in the present thesis. Therefore, complementary historical information of past flooding events was collected (IMIP 2005). The information provided by IMIP was incorporated in the present work in order to complement flooding hazard model and would be included in the final derived flooding risks for the study area performed in the results Chapter 6.

3.3.7 Flooding hazard and flooding risk models.

Once addressed the flooding hazard map within the study area the expected flooding risk from Juárez city would be addressed in terms of the flooding hazard previously explained. In order to assess this risk model, a vulnerability model is needed. These models would be performed using four vulnerability layers as:

Population density, landuse, socio-economic level and medical service. The model would be performed using the Geoprocessing module included in the Arc GIS 10.1.

These four vulnerability factors were selected because they represent the more critical vulnerability components for the Juárez city population and were collected from Juárezageb2005_wgs84_area which contain demographic and physiographic features of the study area. This dataset was provided by (INEGI 2007). The construction of this map model is explained in the following paragraphs: Firstly, using Arc-Map 10.1 program. Open the dataset named: Juárezageb2005_wgs84_area which contain demographic and physiographic features of the study area. Secondly, for the four vulnerability factors as: population, landuse, socio-economic level and medical care. open the attribute table, select the column which contains the factor and derive the four shapefiles of vulnerability. Then, go to the layer properties and select the graduated colour pattern more suitable and desired for the project, in the present research were selected five intervals of vulnerability degree with tone of colours café; yellow; green and blue. Once performed this task the program provides five new shape files showing the vulnerability components for different sectors of the city with different colours. Furthermore, these shape-files are proccessed using the geoprocessing module of Arc GIS 10.1. The process involves to overlap the four vulnerability layers, assign a rank of vulnerability degree for eachone and perform the union tool of the geoprocessing module included in Arc GIS 10.1. The final vulnerability map model is allocated in another shapefile and would be saved in a layer which represent the vulnerability map.

Finally, in order to address the flooding risk overlapping of the vulnerability shape file and the flooding hazard layers is needed. The product of Vulnerability model and Flooding hazard would provide the final flooding risk model. In short, the dataset used to address the risk model date back from 2005 because at the census dataset availability of the study area at the moment of the present research. The flooding risk for the three sectors defined on the study area as Northwest Anapra; Centre Juarez and South Centre Juarez and are presented in: Figs. 6.18; 6.19 and 6.20 of the results Chapter 6.

3.3.8 Complementary information regarded to computer modeling programs used in this chapter.

As mentioned at the onset of chapter 2, this chapter would explores subjects related to programs to assess models instead to be presented in the literature review chapter. Then, the present section aboards with more detail two main computer programs to evaluate flooding. Firstly, HEC-RAS version 3.1.3 (2002) which evaluates hydraulic parameters. Secondly, HEC-GeoRAS 3.1.3 (2002, ver. 3.1.3) for Arc-View GIS 3.2 to simulate and model flooding hazard. In addition, to assess Digital Elevation Models (DEM). HEC-RAS (2002). version 3.1.3 US Army Corps of Engineers Hydrologic Engineering Center (2002) developed a HEC-GeoRAS 3.1.3 program that is an extension of HEC-RAS using Arc-View 3.2. This program is designed to process geospatial data for use with the Hydrologic Engineering Center's River Analysis System (HEC-RAS) and import a file containing geometric attribute data from an existing digital terrain model (DTM) and complementary datasets. In Summary, the programme has the capacity to generate flooding models in three dimension and perform the next tasks:

First**,** Create and import a RAS GIS file that contain River reach and station identifiers; cross-sectional cut lines; cross sectional surface lines; cross sectional bank stations; downstream reach lengths for the left overbank; main channel and right overbank; and cross-sectional roughness coefficient. Additional geometric data defining levee alignments, ineffective flow areas. Then, the storage areas are written to the RAS-GIS import file, but, Hydraulic structure data are not written to the import file. After that, water surface profile data and velocity data exported from HEC-RAS may be processed into GIS data sets. Therefore, the programme create a file of geometric data for import into HEC-RAS. It also enables viewing of exported results from RAS. Finally, The import file is created from data extracted from dataset (Arc-View shape-files) and from Digital Terrain Models derived from TIN (Triangulation Irregular Networks).In the following paragraphs are summarized the application process of the programme that is extracted from the User Manual attached to the program.

a) Loading HEC-GeoRAS; b) Starting a new project; c) Setting the work directory; d) Creating contours from TIN; e) Creating RAS Themes; f) Draw stream centreline g) Giving a name to the rivers and reachs; h) Creating Junctions between

the reaches and rivers. i) Delineate the main channel banks; j) Draw the path centrelines; k) Generation of Cross-sectional cut lines; l) Previewing cross sections; m) through the landuse dataset establishing of the roughness coefficients (N manning values); n) Giving the Levee alignment; o) Definition of the ineffective flow areas; p) Definition of the storage areas; q) Attributing RAS themes such as: stream centreline theme, cross-sectional cut lines theme, extract of cross sectional elevations, Manning N values, Levee positions, Ineffective flow areas, storage area completion, r) Generating the RAS GIS import file; Once created the 3D Stream centreline theme and 3D XS cut lines then, write the RAS GIS import file. s) HEC-RAS Hydraulic Analysis; This task is performed in one-dimensional steady flow and unsteady flow analysis of river and stream systems for the different basins. The general steps in using HEC-RAS in concert with GeoRAS is discussed in the following section; i) start a new project in HEC-RAS, ii) Import the RAS GIS import file; iii) Complete the hydraulic structure data; iv) Complete the flow data and boundary conditions; v) Run HEC-RAS; vi) Review results and refine model;

vii) Export results; t) Importing the RAS export file into the GeoRAS module working in the environment of Arc-View 3.2 program and Generating the GIS data from RAS results such as; A)Water surface TIN; B) Flood plain delineation; C) Velocity TIN; D) Velocity grid; E) Finaly, the assessment of the flooding inundation areas area provided in a 3D presentation.

HEC-GeoRAS 3.1.3 (2002) for Arc-View GIS 3.2. Is a powerful computer program specially designed to model many projects associated with geographic, geologic, topographic, hydrologic, physiographic, metrologic, and mostly the concern of the present research focussed on flooding as well landslide modelling. The fundamental reason to use this program for flooding hazard is because the program HEC-Geo RAS mentioned previously, model the flooding hazard in three dimension. Therefore, it is necessary to work with Digital Terrain Model using TIN (Triangulation Irregular Network) instead of using Raster Grid Data set or DEM (Digital Elevation Model). So in this condition, it is possible to model the flooding hazard. On the other hand, the technical problem of using Arc-Map GIS version 9 or more recent is related to its version uncompatibility. The Arc-View 3.2 program has the modules Spatial as well as 3D that are using frequently during the different task associated during the flooding modelling. There are so many tasks performed for the program but because

it is impossible to mention all of these tasks only two fundamental modules are mentioned, these modules are Three dimension (3D) that is used to perform fundamental features such as Digital Terrain model (DTM), Contour levels, Digital Slope Models (DSM), Digital Elevation Models (DEM) Aspect map, and, the basic task to analyse satellital images and identify drainage systems of the different watershed, basins and subbasins for modelling

CHAPTER 4

DYNAMICS OF ALLUVIAL FANS IN THE AREA OF CIUDAD JUAREZ

4.1 INTRODUCTION

This chapter assesses the geological settings of alluvial fans and fluvial terraces for three main sectors located in the study area (see sections 4.2.1 to 4.2.4) their spatial and temporal distribution are presented in sections 4.3.1 to 4.3.5. Sedimentological and topographic analysis in combination with the dating technique named OSL (Optically stimulated Luminescence) as well the use of a prototype model which matches the study area are the main features to assess the data in this thesis. Thus, the link of OSL alluvial fan dating with Bravo River fluvial prototype model is explored (see section 4.2.4 and Appendix 4C, Albuquerque Quaternary Bravo River fluvial model). Finally, to explain the dynamics of these sedimentary structures in relation to their long-term controlling hydrologic processes which produce the ongoing threat of Ciudad Juárez area another three sections are included (see sections 4.3, 4.4 and 4.5). However, to reduce the size of this Chapter, a photoinventory of sample collection points is presented in Appendix 4A.1, figures 4A1.1 to 4a1.5, the remaining figures of this Appendix 4A1 are draft pictures taken during the field work to demonstrate the appearance of the regional fans.

4.2. GEOLOGICAL SETTINGS OF ALLUVIAL FANS

4.2.1 Results of Geological features.

Literature review of the Cenozoic and Quaternary geology of the study area allows understanding of the general geologic map where recent active alluvial fans as well fluvial deposits were developed within the context of tectonic and climate effects in the region (see section 2.1 Figs. 2.1 to 2.10). After that, OSL sample collection and laboratory test for dating of alluvial fan Colorado were performed by Dr. Shannon Mahan of the USGS Denver Colorado Lab (see Table. 4.1). Then, four map layouts are explained in section 4.2.2. Firstly, Northwest sector 1 which comprises Anapra and Snakes areas (Viboras in Spanish) (Figs. 4.1A; and 4.5 to 4.9 and Appendix 4A1, Figs. 4A1.1 and 4A1.2); Colorado Mountain

Front (See Figs. 4.1B; 4.5; 4.6; 4.10; 4.11 and Figs 4A1.3 and 4A1.4 of Appendix 4A1), Centre sector (Figs. 4.1C; 4.5; 4.6; 4.10 to 4.12 and Fig. 4A1.5 and 4.A6 of Appendix 4A1) and Southeast sector (Figs. 4.1D; 4.5; 4.6; 4.12 ;4.13 and Fig. 4A1.5 of Appendix 4A1). In addition, two geological cross sections (A-A' and B-B') were built. Section A-A', which shows how the Anapra sector catchment and depositional areas are clearly separated by their topographic and hydrologic apexes. The other, cross section (B-B') refers to Colorado Mountain Front alluvial fan, which is formed by a stream network system oriented along many NE Normal faults, thus footwall-derived sediments mostly flow debris and mudflow are common in this sector. Furthermore, in upstream areas, the hydrologic parameter of discharge/sediment ratio with a value more than 1 suggests an intense incision activity, whereas, in the downstream areas this parameter is less than 1, producing a long depositional flat areas. Then, piedmont incision and alluvial fills deposits are common. As a result, a terrace shape adopted below 1155 m asl to 1160 m asl by the distal alluvial fans (see red colour rectangles areas of flat alluvial fills Tepeyac Cemetery **TC**, Municipal Cemetery **MC** and Aztecas San Antonio **ASA** which means flat Alluvial fills overlies fluvial terraces (see Figs. 4.1B and 4.1C and Appendices 4A.2 ;4A.3 and 4C;).

4.2.2 OSL dating results of Colorado alluvial fan

Colorado alluvial fan geologic map shows three red stars related to OSL samples and their dating results (See Table 4.1 and Fig. 4.1A). These sample dating results (P1=30,900 and 44,850; P2=41,100 and 69,020 and P3=74,300 years) is a deposition timer of Colorado alluvial fan and the Bravo River fluvial deposits**.** In addition, terraces' coordinates location of all these sites are stored in a database table given within the geologic map. These sites as well fieldwork collection samples methodology were explained in section 3.2.3 Figs. 3.7A; 3.7B and 3.6C.

Sample information	% Water content[a]	K (%)[b]	U (ppm)[b]	Th (ppm)[b]	Cosmic dose[c] additions (Gy/ka)	Total Dose Rate (Gy/ka)	Equivalent Dose (Gy)	n[d]	Age (yrs)[e]
P1	1 (32)	2.28 ± 0.03	1.32 ± 0.07	4.25 ± 0.24	0.23 ± 0.02	3.01 ± 0.10	93.2 ± 2.26	10 (30)	30,900 ± 1,240
Aeolic sand in alluvial fan sediment							135 ± 4.54	16 (30)	44,850 ± 2,080
P2	1 (32)	2.65 ± 0.07	1.09 ± 0.15	4.97 ± 0.37	0.13 ± 0.01	3.26 ± 0.13	134 ± 5.39	9 (30)	41,100 ± 2,300
Aeolic sand in alluvial fan sediment							225 ± 11.3	14 (30)	69,020 ± 4,380
P3	1 (35)	2.24 ± 0.05	0.96 ± 0.11	4.21 ± 0.33	0.15 ± 0.01	2.80 ± 0.11	208 ± 8.53	15 (15)	74,300 ± 4,290
Aeolic sand in alluvial fan sediment									

[a]Field moisture, with figures in parentheses indicating the complete sample saturation %. Ages calculated using approximately 15% of saturation values.

[b]Analyses obtained using laboratory Gamma Spectrometry (high resolution Ge detector).

[c] Cosmic doses and attenuation with depth were calculated using the methods of Prescott and Hutton (1994). See text for details.

[d]Number of replicated equivalent dose (De) estimates used to calculate the equivalent dose. Figures in parentheses indicate total number of measurements included in calculating the represented equivalent dose and age using the minimum age model (MAM). All aliquots passed methodology tests.

[e]Dose rate and age for fine-grained 250-180 microns quartz sand. Exponential + Linear fit or exponential fit used on equivalent dose, errors to one sigma.

Table 4.1. Quartz OSL Data and Ages from urban outcrops around Ciudad Juárez México. Source: Shannon Mahan (2012) OSL USGS Denver Colorado Lab.

4.2.3 Borehole lithologies in alluvial fills and fluvial soils

Stratigraphic columns of 60 boreholes were provided by Sanitation and Water Municipal Committee JMAS (2009).the lithologies of these boreholes form a pattern that allows them to be grouped into three areas. No boreholes were available in the Anapra west sector (See Figs. 4.1A, 4.1C and 4.1D); coordinates of these boreholes are presented in Table 4.2 and the complete cross sections (A-A'; B-B' and C-C') are in appendices 4A4 and 4B. Facies similarities between borehole lithologies and surface deposits were found in the Municipal and Tepeyac Cemeteries as well Aztecas neighborhoods (**MC, TC**, **ASA** flat areas (see Appendixes 4B) and laboratory results samples of fluvial Bravo River and Alluvial fan deposits reported in tables 1 and 2 as well in detailed reports analysis laboratory sheets in Spanish UNIVERSIDAD AUTONOMA DE CIUDAD JUAREZ (See Appendices 4A2). In relation to fieldwork exploration to find Bravo River fluvial deposits a complementary Appendix named 4A3 is included using pictures which reinforce the evidence found with regard to the contact between the two main sedimentary structures.

Cross Section	Borehole ID	UTM Coordinate (X)	UTM Coordinate (Y)
A-A’	13R	358963.67	3510155.30
A-A’	15	360160.66	3511434.35
A-A’	7R	362734.46	3511530.00
A-A’	111	365589.98	3513173.77
B-B’	59	360815.11	3508136.01
B-B’	61	363387.41	3508768.92
B-B’	42	364655.69	3509607.44
C-C’	142	360799.85	3503131.06
C-C’	93	361492.45	3503744.72
C-C’	95	362566.54	3503288.84
C-C’	141	364155.26	3501816.29
C-C’	193	369724.34	3498991.14
C-C’	178	372445.98	3499489.55

Table 4.2. Boreholes location of cross sections in Figs. 4.1C and 4.1D. 1st column means cross section; 2nd column borehole identification and 3rd and 4th columns means UTM coordinates (X and Y). Cross sections A-A’; B-B’ and C-C’ performed in the area of Hueco aquifer center of Juárez city; Red stars=Section A-A’=holes 13, 15, 7R and 111; Blue stars=Section B-B’=holes 59, 61, 42, 145; white stars=Section C-C’ holes 142, 93, 95, 141, 193 and 178; additional Key is showed in the upper part of Figure and refers to the different soils derived from the Pliocene – Holocene of Rio Bravo Formation: Adapted from Hawley and Kernodle (2000) and Satellite Images worked with GIS (ArcMap GIS 9.2, 2009) Source: JMAS (2009) (see Appendices 4B and 4A4).

The boreholes located on the southeastern extreme of Juárez mountains near the Airport (See lilac colour polygon in Fig. 4.1D) as well Barreal basin (see white stars of cross section C-C' in Fig. 4.1D and appendixes 4B and 4A4) are integrated by the holes 142, 93, 95, 141, 193 and 178 basically composed of clay, clayey sand, sandy clay, and fine, medium, coarse and mixed sand mostly of aeolian origin. Thus, evidence of older lacustrine deposits of the Fort-Hancock Formation deposited in the Cabeza de Vaca Lake during early Pleistocene (<2.25 Ma) (Kottlowski, 1958; Strain, 1966; Reeves, 1965; Hawley and Kottlowski, 1969). Ancestral Bravo River ran from west (El Paso Texas) to south (Chihuahua state) along the Mesilla Bolson ending in several lakes including the big lake Cabeza de Vaca located south of Juárez city at elevation of 1250 masl. In short, the soils included in group 1 are in contact with the alluvial fan system derived from Palo Chino and Jarudo streams. These streams are the channels feeders of both Palo Chino and Jarudo alluvial fans therefore the great volume of sediments generated on the catchment source area are transported and deposited in a deep and wide depression basin named the Barreal basin area which was filled with recent playa lake deposits of Quaternary origin. For this reason, the analysis of the cross section C-C' suggests the contact between medial and distal alluvial fans located at 1165 masl (see Fig. 4.6).

Colorado Mountain Front sector 2 has a typical landscape covered by footwall-derived sediments with many NE and NW normal faults. As a result, a stream network system composed of channels with NE transport direction is typical in this sector (see Figs. 4. 1B, 4.1C). In Fig. 4.1B, the white arrows show the preferred sediment transport direction and the red polygons: **ASA** means Aztecas and San Antonio neigbourhoods; **TC** means Tepeyac Cemetery and **MC** which means Municipal Cemetery (see Appendices 4B; 4A2 and 4A3). These deposits overlie these fluvial deposits. The depositional behaviour of these sediments is indicated in geological settings section 4.2 and the geological cross section B-B' of this sector shows the architecture from the high Juárez Mountains to the Bravo River valley depositional areas. Shortly, due to the field work previously mentioned and further association to the previous works mentioned in relation to Pleistocene Bravo River invasion and further incision, the contact between fluvial Bravo River deposits and alluvial fans derived from Juárez moutains was defined (see continuous red colour line on layouts geological maps of Figs. 4.1A, 4.1C and 4.1

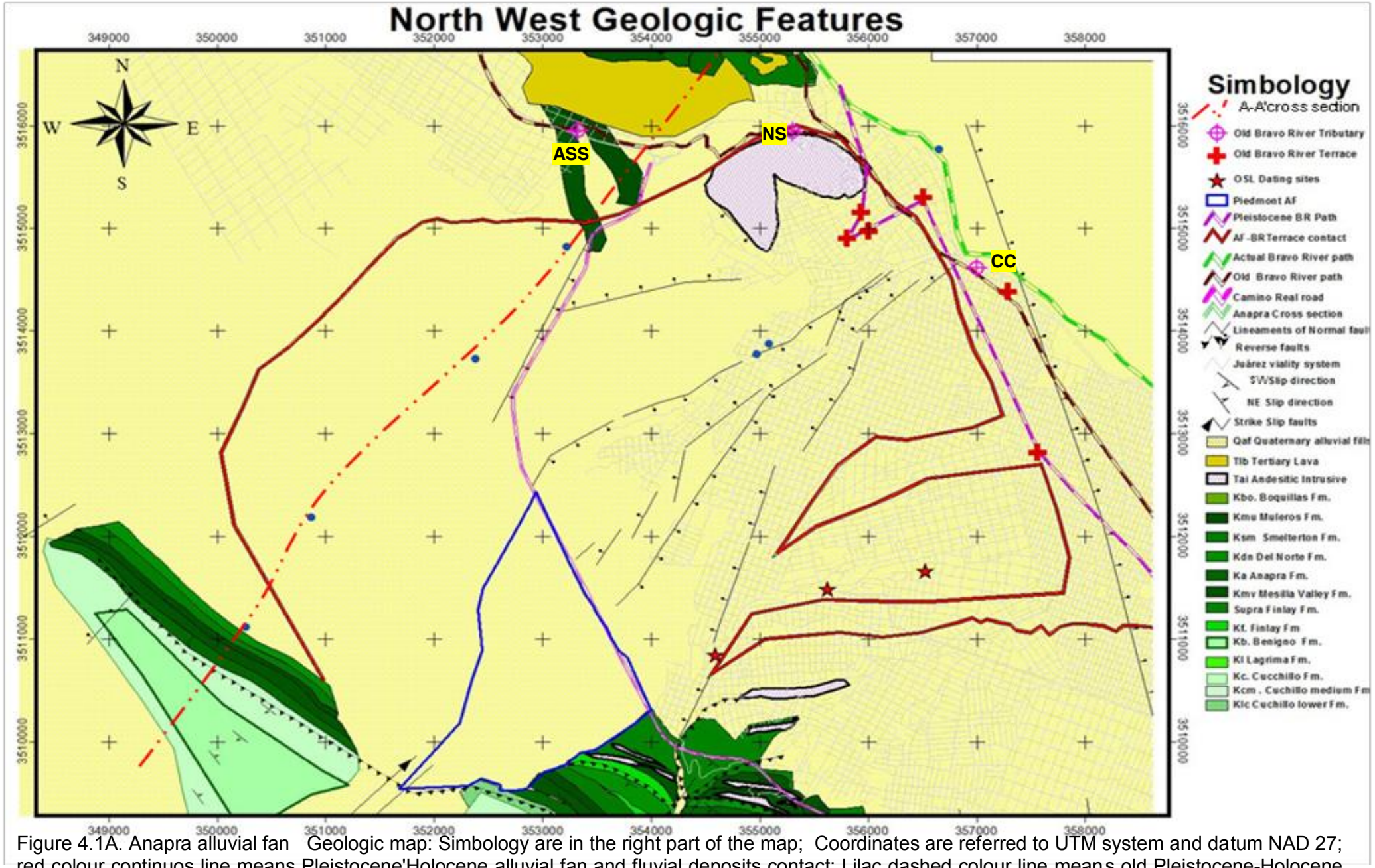

Figure 4.1A. Anapra alluvial fan Geologic map: Simbology are in the right part of the map; Coordinates are referred to UTM system and datum NAD 27; red colour continuos line means Pleistocene'Holocene alluvial fan and fluvial deposits contact; Lilac dashed colour line means old Pleistocene-Holocene Bravo River terraces path and red colour cross means outcrops sites; red stars are OSL sample sites for Colorado fans; (Lilac colour circles inside of yellow boxes = ASA; NS and CC) and Coffee colour dashed line means its path White colour mean the urbanized area of Juárez City: Source: (Drewes and Dyer, 1993) Wacker (1972); Nodeland (1977); García (1970) Digitalized and adapted by David Zúñíga (2011) using (Arc-View 3.2, 2002; Auto-Cad (2009) and ArcMap GIS 9.2, 2009)

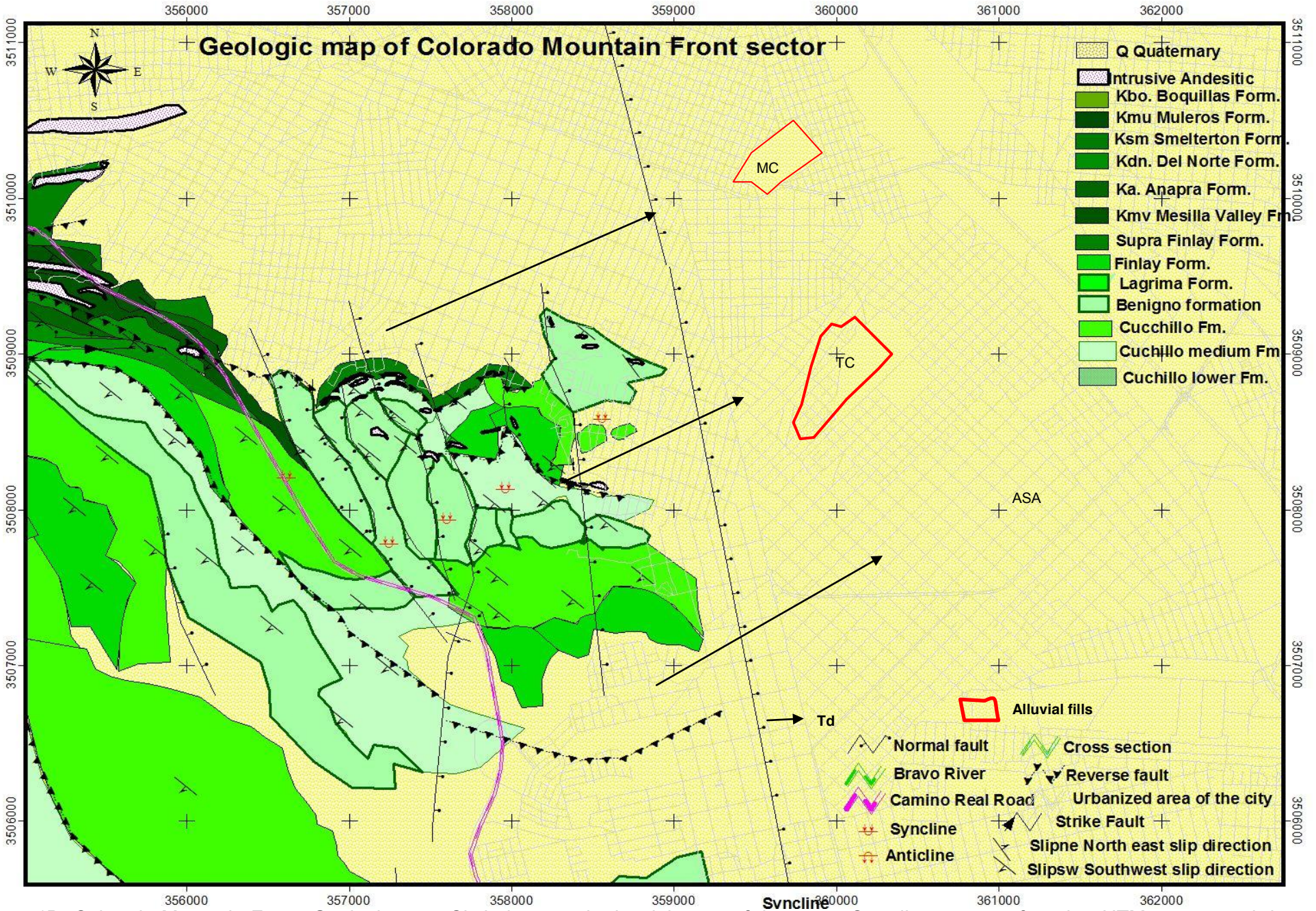

Figure 4.1B. Colorado Mountain Front Geologic map: Simbology are in the right part of the map; Coordinates are referred to UTM system and datum NAD 27; White colour mean the urbanized area of Juárez City: dashed lines mean cross sections (Td) transport direction, (TC)Tepeyac Cementry; (MC) Municipal Cementry and (ASA) Aztecas San Antonio; Source: (Drewes and Dyer, 1993) Wacker (1972); Nodeland (1977); García (1970) Digitalized and adapted by David Zúñiga (2011) using (Arc-View 3.2, 2002; Auto-Cad (2009) and ArcMap GIS 9.2, 2009)

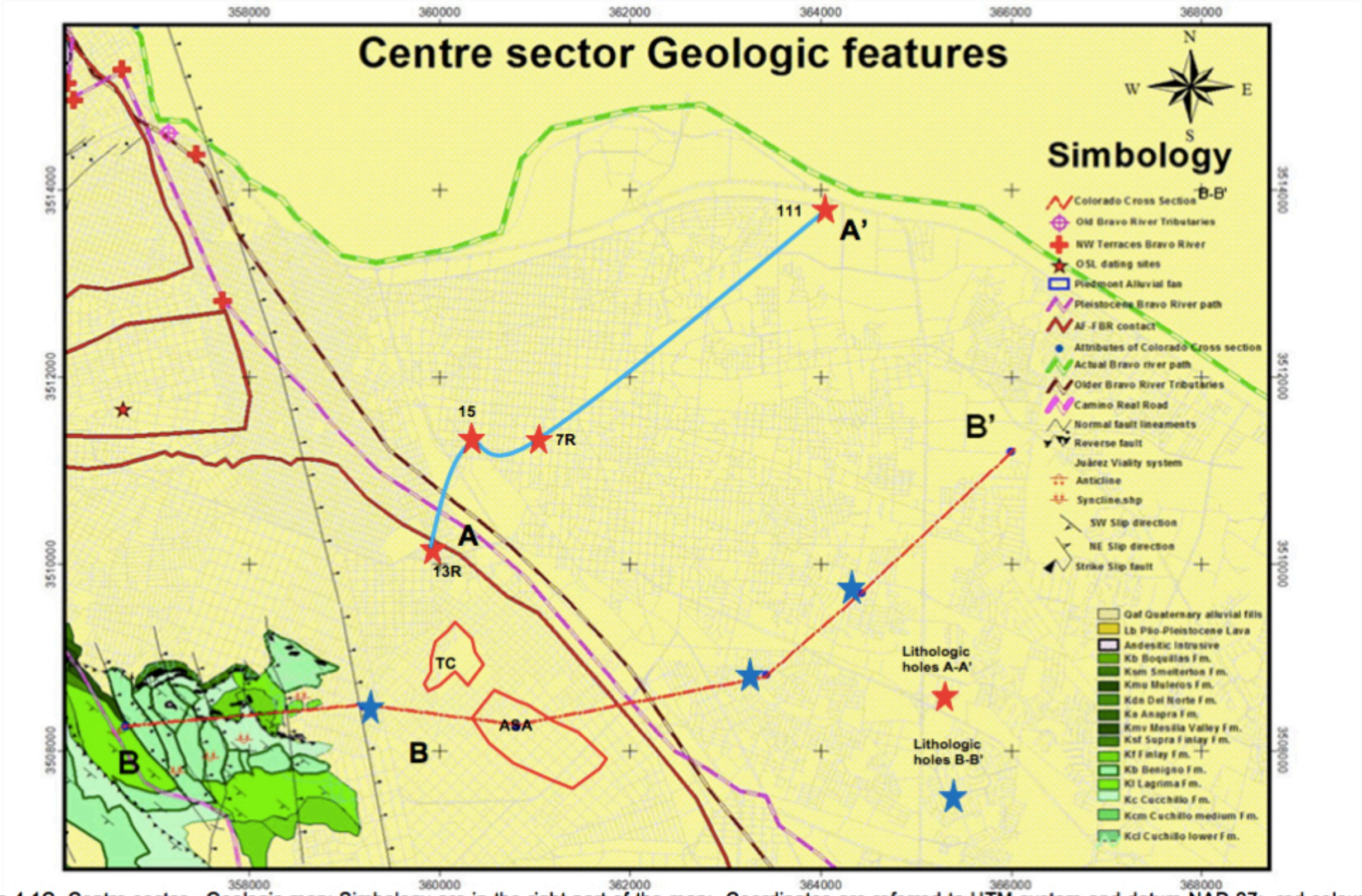

Figure 4.1C. Centre sector Geologic map: Simbology are in the right part of the map; Coordinates are referred to UTM system and datum NAD 27; red colour stars mean the section A-A' and Blue colour stars section B-B': Source: Drewes and Dyer (1993); Wacker (1972); Nodeland (1977); García (1970); Digitalized and adapted by David Zúñíga (2011) using Arc-View 3.2 Auto-Cad (2009) and ArcMap GIS 9.2

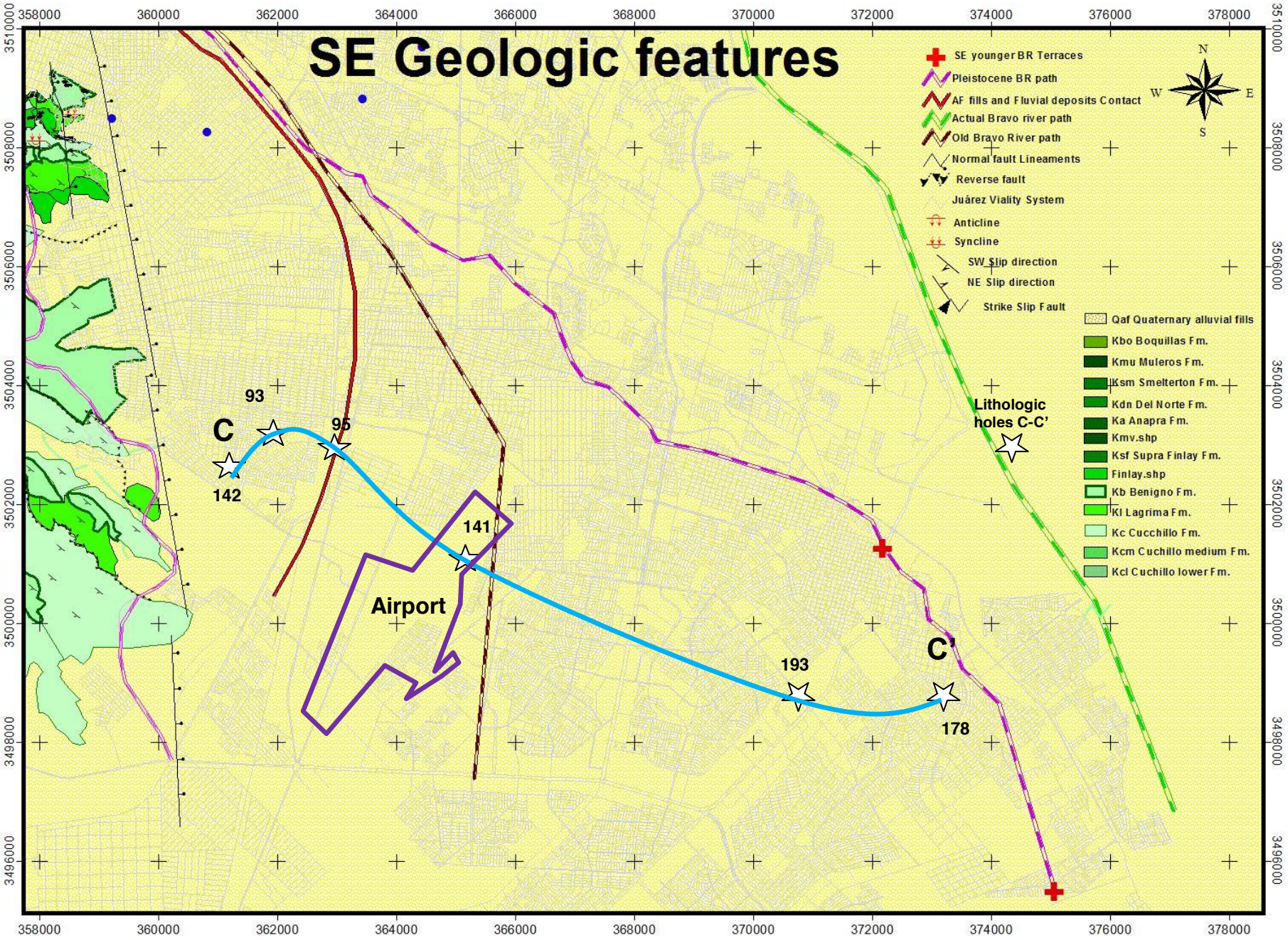

Figure 4.1D. SouthEast sector. Geologic map: Simbology are in the right part of the map; Coordinates are referred to UTM system and datum NAD 27; White colour mean the urbanized area of Juárez City: colour line lilac=Juarez airport; Source: Drewes and Dyer (1993); Wacker (1972); Nodeland (1977); García (1970). Digitalized and adapted by David Zúñiga (2011) using Arc-View 3.2, 2009;Auto-Cad (2009) and ArcMap GIS 9.2, 2009

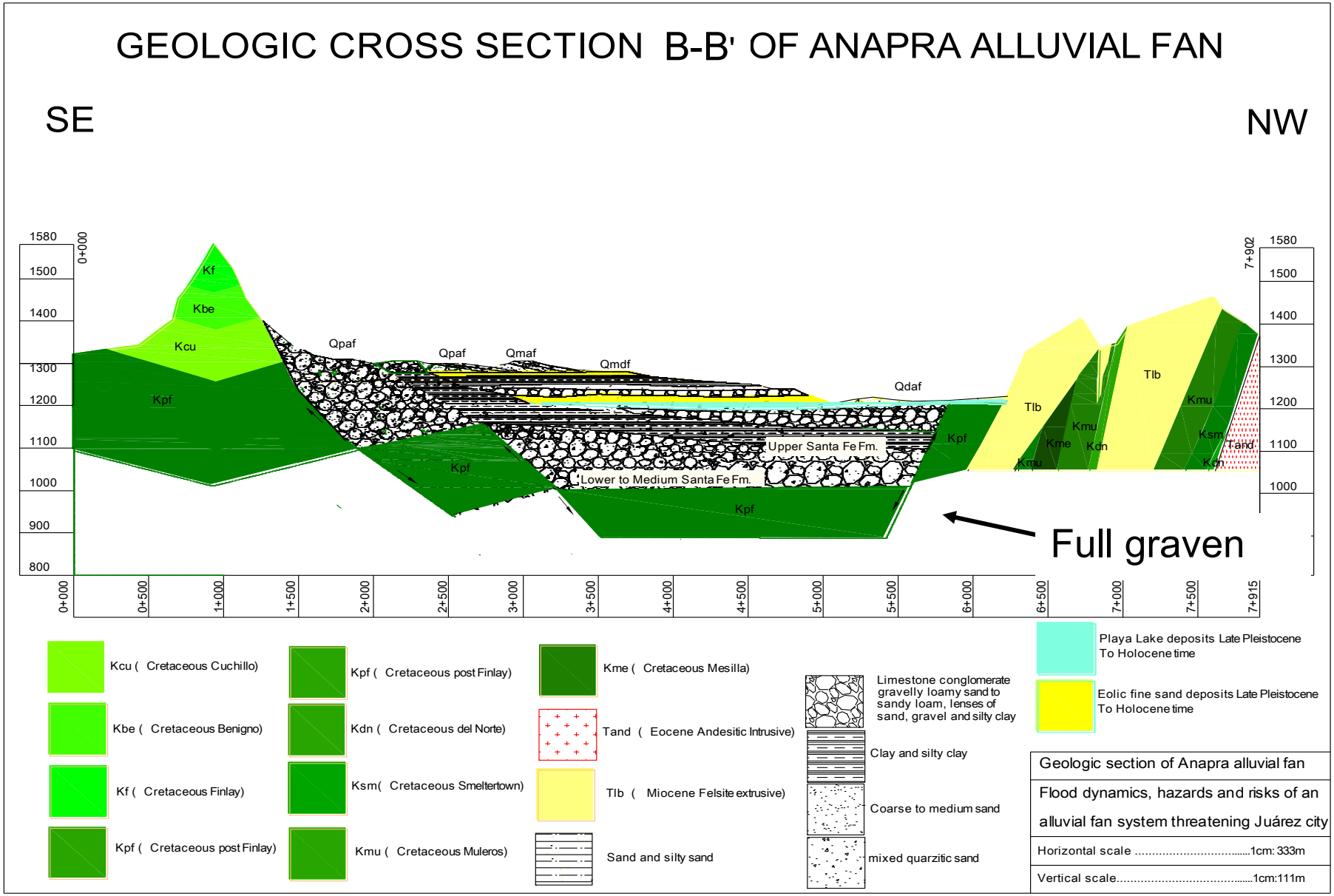

Figure. 4.2 Cross Section Anapra alluvial fan: Symbology as indicated in the Lower part; extension: The black stars= Post-Paleogene volcanogenic deposits and in the upper part includes Lower Santa Fe Formation; The white area are deposits of Lower to Middle Santa Fe Formation CR-Cristo Rey. Created by David Zúñiga (2011) Source: Pazzaglia and Hawley (2004) Auto-Cad (2009), Scales are in the right lower margin surface deposits are alluvial fans mixed with aeolic and playa lake deposits (see simbology).

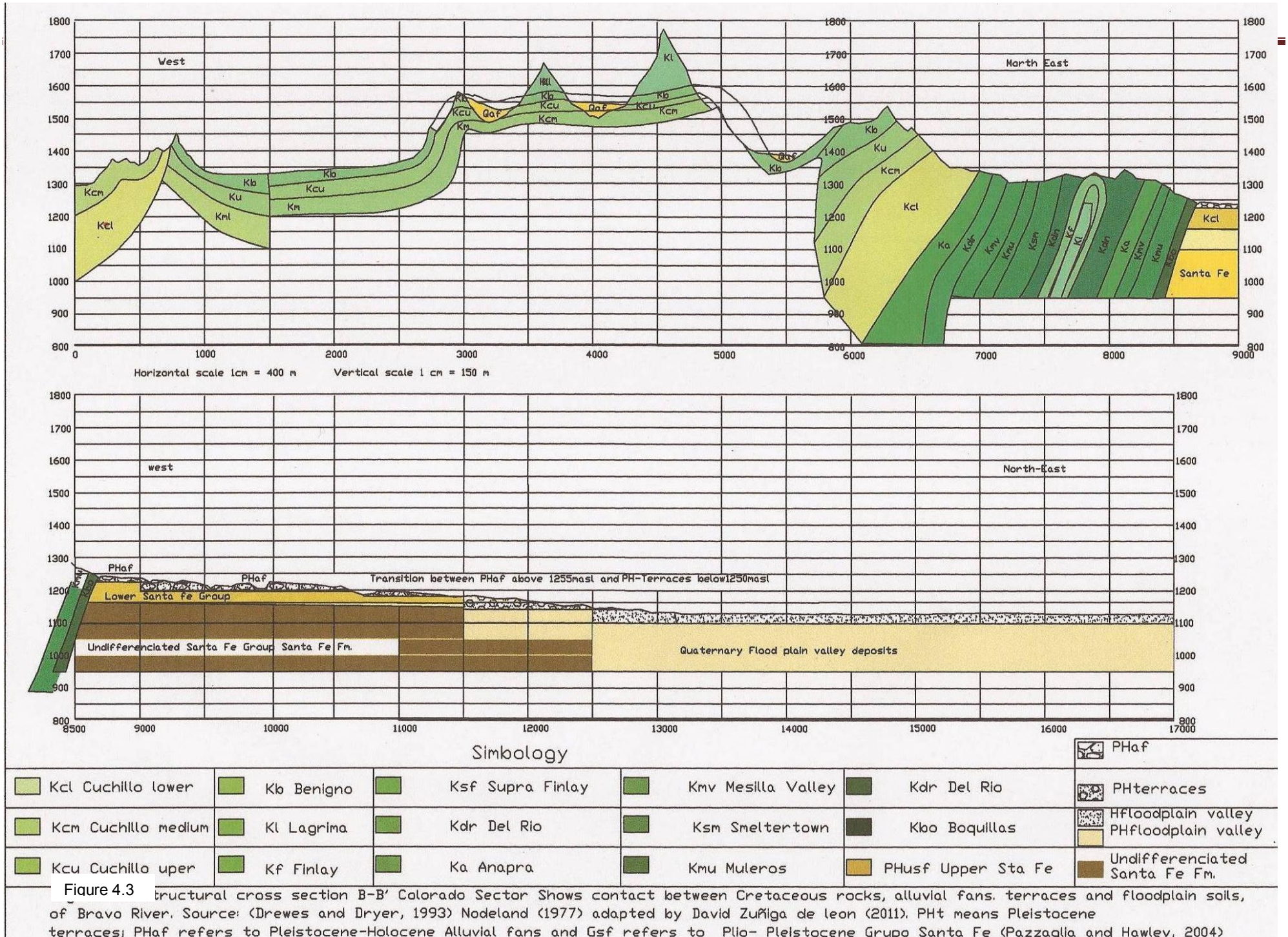

Figure 4.3 tructural cross section B-B' Colorado Sector Shows contact between Cretaceous rocks, alluvial fans. terraces and floodplain soils, of Bravo River. Source: (Drewes and Dryer, 1993) Nodeland (1977) adapted by David Zuñiga de leon (2011). PHt means Pleistocene terraces; PHaf refers to Pleistocene-Holocene Alluvial fans and Gsf refers to Plio- Pleistocene Grupo Santa Fe (Pazzaglia and Hawley, 2004)

4.2.4 Dynamic of fluvial and alluvial sedimentary structures

The fluvial Bravo River model of the study area matches a relict terrace found in the Albuquerque New Mexico area (see a more detailed explanation in Appendix 4C). Fluvial gravel deposits inset within the Edit formation was deposited from 160-100 ka and overlies the Duranes Formation (Connell and Love, 2001). In addition, older Bravo River tributaries' deposits (see Fig. 4.1A pink circles and coffee-coloured hashed line) refers to some fluvial deposits found on the west side of Juárez city, one in Anapra Smart Supermarket **ASS**, another on Norzagaray street located in Felipe Angeles Neighborhood **NS** and the third was located in Coffee Cake site **CC** (see appendices 4A2; 4A3 and Fig. 4.1A)**.**

Furthermore, several authors (Hawley and Kottlowsky, 1969; Hawley et al., 1976; Allen and Anderson, 2000) stated that that younger Bravo River tributaries invaded the region with fluvial deposits during Pleistocene-Holocene time. Thus, it is sensible to suggest at the moment that these deposits maybe younger than 20 to 24 ka (LGM) but more precise dating for these sediments is needed. In this regard in order to confirm and validate the model adopted for the study area alluvial and fluvial structures the 7 remaining OSL dating samples are needed for OSL dating on these ASS, NS and CC sites that are in contact with Mimbres as well Anapra alluvial fan at 1150 m asl.

Additionally, Bravo River terrace contact with anapra alluvial fan deposits marked with red cross were found in the Anapra west sector pink hashed line (see Figs. 4.1A and 4.1B) corresponds to gravels of Edith Formation inset in Segundo alto terrace the Albuquerque Basin located central New México of Lambert (1968). This terrace were formed during Marine Isotope Stage 5 MIS-5; 100 ka to 160 ka (90-98 ka based on dated basalt flows.

Recently, OSL dating was applied by Cole et al. (2008) results from these deposits in the Albuquerque Basin central New México were between 63 Ka to 162 Ka. Then, despite of the big difference between Lambert (1968, 100-160 ka) and

Cole et al. (2007, 63 ka to 162 ka) there is a broad similarities in a whole pointview but more work is needed to dilucidate the model here used. Whereas, on the southeast sector 3, red cross pink hashed line (see Figs. 4.1A and 4.1B) corresponds to younger late Pleistocene MIS-3 and OSL 47 ka to 40 Ma relict of Bravo River terraces equivalent with Primero Alto which comprises Post Santa Fe fluvial deposits of Bravo River in the Albuquerque Basin located central New México terrace of Lambert (1968). In short, the correlation which link the prototype Albuquerque terrace model with that of Juárez city is based on topographic position with respect to actual Bravo River Channel channel position. Thus, Segundo alto terrace of Lambert (1968) is located at 42 m, whereas Primero Alto terrace is located at 18m (see Appendix 4C and in section 2.1.10 Fig. 2.16 of Literature review Chapter 2. Finally, some of the symbols in Figs. 4.1A to 41D are clarified here: a) Bravo River path: Grid line, b) Camino Real Road: Pink line, c) the contact between Alluvial and Fluvial deposits: red line, d) Normal faults lineaments, reverse faults, NE as well SW slip stratification plans of the deformed synclines and anticlines structures. as well location of fluvial Bravo River Terraces.

4.3 RESULTS OF ACTIVE ALLUVIAL FAN DYNAMICS

4.3.1 Geographic location; boundary extension and general description.

In order to show geography, and hydrology the study area a general map is needed and is described in the following paragraphs. The map Fig.4.4 shows: firstly, the UTM coordinates of Juárez city which locate the study area; secondly, three main features **a)** topographic contour levels in red colour, **b)** drainage network system showing the stream order as well main channels in blue colour and **c)** To locate these features within the urbanized area of Juárez city the street system as well urbanized area of the city is illustrated in pink colour (See Fig. 4.4). In addition, Fig. 4.4 is a topohydraulic map, illustrating how the drainage network system has been printed on the landscape.. This map shows topographic contours levels every 5 m; features as Camino Real, Rio Bravo path, lower and upper valley of Bravo River, Hueco and Mesilla bolsons and Barreal basin as well.

Despite increasing urbanization on Anapra port and Barreal–Airport fans, these two extreme sectors remain partially active. Thus, some hydrologic alluvial fans components such as erosion in upstream catchment source areas and deposition in downstream areas are in progress because some reaches of the main channels feeder remain active. For instance, Lomas de Poleo and Anapra port located northwest of Juárez city (see Figs. 4.4, 4.5 and 4.6) these areas were key sites to address alluvial fan dynamics for two reasons. Firstly, Lomas de Poleo was built above thick Pleistocene-Holocene deposits of aeolian origin overlying soils of Camp Rice Formation.

These deposits are located to the east limit of Mesilla bolson vadose zone (**VZMB**) and mark the geologic contact with the younger Anapra alluvial fan located in the northwest of Juárez mountains (Pazzaglia and Hawley, 2004) (see cross section A-A' of Fig. 4.2 and Figs 4.4 and 4.5 These extreme sectors 1 and 3 more likely to alluvial fans are presented first (see Fig. 4.5). After that, Colorado alluvial fan and piedmont alluvial mountain front sector 2 will be presented later in section 4.3.4.

Sections 4.3.2 and 4.3.3 describes the following features: **a)** Main alluvial fans components evolution (See Fig. 4.7) and photo-inventory of points where samples of soil were collected from the Anapra sector (Figs. 4.8, 4.9, Snake and Colorado alluvial fan system (Figs. 4.7, 4.8, and 4.9.

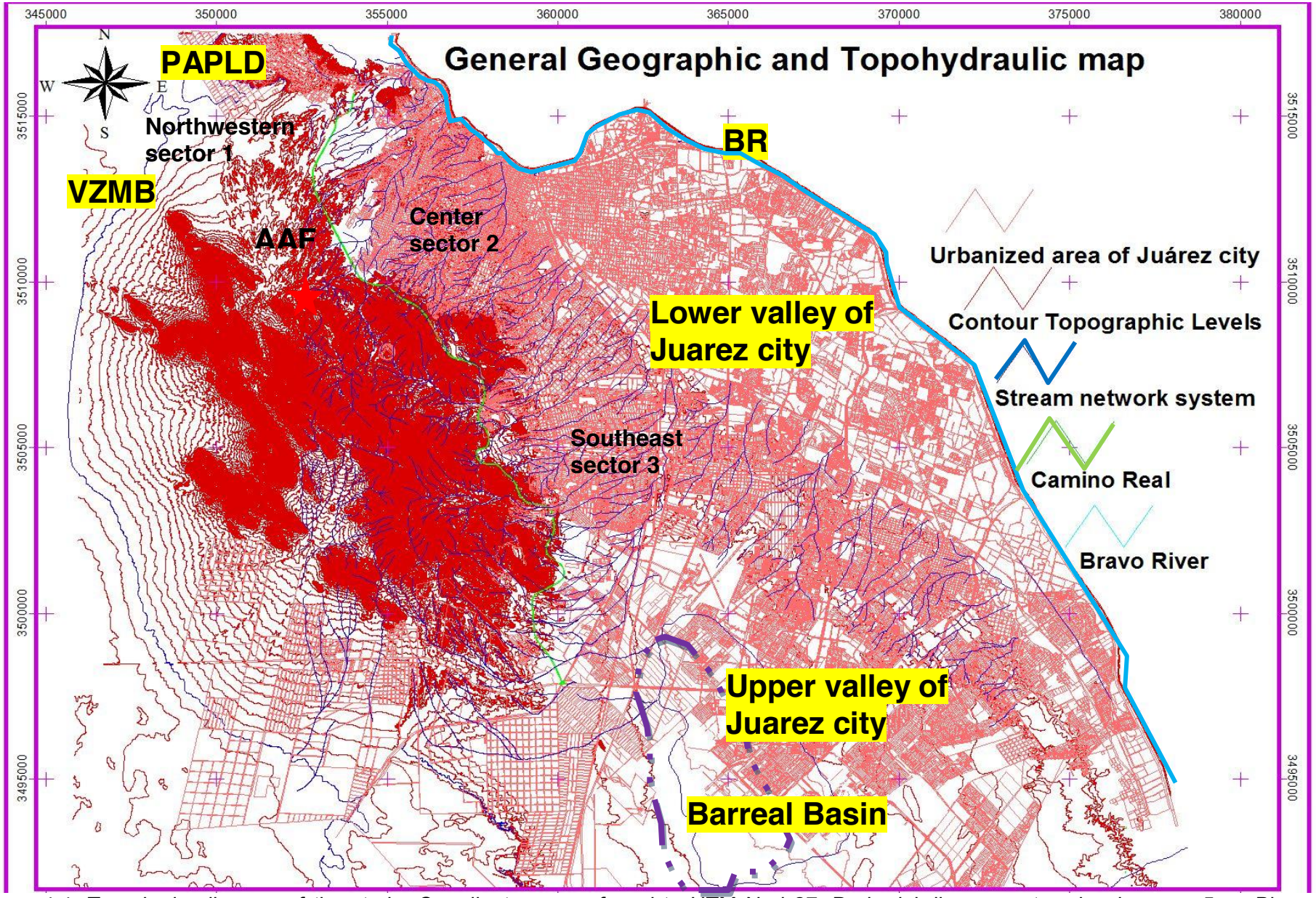

Figure 4.4. Topo-hydraulic map of the study: Coordinates are referred to UTM Nad 27. Dark pink lines =contour levels every 5 m; Blue continuous lines= drainage network; Green line = Camino Real; Blue light lines = Actual Rio Grande path; light pink lines =urbanized area of Juarez city;AAF=Anapra Alluvial Fan;VZMB=Vadoze Zone of Mesilla Basin; BR=Bravo River. Note how the drainage system separate the study area into two valleys an older upper valley (Barreal basin) and a younger lower one. Also, flow direction is clearly defined in all the drainage systems allocated in the different sectors. Created by David Zúñiga (2011). Source: DEM processed using GIS Arc-view 3.2. and Auto-Cad (2009).

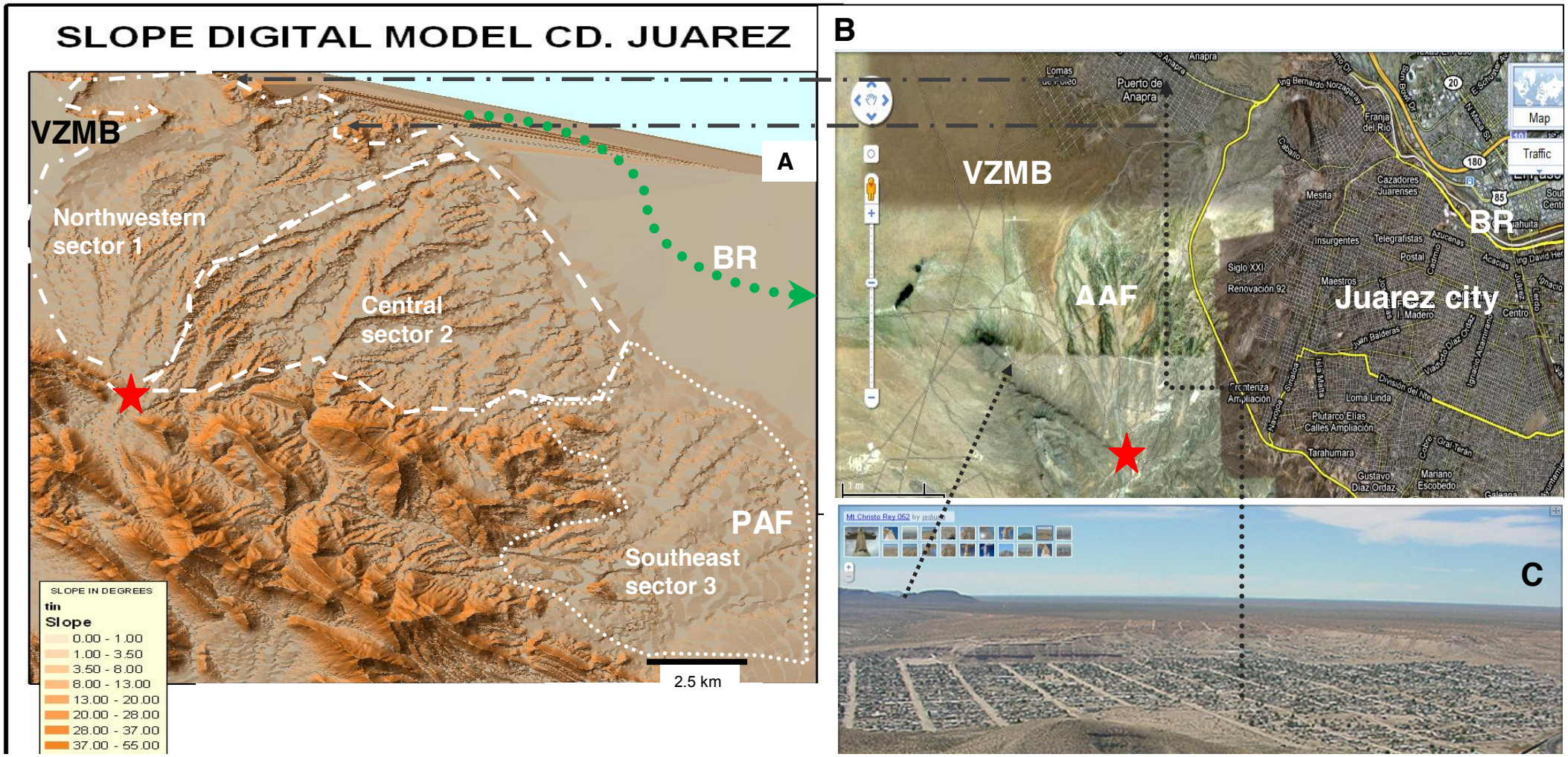

Figure 4.5. A) Shows three sectors of alluvial fans (DSM) Digital Slope Model the terrain gradient light colours means low gradients and bright colours means high gradients. Note in southeastern sector 3, a perfect alluvial fan (PAF) shape is preserved. Instead in central sector is easy to see how the alluvial fan is interrupted by fluvial deposits in the middle of the sector and again the distal alluvial fan appeared close to fluvial valley of Bravo River. B) Shows Anapra sector drained for a channel feeder located in the upstream area of the closed watershed topographic apex (red star) showing in the middle part of alluvial fan. C) Shows a panoramic view of Anapra town and their proximity with Juárez Mountais; BR, Bravo River (green line points in A and continous yellow line in B); PAF, Perfect Alluvial Fan; AAF, Anapra alluvial fan; VZMB, Vadoze Zone Mesilla Basin. Source: Google 2008; and ArcMap GIS 9.3, 2009 to build DSM.

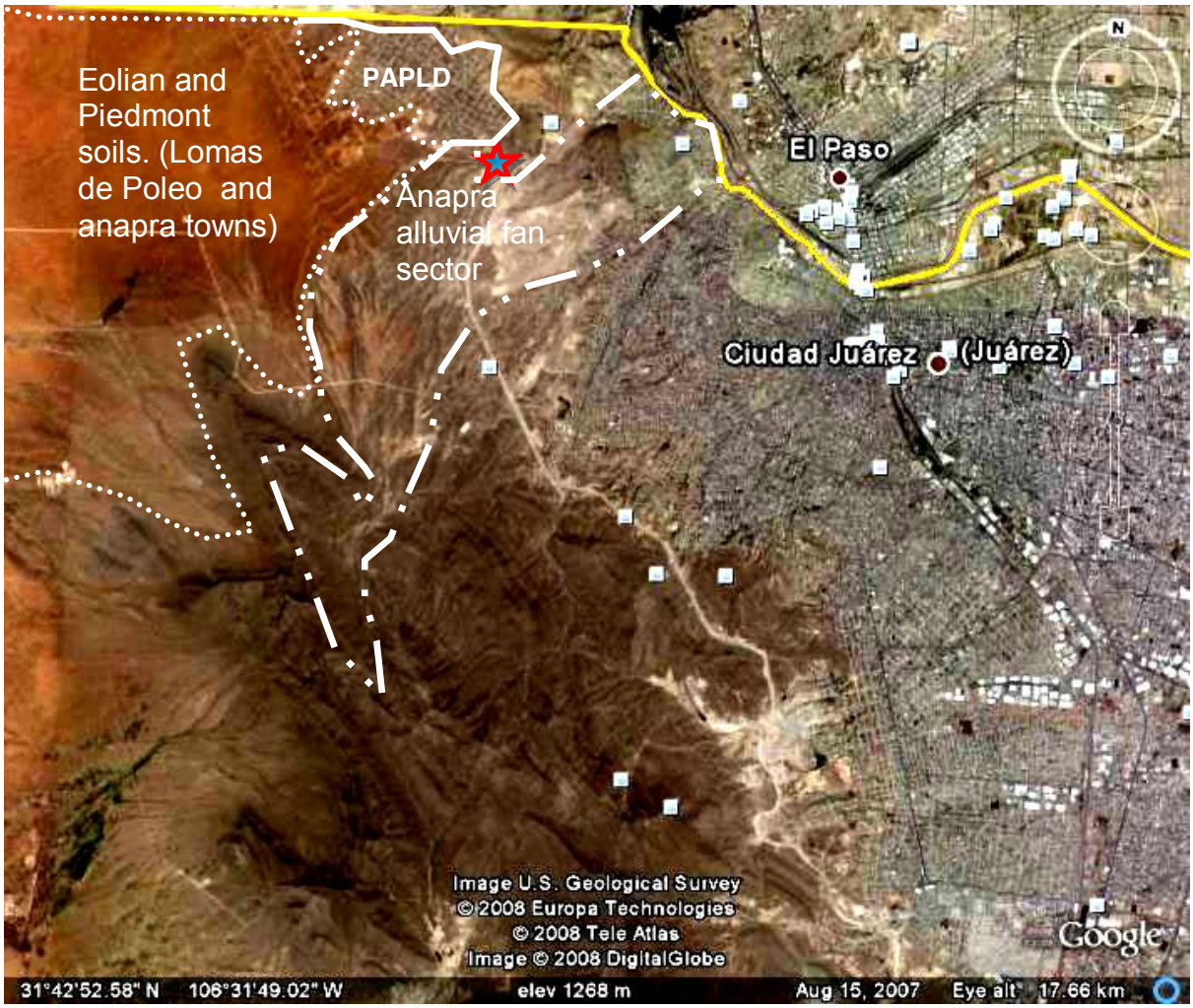

Figure 4.6. Location of the Anapra alluvial fan sector Centre while line: Crossed red symbol=Anapra dyke; Red-yellow colour area limited by dashed white line = Aeolian deposits; Yellow line=Rio Grande; white continuous line (PAPLD)=Puerto Anapra Playa Lake Depression. Source: Image Google Digital (Google 2008); (Wells et al., 1990) and Hack (1941)

4.3.2 Main components and boundary extension of Northwest fans (sector 1)

These main components drainage basin, channel feeder, topographic apex, distributaries channels, hydrologic apex and active depositional lobe were defined following the methodology explained in literature review Chapter 2 (Blair and McPherson, 1998; Bull, 1991; Harvey, 1987; Langford, 1999; Lecce, 1990) (See Fig. 4.7). Furthermore, Fig. 4.8 at the beginning of the next section illustrates the border lines which limit this sector and the influence of the work performed by its hydrologic components as competence and capacity given the geomorphologic expression to Northwest Anapra alluvial fan system (Sector 1).

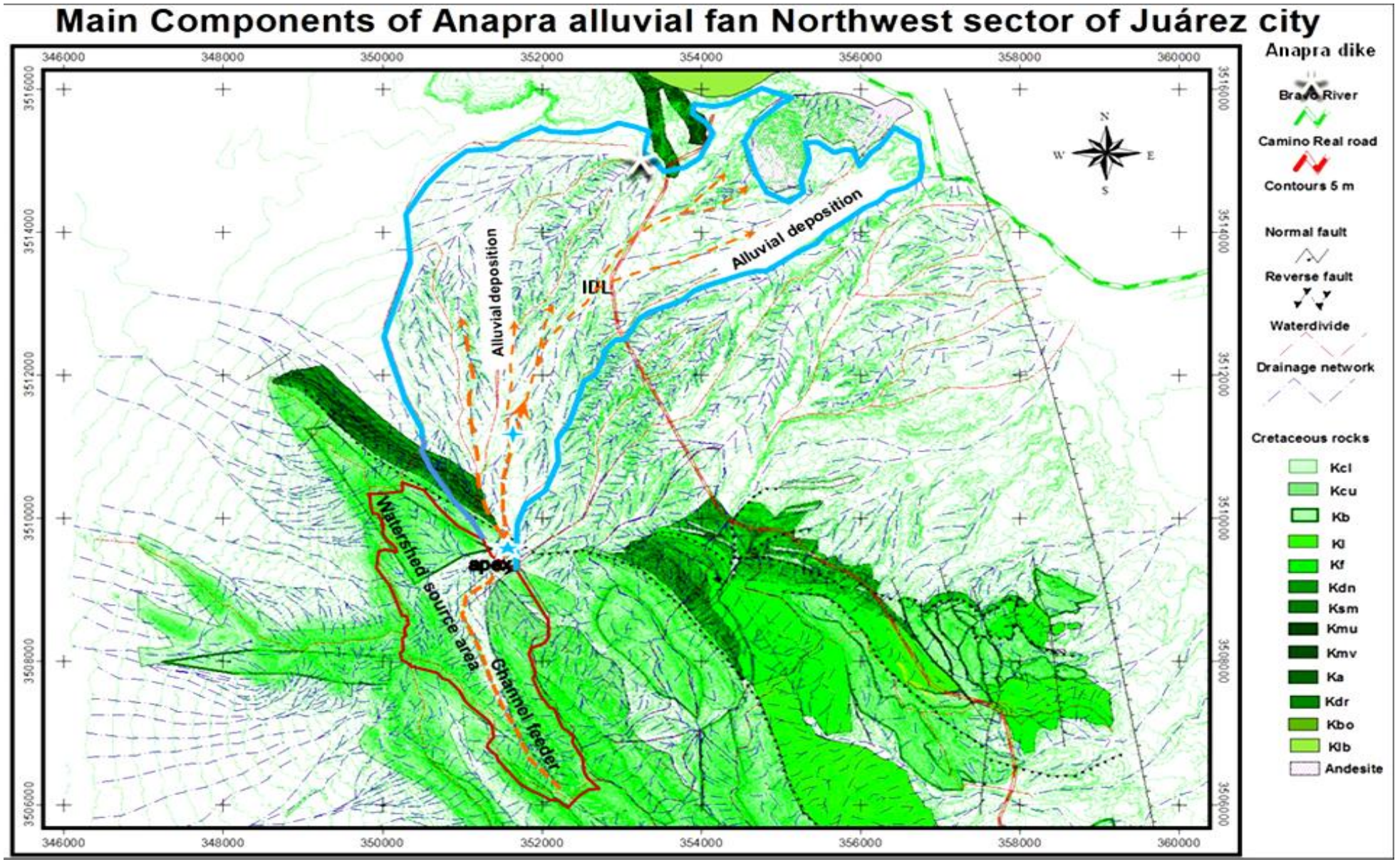

Figure. 4.7. Main components of Anapra alluvial fan: A red continue line= Watershed source area; A blue continue line=Alluvial deposition; A five sides cross=Anapra dyke; apex= Topographic apex; A orange dashed line Channel Feeder; Blue cross= Hydrologic apex A white 5 sides cross= Anapra dyke; Arrows= indicate flow direction of the major and minor streams; Dashed red colour line= Camino Real road; Dashed green colour line = Rio Grande; Geological Symbols are indicated in the right side of the Figure; Coordinate is related to UTM and datum NAD 27. Source: David Zuñiga (2011) using Arc-view 3.2, 2002; Auto-Cad (2009**)** and ArcMap GIS 9.2, 2009)

4.3.3 Anapra alluvial fan sector 1 description.

This fan is located northwest of Juárez city near to Mesilla aquifer and close to Anapra Port neighborhood (see Figs. 4.4 to 4.6) and is composed of two main areas: one corresponds to the catchment source area with A= 5.45 km^2 and channel feeder slope of S=4.94% and the other with an alluvial fan depositional zone of A=32.522 km^2 and channel feeder slope S=2.55%. Both areas maintain a close relationship because the ratio between slope on the channel feeder upward and downward of the topographic apex is such that the slope is approximately twice as steep in the catchment area than in the depositional area.

As a result, the channel feeder delivers a great amount of debris and coarse sediments stored in the footwall catchment source area into the depositional area due to mechanical erosion during glacial periods of the Pleistocene-Holocene time (Ortega-Ramírez et al., 2004). As stated by Ortega-Ramírez et al. (2004), two periods of glacial and interglacial climate causes the channel feeder to construct mostly flow-debris as well sheet-flow which are the more frequent sedimentary structures found in the Anapra alluvial fans (see photo inventory in Appendix 4A1; Figs 4A1.1 to 4A1.5).

The first point visited was: Point 1 photos **a** and **b** are located at UTM 13R 0350187; 3511921 Elev. 1366 m asl and **c** located at UTM 13R 0351620, 3509562; elev. 1370 m asl. (See Figs 4.8 and 4.9 this chapter and Fig 4A1.1 of Appendix 4A1). 2 layers of soils: The lower strata is formed by a big package of boulders, cobbles and poorly sorted gravels (**B-C-GP)** and the upper strata composed of medium cemented cobbles and sandy pebbles mixed with poorly sorted gravels **C-SP-GP** (upper loamy and poorly sorted sandy gravel and fine and soft brown sand lower). Photo **c** shows the channel feeder near to the topographic apex.

As can clearly seen the topographic apex is composed of two principal strata. The lower suggests that high competence of channel feeder to transport these big fragments of rocks and could be certainly classified as flow debris deposited in the proximal area near to topographic and hydraulic apices; this point is the beginning of

the proximal alluvial fans **Qfpc** and the older part of this sector. The second point monitored was located at 13R 0349170; 3511770; elev. 1339 m. The photo illustrates the contact between the western mountain front Cretaceous rocks where the Colorado biggest and longer thrust threatened the study area at point 2 on Fig. 4.9 and geological map of the study area (see Fig. 4.1A). This fault was further reactivated as a normal fault and shows the disposition between the hanging wall Cuchillo Formation older and footwall Anapra Formation younger. This fault has the dip oriented approximately NW 40° / 70SW°.

The third point Photos **a** and **b** of Fig. 4.9, shows the soil composition on the contact at elevation 1339 m. Two strata photo **a** one upper composed of loamy and poorly sorted sandy gravel **SM-SC** and a lower composed by fine and soft brown sand **SC-ML** in this particular area is located in an isolated proximal alluvial fan named **Q1paf**, that was possibly formed during Holocene time, because it has been modified only by deflation and not incision, although it has not been dated in this study. Figs. 4.8; 4.9 and Fig. 4A1.1 of Appendix 4A1 show the classical conical morphology of this alluvial fan and its elevation changes between 1339 m, in the apex and 1260 m in the distal part. In short, this little alluvial fan is composed of piedmont flow debris activated mostly by gravity forces and flow of sediments mixed in a mud matrix that promoted its activation and transportation from the highlands to the deposition lowlands areas given the classical form because there are not any obstacle to avoid the downstream movement of the sediments.

The contact of this alluvial fan in the distal part is clearly covered by fine deposits of aeolian origin mostly sand dunes occurred during the last glaciation event and is described later during the description of the last point visited in this sector. The fourth point is located at 13R 0350369; 3512163 elev. 1293 m. In this point four pictures were taken (see Fig. 4.9 and Appendix 4A1 Fig. 4A1.1 photos **a**, **b**, **c** and **d**) which show composition and soils facies distribution. The point selected to collect samples is located in the wall cave incised by the channel and the samples collected are composed of three layers. A lower layer composed of highly calcium carbonate-cemented cobbles and pebbles mixed with poorly sorted sandy conglomerate **C-P-SP** photo **a** maybe formed during the glacial period of middle

Pleistocene time when aggradations mode had operated. Above this layer another layer of poorly graded gravels packed on a poorly but highly cemented sandy-silty matrix **GP-SP.** In photo **b** two layers were distinguished a lower layer of cobbles and pebbles mixed with highly cemented sand **C-P-SM** and an upper layer composed of gravel mixed with highly cemented and poorly sorted silty sand **GP-SP.** This layer is interpreted as flow debris, also formed contemporaneously to the lower layer.

In the upper part, there are sediments characteristic of sheet-flood composed of poorly sorted and rounded pebble gravels and pebble sands in laminated layers intercalated and packed in high carbonate-cemented matrix (**C-P-SM GP-SP C-P-SP** photo **c** of Fig. 4.9 and Appendix 4A1 Fig. 4A1.1). The three layers observed in this point are interpreted as the ended of the proximal alluvial **Qfpc** elev. 1293 m. In short the elevation range that represents this alluvial fan is between 1350 to 1300 elevation (Figs. 4.8 and 4.9 and Fig. 4A1.2 of Appendix 4A1). This point is illustrated in photo **d** of Fig. 4.9, and shows a little and isolated 5 meter-high island composed of hyper-concentrated flow-debris as well sheet-flood deposits that were eroded and define the beginning of incision operation mode in this area**.** To locate the contact between the end of the middle alluvial fan **Qfmc** and the beginning of the distal alluvial fan **Qfdc** the path of the Puerto la Paz stream that begin in the apex previously mentioned is followed. The outcrops (see photos **e**, **f** and **g**; point 4 and Fig.4.9 and Appendix 4A1, Fig. 4A1.2) observed during the path suggest a persistent migration of the channel feeder shifting so many times and producing lobes and leeves at both sides of the stream. These structures constitute the building block of the alluvial fan and its consequent periods of avulsion that perform the final structure of the alluvial fan.

An important question arises: how, it is possible to recognize during field works the hydrologic apex of the alluvial fan system of Anapra sector and how its main components have been performed its modern landscape. This question is associated with the work performed by the channel feeder during different stages of aggradation and incision, which in the study area have occurred many times during Pleistocene to Holocene time.

With regard to the Anapra fan system, the ratio between the slope on the channel feeder upward and downward of the topographic apex is nearly twice as steep in the catchment area as in the depositional area. Thus a prominent volume of sediments are deposited near the topographic apex during aggradation time. This topographic apex is near to a high fault system named Viboras fault and constitutes the gate which regulates the pass of the catchment sediments from the source area to its depositional area. Consequently in relation to the Anapra fan system this hydrologic apex (1293m asl) is near to the topographic apex (1339m asl) (see Fig. 4.9 and Appendix 4A1 Fig. 4A1.1 point 1 photo c). The best way to identify the hydrologic apex is during fieldwork observation.

Finally, the fact that a lot of sediment is deposited on the upper reaches of the fan has important implications for the flood modelling undertaken in Chapters 5 and 6. The key point is that the HEC-HMS and HEC-RAS models are based on Newtonian fluid flow, which is degraded by excessive sediment load in the water. The removal of the bulk of transported sediment by deposition in the upper fan means that floodwater is relatively clear of sediment, and reduces error in the modelling.

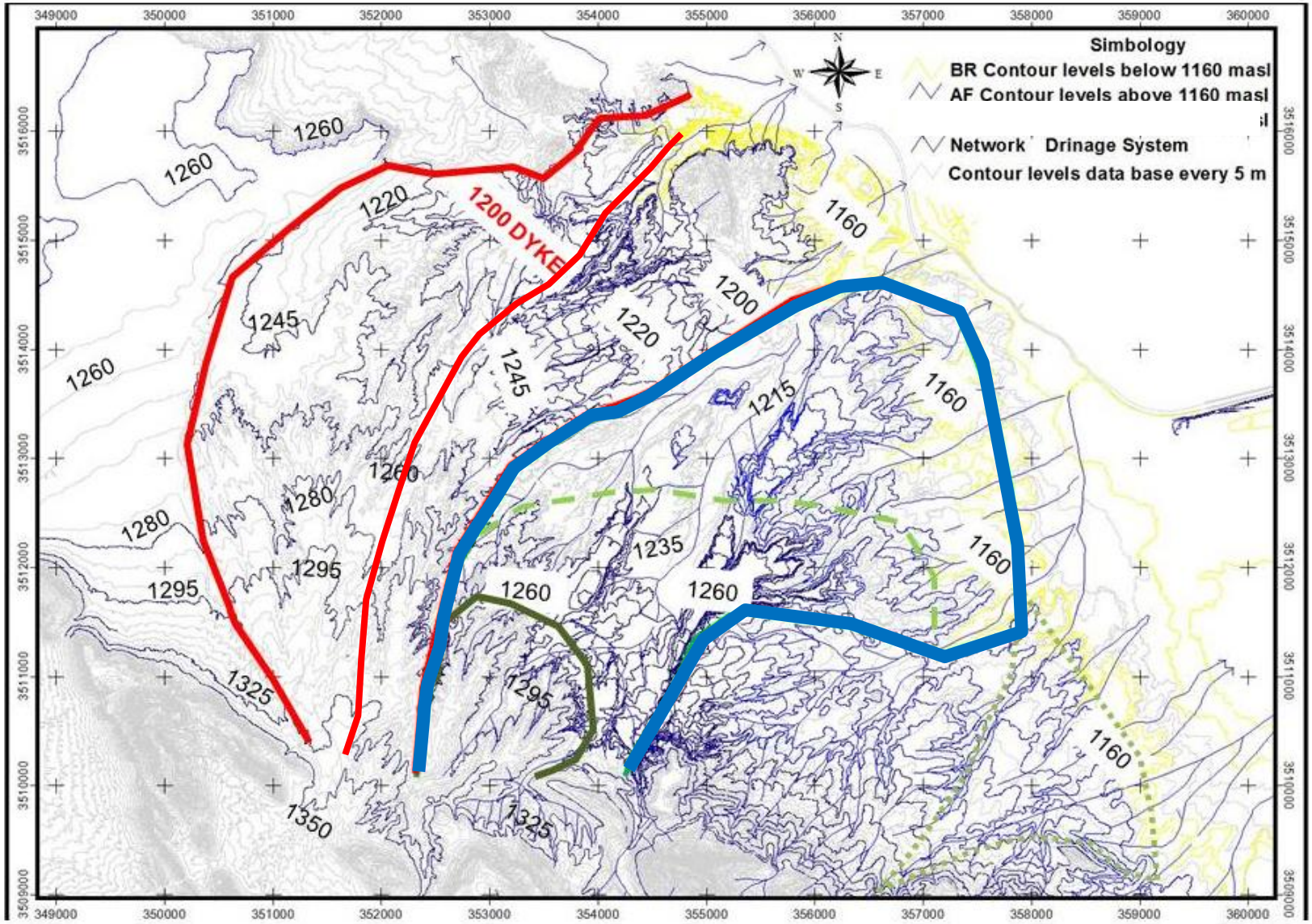

Figure. 4.8. Anapra fan features: A red continuous line= border line of anapra fan; A blue continuous line=Colorado and east Snake Alluvial fan border line. Between blue and red lines is west Snake . Green dashed clolour line = dissection of Colorado alluvial fan and point dashed green line is an isolated Colorado mountain front fan ; Coordinate is related to UTM and datum NAD 27. Created by David Zuñiga (2012) using Arc-view 3.2, 2002; Auto-Cad (2009**);** ArcMap GIS 9.2, 2009.

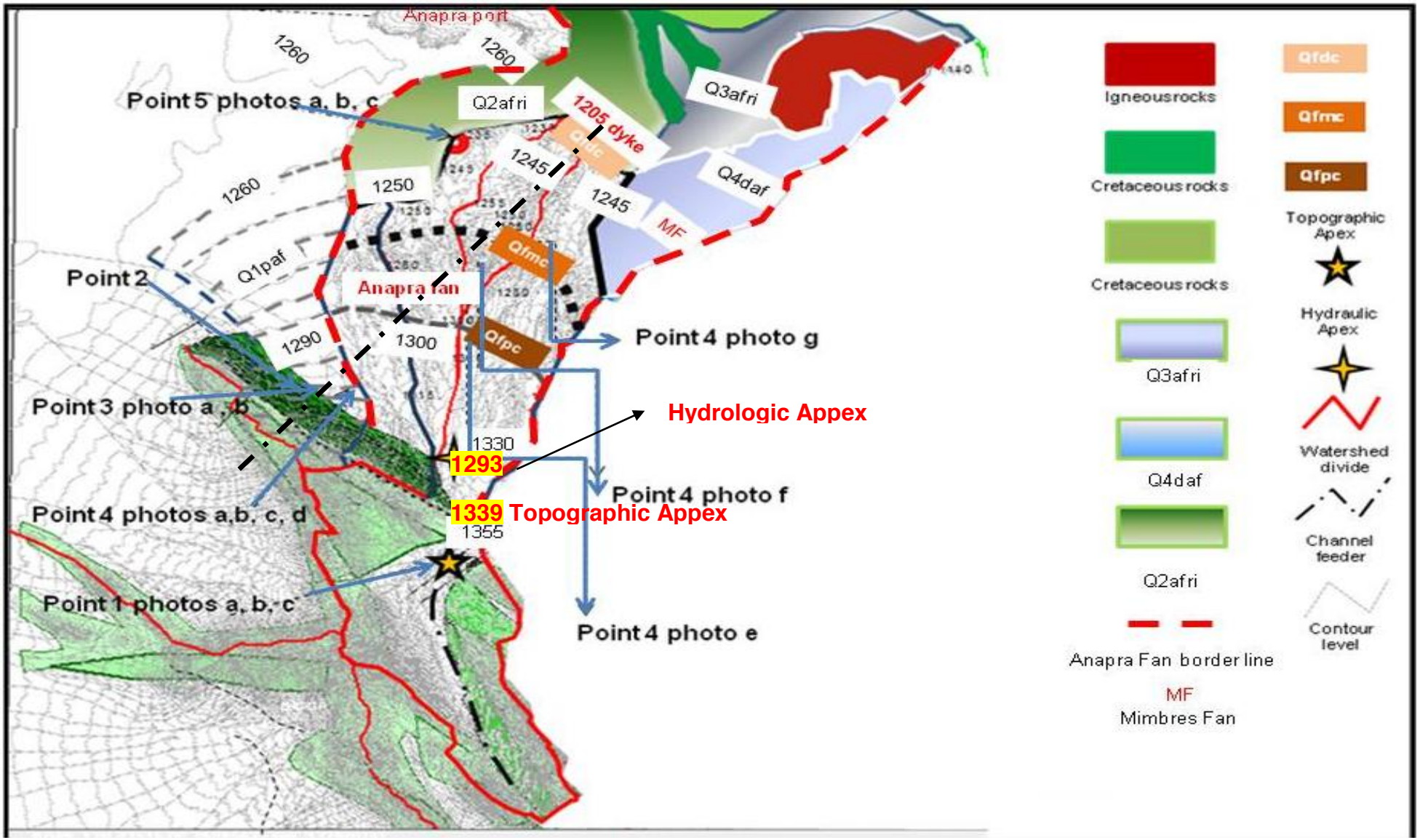

Figure 4.9. Shows:Qfpc= proximal (c) alluvial fan; Qfmc= medial (c) alluvial fan; Qfdc=distal (c) alluvial fan; Q4daf= distal alluvial fan 4; Q3afyri= Fluvial fans from young tributaries of the Rio Grande; Q2atri= fluvial fans from tributaries of Rio Grande; C-C' Cross (See Fig4.2).See additional simbology in the upper rigth part of Figure Created by David Zuñiga (2011) using Arc-view 3.2, 2002; Auto-Cad (2009); ArcMap GIS 9.2, 2009 and Laboratory of Soils mechanics of Juárez University UACJ (2009).

In photo **e** (Fig. 4A1.2 of Appendix 4A1) it is possible to appreciate the thickness of the conglomerate covered on the upper and lower layers, a robust intercalation of sheet-flow and mudflow that together have approximately 8 m of high at both sides of the stream (13R0350960 3512969 Elev. 1270m). In photo **f** a more clear aspect of the composition of the flow-debris layer deposited adjacent to channel feeder is illustrated and in photo **g** located at 13R 0351146; 3513504 Elev. 1261m constitutes the contact between unsorted gravelly sand conglomerate and sandy soil where the end of **Qmfc** is located. The main characteristic of these sediments are the low cementation of sandy soils of aeolic origin deposited in Pleistocene-Holocene time. In conclusion the interval of elevation for this alluvial fan segment correspond to1300 m and 1260 m (see Figs. 4.8, 4.9 and Fig. 4A1.2 of Appendix 4A1).

Finally, the last point visited in this sector is located at Anapra Port also named Anapra. This point 5 include 3 photos; **a**, **b** and **c**, in photo **a** 13R 0351066; 3515296; elev. 1265m (Figs. 4.8, 4.9 and Fig. 4A1.2 of Appendix 4A1) illustrate the fresh, lower, wet and fine sand samples that were collected, taking advantage of the construction of the Santa Teresa road. Photo **b** shows the moment of sand sample collection where it is possible to see the poor sorted and Low plasticity silty sand **LPSM**. This soil facies suggest Late Quaternary river deposits. The previous findings are consistent with Pazzaglia and Hawley (2004) who stated that: In the Paso del Norte area close to Anapra port the water level of lakes during late Pleistocene and early Holocene were in the order of 100 m higher than those prevailed during late Quaternary. A 40 cm layer of high plasticity white color and evaporitic sand **HPEVSPS** (See photo **c** point 4) suggest a low energy and high temperature environment. The elevation registered of 1265 m mark the limit of the isolated alluvial fan **Q1paf** described in the second point of this section (see Fig. 4.9 and Fig. 4A1.2 of appendix 4A1).

In previous paragraphs is explained the progress of the Anapra alluvial fan down to Anapra port. However it is important to draw attention to the boundaries of this area The north-side is the Cristo Rey uplift that formed a little deep full graben and is presented in cross section of Fig. 4.2. The NE side of footwall sediments derived are composed of marine and volcanic sediments with a wedge of upper intra-basinal playa sediments of Anapra dyke which is one many depressive areas

filled with fluvial Bravo River deposits. (See section 4.6) and Aeolian reworked sediments of the recent Pleistocene-Holocene period (See Fig. 4.2).

The Northeast side of the Anapra alluvial fan is described in the following paragraphs. The contact of this medial alluvial fan segment are; **Q2afri, Q3afri and Q4daf** (Figs. 4.8 and 4.9) and are intercalated with deposits of the Bravo River. In this section will be described **Q2afri**, **Q3afri** and **Q4daf** (Fig. 4.6) are described in the following sector that corresponds to the central sector of Snake and Colorado alluvial fans system.

Close to Anapra, the Bravo River runs along two uplifts Franklin and Juárez Mountains. The river bed is as much as 300 m wide valley and its powerful channel and tributaries have been received nearly 25 m of saturated alluvial fills. Furthermore, in the study area the Hueco Bolson varies from 1190 m to 1220 m and the sediments layer of these alluvial fills is as much as 18m to 30m (Tigth, 1905 and Tolman, 1909). In addition, these soils are intercalated with younger Aeolian as well local playa depressions fills.

There is a sector of the Bravo River valley which separates El Paso Texas and Juárez city along approximatelly 65 kms. This sector has a variable flood elevation segment of 1132 m to 1135 m between The Fabens town and San Elizario island located in El Paso Texas area (Hawley and Kernodle, 2000; Gile et al., 1981). Summarizing the previous works already presented and the field work done in this distal alluvial fan segment permits assessment of its temporal and spatial distribution and to conclude that this distal segments **Q2afri** and **Q3afri** (see Fig. 4.6) are composed in the lower part by reworked pedogenic calcretes and in the upper parts by fluvial facies such as silty clay ***SM***, clay ***C*** and sand ***S*** mostly facies derived by arroyo tributaries of the Bravo River deposited during middle Quaternary time (130 ka) (Hawley and Kernodle, 2000; Gile et al., 1981). Actually these soils are preserved in the study area and were formed as a result of the incision regime that prevailed. Consequently the bed of the river shows approximately 30 m of erosion. Fieldwork and sample collection is presented in the description of the next sector.

4.3.4. Photo description and evolution of Snake and Colorado fans sector

The second sector integrated by Snake and Colorado alluvial fans is located southeast of Anapra fan sector 1 and Northwest of Palo Chino and Jarudo alluvial fan. The proximity of these two alluvial fans and the influence of the fluvial Bravo River soils (see Appendixes 4B; 4A2 and 4A3) during the initial stage of its developed has impacted in its irregular morphology. In addition, this sector is strongly dissected by fluvial channels marked by scarp lineaments clearly distinguished in satellite images, contour levels, as well by the form of the drainage network system. Streams and rivers always follow faults to make their path. Then, to locate and analyze these features the use of satellite images as well the study of regional geology of the study area were used; see geologic and topohydraulic maps (Figs. 4.1 and 4.4) and the main components map (Fig. 4.7).

Faulting and failuring on this centre sector began during volcanism of Eocene-Miocene (36.6 to 23.7 Ma) and even during Miocene to Pliocene time (23.7 to 5.3 Ma) (Mack and Seager, 1995). Therefore, as a result of this volcanism period a great volume of sediments derived from erosion were deposited (Mack and Seager, 1995). In addition, scarps and lineaments oriented NW as well NE direction are clearly observed in satellite Images dataset and the existence of Franklin Mountain Uplift, Cristo Rey and Juárez Uplifts and their associated Normal Faults Lovejoy (1976e).

All the previous remarks, suggest the possibility that in this area a transfer zone may be exist, associated with change in the principal rift direction mostly during Pliocene-Pleistocene time (5.3 to 1.6 Ma) as a result of tensive strength in a younger rift Bravo River stage (Mack and Seager, 1995).

Consequently, a great volume of sediments was deposited and transported in many directions by the main streams within the heterogeneous topographic space produced by faulting. Obviously the resulted landscape derived from these differences in uplifting and deposition is in fact reflected in the stream network system and the sedimentary structures derived. In this sector the main geometric components which influence the alluvial fan behaviour as well its spatial geomorphology and development are presented in the following paragraphs. Firstly, the alluvial fan named west Snake fan in the catchment source has an area of Aw= 5.9 km^2,, while the slope channel feeder is Sw=3.84%. The other, named east Snake

fan in the catchment zone has an area of Ae= 3.12 km^2, while the slope of channel is Se=3.65%. However, in the fan depositional area both have Adw=5.33 km^2 and S=2.55%. With respect to the Colorado fan the two main components of the system are: a) n the catchment source area (Ac=11.9 km^2; S=4.23%) while b) in the fan alluvial depositional area both parameters are A=32.522 km^2, including the mountain front alluvial fans; S=2.55%.

The others alluvial fans bordering the mountain front that are included in this sector are mostly flow debris completely free to move, these footwall-derived sediments discharge directly in depressive areas of the urbanized area of the Juárez City and in the recently constructed Camino Real road. The main process that were active through geological time were secondary processes that produced loss of shear stress in the mass of sediments due to an increment in the pore pressure that promoted the progress of failure planes. These alluvial fans are named Colorado and Palo Chino mountain front alluvial fan **CMF** and **PCHMF**.

Due to their unconfined condition these fans exhibit an irregular morphology appreciated in the drainage network system. The high gradient of the streams and their associated competence caused deposition of great amount of big debris such as cobbles in the upper and middle areas with intercalation of Lobes and levees (formed mostly during aggradation mode) interrupted by some gullies formed mostly during incision mode. These structures constitute the building block of the alluvial fans and were derived from different periods of avulsion during the climatic mode (glacial and Intergalacial of the Pleistocene time). The first part of the alluvial fan corresponds to the frontal mountain confined alluvial fans named (**CFM** and **PCHMF**). These fans are formed by three main segments named (**Qfpb**, **Qfmb**, **Qfdb**, **Qfpc**, **Qfmc** and **Qfdc**) (Fig. 4.11).

In short, the sector here mentioned is integrated mostly of frontal mountain alluvial fans with footwall derived sediments mostly formed by cobbles and gravels in the upper parts of the little wedge provided in hanging wall and because its dip orientation downstream direction. Mostly Upper Santa Fe Group Fort Hancock Formation is very common in the contact around these piedmont alluvial fans.

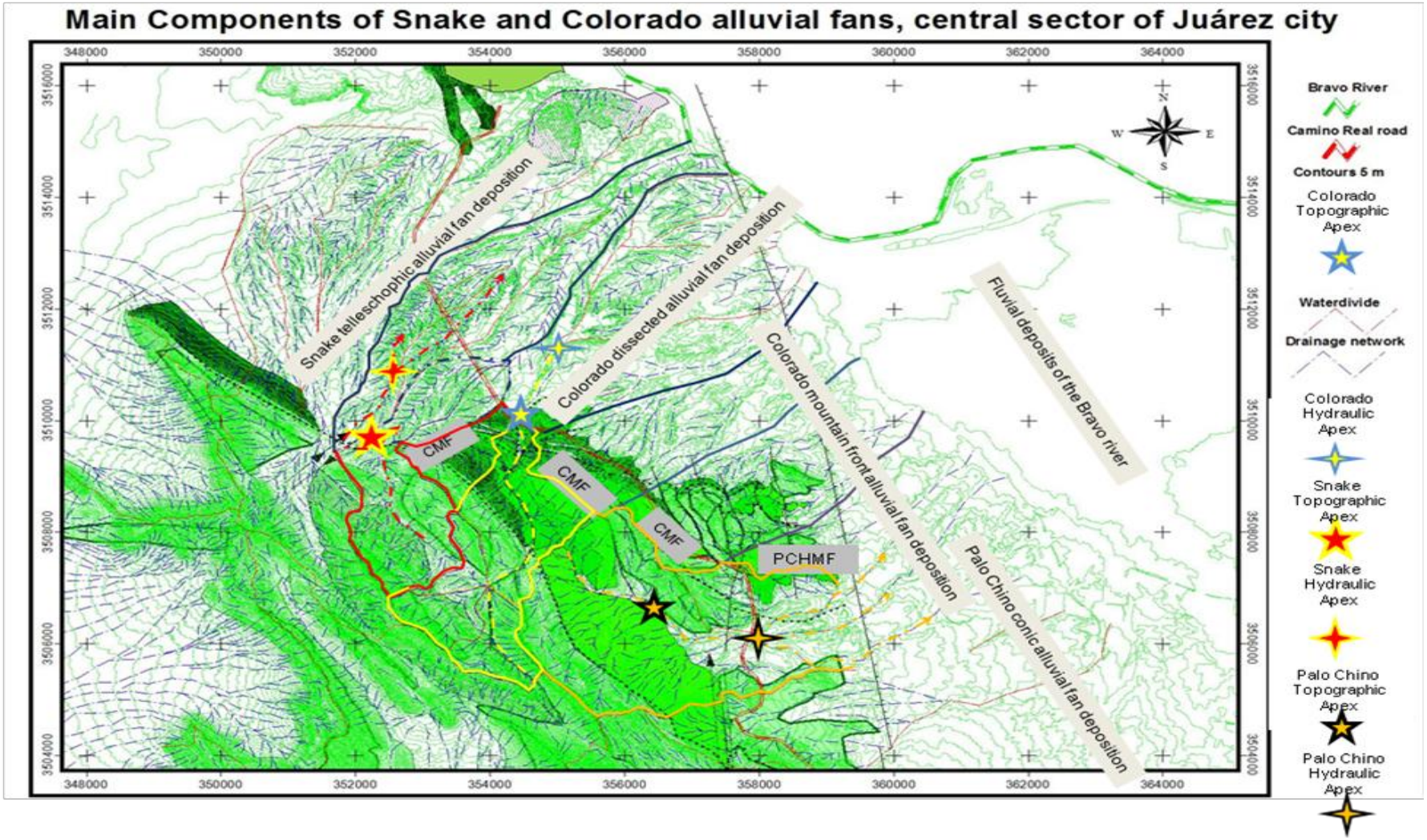

Figure 4.10 Snake and Colorado Alluvial fan main components of central sector; CMF=Colorado Mountain Front; PCHMF=Palo Chino Mountain Front; Red line=Snake Catchment; Yellow line=Colorado catchment; Red dashed line=Snake Channel Feeder; Yellow light dashed line=Snake channel Feeder; Blue line=drainage network of CMF and PCHMF depositional areas; Yellow black line=Palo Chino catchment area; symbology are indicated at the left side of Figure. Coordinate UTM and NAD 27 Datum: Created by David Zúñiga using : Arc-view 3.2, 2002; Auto-Cad 2009

Colorado and Palo Chino Mountain Front alluvial fans are composed of poorly sorted cobbles, pebbles and sand mixed with mud, clay and silty sand prone to landslides, mudflow and gravity mass flows. The footwall derived sediments previously described were deposited within a short length hanging wedges located downstream with progress in the NW and NE direction adopting an irregular path of the drainage system network. These uplifts and subsidence blocks are composed mostly by flow debris as well sheet flood soils, which are the typical building blocks to this irregular depressive and scarped topography sector. Furthermore, as a result of normal faulting the younger Miocene–Pliocene Fort Hancock Formation are in contact with Cretaceous as well volcaniclastic rocks visible in some cuts done in the Camino Real Road.

The first point located at coordinates 13R 0354818; 3510056; and elev. 1262 m asl along the Camino Real road (km 11+700 CR) is composed of the following type of soils given in the photo inventory See Fig. 4.12 and Photo 1 Fig. 4A1.3 Appendix 4A.1 showing a sequence of three soil layers 17m; 12 m and 16 m thick of highly cemented and poorly sorted gravel and sand conglomerate mixed with highly cemented as well medium plasticity silt and clay (**HCPS-GCC-SM-SC MP).** The highly cemented condition of this soil suggests that this proximal segment corresponds to the oldest alluvial fan of the Colorado stream. The soils layers are distributed in three facies; highly cemented limestone conglomerate mixed with poorly sorted silt and sandy clay of medium plasticity **HCLTC-PSM-SC MP** the other of highly cemented fine and poorly sorted sand, mixed with silty sand and silty clay **HCFPS-SM-SC MP** finally the other layer is high concentrated and poorly sorted sand mixed with silty sand and sandy clay of medium plasticity **HCPS-SM-SC-MP** (see Figs. 4.11, 4.12 and Appendix 4A1, Fig. 4A1.3).

The second point located at coordinates 13R 0353838; 351105; and elev. 1254 m along the Camino Real road 10+800 is formed by two layers. A lower layer of medium cemented limestone conglomerate poorly sorted silty sand and silty clay **MCLTC-PSM-SC MP** and an upper layer of highly cemented limestone conglomerate poorly sorted silty sand and silty clay **HCLTC-PSM-SC MP**. In this point the soils facies are similar to the first point and correspond to proximal segment of the Snake alluvial fan system (Figs. 4.11, 4.12 and Fig. 4A1.3 of Appendix 4A1)

The third point is located at coordinates 13R 0354160; 3510359; and elev. 1281m along the Camino Real road km. 10+380 (Fig. 4A1.3 of Appendix 4A1)**.** Three layers were monitored in this point. Firstly, a 2 m thick intermediate layer of cemented silty sand mixed with sandy clay layer **C-SM-SC** and two extreme 4 m layers of windy sands mixed with low plasticity silt and low plasticity mud **WS-ML-OL**. Soils composition at this point suggests the influence of climatic change during glacial when high production of coarse to medium grains sands were derived, whereas during interglacial periods a more fine sands were produced. Thus, it is strongly suggested that soils are younger than the conglomerate and were produced in Pleistocene time. For this reason, the sediments represent the medial segment of Snake alluvial fans and Colorado alluvial fans (Figs. 4.11, 4.12 and Fig. 4A1.3 of Appendix 4A1).

The fourth point monitored is located at coordinates 13R0354448; 3510306; elev. 1256 m (see Figs. 4.11, 4.12 and Fig. 4A1.3 of Appendix 4A1). This point constitutes evidence that much mudflow and flow debris have deposited as a consequence of some fine and plastic layers which are intercalated into the mass of soils. At this point there are three layers: Firstly, in photo 1 a panoramic view of the monitored area is presented and in photo 2, an intermediate layer of low plasticity clay ***CL***; Secondly, a lower cemented clayey and poorly sorted gravel conglomerate mixed with sandy clay ***LCPGCP-SC***. Finally, an upper layer of low cemented and poorly sorted gravel conglomerate mixed with sandy clay and clay of low plasticity ***LCGC-PSC***.

In addition, in photo coordinates 3 13R 0354378 UTM 3510304 Elev. 1262 m, a sequence of two soils strata are presented: a lower layer formed by low cemented and poorly sorted gravel conglomerate mixed with sandy clay ***LCPGCP-SC*** and an upper strata of low cemented gravel conglomerate mixed with poorly sorted sand conglomerate ***LCGC-PSC***. The five point Photo 5 is located at coordinates 13R 0354794; 3511085; and elev. 1235m (see Figs. 4.11, 4.12 and Fig. 4A1.3 of Appendix 4A1) and has two layers: a high plasticity red clay ***RCH*** intercalated with Quartzite silty sand mixed with low plasticity red clay ***QMS-RCL***. These soils are in the medial Colorado alluvial fan **Qmfb and Qmfc**. Regarded to this sector, an alternative model suggest that the contact between the proximal alluvial fan end

segment **Qfpb, Qfpc** showed in Figs. 4.11 and 4.12 and **Qfpd** presented in Fig. 4.11 and 4.12 is with fluvial river deposits at elevation 1235 masl (see Appendix 4C).

The five point (see Photo 5 Fig. 4.12 and Fig. 4A1.3 of Appendix 4A1) is located near to Juan Balderas street at coordinates 3R 0355723 UTM 3511681; elev. 1235 m. In this point four different soils types were monitored: A lower layer of medium plasticity fine silty sand ***SM***, overlaying a little layer of medium plasticity red clay ***RCM***; and then a layer of poorly sorted pebble sand mixed with silty sand ***PSP-SM***. Finally, an upper layer composed of cobbles and gravels conglomerate medium cemented and mixed with pebble sandy clay with little or no cementation ***MCGC-PSC***. The previous layers of soils strongly suggest the characteristic building block sheet-flow and debris-flow facies dominated by Colorado stream basically represented by lobes or leeves developed in stages of climatic change of the middle to late Pleistocene. This segment of medial alluvial fans comprises an intermittent sequence of this structure over the Colorado alluvial fan.

The sixth point Fig. 4.12 and Fig. 4A1.4 of Appendix 4A1 is located on the Chihuahua neighbourhood at coordinates 13R0356277; 3512122; and elev. 1215 m. The photo shows clearly the unconfined and uncemented condition of a low plasticity and poorly sorted fine sand mixed with silty sand maybe of aeolic origin ***LP-SP-SM*** this site is the contact between proximal and medial Snake and Colorado alluvial fans. For reasons of inaccessibility there not were possible to visit a similar elevation point located on the Snake alluvial fan that present similar facies and maybe represent the contact of the proximal and medial alluvial fan. It is possible that **Qfma** equal to **Qfmb** (see Fig. 4.12 and Fig. 4A1.4 of Appendix 4A1). The previous deposits are derived from the Bravo River and is presented in Appendix 4C.

The point seven (Photo 8 Fig. 4.12 and Fig. 4A1.4 of Appendix 4A1 with coordinates 13R 0356085; 3514610; and elevation1161 m) has two layers of soils: the lower layer is composed of poorly sorted quartzite sandy clay ***QPSC*** and the upper layer is formed of quartzite poorly sorted silty sand (***QPSM***). The two layers are of volcanic origin and are located within the segment of medial to distal Snake alluvial fan **Qfma** to **Qfda** (See Fig. 4.12 and Fig. 4A1.4 of Appendix 4A1). The Point for Photo 9 is located at coordinates 13R 0352802; 3512650; and elev. 1256m (See Fig. 4.12 and Fig. 4A1.5 of Appendix 4A1). Three layers were monitored. A lower layer of unconsolidated cobbles pebbles and silty sand conglomerate ***UC-CPSM*** and

intermediate layer of unconsolidated cobbles and pebbles poorly sorted sands mixed with silty sand ***UC-CPSP-SM*** and finally an organic silt of low plasticity white colour of evaporitic origin ***ML-OL*** The presence of the last layer white silty organic soil suggest an evaporitic environment of deposition that maybe took place during the invasion of the tributaries of the Rio Bravo during the Pleistocene-Holocene time when many depressions were covered with water and were lakes, possibly contemporaneous with Anapra Port discussed in sector Anapra. This suggestion is considered because the elevation of this point (1256 m) is similar to the elevation of point of Anapra 1265 only 9 m of difference. However, future work may allow these sediments to be dated.

Tenth point (see photo 10). This point is located at coordinates 13R 0356405; 3514674; and elev. 1149m (See Fig. 4.12 and Fig. 4A1.4 of Appendix 4A1). The soils found were composed by two layers of pebble gravels and sand without plasticity and unconfined typical of fluvial origin ***RGS*** and another layer composed of sandy clay ***CS*** These two layers are alternated and formed a levee of approximately 10 meters high. The presence of these layers strongly support the view that the river valley deposits during aggradational periods were deposited over the distal segment of the Anapra as well as Snake alluvial fans and then during the incision time actually active. “The Bravo River has cut the alluvial fans as well the deposits of the Rio Bravo distributaries” (Hawley and Kennedy, 2004; Gile et al., 1981; Leeder et al., 1996a; Leeder et al., 1996; Hawley and Kernodle, 2000, Table 2). In summary this point represents the limit of the distal alluvial fan Snake as well Anapra fan previously discussed **Qfda**; **Qdfb1**; **Qfdb1**; **Qdfc** (See Figs. 4.11, 4.12 and Fig. 4A1.4 of Appendix 4A1).

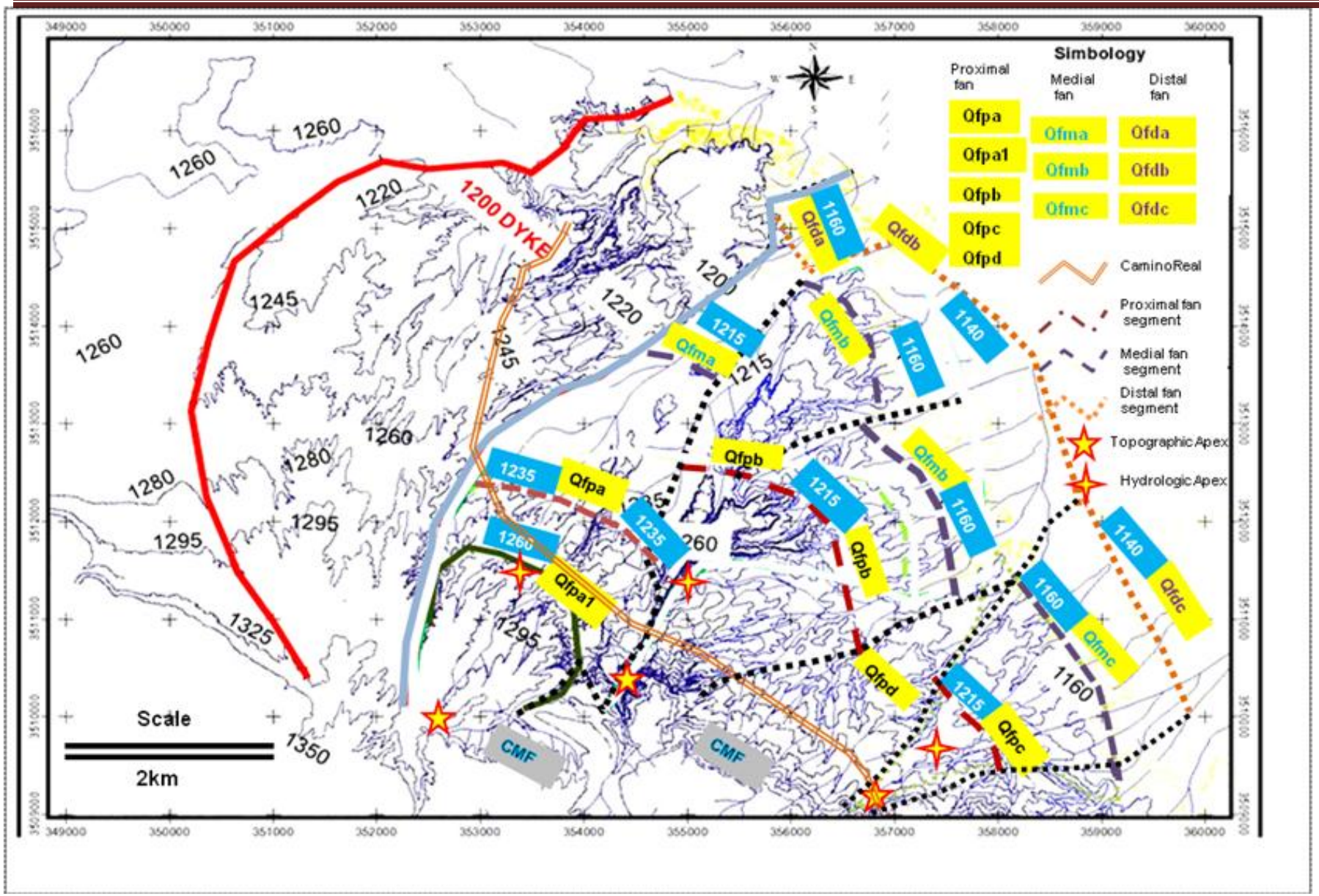

Figure 4.11. Symbology for proximal, medial and distal segments of alluvial fans (Yellow bars) are linked with elevation see (blue bars). their border with dash black colour lines. (CMF) means Colorado Mountain Front; and (PCHMF) means Palo Chino Mountain Front alluvial fans. See figure 4.12 for geographic location of sample collection and photoinventory as well drainage features. Created by David Zúñiga (2012). using Auto Cad 2009 and Arc-

123

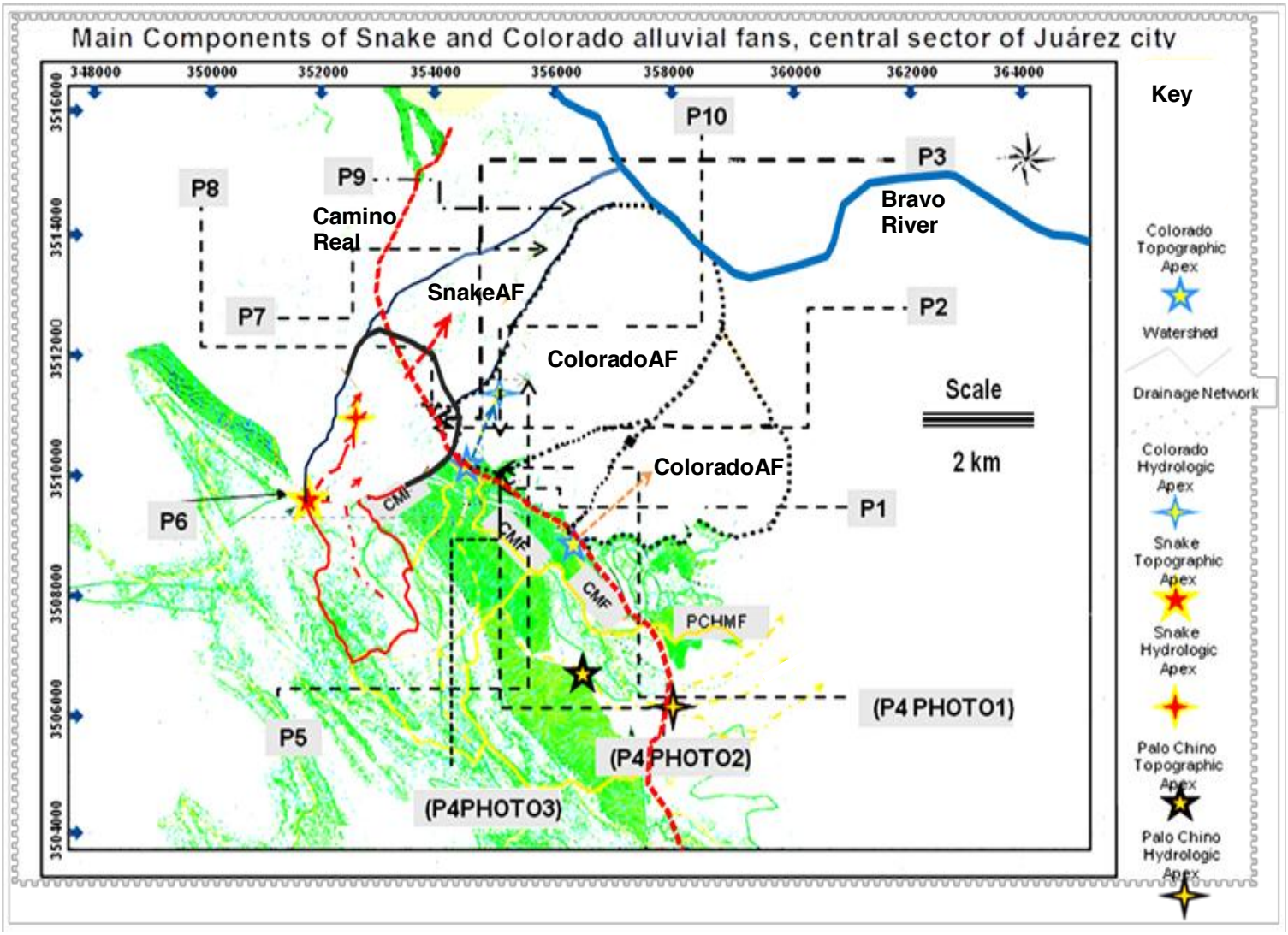

Figure 4.12. Nine sites of sample collection are presented in Figs. 4A1.3 and 4A1.4 of Appendix 4A1 indicated as P1 to P10 These figures show geographic coordinates and soils facie of the nine sites visited. On the right and lower side of the figure the main alluvial fans components as channel feeder, Topographic and Hydrologic apex are shown. Channel feeder transport direction of Snake is marked in red colour dashed arrow line; Channel feeder of Colorado fan is marked by a blue dashed arrow line and Channel feeder of piedmont alluvial fans are indicated in marrow dashed arrowed line. (CMF) means Colorado Mountain Front; and (PCHMF) means Palo Chino Mountain Front Alluvial fans. Geographic location of alluvial fans Snake and Colorado is presented in: PN= Point number collection; PNPHOTO= Photo number. Coordinates are in UTM Nad 27 geographic coordinate sistem. Facies details and soils classification was done using the Unified Soil Classification System (USCS) and are described in detail in appendices 4A1, 4A2 AND 4A3; Created by David Zúñiga (2012) using Arc View 3.2 and, Unified Soil Classification System USCS (2011), and Laboratory of soils mechanic of Juárez University UACJ (2009).

4.3.5 Palo Chino and Jarudo alluvial fan Photo inventory and Evolution

The proximal segment of south-eastern Palo Chino fan is composed as follows. Firstly, three strata of hyper-concentrated limestones conglomerates point 1 photo 1 in Figs. 4.14 and Fig 4A.5 of Appendix 4A1 at coordinates 13R 0357857; UTM 3506388; elev. 1279 m asl, along Camino real road km. 16+100. The upper layer is a highly cemented limestone conglomerate composed of boulders gravels mixed with silty sand of high plasticity (**BGHCLTC-SM-HP**). An intermediate layer of poorly sorted silty sand mixed with highly cemented sandy clay (**PS-SM-SC-HC**) and a medium cemented silty sand and silty clay lower layer (**SM-SC**).

Secondly, point 2 photo 2 in Figs. 4.14 and Fig 4A.5 of Appendix 4A1 is located at coordinates 13R 0359871; UTM 3503075; along the Camino real road km 22+000 elevation 1270 m asl also is comprised by three layers: an upper layer 4.7 m of highly cemented boulders and sandy gravel conglomerate (**CBGS**), an intermediate layer of 3.4 m of cemented boulder cobbles and poorly sorted sand conglomerate (**BRCSPC**) another layer of 1.65 m of cemented boulder limestone conglomerate (**LTBC**) and finally a lower layer of 3.45 m of highly cemented boulder and cobble conglomerate (**BCHC**).

Briefly, the point 1 photo 1 located at the Camino Real road (km. 16+100) elevation 1279 m, corresponds to the proximal segment of Palo Chino Alluvial fan. It is older because it was captured from initial normal faulting development stages. This fault dips in an east direction and the subsequent deposition of mountain front footwall derived sediments filled the little wedges lifted in the hanging wall were the building block of the alluvial fan in the proximal area (see geological map Figs. 4.1 and 4.14). The second point located at elevation 1279 m is only 9 meters above the first point and due to facies similarities; it's possible that both being contemporaneous therefore are also in the proximal segment of the alluvial fan system.

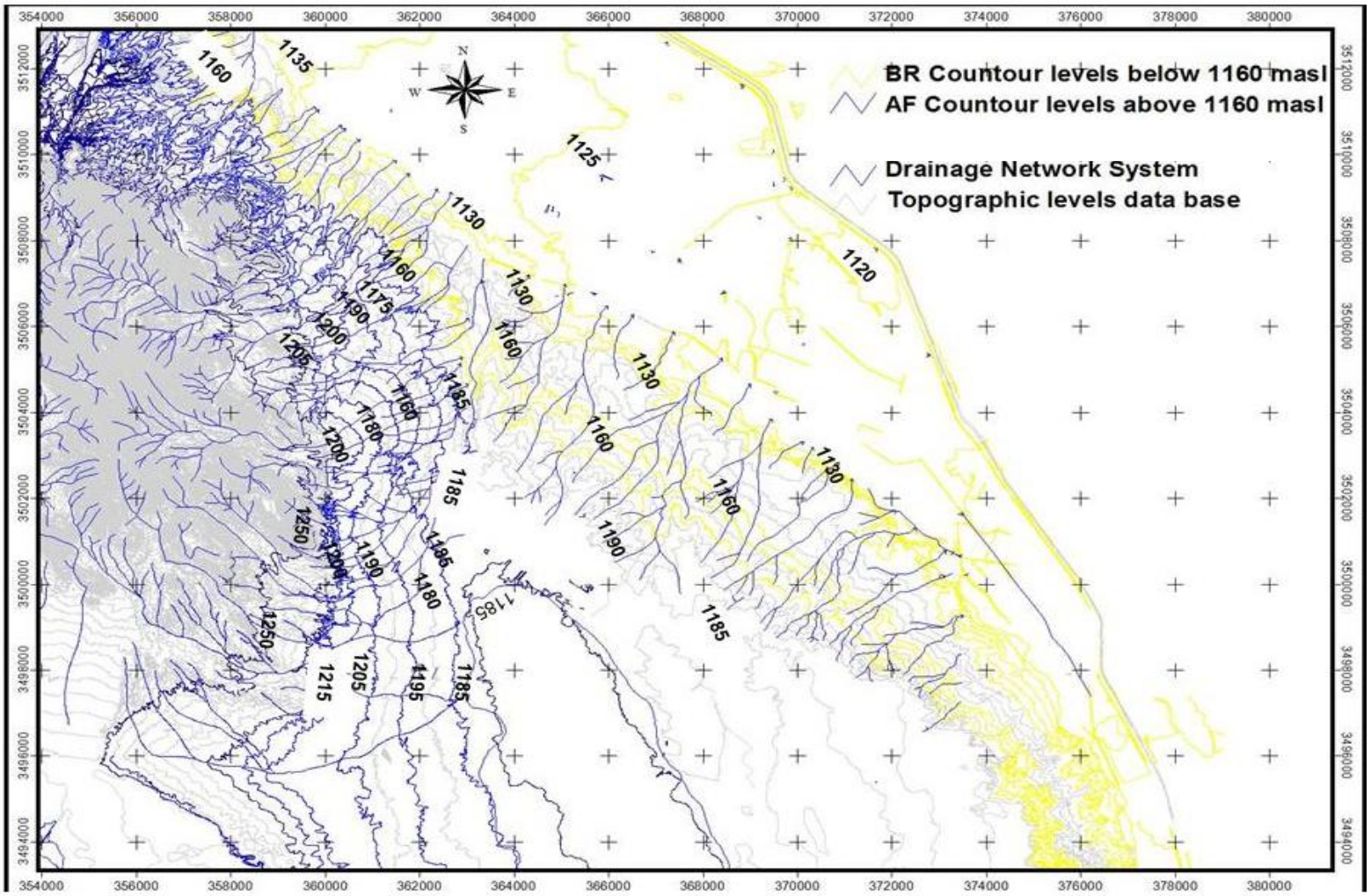

Figure 4.13. Complementary Topo-hydraulic map of the Palo Chino and Jarudo alluvial fan (Sector 3). Coordinates UTM and Datum Nad 27. Contour Levels of the alluvial fan are marked in colour blue and Floodplain and Fluvial fills are marked in yellow colour. this figure is complementary of figure 4.13 and shows more clearly how contour levels elevation adopts the alluvial fan shape. Instead, Figure 14 shows in green colour topography but shows also geology and hydrology maps the hydraulic Created by David Zúñiga (2011) using: Auto-Cad (2009) and Arc-vie 3.2.

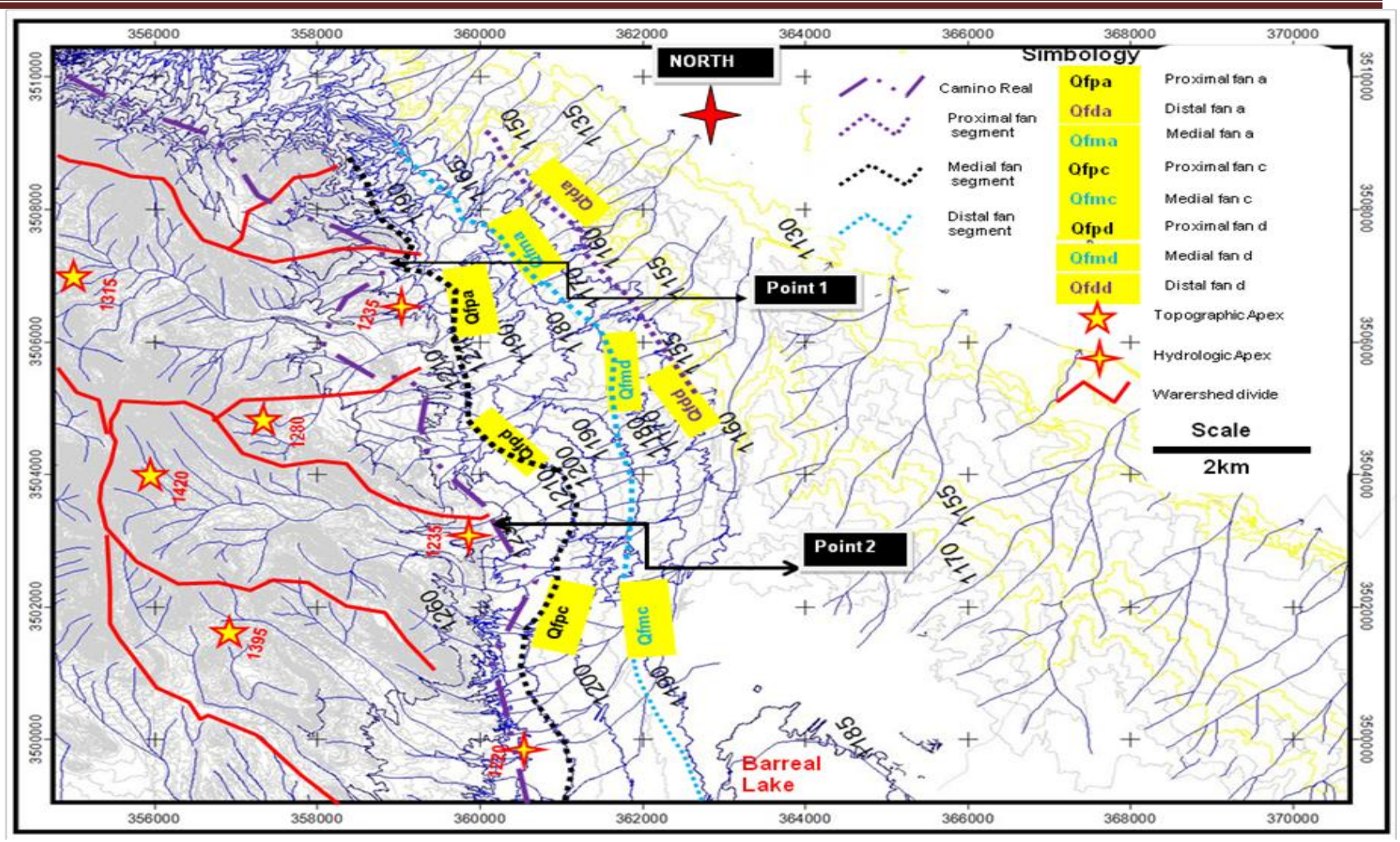

Figure 4.14. Complementary Top hydraulic map of the Palo Chino and Jarudo alluvial fan (Sector 3). Coordinates UTM and Datum Nad 27. Contour Levels of the alluvial deposits and drainage network system are marked in colour blue and Floodplain and Fluvial fills are marked in yellow colour, Note that point 1 and point 2 are sites of photo inventory and sample collection and are Fig. A1.5 of Appendix A1. Watershed divide is marked in red colour line. Created by David Zúñiga (2011) using Auto-Cad (2009) and Arc-view 3.2, 2002).

The main hydrological components of the system illustrated in Fig. 4.14 constitutes a source or sediments open to tributaries of the Palo Chino as well Jarudo streams. This perfect conical form is clearly defined by the contour levels distribution being more evident in the junction between the alluvial fan deposits and the intercalation of sediments derived by the ancestral Rio Grande that occurred during late Pleistocene and Holocene time (see Mack and Leeder, 2004**;** Hawley and Kennedy, 2004**;** Hawley and Kernodle, 2000; Gile et al., 1981; Leeder et al., 1996 and Leeder et al., 1996a).

In addition, the geologic layouts maps (Figs. 4.1A to 4.1D) show a large normal fault passing through Juárez city together with many normal minor adjacent faults. The faults influenced the morphology and evolution of this alluvial fan because the existence of different wedge depressions due to uplifts (footwall) and subsidence (hangingwall) events. Consequently, the balanced contribution between space formed during tectonics of Pliocene and Pleistocene time when subsidence and uplift occurred and the corresponding period of substantial deposition occurred during the climatic operation mode of Pleistocene- Holocene time due to a subsequent period of aggradations mode occurred during glacial and interglacial periods. These events have provided the accommodation space for deposition principally by flow debris and sheet flood soils deposited in the highest and intermediate elevation of the Juarez mountains as can be clearly seen on the photos of point 1 and 2 located along the cuts left during the Camino Real construction see (Fig. 4.12).

5. Summary

This chapter shows the range of alluvial fan structure and distribution, and provides a detailed geography of the fan system. This provides important information about the fan processes, and leads in the next two chapters to modelling of flooding treatening on the alluvial fans network located in the Juárez city study area

5.1 INTRODUCTION: FLOOD ASSESSMENT USING MODELS

Following from Chapter 4 this chapter explores the effects of rainfall and subsequent flooding on the city using the SCS (1986) approach within the HEC-HMS (2002) modelling program (detailed in Appendix 5.1). Flood modelling is especially important in view of a changing global climate that might influence flood patterns in the region. The flood development of the study area is typical of summer episodic storms strong enough to produce inundation in many urbanized areas. These short-time storms may be of one-hour duration inversely associated with their frequency, intensity and duration. The 24HMR (=24 hour maximum rainfall is the most intense single rainfall event in any one 24-hour period for each year) during the period 1969-2007 is shown in Fig. 5.1 and recorded the maximum value in 1973 with 80.2 mm, instead of 1998 when 24HMR recorded was only 16 mm. Figs. 1.6 and 1.8 (Chapter 1) show the effects of the more recent flooding event occurred in June 2006 and the historic flooding events between 1827 and 2007 when the Bravo River moved from the Mexican to the American side in 1864 is reported in Figs. 1.9 and 1.10 of Chapter 1.

YEAR	24HMR (mm)	YEAR	24HMR (mm)	YEAR	24HMR (mm)	YEAR	24HMR (mm)
1969	22.80	1979	26.50	1989	37.30	1999	22.00
1970	36.20	1980	33.00	1990	62.00	2000	66.80
1971	55.50	1981	46.50	1991	40.00	2001	80.00
1972	41.90	1982	56.10	1992	44.00	2002	18.50
1973	80.20	1983	38.70	1993	27.40	2003	25.00
1974	52.70	1984	58.40	1994	NI	2004	28.00
1975	63.00	1985	30.50	1995	NI	2005	32.00
1976	51.10	1986	39.60	1996	24.00	2006	59.00
1977	28.70	1987	70.50	1997	19.00	2007	36.00
1978	62.50	1988	35.60	1998	16.00		

Figure 5.1. Historical rainfall of 24HMR for the study area from 1969-2007 (37 years of data. 24HMR = 24-hour maximum rainfall, and refers to the single largest event of rainfall over a 24-hour period each year). The Figure shows the year of the rainfall event (Cols.1, 3, 5 and 7) and intensity in mm (Cols. 2, 4, 6 and 8). Source: CNA (2007). These data are the basis of the flood modelling described in this Chapter.

5.2. HEC-HMS COMPUTER PROGRAM FOR FLOOD MODELLING AND HYDROGRAPHS

This method evaluates the water stored in control structures named dykes which were constructed to prevent inundation in the valleys and urbanized area of Juárez city. In addition, this program produces hydrographs which show peak discharge predicted for reaches, basins and sub-basins. However, due to incomplete rainfall records of Ciudad Juárez, it is necessary to use extreme event statistical methods applied to 24HMR data (See, Fig. 5.1 above). Since one hour is a more realistic assessment of the time for rainfall to develop into flooding in Juárez, it is further necessary to convert 24HMR data into one-hour data using other statistical methods. In the following paragraphs are presented in hierarchical order the sequence of assignments developed in order to assess the design hyetograph.

5.2.1 Rainfall data collection.

Fundamental information of historical 24 hours maximum rainfall (24 HMR) in the study area during the last 37 years was provided by the governmental offices of México (CNA, 2007). Fig. 5.1 suggests that the rainfall design of the study area is associated with events of high intensity and short duration. These events are produced by low-pressure systems derived from the convergence of cold and warm fronts causing convective storms (INEGI, 2002; NOAA, 1961 and NOAA, 2004).

5.2.2 Statistical approaches to assess the design hyetograph for 24 HMR.

The observed rainfall during the period analysed was used to estimate future rainfall and two widely used statistical approaches that fit with the rainfall behaviour observed in the study area were applied. These two PDFs (Probability Distribution Functions) are: **a)** Gumbel Extreme Value type 1 (GEV1) (See Appendix 5.2) and **b)** Log Pearson III (See Appendix 5.3 detailed results table). Both statistical approaches are applied in order to predict 24HMR (Ponce, 1994).

5.2.2.1 Gumbel EV1 Probability distribution function.

This approach is explained in details in Appendix 5.2 which contains a stage by stage procedure of the Gumbel EV1. Thus, in this chapter only the results are presented below (See Figs. 5.2, 5.3, 5.4 and 5.5)

Col. 1	Col. 2	Col. 3	Col. 4	Col. 5	Col. 6
Year	(24HMRmm)	(24HMRmm)	m	N+1	m/N+1=(1/Tr)=(Pe)
1969	22.80	80.20	1	38	0.026
1970	36.20	70.50	2	38	0.053
1971	55.50	66.80	3	38	0.079
1972	41.90	63.00	4	38	0.105
1973	80.20	62.50	5	38	0.132
1974	52.70	62.00	6	38	0.158
1975	63.00	59.00	7	38	0.184
1976	51.10	58.40	8	38	0.211
1977	28.70	56.10	9	38	0.237
1978	62.50	55.50	10	38	0.263
1979	26.50	52.70	11	38	0.289
1980	33.00	51.10	12	38	0.316
1981	46.50	46.50	13	38	0.342
1982	56.10	44.00	14	38	0.368
1983	38.70	41.90	15	38	0.395
1984	58.40	40.00	16	38	0.421
1985	30.50	39.60	17	38	0.447
1986	39.60	38.70	18	38	0.474
1987	70.50	37.30	19	38	0.500
1988	35.60	36.20	20	38	0.526
1989	37.30	36.00	21	38	0.553
1990	62.00	35.60	22	38	0.579
1991	40.00	33.00	23	38	0.605
1992	44.00	32.00	24	38	0.632
1993	27.40	30.50	25	38	0.658
1996	24.00	28.70	26	38	0.684
1997	19.00	28.00	27	38	0.711
1998	16.00	27.40	28	38	0.737
1999	22.00	26.50	29	38	0.763
2000	66.80	25.00	30	38	0.789
2001	18.00	24.00	31	38	0.816
2002	18.50	22.80	32	38	0.842
2003	25.00	22.00	33	38	0.868
2004	28.00	19.00	34	38	0.895
2005	32.00	18.50	35	38	0.921
2006	59.00	18.00	36	38	0.947
2007	36.00	16.00	37	38	0.974

Figure 5.2. Excedence probability (Pe) derived from the Gumbel Statistical approach (Col. 1, year of event; Col. 2, rain event recorded; Col. 3, rainfall event ordered from highest to lowest values; Col. 4, ranked number (m); Col. 5, number of events plus 1 (in this case it is 38); col. 6, formulae to evaluate (Pe) and Tr, return period of 24HMR.

A brief explanation of the parameters used in Fig. 5.3 is needed: The results of 24HMR predicted for different return periods using the Gumbel Extreme Value type 1 probability distribution function is illustrated by Ponce (1994, pp. 223, 224 and

225). Col. 1, return period (Tr) of the 24 HMR random variable equal to the inverse of (Pe); Col. 2, excedence probability (Pe), the values assumed for the Gumbel variate (y) are in function of Tr defined in Col. 1; Cols 3, 4 and 5 and are part of formulae (d) (given in appendix 5.2); Col 6, (K) is the value estimated for the Gumbel variate (y) that is explained in more detail after the table of Fig. 5-4. Col. 7 is the value predicted of the maximum rainfall event for 24 HMR and different return period given by: Rmax=Xm+K(s); where (Xm) and (s) are the mean and standard deviation value of the random variable 24HMR respectively (see appendix 5.2).

Col. 1	Col. 2	Col. 3	Col. 4	Col. 5	Col. 6	Col. 7
Tr	**P(e)**	**Tr/(Tr-1)**	**Ln(Tr/Tr-1)**	**(-LnLn(Tr/Tr-1))**	**K**	**Rmax (mm)**
1.05	0.95	21	3.0445	-1.1133	-1.4596	14.84
1.11	0.9	10	2.3116	-0.8379	-1.2168	19.14
1.25	0.8	5	1.6094	-0.4758	-0.8975	24.79
2	0.5	2	0.6931	0.3665	-0.1545	37.94
5	0.2	1.25	0.2231	1.4999	0.8449	55.63
10	0.1	1.11	0.1053	2.2503	1.5068	67.35
25	0.04	1.04	0.0408	3.1985	2.3430	82.15
50	0.02	1.02	0.0202	3.9019	2.9633	93.13
100	0.01	1.01	0.0100	4.6001	3.5791	104.03
200	0.005	1.00	0.0050	5.2958	4.1926	114.88

Figure 5.3. shows the results of 24HMR predicted for different return period using the Gumbel Extreme Value type 1 probability distribution function. In this table, Tr = return period, Pe = Probability of excedence for expected rainfall values, Rmax = maximum rainfall the meanings of Col.1 to Col.7 are explained in the upper paragraph. Source of calculation method: Ponce (1994).

In addition, Fig. A5.2.1 (Appendix 5.2), the values; Yn=0.5418 and σn=1.1339 for N = 37 were obtained. Additionally, a simple statistical evaluation of the mean value (Xm) and Standard Deviation (s) for the random variable (24HMR) listed in Col. 2 of Fig. 5.3 enable to evaluate the mean value Xm= 42.35 mm. and Standard Deviation s=17.152 mm. of the random variable (24HMR).

5.2.2.2 Log Pearson Type III Probability Distribution Function.

This statistical approach is similar to GEV1 and was applied in the present research for two reasons. Firstly, because it is widely used to simulate flooding in areas of

dendritic drainage with desert climatic conditions like that prevailed in the study area; and secondly it gives comparison, and helps to validate and reinforce the results from the Gumbel EV1 method. The results are shown in Fig. 5.4.

Col. 1	Col. 2	Col. 3	Col. 4	Col. 5
Return Period (Tr) in years	**P(exc) (%)**	**K**	**yi(LogR)**	**24HMR (mm)**
1.05	95	-1.596	1.2793	19.02
1.11	90	-1.2623	1.3404	21.89
1.25	80	-.8497	1.4159	26.06
2	50	-0.027	1.5664	36.84
5	20	0.832	1.7236	52.92
10	10	1.2975	1.8088	64.38
25	4	1.8059	1.9019	79.78
50	2	2.140	1.9630	91.83
100	1	2.4456	2.0189	104.44
200	0.5	2.7257	2.0702	117.54

Figure 5.4. Log Pearson III model prediction of 24HMR for different return periods. Similarly to Gumbel method Log Pearson Type III uses the reciprocal association between the return period (Tr) in years, of the random variable 24HMRand the probability of exceedence P(exc) of the random 24HMR variable both indicated in cols. 1 and 2. Col. 3 frequency factor (K). The Log Pearson III variate (formula 2) is applied and registered in col. 4. Finally, the results given in col. 5 for the random variable 24HMR for several return periods are obtained assessing the antilogarithms of col. 4.

The evaluation of 24HMR predicted using Log Pearson Type III Probability Distribution Function and is presented in appendix 5.3. Here, only the tabulated results are given in Fig. 5.5 below.

Log Pearson III Probability method considers a double logarithmic scale for the Probability Distribution Function (PDF) in function of the random variable P(24HMR) for each of the several probability levels P(j); P(24HMR)i...(1), col.7 of figure A5.3.1 Appendix 5.3. Also, use LogP(24HMR)=Ym+Kj*Sy (2) col. 4 Figure A5.3.1 appendix 5.3, where Kj, is the factor given in col. 3 of Figure A5.3.1 Appendix 5.3 in function of the probability Pj.

Summarizing, the process to address 24HMR requires six steps: Firstly, identify the annual P(exc) during the design period; Secondly, evaluate the Logarithms of the annual historical P(24HMR); Thirdly, calculate the mean (Ym),

Standard Deviation (Sy), Skew Coefficient (Cs) of the Logarithms (Yi); then, calculate the logarithms of P(24HMR) for each of the several probability levels (Pj); After that, calculate the P(24HMR) for each probability level (Pj); Then, the 24 hours maximum rainfall was obtained with the antilogarithm of Yi(log R) which is indicated in (Col 5 of Fig. A5.3.1 Appendix 5.3) Finally, in Fig. 5.5 is presented the graphic results of Log Pearson type III Distribution.

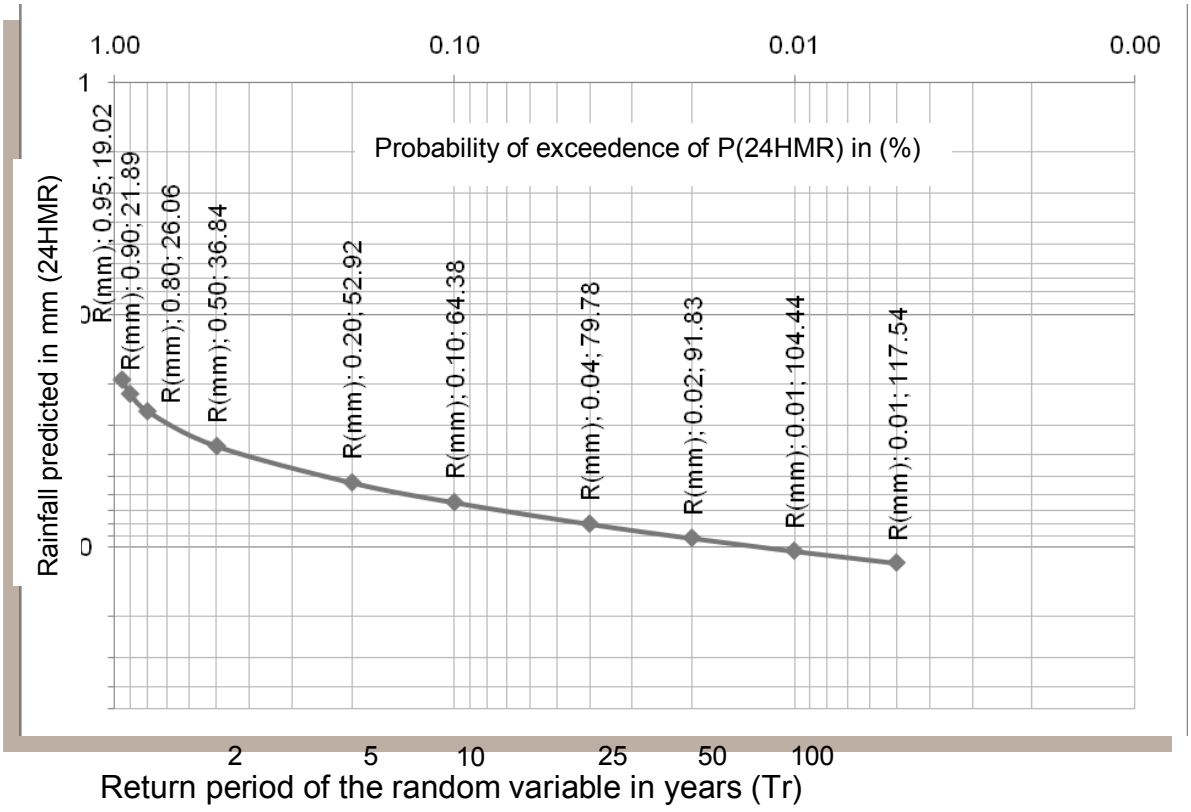

Figure 5.5. Graphic of Log Pearson Type III Probability Distribution Function (PDF) shows the results of the design rainfall (24HMR) for different return periods (Tr). The graphic is a double logarithmic scale; the Horizontal axis represent the probability of exceedence of the random variable (24HMR) as the reciprocal of the return period of random variable in terms of its frequency. In the vertical axis there are the rainfall design predicted of the random variable in (mm): Source of calculation method: Ponce (1994).

Conclusion: Both approaches (Gumbel and Log Pearson III) predict similar values for 24HMR. GEV1 gives: 14.84 mm, 19.14 mm, 24.79 mm, 37.94 mm, 55.5 mm, 67.35 mm, 82.15 mm, 93.13 mm, 104.13 mm and 114.88 mm. Log Pearson Type III PDF predicts; 19.02 mm; 21.89 mm; 26.02 mm; 36.84 mm; 52.92 mm; 64.38 mm; 79.78 mm; 91.83 mm; 104.44 mm and 117.54 mm which are similar and help to

verify the method. A comprehensive analysis of the previous data suggests that Log Pearson Type III PDF predicts higher values for; 1.05 year, 1.11 year, 1.25 years of return periods (Tr) instead, for 2, 5, 10, 25 and 50 years values of GEV1 are highest. However, for 100 and 1000 years of Tr, Log Pearson Type III PDF again predicts higher values than GEV1.

5.2.2.3 Design storm for the study area using Cheng-Lung-Chen approach.

After assessing the 24HMR data, another probabilistic approach is used to extend the predictions into a design (=modelled) storm that would be applied to build the hyetograph in an appropriate timescale required for the study area. Studies performed by Cheng (1983) contain statistical approaches for design rainfall formulae for many countries of the United States including Arizona, New Mexico and El Paso Texas. El Paso Texas and Juárez city have practically the same climatic and regional conditions (see appendix 5.3A), Results derived from Cheng (1983) approach for three different return periods: 10 years, 50 years and 100 years were obtained: 37 mm; 50.5 mm and 55.5 mm respectively.

$R_1^{10} = (0.35 \times \mathrm{Ln}(T_r) + 0.76) \times (0.54 \times (t)^{0.25} - 0.50) \times (R_1^2) = 37.0$ mm; (Bell 1969)

$R_1^{50} = a_* R_1^{10} \mathrm{Log}(10^{2-f} \times T^{f-1})/(t+d)^n = 50.5$ mm; (Cheng 1983)

$R_1^{100} = a_* R_1^{10} \mathrm{Log}(10^{2-f} \times T^{f-1})/(t+d)^n = 55.5$mm; (Cheng 1983)

5.2.2.4 Hyetograph for the study area.

Hyetograph is the graphic representation of the design storm. The vertical (y) axis shows rainfall in mm and the horizontal (x) axis represents the rain time interval in min on the horizontal axis. In gauged areas this information comes from existing stations that record the rainfall variation over specific period of time. In these conditions the hyetograph is constructed directly. However, in the study area, information for the historic rainfall design was recorded for 24hour duration and the storm design for 1 hour was derived using Cheng (1983) without temporal variation during one day as well as during an hour. For this reason, the hyetograph built is synthetically and suggests a distribution with intervals of time of 5 min and rainfall

depth variation in the rising limb increments of 1 mm to 3 mm approximately and in the recessing limb descending decrements were of 1mm to 3 mm. The maximum value was located in the middle with 10 mm adopting a bell shape. In short, this un-gauged hyetograph (See Fig. 5.6) is entirely hypothetical. On the other hand, the time distribution of the storm occurrence is irrelevant and was considered from 3:00 PM to 4:00 PM because this was the date of the storm event recorded in the study area in June 2006.

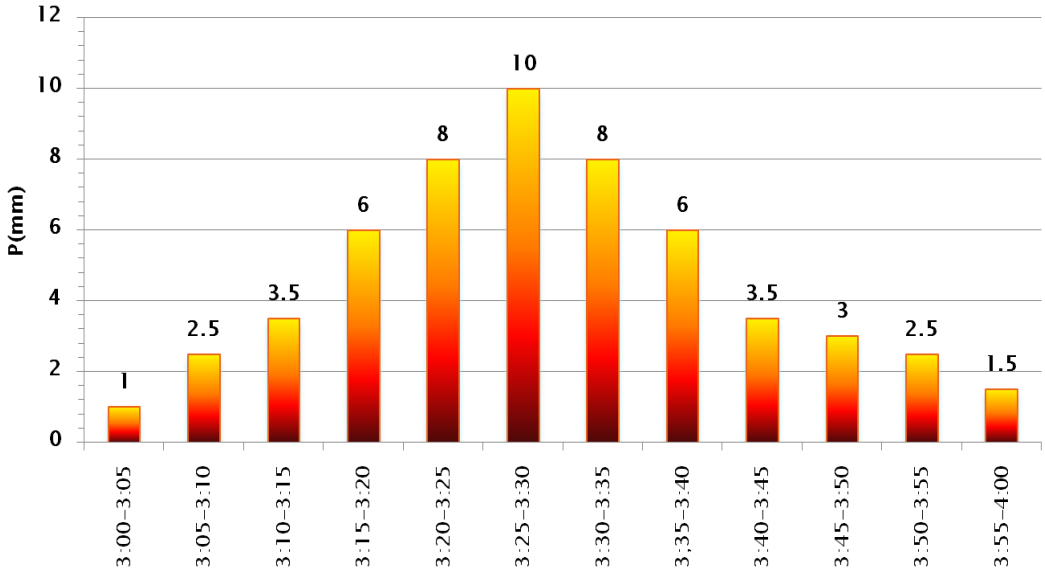

Figure 5.6 Hyetogram for the study area that shows the depth-rainfall-duration occurred for a recurrence interval of 100 years that corresponds to the design storm. Source of calculation method to produce this graph: Cheng (1983).

5.3 HYDROGRAPH DEVELOPMENT USING THE CN METHOD OF SCS (1986)

Once the design hyetograph of Fig. 5.6 has been constructed then the hydrographs are assessed. Appendix 5.4 explains the CN method in a general context and the results are presented in Appendix 5.4.2 to 5.4.9. In addition, the methods chapter also details methodology to assess the parameter named Curve Number (CN) described by the Soils Conservation Service of the USA (SCS 1986) is a key feature and was used for two reasons: firstly, this method is widely used in some areas of the United States as Arizona, New México, and Texas along with others; and secondly it has proved its ability to simulate flooding in urbanized areas

as well as in diverse land-use environments (See Appendix 5.4 and Fig. Fig. A5.4.1A).

5.3.1 (CN) Method description. This section is explained in Appendix 5.4 and describes the methodology involved in the method. This is an empirical method that was derived from the simulation of many land-use terrains and soil types against a predicted runoff (See Appendix 5.4; Fig. Fig. A5.4.1A).

5.3.2 Basin and sub-basins Location and CN parameters determination

The study area consists of 8 basins named as: Jarudo, Anapra, Center, Airport, Barreal, Bravo River, Acequias and Chamizal. To define the watershed divide of these basins and sub-basins, the use of contour levels every 5m was made; satellite images of the study area as well the use of Auto-Cad and Arc-Map computers programs were applied (Fig. 5.7).

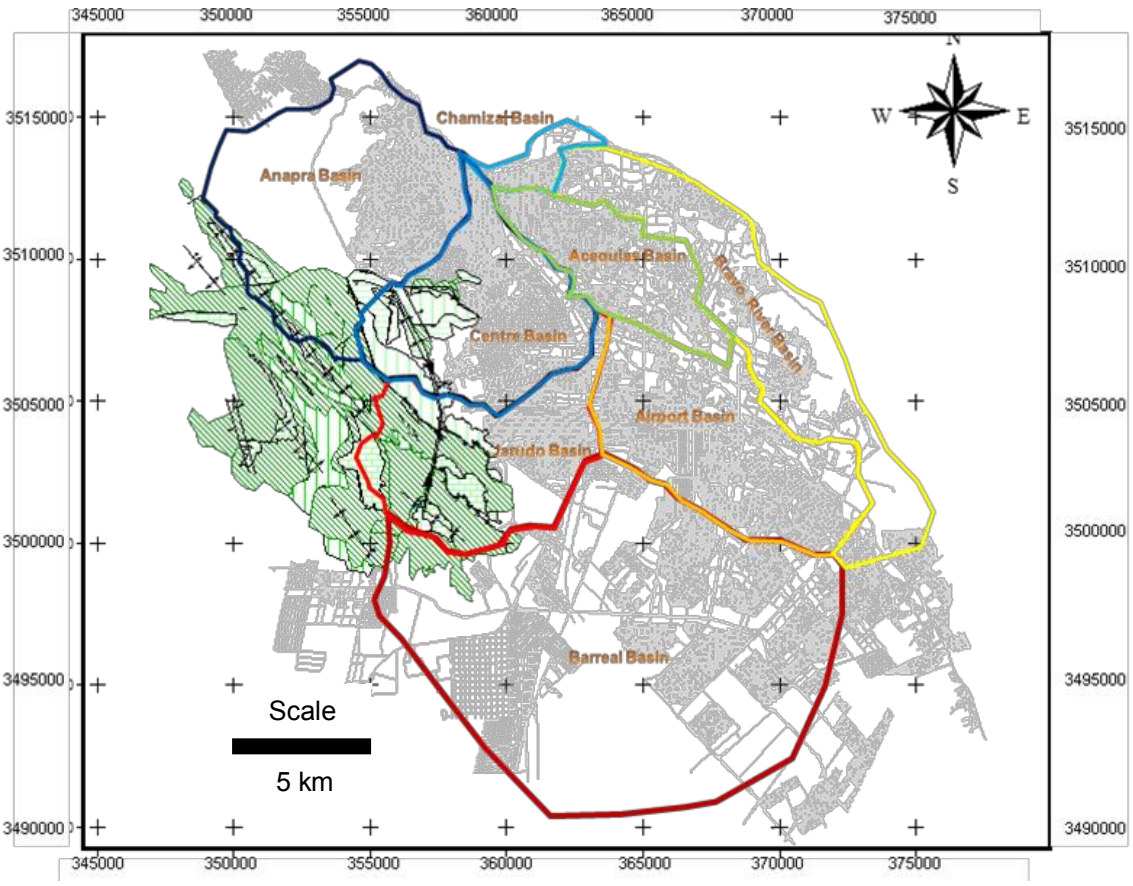

Figure 5.7. General map of study area showing locations of the eight basins defined to flood modelling, and described in the sections below. This map was created using Arc-Map 9.2 (2011); Auto-Cad (2009) and satellite images provided by IMIP (2007).

Basins and sub basins in the study area are presented in sections 5.3.2.1 to 5.3.2.8 detailing the connection between their hydraulic components as: streams, reaches, joints, dykes and Bravo River. Furthermore, the water stored in retention basins behind dykes during the flooding hazard event is compared with storage capacity in order to evaluate their behaviour.

5.3.2.1 Jarudo sub-basin location and network distribution description.

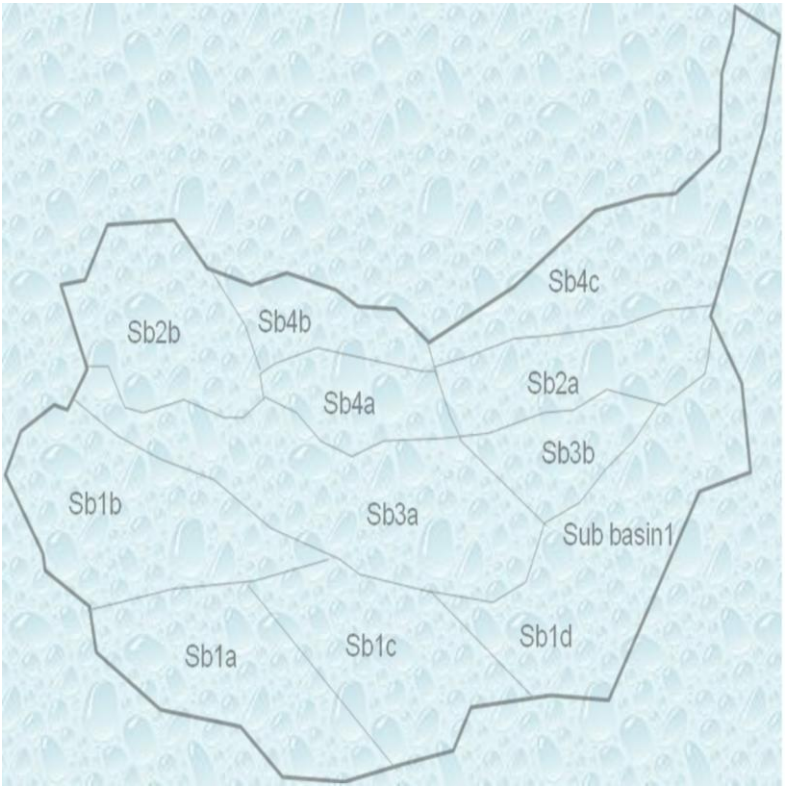

Figure 5.8. shows the distribution of sub-basins within Jarudo Basin. Width of basin at its widest point is 5.15 km.

The main components and hydraulic structures of Jarudo Basin are twelve sub-basins, ten convergence points, eight reaches and nine dykes (see Figs. 5.8 and 5.11). Basically, the main driver is the Jarudo stream that begins in Sub-basin 1a with a stored water volume of 161,400 m^3; this sub basin discharges into DP1 dyke (see Figs. 5.9 and 5.10). This dyke has a storage capacity of 40,000 m^3 (see Fig. 5.11) then a deficit of 121,400 m^3 suggests bad behaviour (Fig. 5.11). This volume DP1 (121,400 m^3) is joined with Sub-basin 1b (150,000 m^3, see Fig. 5.9) and runs downstream to discharge into dyke (DP2=271,400 m^3). Therefore, DP2 with a

storage capacity of 10,000 m^3 (Fig. 5.11) has a bad behaviour with a deficit of 261,400 m^3 (Fig. 5.9 and 5.11). In addition, two sub-basins Sb1c and Sb1d with volume of 39,200 m^3 and 52,700 m^3 (Fig. 5.9) gives a total of 91,900 m^3 drained downstream. Then, a total of 353,300 m3 of water would spill over to dyke DOR (=353,300 m^3), which suggests a bad behaviour because of its storage capacity of 260,000 m^3 (see Fig. 5.11). Similarly, three streams tributaries of Jarudo stream are connected to it. Firstly, three sub-basins (2a, 2b, and 3b) with 45,100 m^3, 96,700 m^3, 50,000 m^3 respectively are joined (Figs. 5.9 and 5.10). The highest sub-basin 2a discharges into the dyke DCM with storage capacity of 3,600 m^3, it exhibits bad behaviour because of a deficit of 41,500 m^3 (Fig. 5.11). A total volume of 188,200 m^3 is accumulated in junction JDORSOR; this volume drains to dyke SD with storage capacity of 150,000 m^3 (Figs. 5.9; 5.10 and 5.11), a deficit of 38,200 m^3 that suggests bad behaviour. The other two tributaries of the Jarudo basin have three dykes named CD, GD, and RD have storage capacity of 90,000 m^3, 0 m^3 (see below) and 150,000 m^3 respectively (Fig. 5.11). Sub-basin 3a with 268,100 m^3 drains to CD dyke so it has a deficit of 178,100 m^3 (Figs. 5.9, 5.10 and 5.11). This volume and the volume of sub-basin 1 (231,600 m^3) give a total volume of 409,700 m^3 and would be drained until junction JCB (See Fig. 5.10). Sub-basin 4a with volume 87,400 m^3 drains to dyke GD that has NO storage capacity because the water invaded homes and all the water drained by sub-basin 4a is distributed over the streets (deficit = 87,400 m^3 (see Fig. 5.11). Sub-basin 4b drains 185,300 m^3 into RD dyke which has a storage capacity of 150,000 m^3 so this dyke has a deficit of 35,300 m^3 (Figs. 5.9, 5.10 and 5.11) that suggest bad behaviour. Finally, Sub-basin 4c drains 112,700 m^3 and together with the 35,300 m^3 overspill from dyke RD discharges a total of 148,000 m^3 into dyke TCD with storage capacity of 2000 m^3; a deficit of 146,000 m^3 is evidence of inadequate behaviour. In brief it is clear that only one structure showed good behaviour.

5.3.2.1.1 (CN) Curve Number coefficient determination method for Jarudo basin

The CN parameter was estimated using values given in Fig. A5.4.1A of Appendix 5.4. The terms involved as well the process to obtain the CN coefficients are explained in Appendix 5.4. The first part in the process is to divide the sub-basin into

homogeneous areas with similar land-use. After that, using the table given in Fig. 1, and data in Appendix 5.4 the CN parameters were addressed.

5.3.2.1.2 Concentration time and Lag-time evaluation for Jarudo basin.

Concentration time and Lag-time are fundamental features which were evaluated using Kiprich's equation: $T= 0.000325[L/Ss^{0.5}]^{0.77}$; Tc=concentration time in hours; L=length of the stream in meters; Ss=gradient of the main stream. Main stream length was evaluated with Auto-Cad and Arc-Map programs. Physiographic and hydrologic parameters are: A (area); Is (Impervious surface); Ia (Initial abstraction) are parameters also needed for HEC-HMS flooding simulation.

5.3.2.1.3 Peak discharge and water storage using HEC-HMS for Jarudo basin.

HEC-HMS method was used for peak discharge and water volume calculation (Figs. 5.10 and 5.11) shown the volume of water stored and peak discharge for the different sub-basins within the Jarudo basin. The stored volume of water in m^3 is assessed by simple multiply the area of the sub-basin in m^2 by the direct runoff (Q) in meters that is given for the CN of SCS (1986) unit hydrograph. The following formula complement the explanation of this method.

$Q = (P-I_a)^2 /(P-I_a) +S = (P-0.2S)^2/(P+0.8S)$.....a

Where: Q= volume of accumulated runoff (mm)

P = accumulated rainfall (Potential maximum rainfall) (mm)

S= Potential maximum retention of rainfall in the watershed at the beginning of the storm (in mm) which depends on soil and watershed cover conditions. In theory its values vary between (0-100) but for practical reasons values they are 98 (paved areas) and 68 (unpaved areas) are adopted, defined by formula (b):

$S = (2540-254*CN)/CN$.....b

I_a=Initial abstraction including surface storage interception and evaporation (in mm) is highly variable, but generally is correlated with soil and cover parameters. Through the study of many small agricultural watersheds, Ia was found to be approximately (I_a=0.2S).

Fig. 5.9. below summarizes the peak discharge (PD) and stored water (SW) for sub basins of the Jarudo basin.

Sub-basin	Sb4a	Sb4b	Sb4c	Sb3a	Sub-basin-1	Sb2a	Sb2b
P.D (m^3s^{-1})	43.1	78.5	35	103.4	32.9	14.9	26.7
SV (m^3)	87,400	185,300	112,700	268,100	231,600	45,100	96,700
Sub-basin	**Sb3b**	**Sb1a**	**Sb1b**	**Sb1c**	**Sb1d**		
P.D (m^3s^{-1})	16.9	29.5	35.0	13.9	8.1		
SV (m^3)	50,000	161,400	150,000	39,200	52,700		

Figure 5.9. Peak discharge (PD) and stored water (SW) for sub-basins in the Jarudo basin. The results indicated were derived by the HEC-HMS programme. Following the methodology previously described. Source of the method: SCS (1986) in HEC-HMS flooding simulation.

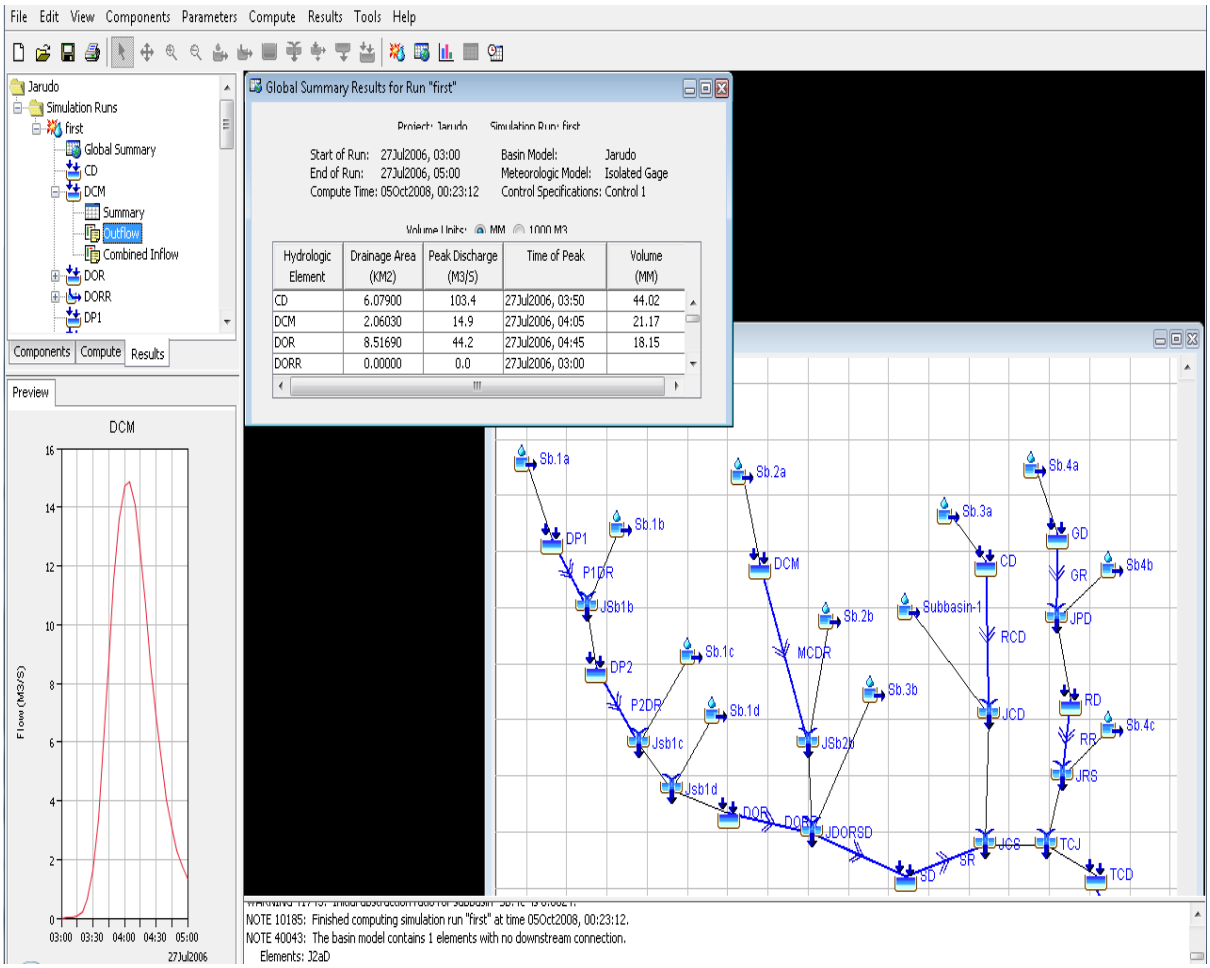

Figure 5.10. HEC-HMS simulation flooding hazard model components for the Jarudo basin. Source of the method: HEC-HMS (2002; version 3.1.0 Army Corps of Engineers of Texas).

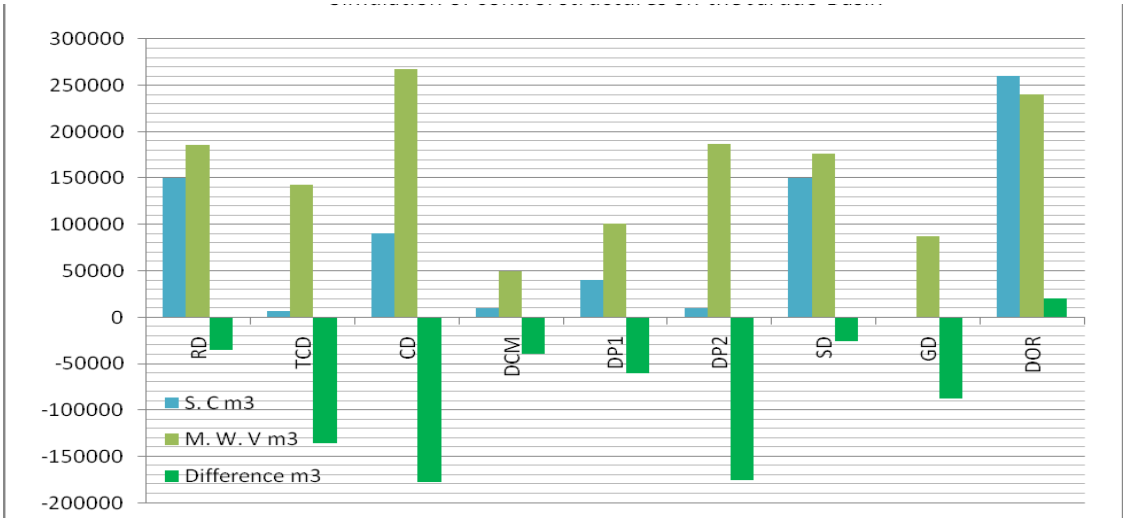

Figure 5.11. Twelve structures with storage capacity (S.C.) versus HEC-HMS simulation flooding water volume (M.W.V.) for Jarudo basin. Negative bars indicate the part of the basin where dykes are expected to fail during flooding events. Abbreviations are given in the text**.** Source of data for calculations: IMIP (2005)

5.3.2.2 Anapra basin network distribution and description.

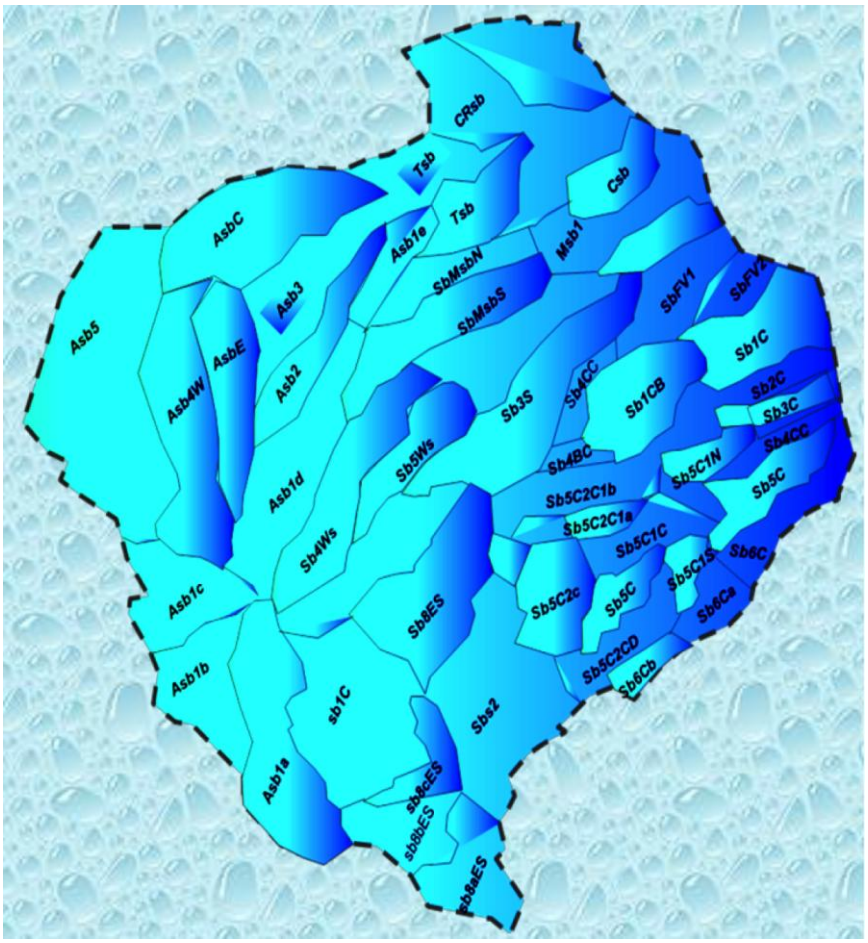

Figure 5.12. Anapra sub basin distribution. Width of basin at its widest point is 10.1 km.

5.3.2.2.1 Description of Anapra drainage system.

Anapra Basin geographic location is shown in Fig. 5.7 and is located mostly over alluvial fans; it has an area of 70.33 km^2 and formed by 60 sub-basins, 27 control regulation structures and 18 dykes (see Figs. 5.13, 5.14 and 5.15).

5.3.2.2.2 Ladrillera Stream Sub-basin (LSb). This sub-basin is located in the northern part of the city (Fig. 5.12) and discharges 35,300 m^3 directly to two 1.35 m by 1.25 m floodgates of the Bravo River (SBR1). These floodgates, with 0.72 m^3/sec of capacity are working unsatisfactorily. For this reason, sediments accumulate in the lowest areas.

5.3.2.2.3 El Tapo stream sub-basin (LSb) (Figs 5.12 and 5.14) show that this sub-basin is drained by El Tapo stream and is divided into two sectors by the Benito Juarez dyke (Figs 5.13 and 5.14): Firstly, in the upper part, there are two tributaries. One, begins with sub-basins AsbE (47,000 m^3) and Asb4W (44,700 m^3) (Figs. 5.13 and 5.14) which are joined in Junction 2; then, using Reach 3, continues until Junction 4. At this point, AsbC (49,600 m^3) is joined. All the water concentrated in Junction 4 is collected by the Benito Juarez Dyke. Then, another Sub-basin Asb5 (89,800 m^3) is joined (Figs. 5.13 and 5.14). Moreover, the east tributaries which originate in the upper mountains: Asb1a (43,700 m^3), Asb1b (26,900 m^3) and Asb1c (24,600 m^3) are joined at Junction 1 and then transited through Reach 1 until Junction 3 where Asb1d (41,300 m^3) is joined (Figs 5. 13 and 5.14). Then, water is conducted through Reach 2 until the Dyke, where, sub-basins Asb2 (32,500 m^3), Asb3 (31,700 m^3) and Asb1e (12,500 m^3) drain downwards until the Dyke. As a result, a total volume of 443,800 m^3 is drained by these eleven sub-basins associated with the Dyke called Benito Juarez dam (See Figs. 5.13; 5.14 and 5.15). Therefore, this dyke with storage capacity of 1 Mm^3 (IMIP 2005) is working at 44.4 % of its capacity (Fig. 5.15). Furthermore, the lowest part of this basin is driven by El Tapo stream that connects the dyke through Reach el Tapo formed by two sub-basins CRSb (37,800 m^3) joined in Junction 5. Another reach, Del Tapo and another joint Del Tapo 2, is incorporated. At this point, the sub-basin Tsb (31,400 m^3) is connected (Figs. 5.13 and 5.14). This lower part drains 69,200 m^3 directly to the Bravo River discharging through two floodgates 3 and 4 (1.35 m by 1.25 m each one) with total capacity of 0.72 m^3/sec (See Fig. 5.36). The high gradient of this stream (average 3.3%) provokes important sediment transportation and deposition that during rainfall season; people who live around this sub-basin are affected.

5.3.2.2.4 Cocotla stream Sub-basin CSb. This isolated stream (Fig. 5.12) drains 51,500 m^3 directly to the Bravo River CSb (Figs. 5.13 and 5.14) using two floodgates of 1.35 m by 1.25 m each one named 5 and 6 with capacity of 0.72 m^3/sec (See Fig. 5.36). Felipe Angeles Neighbourhood is the more important community affected during flooding because the inadequate design of the floodgate system.

5.3.2.2.5 The Mimbres Sub-basin stream. This stream is the main driver (See Figs. 5.12 and 5.14) and during rainfall season works like stream and the rest of the year works like a street. It is completely paved and has a gradient of 2.5 %. There is only one regulation control structure (Tabaco Dyke) located in Navojoa street between Tonala and Juchitan streets. The characteristics of this dyke are: Storage Capacity 9,000 m^3 (Fig. 5.14), curtain length 94 m, curtain height 4.7 m. (IMIP 2005).

5.3.2.2.5a Mimbres Sub-basin stream tributary north (SbMbN). It is northern to SbMsbS (Fig. 5.12) and discharges 30,900 m^3 (Fig. 5.13) directly to The Tabaco Dyke that has storage capacity of 9,000 m^3 (IMIP 2005) (Figs. 5.14 and 5.15). Thus, this control structure overspill 21,900 m^3 and does not work satisfactorily. The connection of this dyke with the rest of the sub-basin is through a natural reach Reach 2M and a convergence in 1M (Figs. 5.12; 5.13; 5.14 and 5.15).

5.3.2.2.5b Mimbres Sub-basin stream tributary south SbMsbS *(Fig. 5.12)*. It is located above the Tabaco Dyke and drains 71,500 m^3. This volume will be added downstream until the Bravo River through the Junction 1M, where sub-basin SbMsbN drains 21,900 m^3 is joined. Therefore, a total volume of 93400 m^3 is transited trough a natural reach R1M and finally connected to the Bravo River (Figs. 5.12 and 5.14).

5.3.2.2.5c Mimbres sub-basin stream Msb1 (Fig. 5.12). It is located in the lowest part of the basin and discharges 93,200 m^3 to the Bravo River RBS. This volume drains to Bravo River trough three floodgates of 1.35 m by 1.35 m each one (7, 8 and 9) the gates capacity is 1.08 m^3/sec (Figs. 5.12; 5.14 and 5.36).

5.3.2.2.6 Snake Stream sub-basin (Fig. 5.12) this sub basin is divided into two sub-basins: Snake West and Snake East and is originated in the highest Juarez mountains ending on the Bravo River. One, west Sub-basin Sb4WS drains 50,000 m^3 through Pico de Aguila Dyke (DPA=storage capacity 150,000 m^3 (IMIP 2005)). Thus, the dyke exhibits good behaviour (See Fig. 5.15). After that, water drains downwards through natural reach RSa and convergence point J5S. The east sub-basin Sb5WS drains 18,100 m^3 to Puerto la Paz Dyke (DPLP) which has a storage

capacity of 50,000 m^3 (IMIP 2005) and also works satisfactorily (Fig. 5.15). Then it is connected downward through a natural reach Rsa and a convergence point J3S (Figs. 5.13 and 5.14). Additionally, in the lowest part of the West Snake stream, there are two sub-basins named Sb3S *(63,200 m^3) and SbS2* (54,400 m^3) which are connected through junction J3S. Finally, the sub-basin SbS1 (32,700 m^3) is connected to the Bravo River in SV (150,300 m^3). As a result, the Bravo river in SV is 150,300 m^3 (Figs. 5.12; 5.13 and 5.14).

5.3.2.2.7 Sub-basin named Francisco Villa stream SbFV2 *(Fig. 5.12)*. This basin drains a volume (38,400 m^3) and is stored in depressive areas like natural dykes the remained produces inundation problems in the surrounded areas (Jc19). Moreover, sub basin SbFV1 discharges 49,300 m^3 and drains its water until Acequia Madre that also is distributed in the adjacent topographical depressions finally its discharges in junction Jc17 (Figs. 5.12; 5.13 and 5.14).

5.3.2.2.8 Sub-basin east branch of Snakes stream *(Fig. 5.12)*. This basin originates in the highest Juárez mountains beginning with three sub-basins; Sb8aES (22,000 m^3), Sb8bES (18,000 m^3) and Sb8cES (11,200 m^3). These three sub-basins are joined in junction J4S through a natural reach RS1. Then, a sub-basin named Sb8ES (54,600 m^3) is connected to Gasera Dyke (GD). This dyke receives a volume of 105,800 m^3 and because it has 150,000 m^3 of storage capacity (See Fig. 5.14) (IMIP 2005) its behaviour is good. Moreover, the GD dyke is joined to Fronteriza dyke DF through natural reach RS2, convergence point J2S and natural reach RDF. The Fronteriza dyke recently was converted into an energy releaser structure (Figs. 5.12, 5.13; 5.14 and 5.36). There is another tributary stream Sb3V1 that drains 6,600 m^3 to Jazou Dyke DJ as well as Sub-Station dyke DSE using R2c natural reach, convergence point (Jc16) and natural reach Rc7. Also, at convergence point Jc16, there are connected three sub-basins Sb1CC (85,800 m^3), R4C (9700 m^3) and Sb1CB (81,800 $m^{3`}$). These three sub-basins drain to convergence point Jc16 where another sub-basin is connected Sb1C with (83,300 m^3). Finally, these sub basins are drained until the Acequia Madre convergence point Jc15 that receives 260,600 m^3 of water (Figs. 5.12, 5.13 and 5.14). The dyke's behaviour is described in the following paragraphs. Firstly, the storage capacity of Gasera Dyke DG is 150,000 m^3 (IMIP

2005) and the predicted volume was 105,800 m^3. Thus, this dyke is working to 70.5 % of its capacity (Fig. 5.14). The Jazou Dyke DJ has 7,000 m^3 of storage capacity (Fig. 5.15) (IMIP 2005). It has an estimated flooding 6,600 m^3 and will be working at 94.2 % of its capacity (Fig. 5.15). The Sub-Station Dyke DSE has a 1,000 m^3 storage capacity (Fig. 5.15) (IMIP 2005) represents an auxiliary support to Jazou dyke due that both dykes are in the same sub-basin (Figs. 5.12, 5.14 and 5.15).

5.3.2.2.9 Sub-basin stream Mezquite Sb3C. This isolated sub-basin drains a total volume of 19,500 m^3 directly to the Bravo River and it is represented in the HEC-HMS model by (Jc13) (Figs. 5.12, 5.13 and 5.14).

5.3.2.2.10 Sub-basin Altavista stream Sb2C. Drains 38,800 m^3 and drains directly to the Bravo River (Figs. 5.12, 5.13 and 5.14). This sub-basin has two regulation control dykes (Acacias) and (Gardenias) located in Acacias and Datileras streets respectively. However, these dykes are completely invaded and their storage capacity is insignificant and does not contribute in any form to regulate the flooding events. Water spilling over the surrounded area of this sub-basin produces sediment accumulation during flooding events. This sub-basin discharges in the Bravo River at Jc14. Sub basin named Sb4BC drains a volume of 30,000 m^3 to Jesus Garcia Dyke DJG through a convergence point Jc10 following its course through a natural reach RC10 until convergence point Jc11. After that, Sb4ACOL drains 19,000 m^3 to Dyke Balderas DB then, the stream continues downwards through a natural reach R9C until convergence point Jc11. At this joint, another sub-basin is connected, Sb4CC draining 26,000 m^3. Finally a volume of 75,000 m^3 will follow until convergence point Jc12 and incorporates to the Bravo River using the Viaduct named Gustavo Diaz Ordaz (Figs. 5.12, 5.13, 514 and 5.15). Balderas Dyke DB with 8,000 m^3 of storage capacity (Fig. 5.15) (IMIP 2005) will receive a volume of 19,000 m^3 (237.5% of its capacity) there is a deficit of 11,000 m^3. Similarly, Jesus Garcia Dike DJG with a storage capacity of 2,000 m^3 (IMIP 2005) will receive 30,000 m^3 (1500% of its capacity) (Fig. 5.15) so there is an excess of 28,000 m^3. The other sub-basin Sb4CC with volume of 26,000 m^3 is joined with the volume produced by over-spilling dykes, given a total volume of 65,000 m^3 drained until junction Jc12 (Figs. 5.12, 5.13. 5.14 and 5.15).

5.3.2.2.12. Sub-basins located on the upper level which connect directly to joint (Jc8) are: Firstly, Sb5C2C1b (42,300 m^3) and Sb5C2C1a (15,000 m^3) (Figs. 5.13 and 514). Secondly, the intermediate sub-basins that connect with convergence point (Jc8) but have an intermediate control structure dyke are: Sb7C (1600 m^3) the Nueva Zelanda Dyke DNZ 15,000 m^3 storage capacity (IMIP 2005) will be worked appropriately (10.6% of its capacity) (Fig. 5.15). This volume is controlled by this dyke that is linked in Jc8 and R16c. Sub-basin 5b5C2C (38,700 m^3) (Figs. 5.13 and 5.14) drains to Guadalajara Izquierda dyke DGI through convergence point Jc6. The dyke DGI has a storage capacity of 60,000 m^3 (IMIP 2005) greater to the predicted flooding hazard event (38,700 m^3), thus would worked at 64.5% of its capacity) (Fig. 5.15). This dyke is connected by Jc8 through a natural reach rc15. Sub-basin 5b5C2Ca (35,800 m^3) discharges in Hawaii Dyke DH, storage capacity 12,000 m^3 (IMIP 2005). As can be see this dyke does not have enough storage capacity and will overspill a volume of 23,800 m^3 (298.3% of its capacity) (See Fig. 5.15). Water excess will drain until convergence point Jc8 through a natural reach R13C. Sub-basin Sb5C2C1 (27,100 m^3) (Figs. 5.13 and 5.14) will discharge in Cozumel Dyke DC storage capacity 2,000 m^3 (Fig. 5.15) (IMIP 2005) less than the predicted volume (1,355% of its capacity) then, this dyke would overspill 25,100 m^3 to convergence point Jc8 using a natural reach R19C (Figs. 5.13 and 5.14). Water volume accumulated in this upper platform derived from the dykes' over-spilling of Hawaii DH and Cozumel DC is 48,900 m^3 excess joining on convergence point (Jc8). This volume is added to 57,300 m^3 derived from Sb5C2C1a and Sb5C2C1b sub-basins given a total volume of 106,200 m^3 accumulated convergence point (Jc8) (Figs. 5.12, 5.13, 5.14 and 5.15).

5.3.2.2.13. The intermediate level has three sub-basins connected directly to convergence point. Jc5: SB5C1N (7,800 m^3), Sb5C1C (8,800 m^3) and Sb5C1S (9,100 m^3) (Figs. 5.12; 5.13 and 5.14). In addition, there are two branches each one with one control structure. One is a west tributary of Colorado stream drains Sb8C (6,100 m3), this sub-basin drains to Caballerizas Dyke DCAB with 3,000 m^3 storage capacity (IMIP 2005). It is clear that this dyke would not work appropriately (203% of its capacity) and will have an excess of 3,100 m^3 during the flooding hazard event.

This sub-basin is connected to convergence point Jc5 through R17C ending in convergence point Jc9 (Figs. 5.13, 5.13 and 5.14).

5.3.2.2.14. The East branch of this sector represented by Sb5C2CD (40,300 m^3) (Figs. 5.13 and 5.14) is connected to Tarahumaras dyke DTa and has 8,000 m^3 storage capacity (IMIP 2005) which represents (503.7% of its capacity) (Fig. 5.15). Thus, there is predicted to be overspill of 32,300 m^3 during a flooding event. These sub-basins are joined in convergence point Jc5 through reach Rc12 (Figs. 5.13, and 5.14).

5.3.2.2.15. The lower Colorado Stream has only one sub-basin connected directly to Junction Jc7 Sb5C1I (55,800 m^3) (Figs. 5.13 and 5.14). Thus, water volume accumulated in Jc7 is 140,100 m^3 derived for three sub-basins connected directly. In addition the volume derived from dykes over-spilling in the upper platform DH and DC 48,600 m^3 and the intermediate platform over-spilling dyke DCAB 3,100 m^3 and DTa 32,300 m^3 gives a total accumulated overspilling in convergence point Jc7 of 224,100 m^3 (Figs. 5.13, 5.14 and 5.15).

5.3.2.2.16 Luis Echeverria and Francisco Covarrubias neighbourhoods is composed of four sub-basins, two control structures (dykes) and four junctions. The sub-basins are; Sb6ColB which drains 8,000 m^3 into Ecatepec dyke (DEcat) with 3,000 m^3 storage capacity (IMIP 2005) would operate at 267% of its capacity during a flooding hazard event and would be over-spilled by 5,000 m^3 (Fig. 5.15). Then a natural reach Rc11 Tiradores del Norte stream would transport this volume until convergence point Jc3 (Figs. 5.12; 5.13 and 5.14).

5.3.2.2.17 Sub-basin Sb6Cb. This sub-basin discharges 4,000 m^3 directly to convergence point Jc1 through a tributary of Tiradores del Norte stream (Figs. 5.13 and 5.14).

5.3.2.2.18 Sub-basin Sb6Ca. This sub-basin drains 5,200 m^3 to dyke Covarrubias (DCov) with storage capacity 5,000 m^3 (IMIP 2005). Therefore, this dyke would work at 104 % of its capacity (Fig. 5.15). Thus, 200 m^3 of excess of water would overspill

during the flooding hazard event. Finally, this volume is drained to (Jc2) along a natural reach Tiradores del Norte Stream RC10 (Figs. 5.13 and 5.14).

5.3.2.2.19 Sub-basin Sb6C. Discharges 56,600 m^3 of water through convergence point Jc2 using Tiradores del Norte Stream (Figs. 5.13 and 5.14).

5.3.2.3. (CN) Curve Number coefficient of Anapra basin (see Appendix 5.4.2)

Information for this is provided in Appendix 5.4.2.

5.3.2.4 Concentration time and Lag-time of Anapra basin. (See appendix 5.4.*2*)

Information for this is provided in Appendix 5.4.2.

5.3.2.5. Peak discharge and store water using HEC-HMS for Anapra basin

HEC-HMS programme were applied using the CN method defined by SCS (1986) to evaluate peak discharge and water store volume for the flooding hazard event. Figs. 5.14 and 5.15 show the volume of water stored as well as peak discharge for different sub-basins within the Jarudo basin and Fig. 5.13 shows the sub basin distributions. The volume of water stored (in m^3) was assessed by simple multiply the area of the sub-basin (in m^2) by the direct runoff (Pe) in (mm) that is given for the CN of SCS (1986) unit hydrograph.

Sub-basin	Asb1a	Asb1b	Asb1c	Asb1d	ASb1e	ASb2	Asb3	Asb4W	R4c
P.D (m^3s^{-1})	13.6	8.4	7.6	12.6	3.9	10.1	12.1	17.1	4.1
SV (m^3)	43,700	26,900	24,600	41,300	12,500	32,500	31,700	44,700	9,700
Sub-basin	Asb5	AsbC	AsbE	CRSb	CSb	LSb	Msb1		
P.D (m^3s^{-1})	34.4	19.0	17.3	16.7	22.5	15.6	31.7		
S V (m^3)	89,800	49,600	47,000	37,800	51,500	35,300	93,200		
Sub-basin	Sb1C	Sb1CB	Sb1CC	Sb2C	Sb3C	Sb3S	Sb3V1		
P.D (m^3s^{-1})	34.2	34.3	28.3	15.9	8.0	17.8	3.5		
SV (m^3)	83,300	81,800	85,800	38,800	19,500	63,200	6,600		
Sub-basin	Sb4ACOL	Sb4BC	Sb4CC	Sb4WS	Sb5C1I	Sb5C1C	Sb5C1N		
P.D (m^3s^{-1})	7.8	11.2	11.4	14.2	18.4	3.8	3.7		
SV (m^3)	9,000	30,000	26,000	50,000	55,800	8,800	7,800		
Sub-basin	Sb5C1S	Sb5C2C1a	Sb5C2C1b	Sb5C2Ca	Sb5C2CD	Sb5C2CI			
P.D (m^3s^{-1})	3.7	6.5	17.4	14.8	16.6	12.2			
SV (m^3)	9,100	15,000	42,300	35,800	40,300	27,100			
Sub-basin	Sb5WS	Sb6C	Sb6Ca	Sb6Cb	Sb6ColB	Sb7C	Sb8aES	5b5C2C	
P.D (m^3s^{-1})	5.0	16.4	2.6	2.0	3.9	0.9	9.5	15.7	
SV (m^3)	18,100	56,600	5,200	4,000	8,000	1,600	22,000	38,700	
Sub-basin	Sb8bES	Sb8C	Sb8cES	Sb8ES	SbFV1	SbFV2	SbMbN	SbMsbS	
P.D (m^3s^{-1})	7.0	3.0	4.0	21.4	22.3	16.8	10.4	17.6	
SV (m^3)	18,000	6,100	11,200	54,600	49,300	38,400	30,900	71,500	
Sub-basin	TSb	R4c	SBR1	SbS1	SbS2	SCSb	SV		
P.D (m^3s^{-1})	14.7	4.1	15.6	9.3	14.3	22.5	38.4		
	31,400	9700	35,300	32,700	54,400	51,500	149,600		

Figure 5.13. Peak discharge and stored water for sub-basins allocated on the Anapra basin. P.D=Peak Discharge and SV = storage water volume. Source of calculation methods: SCS (1986) and HEC-HMS programme.

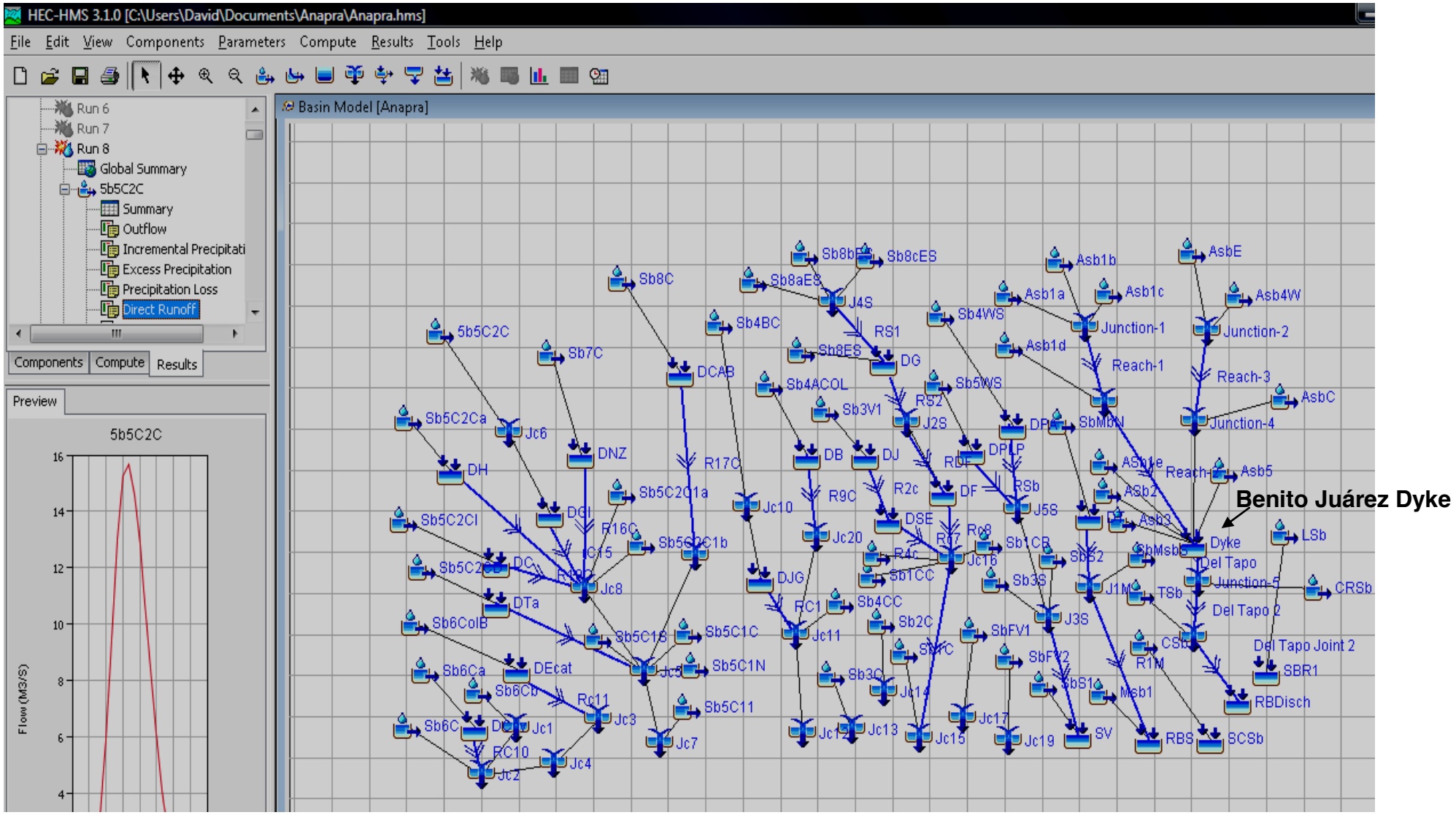

Figure 5.14. HEC-HMS simulation flooding hazard model components for the Jarudo basin. Source of model diagram HEC-HMS (2002, version 3.1.0 Army Corps of Engineers of Texas).

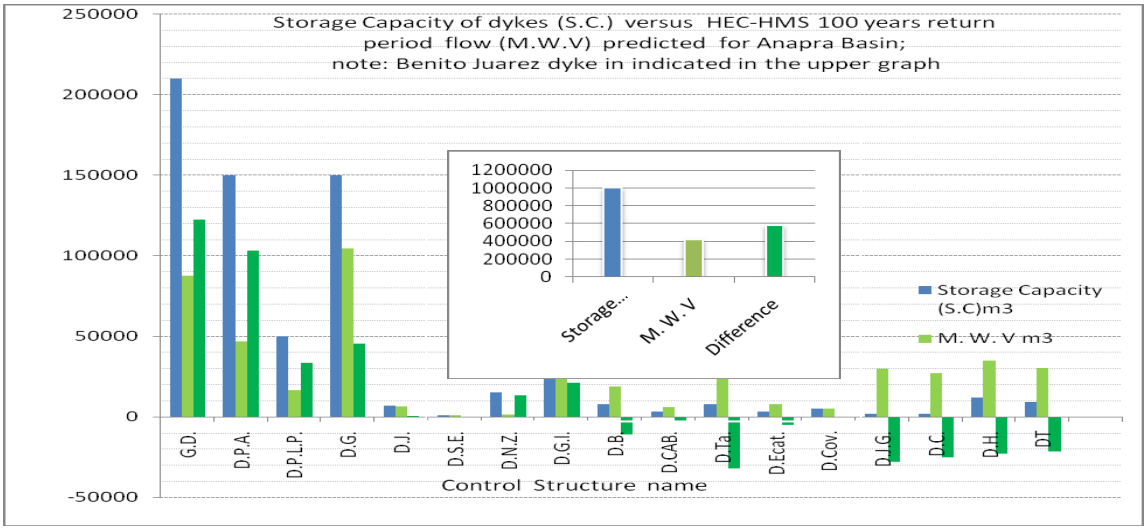

Figure 5.15. Structure storage capacity (S.C) versus HEC-HMS simulation flooding water volume for Anapra basin. Negative bars indicate the part of the basin where dykes are expected to fail during flooding events: Source of data for the storage capacity IMIP (2005).

5.3.2.3. Center Basin network distribution and description.

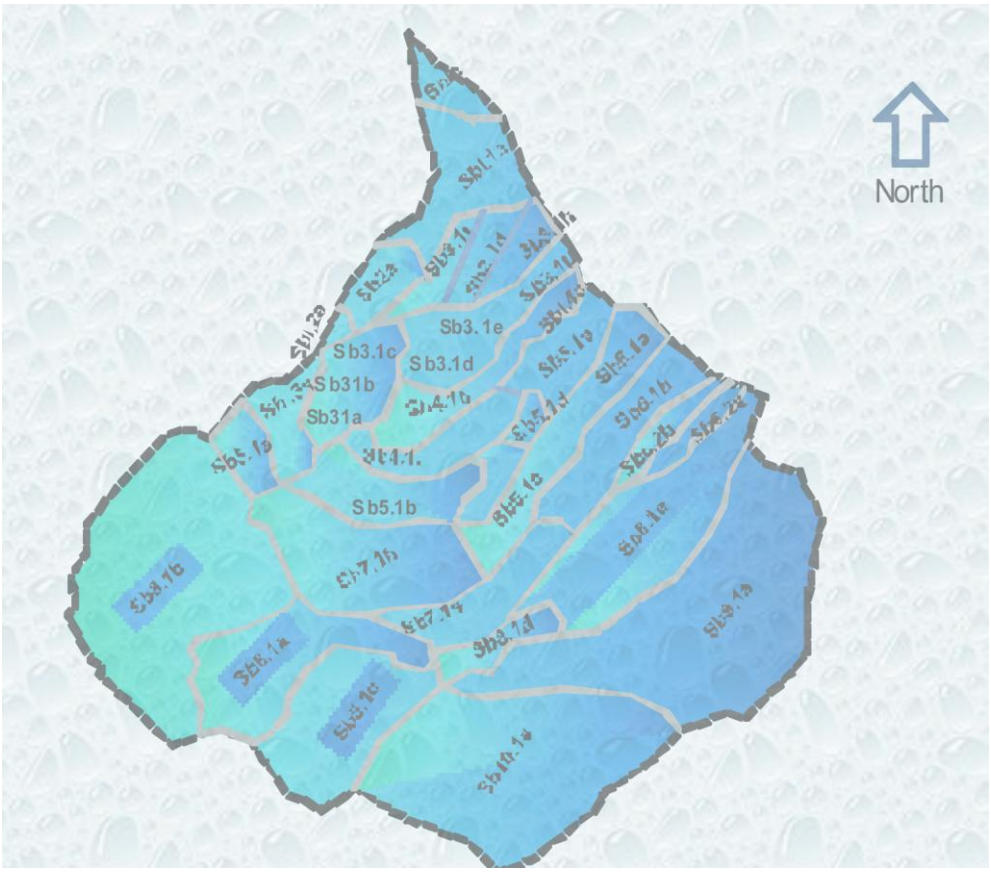

Figure 5.16. Center Basin sub-basin distribution. Width of basin at its widest point is 8.2 km.

5.3.2.3.1 Description of Centre basin drainage system.

The Center basin is formed by 34 sub-basins 14 dykes, 6 sewers, has an area of 42.4669 km^2 and is drained by 13 streams and tributaries: Mariano Escobedo, Monterrey, Panteon, Basurero, Tepeyac, San Antonio, Mercado Ornelas, Calos Amaya Norte, Carlos Amaya Sur, Del Indio, Libertad and Libertad CBTI.

5.3.2.3.2 ***Sub-basin stream Sb1a*** is Located in the historical center of the city and drains 22,000 m^3 directly to Acequia del Pueblo J1a from 16 de Septiembre street until Bravo River and from Colorado stream until Francisco Villa street. This isolated sub-basin produces inundation problems mostly in commercial areas (see Figs 5.16 and 5.17).

5.3.2.3.3 Montemorelos Sub-basin stream Sb1.4a. Drains 10,500 m^3 through Montemorelos sewer with capacity 3,000 m^3 (IMIP 2005) would operate at 350 % of its capacity during the flooding event (Fig. 5.19). 7500 m^3 of water flow overspill to convergence point J3-4 which also receives flow of Sb1.3a (16,400 m^3) where Division del Norte sewer with 6,000 m^3 storage capacity (IMIP 2005) would work at 398% of its capacity this volume (17900 m^3) is conducted until junction J3-4-2 (Figs 5.18 and 5.19). In addition, it receives water from Melchor Ocampo Sub-basin Sb1.2a (6,300 m^3). Here is Melchor Ocampo sewer with 4,000 m^3 capacity (IMIP 2005). It is going to operate at 605% of its capacity so will overspill 20,200 m^3 (Figs. 5.18 and 5.19). Then, Sb1.1a (97,500 m^3) is joined in convergence point J1,2,3,4a and in this junction the Acequia Madre will receive 117,700 m^3 of volume by the flooding event. Three sewers; Melchor Ocampo, Montemorelos and Division del Norte, located in neighbourhoods named similarly are little bridges that function like regulation structures (sewers) but not are considered like retention control at all (dykes). Also, because this area is mostly paved and urbanized, there are many inundation problems. The principal stream driver of the sub-basins already described is Mariano Escobedo stream that finished in junctions J1, 2, 3 and 4a. Finally the neighbourhoods located in this sector are: Melchor Ocampo, Division del Norte, Montemorelos, Vicente Guerrero and Mariano Escobedo (Figs. 5.16, 5.17 and 5.18).

5.3.2.3.4 Sub-basin Monterrey Stream Sb2a. Drains 80,900 m^3 through Monterrey stream directly to Acequia del Pueblo channel J2a. In this sub-basin there is not any regulation control structure so during the flooding hazard events water discharge directly in urbanized areas basically in streets close to neighbourhood Monterrey mixing with sanitary drainage system water (Figs. 5.18 and 5.19).

5.3.2.3.5 Sub-basin Panteon stream originates in the Juárez Mountains and discharges in the Acequía del Pueblo JAP3. Approximately 95 % is paved, mostly urbanized and there are six control structures. Firstly, in the upper part, La Bible Dyke DLB with 56,000 m^3 storage capacity (IMIP 2005), Pantitlan Dyke DP with 7,000 m^3 storage capacity (IMIP 2005) (Figs. 5.17; 5.18 and 5.19)., Juan Mata Ortiz DJMO with 15,000 m^3 storage capacity (IMIP 2005), Rafael Velarde Dyke DRV with 15,000 m^3 storage capacity (IMIP 2005), Miguel Ahumada sewer 4,000 m^3 capacity (IMIP 2005), and Ayutla sewer 500 m^3 capacity (IMIP 2005), Additionally, this sector is composed of nine sub-basins; Sub-basin Sb3.1a (20,200 m^3) discharges directly to La Bible Dyke DLB so work to 36% of its capacity. Sb3.1b (27,500 m^3) discharges directly to Pantitlan Dyke DP so it will be working to 393% of its storage capacity and will over-spill 20,500 m^3 during flooding hazard events, the Dyke La Bible is connected through dyke Pantitlan DP through a natural reach RLB. Sb3.1.c discharges (9000 m^3) directly to Juan Mata Ortiz Dyke DJMO that will be working to 60% of its capacity (Figs. 5.17; 5.18 and 5.19). Sb3b1d discharges (48,800 m^3) directly to Rafael Velarde Dyke DRV this dyke is connected through natural reaches RDP, RDJMO and natural reach RFV and drains 69,300 m^3 so will be working at 462% of its capacity over-spilling 54,300 m^3 (Fig. 5.19) downwards during the flooding event. This volume goes downward until the intermediate platform joint JAA. In this intermediate platform there are connected three sub-basins: Sb3.1e (9,300 m^3); Sb3.1f (7,200 m^3) and Sb3.1g (18,500 m^3). As a result, in the intermediate platform JA 89,300 m^3 of water will be concentrated during the flooding events (Figs. 5.17; 5.18 and 5.19).

5.3.2.3.6. The lower platform of Panteon Basin is formed by two sub-basins which discharge directly to Acequia del Pueblo channel JAP3: Sb3.1h (36,600 m^3) and Sb3.1i (13,800 m^3). A total volume of 139,700 m^3 would be discharged directly to

JAP3. In this lower platform the volume of water drained causes many inundation problems to homes located in the surrounding areas: Obviously, the Channel (Acequía del Pueblo) does not provides any solution because the drains capacity is completely lower than the flooding volume (Figs. 5.17; 5.18 and 5.19).

5.3.2.3.7 Sub-basin Older Landfill Stream. This Basin is divided in two micro sub-basins: One upper Sb4.1a (23,200 m^3) its regulated by Copaltepec Dyke located in Galeana neighbourhood between streets Copaltepec and Teotepec CD with 24,000 m^3 of storage capacity (IMIP, 2005). Thus, this dyke would be working at 96.6% of its capacity during hazard flooding. In addition, Sb4.1b (33,500 m^3) is connected to JAP4 through a natural reach RDCAP and discharges directly to Acequia del Pueblo channel (Figs. 5.17; 5.18 and 5.19).

5.3.2.3.8 Sub-basin Tepeyac stream. It is drained by two main tributaries and four dykes; three located in the highest south tributary are named as follows. First, Carlos Amaya DCA (10,000 m^3 storage capacity (IMIP 2005)) receives flow from Sub-basin Sb5.1b (22,700 m^3); this dyke will be operating to 227% of its capacity, also over-spilling 12,700 m^3 downward until dyke Mayas through a natural reach RDCADM (Fig. 3.20). Second, Sb5.1a (51,500 m^3) discharges to Usumasintas dyke DU with storage capacity 15,000 m^3 (IMIP 2005)). Thus, it would be working at 343% of its capacity and will over-spill 36,500 m^3 to Mayas Dyke DM through a natural reach RDUDM. Third, Sb5.1c (17,100 m^3) drains to Dike Mayas 53,600 m^3 DM storage capacity 80,000 m^3 (IMIP 2005) (See Fig. 5.19). Thus, it will be operating during the flooding hazard event to 67 % of its capacity and will be strong enough to regulate the volume of the three sub-basins. Then, Maya Dyke is connected to Teloloapan Dyke DT through a natural reach RDMDT. The other Sub-basin Sb5.1d (10,800 m^3) drains to Teloloapan Dyke DT with 10,000 m^3 storage capacity (IMIP 2005) (See Fig. 5.19) so it will be working at 108 % of its capacity and will over-spill 800 m^3 downwards to the lower platform located in the connection with Acequia del Pueblo channel JAP5 through a natural reach RDTAP. Finally for Sb5.1e (49,300 m^3), all the water (49,300 m^3) goes into convergence point JAP5 and will continue through the Acequia del Pueblo Channel (Figs 5.17; 5.18 and 5.19).

5.3.2.3.9 San Antonio stream Sub-basin. It is mostly urbanized and has its origin in the Juárez Mountains is regulated by Palo Chino Dyke DPCH with 50,000 m^3 storage capacity (IMIP 2005), it is located in Libertad neighbourhood between Basalto and Marfil streets and receives the water of Sub-basin Sb6.1a (46,400 m^3) so the dyke DPCH will be working at 93% of its capacity (Figs. 5.17; 5.18 and 5.19). This runoff continues until Acequia del Pueblo JAP6 through a natural reach RPCHSA. Sb6.1b (71,800 m^3) will be draining until acequia del Pueblo Channel JAP6 during the flooding event (Figs. 5.17; 5.18 and 5.19).

5.3.2.3.10 Sub-basin Sb6.2a. It is drained by a Tepeyac stream's tributary (14,600 m^3) and separated by construction and topographic reasons of the main original stream and discharges directly to the Acequia del Pueblo JCAN (Figs. 5.17 and 5.18).

5.3.2.3.11 Sub-basin Sb6.2b. It is an isolated and disconnected tributary branch of Tepeyac stream and discharges (16,400 m^3) directly to Acequia del Pueblo channel in convergence point JAP6b (Figs. 5.17 and 5.18).

5.3.2.3.12 Mercado Ornelas Stream Sub-basin. This sub-basin is completely urbanized and is regulated by El Hoyo Dyke DEH 30,000 m^3 storage capacity (IMIP 2005). Sub-basin Sb7.1a (44,000 m^3) drains directly to the dyke thus it will be working during a flooding event at 146.6 % of its capacity and will over-spill 14,000 m^3 to the Acequia del Pueblo channel JAP7 through a natural reach REHAP. Sb7.1b (65,900 m^3) drains directly to Acequia del Pueblo channel JAP7 this volume is joined with the excess overspilling 14,000 m^3 of El Hoyo Dyke **DEH** so its represents 79,900 m^3 that will be transported by Acequia del Pueblo JAP7 Dyke. El Hoyo dyke is located in a topographic depression formed as a result of the construction of Carlos Amaya Boulevard and normally is used like a market area during weekends is located in the Carlos Amaya Boulevard (Figs. 5.17; 5.18 and 5.19). Sub-basin El Indio stream begins in the highest part of the Juárez mountains and drains to Acequia del Pueblo Channel. Approximately 80 % of the area is urbanized and paved. Also, it has four regulation structures. Three dykes are located in the upper platform; Trituradora Dyke TD has 200,000 m^3 storage capacity; Asfalto sewer with

10,000 m^3 and Board Juarez mountains park with 200,000 m^3 storage capacity (IMIP 2005). The other control structure is located in the middle platform of this sub-basin named sewer Chocholtecas with 6,000 m^3 of storage capacity (IMIP 2005). In addition, there are two sewers located in Fernando Borreguero and Juan Gabriel Streets but due to their null storage capacity there are not considered as control structures in this analysis (Figs. 5.17; 5.18 and 5.19).

5.3.2.3.13 Asfalto Sub-basin stream Sb8.1b. Drains (62,000 m^3) directly to Asfalto Sewer (10,000 m^3 storage capacity) located in Asfalto Street. This structure during the flooding hazard event will be working at 620% of its capacity consequently 52,000 m^3 of water excess will over-spilled downwards (Figs. 5.17; 5.18 and 5.19).

5.3.2.3.14 Board Juarez Mountains Sub-basin Sb8.1a. Originates in the Juarez Mountains draining (124,800 m^3) along tributaries of El Indio Stream until a Board Juárez Mountain Park Dyke. This dyke is located in the older militar field (Campo Militar in spanish) and during flooding hazard event will be working at 62.4% of its capacity and will work appropriately (Figs. 5.17; 5.18 and 5.19).

5.3.2.3.15 Trituradora Dyke Sub-basin Sb8.1c. Discharge (63,900 m^3) in the dyke, similarly named and located inside the ASPA company installations and will be working during the flooding hazard event at 32% of its capacity so it's a satisfactory regulation of water (Figs 5.17; 5.18 and 5.19). As a result the total water volume derived by the higher platform which is accumulated in Sink-1 (Trituradora Dyke) so it will over-spill downwards to lower platform a total volume of 46,500 m^3 during the flooding hazard event. This Sink-1 is connected to Chochultecas sewer (ACH) through a Chochultecas stream natural reach RTDAP (Fig. 5.19).

5.3.2.3.16 Chochultecas stream Sub-basin Sb8.1d. Transports (24,200 m^3) water to Chochultecas sewer with 6,000 m^3 storage capacity that will be operating during the flooding hazard event at 403% of its capacity over-spilling 18,200 m^3 downwards until Acequia del Pueblo Channel JAP8. Finally, Sub-basin Sb8.1e (150,000 m^3) discharges directly to Acequia del Pueblo JAP8 (168,200 m^3). The Chochultecas sewer located between Chochultecas and Daniel Garcia streets constitutes the body

of the Chochultecas street and it's completely invaded for constructions and sport installations (Figs. 5.17; 5.18 and 5.19).

5.3.2.3.17 Libertad stream Sub-basin Sb9.1a. This sub-basin drain (229,500 m^3) by the Libertad stream and produces many inundation problems in the Juárez Industrial Park as well as Rivera Lara Street, during flooding events. In addition this volume is incorporated directly to Acequia del Pueblo channel through the junction JAP-9 (Figs. 5.17 and 5.18).

5.3.2.3.18 Libertad 2 CBTI Sub-basin Sb10.1a. Drains (136,200 m^3) and it is located through the west area of Acequia del Pueblo near to Jarudo stream before the intersection with the Drain 2-A. This sub-basin does not has a defined course so during the flooding events the water accumulates on streets provoking inundation basically in the west area of Panamericana and Teofilo Borunda streets. A volume of 365,700 m^3 will drain to JAP-9 (Figs. 5.17; 5.18 and 5.19).

5.3.2.3.19. (CN) Curve Number factor method of Centre basin (Appendix 5.4.3)
Information for this is in Appendix 5.4.3.

5.3.2..3.20. Centre basin Physiographic and hydrologic values (Appendix 5.4.3)
Information for this is in Appendix 5.4.3.

5.3.2.3.21. Peak discharge and store water using HEC-HMS for Centre basin.

HEC-HMS computer program performs hydrologic calculations such as hydrographs and storage volume for the sub-basins allocated within the different basins of the study area. However, before using it physiographic and hydrologic parameters are needed. Such parameters as: area (A); Impervious surface (Is); Initial abstraction (Ia); Concentration time (Tc) and Lag-time. In relation to the area (A), Length and slope of the streams of the sub-basins were evaluated using Auto-Cad program, the land use was identified using satellite Images and the program Arc-Map 9.2 GIS for their interpretation (See appendix 5.4 and Figs. 5.17, 5.18 and 5. 19 below)

Sub-basin I	Sb1a	Sb2a	Sb3.1a	Sb3.1b	Sb3.1c	Sb3.1e	Sb3.1f	Sb3.1g	Sb3.1h
P.D (m^3s^{-1})	7.2	28.1	8.8	15.1	4.6	5.2	3.4	6.8	15.3
S.V (m^3)	22,000	80,900	20,200	27,500	9,000	9,300	7,200	18,500	36,600
Sub-basin	Sb3.1i	Sb3b,1d	Sb4.1a	Sb4.1b	Sb5.1a	Sb5.1b	Sb5.1c	Sb5.1d	
P.D (m^3s^{-1})	7.7	20.7	7.6	10.6	19.7	9.6	6.3	4.4	
S.V (m^3)	13,800	48,800	23,200	33,500	51,500	22,700	17,100	10,800	
Sub-basin	Sb5.1e	Sb6.1a	Sb6.1b	Sb6.2a	Sb6.2b	Sb7.1a	S b7.1b	Sb8.1a	
P.D (m^3s^{-1})	18.1	18.8	16.9	4.4	5.3	15.7	21.7	46.8	
S.V (m^3)	49,300	46,400	71,800	14,600	16,400	44,000	65,900	124,800	
Sub-basin	Sb8.1b	Sb8.1c	Sb8.1d	Sb8.1e	Sb9.1a	Sb10.1a			
P.D (m^3s^{-1})	21.9	19.3	9.1	65.6	60.7	44.9			
S.V (m^3)	62,000	63,900	24,200	150,000	229,500	136,200			
Sub-basin	Sb1.1a	Sb1.2a	Sb1.3a	Sb1.4a					
P.D (m^3s^{-1})	33.9	3.4	8.6	5.5					
S.V (m^3)	97,500	6300	16,400	10500					

Figure 5.17. Peak discharge and stored water for the 34 sub-basins in the Centre basin Source of calculation: SCS (1986).

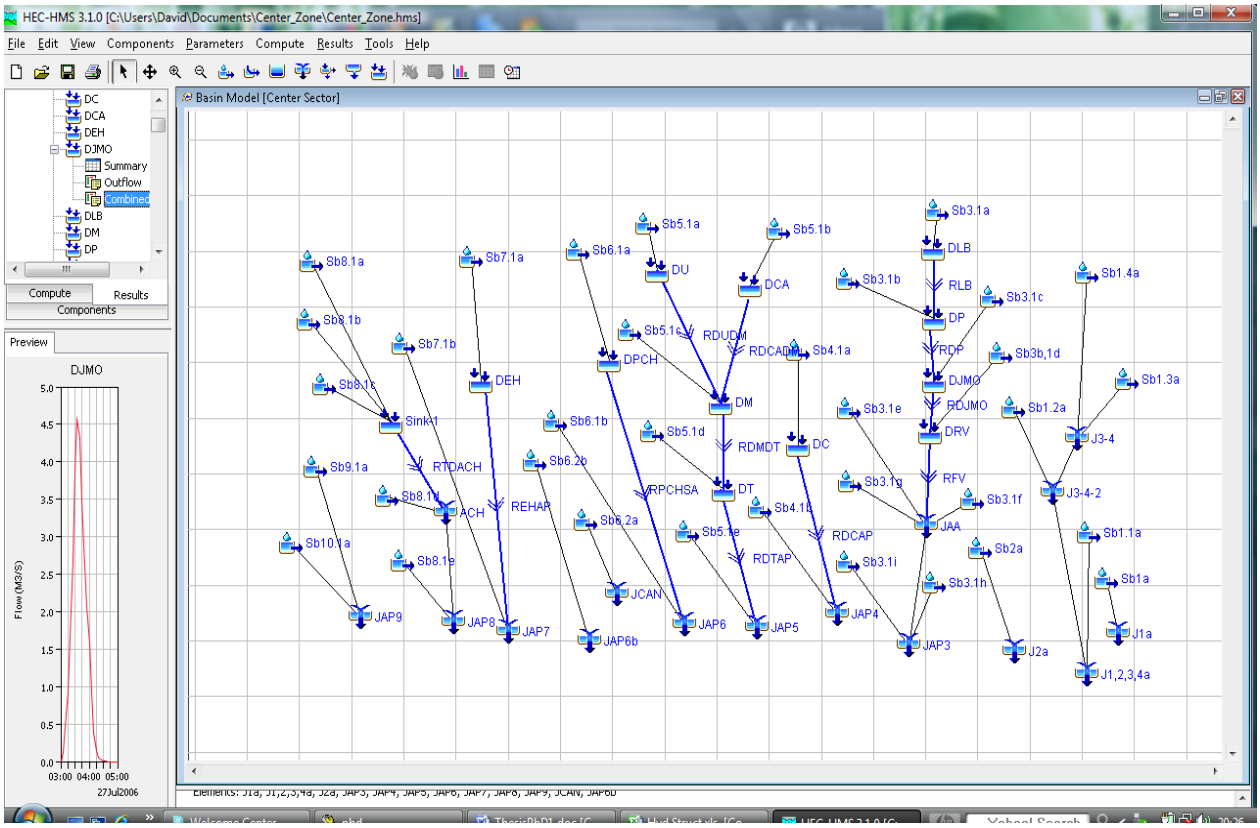

Figure 5.18. HEC-HMS simulation flooding hazard model components for Centre basin. Source of model: HEC-HMS (2002) version 3.1.0.

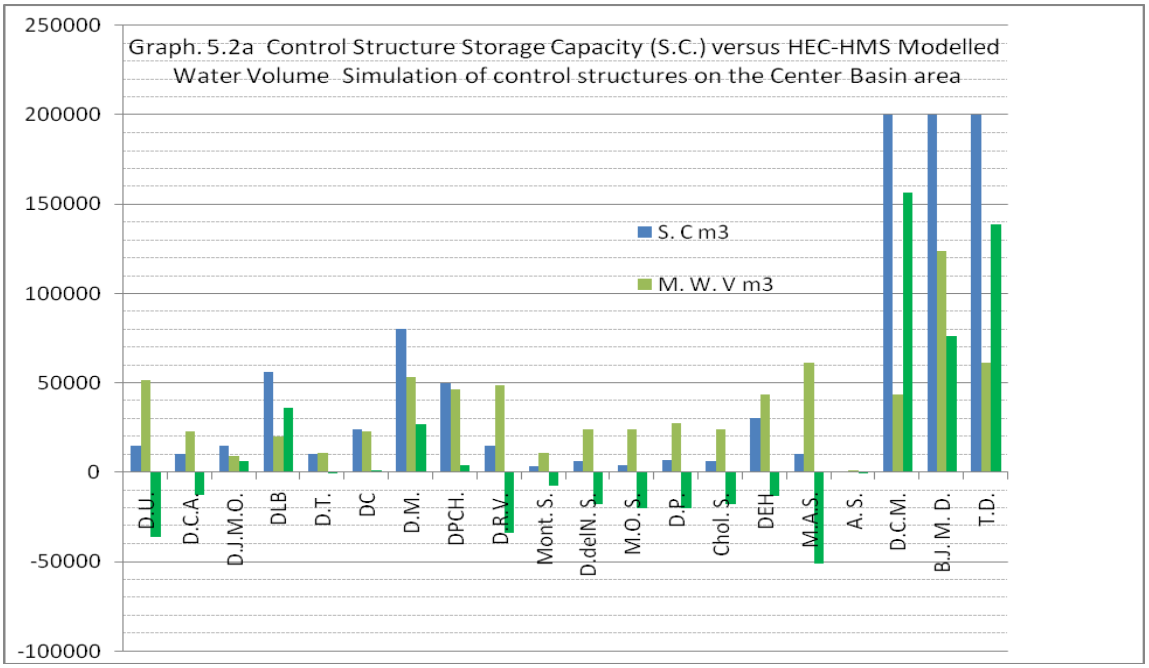

Figure 5.19. Structure storage capacity (S.C) versus HEC-HMS simulation flooding water volume for Center basin. Negative bars indicate the part of the basin where dykes are expected to fail during flooding events. Source of data for the calculation: IMIP (2005).

5.3.2.4 Barreal basin network distribution and description.

The general geographic location of this basin is presented in Fig. 5.7 and sub basins which comprise Barreal Basin is illustrated below in Fig. 5.20. Furthermore, a whole description is presented in section 5.3.2.4.1.

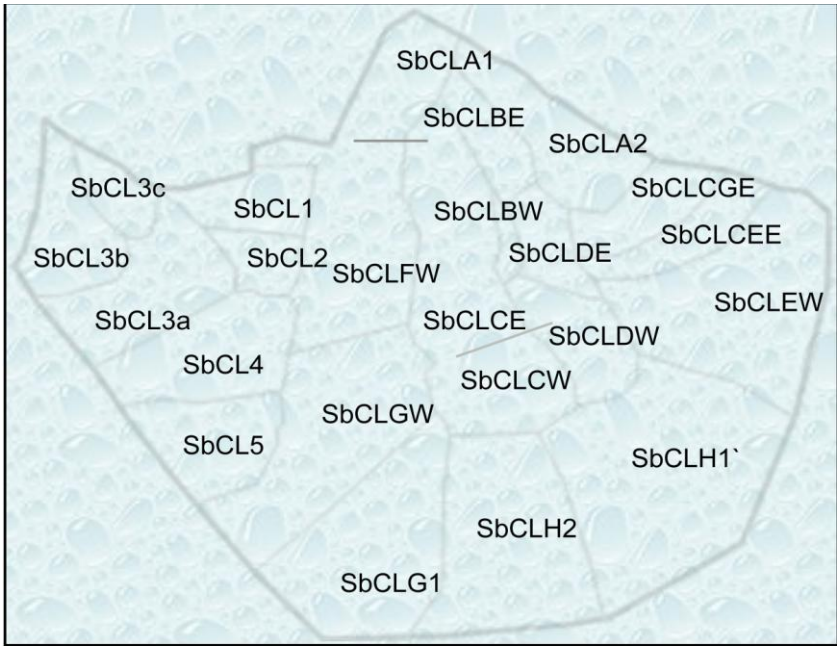

Figure 5.20. Barreal sub-basins location and distribution. Width of basin at its widest point is 13.4 km.

5.3.2.4.1 Description of Barreal basin drainage system.

Barreal Basin is formed of 23 Sub-basins, covers an area of 178.62 km^2 and it is located south of the study area with the following limits. In the north is, Casas Grandes Highway beginning near to Villa Esperanza neighbourhood. Then, following to the east until Juan Gabriel Boulevard and along the railway until its intersection with the Airport and following through the east passing the Benito Juarez roundabout. Finally, its continues until the terraces that limited this Basin with the south as well as to west (see Figs. 5.7; 5.20; 5.21 and 5.22)

The hydrologic behaviour of this basin corresponds to a closed lacustrine basin basically constituted by layers of aeolian fine sand and silt in the highest elevation and in the lowest elevations silts and clay soils. In general streams have low gradient and the average flow direction is from north to the basin center causing inundation during the flooding. In its central part has an area of approximately 6 km^2 and the water table rises about 40 cm in average during flooding historic events. The lowest area of the basin is located in the intersection of Victoria neighbourhood and Airport highway. The main neighbourhoods located in this sector are: Santa Elena, Valle Dorado 1, 2 and 3, Granjas Polo Gamboa, Pablo Gomez, Panamerican Industrial Park, South area of the Airport, Los Cipresses Neighbourhood, Fuente Alto

Neighbourhood, Haciendas del Bosque, Victoria, Rincones de Salvarcar, Municipio Libre, Central de Abastos, Juarez Industrial Park and El Mezquital Neighbourhood.

5.3.2.4.2 Sub-basin SbCLA2. This sub-basin is mostly urbanized, drains 236,200 m^3 it is connected to JCB. This sub-basin is located near to the International Airport and it is limited from Oscar Flores Boulevard along Airport Boulevard and De las Torres Avenue (Figs. 5.20; 5.21 and 5.22).

5.3.2.4.3 Sub-basin SbCLA1. Drains 605,100 m^3 it is connected with Junction BBFJ drains 1268.8 m^3 and it is located to the west of Oscar Flores Boulevard and to the North of sector IV, between the Airport and Las Torres avenue intersection. (Figs. 5.20; 5.21 and 5.22).

5.3.2.4.4. In this sector three sub-basins are connected, as follows. SbCL3a that drains 175,200 m^3; SbCL3b that drains 88,600 m^3 and SbCL3c that drains 46,000 m^3. These represent the biggest area of this sub-basin and are connected to junction JSE2 accumulating a total volume of 309,800 m^3. These three sub-basins drain to the older dyke named Santa Elena located to the west of the railway and to the north of Casas Grandes Highway. In this area the urbanization is approximately 20% and its soils are constituted predominantly by terraces formed by sand and silts partially consolidated. The more important neighbourhood is Granjas Santa Elena (Figs. 5.20; 5.21 and 5.22).

5.3.2.4.5 Sub-basin SbCL2. Drains 46,400 m^3 and is limited to the north for Sub-basin SbCL1 and to the west for Panamericana highway, its water flows until the Santa Elena old dyke located to the south near to SbCL4 Sub-basin, then it is connected to Junction JFP where 356,200 m^3 acummulates. Another sub-basin located near to Benito Juárez roundabout named SbCL1 drains 104,700 m^3 and flows parallel to Casas Grandes Highway from west to east direction crossing Panamericana highway following until the lowest part of the sub-basin where it is connected to Junction JCG with total flow of 460,900 m^3 (Figs. 5.20; 5.21 and 5.22)

5.3.2.4.6 Sub-basin SbCLBW drains 113,500 m^3 and it is connected to JCLPO (574,400 m^3). This sub-basin located at the east of the sector is mostly urbanized and there are some absorption holes which represent an option to reduce the concentration of water in the lowest areas. The other sub-basin is SbCLBE 89,300 m^3, it is located at the south of the Panamericana highway and Las Torres avenue and connected in junction JCLPO. Finally, this sub-basin discharges in junction JCLA1 and BBFJ which have a total of 1,124,600 m^3) (Figs. 5.20; 5.21 and 5.22).

5.3.2.4.7 Sub-basin SbCL4 drains 113,600 m^3 it is connected to junction JCL4, W 354,700 m^3 and is located at the south of the Sub-basins SbCLA2 and SbCLA1, Secondly, SbCLCW drains 241,100 m^3 and it is connected in junction JCL4, W, located at the west of Panamericana highway an area in development. Another sub-basin SbCLCE 13,300 m^3 it's connected to junction J4 (368,000 m^3) (Figs. 5.20; 5.21 and 5.22).

5.3.2.4.8 Sub-basin SbCLDW drains (84,700 m^3) it is connected to junction J5 (154,800 m^3) its junction is sited at the central depressed part of the basin and represents the perfect receptor of the other sub-basin SbCLDE 70,100 m^3, it is an area in development located to the east of Panamericana highway (Figs. 5.20; 5.21 and 5.22).

5.3.2.4.9 Sub-basin SbCL5 drains (86,900 m^3) it is connected to junction J5-FW (351,900 m^3). In addition at the same junction converges the sub-basin SbCLFW (265,000 m^3). SbCLEW (57,000 m^3) is connected with junction J6 (495,300 m^3). SbCLEE (86,400 m^3) discharge also in Junction (Figs. 5.20, 5.21 and 5.22).

5.3.2.4.10 Sub-basin SbCLGW drains 284,400 m^3, it is connected to (J7; 594,700 m^3). In this junction also is connected the sub-basin SbCLG.1 (203,700 m^3). In addition in the same junction J7 is connected the sub-basin SbCLGE (106,600 m^3) (Figs. 5.20; 5.21 and 5.22).

5.3.2.4.11 Sub-basin SbCLH2 drains (216,100 m^3) is connected to junction J8 (572,100 m^3). At the same junction is connected SbCLH.1 (356,000 m^3) (Figs. 5.20; 5.21 and 5.22).

5.3.2.4.12 (CN) Curve Number coefficient Barreal basin (Appendix 5.4.4)

Information for this is in Appendix 5.4.4.

5.3.2.4.13 Physiographic and hydrologic values of Barreal (Appendix 5.4.4)

Information for this is in Appendix 5.4.4.

5.3.2.4.14 Peak discharge and store water using HEC-HMS for Barreal basin.

HEC-HMS method was used for peak discharge evaluation and storage volume of water from the flooding. Furthermore, Figs. 5.21 and 5.22 show the results of Barreal basin. It is important to mention that HEC-HMS program use the CN method defined by SCS (1986). Fig. 5.21 shows peak discharge and stored water for sub-basins located in Barreal basin.

Sub-basin Identification	**SbCLA2**	**SbCLA1**	**SbCL3a**	**SbCL3b**	**SbCL3c**
Peak Discharge (m^3s^{-1})	63.3	119.3	38.4	19.8	15.0
Stored Volume (m^3)	236,200	605,100	175,200	88,600	46,000
Sub-basin Identification	SbCL2	SbCL1	SbCL4	SbCLBW	SbCLBE
Peak Discharge (m^3s^{-1})	9.4	22.2	21.2	26.5	17.9
Stored Volume (m^3)	46,400	104,700	113,600	113,500	89,300
Sub-basin Identification	SbCLCW	SbCLCE	SbCLDW	SbCLDE	SbCL5
Peak Discharge (m^3s^{-1})	54.5	5.9	22.1	18.9	16.1
Stored Volume (m^3)	241,100	13,300	84,700	70,700	86,900
Sub-basin Identification	SbCL2FW	SbCLEW	SbCL4	SbCLGW	SbCLG1
Peak Discharge (m^3s^{-1})	54.0	12.9	21.2	78.4	41.5
Stored Volume (m^3)	265,00	57,000	113,600	284,400	203,700
Sub-basin Identification	SbCLGE	SbCLH2	SbCLH1		
Peak Discharge (m^3s^{-1})	21.7	41.4	89.2		
Stored Volume (m^3)	106,600	216,100	356,000		

Figure 5.21. Peak discharge and stored water for sub-basins allocated on the Barreal basin. The results indicated were derived by HEC-HMS programme: Source of the method SCS (1986) in HEC-HMS flooding simulation.

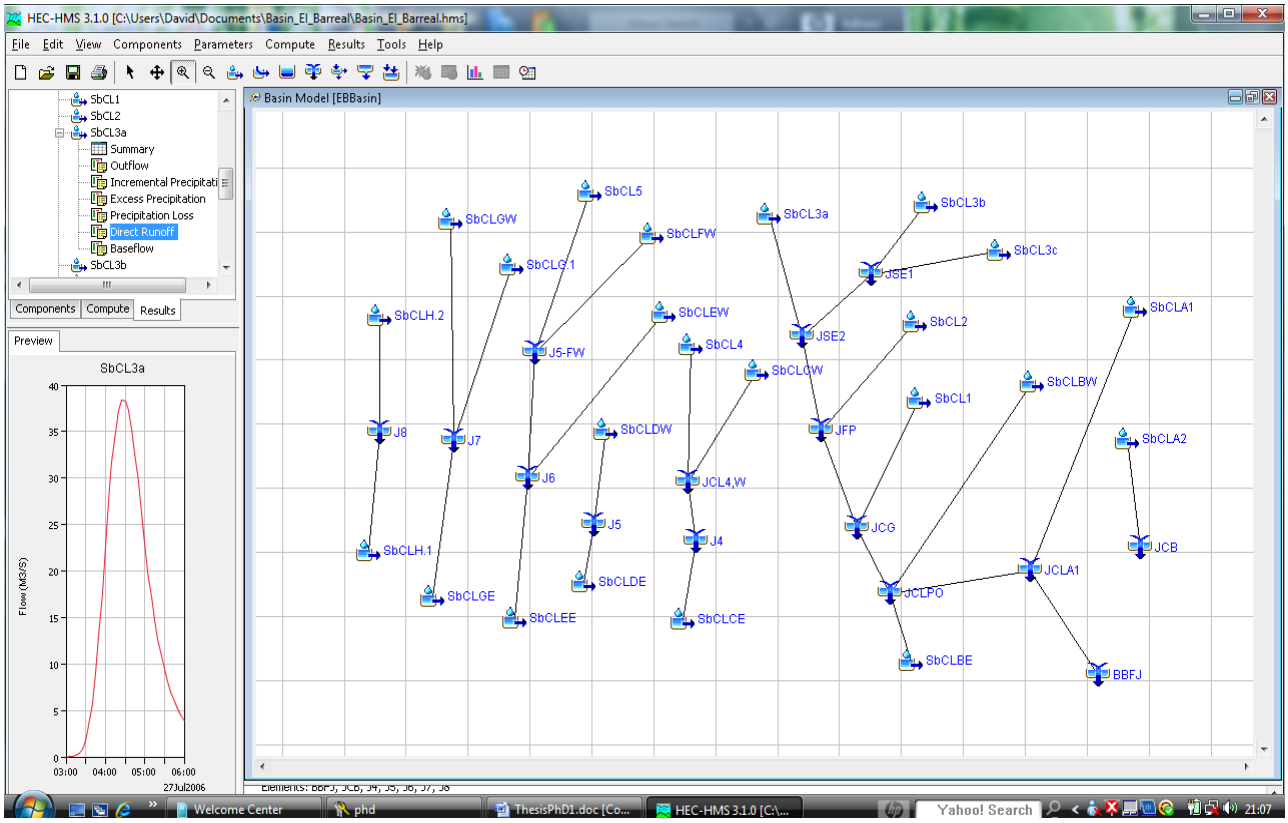

Figure 5.22. HEC-HMS simulation flooding hazard model components for Bareal basin. Source of the method HEC-HMS (2002) version 3.1.0.

5.3.2.5 Airport basin network distribution and description.

The general geographic location of this basin is presented in Fig. 5.7 and sub basins which comprises Airport basin are illustrated below in Fig. 5.23. Furthermore, a whole description is presented in Section 5.3.2.5.1.

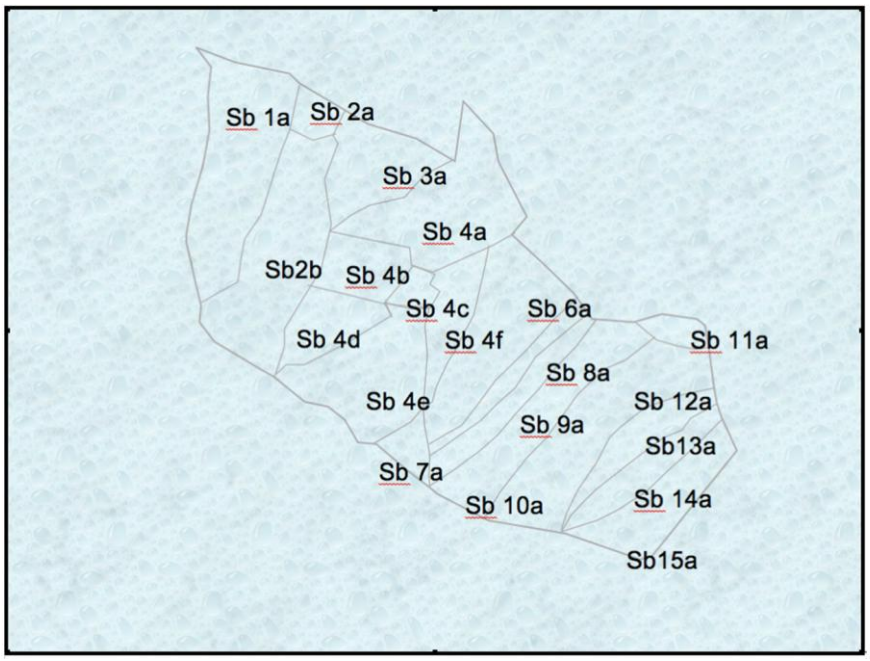

Figure 5.23. Airport sub-basin distribution. Width of basin at its widest point is 5.13 km.

5.3.2.5.1 Description of Airport basin drainage system.

5.3.2.5.2 Airport Basin. This Basin with a total area of 57.2936 km^2 has 2 sewers (Figs. 5.7; 5.23; 5.24; 5.25 and 5.26) and it is limited to: the west, Oscar Flores Boulevard; the east, Juarez-Porvenir Boulevard; the south, Barreal lake and to the north, the drain 2-A and Acequia del pueblo channels. However, it does not discharge into these channels because there is no collector to connect them. Also, there are three little control structures (Figs 5.23; 5.24; 5.25 and 5.26).

5.3.2.5.3 Lomas del Rey Stream Sub-basin Sb.1a. This sub-basin located to the west of Panamericana highway collects 324,200 m^3 of water derived from Lomas de San Jose, Colinas de Juarez, Lomas del Rey, La Cuesta and Las Arenas neighbourhoods. This flow discharge in the Central Park, located near to the intersection of Panamericana and Teofilo Borunda streets without any control structure. Here the drain 2-A is located. However, this sub-basin begins draining from the south of Zaragoza Boulevard to the north so that water flows from streets going to Panamericana Boulevard and discharging into the Central Park finally water finishes in convergence point JTB=324,200 m^3 (Figs. 5.23; 5.24; 5.25 and 5.26).

5.3.2.5.4 Airport Stream Sub-basin Sb.2a. This sub-basin is located in the upper part of the stream approximately at the middle of the airport installations, drains 35,700 m^3 from south to north collecting the runoff from: Airport, Oasis, Del Real, Erendira, Lino Vargas, Loma Linda, and Luis Donaldo Colosio Neighbourhoods. This stream driver discharges in some terrains located to the north of Luis Donaldo Colosio Neighbourhood and it is connected in junction JCLML 35,700 m^3 (Figs. 5.23; 5.24; 5.25 and 5.26).

5.3.2.5.5 Airport stream sub-basin Sb.2b. Drains 303,700 m^3 and is originated inside the airport terrains draining water and crossing Erendira, Luis Donaldo Colosio, Del Real, and Airport neighbourhoods, then, discharges into the drain 2A located between Panamericana highway and Paseo de la Victoria Boulevard. However, this water does not flow completely to the drain 2A. For this reason, there are many areas located in Luis Dolando Colosio neighbourhood which are inundated during flooding events. The discharge point of this sub-basin is JCLML=303,700 m^3 and JD2a=303,700 m^3 (Figs. 5.24; 5.25 and 5.26).

5.3.2.5.6 Morelia stream sub-basin Sb.3a. This sub-basin drains 164,900 m^3, it originated in Vista del Valle neighbourhood and has two main tributaries; one discharges in some agricultural terrains that are located between drain 2-A and Paseo de la Victoria Avenue. The other is located in Mission de los Lagos Club. However, this sub-basin does not have any control structure and water is stored in urbanized areas (Figs. 5.24; 5.25 and 5.26).This sub-basin begins in the upper part of Jilotepec Boulevard crossing the eastern part of Erendira, Vista del Valle and Yolanda neighbourhoods. Then, before crossing Paseo de la Victoria Boulevard, it continues downwards until some agricultural terrains located closely to Paseo de la Victoria Boulevard (Morelia Park). Finally, the discharges of this sub-basin are indicated by junction J3aD=164,900 m^3 (Figs. 5.24; 5.25 and 5.26).

5.3.2.5.7 Maximo Favela and Zafra Sub basins. Tapioca stream is the main driver of these sub-basins which are located in the upper platform are mostly urbanized with a high development. Similarly to the majority of the surrounded sub-basins its

flow runs through streets of the area provoking many inundation during the flooding hazard events mainly in the following neighbourhoods: Infonavit Aeropuerto, El Granjero, Lucio Blanco, Colinas de Juarez and Solidaridad. There is three little regulation structures completely filled with sediments and garbage: Maximo Favela Sewer, Zafra Sewer and Airport Board that have limited size and practically null storage capacity no more than 3,000 m^3 each other (IMIP 2005) (Figs. 5.24; 5.25 and 5.26). These two sub-basins are located in the upper platform: Sb.4a 228,400 m^3 and Sb.4b 97,000 m^3) discharge in DBA=5500. and are represented in the simulation HEC-HMS model. These structures will work during the flooding event at 5916% of their capacity and will over-spill a volume of 319,900 m^3 during the flooding hazard event. Finally, water over spilling of the last sub-basin drains downward until the junction JMFZ=665600 m^3 through a natural reach RDBA=345,700 m^3 where three sub-basins Sb4c=26200 m^3, Sb4d=101,700 m^3 and Sb4e=217,800 m^3 are connected (Figs. 5.24; 5.25 and 5.26).

5.3.2.5.8 Board Airport sub-basin. It is composed of three sub-basins located in the intermediate and lower platform of the Airport Basin: Sub-basin Sb.4c (0.526 km^2, 10.5 m^3s^{-1} peak discharge and 26,200 m^3) is located at the end of the airport runway closely to Aquiles Serdan Street of airport neighbourhood (Figs. 5.23; 5.24 and 5.25). Intermediate Platform airport sub-basin Sb.4d drains 101,700 m^3 through a tributary of Tapioca Stream connected to Maximo Favela 2,500 m^3 storage capacity (IMIP 2005) and Zafra (3,000 m^3 storage capacity) (IMIP 2005). It is located in a completely urbanized area integrated by Solidaridad, Granjas, Alcaldes and Airport neighbourhoods (Figs. 5.24; 5.25 and 5.26).

Intermediate Platform Airport sub-basin Sb.4e drains 217,800 m^3 is a mostly urbanized area connected the Airport platform. Water received from this sub-basin as well as sub-basins Sb.4c and Sb.4d continue until control structures Maximo Favela as well as Zafra sewers JMFZ, where a total of 665,600 m^3 will be accumulated during flooding events (Figs. 5.24 and 5.25). Airport Platform Sub-basin Sb.4f (0.864 km^2, 21.3 m^3s^{-1} peak discharge and 43,100 m^3) its sub-basin is joined in Junction JBDA, where a total volume of 698900 m^3 will be accumulated during the flooding event J42Ad (Figs. 5.24 and 5.25).

5.3.2.5.9 Arcadas stream Sub-basin Sb.5a. It is located in the urban area of the city crossing some important Boulevards such as: De Las Torres, Jilotepec and Paseo de la Victoria. Stream discharges near to drain-2A closely to acequia Madre. Additionally, there is no control structure in this sub-basin that is located inside the arcades neighbourhood. The hydrological parameters obtained for this sub-basin in the simulation HEC-HMS model were: 1.813 km^2, 37.1 m^3s^{-1} peak discharge and 90,300 m^3 and its discharge is represented by junction J5A2aD (Figs. 5.24 and 5.25).

5.3.2.5.10 Salvarcar stream sub-basin Sb6a. Drains 228,400 m^3. Salvarcar stream is the driver for this sub-basin and their lower limit is defined by the Acequia Madre. Also, it is mostly urbanized and is composed of Morelos I, II, III, and IV neighbourhoods as well as for the Intermex Industrial Park. Moreover, there is no control structure in this sub-basin and its stream follows a south to north direction beginning in the intersection of De las Torres Boulevard and Mitla street. This sub-basin also receives the water flow generated in Torres del Sur, Intermex Industrial Park and Torres del PRI, Porfirio Siva, Valle Dorado neighbourhoods as well as Industrial zone Henequen. The discharge basically concentrates mainly in Tamaulipas street crossing Jilotepec Boulevard producing inundation in Arcade's neighbourhood. Finally, this sub-basin is connected in the simulation HEC-HMS model by J5S2aD=228,400 m^3 (Figs. 5.24 and 5.25).

5.3.2.5.11 La Rosita roadway stream Sub-basin Sb.7a. Drains 23,300 m^3. This little Sub-basin named La Rosita roadway stream is located in Salvarcar neighbourhood cross the Jilotepec Boulevard and does not have any regulation control structure exist. Its area is limited by Salvarcar neighbourhood between Zaragoza and Jilotepec Boulevards, discharging on Queretaro and San Luis streets In an area completely urbanized. The water discharges are represented in the HEC-HMS modelling by junction JLR2aD (Figs. 5.24 and 5.25).

5.3.2.5.12 Tabasco Stream Sub-basin Sb.8a. Drains 24,200 m^3 it's limited by Acequia Madre and begins inside the urbanized area of Salvarcar neighbourhood crossing the Jilotepec Boulevard and provoking many inundations problems during the flooding event in the Salvarcar neighbourhood. In the simulation HEC-HMS

model the connection of this sub-basin representation is indicated by junction JTS2Ad (Figs. 5.24 and 5.25).

5.3.2.5.13 Morelos I stream sub-basin Sb.9a. Drains 63,300 m^3 and it's limited by Acequia Madre and does not have any control structure, begins draining approximately on Santiago Troncoso street to the east of Intermex Industrial Park (Rinconada de las Torres neighbourhood) running in a northeast direction discharging in the main channel approximately 250 meters before its intersection with the Manuel Gomez Morin Boulevard. In addition, this sub-basin provokes inundation in its surrounded terrains. Along its trajectory this stream crosses Rinconada de las Torres, Colinas del Sol, Bosque Bonito, El Fortin, Simon Rodriguez and the East part of the Salvarcar neighbourhoods. It is represented by the HEC-HMS simulation model by junction JM12aD (Figs. 5.24 and 5.25).

5.3.2.5.14 Morelos II stream sub-basin Sb.10a. Drains 140,400 m^3 and is limited by Acequia Madre Channel is completely urbanized and does not have any control structure. Its stream pattern is parallel to Morelos I stream but begins on Ramon Rayon Boulevard following to ampliacion de las Torres Del Sur, Paseo de las Torres and Rinconada de las Torres I and II. Then it crosses the same neighbourhoods as Morelos I stream cross. Finally, its discharges are produced on the intersection between Acequia Madre channel and Manuel Gomez Morin Boulevard producing important inundation in this area as well as Morelos II neighbourhood. Its junction is represented by JMII.2aD (Figs. 5.24 and 5.25).

5.3.2.5.15 Insurgentes stream Sub-basin Sb.11a. Drains 14,700 m^3, it's a little sub-basin limited by a parallel collector that discharges to Acequia Madre Channel, is originated in the middle of the urbanized area and does not have any regulation structure. Moreover this stream is located in Zaragoza town discharging to the south of the Juarez Porvenir highway nearly to Villa Bonita and Paseos de Zaragoza neighbourhoods. Finally, its volume is drained and accumulated along the intersection of Juarez Porvenir highway and the joined of Zaragoza stream. Its junction is represented in the HEC-HMS simulation model by JM22aD (Figs. 5.24 and 5.25).

5.3.2.5.16 Zaragoza stream sub-basin Sb.12a. Drains 175,400 m^3 and also runs parallel to Acequia Madre collector that intercepts the drained water. It originated in Zaragoza town and does not have any control structure. It begins flowing from Mission de los Lagos, and Horizontes del Sur steep II neighbourhoods as well as Thomson Industrial Park zone. Then it crosses Horizontes del Sur steep I, part of Praderas del Sur, Praderas del Henequen, Manuel Valdez and Zaragoza neighbourhood. Moreover, it continues through Independencia Boulevard until its discharge located on the south side of Juárez-Porvenir highway approximately 200 meters from the intersection of these two Boulevards. Finally, its junction is represented by JZS2aD in the HEC-HMS simulation model (Figs. 5.24 and 5.25).

5.3.2.5.17 El Papalote stream sub-basin Sb13a. Drains 47,700 m^3 and similarly as Zaragoza stream sub-basin, is limited by the same collector parallel to Acequia Madre channel, located in urbanized area of Zaragoza town and doesn't have any regulation structure. It flows parallel to Independence Boulevard since Zaragoza Boulevard until Valle de Juarez Street then follows to north-east until Juarez-Porvenir Boulevard where finally discharges at the intersection of this boulevards provoking many inundations. Its junction is represented in HEC-HMS model by JPS2aD (Figs. 5.24 and 5.25).

5.3.2.5.18 Independencia Stream Sub-basin Sb.14a. Drains 53,400 m^3 and its limited by Acequia Madre channel, originates in an urbanized area of Papalote residential from the east side of Independencia Boulevard but more separated than Zaragoza stream. Since Airport Boulevard until Zaragoza Boulevard goes to Juarez Porvenir highway crossing Heroes de Mexico, Patria and Praderas de Oriente neighbourhoods. Its junction is represented by JIS2aD in the HEC-HMS simulation model (Figs. 5.24 and 5.25).

5.3.2.5.19 Patria stream sub-basin Sb.15a. Drains 152,800 m^3. It originated in the urban area and does not have any regulation structure. It begins draining in Santiago Troncoso street north to Fray Garcia de San Francisco Street and Manuel Clothier Residential neighbourhood. Then, it crosses Tierra Nueva neighbourhood

discharging in terrains closed to Puerto Dunquerque Street. The junction where this sub-basin discharges is represented in the HEC-HMS model by JP2aD (Figs. 5.24 and 5.25).

5.3.2.5.20 C.N and Hydrologic parameters of Airport basin (Appendix 5.4.5)
Information is provided in Appendix 5.4.5.

5.3.2.5.21 Concentration time and Lag-time for Airport basin (Appendix 5.4.5)
Information is provided in Appendix 5.4.5.

5.3.2.5.22. Peak discharge and storage of water using HEC-HMS for Airport basin.

HEC-HMS method was used for peak discharge evaluation and store volume of water from the flooding. Furthermore, Figs. 5.24 and 5.25 show the results of Airport basin. It is important to mention that HEC-HMS program use the CN method defined by SCS (1986).

Sub-basin	Sb.1a	Sb2a	Sb.2b	Sb3a	Sb4a	Sb4b	Sb4c	Sb4d
P.D m^3s^{-1}	88.9	*13.1*	66.0	60.4	73.4	41.3	10.5	33.5
S.V (m^3)	200	35,700	303,700	164,900	228,400	97,000	26,200	101,700
Sub-basin	Sb4e	Sb.4f	Sb.5a	Sb6a	Sb.7a	Sb8a	Sb9a	
P.D (m^3s^{-1})	73.4	21.3	37.1	71.2	10.9	11.8	19.8	
S.V (m^3)	217,800	43,100	90,300	228,400	23,300	24,200	63,300	
Sub-basin	Sb10a	Sb.11a	Sb.12a	Sb13a	Sb.14a	Sb15a		
P.D (m^3s^{-1})	39.3	3.3	44.8	17.0	17.2	49.1		
S.V (m^3)	140,400	14,700	175,400	47,700	53,400	152,800		

Figure 5.24. Peak discharge and stored water for sub-basins allocated on the Airport basin. Source of data for calculation: SCS (1986).

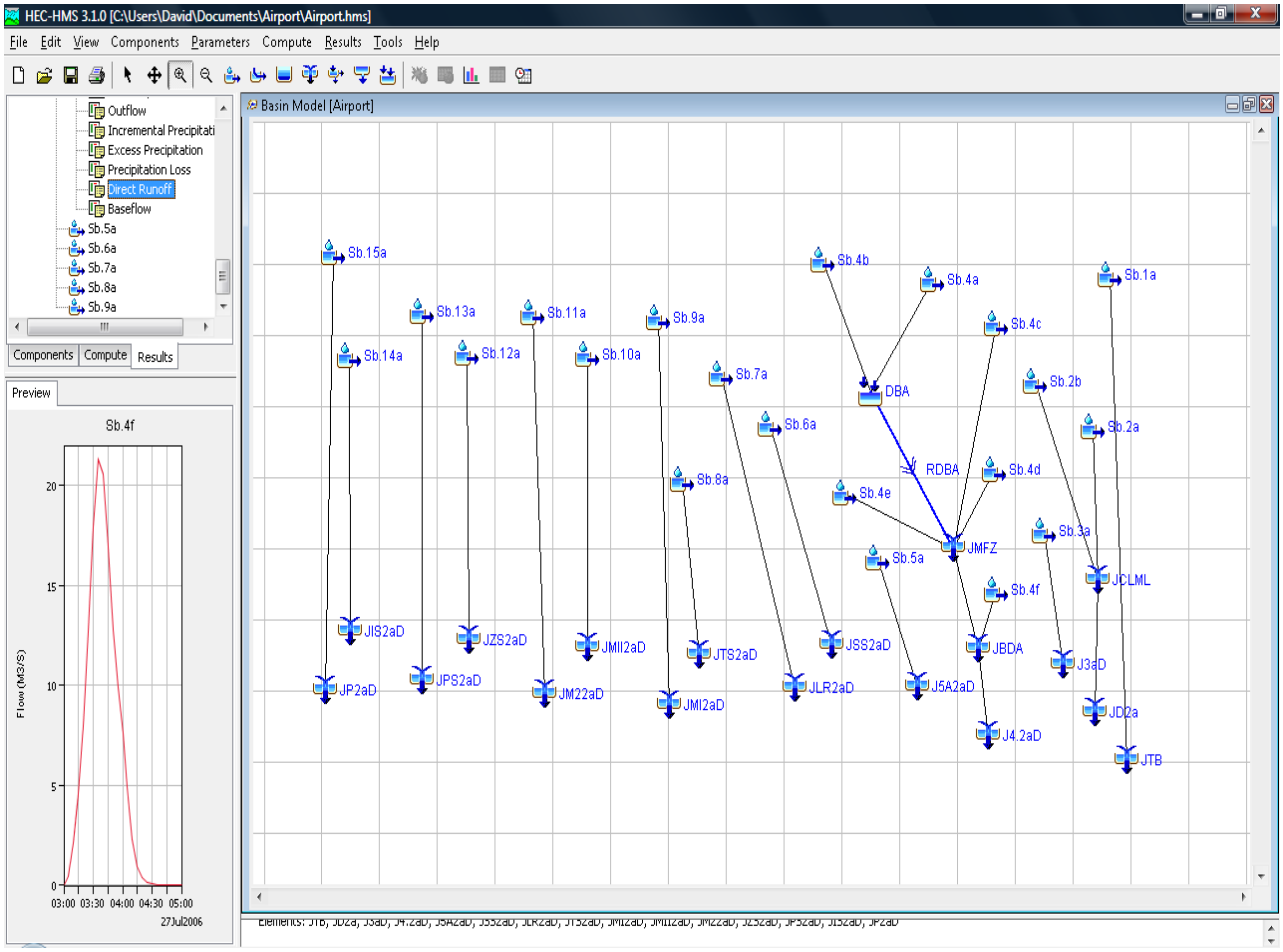

Figure 5.25. HEC-HMS simulation flooding hazard model components for Airport basin. Source of the method HEC-HMS (2002) version 3.1.0.

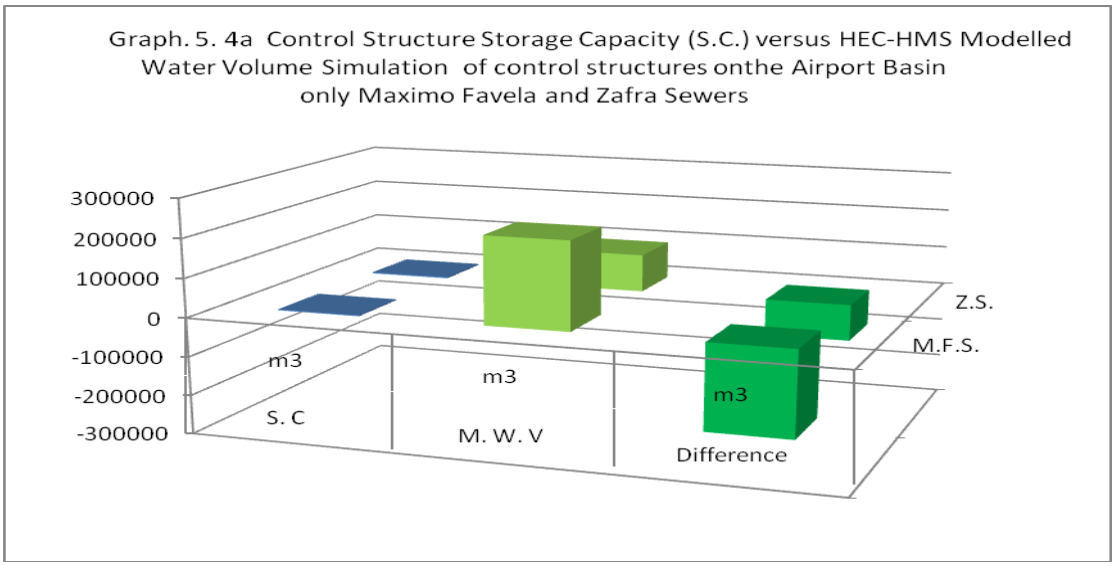

Figure 5.26. Structure storage capacity (S.C) versus HEC-HMS simulation flooding water volume for Airport basin. Negative bars indicate the part of the basin where dykes are expected to fail during flooding events. Source of calculation: IMIP (2005).

5.3.2.6 Bravo River basin network distribution and description.

The general geographic location of this basin is presented in Fig. 5.7 and sub-basins which comprise Bravo River basin are illustrated below in Fig. 5.27. Furthermore, a full description is presented in section 5.3.2.6.1.

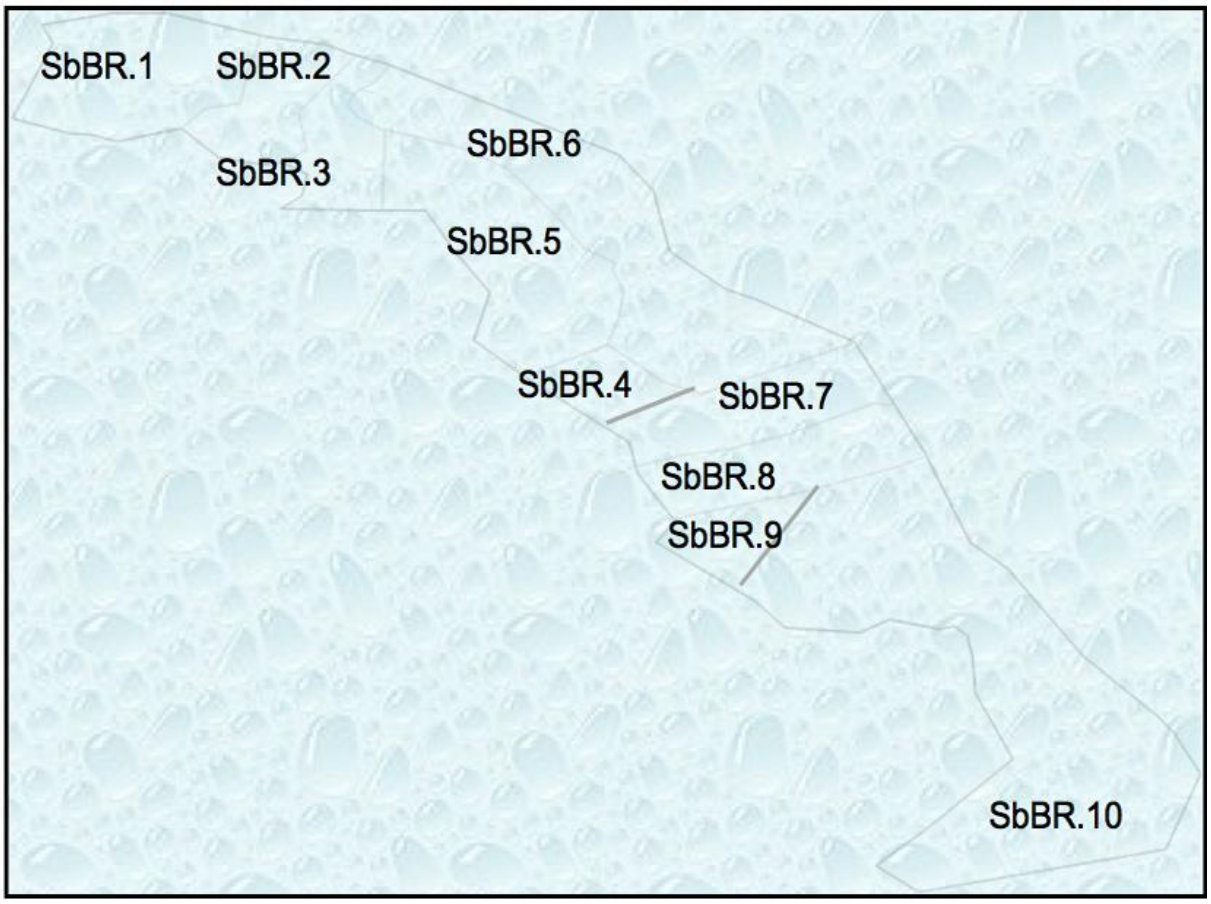

Figure 5.27. Bravo River sub-basin distribution and location. Width of basin at its widest point is 3.4 km.

5.3.2.6.1 Description of Bravo River basin drainage system.

5.3.2.6.2 Bravo River Basin. The area of this basin is 59.018 km^2 (Figs. 5.27 and 5.28) and it is limited to: The north-northwest, by the Bravo River border and Americas Avenue. To the south-southwest, by Acequia Madre. Land-use of the area is fundamentally Commercial, Industrial and of Services. It is equipped with a good transportation system mostly urbanized and paved. In addition, there are a lot of Government offices, business and enterprises as well as factories installed in the area. Topographically, this sector is flat with low slope and not connection with other

areas. Therefore, its drains to Bravo River through an interceptor drain. However, there are other areas that are affected by inundations because of the low runoff capacity of these undefined streams course. Also, because, there are not any control structures in the area (Figs. 5.28 and 5.29).

5.3.2.6.3 Sub-basin Bravo River 1 SbBR.1. This basin includes neighbourhoods of: Americas, Cordova-Americas, Patricia Mayorga, Los Naranjos, Los Olmos, Santa Monica, Vista del Norte, Fovissste-Chamizal, Rincon's del Campanario, Pronaf and Monumental among others. Its land-use is basically residential as well as Industrial. It is limited by the Bravo River, Acequía Madre and Americas Avenue. The main water concentration is located near to the intersection of Melquiades Alanis and Plutarco Elias Calles Streets (Francisco Villa Neighbourhood). In addition, there is a natural depressive area in Americas and Del Charro Intersection streets. This sub-basin is connected to junction J1 which discharges a total of 295,000 m^3 (Figs. 5.28 and 5.29).

5.3.2.6.4 Sub-basin Bravo River 2 SbBR2. This basin is limited to the south, by Paseo Tríunfo de la República and Gómez Veleta streets, to the west, by Valentín Fuentes Avenue and to the north, by the Bravo River. There are a lot of industrial parks as well as residential homes allocated on the area. One of the most important water concentrations is located near to Fidel Velazquez neighbourhood between the Arizona and Rafael Perez Serna streets; in addition, this problem is aggravated because there is not any control structure to mitigate inundation problems. This sub-basin is connected to junction J2 which drains 137,300 m^3 (Figs. 5.27, 5.28 and 5.29).

5.3.2.6.5 Sub-basin Bravo River SbBR3. It is limited as follows: to the east, by sub-basins SbBR4 and SbBR5 where the Valentín Fuentes Industrial park is installed and to the north, sub-basin SbBR2. The biggest inundation problems of this sub-basin are located on Tomas Fernandez and Vicente Guerrero intersection as well as, in the intersection of Paseo Triunfo De La Republica Street and Acequía Madre. Here, there is a sector of 2 km^2 where water rise nearly 20 cm or 40 cm in depth during flooding events. Another big problem is related to Infection because sanitary and

pluvial water mix together during flooding events. Finally this sub-basin is connected to junction J3 (Figs. 5.28 and 5.29) where it drains 152,000 m^3 (Figs. 5.27, 5.28 and 5.29).

5.3.2.6.6 Sub-basin Bravo River 4 SbBR4. It is limited to the north, by the Bravo River, to the east, by Las Industrias Avenue, to the south, by Vicente Guerrero Street, and to the west, by SbBR2 and SbBR3 sub-basins. Furthermore, urbanization in this sub-basin has been increased covering approximately 65 % of the sub-basin area. Therefore, some homes developments such as: Alameda, Arboledas and Residential neighbourhoods are increasing quickly. The sub-basin presents some inundation areas with nearly 50 % of the total area. One of the reasons of this problem is because this sub-basin is limited to the north by a boundary that is not connected to the Bravo river water flow, Similarly to sub-basin SbBR2 water concentrates in some local collector streets mainly in flat and depressive areas. Finally, its sub-basin is connected to Junction J4 draining 124,300 m^3 (Figs. 5.27, 5.28 and 5.29).

5.3.2.6.7 Sub-basin Bravo River 5 SbBR5. It is limited; to the north, Sub-basins SbBR4 and SbBR6; to the east, Las Torres Ave; to the west, Acequía Madre and Sub-basin SbBR3. In this sub-basin are allocated the Hippodrome as well as one of the most important Industrial parks (Bermudez Industrial Park). In addition, another important residential neighbourhood located in the area is (Campos Eliseos). This sub-basin exhibits a flat topography and consequently many inundation areas occurred during flooding events. The most affected is located on the intersection of Tomas Fernandez and Vicente Guerrero streets. Finally, this sub-basin is connected to junction J5 draining 347,600 m^3 (Figs. 5.27, 5.28 and 5.29).

5.3.2.6.8 Sub-basin Bravo river 6 SbBR6. Drains 329,000 m^3 (Figs. 5.27 and 5.28) and it is limited; by the Bravo River at northeast margin. Las Torres Avenue, in the south and in the west by the SbBR4 and SbBR5 sub-basins. An important part of this area is urbanized and some neighbourhoods were recently constructed. Some of the most important residential areas are between others Valle Verde and Alameda neighbourhoods. Normally water flows through the centre of the sub-basin producing

inundation areas in approximately 50% of its total area and it is connected at J6 (Figs. 5.28 and 5.29).

5.3.2.6.9 Sub-basin Bravo River 7 SbBR7. It is a mostly developed sector and it is limited by the Bravo River in the northeast, by Acequía Cordero in the south and by De las Torres Avenue in the west. The more important inundation area of this sub-basin is located along the left side of Acequía Cordero where many home developments have been constructed recently. The land-use of the area is predominantly residential. In addition, water concentrates in some depressed undeveloped natural areas and stays there until their infiltration or evaporation so it is a big human risk for infectious. Finally, this sub-basin is connected to junction J7 draining 171,100 m^3 (Figs. 5.27, 5.28 and 5.29).

5.3.2.6.10 Sub-basin Bravo River 8 SbBR8. It is limited; to the south, by sub-basin SbBR9 along a parallel line until Gómez Morin Boulevard; to the west, through north of Las Torres Avenue until their intersection with sub-basin SbBR7; finally, to the northwest by the Bravo river. The land-use in this area is mostly agricultural but recently this area has been developed with many residential homes. Similarly to sub-basin SbBR7 and SbBR6, water concentrates in depressive flat areas provoking obvious flooding problems to people in contact with it. This sub-basin is connected to junction J8 draining 233,400 m^3 (Figs. 5.27, 5.28 and 5.29).

5.3.2.6.11 Sub-basin Bravo River 9 SbBR9. Drains 179,100 m^3 (Figs. 5.27 and 5.28).and it is limited; to the south, Acequía Madre since Torres avenue until its junction with Acequía del Pueblo and drain 2A, then following through west its limits are Torres avenue, and to the north, with sub-basin SbBR10. This sub-basin has approximately 60 % of urbanized area and water concentrates mostly on the south side of Manuel Gómez Morin Boulevard. Close to Satellite neighbourhood. Its connection is at J9 (Figs. 5.28 and 5.29).

5.3.2.6.12 Sub-basin Bravo River 10 SbBR10. Drains 770,000 m^3 (Figs. 5.27 and 5.28). It is the biggest sub-basin of the Bravo river basin and is located as a band between the Bravo River and Acequía Madre. Since Quintas Del Valle

neighbourhood until approximately 1 km southwest of Independency Boulevard. Within, this area, there are the Bravo Industrial park as well Zaragoza International bridge. In addition, this sub-basin has important streets such as: Gomez Morin, Ramon Rayon, independence and others. It is connected to Junction J10 (Figs. 5.28 and 5.29).

5.3.2.6.13. C.N and hydrologic parameters Bravo River basin (Appendix 5.4.6)
Information is provided in Appendix 5.4.6.

5.3.2.6.14 Concentration time and Lag-time for Bravo River basin (Appendix 5.4.6)

Information is provided in Appendix 5.4.6.

5.3.5.6 Peak discharge and storage of water using HEC-HMS for Bravo River basin.

HEC-HMS method was used for peak discharge evaluation and store volume of water from the flooding. Furthermore, Figs. 5.28 and 5.29 show the results of Bravo River basin. It is important to mention that HEC-HMS program use the CN method defined by SCS (1986). Fig. 5.28 shows peak discharge and stored water for sub-basins in Bravo River basin.

Sub-basin	SbBR.1	SbBR.2	SbBR.3	SbBR.4	SbBR.5	SbBR.6	SbBR.7
P.D (m^3s^{-1})	64.1	29. 3	35.8	43.2	90.9	86.1	52.3
SV (m^3)	295,000	137,300	152,000	124,300	347,600	329,000	171,100

Sub-basin	SbBR.8	SbBR.9	SbBR.10
P.D (m^3s^{-1})	52.2	52.4	168.5
S.V (m^3)	233,400	179,100	770,000

Figure 5.28. shows the results of the concentration time as well as the Lag-time for the sub-basin located within the Bravo River basin. Source of calculation in this Figure: (Kiprich,1940 in: Loukas & Quick, 1995).

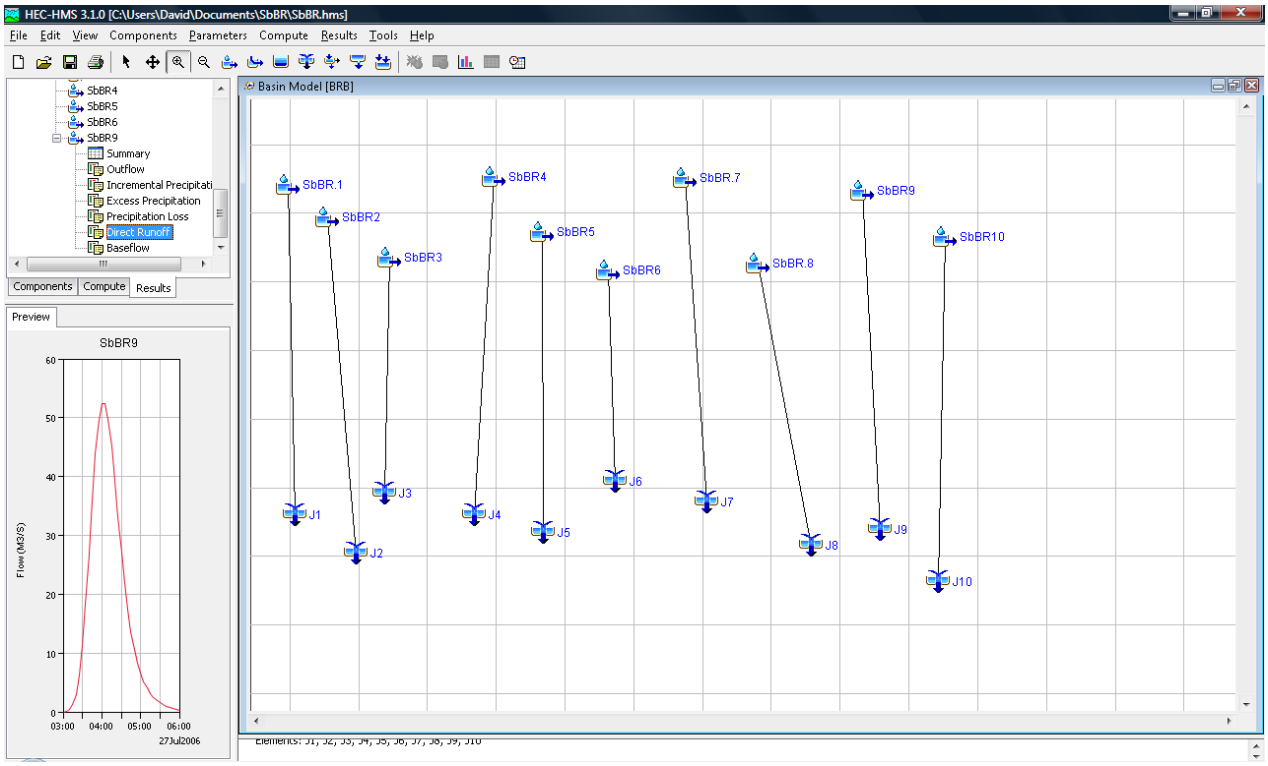

Figure. 5.29. HEC-HMS simulation flooding hazard model components for Bravo river basin. Source of model: HEC-HMS (2002) version 3.1.0.

5.3.2.7 Acequias basin network distribution and description.

The general geographic location of this basin is presented in Fig. 5.7 and sub basins which comprises Acequias basin are illustrated below in Fig. 5.30. Furthermore, a whole description is presented in section 5.3.2.7.1

5.3.2.7.1 Description of Acequias basin drainage system

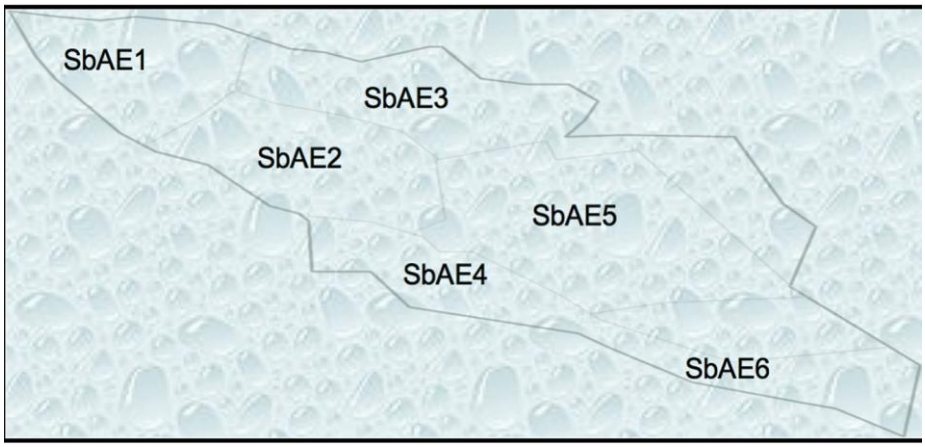

Figure 5.30. Acequias Basin and sub-basin distribution. Width of basin at its widest point is 3.6 km.

5.3.2.7.1 Description of Acequias basin drainage system.

This basin is limited by Bravo River, Airport, Centre and Chamizal basins (Figs. 5.7; 5.30; 5.31and 5.32) has an area of 28.7070 km^2. This basin basically is integrated by six neighbour sub-basins that drain through the central lowest areas. In addition, this problem is aggravated due to over-spilling of Acequía del Pueblo and also because drain 2A, does not have enough store capacity during flooding events. The next paragraphs show the sub-basins composed by this basin (Fig. 5.30).

5.3.2.7.2 Sub-basin SbAE1. This sub basin is limited: to the southwest Acequía del Pueblo where there are located some neighbourhoods such as: Ex-hippodrome, El Barreal and Partido Romero between others and to the north, by Paseo Triunfo de la Republica street. This sub-basin has a flat geometry with low gradient that cause water concentration in two sectors: One, in the intersection of Juan Gabriel, 16 de Septiembre and Insurgentes streets. The other, in the intersection of Insurgentes and Reforma streets. The connection of this sub-basin is through J1 where 198,800 m^3 water volumes is drained (Figs. 5.30, 5.31 and 5.32).

5.3.2.7.3 Sub-basin SbAE2. This sub basin is limited to the west by 2 de Abril Street and to the north by Acequia Madre. This sub-basin is geometrically formed as a long band along the Francisco Marquez and Tecnológico streets. Similarly to sub-basin SbAE1, this sub-basin has two inundation areas. One located in the intersection of the Raza and Charro streets and the other in Adolfo Lopez Mateos and Plutarco Elias Calles streets. Finally, this sub-basin drains 179,400 m^3 through junction J2 (Figs. 5.31and 5.32).

5.3.2.7.4 Sub-basin SBE3. This sub basin is limited to the north by Oscar Flores and Valentín Fuentes streets and to the Southwest, Acequía del Pueblo. Like SbAE1 and SbAE2 has a very flat surface and the average slope is in the order of 0.5%, finally, this sub basin spill 184500 m^3 (Figs. 5.31 and 5.32).

5.3.2.7.5 Sub-basin SBAE4. This sub basin runs from Tecnológico to Industrias street along Acequía del Pueblo until Valentin Fuentes Street and then finishes in

Ejercito National Avenue. This sub-basin which is the biggest of the sector basically concentrates its flooding in Virreyes, Real de San Jose and Seminario Neighbourhoods. Finally, it drains 298,500 m^3 to J4 (Figs. 5.31 and 5.32).

5.3.2.7.6 Sub-basin SbAE5. The path of this sub basin runs, from the west, along the Acequía del Pueblo, beginning in Ramon Rivera Industrial Park until the Residential Gardens Neighbourhood. After that, continues through Northeast until Camino Viejo San José which is located at the North parallel to Ejercíto Nacional Avenue. In this sub-basin during flooding events approximately 60% of its area is inundated principally near to Tecnológico Street and Acequía del Pueblo intersection. This sub-basin is connected at junction J5 draining 108,000 m^3 (Figs. 5.31 and 5.32).

5.3.2.7.7 Sub-basin SbAE6. This is partially urbanized and defined by a triangular geometry formed by Acequía Madre, Drain 2A and sub-basins SBAE4 and SbAE5. From Acequia Madre the sub-basin is limited since Gómez Morín Street until their intersection with drain 2A. The more important inundation area is located on Acequía Madre and Drain 1A near the Ejercito Nacional Avenue. Approximately 25 % of water is accumulated in this area; the rest is distributed over streets and residential areas as well as recreational areas. Finally, it's connected to junction J6 where spill 211,300 m^3 (Figs. 5.31 and 5.32).

5.3.2.7.8 C.N and hydrologic parameters Acequias basin (Appendix 5.4.7)
Information is provided in Appendix 5.4.7.

5.3.2.7.9 Concentration time and Lag-time for Acequias basin (Appendix 5.4.7)
Information is provided in Appendix 5.4.7.

5.3.2.7.10 Peak discharge and store water using HEC-HMS for Acequias basin.

HEC-HMS method was used for peak discharge evaluation and storage volume of water from the flooding. Furthermore, Figs. 5.31 and 5.32 show the results of Acequias basin.

Sub-basin	SbAE1	SbAE2	SbAE3	SbAE4	SbAE5	SbAE6
P.D (m^3s^{-1})	43.2	30.9	34.5	51.6	24.1	34.5
S.V (m^3)	198,800	179,400	184500	298,500	108,000	211300

Figure 5.31. Peak discharge and stored water for sub-basins located in the Acequias basin.

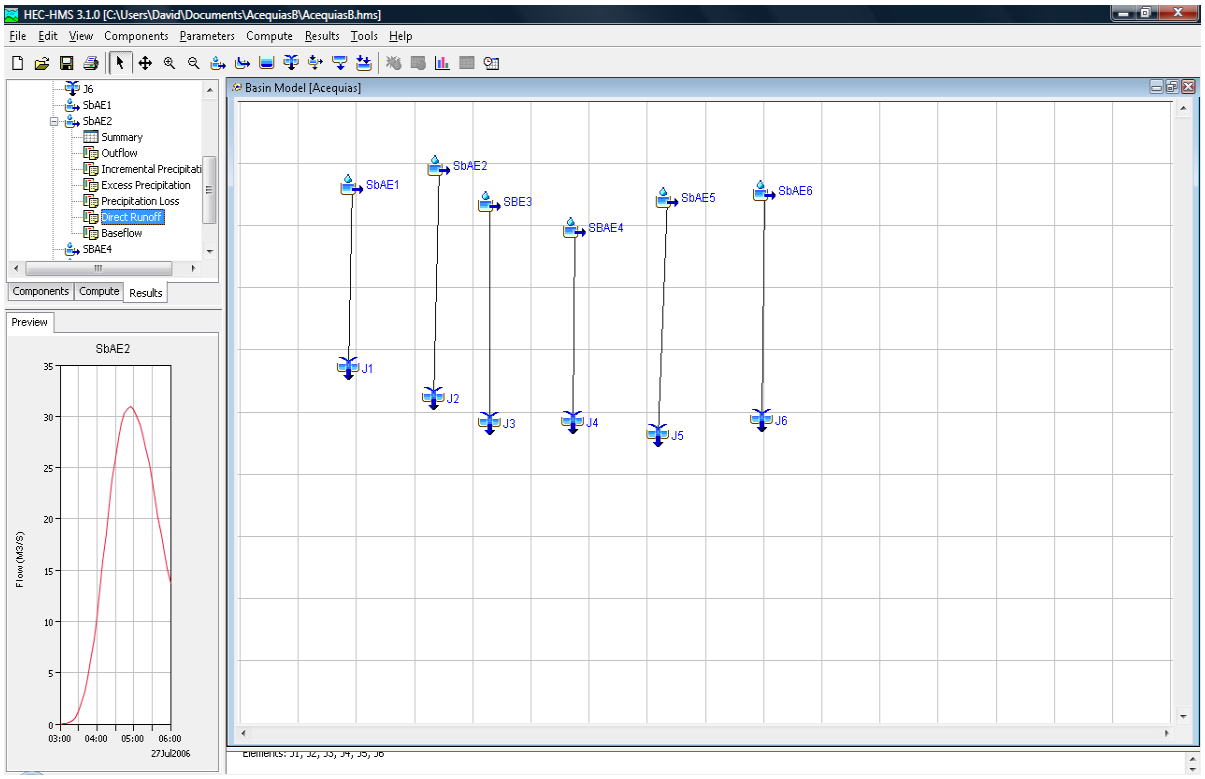

Figure 5.32. Peak discharge and stored water for sub-basins located in the Acequias basin.

5.3.2.8 Chamizal basin network distribution and description.

The general geographic location of this basin is presented in Fig. 5.7 and the sub basins which comprises Chamizal basin are illustrated below in Fig. 5.33. Furthermore, a whole description is presented below in section 5.3.2.8.

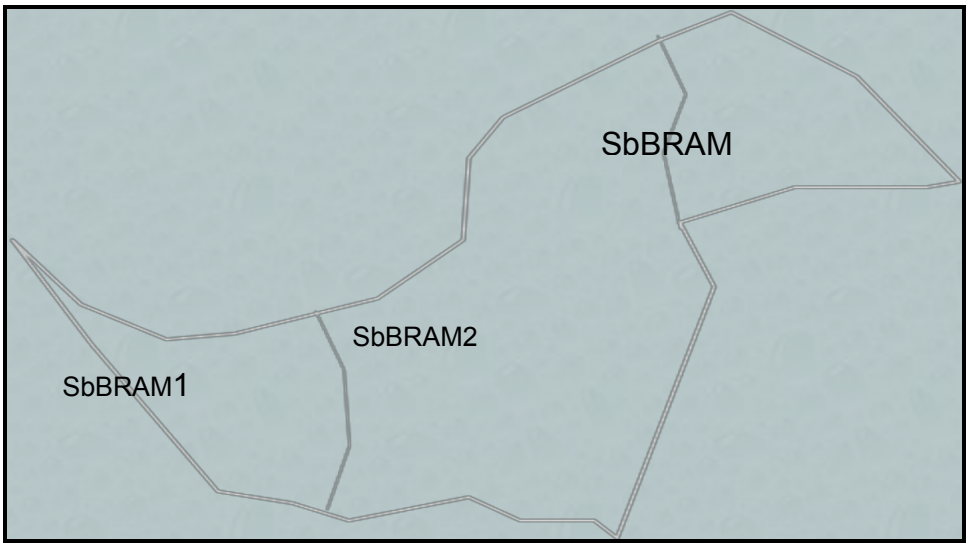

Figure 5.33. Chamizal sub-basin distribution.Width of basin at its widest point 2.1 km

5.3.2.8 Chamizal basin network distribution and description.

5.3.2.8.1 Description of Chamizal basin. Chamizal Basin located near to the old centre of the city has an area of 6.058 km^2. Basically, the land-use of this sub-basin is predominantly recreational as well as services there are many government offices. It is mostly paved and urbanized with an important transportation system. This transportation system is frequently affected during flooding events. Also, in this sub-basin is located the Santa Fe International Bridge near to the centre of the city and the Cordova-Americas International Bridge near to the Chamizal Park. These two bridges provide the communication between two cities of Juárez city and El Paso Texas city. Topographically this sub-basin is characterized by low slope 0.5%. In the following paragraphs the sub basins enclosed to Chamizal basin are described.

5.3.2.8.2 Sub-basin Bravo River AM1 SbBRAM1. Located between Bravo River and Acequía Madre this sub-basin drains 61,800 m^3 (Figs. 5.34 and 5.35) have two big inundation areas. One, located in the intersection of Francisco Villa and Malecón streets near to the Municipal Government building and the other in Acequía Madre, Bravo River and Francisco Villa Street, near to the fire station building office. This

area is mostly paved and urbanized and during flooding events the transportation system is affected. This sub-basin is connected to junction J1 (Figs. 5.34 and 5.35).

5.3.2.8.3 Sub-basin Bravo River AM2 SbBRAM2. This sub basin drains 141,500 m^3 (Figs. 5.34 and 5.35) and is located in the central area of the city the limits are: the Bravo River to the north; Acequía Madre to the south and to the east Americas Avenue. Similarly, the other sub-basins in the area are mostly urbanized and paved. Its land-use is predominantly commercial and of services and topographically presents the same characteristics as SbBRAM1. A big part of the Chamizal Park and some residential areas such as: Hidalgo, Americas and Margaritas neighbourhoods are vulnerable during flooding events. In addition, this sub-basin is located near to the older course of the Bravo River already converted in recreational park as well as a corridor where a street system and the Chamizal Park are important structures. Finally, this sub basin discharges in J2 (Fig. 5.35).

5.3.2.8.4 Sub-basin Bravo River AM3 SbBRAM3. Located northwest of International Cordova-Americas bridge and limited by: the Bravo River to the north and by Americas and Heroico Colegio Militar avenues to the south it drains 45,100 m^3 (Figures 5.34 and 5.35). It adopts a similar geometrical and topographical characteristics to SbBRAM2 with land-use mostly recreational. The street system is composed for primary streets fundamentally and exhibits a few inundation connecting convergence point J3 (Fig. 5.36).

5.3.2.8.5. C.N and hydrologic parameters Chamizal basin (Appendix 5.4.8)

Information is provided in Appendix 5.4.8.

5.3.2.8.6. Concentration time and Lag-time for Chamizal basin (Appendix 5.4.8)

Information is provided in Appendix 5.4.8.

5.3.2.8.7. Peak discharge and storage of water using HEC-HMS for Acequias basin.

Sub-basin	SbBRAM1	SbBRAM2	SbBRAM3
P.D (m^3s^{-1})	14.8	33.9	12.6
S.V (m^3)	61,800	141,500	45,100

Figure 5.34. Peak discharge and stored water for sub-basins located in the Chamizal basin

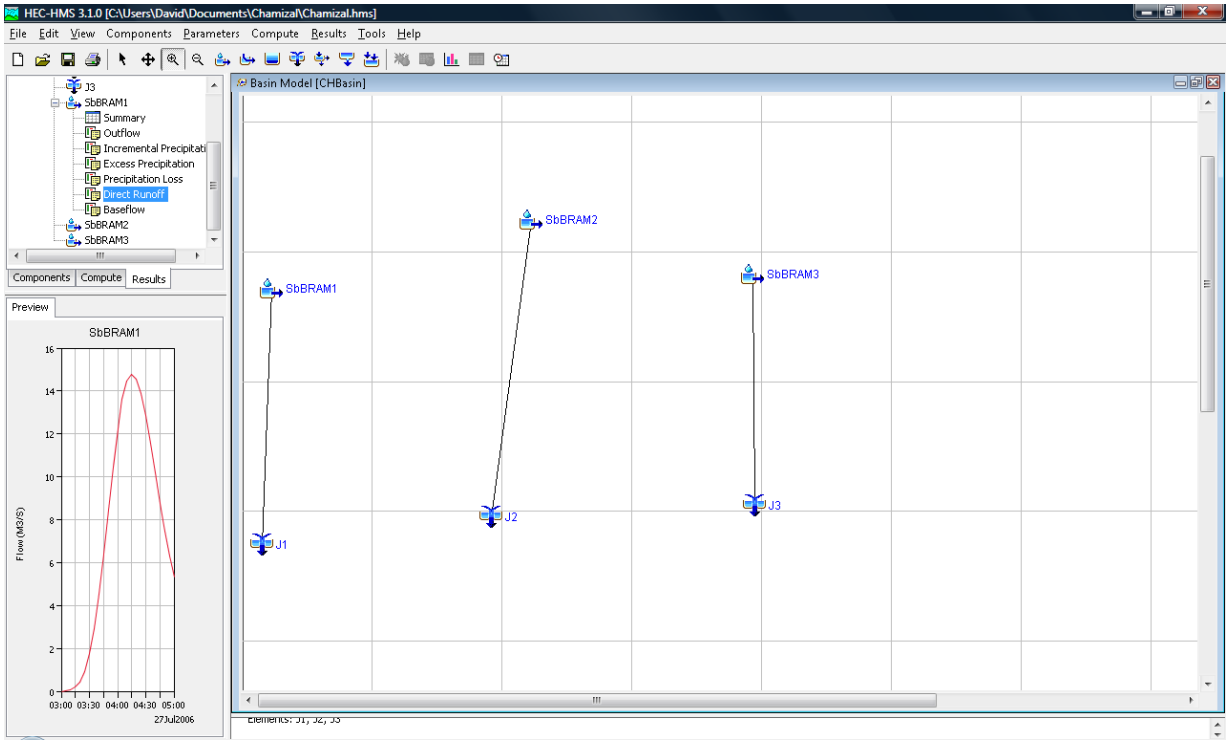

Figure 5.35. HEC-HMS simulation flooding hazard model components for Chamizal basin. Source for the model HEC-HMS (2002) version 3.1.0.

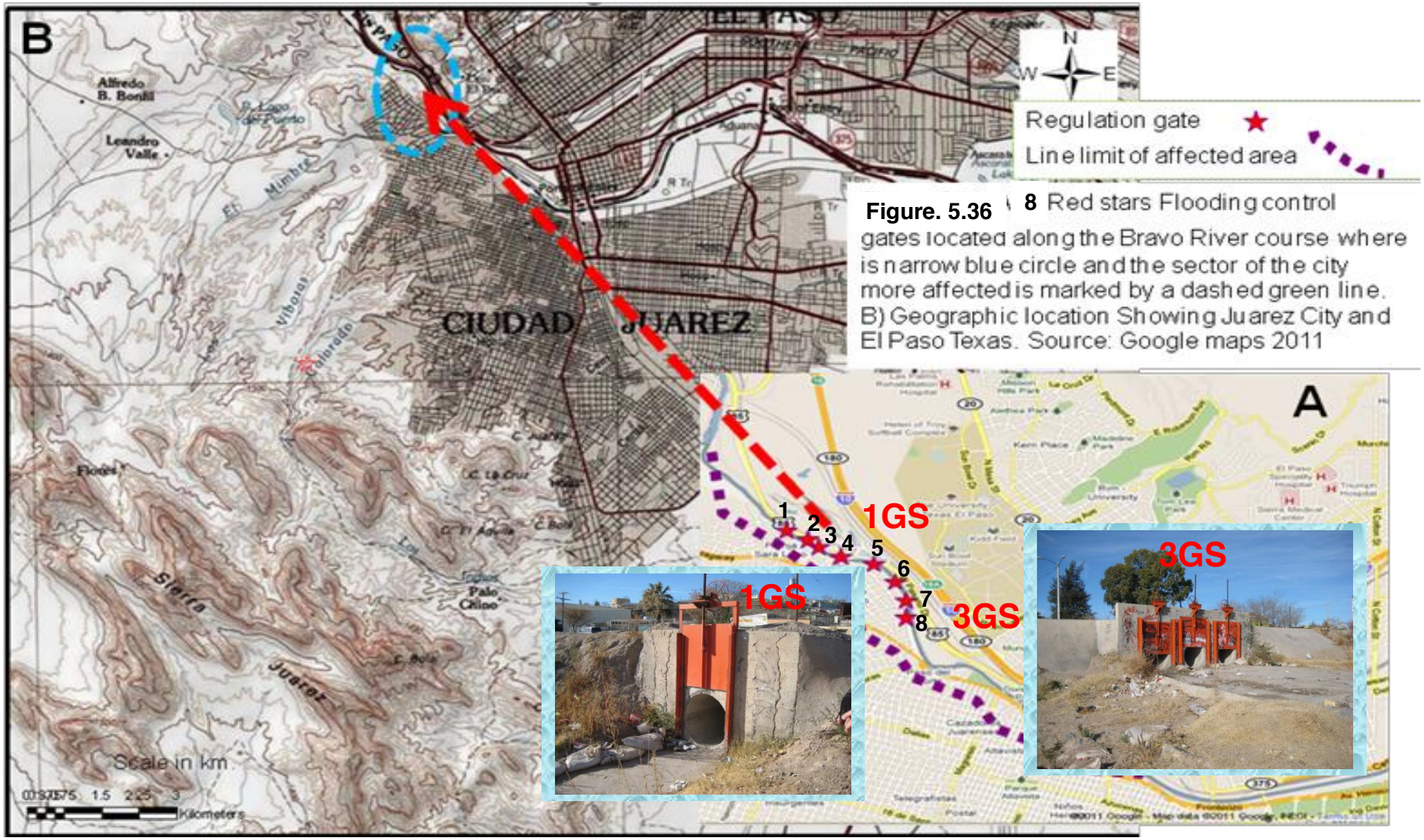

Figure. 5.36 gates located along the Bravo River course where is narrow blue circle and the sector of the city more affected is marked by a dashed green line. B) Geographic location Showing Juarez City and El Paso Texas. Source: Google maps 2011

Figure 5.36. Map of locations of sluice gates allowing floodwaters to exit to the Bravo River in the Chamizal Basin area. The inset picture of 1GS means a 1 gate system the dimensions of which are: 1.35 m by 1.25 m. Points indicated in the map along the Bravo River, for Points 1 to 7, are 1GS. At point 8 there is a 3GS which means three gates of 1.35 m by 1.25 m each one.

CHAPTER 6

6.1 INTRODUCTION

Three main computer programs: HEC-HMS (2002); HEC-RAS (2002); and the version 3.2 of Arc-View (2002) with HEC-GeoRAS (2002) module included are used here to assess the flooding hazard of the study area. Thus, hydrographs derived from HEC-HMS model comprise 8 basins (see Chapter 5). However, in this chapter only two basins located in the medial active alluvial fan system were addressed; Anapra and Center basins. The reason to focus on only these two basins is because they cover the most active part of the fan system and present the greatest threat of Juárez city. The following sections show the design storm and the HEC-HMS (2002) hydrographs derived from different streams and reaches located in Anapra and Center basins (see Figs. 6.1 to 6.4).

6.2 OVERVIEW OF DESIGN STORM IN THE STUDY AREA

6.2.1. Design hyetogram to model HEC-HMS hydrographs

The hyetogram of the study area was assessed in Chapter 5 (see Fig. 5.7) using the Cheng (1983) probabilistic approach. This approach was used because it is more suitable and widely applied in desert areas like that of Ciudad Juárez. The design storm was assessed in Chapter 5, Section 5.2.2.3 for three return periods of: Tr 10 years=37 mm; Tr 50 years=50.5 mm. and Tr 100 years=55.5 mm; in each case the rainfall in mm per storm is that expected for the respective return period.

6.3 HYDROGRAPH DESIGN

6.3.1. Introduction

The area studied for the active alluvial fan system is located inside two big basins named Anapra basin (Fig. 6.1) and Center basin (Fig. 6.2). Furthermore, stream network discharge and water volume stored in these basins and control regulation dykes were derived from HEC-HMS (2002) program simulation and were assessed in Chapter 5. This section briefly reproduces those related to Anapra and Center basins as mentioned at the onset of this introduction section. Moreover, in Figures 6.3 and 6.4 the peak discharges of these two basins are provided

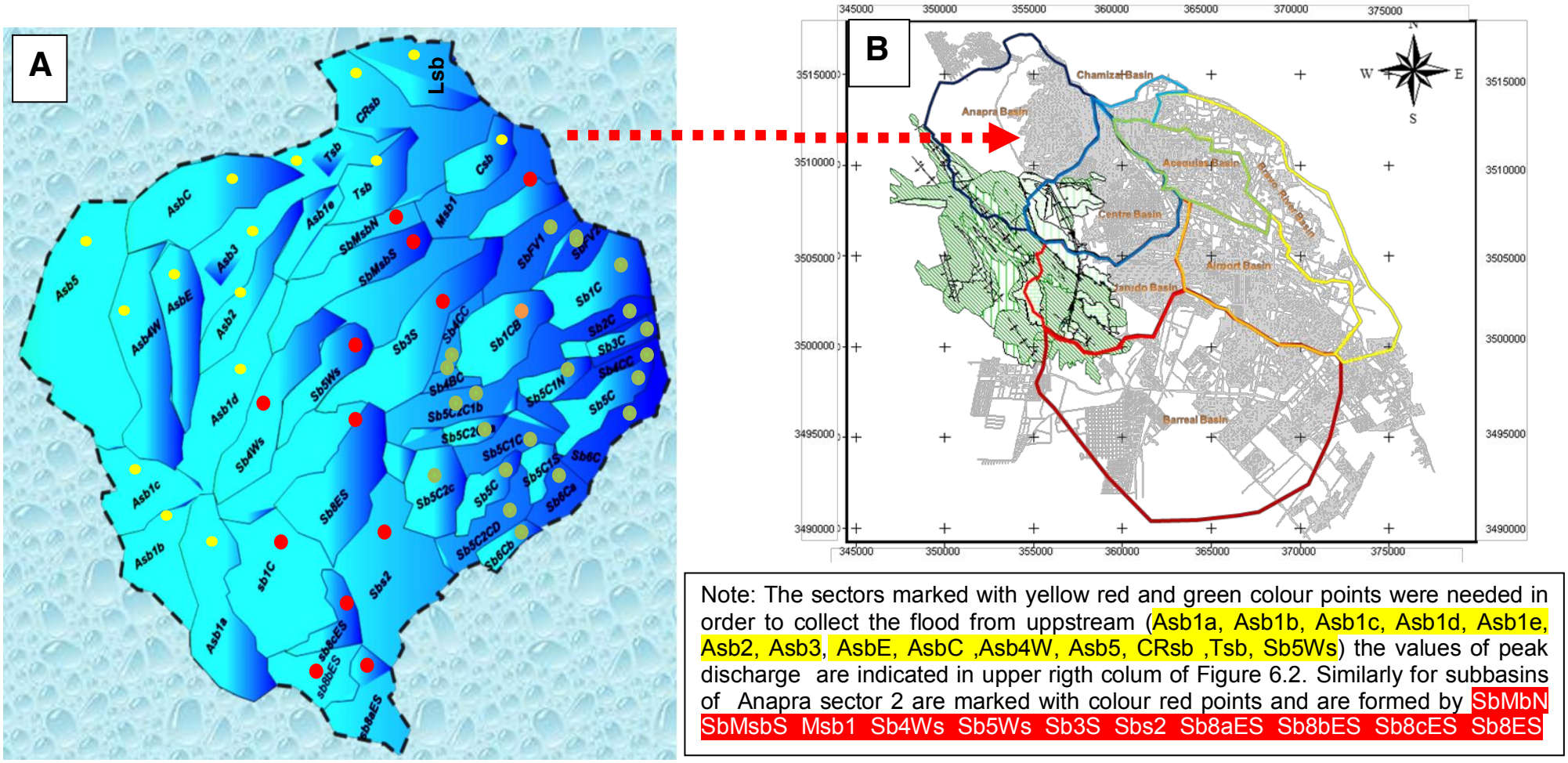

Note: The sectors marked with yellow red and green colour points were needed in order to collect the flood from uppstream (Asb1a, Asb1b, Asb1c, Asb1d, Asb1e, Asb2, Asb3, AsbE, AsbC ,Asb4W, Asb5, CRsb ,Tsb, Sb5Ws) the values of peak discharge are indicated in upper rigth colum of Figure 6.2. Similarly for subbasins of Anapra sector 2 are marked with colour red points and are formed by SbMbN SbMsbS Msb1 Sb4Ws Sb5Ws Sb3S Sbs2 Sb8aES Sb8bES Sb8cES Sb8ES

Figure 6.1. Anapra Basin and its sub-basins locations: A) Shows the sub-basins located in Anapra basin. B) Shows its geographical location in UTM Coordinates: Created by David Zúñiga (2012) using HEC-HMS (2002) version 3.1.0. and Arc-View (2002).

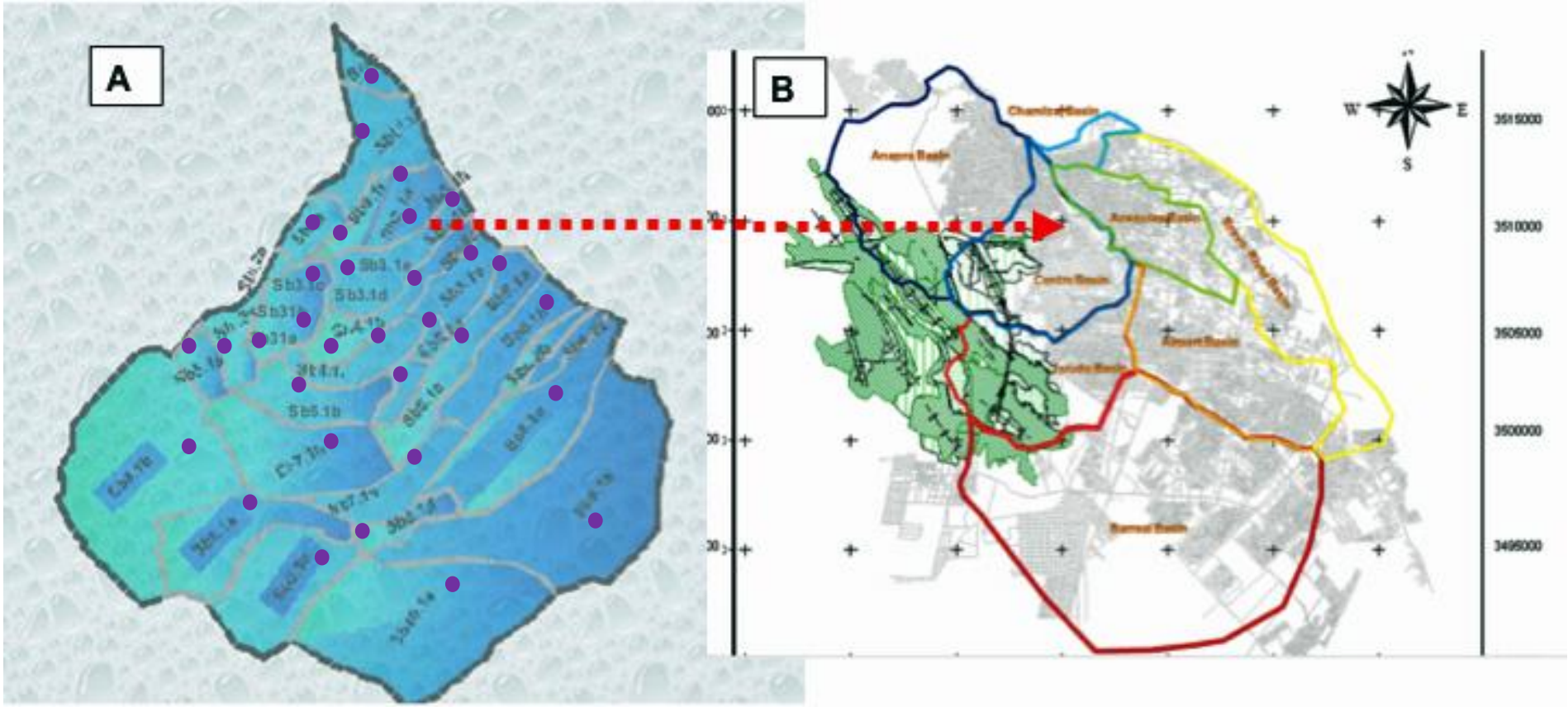

Figure 6.2. Center Basin and its sub-basins locations: A) Shows the sub-basins B) Shows its geographic location in (UTM) coordinates: Green colour points on Figure 6.1 means Colorado sector 1; blue colour points (Colorado sector 2). Peak discharge for 100 years return periods derived from HEC-HMS are shown in Fig. 6.3. TZ reaches zones indicated in column 2 of upper rigth table of Fig 6.3 were found similarly to that of Anapra basin. Created by David Zúñiga (2012) using HEC-HMS (2002) version 3.1.3

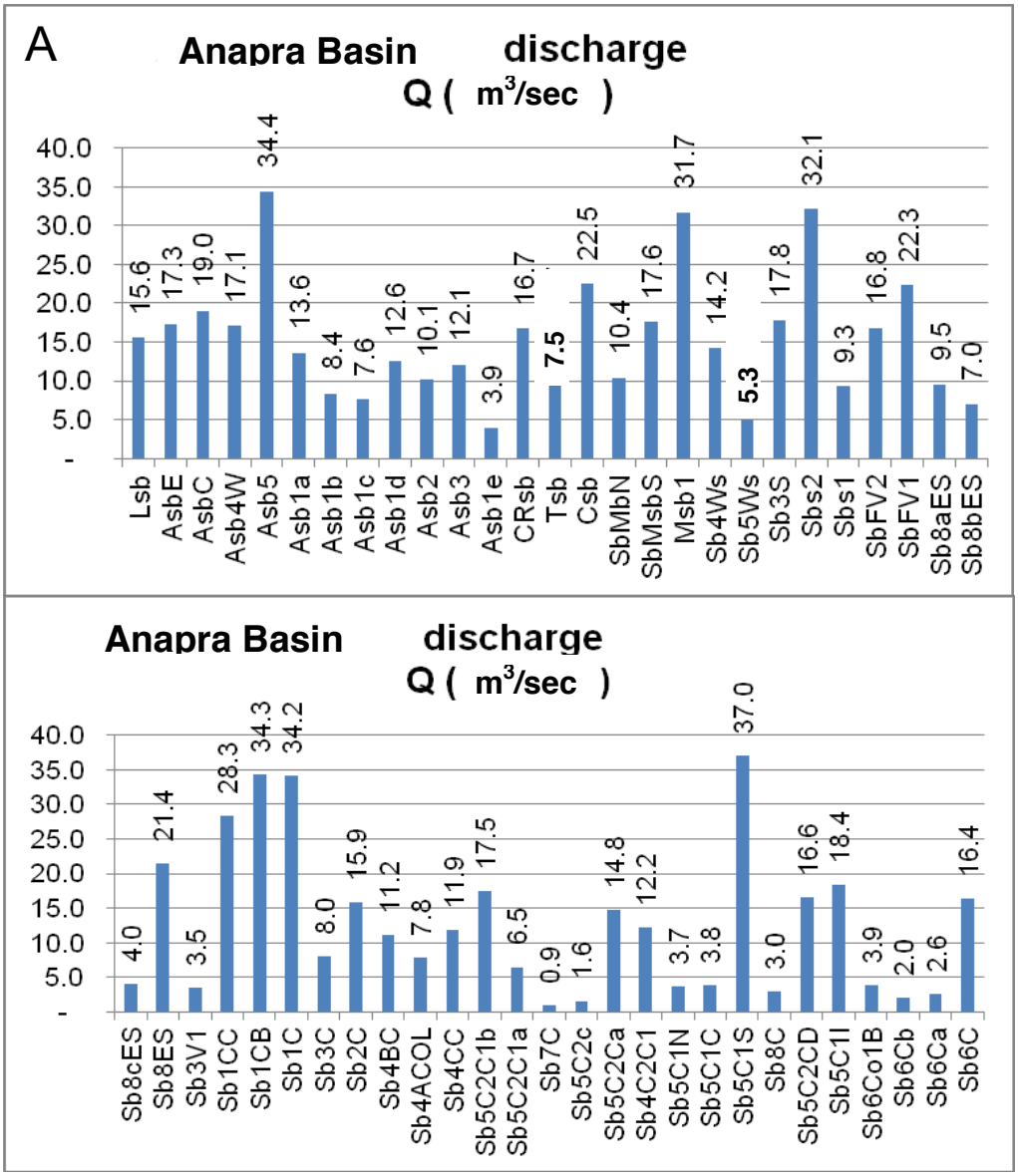

Sub-basin	TZ Q 100y m^3s^{-1}
AsbE	17.3 (Aw1)
AsbC	19.0 (Aw1)
Asb4W	17.1 (Aw1)
Asb5	34.4 (Aw2)
Asb1a	13.6 (Aw4)
Asb1b	8.4 (Aw4)
Asb1c	7.6 (Aw4)
Asb1d	12.6 (Aw4)
Asb2	10.1 (Aw3)
Asb3	12.1 (Aw2)
Asb1e	3.9 (Aw3)
CRsb	16.6 (AC)
Tsb	7.5 (AC)
Sb5Ws	5.3 (AC)
SbMbN	10.4 (M1)
SbMsbS	17.6 (M2)
Msb1	31.7 (M3)
Sb4Ws	14.2 (sw1)
Sb5Ws	5.0 (se5)
Sb3S	17.8 (sw2)
Sbs2	14.3 (sw3)
Sbs1	9.3 (sw4)
SbFV2	16.8 (Fv2)
SbFV1	22.3 (Fv1)
Sb8aES	9.6 (se1)
Sb8bES	7.0 (se5)
Sb8cES	4.0 (se3)
Sb8ES	21.4 (se1)
Sb3V1	3.5 (se2)
Sb1CC	28.3 (se4)
Sb1CB	34.3 (se6)
Sb1C	34.2 Sb1C
Sb3C	8.0 Sb3C
Sb2C	15.9 (FO)
Sb4BC	11.2 (4BC1)
Sb4ACOL	7.8 (4BC2)
Sb5C2C1b	17. 5(Jc8.5)
Sb5C2C1a	6.5 (Jc8.4)
Sb7C	0.9 (Jc8.3)
Sb5C2c	11.4(8C4)
Sb5C2Ca	14.8(Jc8.1)
Sb5C2C1	12.2 (Jc8.2)
Sb5C1N	3.7 (8C3)
Sb5C1C	3.7 (8C2)
Sb5C1S	3.9 (Gl.3)
Sb8C	3.0 (8C1)
Sb5C2CD	16.6(5C11.1)
Sb5C1I	18.4(5C11.3)
Sb6Ca	2.6 (Gl.1)
Sb6C	16.4 (Gl.2)

Figure 6.3. Peak deschage of Anapra basin A) Below blue barrs are subbasins names and above are discharge in m^3/sec (Q). **B)**.Yellow colour box= Anapra sector 1; red box=Anapra sector 2 and green colour box = Center sector 1 Table of Figure 6.3 indicates the name of sub-basin and the link with the transference zones (TZ) selected in order to perform the hydrograms routing through the sub-basin reaches. 1) The symbols in parentheses of column 2 (TZ) mean the name of the streams which drains its sub-basins from upstream to downstream. For instance, (sub-basins AsbE, AsbC and Asb4W converge in a common point thus W1=53.4 m^3/sec and the value is the predicted 100 yrs return period discharge. Similarly, the streams which are connected through transference zone are shown in columns 1 and 2 of the upper rigth table (See Fig. 6.5 and 6.6 to 6.10). 2) In Fig 6.1 are indicated the Anapra sector 1 subbasins marked by a yellow colour point which are inside os Anapra basin. Red colour boxes correspond to Anapra Sector 2. The discharge selected to map the flooding is that which corresponds to 100 yrs return period. Created by David Zúñiga (2012) using HEC-HMS (2002) version 3.1.3 and SCS (1986).

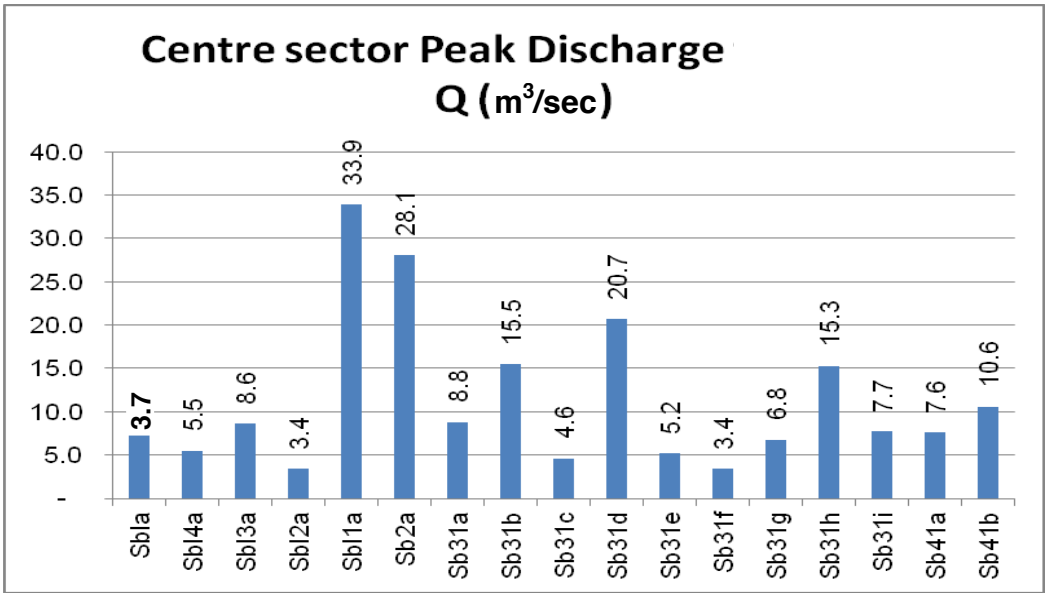

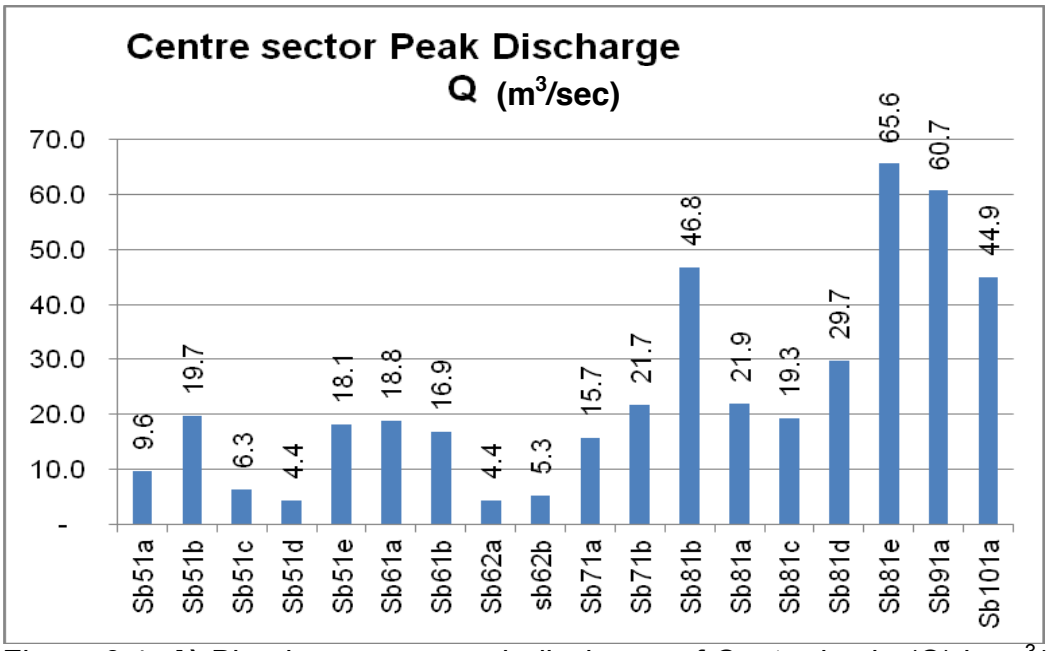

Sub-basin	TZ Q 100y m^3s^{-1}
Sbla	3.7(5C11.2
Sbl4a	5.5(First1)
Sbl3a	8.6(First3)
Sbl2a	3.4(First2)
Sbl1a	33.9(First5)
Sb2a	28.1(First4)
Sb31a	8.8(Snd1)
Sb31b	15.1(Snd2)
Sb31c	14.6(Snd3)
Sb31d	20.7(Snd4)
Sb31e	5.2(Snd6)
Sb31f	3.4(Snd5)
Sb31g	6.8(Snd7)
Sb31h	15.3(Snd9)
Sb31i	7.7(Snd8)
Sb41a	7.6(Third1)
Sb41b	10.6(Third2)
Sb51b	19.7(Four1)
Sb51a	9.6(Four2)
Sb51c	6.3(Four3)
Sb51d	4.4(Four4)
Sb51e	18.1(Four5)
Sb61a	18.8(Five1)
Sb61b	16.9(Five2)
Sb62a	4.4(Six1)
sb62b	5.3(Six2)
Sb71a	15.7(Seven1)
Sb71b	21.7(Seven2)
Sb81a	46.8(Eigth1)
Sb81b	21.9(Eigth2)
Sb81c	19.3(Eigth3)
Sb81d	9.1(Eigth4)
Sb81e	65.6(Eigth5
Sb91a	60.7(Eigth6)
Sb101a	44.9(Eigth7)

Figure 6.4. **A)** Blue bar means peak discharge of Center basin (Q) in m^3/sec for a return period of 100 years. On the x-axis the sub-basin names are indicated and in y- axis the peak discharge (Q) in m^3/sec. Blue colour box means Center sector 2 Note: Column 1 of upper rigth table indicate the name of sub-basin which converge with the transference main zones selected in order route the sub-basin hydrographs through the main reaches. (See the blue colour box and symbols in parentheses of upper rigth column 2 TZ that mean the name of the main stream which drains its sub-basin). For instance, Sb81e in blue bar graph = 65.6 m^3/sec is linked to transference zone (Eigth5) and the value is the predicted 100 yrs return period discharge is 65.6 m^3/sec; 2). The differents subbasins of this sector are marked with blue points in the Fig. 6.2. The discharge selected to map the flooding is that which corresponds to 100 yrs return period. Created by David Zúñiga (2012) using HEC-HMS (2002) version 3.1.3 and SCS (1986).

6.3.2. Discharge results (Hydrographs) for Anapra and Center sector and why were divided into sectors.

HEC-HMS model was applied to eight basins and was described in detail in Chapter 5 for three different return periods of the design storm: Tr=10 years, Tr=50 years and Tr=100 years. However, in the present chapter only the predicted discharge which produces flooding hazard to 100 years return period and their associated hydrographs evaluated in chapter 5 are extracted to assess flooding in active alluvial fan areas. The reason to use 100 years of return period instead of 50 or even 25 years which eventually are used in many Civil Engineering works is because this is the period which defines the design storm which produce the flooding hazard discussed on Chapter 5. Also, a 100-year return period is commonly used in flood predictions elsewhere (for example the Environment Agency website flood maps in the UK readily available online). The reason to divide Anapra and Center Basin in sectors is becasue basin hydrographs obtained from HEC-HMS should be routed upstream to downstream along reaches and streams of sub basins therefore transference zones and sectors from them are needed (See Figs 6.1 to 6.4). After that, results was evaluated by another program which performn energy and continuity equations. This program (HEC-RAS) is described in Chapter 3 and the resulting hydrographs are reproduced in Figs. 6.3 and 6.4. After that, these hydrographs were linked with the sub-basins using an identification name given in (Figs. 6.1 and 6.2) of Anapra and Center basins. The drainage network system is composed by many tributaries which converge to the main streams passing trough intermediate streams from upstream to downstream then sub-basins discharge or hydrographs are routing by HEC-RAS flow calculation using transference zones which routed these hydrographs along the main sub-basin streams (see section 6.4.2, tables of Figs. 6.3 and 6.4).

6.4. Flooding Hazard model methodology

6.4.1. *Introduction*

Assessing the flooding hazard model for the active alluvial fan system is the main aim of the present research. The model used in this thesis was described in depth in Chapter 3 and is widely used to perform flooding hazards. It is divided into

three main parts. Firstly, Pre-HEC-GeoRas; Secondly, HEC-RAS and Finally, Post HEC-GeoRas modules. Thus, in order to assess the flooding hazard over the active alluvial fan system the use of a digital three-dimensional method is needed. This method is a Pre-Processor and Post-Processor HEC-GeoRAS computer program, which works within the Arc-View 3.2 GIS environment. These modules create a data exchange file consisting of streams geometry extracted from a Triangular Intregrated Network (TIN) model created in Chapter 3 (see section 3.1.2 to 3.1.5 and Fig. 3.1; section 3.3; 3.3.1 to 3.3.8). In addition, Manning coefficients (n), contraction and expansion coefficient, geometric data and flow hydrographs were addressed using HEC-RAS (2002) ver. 3.1.3 computer program. All the previous issues mentioned were processed using the fundamental hydraulic energy equation concept. This concept is further applied in the computer program HEC-RAS (2002) ver. 3.1.3.

6.4.2. HEC-RAS Transference reaches zones for flow model application.

As stated in section 6.3.2 to apply HEC-RAS (2002) flooding hazard model, transference reach zones between the catchment source and depositional areas of active alluvial fans are needed. These transference zones sectors are presented in the following paragraphs: **Firstly**, Fig. 6.5 shows five streams which discharge in transference zone of Anapra basin sector 1 formed by: W1 (Fig. 6.6); W2 (Fig. 6.7); W3 (Fig. 6.8); W4 (Fig. 6.9) and AC (Fig. 6.10) (See Fig 6.1 yellow colour points and yellow colour box of Fig. 6.2). These reaches transited the discharge derived by HEC-HMS (See Fig. 6.3 above) also illustrated in Fig. 6.6 The previous work already performed to characterise the transference zone of sector 1 were applied also for the remaining transference zones sectors described after Fig. 6.11.Further application of HEC-RAS (2002) presented in section 6.4.3 leads to flooding hydraulic calculations based on the energy equation which is given in HEC-IFH (1992) and HEC-1 (1998) Hydraulic Reference Manuals. **Secondly**, The stream network which corresponds to transference reaches zones of sector 2 were defined similarly to sector 1 and were referred to Anapra basin, described in the Appendix 6A. The three streams which integrate transference zones of Anapra basin sector 2 (See FFig. 6.1 red colour points and red box of Fig. 6.2 and also see Appendix 6A) are: M1 (Fig. 6A.1), SW1 (Fig. 6A.2) and Snake (Fig. 6A.3). The discharge assigned to these transference reaches zones was derived by HEC-HMS (See Fig. 6.3) also illustrated below in (Fig. 6.5).

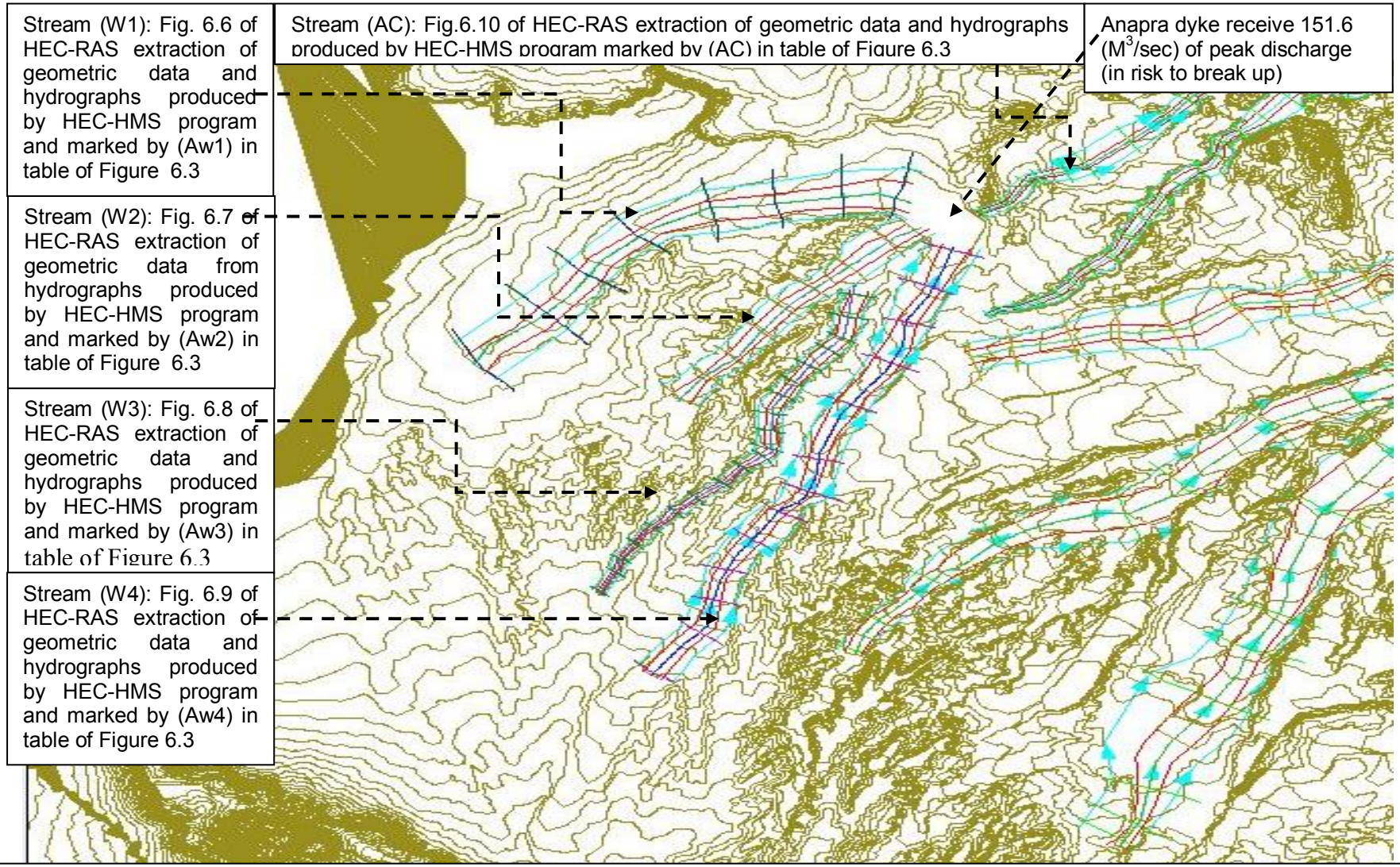

Figure 6.5. Link between the transference reaches zone 1 performed over the DEM during Pre-GeoRAS processor module and the associated flooding profile given in the previous link between HEC-HMS (2002) hydrographs and the reaches that are routed by HEC-HMS hydrographs, Green colour lines means countour levels every 5 m. Created by David Zúñiga (2012) using Arc-view 3.2 with HEC-GeoRAS pre and Post processor: 3D and spatial extensions.

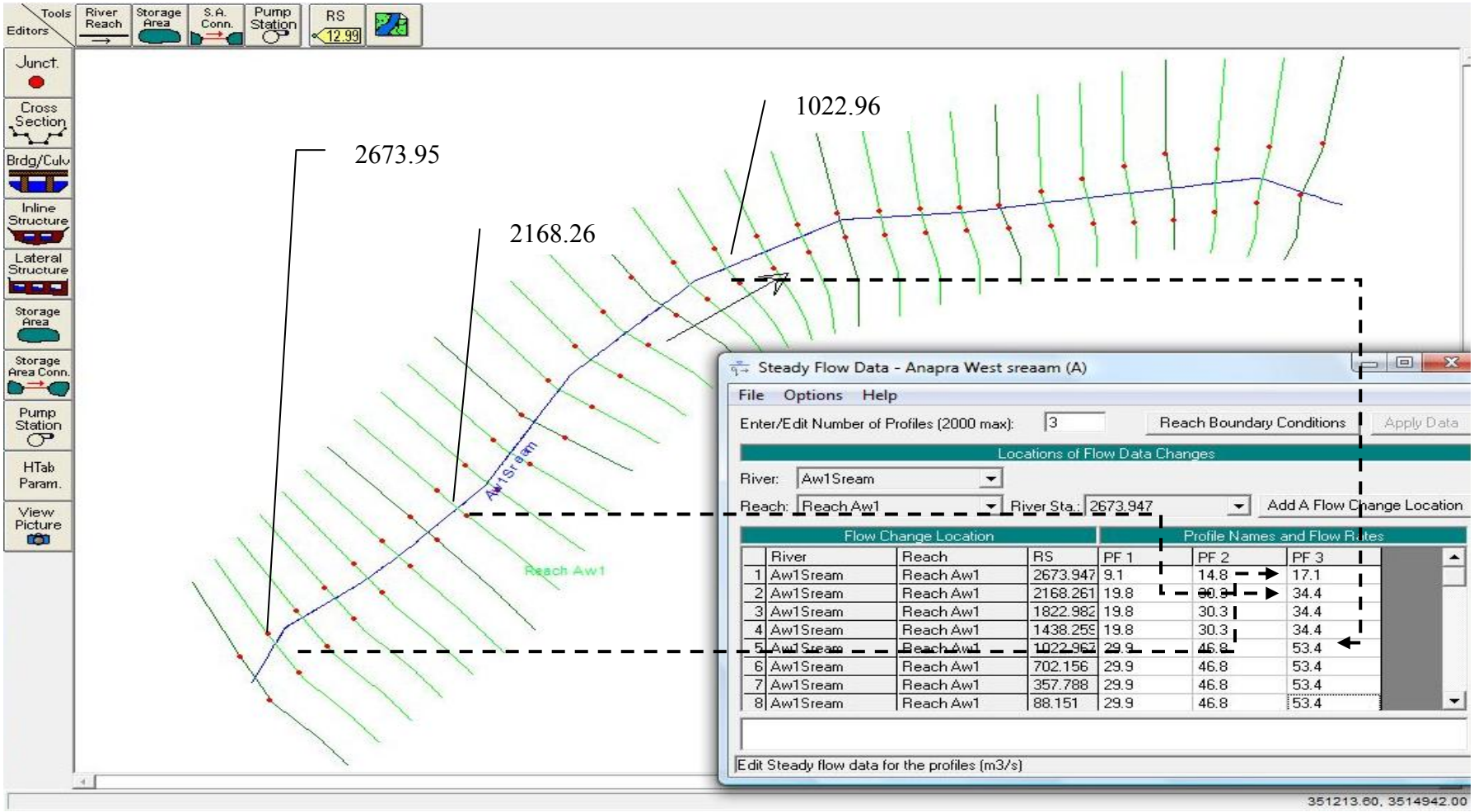

Figure 6.6. Association and organization of HEC-HMS hydrographs plans for flooding hazard plan (PF3 to Tr 100 years) into the HEC-RAS program. This stream driver corresponds to (Aw1) transference reach zone 1 which comprises subbasins: AsbE=17.1, AsbC=17.1 and Asb4W=19.0 m^3/sec (See yellow box of TZ column of Fig. 6.3). Created by David Zúñiga (2012) using HEC-RAS (2002) version 3.1.3.

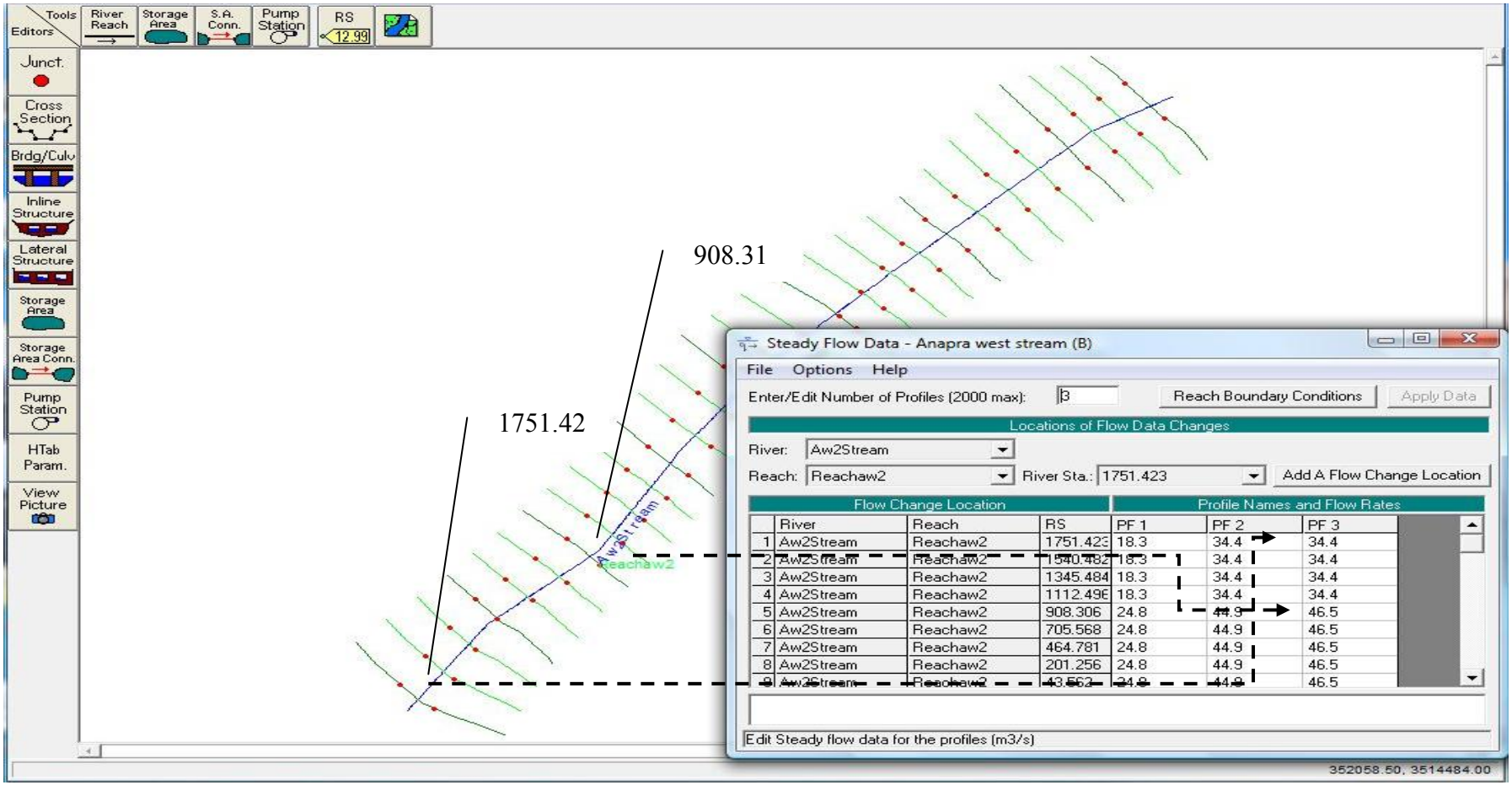

Figure 6.7. Association and organization of HEC-HMS hydrographs plan for flooding hazard (PF3 to Tr 100 year) into the HEC-RAS program. This stream driver corresponds to (Aw2) transference reach zone 1 which comprises subbasins: Asb5=34.4 and Asb3=12.1 =46.5 m^3/sec (See yellow box of TZ column of Fig. 6.3). Created by David Zúñiga (2012) using HEC-RAS (2002) version 3.1.3.

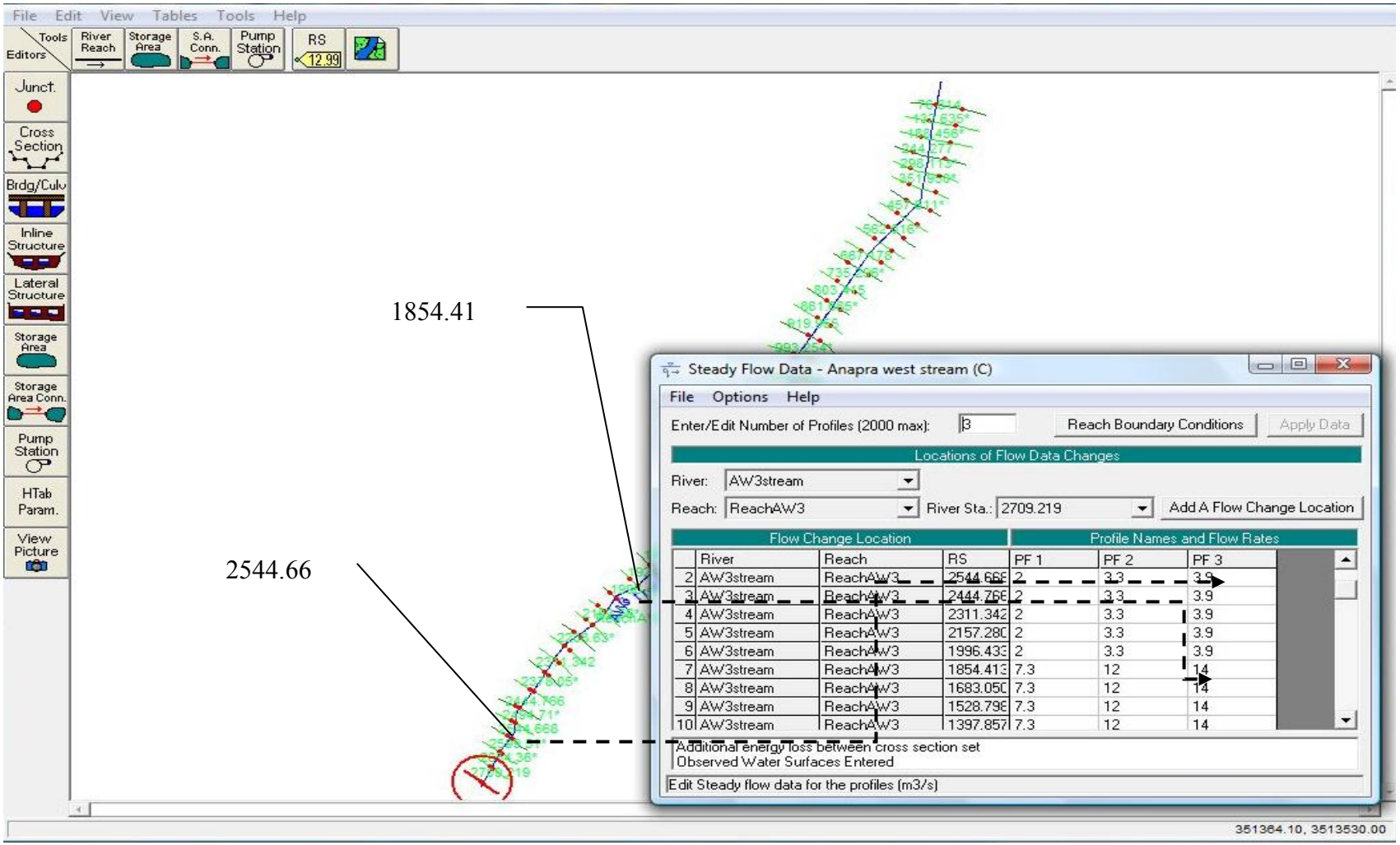

Figure 6.8. Association and organization of HEC-HMS hydrographs plan for flooding hazard: (PF3 to Tr 100 year) into the HEC-RAS program. This stream driver corresponds to (Aw3) transference zone reach 1 which comprises subbasins: Asb1e=3.9 and Asb2=10.1 =14.0 m^3/sec (See yellow box of TZ column of Fig. 6.3). Created by David Zúñiga (2012) using HEC-RAS (2002) version 3.1.3

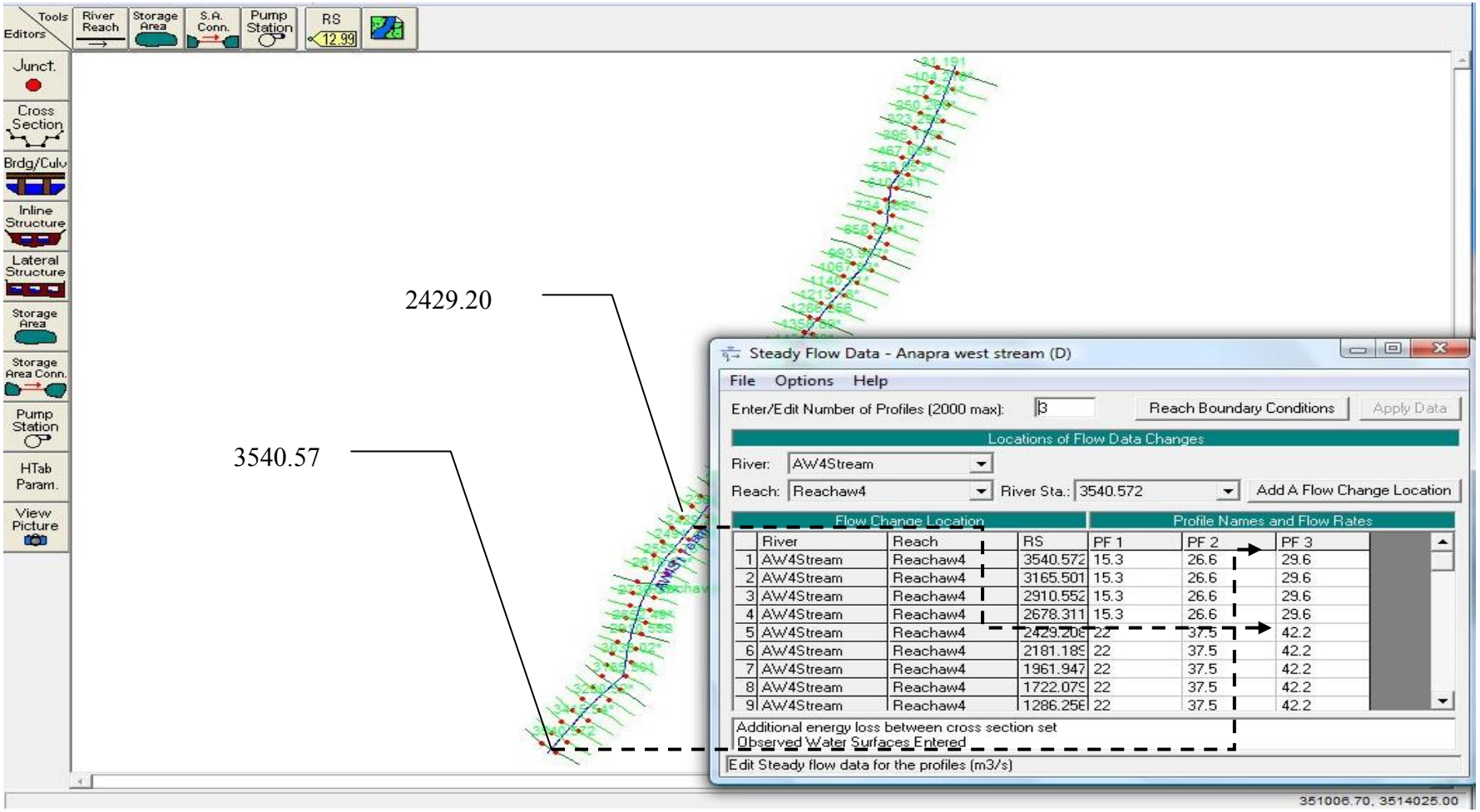

Figure 6.9. Association and organization of HEC-HMS hydrographs plan (PF3 for Tr 100 year) into the HEC-RAS program. This stream driver corresponds to (Aw4) transference reaches 1 which comprises subbasins: (Asb1a=13.6 and Asb1b=8.4, Asb1c =12.6) = 29.6 m^3/sec and Asb1d = 12.6 m^3/sec then a total volume of 42.2 m^3/sec is collected by this reach , (See yellow box of TZ column of Fig. 6.3). Created by David Zúñiga (2012) using HEC-RAS (2002) version 3.1.3.

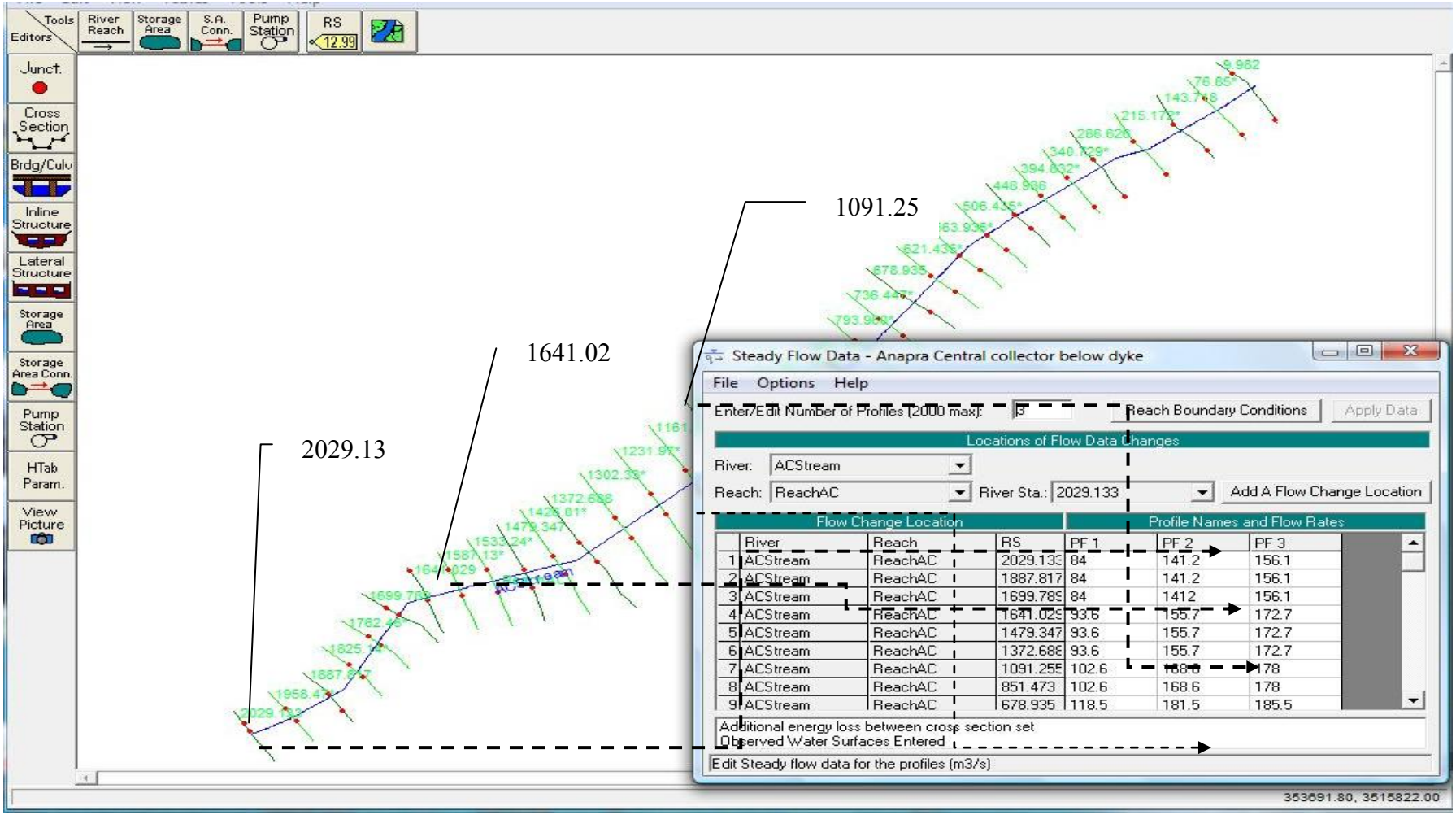

Figure 6.10. Anapra basin. Association and organization of HEC-HMS hydrographs plan: (PF3 to Tr 100 year) into the HEC-RAS program:This stream driver corresponds to (AC) transference reach zone 1 which comprises Benito Juarez dyke=156.1 m^3/sec and downward, subbasins: (CrSb=16.7, Asb5Ws=5.3, Tsb =7.5 then a total volume of 185.5 m^3/sec is collected by this reach . Created by David Zúñiga (2012) using HEC-RAS (2002) version3.1.3

*Note***:** Before moving with the explanation process to create transference reach zones for the different sectors a brief explanation is needed. Based on the stream network discharge evaluated though HEC-HMS model in chapter 5 (listed in Figures 3 and 4) different transference zones were assigned to the new reaches which will route the discharge derived from HEC-HMS. Therefore, these new reaches would transport the discharge in deposition areas and must be assigned with a new name such as those listed below in the next paragraphs.

Thirdly, streams which discharge in transference reach zones of sector 1 Center basin were defined similarly to those given to sectors 1 and 2 of Anapra basin and are given in Appendix 6A, Fig. 6A.4: (FV1, Fig. 6A.5; FV2, Fig. 6A.6; Sb1C, Fig. 6A.7; First one test, Fig. 6A.8; Sb3C, Fig. 6A.9; 4BC, Fig. 6A.10; 5C11, Fig. 6A.11; Sb8C, Fig. 6A.12; Jc8, Fig. 6A.13 and GI, Fig. 6A.14) (See green points on Figs 6.1. and green box on Fig 6.2 The assigned discharge to transference reaches zones was derived by HEC-HMS (See Fig. 6.3).

Finally, the stream network which discharges in transference reach zones of sector 2 of Center basin were defined similarly to sector 1 and 2 of Anapra baisin and sector 1 of Center basin (See Fig. 6A.15, Appendix 6A) which shows eight streams that connect transference zones of Center Basin sector 2 (See Blue colour points of Fig. 6.2 and blue box of Fig.6.4) formed by: (FirstCS, Fig. 6A.16; S^{nd}CS, Fig. 6A.17; Three, Fig. 6A.18; Four, Fig. 6A.19; Five CS, Fig. 6A.20; Six CS, Fig. 6A.21; Seven CS, Fig. 6A.22 and Eight CS, Fig. 6A.23). The discharge assigned to these transference reaches zones was derived by HEC-HMS (See Fig. 6.4).

These transference zones are needed because the HEC-RAS method that use steady and gradually varied flow could not applied in mountainous areas with slope steeper than 6% or where turbulent flow is expected. Therefore it is important to connect these sub-basins with the main reach drivers from upstream to downstream areas in order to route the peak discharge obtained by HEC-HMS (2002) computer programs.

6.4.3 Flooding results using the HEC-RAS computer program.

6.4.3.1 Methodology to assess flooding hazard.

Once the geometric data of streams located within these four sectors were addressed, the following steps were performed. **A)** Assume steady flow mode and a water surface elevation at upstream or downstream cross sections if a supercritical profile is being calculated. **B)** Based on the assumed water surface elevation determine the corresponding total conveyance and velocity head. **C)** With values derived in step B, compute S_f (friction losses) and solve equation 6. 2. **D)**. From the values obtained in step B compute Sf and solve equation 6. 1. **E)** Compare the computed value of WS2 with the value assumed in step B; repeat steps B through E until the values agree within (0.01 feet) = (0.003m). on the user defined tolerance HEC-1 (1998) (see Hydraulic Reference Manual).

Following with the flooding methodology the main issue was to export from Arc-view 3.2 to HEC-RAS streams geometry. This task was done using the Pre-GeoRAS processing module. After that, using HEC-RAS (2002) ver. 3.1.3 and with the flow expected to the design storm derived from HEC-HMS (2002) 3.1.0 for 10; 50 and 100 years of return period flooding was evaluated (see Fig. 6.11, next page of this chapter and the whole results are shown in Appendix 6B, Figs. 6B.2 to 6B.27. After that, flooding resulted from HEC-RAS (2002) was exported into Arc-View 3.2. Finally, using Post-processing GeoRAS module of Arc-View 3.2 the flooding hazard model for all the streams allocated within the active alluvial fan system were addressed.

Results of flooding hazard reaches profile and water cross section surface for Anapra and Center basins are described next: For Anapra basin: Appendix 6B; Figs. 6B.1 to 6B.4 (AW2, AW3, AW4 and AC) correspond to Anapra basin of sector 1 (See Fig. 6.5) and (Figs. 6B5 to 6B7, Appendix 6B which integrate the streams M1; SW1 and Snake west and east) correspond to (Anapra basin sector 2).

With regard to the Center basin that is also divided in two sectors: sector 1 integrated by the streams; (FV1, FV2, Sb1C, First one test, 5C11, Sb3C, SB4BC, Jc8 and SB8C and SbGI) see Appendix 6B, Figs. 6B.8 to 6B.15; Center sector 1 is integrated by the streams; FirstCS, SndCS, ThirdCS, FourCS, FiveCS, SixCS, SevenCS and EigthCS (see Appendix 6B Figs. 6B.16 to 6B.22) (See also Figs. 1 to 4 at the onset of this chapter for location basin location).

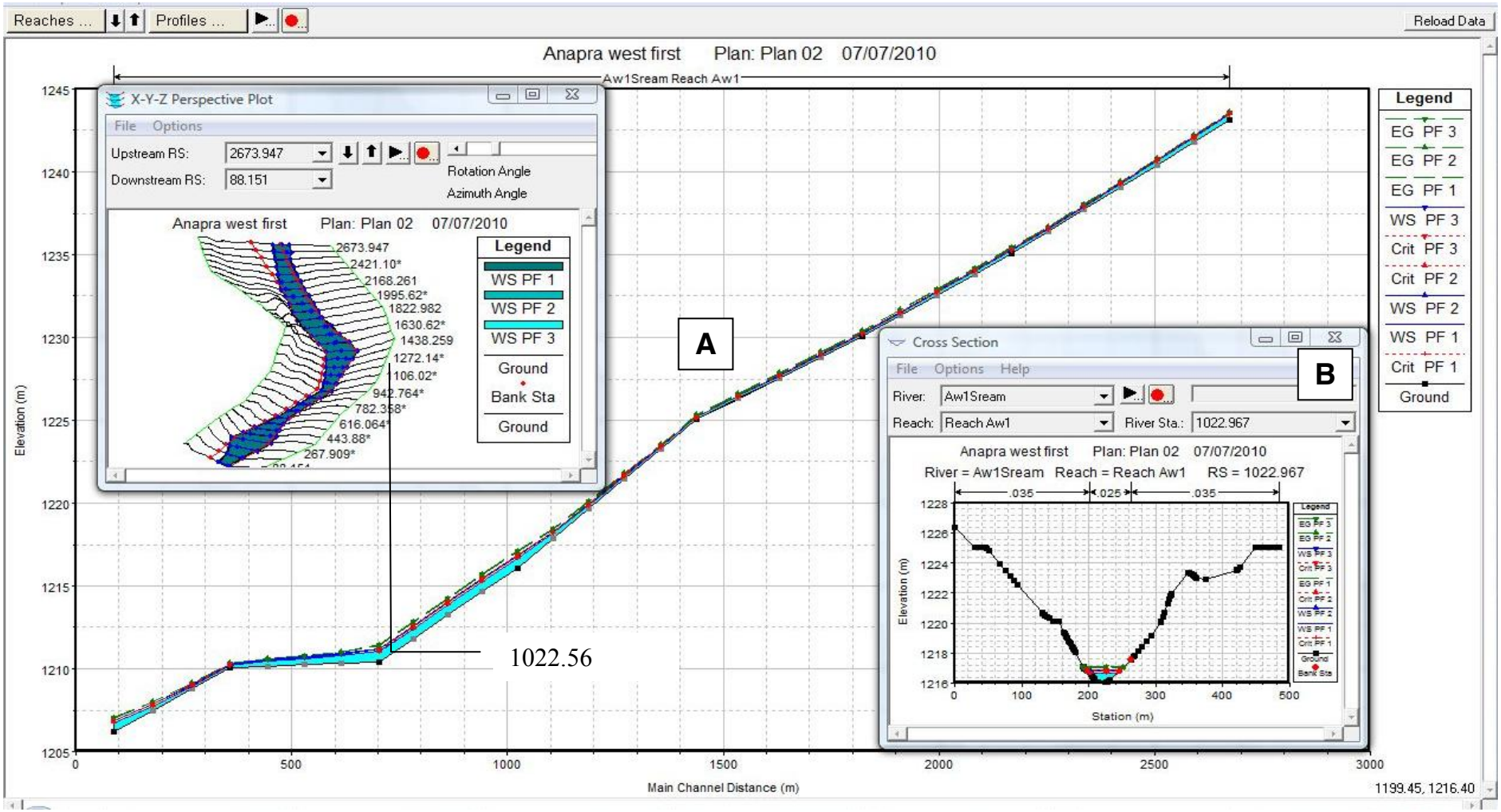

Figure 6.11. Water Surface elevation of stream AW1: 10 years (PF1); 50 years (PF2) and 100 years (PF3) return periods: A) Shows a perspective view of the profile. B) Shows a cross section of water surface that corresponds to station 1022.067 of the stream. (See map location in Figure 6.5 and Figs. 6.1 and 6.3 at the onset of this chapter). Created by David Zúñiga (2012) using HEC-RAS (2002) version 3.3.

6.4.3.2 Summary of the flooding results using HEC-RAS.

A steady flow model was performed using HEC-RAS computer program to simulate flooding hazard model. Thus, water surface elevation of streams comprised the Anapra sector (AW1, AW2, AW3, AW4, AC, M1 and SW1) for return periods: (10 years, PF1; 50 years, PF2 and 100 years, PF3) were evaluated and are presented in Appendix 6.2B, Figs. 6B.1 to 6B.7 In addition, the stations location of cross sections corresponding to major streams draining watersheds in Anapra and Center basin areas also are presented. Finally, in both profiles and cross sections (WS1 to PF1, WS2 to PF2 and WS3 to PF3 are referred to water surface elevation from different flow plans as: P1 to 10 years return period; P2 to 50 years return period and P3 to 100 years return period of the design storm.

Furthermore, in order to address the flooding hazard HEC-RAS (2002) the following steps were performed: Firstly, once the geometry data from Pre-GeoRAS processor module of Arc-View 3.2 are imported, the cross sections must be updated using HEC-RAS (2002) with the Manning roughness coefficient (n). After that, the banks were revised for all the cross sections which also would be filtered in order to have at least 500 points by section. Secondly, the design flow already evaluated in Chapter 5 using HEC-HMS (2002) hydrographs for 10 years, 50 years and 100 years return period should be assigned into HEC-RAS program considering steady flow conditions. Finally, the flow plan would be selected in agree with the desired flooding scenario as 100 years return period selected to Juárez City.

Hydraulic reference manual named HEC-IFH (1992) uses hydraulic concepts of energy as well continuity equation in order to transit the hydrographs, instead of HEC-HMS hydrographs generated using hydrology concepts associated with main components of the hydrologic cycle such as rainfall. HEC-RAS program works with Arc-View GIS version 3.2 and spatial modules included to extract the geometric data of streams from the DEM of the study area (See sections 3.3.2 to 3.3.5 of methods Chapter 3). This geometric data are exported into the HEC-RAS program. After that, a Pre-processing module named Pre-GeoRAS included in Arc-View 3.2 allow the extraction of geometric data of stream centrelines, stream bank lines, stream flow lines and cross sections of the streams. Then, geometric data are exported into the HEC-RAS program in order to perform analysis and update the flow plan suitable for

the flooding hazard model. Moreover, the program evaluates the flow plan profiles which are analyzed and checked again, the results given for HEC-RAS are exported to Arc-View 3.2 where the program reads it, and finally applying the Post HEC-GeoRAS the exported file is open and performs the GIS themes created such as cross sections cut lines, streams centreline, bounding polygons, water surface TNS and flood plain polygons.

The use of Arc-View 3.2 Pre-GeoRAS module as well the Triangulated Integrated Network (TIN) of the digital elevation model (DEM) and contour levels offset every 5 and 1 meters were used in order to extract geometric data for main reaches of the streams located in the transference zones of the alluvial fan system: Anapra sector 1 (Figs. 6.1, 6.3 and 6.5, this chapter); Anapra sector 2 (See Figs 6.1 and 6.3 this chapter and Fig. 6A.4, Appendix 6A); Center sector 1 (See Figs 6.1 and 6.3 of this chapter and Fig. 6A4, Appendix 6A) and Center sector 2 (See Figs. 6.2 and 6.4 this chapter and Fig. 6A.15, Appendix 6A). After that, the HEC-RAS program was used to open this exported geometric data and the organization of the different hydrographs that contain the flow plan evaluated by HEC-HMS assigned. This process of flow assignation and organization was achieved through the link between the hydrographs obtained in HEC-HMS program and the main reaches that would route these hydrographs. The procedure followed during HEC-RAS application is a repetitive task that requires 26 pages to illustrate its results as: Watersurface elevation of stream: 10 years (PF1); 50 years (PF2) and 100 years (PF3) return periods.

6.4.4 Arc-view 3.2 and HEC-GeoRAS Post-processor

6.4.4.1. Overview of main tasks

A brief description of main tasks already done are presented in the following paragraphs related to the four network geometric stream sectors derived using HEC-RAS program as was mentioned in this chapter as well the attached appendix.:

A) Network stream system that integrate Anapra sector 1 (see yellow points of Fig. 6.1 and yellow box of Fig 6.3) are: (W1, Fig. 6.6; W2, Fig. 6.7; W3, Fig. 6.8; W4, Fig. 6.9 and AC, Fig. 6.10).

B) The stream network formed by Anapra sector 2 are: (M1, Fig. 6A.1, Appendix 6A; SW1, Fig. 6A.2 Appendix 6A and Snake (See red colour points Fig 6.1 and red colour box of Fig 6.3) and Fig. 6A.3, Appendix 6A).

C) The streams network comprised by Center sector 1 (See gree colour points of Fig. 6.1 and green colour box of Fig. 6.3) are in Appendix 6A as: (FV1, Fig. 6A.5; FV2, Fig. 6A.6; SB1C, Fig. 6A.7; first one test, Fig. 6A.8; SB3C, Fig. 6A.9; 4BC, Fig. 6A.10; 5C11, Fig. 6A.11; SB8C, Fig. 6A.12; Jc8, Fig. 6A.13 and G1, Fig. 6A.14).

D) The steam network which integrate Center Sector 2 (See bue colour points of Fig. 6.2 and blue colour box of Fig. 6.4) are in Appendix 6A as: (FirstCS, Fig. 6A.16; SndCS, Fig. 6A.17; ThirdCS, Fig. 6A.18; FourCS, Fig. 6A.19; FiveCS, Fig. 6A.20, SixCS, Fig. 6A.21; SevenCS,Fig. 6A.22 and EigthCS, Fig. 6A.23) Secondly, these hydraulic data previously evaluated in HEC-RAS were exported into the master program Arc-view 3.2 with HEC-GeoRAS. After that, using the post GeoRAS processor the flooding hazard of the sectors previously mentioned were assessed.

6.4.4.2. Flooding hazard models with 5m and 1m resolution DEM

The flooding hazard model of Juárez city was assessed using two DEMs. The first one using contour levels offset every 5 m and the other with contour levels offset every 1m. DEM flood model of 1m resolution was applied on areas of the city which are particularly under threat from flooding, so in the maps later in this chapter, the 1m flood maps cover small areas of particular concern.

6.4.4.2.1. Flooding in flat valley areas.

Summarizing, as the resolution obtained from DEM of 5m as well 1m was not good enough to assess flooding hazard in flat areas then complementary historical information of past flooding events was collected. This information provided by IMIP (2005) contains areas of frequent inundation, which damage the city when catastrophic flash flood events occurs, such as that occurred in June 2006 with 59 mm of rainfall in only 45 minutes (see Figs. 1. 5 and 1.6 of Chapter 1). In summary

(Figs. 6.12; 6.13 and 6.14) the flooding hazard threatening the study area is shown in three sectors. Northwest, Centre and Southern and Southeast. In these figures the flooding hazard maps are illustrated upon a series of TIFF format Raster Satellite Images with spatial reference defined by NAD_1927_UTM_Zone _13N and with a D_North_American_Datum which were joined together using a rectify process in order to cover the entire satellite map of the study area.

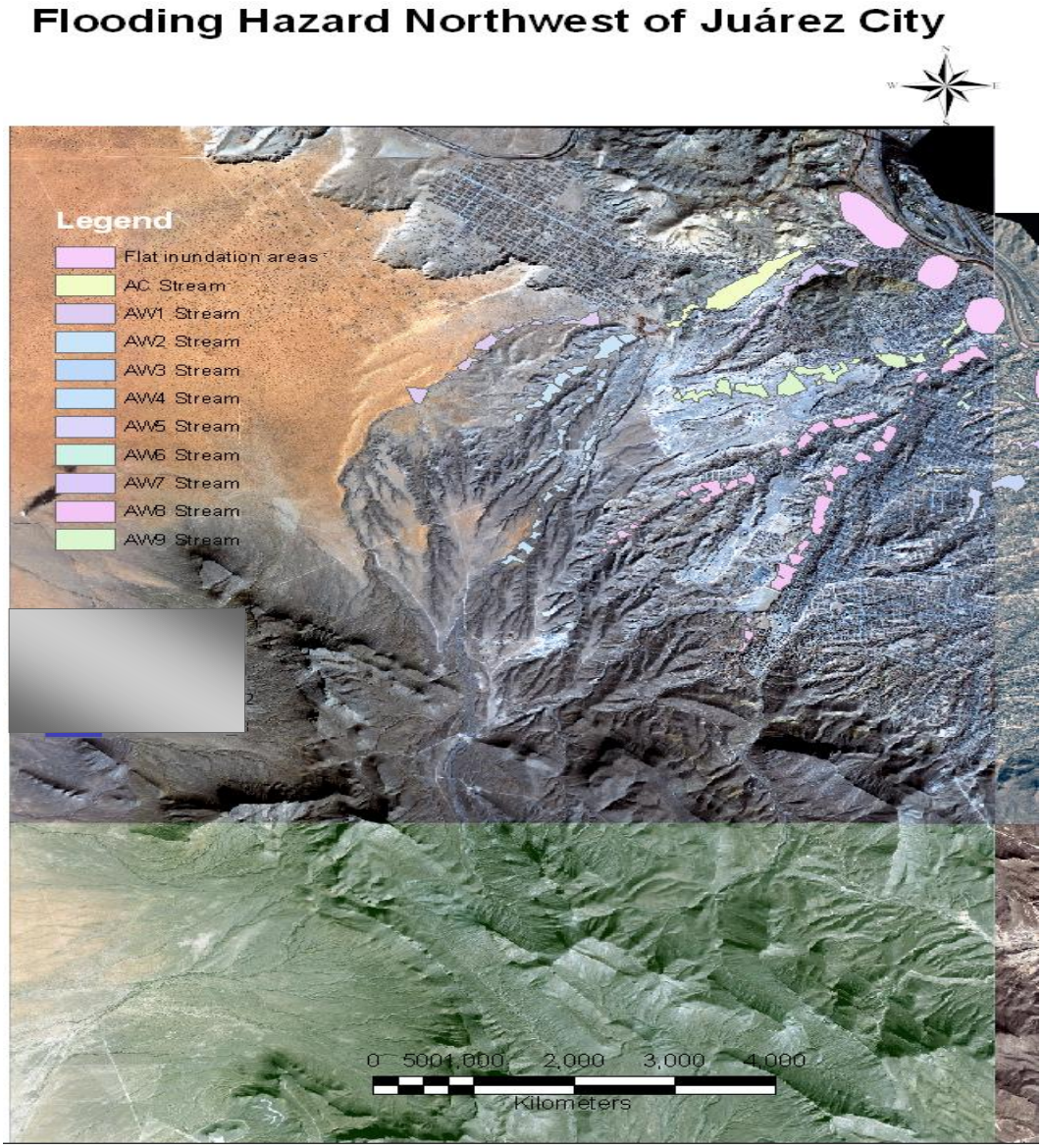

Figure 6.12. Flooding Hazard model for the Northwest sector of Juárez City: Figure shows only one of the 13 satellite Images used and the total Images are presented in Fig. 3.3 methods chapter 3 In the upper part, there is the legend of streams inundation areas in colours for nine streams northwest of the study area. Source: Satellite Images of the study area: IMIP (2007); Arc-view GIS 3.2 version with pre and processing HEC-GeoRAS.

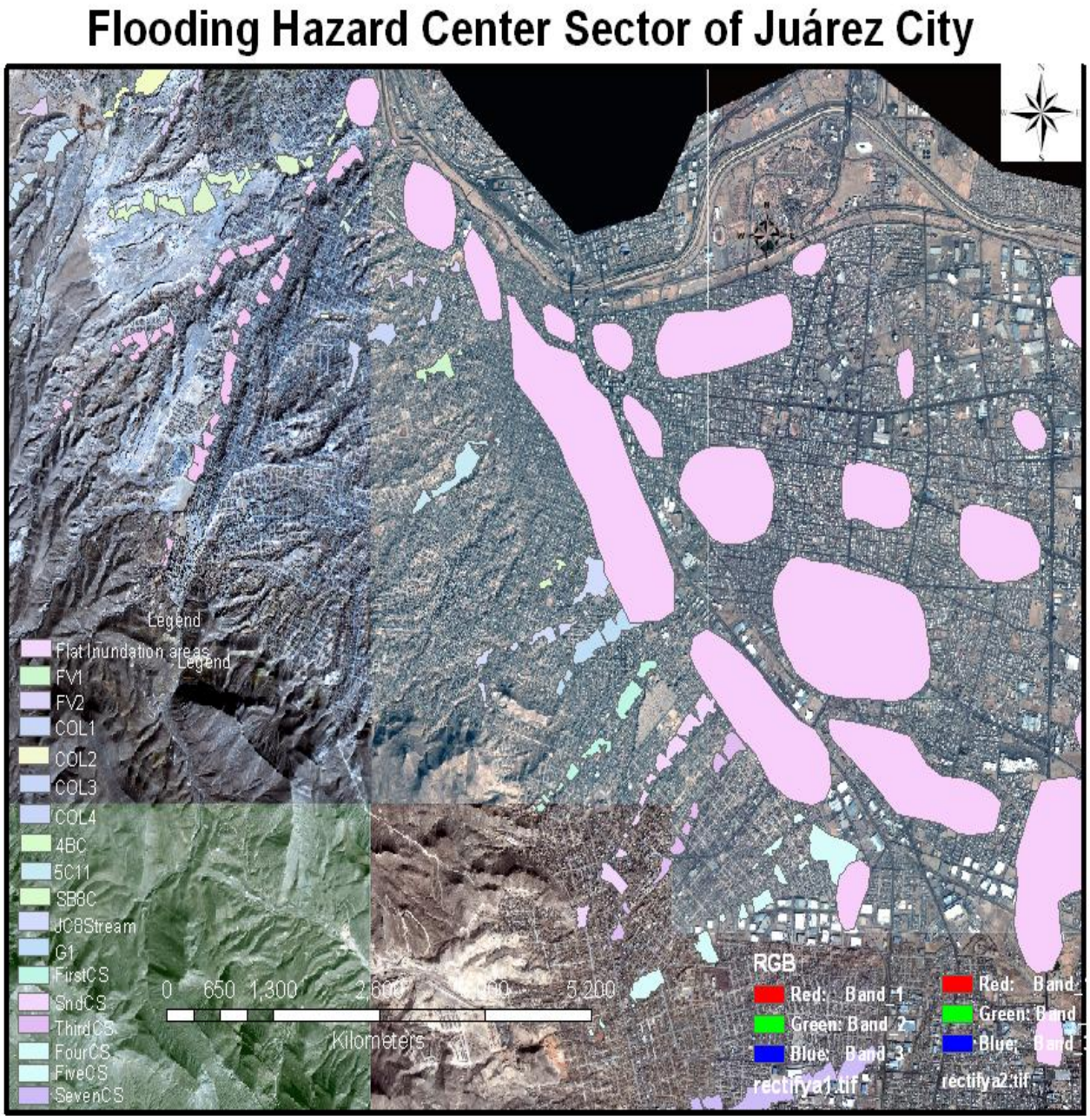

Figure 6.13. Flooding Hazard model for the Center sector of Juarez City: Figure. shows only two of the 13 satellite Images used the total Images are presented in figure 3.3 of methods chapter 3 (rectifya1 and rectifya2 RGB 3 colour band); also in the lower left part of the figure. there is a legend of stream and inundation areas in colours for the streams allocated. Source: Satellite Images of the study area: IMIP, (2005, 2007); Arc-view GIS 3.2 version with pre and processing HEC-GeoRAS.

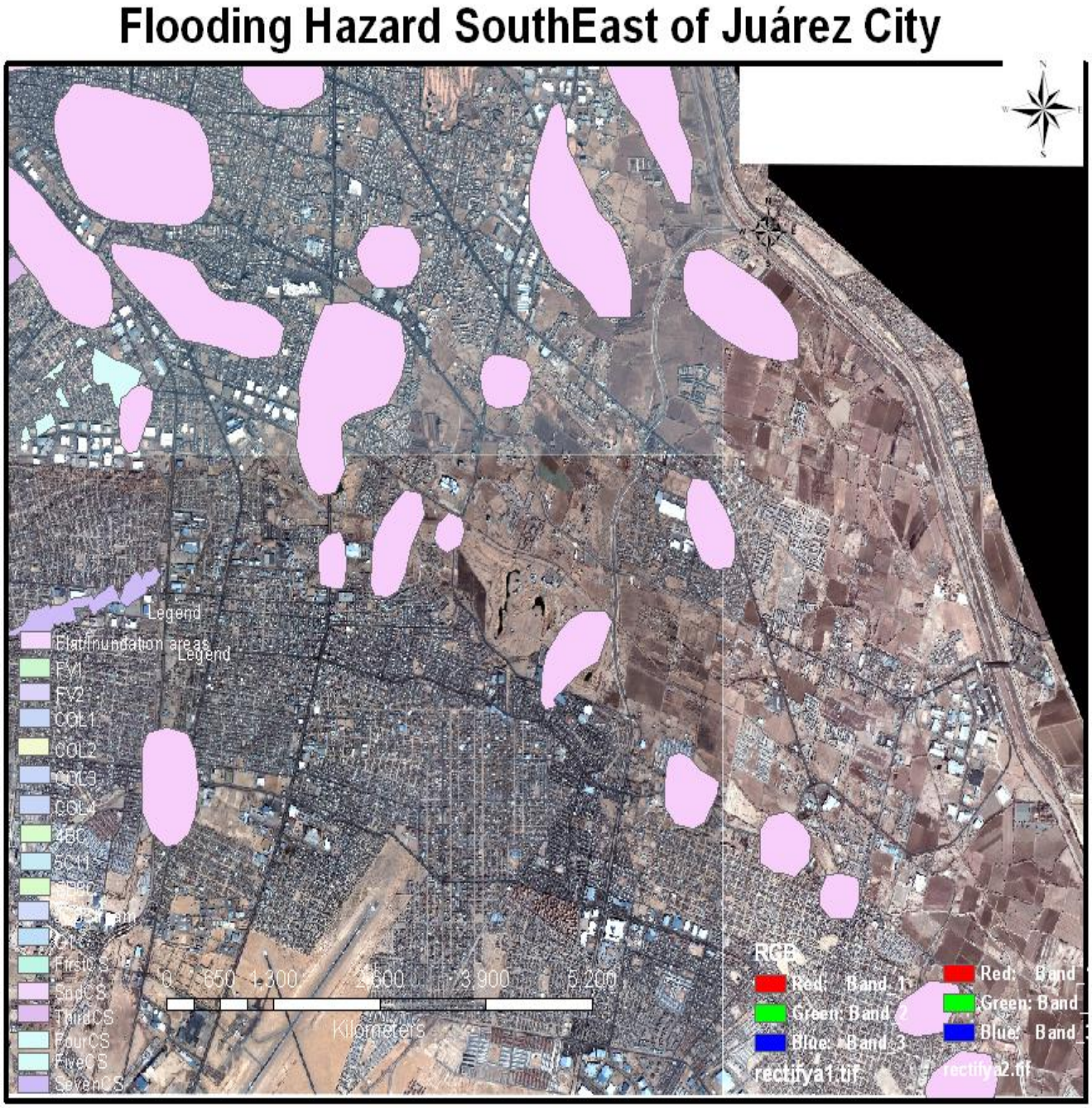

Figure 6.14. Flooding Hazard model for the Southeast sector of Juarez City: Figure shows only two of the 13 satellite Images used the total Images are presented in figure 3.3 of methods chapter 3 (rectifya1 and rectifya2 RGB 3 colour band); also in the upper part there is the legend of streams inundation areas in colours for streams allocated Northwest of the study area. Source: Satellite Images of the study area: (IMIP, 2005, 2007) Arc-view GIS 3.2 version with pre and processing HEC-GeoRAS Flooding hazard maps derived from 1m digital elevation model were insert within an scanned digital raster sheet. This map is scaled to 1:50,000 and is a Topographic chart for the study area named (H13A25.Gif) and corresponds to ITRF.

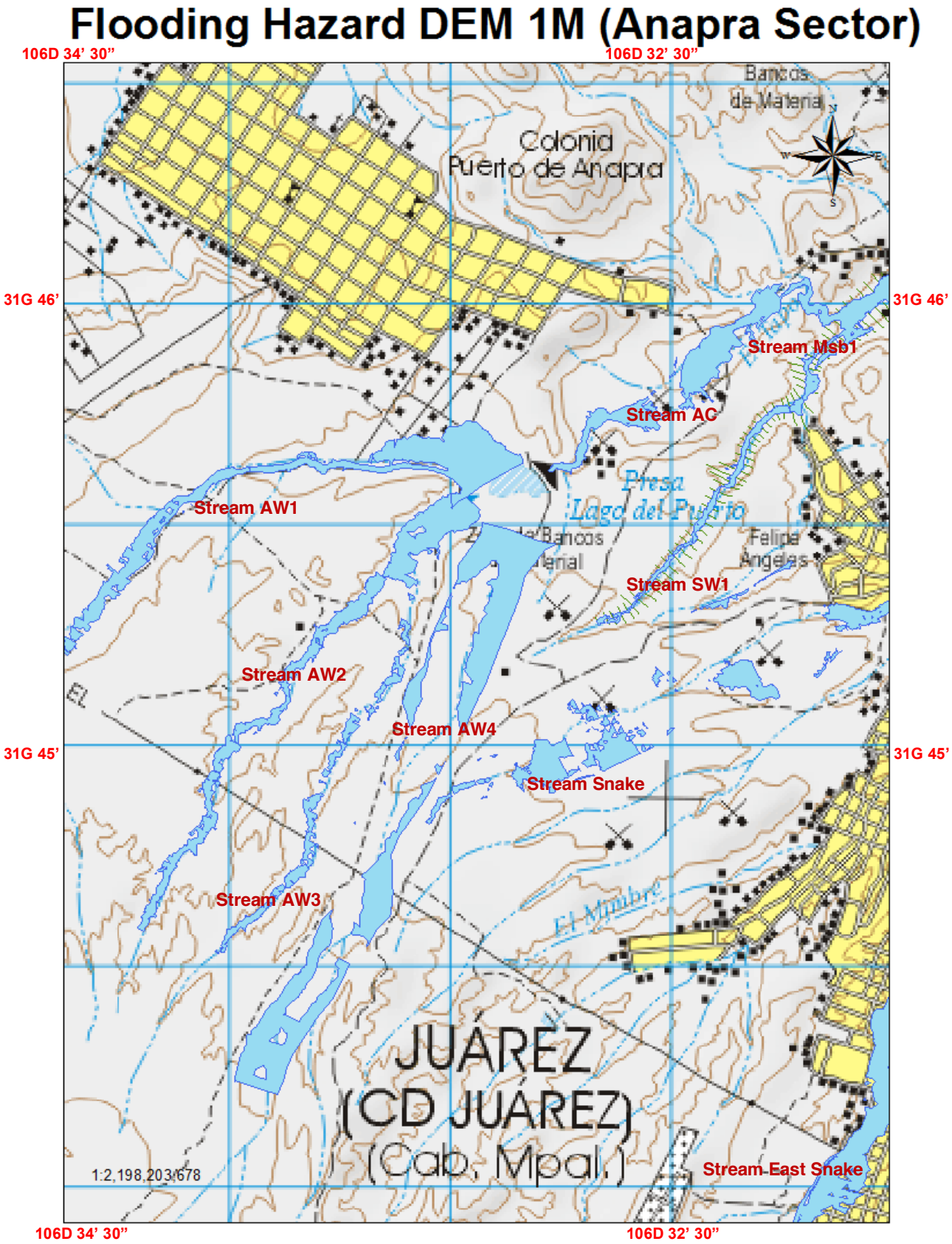

Figure 6.15. Flooding hazard model derived from 1m DEM resolution for the Anapra sector. Blue colored areas correspond to flooding extension and text in red color indicate the name of the stream; Pink color polygons are flat inundation areas Contour levels are marked as red lines. Yellow color means urbanized area and white color inside are streets: Source of data for this map: UACJ (2011); IMIP (2005) Created by David Zúñiga (2012) using Arc-view 3.2 with HEC-GeoRAS with pre and post-processor module. INEGI (1988) Topographic Chart H13A25.

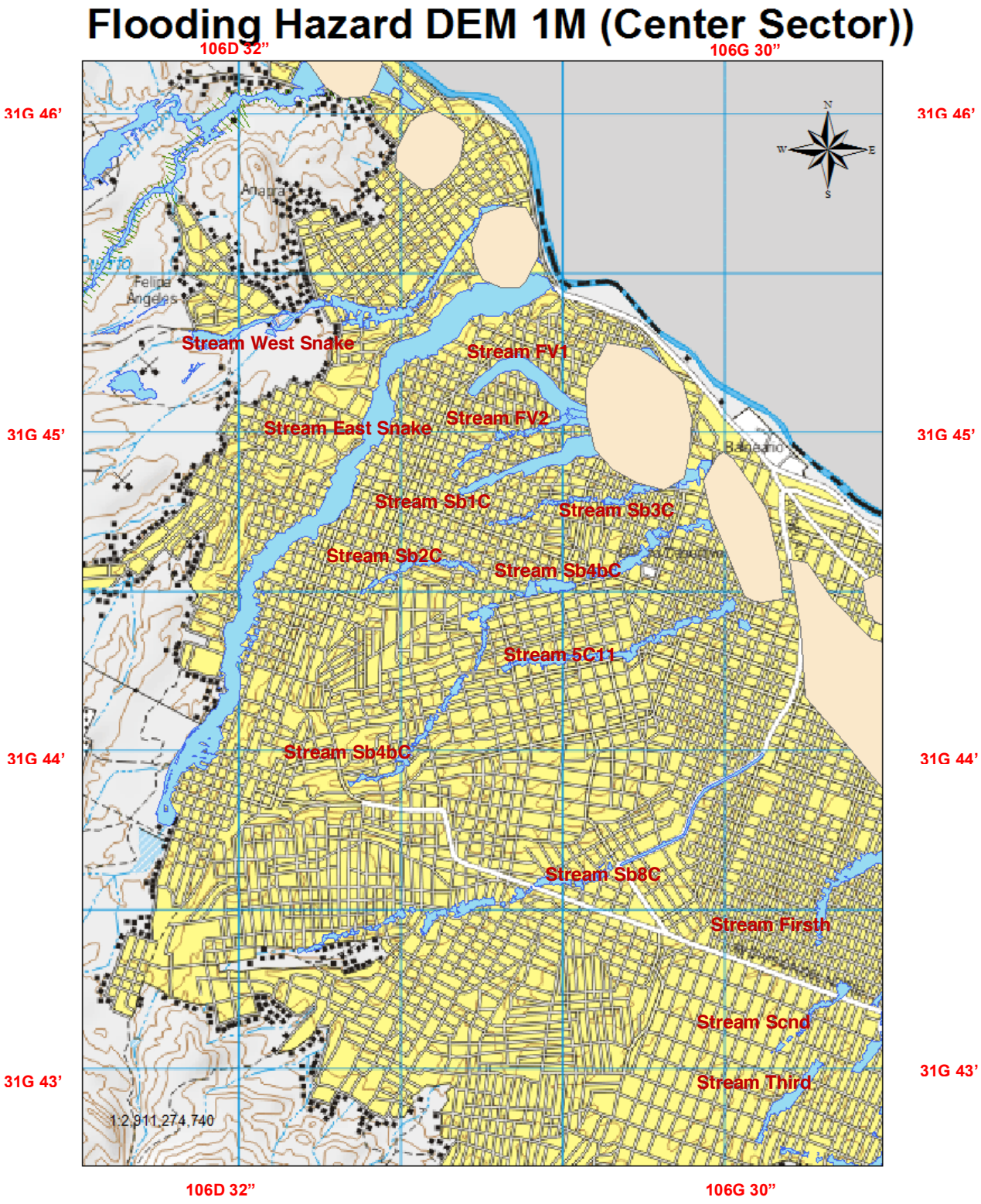

Figure 6.16. Flooding hazard model derived from 1m DEM resolution for the centre sector. Blue colored areas correspond to flooding extension and text in red color indicate the name of the stream; Pink color polygons are flat inundation areas Contour levels are marked as red lines. Yellow color means urbanized area and white color inside are streets Source of data for this map UACJ (2011); IMIP (2005); INEGI (1988): Created by David Zúñiga usisng Arc-view 3.2 with HEC-GeoRAS with pre and post-processor module:) Topographic Chart H13A25.

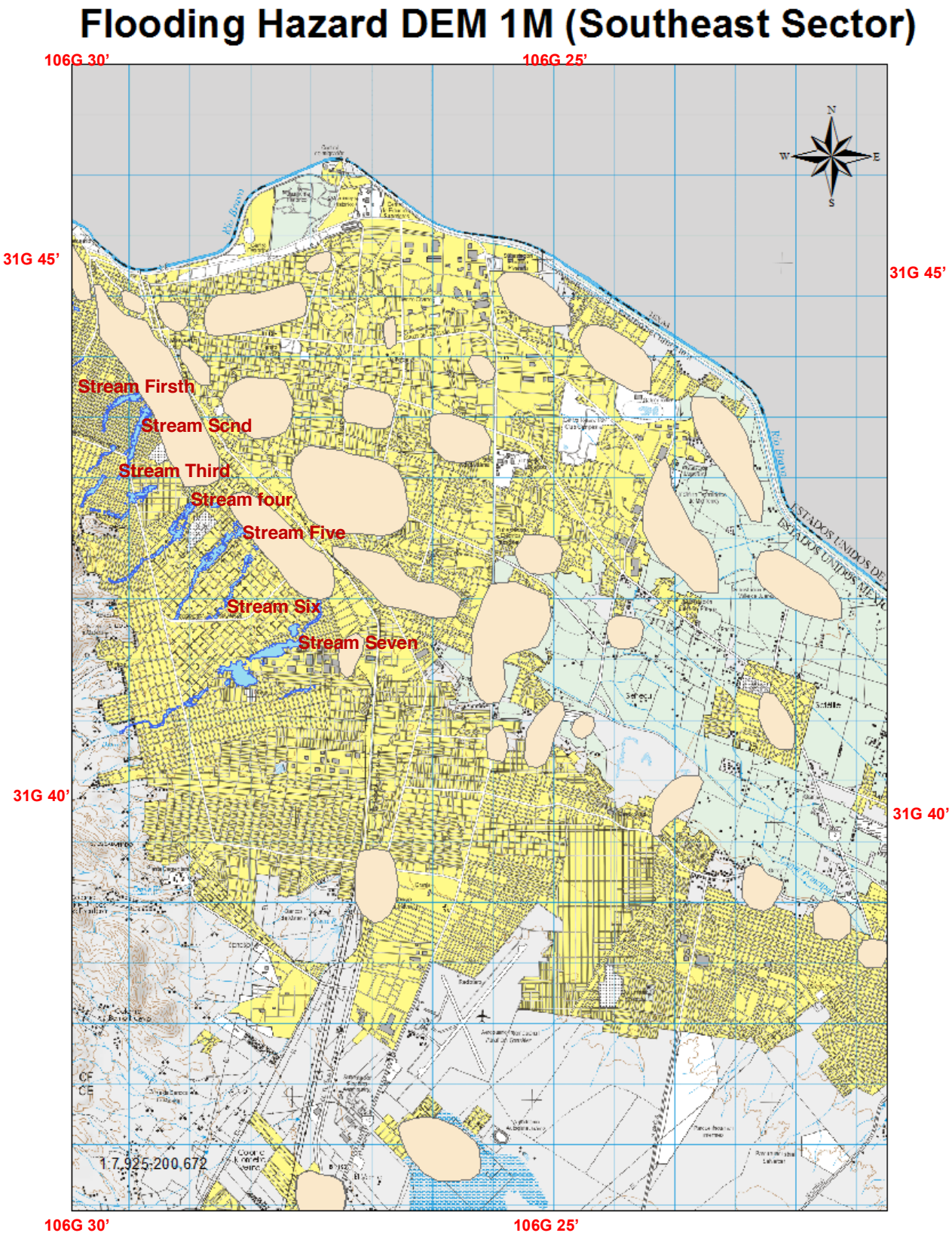

Figure 6.17. Flooding hazard model derived from 1m DEM resolution for the Southeast sector. Blue colored areas correspond to flooding extension and text in red color indicate the name of the stream; Pink color polygons are flat inundation areas Contour levels are marked as red lines. Yellow color means urbanized area and white color inside are streets: Data for this map from: UACJ (2011); IMIP (2005); INEGI (1988) Topographic Chart H13A25. Created by David Zúñiga (2012) using Arc-view 3.2 with HEC-GeoRAS with pre and post-processor module.

6.4.4.2.2. Flooding risk model from Vulnerability matrix based in: population density (Pd); Landuse (LU); Medical Services (MS) educational level (SD).

The vulnerability model to assess the flooding risk for the study area is based in four main components. These components are: Population density (Pd)=40%; Landuse (LU)=20%; Medical Services (MS)=20% and educational level (called Scholarly Degree in this analysis (SD)=20% were updated using the dataset named "Juárezageb2005_wgs_84_Area" Juárez University (2005). Briefly, the process to perform this model starts by opening the dataset mentioned in the previous paragraphs. After that the four different matrixes as: Pd; LU; MS and SD were derived from the program Arc-GIS 10.1. These four themes were processed using the command intersection of the geoprocessing Arc-GIS 10.1 module. Before to acquire the vulnerability results theme values as: (Pd=40%; Lu=20%; SD=20% and MS=20%) were introduced into the geoprocessing module of Arc-GIS 10.1. A detailed explanation of the vulnerability matrix is presented in Appendix 6C.

In this chapter the flood risk model is addressed for three sectors. In fact, to assess the flooding risk two key features are needed. Firstly, the flooding hazard model which are illustrated in (Figs. 6.15 to 6.17) and the vulnerability model shown in Appendix 6C. Furthermore, by definition risk is the product of hazard and vulnerability then the flood risk could be represented by the overlapping and intersection of these two features (see Figs. 6.18 to 6.20). Therefore, considering the simple product (intersection) of these two matrixes given in a geospatial form it becomes possible to assess the risk of flooding.

The risk layout maps given in Figs. 6.18, 6.19 and 6.20 are composed of the vulnerability as a background and the flooding hazard formed by streams and flat areas in transparent shapes of three sectors (sky blue, dark blue and red colours). These streams overlie the five vulnerability levels by colour Low, Medium, Medium to High, High and very High vulnerability. Finally, the result of these overlapping layers allows proposing five risk levels for the study area as: Low Risk (LR); Medium Risk (MR); Medium to High Risk (MR to HR); High Risk (HR) and Very High Risk (VHR).

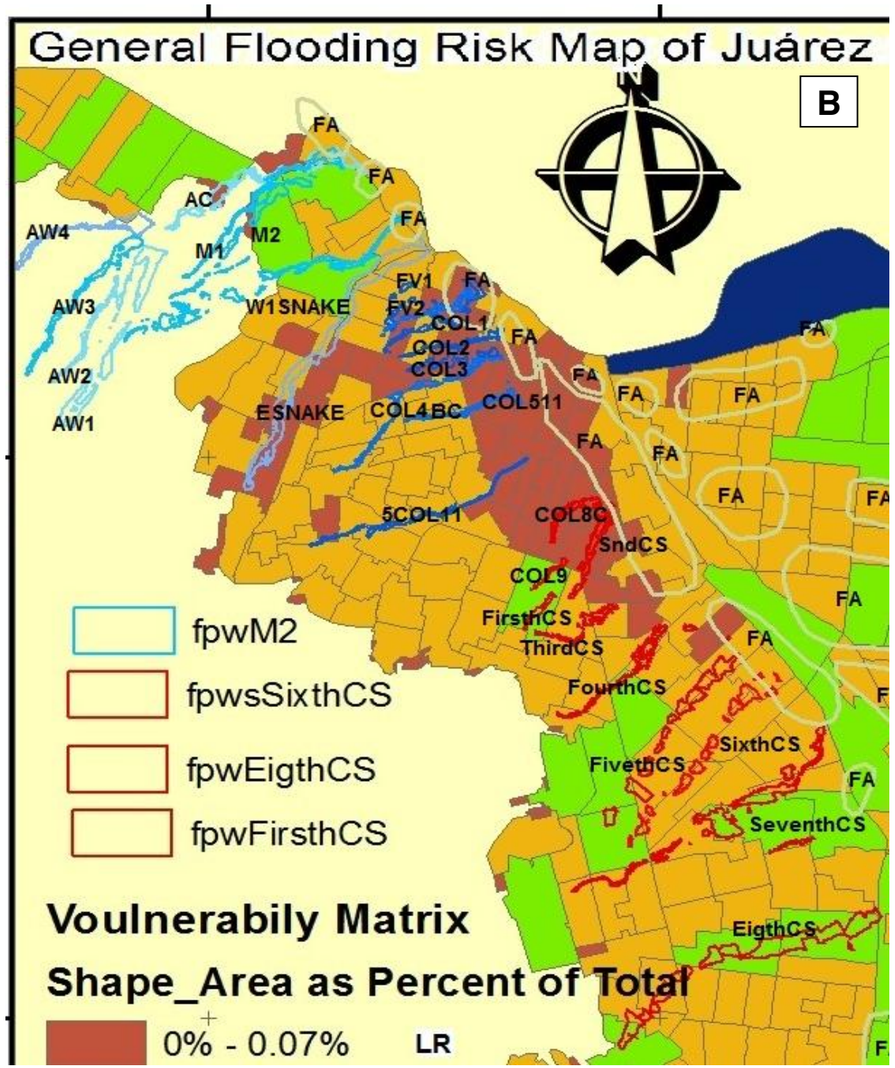

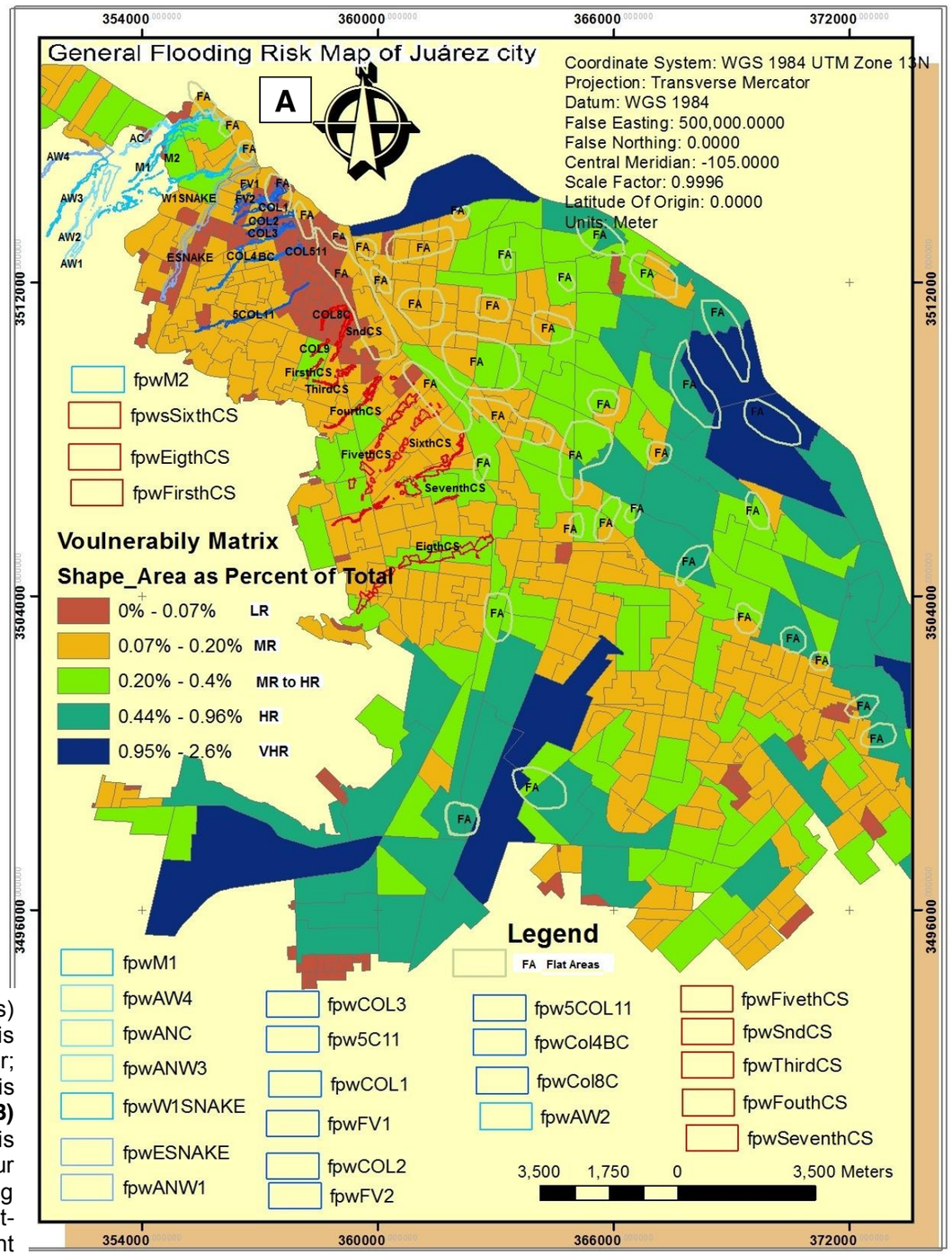

Figure 6.18. A) General Flood Risk map related to the whole study area (Northwest and centre sectors) derived from the flooding hazard map using 1m DEM resolution and Vulnerability model. The map is divided in 5 risk levels: (VHR, dark blue colour; HR, dark green colour; MR to HR , Light green colour; MR, dark yellow colour and LR, opaque red colour) Note, also simbology for streams allocated in this sector corresponds to different colors for the flooding hazard layer model and FA means flat areas. **B)** Shows an enlarged view of the three sectors allocated in the study area: Sector Anapra-Snakes is coloured ligth blue colour and there is no risk in this sector; Sector center is marked in blue dark colour and eastern sector is coloured in red colour. Created by David Zúñiga (2012) using Juárezageb2005_wgs_84_Area. INEGI (2007) and Arc-view 3.2 with HEC-GeoRAS with pre and post-processor module and Arc-GIS 10.1 (2011): IMIP (2005); Simbology is included for the different features.

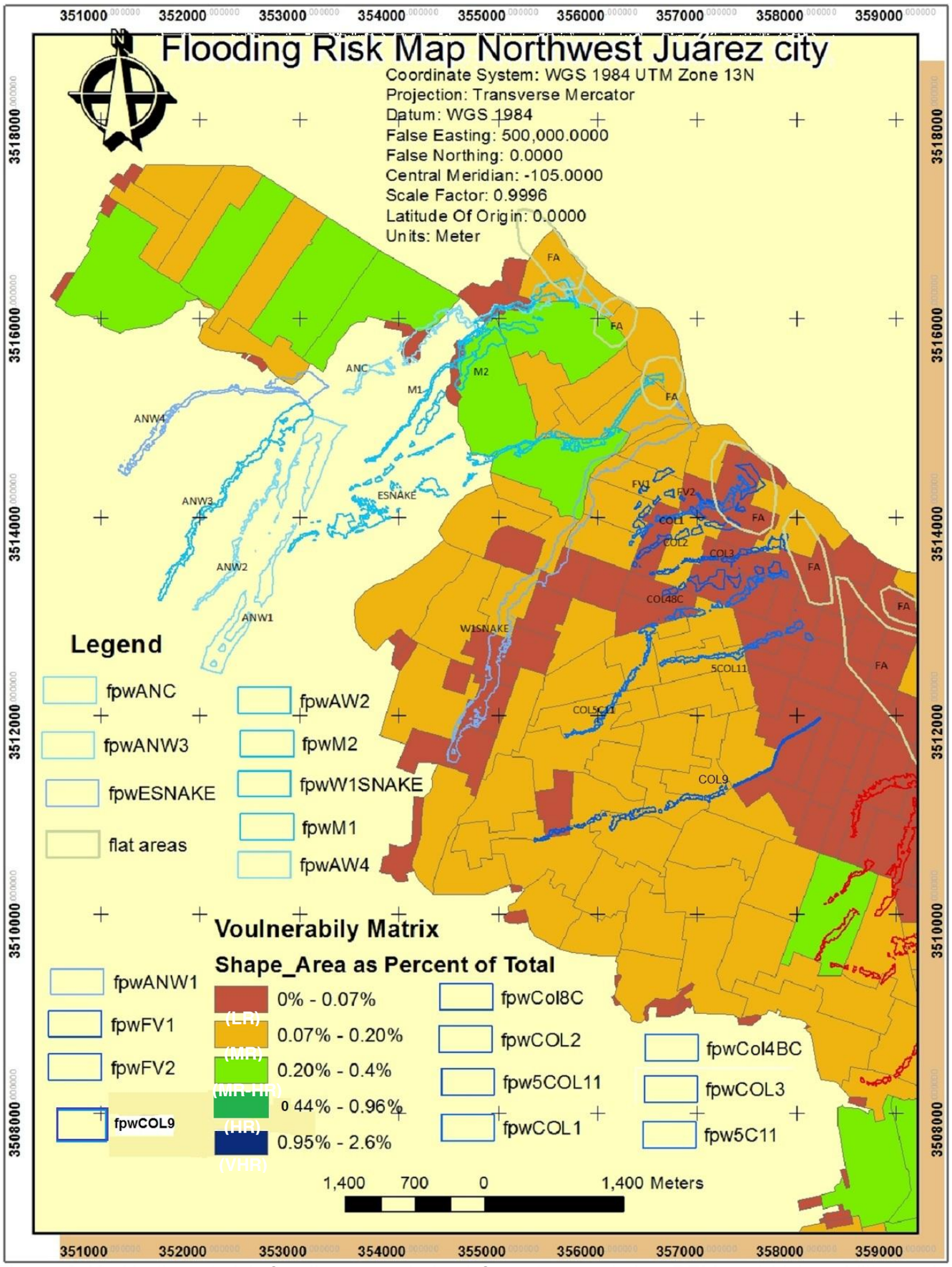

Figure 6.19. Northwest risk flooding map derived from 1m resolution DEM and Vulnerability mode derived from demographic census data set.Flooding Hazard along main streams are named in the legend as well over the map. The risk is divided in 5 risk levels: (VHR, Very High risk; HR, High Risk; MR- HR Medium to High Risk; MR, Medium Risk and LR, Low Risk) Note, Flat areas (FA) means flat areas and are indicated in transparent ligth green colour poligons. Sector Anapra-Snakes is coloured ligth blue colour and there is no risk in this sector due no urbanization is prevailed in this area; Sector center is marked in transparent blue dark colour and eastern sector is coloured in red colour. Created by David Zúñiga (2012) using Juárezageb2005_wgs_84_Area. INEGI (2007) and Arc-view 3.2 with HEC-GeoRAS with pre and post-processor module and Arc-GIS 10.1 (2011): IMIP (2005). Simbology is included for the different features.

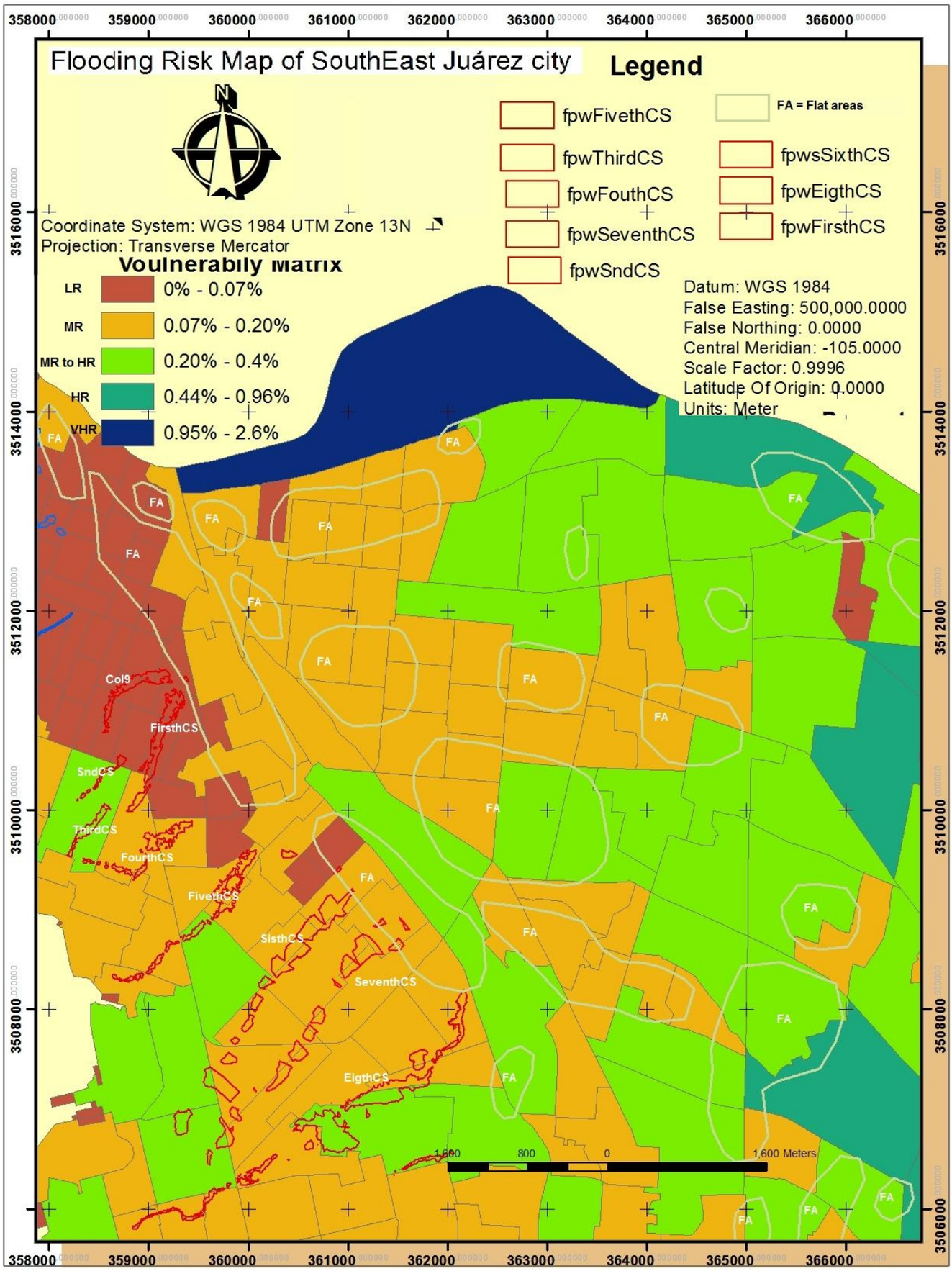

Figure 6.20. Southeast risk flooding map derived from 1m resolution DEM and Voulnerability mode derived from demographic census data sets. Flooding Hazard along main streams are named in the legend as well over the map (white text). The risk is divided in 5 risk levels: (VHR, Very High risk; HR, High Risk; MR- HR Medium to High Risk; MR, Medium Risk and LR, Low Risk) Note, Flat areas (white text, FA) means flat areas and are indicated in ligth green colour transparent poligons. Main streams flooding risk of eastern sector is coloured in transparent red colour overlaying the vulnerability model. Created by David Zúñiga (2012) using Juárezageb2005_wgs_84_Area. INEGI (2007) and Arc-view 3.2 with HEC-GeoRAS with pre and post-processor module and Arc-GIS 10.1 (2011): IMIP (2005). Simbology is included for the different features.

Juárez, along with many other cities the world, is not properly prepared to face flooding hazard events like that named "Sandy" which occurred in New York area of USA in November 2012. Thus, in order to mitigate the effects of this natural disaster some actions should be implemented by govermental autorities. Major aspects of the Ciudad Juárez flood risk, are detailed below:

A) Urban areas lacking impermeable pavement combined with high soil permeability have high infiltration rates. Consequently, some neighborhoods as Lomas de Poleo and Felipe Angeles located Northwestern of the city were not affected by flood risk. The flooding hazard model along streams of this sector is marked with low intensity blue colour overlying over a zero vulnerability level (0). This situation suggests no flood risk in these areas because the intersection or product between flooding hazard and vulnerability means mathematically zero (0).

B) In the remaining sectors: Anapra-Snakes, Center, and South-East the behaviour between flooding hazard of the streams and their associated vulnerability produces their flood risk as indicated in the Figs. 6.18, 6.19 and 6.20. These flooding risk levels are the product between vulnerability level and flooding hazard areas defined and explained during this chapter.

Summarizing, the concept of risk means the product between flooding Hazard and vulnerability level, therefore mathematicaly it is possible to assess these features using programs which work with spatial dataset (mostly raster format representations).

In the present work, in order to perform the vulnerability model the geoprocessing module included in Arc-GIS 10.1 was applied. This program model was explained at the onset of this section and was applied firstly. After that, using the application of geo-prossessing module some themes as: LU, Pd, SD and MS were derived from the dataset named "Juárezageb2005_wgs_84_Area". Furthermore, the resulting vulnerability matrix is a mathemetical addition (+) acquired using union in the geoprocessing module. Thus, due to the correspondence between geographic coordinates, scale and cellsizes of the spatial raster format of the shapefiles it is possible to create the vulnerability map for the study area. After that, as mentioned before intersection or product between vulnerability level and flooding hazard gives the Flood Risk Maps presented in the present chapter.

CHAPTER 7 DISCUSSION

7.1 INTRODUCTION TO DISCUSSION

As stated in the introduction (Chapter 1) the overall aim of this thesis is to assess the dynamics of the alluvial and fluvial systems upon which Juárez city is built, with particular emphasis on flooding threatening the city from the nearby mountains. Thus, the work is an integrated approach to understand fan dynamics and apply this in a practical sense, to assist planning of flood mitigation. In short, this research consists of two major areas of study, repeated here from Chapter 1:

1. Analysis of the processes of alluvial fan evolution in the study area that include: the nature of rock formations and their susceptibility to erosion; location of the key sources of sediment feeding the streams as well their capacity and competence.
2. Analysis of the hazards threatening the population of Ciudad Juárez, that result from the alluvial fan processes which include: flood maps using GIS, modeling of flooding, and its effects on the city's population. This may assist hazard mitigation planning in the city.

In order to achieve knowledge in these two areas, there are several questions which form the basis for this discussion. Thus, for clarity these are repeated in the following paragraphs.

1. What are the behavioural responses of the alluvial fans and the Bravo River fluvial systems in relation to local topography and climatic change in recent geological history?
2. What is the flooding threat to the city, how has it changed in recent years, and how might it change in future decades?
3. What is the effect of current engineering works on the Bravo River and in the area of the city that have modified the natural processes of the river streams and fans, and how would these need to be modified to mitigate the flooding threat?

This discussion chapter addresses these questions, analyzing the results presented in the previous chapters. Therefore, this chapter is divided into three sections, to address the three questions stated above. Then, a general summary section gives the overall outcomes of the discussion.

7.2. FAN SYSTEM AND BRAVO RIVER FLUVIAL SYSTEM IN RELATION TO TOPOGRAPHY AND CLIMATE CHANGE IN RECENT HISTORY

The Bravo River system and Juárez Mountains streams developed during recent geological time to produce a variable landscape which can be broadly divided into three major areas: A) The northwest sector composed of Anapra alluvial fan (See Fig. 4.1A); B) the central sector comprised of west and east Snakes streams, as well Colorado and mountain front fan system (see Fig. 4.1C); and C) the southeast sector which integrates the Palo Chino and Jarudo fan system (see Fig. 4.1D). Their evolution is linked to topography and climate change. Therefore, in the following three sections their differences and similarities are discussed.

7.2.1 Fan and River response to local topography

Topographic components have influenced spatially and temporarily the alluvial and fluvial systems evolution of the study area: one, associated with the Bravo River sediments invasion, the other with the internal alluvial fan evolution of each sector.

North-west of Juárez city Playa Lake Deposits of Anapra Port (PLDAP) (see Chapter 4; Figs. 4.4, 4.6 and 4.8) preserved the Bravo River limit at elevation 1260 m asl. This river margin also is observed southeast of Juárez Mountains (see Fig. 4.12). Therefore, during Pliocene to Early Pleistocene time (c. 3 to 1 Ma) Bravo River flowed in the study area forming the Hueco and Mesilla basins (see Gile et al., 1981; Mack and Seager, 1990; Leeder et al., 1996 and Mack et al., 1997; Mack et al., 2006). However, climatic fluctuations seem likely to have changed their nature, as can be seen in Fig. 2.19 which shows how the obliquity 41 ka cycle prevailed during Early Pleistocene time, switching to the 100 ka eccentricity system later in the

Pleistocene (see section 2.2.2). In the early Pleistocene, the Bravo River filled the ancient Cabeza de Vaca Lake underlying Barreal Basin southeast of Juárez city (Mack et al., 2006) (See Fig. 4.4). After that, Bravo River tributaries during middle to late Pleistocene flowed from northwest Mesilla basin and Hueco basin located east of Juárez city and may have deposited high volumes of soils of the Fort-Hancock and Camp Rice Formations (Strain, 1966; Hawley, 1975; Gustavson, 1991).

However, also throughout the Pleistocene, alluvial fans developed; of importance are the Snakes, Colorado and the adjacent mountain front piedmont fans (Sector 2) draining together downwards to connect with fluvial and terrace deposits of the Bravo River (see yellow and red colour lines in Fig. 4.8) resulting in lateral and vertical transition between Anapra and Colorado fans. As a result many incision and aggradation events occurred during Pleistocene-Holocene time. The detailed history and palaeohydrological evolution of the region is difficult to determine because of the presence of the city covering and disturbing most of the evidence. However, in an attempt to address this, the OSL dating technique was applied in a preliminary study on the youngest parts of the fans in critical locations.

Three sample sites were chosen for OSL dating to help constrain the history of the alluvial fans. These three were part of a set of 10 samples collected, but only 3 were analysed due to time and resource constraints during the period of producing this PhD. The samples are located on the Colorado fan and were selected in order to understand the most recent history of the fan system. See aerial image in Fig. 3.5, and the three red stars on the map in Fig. 4.1A. for overall distribution of the sites, and Figs. 3.5A-C for detailed photographs of each site. Consistency of material was achieved by sampling aeolian sands for all three samples. In each site, the local stratigraphy shows that the aeolian sands sampled for OSL dating are overlain by conglomerates (see Figs. 3.5A-C); this stratigraphy shows episodes of aeolian deposition followed by renewed fan activity. The results fall into Oxygen Isotope Stages 3-5 as follows: (30,900 and 44,850 years) (Sample P1, elevation 1252 m [see Fig. 3.5A], within OIS 3) ; (41,100 and 69,020 years) (Sample P2, elevation 1201 [see Fig.3.5B], around the border between OIS 4-3) and 74,300 years (Sample P3, elevation 1241 [see Fig.3.5C], very latest OIS 5).

The fact that the local stratigraphy in each case is similar (aeolian sand overlain by conglomerate) shows the same processes were taking place on the Colorado Fan

at different times. Furthermore the three dates range between the latest OIS 5 and later part of OIS 3, thereby representing deposition during both glacial and interglacial phases. Also, these sites are all located at relatively higher topographic positions compared to the active flooding in the city, and are obviously higher than the Bravo River.

A key problem in analysis of the fans is that the fan system has been dissected and extensively covered by modern building of Juárez City on the fan; therefore determining the geometric relationships between the various parts of the fans is made effectively impossible by human intervention. However, it may be expected that the uppermost exposed deposits in any one site will give the best opportunity to assemble age data for the more recent fan evolution. Topographically lower parts are occupied by roads and homes, with almost complete coverage of the ground surface. Any exposed surfaces of unconsolidated sediments where original stratification cannot be demonstrated are unreliable for dating because of the possibility of reworking by human action. The three samples dated were collected from prominent sites of in-place sediments with clear stratigraphy, selecting aeolian sediments that are more reliable for dating, and are not in the topographically lower sites. However, Figs. 3.5A-C show the sampled material is from the uppermost aeolian sediments in the sample sites and therefore are the youngest available reliable sites. They give older ages than were expected, and suggest that these parts of the fan system became inactive at an older time. However it is very clear from the topography of the fan system and the continuing flooding of the city that the hydrological system has been continually active through the Pleistocene to modern times. Therefore, it seems likely that the older (dated) fans were eroded by more recent activity that cannot be satisfactorily dated because of the presence of the city that has covered and disturbed most of the sedimentary deposits. Thus, although making firm interpretations from only three dates is not possible, the three dates provide valuable constraints on the history of the area.

The consequence of these three dates and the arguments presented above is that there is no clear evidence of a relationship between glacial/interglacial cycles on one hand, and sedimentary process on the other hand. The proximity of the fans to the Juárez Mountains, and the repeated similar stratigraphy in the three sample sites, suggest that local climatic changes, perhaps influence by the steep topography

of the mountains, was the major control on fan formation. It is also possible that the regional topography from Juárez Mountains, across the Hueco Basin to the Franklin Mountains to the north, created a regional climatic environment that was more influential than the global glacial/interglacial cycles. Support for this suggestion comes from recent work on the Rio Grande terraces in the Albuquerque area of New Mexico (Cole et al., 2007), which shows that there is no clear relationship between terrace age and climate in the Albuquerque area. Cole et al. (2007, Fig.7) show that terrace dates from a variety of dating methods are scattered through OIS-6 to OIS-1, with no firm pattern.

In order to explore the history of the fans further, the connection between the Juárez fans and Bravo River terrace system was examined. In Fig. 4.1A, a series of red crosses marks the locations of fragments of older Bravo River terraces (undated); these cross the positions of the distal parts of the alluvial fans and it is likely that the fans and terraces interfinger. Borehole records provided in the Appendices for Chapter 4 demonstrate a long history of shifting clastic deposits, although these were paper records, and access to the sediments was not possible. Nevertheless, these borehole records show fluctuating energies and inputs from both the fan system and prehistorical Bravo River. Finally, comparison was made between the Juárez OSL dates and dates of similar ages elsewhere in the region, with reference to work near Albuquerque in USA (Cole et al., 2007; Hall et al., 2008) where OSL dates of 63 Ka to 98 Ka (dated by those authors) give comparable ages to the Juárez fans.

Hawley (1975) stated that during the period from the Last Glaciation Maximum to early Holocene time (25 ka to 10 ka) the Bravo River valley filled with 18 to 30m of basal channel pebbles to cobbles and sandy gravels. Therefore, if this is true the recent deposits located nearly to elevation 1160 m asl along Municipal Cementery (**MC**) Tepeyac Cemetery (**TC**) and Aztecas San Antonio neighborhoods (**ASA**) (see, Figs. 4.1B, 4.1C, sections 4.2.1 ,4.2.2 and 4.2.3) as well some consolidated Felsite and Andesite outcrops located nearly to Anapra, Felipe Angeles and Cristo Rey mountains named **ASS**, **NS** and **CC** (see crossed pink circles and ashed coffee line Fig. 4.1A) would link with older Bravo River tributaries (see section 2.1.6) (Hawley, 1975). Finally, the likely youngest incision that occurred during Holocene time is associated with the lowest buried preserved terraces identified in boreholes cross

section at elevation 1140 m asl (the details of these can be found in: section A-A' red stars boreholes 13R, 15, 7R and 111; also section B-B' blue stars boreholes 59, 61 and 42 of Fig. 4.1C and Table 4.2). Furthermore, about 60 km north of the study area, Bravo River terraces deposits were found in relict basin floors named Lower and Upper la Mesa in the vicinity of Tortugas mountains located in New México at coordinates (32º16' N 106º45W elevation 1194m asl; see Gile et al. 2007 Desert Project study, Figs.1, 4 and 10). These terraces were found in Jornada I, 700-500 ka; Tortugas, 500-250 ka; Picacho, 250-100 ka; Leasburg, 15-10 ka; Fillmore 700-0.1 ka and finally the modern Bravo River valley floodplain). The previous fluvial deposits were correlated with carbonate horizons (see Fig. 4 of Gile et al., 2007). Because of the Holocene incision the area located along the Bravo River 150 km north of the study area it is reasonable to suppose that the Bravo River terraces were formed at comparable ages, and supports the view that the aeolian sediments of the late Pleistocene developed on the fans from erosion of the Juárez Mountains, followed by incision into the older fan system. Thus there is good reason to suppose that after 31 ka (the youngest of the three OSL dates in this study), the fan system was incised by the Bravo River.

7.2.2. Fan and River response to Climate change.

The ancestral hydrologic apex of the Anapra alluvial fan originally was located at elevation 1293 m asl (see Figs. 4.1A, 4.2 and 4.9), during Pliocene to Early Pleistocene time (c. 3 to 1 Ma) (see Gile et al., 1981; Mack and Seager, 1990; Leeder et al., 1996 and Mack et al., 1997; Mack et al., 2006). After that, during Pleistocene-Holocene time at least two further catastrophic climate change events caused incision again and other shifts of the channel feeder took place from 1293 m asl to nearly 1260 masl (see Figs. 4.1A, 4.2 and 4.9 and Strain, 1966; Hawley, 1975; Gustavson, 1991). Finally, again the channel feeder shifted from 1260 m asl to 1215 m asl (see Figs. 4.1A, 4.2 and 4.9 and Hawley, 1975; Gustavson, 1991). As a result, it is sensible to suggest an alluvial fan dynamicity which developed the modern landscape constructing a proximal, medial and distal fans segments model for Anapra northwest (see Fig. 4.9). A similar fan evolution is suggested for Colorado and Snakes alluvial fan models. It may be speculated that during Pleistocene time

the east and west Snake streams were captured by the ancestral Bravo River tributary at elevation of 1215 m asl. In this regard, the influence of tectonics is perhaps the reason of the Colorado fan shift (see continuous red line of Fig. 4.1A, 4.1C and 4.1.D. Future work may be able to clarify controls on these shifts, which may be related to activity on the Arroyo De Las Viboras (ADLV) fault recently described by Avila (2011) as being an active fault today. In this respect, future field and laboratory work is planned on calcretes (Machete 1985; Bachman and Machete 1977) taking advantage of the abundant outcrops in the region of calcrete or calcic soils (regionally known as caliche conglomerates), which should be datable. Bachman and Machete (1977, Fig. 38 and 39) assembled data on calcretes in New Mexico, not far from the study area, in a range of papers published mostly in the early 1970s, and this work shows accumulation of calcretes at various times in the latter half of the Quaternary period. Bearing in mind these studies are somewhat older and therefore perhaps less well-constrained than more recent years, of considerable potential significance for this PhD study is the correlation diagram presented by Bachman and Machete (1977, Fig. 39), that shows three areas with a calcrete formed at around 70-75 ka, near Albuquerque, San Acacio and Las Cruces. In the Las Cruces area, the calcrete ages are given for different parts of the sedimentary basin (Bachman and Machete 1977, Fig. 39, right-hand column). Thus the border and valley of the area have calcrete dates ranging from 100+/-50 ka to 50 ka, whereas the basin ("bolson") is more tightly constrained to 75 ka. In comparison with the Juárez fans, the oldest OSL date from this PhD is 74 ka in aeolian sands, consistent with an episode of aridity around the end of OIS 5, going into the start of the glacial phase of OIS 4 (the boundary between OIS 5 and 4 is about 75 ka). It is perhaps significant that this more tightly constrained calcrete age is from the bolson, which is expected to be wetter for longer since it is expected to be the area where standing water would persist. In contrast, in the valley and border areas, desiccation may have been more easy to achieve, thus periods of drying spread over a longer time period might explain the longer range of dates in the valleys and border areas. Thus a pervasive episode of aridity around 75 ka might explain the presence of calcrete in the New Mexico bolsons studied by Bachman and Machete (1977). Younger calcrete ages from the Las Cruces area have ages ranging from 25 - 20 ka, all younger than the youngest OSL date of 31 ka in Juárez. Only further dating in

Juárez could identify whether or not there was a younger arid episode in the Juárez area, but it is important to note that the OSL date sites were chose deliberately to sample the youngest parts of the Juárez fans, so that any evidence of younger arid phases may have been removed, or the sediments were never deposited. Bachman and Machete (1977, Fig. 38, central graph) compiled slightly different calcrete age data from the Las Cruces area of New Mexico, with ages from ca. 100 - 50 ka and from ca. 20 - 12 ka; thus there is a gap between 50 - 20 ka when no calcrete formed, crossing the youngest OSL date from Juárez. However, the earlier set of ages in Las Cruces area contains the 60 ka OSL date from Juárez. Therefore there is a little inconsistency between the two compiled datasets presented in Bachman and Machete (1977, Figs. 38 and 39), which is perhaps not surprising since they are presented as tentative, in that paper. Nevertheless, the overall conclusion that can be drawn from this comparison is that around 75 - 70 ka there was an episode of aridity that affected both the Las Cruces area of New Mexico and the northern Mexican alluvial fans in Juárez, while younger dates show more localized effects of aridity.

7.3 FLOODING FEATURES THREATENING JUÁREZ CITY

Flood threats must take into account two major aspects, discussed in the remainder of this chapter: A) flood issues related to the Bravo River, which was dammed in 1916 (Elephant Butte Dam, USA) changing its previous natural controls and fixing its channel position; and B) the historical pattern of flooding from the Juárez Mountains together with the models based on HEC-HMS and HEC-RAS predictions in Chapters 5 and 6. The two subsections below consider the current flood threat, changes in recent years and potential threat in future decades.

7.3.1 Current and historical flood threats to Juárez city

Historical descriptions of floods and flood damage are recorded in the “Diario de Juárez” local newspaper and UTEP library microfilm sequence frames (See Appendix 1A). These publications reported a major flooding event in 1827 when catastrophic flooding left only the Church named “Mission of Nuestra Señora de

Guadalupe" standing. In addition, two flooding events related to the shift of Bravo River occurred in 1852 and 1864 these reports are also associated with precipitation disasters (see Appendix 1B). During the 1864 flood, many Mexican terrains were affected by channel change, for example in the Chamizal area, which limits the Mexican/USA border (see Figs. 1.8, 1.9 and 1.10). Moreover, major flooding in 1897 changed the Bravo River trajectory which led to formation of the "Cordova Island" (Fig. 1.10, Chapter 1). The historical records show the sporadic nature of flooding, but since 1916, there has been less threat since the construction of the Butte Dam. Nevertheless, the Mexican and US authorities constructed robust levees in the area between El Paso and Ciudad Juárez, since rainfall upstream of Juárez in the Bravo River (=Rio Grande) leads to a serious threat to the regions of the city bordering the river. Note that flood defenses are very well constructed on the American side, leading to the potential for worse flooding in Juárez since little water would escape north into El Paso Texas. A clear demonstration of the current danger of flooding is the largest recent flood registered on August 03, 2006, with 59 mm rainfall in less than 1 hour (see Fig. 1.5). Personal memories are valuable records, for example, "Talavera García remembered that since 50 years the Bravo River never rose as much as today" (See Appendix 1A, 08/03/2006 report of Diario de Juárez Local Newspaper) He said that in 1925, the river rose in a way that practically covered the Cuauhtémoc sector. He commented that the river again rose on July 16th, and on August 6th 1954 but, in 1960 began to become more dry. On the other hand Raul Luevano Engineer of Water Meeting Office said that the Bravo River may flow a 450 m^3/s similar to that registered in 1950.

Mack and Leeder (1998) reported four events of change of position of the Bravo River channel along Mesilla bolson west of Organ-Franklin-Juárez Mountains just before the completion of Elephant Dam in 1916. One, during 1844 and 1852 to the north of Mesilla basin and three more during 1903 and 1912 south to the basin. Thus, the Bravo River power caused lateral erosion with further changes in the river trajectory, reducing sinuosity and river enlargement by 1893; 1903, and 1912 Bravo River locations near to Doña Ana and La Mesa (see Fig.1C2 of Appendix 1C) (Mack and Leeder, 1998). Nevertheless, river channel changes are effectively impossible nowadays because of the control by Elephant Butte Dam and the constructed levees.

Therefore, because of the control of the river, the flooding threat to the city is from the mountains, principally associated with episodic summer storms of high intensity and short duration. Nevertheless, there is still a flood threat from the river, during times of heavy rainfall, and although the levees have been built up, the possibility of overtopping into the surrounding topographically lower occupied land continues. The key difficulty is that the sluice gates, that normally allow drainage of mountain floods into the river, would not be usable in a case of double flooding (river and mountains simultaneously). Water is not the only threat; sediment load carried by floods adds to the problem, due to incision by the river during flooding. Incision and sediment production are complex; Lindsey and Van Gosen (2010) stated that incision or vertical erosion occurs just before lateral erosion takes place because stream power/resisting power ratio is less than 1. In addition, when sediment supply is important stream power becomes near to resisting power and the factor could become 1 (equilibrium). Finally if sediment supply is very high, then stream power is higher than discharge power and the factor could become more than 1. Thus, deposition would take place. Therefore, in agreement with Lindsey and Van Gosen (2010) theory it is possible to conclude that high summer discharge events like those presented in the study area during the “Chamizal case” (Mack and Leeder, 1998) promotes incision. With regard to the flood modeling, although sediment is carried into the city by flooding, most sediment is retained in the detention basins in the upper reaches of the fans, so that the effect of the additional mass of sediment on the model parameters is likely to be within acceptable limits to maintain validity of the modeling. Note also that the flood modeling refers to the city floods, and will be most accurate in the areas where a) there is less sediment load because it is deposited higher up, and b) there are more inhabited places.

Therefore, episodic storms of short duration and high intensity are the flooding threat of the study area, and the reader is reminded of the mean annual precipitation recorded from the period of 1852 to 1905 was 223 mm with a mean temperature of 16.4^0 C (Mueller 1975). Also for the same period the lowest annual precipitation registered was 88 mm, while the highest was 434 mm occurred during the year of 1905 with 50% distributed during the July, August and September months (Mueller 1975). Higher rainfall is due to meeting of two wind fronts, one warm from the Gulf of

México and another cold, derived from the Pacific Ocean. Thus, the final place where these storms split into tropical depressions is the study area mostly Juárez Mountain (Mueller 1975). Furthermore, the El Niño Southern Oscillation (ENSO) has been a threat to Juárez city in recent times, producing anomalies in the atmospheric pattern (Andrade and Sellers, 1988 and Reynolds, 1997); thus, in El Paso Texas, stronger ENSO events caused precipitation increment especially during autumn at the onset of an ENSO event, and also during the following spring (See sections 2.2.2 to 2.2.5 Figs. 2.17, to 2.25). The difference between flood threats in El Paso and Juárez is that in El Paso, the flood defences have been engineered to generate wide spillways away from habitation, to carry floodwaters from the Franklin Mountains to the river, which exacerbates the danger of river flooding on the Mexican side, where the levee defenses are less robust (personal observations by the author). Significant river discharge differences have been observed during the seasons of the year, The average year river discharge have been evaluated as being less than 283 m^3/s (Mueller 1975). In summary, the conclusion is that nowadays the threat of flooding pattern of the Juárez city has been increased with more precipitation. Rainfall information of the study area is available for the period 1969 to 2009 (See Fig. 1.5 Chapter 1); and average yearly accumulated precipitation is available for 1957 to 2009 (See Fig. 1.3 and Section 1.4). The modeled rainfall threat derived from the design storm for the study area was 55.5 mm in 1 hour for a 100 years return frequency (see hyetogram Fig. 5.7 of Chapter 5) is consistent with the current experience of flooding in Ciudad Juárez.

7.3.2 How might the flood threat change in future decades?

Predicted results from modeling in Chapter 5 suggest an increasing future flooding in the study area for two main reasons. Firstly, Andrade and Sellers (1988) strongly suggest important shifts provoked by ENSO in the precipitation pattern in recent times, this is likely to worsen as a result of global warming which is most likely to affect the study area. This conclusion is supported by Reynolds (1997) who related rainfall to ENSO in the El Paso Texas area. In El Paso Texas, seasonal precipitation during moderate to strong ENSO events, especially during the autumn of an ENSO onset year and the following spring is affected by moderate to strong ENSO events.

Secondly, the high urbanization rate of Juárez city is the other factor that would be expected to lead to decreased retention of floodwaters, which cannot drain easily.

A brief analysis of datasets indicate that two highest precipitation events occurred during the period mentioned above are: Firstly, 464 mm occurred during the year of (1884) with 70% (325 mm) falling during August September and October months. Secondly, in 2006 with a total annual rainfall of 444 mm but 68% was during August (174 mm) and September (127 mm). In this regard, a controversy emerges due to two historical flooding event occurred on August 24th and 26th of 1890 year caused many disasters affecting 80 families (see appendix 1A). However, in (Appendix 1 Fig. 1.1) yearly and monthly accumulated precipitation recorded in El Paso Texas is 215 mm during 1890 with only (82.5 mm) during August. Therefore, it is contrary to the trend observed by Andrade and Sellers (1988) and Reynolds (1997) who stated that for El Paso Texas, stronger ENSO events caused increment in precipitation especially during autumn at the onset of an ENSO event, and also during the following spring (see Figs. 2 to 4 in Appendix 1).

7.4. EFFECT OF ENGINEERING WORK IN FLOOD MITIGATION

7.4.1 Fluvial process of the Bravo River affected by dam construction

Bravo River channel hydrological capacity and competence have built the modern regional landscape over the last few million years. However, the river's ability has reduced since the early 20th century due to construction of two control structures located upwards north of the study area: Elephant Butte Dam with geographic coordinates (G.C. North 33.201522, East -107.187538), and Caballo Dam 20 miles downwards of Elephant Buttle Dam (G.C. North 32.905544, East -107.296994). These flow regulation structures have impacted the Bravo River channel behaviour due to reduction in discharge, capacity and competence downstream of the dams so that the Bravo River channel has been deactivated in its capacity to construct terraces. Thus, the bedload of the ancient Bravo River floodplain is composed mainly of a pebbly sand multilayer of 8 km-wide floodplain. Thus, periodical spring floods derived from headwaters and snowmelt during 68 years of data information are

evidence that the main channel of the Bravo River has extended its floodplain approximately by 1300-100 m and had increased its sinuosity in the order of 1.9-1.2 (Mack and Leeder, 1998).

7. 4.2 Engineering works that affect the natural processes of alluvial fans.

The study area has been affected enormously during the last decades as a result of urbanization works associated with an expanding population that is now 1.3 million, having tripled from about 400,000 in the 1970s. These changes have deactivated the alluvial fan system and thus interfered with the natural fan processes, leading to an imbalance of the alluvial aquatic and sedimentary activity. Thus, big hydrographs with high peak discharge and little concentration time are produced due to high effective runoff (see section 5.2.2.4 and Fig. 5.7 in chapter 5).

Three big sectors located in the study area illustrate this environmental problem at various scales. The Northwestern sector located in Anapra neighborhood is the least affected. Here, the natural conditions are still preserved and the alluvial fan system components are still active (see Figs. 4.6 and 4.9 of results Chapter 4). Thus the alluvial fan in this sector is still active but its stability is in danger because recently the city has been growing in the Anapra direction. On the other hand, the Centre sector as well Southeast sectors are more affected because of construction of many artificial dykes for flood retention (that the modeling in Chapter 5 shows to be largely inadequate). The Central Sector, comprising east Snake and Colorado alluvial fans (see Figs. 4.7; 4.8 and 4.9) is the most affected by urbanization works because of its high population density and also because of the poor quality of dykes. The natural processes are also interrupted because the sediments are caught by dykes in the upper reaches of streams, part of the process of preventing the natural formation of alluvial fans (the fans are also arrested by the widespread streets and building construction across them). In short, the results emerged from Chapters 5 with regard to flooding prediction show that only 18 of 47 dykes monitored would be expected to able to resist flooding hazard events (see Figs. 5.11; 5.15; 5.19; and 5.26 of Chapter 5).

7. 4. 3 How could these flood-prevention measures be modified to mitigate the flooding threat?

To mitigate the flooding threat of the city it is necessary to update building regulations mostly those nearly to homes avoiding building permissions within the flooding area of all the main streams. In addition, the following recommendations for auxiliary works to regulate the flow with strong enough structures systems.

1) The Juárez population is mainly located in flat Bravo River valley areas. There, a surface layer of clay, clayey silt and clayey sand with infiltration rates below 0.05 cm/hr is observed. Consequently, to mitigate the flooding risk assessed in (Chapter 6 section 6.4.4.2.1 and Figs. 6.15 to 6.17) the following measures are proposed. Firstly, for flat areas assign new land use as parks or recreation and design the control structures and absorption wells needed to drain the water stored to recharge it to the groundwater. Secondly, for private sector areas which are under construction or proposal, the Municipal Government should negate permission to build homes, commercial or industrial developments in these areas.

2) A program of main stream channeling must be designed to contain flood discharge of 100 years return period equipped with control structures to regulate the stream discharge from tributaries which would discharge to the main streams in the areas of: Anapra, Mimbres, Snakes Colorado, Pantheon, del Indio, Jarudo, Palo Chino and Barreal Streams.

3) Strengthening of all flow regulation structures (dykes) in order to adapt them hydraulically and structurally to the flooding discharge and water stored defined for the design flooding hazard (See point 8.2.1 section 8.2 of conclusion chapter 8).

4) The 13 flow control gates system installed on the west bank (=Mexican side) of Bravo River between the North International boundary and Gustavo Diaz Ordaz neighborhood need to be redesigned to solve inundation problems that frequently occur when the Bravo River overspills and Juárez Mountain flooding happen simultaneously.

5) Engineering works like streets and highways as Camino Real are basic to improve transportation and communication issues. However, these works also impact the behavior of flooding and its consequences. Also, high urbanization rates have caused less infiltration rates and shorter concentration and lag times.

Therefore, high stream discharge and water storage in inundation areas and dykes are expected. For this reason, engineering works shall be carefully planned and designed according to the flooding hazard predicted. Finally, construction regulation should restrict works in areas of active alluvial fan and terraces. Then, it is urgent to repair dykes, and redesign them as well as the regulation gates installed along the Bravo River in order to solve efficiently the inundation problems summarized in Fig. 8.2.1 in the Conclusion Chapter 8.

CONCLUSIONS

This chapter states the outcomes of this thesis in relation to the major questions of the aims stated in Chapter 1. Therefore, the outcomes are summarized first, followed by recommendations.

8.1 Main outcomes of this study

8.1.1. Ciudad Juárez is constructed on an alluvial fan system developed from the Juárez Mountains to the southwest, and interlayered fluvial deposits from the Bravo River (=Rio Grande) to the north and northeast. The city and its deposits lie in the Hueco Basin through which the Bravo River flows from Texas. Fieldwork and laboratory grain size investigation demonstrates that the alluvial fan system consists principally of aqueous flood deposits but is interlayered with aeolian sands. Three OSL dates on aeolian sands in the topographically higher parts of the Colorado Fan (located through the centre-west of Juárez City) reveal ages of 31 ka, 60 ka and 74 ka, demonstrating a pervasive arid climatic state and intermittent episodes of flooding. These dated deposits are in small sites between building developments which otherwise have disturbed and covered a very large part of the fan surface. Thus, while it will be impossible to reconstruct the fan system in detail, these deposits and dates demonstrate the dynamicity of the alluvial system. These dates are also rather old, and therefore indicate that the more recent palaeohydrological processes in the Hueco Basin, leading to the modern position of the Bravo River are likely to have incised during the late Pleistocene, but more dating is required to develop this.

8.1.2. Flood modeling using standard methods and software (HEC-HMS and HMS-RAS on a GIS platform) is consistent with historical and recent flood data to show that there is a significant continuing flood threat to many parts of Juárez City, in particular those areas of the central part that are also the most populated areas. Vulnerability maps include both position and socio-economic status to demonstrate an important threat. More specifically, the greatest threat of inundation by flash flooding is mostly in northwestern Juárez city in the ladrillera de Juárez and Benito Juárez neighborhoods. In this area a system of 13 little regulation rectangular gates of 1.35 m by 1.25m are installed in the levees of the Bravo River; the capacity of these gates is (0.36 m^3/sec each). However only 4 work properly (see section 5.3.2.2.1 description of Anapra basin system; section 5.3.2.2.2 Ladrillera

stream subbasin (LSb) (2 gates); section 5.3.2.2.3 El Tapo stream (2 gates); section 5.3.2.2.4 Cocotla stream subbasin (Csb) (2 gates); section 5.3.2.2.5c Mimbres subbasin (Msb1) (3 gates). These 9 gates don't work properly because lack of capacity. Thus, an important reflection emerges. For instance, eventually, during the storm season the Bravo River receives high amounts of rainfall derived from Colorado; Arizona; New México and El Paso Texas. However, at the same time the river receives high discharges derived from Juárez mountains. As a result, water running from the Bravo River overspills because the little regulation gates are closed in order to avoid inundation problems on Ladrillera de Juárez, Felipe Angeles, Mimbres and Norzagaray streets (see Fig. 5.36 of Chapter 5). On the other hand, when episodic storm occurred in Juárez mountain the flooding is running but the gates are closed and consequently a big inundation problem undergone.

8.1.3. Flood threat comes from two sources: A) the Bravo River (=Rio Grande), which, despite its controlling dams in the USA and the levees constructed to protect Juárez and El Paso, is subject to overspill on the less well-protected Mexican side to threaten properties near the river; B) flash floods from Juárez Mountains, which can develop within an hour, and likely to overcome most flood defence measures. Because of increasing instability in global climate, and the location of northern México in a region of predicted climate change, the threat of flooding is likely to worsen in the near future. The results of modeling show that in the medium to long-term future the area is likely to be subject to stronger events. If such floods come from both the Bravo River and the Juárez Mountains at the same time, then there is a potential for catastrophic floods. Thus the floodgates in the Bravo River levee, that are opened to allow flash floods to drain to the river, and closed to prevent Bravo River flooding, will be ineffective.

8.1.4. Urbanization in the study area has provoked more flooding as a result of a reduction in permeability of the natural soils. Furthermore, major streams have been paved and channelized or pipelined in order to conduct the water. Then, in order to protect people from flooding on these areas to build conduction water channels from the topographic apex near to the mountain front until the control regulation structures (dykes) is needed flooding hazard maps for main streams of the study area (see Chapter 6, Figs. 6.15; 6.16 and 6.17). Moreover, the consequent loss of soil permeability increases the runoff and the sediments eroded in the source areas are transported downstream and captured for small and weak

dikes constructed located in the downstream areas. As a result the other physical feature which has been affected is the inactivation of the alluvial fan system located in the central sector near to Juárez Mountain.

8.2. Recommendations for mitigation of flooding problems

The results of this work show that some major measures are required in Juárez City to mitigate the flooding problems, as follows:

8.2.1. Dykes are common engineering structures in Juárez City to regulate water flow. Modeling in this resaerch shows that 18 of 47 dykes monitored through the application of HEC-HMS computer program work properly because have more storage capacity than the predicted flood hazard for 100 yrs return period (see Figs. 5.11; 5.15; 5.19 and 5.26 of the results HEC-HMS results Chapter 5). However, the problem here is that perhaps these structures were not structurally well designed and also not correctly located. Therefore, it is recommended to review and update properly their design.

8.2.2. The south (Mexican side) bank of the Bravo River defenses which separate Juárez city and El Paso Texas should be reinforced and compacted in order to avoid failure and water infiltration due to loss of shear strength during flooding events.

8.2.3. Designing a relocation program of people who live on main streams flooding areas illustrated in flooding hazard maps of Figs. 6.15, 6.16 and 6.17. These people must leave 15 m of unbuilt land on each side of the streams axes.

8.2.4. Installation of hydrologic stations to measure the temporal distribution during the day, months and years of precipitation, temperatures and evaporation in mountainous zones as well as in valleys should be provided mostly should be installed along main streams mentioned in point 8.2.3.

8.2.5. Discharge and runoff gauge installation in all the main streams of the Juárez city area (see Figs. 6.15 to 6.17). Also, direct measures of concentration time for all the flooding events.

8.2.6. Design of a Contingency Plan in order to help and evacuate people in case of flooding disasters.

References

Allen, B. D. and Hawley, J. W. 1991. Lake Estancia basin tour, in Hawley, J. W., and Love, D. W. (Eds.), Quaternary and Neogene landscape-evolution: A transect across the Colorado Plateau and Basin and Range provinces in west-central and central New Mexico*, New Mexico Bureau of Mines and Mineral Resources*: Bulletin 137, 130-134.

Allen, B. D. 1993. Late Quaternary lacustrine record of paleoclimate from Estancia Basin, Central New Mexico, USA [Ph.D. dissertation]: Albuquerque, University of New Mexico, 94 pages.

Allen, B. D. and Anderson, R. Y. 2000. A continuous, high-resolution record of late Pleistocene climate variability from the Estancia basin, New Mexico: *Geological Society of America Bulletin*, 112, no.9, 1444-1458.

Andrade, E. R. Jr. and Sellers, W. D. 1988. El NIño and its effect on precipitation in Arizona and Western New Mexico, *Journal of Climate*, 8, 403-410.

Arc-View 3.2, 2002 Free Arc-View 3.2 Program Available in: http://rapid4me.com/?q=arcview+3.2+free. Date: December, 2012.

Auto-Cad, 2009. Free tutorial. Available in: www.brothersoft.com/autocad-238265.html. Date May 5, 2011.

ArcMap GIS 9.2, 2009 Using HEC-GeoRAS with Arc-GIS 9.2. Available in: www.flumen.upc.edu/admin/files/cursos/25.pdf. Date May 5, 2011.

ArcMap GIS 9.3, 2009 Using HEC-GeoRAS with Arc-Gis 9.3. Available in: Web.ics.purdue.edu/~vmerwade/education/georastutorial.pdf. Date: May, 5, 2011.

ASTM. 1985. Classification of Soils for Engineering Purposes. *Annual book of ASTM Standards*, D 2487-83, 04.08, *American Society for Testing and Materials*, 1985, pp. 395-408.

Blair, T. C. and McPherson, J. 1998. Recent debris-flow processes and resultant form and facies of the dolomite alluvial fans, Owens valley, California. *Journal of Sedimentary Research*, A68, 800-818.

Blair, T. C. and McPherson, J. 1994. Alluvial fans and their natural distinction from rivers based on Morphology, hydraulic processes, sedimentary processes and facies assemblages. *Journal of Sedimentary Research*, A64, 450-489.

Bull, W.B. 1968. Alluvial fans, *Journal of Geology Education*, 16, 101-106

Bull, W. B. 1991. Geomorphic responses to climatic change. *Oxford University Press, New York*, 326 pp.

Bell, F. C. 1969. "Generalized Rainfall-Duration-Frequency Relationships, " *Journal of the Hydraulics Division*, ASCE, Vol.95 No, HY1, Proc. Paper 6357, Jan., 1969, pp. 311-327.

Bachman, G. O. and Machete, M. N. 1977. Calcic soils and calcretes in the southwestern United States. UNITED STATES DEPARTMENT OF THE INTERIOR *GEOLOGICAL SURVEY Open-File Report 77-794*.
Available in: http://pubs.usgs.gov/of/1977/0794/report.pdf Date: December, 2012.

Cheng, L. Ch. 1983. Rainfall Intensity-Duration-Frequency Formulas. *Journal of Hydraulic Engineering*, 109 (12), 1603-1621.

Cole, J.C., Mahan, S.A., Stone, B.D. and Shroba, R.R. 2007. Ages of Quaternary Rio Grande terrace-fill deposits, albuquerque area, New Mexico: U.S. Geological Survey, Denver Colorado. *New Mexico Geology*, Volume 29, Number 4, November 2007 Available in:http://geoinfo.nmt.edu/publications/periodicals/nmg/downloads/29/n4/nmg_v29_n4_p122.pdf

CNA. 2008. Total annual accumulated precipitation recorded in Juárez city during the period from 1957 to 2008. Collected personally in printed paper. National Water Commission Office of Ciudad Juárez, Chihuahua México. Date: Enero 2008. and
Information of Average monthly accumulated precipitation recorded in Juárez city during the period from 1957 to 2008. National Water Commission Office of Ciudad Juárez, Chihuahua México. Date: Enero de 2008.

CNA, 2007. Information of maximum daily precipitation events during the period from 1969 to 2006 (37 years) were collected personally in printed paper. National Water Commission Office of Ciudad Juárez, Chihuahua México. Date: Enero de 2007.

Collins, E. W. and Raney, J. A. 2000. Geologic map of west Hueco Bolson, El Paso region, Texas: The University of Texas at Austin, Bureau of Economic Geology, Open-File Map, scale 1:100,000.

Connell, S. D. and Love, D. W. 2001. Stratigraphy of middle and upper Pleistocene fluvial deposits of the Rio Grande (Post Santa Fe Group) and the geomorphic development of the Rio grande valley, northern Albuquerque basin, central New Mexico: *New Mexico Bureau of Geology and Mineral Resources*, Open File Report 454C, p. C1–C12.

Connell, S. D., Allen, B. D. and Hawley, J. W. 1998. Subsurface stratigraphy of Santa Fe Group from borehole geophysical logs, Albuquerque Area, New Mexico: *New Mexico Geology*, 20(1), 2-7.

Drewes, H. and Dyer, R. 1993. Geological map and structure sections of the Sierra Juárez, Chihuahua, México scale 1:12,500 MAP 1-2287. U.S. *Geological Survey miscellaneous investigations.*

Diaz-Pereira, D., Ochoa-Martinez, C.A, Perez-Sesma, J.A. 2005. Ecuaciones de LLuvia intensa generalizada para obtener precipitaciones maximas de corta duracion. GEOS, Vol. 25, No. 2.

ESRI, 2011. Tutorials for ArcGIS 9.2 Desktop Help. Available in: http://webhelp.esri.com/arcgisdesktop/9.2/index.cfm?Topicname=tutorials. Date: 15/07/2011. and Tutorials for ArcGIS 9.3 Desktop Help. Available in: http://www.esri.com/software/arcgis/arcgis10/index.html. Date: 15/07/2011.

El Diario de Juárez Newspaper. 2010. Information regarded to disasters from 1827 to 2007 taken from different editions of Diario de Juárez Newspaper. Juárez City of Mexico. Date: December 2007.

El Diario de Juárez Newspaper. 2008. Landslide occurred in July 2008 in the Camino Real road. Available in: www.diario,com,mx/multimedia.php?video_id=97d0145823aeb8ed80617be62e08bdcc&p=73) Date accessed: September 2008.

García, R. 1970. Geology and Petrography of Andesite intrusions in and near El Paso, Texas. The Universty of Texas at El Paso (UTEP). *Master's Thesis*: Available in http://proquest.umi.com/dissertations/Previous_ALL EPOO877. Date: December, 2008

Google. 2007 to 2009. Satellite Image of the Study area and Map of America. Available in: www.maparchive.org/.../north_america_ref02.jpg. Date: 23/05/ 2009.

Gile, L. H., Hawley, J. W. and Grossman, R.B. 1981. Soils and geomorphology in the Basin and Range area of southern New Mexico-guidebook to the Dessert Project: *New Mexico Bureau of Mines and Mineral Resources Memoir* 39, 222p.

Gile, L. H., Peterson, F. F. and Grossman, R. B. 1966. Morphological and genetic sequences of carbonate accumulation in desert soils: *Soil Science*, 101(5), 347-360.

Gill, T.E., Collings, T.W. and Novlan, D.J. 2009. Variable impacts and differential response to flash flooding in the Paso del Norte metroplex (El Paso, Texas, USA / Ciudad Juárez, Chihuahua, Mexico) Department of Geological sciences, *University of Texas at El Paso (UTEP):* Available in: <http://ams.confex.com/ams/pdfpapers/148065.pdf> [March 12, 2009].

Gumbel. E.J. 1958. "Statistics of Extremes". Irvington, New York: *Columbia University Press in*: Ponce (1994).

Gustavson, T.C. 1991. Arid basin depositional systems and palaeosols: Fort Hancock and Camp Rice Formations (Pliocene–Pleistocene), Hueco Bolson, west Texas and adjacent Mexico. *Texas Bureau of Economic Geology Report of Investigations,* 198 (49 pp.).

Grossman, R. B., Monger, H. C., Gile, L. H., Hawle, J. W. 2007. The Desert Project-An Analysis of Aridland Soil-Geomorphic Processes. Bulletin 798. NM State University. Available in: aces.nmsu.edu/pubs/research/weather_climate/BL798.pdf. date: Nov. 2012.

Hall, S.A., Goble, R.J. and Raymond, G.R. 2008. OSL ages of upper Quaternary eolian sand and paleosols, northwest Albuquerque Basin, New Mexico. May 2008, *New México Geology* 39. Number 2, volume 30. Available in: http://geoinfo.nmt.edu/publications/periodicals/nmg/downloads/30/n2/nmg_v30_n2_p39.pdf
Hack, J. T. 1941. Dunes of the western Navajo Country: *Geophysical Review*, 31(2), 240-263.

Hall, S. A. 1977. Late Quaternary sedimentation and paleoecologic history of Chaco Canyon, New Mexico: *Geological Society of America Bulletin*, 88, 1593-1618.

Hawley, J. W. and Kernodle, J.M. 2000**.** Overview of the hydrogeology and geohydrology of the ed., Proceedings of the 44th Annual New Mexico Water Conference: *New Mexico Water Resources Research Institute Report* 312, 24pp.

Hawley, J. W., 1993a, Geomorphic setting and late Quaternary history of pluvial-lake basins in Hawley, J. W., Bachman, G.O. and Manley, K., 1976, Quaternary stratigraphy in the Basin and Range and Great Plains provinces, New Mexico and western Texas; in Mahaney, W.C., 69 ed., *Quaternary Stratigraphy of North America*: Stroudsburg, PA, Dowden, Hutchinson, and Ross, Inc., p. 235-274.

Hawley, J. W., Bachman, G.O. and Manley, K. 1976. Quaternary stratigraphy in the Basin and Range and Great Plains provinces, New Mexico and western Texas; in
Hawley, J. W., Hibbs, B. J., Kennedy, J. F., Creel, B. J., Remmenga, M. D., Johnson, M., Lee, M. M. and Dinterman, P. 2000. Trans-International Boundary aquifers in southwestern New Mexico: New Mexico Water Resources Research Institute, New Mexico State University, prepared for U.S. *Environmental Protection Agency-Region 6 and International Boundary and Water Commission; Technical Completion Report.*

Hawley, J. W., Kottlowski, F. E., Seager, W. R., King, W. E., Strain, W. S. and LeMone, D. V. 1969. The Santa Fe Group in the south-central New Mexico border region: in Border stratigraphy symposium: *New Mexico Bureau of Mines and Mineral Resources*, Circular 104, 52-76.

Hawley, J.W. 1969. Notes on the geomorphology and late Cenozoic geology of northwestern Chihuahua. *New Mexico Geol. Soc. Guidebook*, 20th Field Conf., 131–142.

Hawley, J.W., 1975. Quaternary history of Dona Ana County region, southcentral New Mexico. *New Mexico Geological Society, Guidebook* 26, 139–150.

Hawley, J.W., 1981. Pleistocene and Pliocene history of the international boundary area, southern New Mexico. *El Paso Geological Society Field Trip Guidebook*, pp. 26–32.

Hawley, J.W. and Kennedy, J.F. 2004. Creation of a Digital hydrogeologic framework model of the Mesilla Basin and southern Jornada del Muerto Basin: *NM Water Resources Research Institute. Technical Completion Report*, 105p. CD-ROM.

Hawley, J.W., Kottlowski, F.E. 1969. Quaternary geology of the south-central New Mexico border region. *New Mexico Bureau of Mines and Mineral Resources*, Circular 104, 89–115.

Holliday, V. T. 1989. Middle Holocene drought on the Southern *High Plains: Quaternary Research*, 31, 74-82.

Holliday, V.T. 2000 Folsom drought and episodic drying on the Southern High Plains from 10,900-10,200 14C yr B.P: *Quaternary Research*, 53, 1-12.

Hooke, R.L. 1967. Process on arid region alluvial fans. *Journal of Geology* 75, 438-460.

HEC-RAS 3.1.3. 2002. Hydrologic Engineering Centre-River Analysis System Available in: :www.hec.usace.army.mil/software/hecras/documents/hydref/cvr_incvr_toc.pdf. Date: may 5, 2011

HEC-HMS 3.1.0. 2002. (Hydrologic Engineering Center-Hydrologic Modeling System). Available in: www.hec.usace.army.mil/software/hec-hms/ Date: may 5, 2011

HEC-1. 1998. Flood Hydrograph Package: User's Manual. Hydrologic Engineering Center. U.S. *Army Corps of Engineers, Davis, CA.*

HEC-IFH. 1992. Hydrologic Engineering Center. Interior Flood Hydrology Package: User's Manual. U.S. Army Corps of Engineers, Davis, CA.

HEC-GeoRAS 3.1.3. 2002 for Arc-View GIS 3.2. Available in: www.hydroeurope.org/jahiawebdav/site/hydroeurope/groups/team9/public/gisreference material/HecGeoRAS42_User Manual.pdf. Date: May, 2011

Hall, A. S., 2008. OSL ages of upper quaternary eolian sand and paleosols, northwest Albuquerque Basin, New Mexico. *New Mexico Geology* Volume 30, Number 2 May 2008.

INEGI. 1983. Geological Chart H 13-1 of Cd. Juárez scale 1:250,000. Instituto Nacional de Estadistica Geografia e Investigacion, Date: Enero de 2009.

INEGI. 1988. Topographic Chart H 13A25 of Cd. Juárez scale 1:50,000. . Instituto Nacional de Estadistica Geografia e Investigacion, Date: Enero de 2009.

INEGI. 2007. Juárezageb2005_wgs_84_Area. Informatic, Instituto Nacional de Estadistica Geografia e Investigacion, Date: Enero de 2009.
Demographic data sets regarded to population density.

INEGI. 2002. Demographic and Physiographic features of the Ciudad Juárez area. Instituto Nacional de Estadistica Geografia e Investigacion, Date: Enero de 2009.

IBWC. 2006. International Border Water Commision. UNIES-UNITED NATIONS (1906) International Border Agremment between Mexico and Unites States of America. "The Chamizal case". Available in: untraty.un.org/cad/riaa/cases/VolX1/309-347.pdf. date: December, 2012.

IMIP. (2005) Plan de Desarrollo Urbano de Ciudad Juárez, Instituto Muinicipal de Investigacion y Planeacion "Plan Sectorial de Manejo de Agua Pluvial. Ayuntamiento de Juárez. 380 pages.

IMIP. (2007) Contour levels dataset every 5 meters of the study area; Topographic chart; Aerial photo; Digital Elevation Model and Sattelite Images of the study area. Instituto Muinicipal de Investigacion y Planeacion de Ciudad Juárez, México.

JMAS. 2009**.** Boreholes lithology of the study area provided by: Junta Municipal de Aguas y Saneamiento de Ciudad Juárez, Chihuahua México. Date: Enero de 2009.

Kelley, S. A. and Chapin, C. E. 1995. Apatite fission-track thermochronology of the southern Rocky Mountain-Rio Grande rift-western High Plains provinces: *New Mexico Geological Society Guidebook* 46, 87-96.

Kelley, S. A. and Chaplin, C. E. 1997. Cooling histories of mountain ranges in southern Rio Grande rift based on apatite fission-track analysis-reconnaissance study:*New Mexico Geology*, 19, 1-14.

Kelley, S. A., Chapin, C. E. and Corrigan, J. 1992. Late Mesozoic to Cenozoic cooling histories of the flanks of the northern and central Rio Grande rift, Colorado and New Mexico: *New Mexico Bureau of Mines and Mineral Resources*. Bulletin 145, 40 pages

Kottlowski, F. E. 1958. Geologic history of the Rio Grande near El Paso. West Texas *Geological Society Guidebook*, 46–54.

Kiprich, Z. P. 1940. Time of concentration of small agricultural watersheds. Civ. Eng. 10(6), 362, IN: Linsley, R., Kohler, M.A. & Paulhus, J.L.H. (1982) *Hydrology for Engineers. McGraw-Hill, New York, USA*.

Kevin T. P. and Lewis. A. O. 1997. An Introduction to Global Environmental Issues. Second Edition, *Routledge Taylor & Francis Group. New York*.

Langford, P. R. 1999. The Miocene to Pleistocene filling of mature extensional basin in Trans-Pecos Texas: geomorphic and hydrologic controls on deposition. *Journal of Sedimentary Geology*, 128, 131-153.

Lambert, P. W. 1968. Quaternary stratigraphy of the Albuquerque area, New Mexico [PhD. Dissertation]. *Albuquerque University of New Mexico*, 329 p.

Lecce, A. S. 1990. The alluvial Fan Problem. Chapter 1. Alluvial Fans: A Field Approach edited by A.H. *Rachocki and Church. John Wiley & Sons Ltd*.

Leeder, M. R., Mack, G. H. and Salyards, S. L. 1996. Axial-transverse fluvial interactions in half-graben: Plio-Pleistocene Palomas basin, southern Rio Grande rift, New Mexico, USA. *Basin Research* 12, 225–241.

Leeder, M. R., Mack, G. H. and Salyards, S. L. 1996a. Axial-transverse fluvial interactions in half-graben: Plio-Pleistocene Palomas basin, southern Rio Grande rift, New Mexico, USA. *Basin Research* 12, 225–241.

Leeder, R. M and Mack, G. 2009**.** Basin Fill Incision, Rio Grande and Gulf of Corinth Rifts: Convergent Response to Climatic and Tectonic Drivers (pages 9-27)

Leopold, L. B. 1951. Pleistocene climate in New Mexico: *American Journal of Science*, 249, 152-168.

Lindsey, D.A. and Van Gosen, B.S. 2010. Processes of Terraces Formation on the Piedmont of the Santa Cruz River Valley During Quaternary Time, Green Valley-Tubac Area, Southeastern Arizona. *Scientific Investigation Report 2010-5028. U.S. Geological Survey.* of North America. *The Geological Society of America* V.K-2, pp. 353-371.

Loukas, A. and M. C. Quick. 1996. Spatial and temporal distribution of storm precipitation in southwestern Bristish Columbia. *Journal of Hydrology* 174: 37-56, 1996.

Love, D. W. and Young, J. D., 1983, Progress report on the late Cenozoic geologic evolution of the lower Rio Puerco: *New Mexico geological Society Guidebook* 34, p. 277-284.

Lovejoy, E. M. P. 1976e. Geology of Cerro de Cristo Rey Uplift, Chihuahua and New Mexico. *New Mexico Bureau of Mines & Mineral Resources. Memoir* 31, 11-26.

Loukas, A. and Quick, M .C. 1995. Physically-based estimation of lag time for forested mountainous watersheds. *Hydrological Sciences- Journal- des Sciences Hydrologiques*, 41(1), 1-19.

Machette, M. N., 1985, Calcic soils of the southwestern United States, in: Weide, D.L., ed., Quaternary soils and Geomorphology of the American southwest: *Geological Society of America Special Paper* 203, p.1-42.

Machette, M. N., Long, T., Bachman, G. O. and Timbel, N. R. 1997. Laboratory data for calcic soils in Central New Mexico: Background information for mapping Quaternary deposits in the Albuquerque basin: *New Mexico Bureau of Mines and Mineral Resources,* Circular 205, 63p.

Mack, G. H., James, W. C. 1993. Control of basin symmetry on fluvial lithofacies, Camp Rice and Palomas Formations (Plio-Pleistocene), southern Rio Grande rift, USA. In Marzo, M., Puigdefabregas , C. (Eds), Alluvial Sedimentation. *International Association of Sedimentologists Special Publication,* 17, 439-449.

Mack, G. H., Seager, W. R., Leeder, M. R., Arlucea-Perrez, M. and Salyards, L. S. 2006. Pliocene and Quaternary history of the Rio Grande, the axial river of the southern Rio Grande rift, *New Mexico, USA. Earth Science Reviews*, 79, 141-162.

Mack, G. H. and Leeder M. R. 1998. Channel shifting of the Rio Grande, southern Rio Grande rift: implications for alluvial stratigraphic models. *New México, USA. Sedimentary Geology Bulletin,* 117, 207-219.

Mack, G. H. and Leeder, M. R. 1999. Climatic and Tectonic controls on Alluvial fans and axial fluvial sedimentation of the Camp Rice and Palomas Formations (Plio-Pleistocene) in the southern Rio Grande Rift. *Geological Society of America Bulletin*, 102, 45-53.

Mack, G. H., Love, D. W. and Seager, W. R. 1997. Spillover models for axial rivers in regions of continental extension: the Rio Mimbres and Rio Grande in the southern Rio Grande rift, USA. *Sedimentology*, 44, 637–652.

Mack, G. H., Salyards, S. L. and James, W. C. 1993. Magnetostratigraphy of the Plio-Pleistocene Camp Rice and Palomas Formations in the Rio Grande rift of southern *New Mexico. American Journal of Science*, 293, 47-77.

Mack, G. H. and Seager, W. R. 1990. Tectonic control on facies distribution of the Camp Rice and Palomas Formations (Plio-Pleistocene) in the southern Rio Grande rift. *Geological Society of America Bulletin*, 102, 45–53.

Mack, G. H. and Seager, W. R., 1995. Transfer zones in the southern Rio Grande rift. *Journal of the Geological Society of London*, 152, 551–560.

Mack, G. H., Seager, W. R., and Kieling, J. 1994. Late Oligocene and Miocene faulting and sedimentation and evolution of the southern Rio Grande Rift, New Mexico, USA. Sedimentary Geology Bulletin, 92, 79-96.

Morrison, R.B. (1991) Quaternary geology of the southern Basin and Range province in Morrison, R.B. ed., Quaternary non-glacial geology: Conterminous U.S.: Boulder, Colorado, Geological Society of America, The Geology of North America v K-2, p 353–371.

Mueller, J. E. 1975. Restless River: International Law and the Behavior of the Rio Grande. *Texas Western Press, El Paso*.

National Park Service 2008. Chamizal “Two inundations and one buried for the Peter property” National Park Service U.S. Department of the Interior, Chamizal National Memorial. Available in: www.nps.gov/cham/hystoryculture/upload/FloodsSPANISH.pdf. Date: July, 15/ 2011.

Nodeland, S. 1977. Cenozoic Tectonic of Cretaceous rocks in the Northeast Sierra de Juárez, Chihuahua, México. The Universty of Texas at El Paso (UTEP). Master's Thesis: Available in http://proquest.umi.com/dissertations/Previous_ALL EPOO877.
Open-File Report 391, 28 pages.

NOAA. 2009a. Rainfall Frequency/Magnitude Atlas for the South-Central United States. (SRCC Technical Report 97-1 Geoscience Publications Department of Geography and Anthropology Lousiana State University Baton Rouge, LA 1997.
http://www.srh.noaa.gov/epz/climat/rain/elpmonthlyprecip.html available in website Information of monthly and annual precipitation from 1878 to 2008.

NOAA. 2009b. Weather Almanac, 2001 El Paso, Texas (ELP) Daily maximum rainfall (24HMR) Occurred in El Paso, Texas for years (1941, 1943, 1945, 1956, 1958,, 1960, 1966, 1968, 1984, 1986, 1987 and 1992).

NOAA. 2004. Precipitation-Frequency Atlas of the United States: Volume 1 Semi Arid Southwest (Arizona, Southeast California, Nevada, New Mexico, Utah). National Weather Service (Atlas 14) U.S. Department. of Commerce, Silver Spring, MD.

NOAA 1961. Rainfall Frequency Atlas for the United States for Durations from 30 Minutes to 24 Hours and Return Periods from 1 to 100 Years. Technical Paper 40 National Weather Service. (U.S. Department of Commerce, Washington, DC).

Ortega-Ramírez, J., Bandy, A., Valiente-Banuet, J., Urrutia-Fucugauchi, C.A., Mortera-Gutierrez, J., Medina-Sánchez., G. and Chacon-Cruz J. 2004. Late Quaternary evolution of alluvial fans in the Playa, El Fresnal region, northern Chihuahua desert, Mexico: Palaeoclimatic implications, Geofisica Internacional, 43(3), 445–466.

Pazzaglia, F.J., Hawley, J.W., 2004. Neogene (rift flank) and Quaternary geology and geomorphology. In: Mack, G.H., Giles, K.A. (Eds.), The Geology of New Mexico. New Mexico Geological Society, Special Publication, 11, 407–437.

Ponce, V. M. 1994. Chapter 6. Engineering Hydrology Principles and Practices. Online Computational resources. Available at: Ponce.tv/330textbook_hydrology_chapters.html. and Chapter 6 (Frequency Analysis) is available in:ponce.tv/textbookhydrologyp204.html. Date: December 15, 2012

Reeves, C. C., jr. 1965. Pluvial Lake Palomas, northwestern Chihuahua, Mexico and Pleistocene geologic history of south-central New Mexico Geological Society, Guidebook, 16, 199-203.

Reynolds A. J. 1997. El Paso Texas Precipitation and its relationship to The El niño/ Southern Oscillation (ENSO). Available in: www.srh.noaa.gov/epz/?n=research_papers_jaelnino. Date: July; 2011.

Seager, W. R., Clemons, R. E., Hawley, J. W. and Kelley, R. E. 1982. Geology of northwest part of Las Cruces 1º x 2º sheet, New Mexico: New Mexico Bureau of Mines and Mineral Resources Geologic Map, GM-53, scale 1:125,000, 3 sheets.

Seager, W. R., Hawley, J. W., Kottlowski, F. E., and Kelly, S.A. 1987. Geology of east half of Las Cruces and Northeast El Paso 1x2 sheet, New Mexico: New Mexico Bureau of Mines and Mineral Resources Geologic Map 57, scale 1:125,000.

Seager, W. R., 1981. Geology of Organ Mountains and southern San Andres Mountains, New Mexico. *New Mexico Bureau of Mines and Mineral Resources, Memoir* 36 (97 pp.)

Smith, G. A., 1994, Climatic influences on continental deposition during late-stage filling of an extensional basin, southeastern Arizona: Geological Society of America Bulletin, v. 106, Socorro, New Mexico: Socorro, Rocky Mountain Cell*, Friends of the Pleistocene Field.*

Spaulding, W. G., Leopold, E. B., and Van Devender, T. R. 1983 Late Wisconsinan States: *Princeton, NJ, Princeton University Press*, 433-451.

Strain, W. S. 1966. Blancan mammalian fauna and Pleistocene formations, Hudspeth County, Texas. Texas Memorial Museum Bulletin 10 (55 pp.).stratigraphy, Animas Valley, *New Mexico, Quaternary Research*, v. 50, p. 283-289.

Swift, D. 1973. Lithofacies of the Cuchillo Formation, southern Sierra de Juárez Chihuahua, México. . The Universty of Texas at El Paso (UTEP). Master's Thesis: Available in http://proquest.umi.com/dissertations/Previous_ALL EPOO877.

SCS. 1986. Urban Hydrology for Small Watersheds. Soil Conservation Service Technical Release 55: Department of Agriculture, Washington, DC.

Tedford, R. H. 1981 Mammalian biochronology of the late Cenozoic basins of New Mexico*: Geological Society of America Bulletin*, Part I, 92, 1008-1022.

Tight, W. G. 1905. Bolson plains of the Southwest: American Geologist, v. 36, p. 271-284. *Geological Society of America Bulletin*, Part I, 92, 1008-1022.

Tolman, C. F. 1909. Erosion and deposition in southern Arizona bolson region: *Journal of Geology*, 17, 136-163.

TR 55. SCS 1986**.** Urban Hydrology for Small Watersheds. Edited by: USDA Soils Conservation Service (SCS); Now: *Natural Resource Conseravion Service (NRCS).* Available in: www.hydrocad.net/ tr-55.htm. Access date: May 6, 2011.

UTEP. 2009. University of Texas at El Paso Library sequences frames. Disasters caused for precipitation occurred in 1891 August 24th and 26. Taken from historic documents CJMA roll 70 sq. 2 fs.

UACJ. 2010. Daily maximum precipitation from the period of 2007 to 2009. The Information was collected personally from the Climatology Laboratory of Civil Engineering Faculty of Juárez University Ave. del Charro # 610 Norte. Ciudad Juárez Chihuahua, México. Phone: 6 88-48-00 and www.uacj.mx/IIT/Laboratorioclimatologia/paginas/pronosticos/paginas

UACJ. 2009. Soil Classification during the period 2009 to 2012. The work was done in the Soil mechanics Laboratory of the Civil Engineering Faculty of Ciudad Juárez University city. For more information ask to Master in Engineering Victor Hernándes Jacobo vihernan@uacj

UACJ. 2011 Countour levels offset every 1m using Lidar Technology provided by Juárez University Mexico. Geographic Information System Laboratory (SIG) of Civil Engineering Faculty of Juárez city University. For more information ask to Master in Engineering Victor Hernándes Jacobo: vihernan@uacj

USCS 2011. Engineering Classification of Soils. Available in: www.sfu.ca/~tafgrc/Courses/Easc313/B-Soil_Classification.pdf Date: May 6, 2011.

Uphoff, T. L. 1968. Subsurface stratigraphy and structure of the Mesilla and Hueco Bolsons, El Paso region, Texas and New Mexico. Master's thesis, University of Texas at El Paso.

Vanderhill, J. B. 1986. Lithostratigraphy, vertebrate paleontology, and magnetostratigraphy of Plio-Pleistocene sediments in the Mesilla Basin, New Mexico. *PhD dissertation, Austin, University of Texas*, 305 pp.

Wacker, H. 1972. The stratigraphy and structure of Cretaceous rocks in north-central Sierra de Juárez Chihuahua, México. The Universty of Texas at El Paso (UTEP). Master's Thesis: Available in http://proquest.umi.com/dissertations/Previous_ALL EPOO877.

Wells, S. G., Bullard, T. F., Condit, C. D., Jercinovic, M., Lozinsky, R. P., Rose, D. E. 1982. Geomorphic processes on the alluvial valley floor of the Rio Puerco: New Mexico *Geological Society Guidebook* 33, 45-47.

Wells, S.G., McFadden, L.D. and Harden, J. 1990. Preliminary results of age estimations and regional correlations of Quaternary alluvial fans within the Mojave Desert of Southern California, in At the End of the Mojave: Quaternary Studies in the Eastern Mojave Desert, edited by R.E. Reynolds, S.G. Wells and R.M. Brady, San Bernardino County Museum Association, Redlands, 45-53.

Wikipedia 2012. The Chamizal Case (México and United States): Dispute Origins (1848-1895); Disputes and Controversy (1895-1963); Chamizal Settlement 1963 and Resolution. Available in: http://en.wikipedia.org/wiki/Chamizal_dispute. Date: December, 2012.

Wolberg, D. 1980. Pleistocene horse skull discovered: *New Mexico Geology*, 2, 29.

Zaprowsky, B, J., F. J. Pazzaglia, and E.B. Evenson 2005. Climatic Influences on Profile Concavity and River incision, *J. Geophys. Res., 110, 1-19pp.*

Appendices

Appendices for this PhD thesis are provided in the following pages.

Important note:
Appendices are included to support Chapters 1, 3, 4, 5 and 6. There are NO appendices for Chapters 2, 7 and 8. In order to facilitate easy comparison between text and appendices, the appendices are numbered according to the chapters, so appendices 1, 3, 4, 5 and 6 support the appropriate chapter. Therefore, because there are no appendices for Chapters 2, 7 and 8, this appendix set does not contain Appendices 2, 7 and 8.

APPENDIX 1A

Figure 1A.1 Directly below this caption shows historical precipitation events that threatened Juárez city during 1827-2007 (Source: Diario de Juárez, the local newspaper (El Diario de Juarez, 2010) and microfilm documents recorded in Library of University of Texas, El Paso UTEP (2009) examined in 2009 by the author. (translation from the original spanish where appropriate).

Date	Event	Source
1827	Catastrophic flooding took everything at its pace and there only remained the Church "Mission of Nuestra Señora de Guadalupe".	El Diario de Juárez 20/12/1999
1852	Floods in Juárez city were registered in documents of the time.	El Diario de Juárez 20/12/1999
1864	Floods in Juárez city were registered in documents of the time.	El Diario de Juárez 21/12/1999
1891 August 24th and 26th	Disasters caused by precipitation such as dyke weakening and approximately 80 families were affected as a result of inundations. The Mexican Ferrocarril company is responsible for the damages caused in homes of families. Taken from historic documents CJMA roll 70 sq. 2 fs	UTEP library Microfilm sequences frames
1897	Floods in Juárez city were registered in documents of the time.	El Diario de Juárez 20/12/1999
08/1917	Floods in Juárez city were caused by the Colorado stream. The whole population had to be advised by the major Melchor Herrera in order to raise	El Diario de Juárez 20/12/1999

	barriers.	
O6/1942	Bridge connected El Paso Texas with Cordova Island was broken as a result of flooding on the Bravo River.	El Diario de Juárez 20/12/1999
10/07/1956	Heavy rainfall causes the overflowing of the Jarudo and Colorado streams. At least 20 persons died.	El Diario de Juárez 20/12/1999
2/01/1993	Landslides and floods caused by rainfall causes fear amongst the families of the zone.	El Diario de Juárez
16/08/1993	Blackouts, accidents, and floods caused by rain and, landslides. There were 18 injured.	El Diario de Juárez
4/06/1994	Reconstruction of devastated houses begins. At least 1,000 familes are in a critical situation.	El Dario de Juárez
2/07/1995	4 died and 60 houses were flooded by storm in Felipe Angeles, Anapra, and Bellavista neighbourhoods. Zaragoza river overflowed.	El Diario de Juárez
06/02/2000	Tornado left 15 deaths and destruction in the city. The worst sector was the viaduct where a bus with 30 passengers was washed into the water course.	El Diario de Juárez
06/03/2000	The drought months finished and the rain came. (Yesterday was registered the first precipitation of the summer season).	El Diario de Juárez
07/19/2002	Warning because precipitation is arriving. Rainfall inundates two collectors of the hydraulic infrastructure and also some neighbourhoods.	El Diario de Juárez
07/21/2002	Two people died as a consequence of the heavy rainfall that fell on the city.	El Diario de Juárez
07/22/2002	A body of a woman was rescued after an intense rescue operative, her body was found in one dyke of the Granjas de Chapultepec neighbourhood.	El Diario de Juárez
02/21/2003	Rainfall inundates 40 sectors of the city.	El Diario de Juárez
05/28/2004	Federal, State, and Municipal authorities alert	El Diario de

	people because a tornado is coming.	Juárez
05/28/2004	Tornado inundated the city and provoked a lot of problems to the transportation system as well as causing damage to homes of people.	El Diario de Juárez
08/13/2005	The city is under emergency (rescue units are rebased for the helping calls of people) the Bravo River and Acequia are over spilling.	El Diario de Juárez
08/13/2005	Condak's Constructor will repair damaged homes (Put in operation technical plan for Villas del Sur neighbourhood).	El Diario de Juárez
08/01/2006	Juárez authorities are asking the Mexican president about financial sources in order to protect against inundation problems.	El Diario de Juárez
08/01/2006	An inventory of 246 homes totally damaged is presented. These homes will be demolished. FONDEN (Natural disasters foundation) will evaluate the tornado disaster.	El Diario de Juárez
08/01/2006	Soil subsidence appears in all the streets, 500 families are evacuated, and water of dykes is pumped because another tornado is coming.	El Diario de Juárez
08/02/2006	Rainfall destroys everything (Municipal authorities put the orange alert that inundations will cause overspill of dykes and the Bravo River has overtopped its banks.	El Dario de Juárez
08/02/2006	Priority to keep safe the population and move families to refuges that are available. People save only essential property because water inundated their homes quickly.	El Diario de Juárez
08/02/2006	Municipal of Juárez declared orange warning; the Bravor Rver and dykes overspilled; these were hours of big concern for Juárez people.	El Diario de Juárez
08/02/2006	Precipitation covers all the Juárez region, also the Praxedis community was affected. Water	El Diario de Juárez

	destroyed 7 homes and many streets were closed.	
08/03/2006	Precipitation left damage for 500 millions of Mexican money (approximately £25,000). Municipal authorities plan to build a viaduct in the Indio stream course.	El Diario de Juárez
08/03/2006	Kindergardens are inundated in the Felipe Angels neighbourhood.	El Diario de Juárez
08/03/2006	Water, mud and tears ("no one comes to help us, we called to 060 and nothing, all our belongings are floating on the water and some were lost on the mud, we need help").	El Diario de Juárez
08/03/2006	The city left completely covered with holes and in some areas the water level raised 2 meters, also there were registered 36 accidents in 52 hours.	El Diario de Juárez
08/03/2006	The water stored in the Fronteriza dyke will be pumped and a cut will be done in the bank in order to drain it. But the water should run over a street where some neighbourhood are located.	El Diario de Juárez
08/03/2006	Talavera García remembered that since 50 years the Bravo River never rose as much as today. He told that in 1925, river rose in a way that practically covered the Cuauhtémoc sector. He comments that the river again rose on July 16th, and August 6th, 1954 but, in 1960 began to dry up. Also, Ing. Luevano, told that the Bravo river may have flowed with a volume of 450 m^3 /s similar to that recorded in 1950s.	El Diario de Juárez
08/16/2006	A tornado provoked many problems in the city (a lot of streets and intersections were closed as a consequence of heavy precipitation).	El Diario de Juárez
08/16/2006	Home developers must create adequate hydraulic infrastructure; public works caused lakes in the	El Diario de Juárez

	San Lorenzo neighbourhoods.	
08/17/2006	Precipitation affects 90% of the State; Affected people are waiting for help for several days.	El Diario de Juárez
08/17/2006	JMAS is monitoring the behaviour of the dykes during precipitation events.	El Diario de Juárez
08/17/2006	People are worried because the Bravo river level is rising (the military and more than 1000 civilians are participating in the evacuation and rescue tasks.	El Diario de Juárez
08/17/2006	Precipitation put public services in problems; A big hole appeared in the pavement of a principal avenue in Ejercito National and Technologic streets.	El Diario de Juárez
09/02/2006	The banks of the Bravo River will be reinforced in Juárez city as well in El Paso, Texas.	El Diario de Juárez
09/02/2006	194 families have been invaded by floodwaters over the bank of the Bravo river they will be relocated.	El Diario de Juárez
09/03/2006	A lot of rain fell, only minor damage, relocation of families only in high-risk cases. President advised the people.	El Diario de Juárez
09/04/2006	Precipitation affects Juárez infrastructure; (holes, inundations, homes damages and damaged cars resulted from precipitation in the city.	El Diario de Juárez
09/04/2006	Juárez, under water; the lowest maximum temperature (for this time of year) in 100 years was registered. Again the Bravo river overspilled. Soil subsidence cause failure on the concrete pavement of the Salomon street in Fronteriza neighbourhood.	El Diario de Juárez
09/05/2006	The evacuation of inundated sectors begins and 3000 telephone lines were affected.	El Diario de Juárez
09/05/2006	Schools cancel academic activities and many sectors were evacuated because heavy	El Diario de Juárez

	precipitation is falling.	
09/05/2006	8 dykes were over spilling red warning (the municipal government of Juárez city is planning to evacuate 2,000 families for their homes).	El Diario de Juárez
09/06/2006	As a result of intense precipitation the dikes: Trituradora, Los Ojitos, La Presa, Safari, and Sierra de Juarez were near to their capacity.	El Diario de Juárez
09/06/2006	Pavement collapses as a consequence of the rainfall at the intersection of Morelia and Lechuguilla streets in the Del Valle neighbourhood.	El Diario de Juárez
09/14/2006	Streets of the city are in the worst condition in their history. There are a lot of holes, fractures, and landslides for everywhere in the city.	El Diario de Juárez
09/14/2006	Fight against holes!: the city presents a catastrophic aspect as a consequence of recent precipitation.	El Diario de Juárez
09/14/2006	Alert for tornado because a lot of rain as well as hail is falling.	El Diario de Juárez
05/17/2007	573 neighbourhoods are at risk. Therefore, the emergency plan is activated.	El Dario de Juárez
05/17/2007	Ten intersections were closed as a consequence of the recent precipitations.	El Diario de Juárez

Figure 1A.1 Flooding events occurred in the study area registered in the Local Newspaper Diario de Ciudad Juárez Chihuahua, México during the period from 1827 to 2007. Including also events recorded at the UTEP El Paso Texas University. Source: (Diario de Juarez, 2010) and (UTEP, 2009)

APPENDIX 1B

NOOA (2009a) The National Weather Service Forecast Office provided monthly and yearly accumulated precipitation from El Paso, Texas during a period of 130 years (See Fig.1B.1).

Year	Jan (in)	Feb (in)	Mar (in)	Apr (in)	May (in)	Jun (in)	July (in)	Aug (in)	Sep (in)	Oct (in)	Nov (in)	Dec (in)	Total (in)
1878							1.25	2.55	0.66	1.02	0.67	0.11	
1879	1.57	0.83	0.18	0.07	T	0.08	2.47	0.35	0.04	0.95	T	0.26	6.80
1880	1.01	T	0.30	0.10	0	T	7.54	3.60	0.80	0.47	0.02	1.53	15.37
1881	0.35	0.24	0.01	0.22	1.83	0.02	8.18	3.15	1.44	1.45	0.50	0.78	18.17
1882	0.64	0.78	0.38	0	0.10	0.43	1.26	2.82	0.40	0	1.46	0	8.27
1883	0.10	0.40	2.09	0.10	0.02	0.04	2.84	1.34	2,51	2.03	0.61	0.84	12.92
1884	0.55	0.84	0.33	0.91	T	0.11	0.46	3.98	3.68	5.15	0.21	2.07	18.29
1885	0.12	0.03	0.34	0.04	1.27	2.63	1.06	0.46	0.22	0.46	0.31	0.37	7.31
1886	0.31	0.44	0.28	T	0.01	1.03	1.62	1.85	1.16	0.80	0.52	0.04	8.06
1887	0.03	0.15	0.32	0.09	0.13	0.34	0.73	1.68	0.94	0.78	0.56	1.01	6.76
1888	0.32	1.51	0.95	0.74	0.15	0.42	1.39	1.32	0.49	1.13	1.32	0.05	9.79
1889	0.76	0.18	0.67	0.04	0	0.28	1.59	0.04	2.64	0.35	0.55	0	7.10
1890	0.72	0.02	0.01	0.06	T	0.63	0.95	3.25	1.81	0.41	0.35	0.28	8.49
1891	0.27	0.09	0.16	0	0.38	0.40	0.06	0.13	0.23	T	T	0.50	2.22
1892	1.25	0.57	0.30	0.11	T	T	1.14	0.07	0.12	0.22	0.93	0.61	5.32
1893	0.02	0.52	0.31	0	2.28	T	2.02	3.15	2.08	T	0.02	0.42	10.88

1894	0.33	0.29	0.13	0.01	0.01	0.01	1.40	0.64	0.40	0.39	0	0.63	4.24
1895	0.65	0.17	0.05	T	2.11	0.21	2.48	2.01	0.28	0.88	1.05	0.31	10.20
1896	1.63	0.14	T	T	T	0.60	2.73	1.09	1.48	2.02	0.04	0.06	9.79
1897	0.54	0	0.05	0.14	0.46	2.17	2.89	2.57	2, 7	0.77	T	0.09	12.41
1898	0.25	0.04	0.43	0.81	0.01	0.46	1.46	1.00	0.50	T	0.16	1.04	6.16
1899	0.06	0.03	0.23	0.88	T	0.61	3.08	0.91	0.64	0.01	0.64	0.21	7.30
1900	0.11	0.43	0.26	0.02	0.41	0.27	2.38	0.43	2.18	1.23	0.23	T	7.95
1901	0.35	0.68	0.47	0.47	0.05	0.39	1.05	0.34	0.82	2.98	1.05	0.03	8.68
1902	0.57	0.01	0	0	T	0.01	3.27	2.85	1.86	0.31	0.49	0.78	10.15
1903	0.61	1.09	0.15	0.54	0.29	2.50	1.19	1.73	3.52	0	0	0.01	11.63
1904	T	0.01	0	0	0.06	0.54	0.59	2.24	3.50	3.51	0.01	0.84	11.30
1905	0.86	1.88	1.46	1.38	0.03	2.12	2.55	0.53	2.29	1.28	2.40	1.02	17.80
1906	0.87	1.37	0.01	0.40	0.90	T	2.02	4.10	1.18	0.44	2.50	1.20	14.99
1907	0.42	T	T	0.07	0.10	0.76	0.35	2.50	0.96	2.52	0.73	T	8.41
1908	0.10	0.26	0.35	0.88	0.01	0	2.07	2.55	T	0.12	0.45	0.15	6.94
1909	0.04	0.18	0.77	0	T	0.05	1.62	0.51	0.60	0.02	T	0.56	4.33
1910	0.21	0.10	T	T	T	1.35	0.60	1.18	0.24	0.02	0.03	0.30	4.03
1911	0.36	0.96	0.43	0.47	0.39	2.36	3.43	0.45	1.00	0.43	0.35	0.25	10.88
1912	0	0.15	0.27	0.96	T	1.27	1.11	2. 8	1.77	0.50	0.80	0.48	10.14
1913	0.49	1.26	0.29	0.14	T	0.91	1.13	0.54	0.60	T	0.97	0.76	7.09
1914	0.03	0.53	0.10	0.47	1.23	1.47	4.91	1.85	0.56	0.80	1.13	3.94	17.02
1915	1.01	0.59	1.34	0.20	T	T	2.45	1.37	2.68	0.18	0.01	0.43	10.26
1916	0.66	0.02	0.34	0.20	0.43	0	0.59	3.07	0.56	1.07	0.52	0.32	7.77
1917	0.32	T	0.07	T	0.14	0.36	0.41	4.39	0.76	T	0.04	0	6.49
1918	1.20	0.01	0.08	0	0.05	0.83	1.52	1.66	0.01	1.03	1.04	0.78	8.21
1919	0.08	0.20	0.62	0.65	0.14	0.27	1.87	0.72	3.30	0.97	0.93	0.12	9.87
1920	1.06	0.83	0.22	0.03	0.03	0.99	0.84	1.33	0.31	0.57	T	T	6.21
1921	0.06	0.26	0.04	0.01	0.31	0.79	2.13	0.35	2.49	0.11	0.22	0.15	6.92
1922	0.30	T	0.16	0.28	0.36	0.05	1.08	0.27	1.07	0.35	0.29	0.09	4.30
1923	0.64	1.41	0.33	0.04	0.01	0.09	0.20	2.96	0.41	0.58	0.53	0.93	8.13
1924	0.40	0.13	0.41	0.32	T	T	3.00	2.58	0.14	0.24	0.01	0.05	7.28
1925	0.03	0.05	T	T	0.59	0.17	1.40	2.16	1.03	0.79	0.02	0.27	6.51
1926	0.54	0.17	1.49	1.11	0.70	0.11	3.31	0.27	2.24	0.89	0.15	0.75	11.73
1927	0.05	0.18	0.28	T	0	0.10	2.52	1.34	1.04	0.02	T	0.72	6.25
1928	T	0.71	0.05	0.22	0.96	T	1.15	2.69	0.04	1.47	0.79	0.13	8.21
1929	T	0.29	0.21	T	0.51	0.54	3.01	1.18	0.12	1.60	0.33	0.50	9.29
1930	0.17	016	0.03	T	0.62	0.53	1.33	1.29	0.04	0.75	0.74	0.43	6.09
1931	0.83	0.89	0.38	2.24	0.06	1.34	0.73	2.14	1.10	0.14	0.64	0.30	10.79
1932	0.17	0.68	0.03	T	1.46	0.15	2.28	2.14	2.85	0.53	0	0.65	10.94

1933	0.19	0.23	T	0.09	0.04	2.14	1.34	0.27	0.99	0.60	0.04	0	5.93
1934	0.01	0.12	0.24	0.05	0.37	0.01	0.19	0.60	0.17	0.44	0.21	0.32	2.73
1935	0.24	0.47	0.14	0.02	0.17	0.09	0.16	1.72	1.24	0.14	0.92	0.34	5.65
1936	0.57	0.06	T	0.11	0.56	0.34	0.68	1.94	3.52	0.32	1.32	0.51	9.93
1937	0.12	0.32	0.48	T	0.19	1.05	0.39	0.56	0.48	1.71	0.22	0.91	6.23
1938	1.22	0.17	0.49	T	0.02	2.82	0.60	0.20	2.31	0.19	T	0.28	8.30
1939	0.65	0.08	0.44	0.45	0.01	T	0.60	0.91	0.90	0.93	0.75	0.19	5.91
1940	0.54	0.41	0.02	0.02	0.43	1.87	1.06	0.78	0.25	0.82	1.25	0.31	7.76
1941	0.46	0.46	1.63	1.49	1.23	0.18	1.40	2.13	4.19	1.65	0.48	0.35	15.65
1942	0.14	0.73	0.02	1.04	T	0.52	0.68	3.82	1.03	1.53	0	1.26	10.75
1943	0.25	0	0.07	T	T	1.63	0.92	0.44	1.36	T	1.53	0.82	7.02
1944	0.45	1.42	0.15	T	0.39	1.67	1.52	1.04	0.25	1.30	0.41	0.48	9.08
1945	0.11	0.17	0.64	T	T	0.03	0.47	0.84	0.12	4.31	0	0.05	6.74
1946	1.23	T	0.04	0.36	1.23	0.20	0.71	1.19	1.51	0.41	0.03	1.31	8.22
1947	0.87	T	0.66	0.06	0.68	0.53	0.97	1.63	0.02	0.35	0.53	0.82	7.12
1948	0.25	0.63	0.04	0.11	T	0.96	0.82	1.82	0.03	0.18	T	0.86	5.70
1949	1.84	0.22	0.04	0.05	0.39	0.51	1.18	0.43	1.74	1.50	T	0.86	8.76
1950	0.29	0.26	T	T	0.10	0.11	3.57	0.16	1.32	0.94	0	0	6.75
1951	0.33	0.63	0.59	0.45	T	T	2.48	0.72	0.04	0.43	0.12	0.68	6.47
1952	0.02	0.96	0.92	1.08	0.46	1.14	1.88	1.06	0.07	0	0.23	0.15	7.97
1953	0	0.34	0.12	0.71	0.27	0.53	0.99	0.42	T	0.65	T	0.39	4.42
1954	0.10	T	0.09	0.19	1.26	0.23	0.88	2.37	0.95	0.20	0	0.02	6.39
1955	0.59	0.05	0.18	0	0.26	0.18	3.70	0.70	0.16	0.73	0.15	0	6.70
1956	0.35	1.06	T	0.05	T	1.19	1.10	0.61	0.43	0.01	T	0.04	5.44
1957	0.24	0.46	0.33	0.09	0.10	0.02	2.64	4.11	0.11	2.34	0.74	0.02	11.20
1958	0.74	1.11	2.26	0.05	0.40	1.66	1.36	1.14	6.29	1.98	0.20	T	17.19
1959	0.21	T	0.07	0.15	0.30	0.46	0.40	2.39	T	0.58	0.14	0.29	4.99
1960	0.72	0.37	0.21	0.02	0.04	0.76	3.61	0.77	0.01	0.77	0.11	1.73	9.12
1961	0.41	T	0.29	0.01	T	0.27	2.18	1.40	0.69	0.18	1.63	0.63	7.69
1962	0.94	0.58	0.24	0.10	0	T	1.82	T	3.54	0.55	0.21	0.30	8.28
1963	0.13	0.53	T	T	0.71	0.05	0.52	1.03	0.64	0.55	0.76	T	4.92
1964	T	T	0.99	0.08	0.02	T	0.18	0.76	2.40	0.40	0	0.52	5.35
1965	0.19	0.59	0.03	0.01	0.11	0.66	0.17	0.49	2.12	0.18	0.12	0.74	5.41
1966	0.38	0.20	T	1.08	0.04	2.67	1.17	1.85	1.79	0.01	0.01	0.04	9.24
1967	0	0.04	0.17	0.03	0.05	1.41	0. 8	0.54	1.54	0.09	0.23	0.78	5.72
1968	0.47	1.11	0.85	0.10	T	0.03	5.53	1.71	0.53	0.11	1.35	0.23	12.02
1969	0.05	0.08	0.17	T	0.28	T	1.14	0.28	0.43	0.59	0.63	0.69	4.34
1970	0.03	0.55	0.47	T	0.71	0.73	1.41	0.41	1.01	0.68	T	0.06	6.06
1971	0.17	0.04	0	0.42	T	0.01	2.34	1.59	0.96	1.07	0.14	0.50	7.24

1972	0.44	T	T	0	0.04	1.62	0.71	2.59	1.60	1.25	0.33	0.42	9.00
1973	1.23	1.69	0.60	0	0.29	0.71	2.12	0.73	0.01	0.07	0.08	T	7.53
1974	0.27	T	0.36	0.12	0.05	0.36	2, 2	0.63	6.68	1.90	0.50	0.87	13.95
1975	0.70	0.59	0.19	T	0.03	T	1.11	0.45	2.18	0.25	T	0.71	6.21
1976	0.26	0.52	T	0.30	0.74	0.50	3.17	0.23	1.70	1.20	1.20	0.32	10.14
1977	057	T	0.17	0.09	0.06	0.04	1.09	1.36	0.16	1.65	0.05	0.26	5.50
1978	0.44	0.47	0.07	0	0.57	1.46	0.04	2.18	4.14	2.28	0.45	0.47	12.57
1979	0.77	0.68	T	0.28	0.24	0.03	0.98	2.16	0.41	T	0.04	0.25	5.84
1980	0.54	0.73	0.25	0.31	0.08	T	0.21	1.76	1.90	0.95	0.54	0.04	7.31
1981	1, 1	0.36	0.39	0.65	0.72	0.64	2.08	5.26	0.52	0.53	0.30	0.08	12.63
1982	0.34	0.55	T	0.05	0.19	0.18	1.00	0.48	5.28	T	0.29	2.61	10.97
1983	0.35	0.60	0.45	1.42	0.05	0.23	0.43	0.97	1.51	1.48	0.34	0.16	7.99
1984	0.31	0	0.44	0.01	0.59	3.18	0.69	5.57	0.58	3.12	0.51	1.17	16.17
1985	0.95	0.19	0.59	0.07	0.01	0.10	1.32	1.46	1.47	1.82	0.13	0.05	8.16
1986	0.01	0.39	0.39	T	0.83	3.05	2.66	0.70	0.85	0.45	1.42	1.42	12.17
1987	0.29	0.30	0.49	0.32	0.24	2.24	0.64	2.22	0.89	0.15	0.29	2.87	10.94
1988	0.25	0.70	0.10	0.23	0.15	0.03	3.35	3.46	1.52	0.59	0.24	0.44	11.06
1989	0.11	0.72	0.62	T	0.65	T	1.23	3.06	0.48	0.23	T	0.16	7.26
1990	0.29	0.14	0.41	0.25	0.10	T	3.96	1.98	3.46	0.58	1.34	0.34	12.85
1991	0.82	0.66	0.10	T	0.23	0.01	2.69	2.06	1.82	0.20	0.50	3.29	12.38
1992	1.14	0.16	0.50	0.30	4.22	0.27	0.65	2.11	0.15	0.27	0.28	1.35	11.40
1993	1.34	0.32	0.01	0.12	T	1.47	0.95	2.73	1.32	0.17	0.49	0.71	9.63
1994	0.03	0.23	0.37	0.65	0.80	0.67	0.18	0.02	0.03	0.35	0.54	1.61	5.48
1995	0.26	0.88	0.42	0.04	0.01	1.74	0.28	0.76	3.18	T	0.26	0.23	8.06
1996	0.11	0.19	T	0.49	0	2.36	2.48	1.55	1.24	T	0.16	0	8.58
1997	0.38	0.29	0.64	0.43	0.52	1.11	0.91	1.41	1.55	0.19	0.79	1.14	9.36
1998	0.05	0.15	0.18	0.04	T	0.27	2.07	0.53	0.66	2.14	0.34	0.34	6.77
1999	0.10	0	0.04	T	0.02	1.44	2.00	1.43	1.94	0.56	0	0.63	8.16
2000	0	0.03	0.06	0.28	T	2.45	1.59	0.70	T	0.82	1.06	0.42	7.41
2001	0.06	0.24	0.40	T	0.18	0.30	0.36	1.72	0.30	T	0.60	0.13	4.29
2002	T	1.22	0	0	T	0.35	1.34	0.76	0.48	1.09	T	1.65	6.89
2003	T	1.37	0.18	0.02	T	0.49	0.55	0.66	0.08	0.33	0.52	0.01	4.21
2004	0.37	0.05	0.80	1.06	0.50	0.93	1.70	3.04	0.89	0.39	2.01	0.36	12.10
2005	0.55	1.92	0.08	0.14	0.93	T	0.66	4.35	2.77	1.36	0	T	13.60
2006	0.02	0.28	T	0.01	0.89	0.27	3.17	6.85	4.99	0.92	0.06	0.05	17.51
2007	1.81	0.19	0.02	0.31	1.30	0.51	2.08	0.57	1.71	0.09	1.07	0.46	10.14
2008	0.15	0.16	T	T	0.03	0.48	4.34	2.61	1.52	0.15	0.17	0.27	9.88
MA[1]	0.45	0.46	0.36	0.31	0.44	0.77	1.66	1.61	1.36	0.85	0.50	0.58	8.77
MM[2]	1.84	1.92	2.26	2.24	4.22	3.18	8.18	6.85	6.68	5.15	2.50	3.94	18.29

Mm^3	0	0	0	0	0	0	0.04	T	T	0	0	0	2.22

Figure 1B.2 Precipitation at El Paso and Percent of Normal during Category 3 and 4 ENSO Events. Source: Reynolds (1997)

Onset Year	Category	Autumn Precipitation (in.)	Percent of Normal	Following Spring Precipitation (in.)	Percent of Normal
1899	4	1.29	50	.69	78
1900	3	3.64	142	.99	113
1902	3	2.66	104	.98	111
1905	3	5.97	233	1.31	149
1911	4	1.78	70	1.23	140
1912	3	3.07	120	.43	49
1914	3	5.56	217	1.36	155
1918	4	2.08	81	1.32	150
1919	3	5.20	203	.39	44
1925	4	1.84	72	3.30	375
1926	4	3.46	135	.28	32
1929	3	2.05	80	.65	74
1930	3	1.53	60	2.68	305
1939	3	2.58	101	.47	53
1941	4	6.32	247	1.06	120
1953	3	.65	25	1.54	175
1957	4	3.19	125	2.71	308
1958	4	8.47	331	.52	59
1965	3	2.42	95	1.12	127
1972	4	3.18	124	.89	101
1973	4	.16	6	.53	60
1976	3	4.10	160	.23	26
1982	4	5.57	218	1.92	218
1983	4	3.33	130	1.04	118
Average		3.21	130	1.15	130

Figure 1B.1 Monthly and Yearly maximum accumulated precipitation from El Paso Texas area during the period 1878-2008. Source: NOAA (2009a)

*1 Monthly Average; *2 Monthly maximum; *3 Monthly minimum

Figure 1B.3 Seasonal Precipitation (in.) for Category 3 and 4 ENSO Events from Autumn of Onset Year to Following Autumn. Source: Reynolds (1997)					
Onset Year	Sept-Nov	Dec-Feb	Mar-May	June-Aug	Sept-Nov
1899	1.29	.75	.69	3.08	3.64
1900	3.64	1.03	.99	1.78	4.85
1902	2.66	2.48	.98	5.42	3.52
1905	5.97	3.26	1.31	6.12	4.12
1911	1.78	.40	1.23	5.21	3.07
1912	3.07	2.23	.43	2.58	1.03
1914	5.56	5.54	1.36	3.82	2.87
1918	2.08	.88	1.32	2.86	5.20
1919	5.20	2.01	.39	3.16	.88
1925	1.84	.98	3.30	3.69	3.28
1926	3.46	.98	.28	7.65	1.06
1929	2.05	.83	.65	3.15	1.53
1930	1.53	2.15	2.68	4.21	1.88
1939	2.58	1.14	.47	3.71	2.32
1941	6.32	1.21	1.06	5.02	2.56
1953	.65	.49	1.54	3.48	.98
1957	3.19	1.87	2.71	4.16	8.47
1958	8.47	.21	.52	3.25	.72
1965	2.42	1.14	1.12	5.69	1.81
1972	3.18	3.34	.89	3.56	.16
1973	.16	.27	.53	3.20	9.08
1976	4.10	.89	.23	2.49	1.86
1982	5.57	3.56	1.92	1.63	3.33
1983	3.33	.47	1.04	9.44	4.21
Seasonal Averages 1899-1984	2.56	1.34	.88	3.63	2.56

Figure 1B.4 Autumn, Winter and Spring Season Precipitation (in.) and Percent of Normal During La Niña Events. Source: Reynolds (1997)

Onset Year	Autumn Precip	Percent of Normal	Winter Precip	Percent of Normal	Spring Precip	Percent of Normal
1886	2.48	99	0.22	16	0.54	61
1889	3.54	141	0.74	55	0.07	8
1892	1.27	51	1.15	86	2.59	294
1893	2.10	84	1.04	78	0.15	17
1903	3.52	140	0.02	1	0.06	7
1906	1.18	47	1.62	121	0.17	19
1908	0.57	23	0.35	26	0.77	88
1909	0.62	25	0.78	58	0.00	0
1910	0.29	12	1.62	12	1.29	147
1916	2.14	85	0.64	48	0.21	24
1922	1.71	68	2.14	160	0.38	43
1924	0.39	16	0.13	10	0.59	67
1938	2.50	100	1.01	75	0.90	102
1942	2.56	102	1.51	113	0.07	8
1944	1.96	78	0.76	56	0.64	73
1949	3.24	129	1.41	105	0.10	11
1954	1.25	50	0.66	49	0.44	50
1955	1.04	41	1.41	105	0.05	6
1956	0.44	18	1.34	100	0.52	59
1964	2.80	112	1.30	97	0.15	17
1967	1.86	74	2.36	176	0.95	108
1970	1.69	67	0.27	20	0.42	48
1971	2.17	86	0.94	70	0.04	5
1973	0.16	6	0.27	20	0.53	60
1975	2.43	97	1.49	111	1.04	118
1988	2.35	94	1.27	95	1.27	144
Average	1.78	71	0.87	76	0.54	61

APPENDIX 1C

Mesilla Basin located northwest of the study area has suffered three major events of Bravo River shifts occurred in different parts as:: (1) between I844 and 1852 in the north-central part of the basin, (2) in 1865 in the northern part of the basin, and (3) between 1903 and 19I2 in the southern part of the basin (See Figs. 1C.1 to 1C.3). The historical Bravo River is unique among other rivers described in the literature due to its frequent channel migration. Presented here is the history of channel course changes of the Rio Grande. The historical Rio Grande was a pebbly sand bedload stream, occupying nearly (58 km) floodplain incised about 100 m into Pliocene and early Pleistocene alluvium. Just before to completion of Elephant Butte Dam in 1916, the river experienced late spring floods due to snowmelt near its headwaters (Mack et al., 1998)..

Large scale migration of the Bravo River channel in the order of 17 to 30 km have occurred as in 1865 when this River had a sinuosity of (1.9 to 1.2) and a variable floodplain between (1300- 100 m) all in one flood season. The lateral movement of structures such as: both straight and sinuous stretches, neck cutoff of meander loops, were common processes. These three processes as: meander cutoff, lateral erosion, and avulsion are, the best examples of these processes are highlighted with reference to specific numbered sites on (Figs. 1C1, 1C2 and 1C3). In most cases, the timing of the process can only be bracketed by the dates of the channel surveys. "Neck and chute cutoffs of meander loops are common processes of channel straightening by sinuous rivers". We use neck cutoff as a general term for cutoff involving the transformation of a single strongly curved reach into a single reasonably straight reach. Chute cutoff, in contrast, involves partial cutoff of a meander loop forming a new, but still curved reach. Despite the fact that the historical Rio Grande in the Mesilla Valley was only of moderate sinuosity (< 2), there are several obvious examples of neck cutoff. In the narrow, northern part of the Mesilla Valley, eastward growth of the northernmost meander loop is apparent by comparing the 1903 and 1907 positions of the river (site 1, Fig. 1C2). This broad meander loop experienced a neck cutoff in or just prior to 1912 (Mack et al., 1998).. Bracketed between 1891 and 1912 was downstream migration, clockwise rotation, and eventual neck cutoff of the meander loop at site 2 (Fig. 1C2). In addition, a neck cutoff straightened the chevron-shaped meander of the 1903

channel at site 3 in or prior to 1912, although the timing of this event is not as well constrained as the previous examples, because the 1907 river survey did not extend this far south. There are few well documented meander cutoffs in the main part of the Mesilla Valley, where instead the dominant processes appear to have been lateral erosion and avulsion (Fig. 1C2). One possible example involves the large loop in the 1852 channel near Dona Ana (site 1, Fig. 1C2), which underwent a neck cutoff in or prior to 1893. Two other examples of neck cutoff are evident near Berino (sites 2 and 3, Fig. 1C2). At these locations a progression of change in sinuosity is apparent, from a relatively straight 1893 ***G.H. Mack, M.R. Leeder/Sedimentary Geology 117 (1998) 207-219*** channel, to a substantial increase in sinuosity by 1903, to a return to a straighter channel by 1912 as a result of neck cutoff of the two prominent meander loops. The cutoff at site 3 apparently occurred in the spring of 1906, and was reported by the *El Paso Times* on June 2 of that year:

The Rio Grande has deepened its channel considerably at Berino and in consequence the high water this spring is not near as destructive as it has been in former years. This deepening has been caused by the river cutting across the Morely bend, thus straightening and at the same time shortening its course three miles.

5.2. *Lateral erosion* Lateral, non-avulsive movement of the historical Rio Grande across its floodplain was a common process and was accomplished in two ways: by migration of meander belts and by shifting of relatively straight stretches of the river. An example of the former occurred in the vicinity of Mesilla between 1844 and 1852 (between sites 4 and 5, Fig. 1C2). Here there was a 1 to 2 km westward shift of the meander belt with a minor decrease in channel sinuosity. Many of the meander loops remained in phase, although two loops northwest of Las Cruces became out of phase. Examples of lateral erosion and subsequent course change of low sinuosity stretches of the river are illustrated by the 1893, 1903, and 1912 positions of the channel between Dona Ana and La Mesa (Fig. 1C2). During this time interval the channel locally shifted back and forth by less than a kilometre, although in most stretches there was negligible change in river position and the channel positions are superimposed. It is noteworthy that the 1903 channel in this stretch was relatively straight, but became significantly more sinuous from La Mesa to the southern end of the Mesilla Valley (Fig. 1C2).

The best documented case of lateral channel erosion is shown by the change from the 1852 to the 1889 position of the river in the Hueco basin (Fig. 4). This event received special attention, because the Rio Grande constitutes the international boundary between

Mexico and the United States (Mack et al., 1998). this event, the river migrated south-southeastward as much as a kilometre, leaving in its wake an area of land of disputed ownership called 'El Chamizal' (Fig. 1C3). In accordance with existing treaties between the two countries, El Chamizal would remain part of Mexico if the river had avulsed from its 1852 to its 1889 position, but would belong to the United States if the river had moved by lateral erosion. Accounts by the inhabitants of both El Paso and Ciudad Juarez indicated that virtually all of the channel migration had occurred during spring floods from 1864 to 1868 (Mack et al., 1998). Bank erosion had taken place at a rate of up to 100 m per day, and forests were destroyed before they could be cut down and manmade structures were washed away before they could be moved (Mack et al., 1998). The best documented avulsion of the historical Rio Grande in the Mesilla Valley accounts for the difference in position of the 1852 and 1893 channels near Mesilla (Fig. 1C2) (Mack et al., 1998). . This avulsion took place in the spring of 1865, relocating the river from a few hundred metres east of Mesilla to a position along the western edge of the floodplain as much as 4 km from the town, where it has since remained. The exact node of the avulsion is not documented, but based on the map patterns was probably between Dona Ana and Las Cruces. The avulsed river cut across its former channel about 8 km south of Mesilla, but notably did not rejoin it. Instead the river flowed down the middle of the valley, taking up the course of the 1844 channel 5 km below where it crossed the 1852 channel. Because the 1852 channel was not mapped for more than a few kilometres south of La Mesa, it is not known where, if at all, the post-avulsion channel reoccupied the pre-avulsion channel, although the two channels appear to be converging at their southern immediately below the presumed avulsion node, and ends near La Mesa (Fig. 1C2). Eyewitness accounts by by the magnitude of the shift, as much as 4 km, comlocal residents indicated that this avulsion took place pared to other examples of lateral erosion. However, in one spring flood cycle: no written account of this event has been found. In the spring rise of 1865, the volume of water was so enormous that it took everything before it, and made a mad dash down the valley along the hills on the west -a short cut, which left the town of La Mesilla high and dry upon the opposite bank about a mile away. The valley is described as one vast sheet of water from edge of Las Cruces to the hills on the west, with the site of La Mesilla a strip of island (Mack et al., 1998).

6. **Discussion**

There are several aspects of the record of channel behaviour of the historical Rio Grande in the Mesilla and upper Hueco basins that are pertinent to alluvial sedimentology and stratigraphy. Avulsion occurred in the southern part of the Mesilla Valley between 1903 and 1912 (site 6, Fig. 1C2). Prior to this avulsion, the river was relatively narrow and sinuous, and flowed down the western edge of the floodplain. The avulsion shifted the river to the opposite edge of the floodplain and resulted in a straighter, broader channel. Approximately 20 km from the avulsion node, the post-avulsion channel re-occupied, at least locally, the pre-avulsion channel. The exact time of this avulsion is not known, but may have happened in the spring of 1905, when severe floods affected the southern Mesilla Valley. The river was reported to have broken through its banks at several locations *(Rio Grande Republican,* May 5, *1905; El Paso Times,* May *9* and May 30, 1905), and the town of La Mesa was inundated by 3 m of water (El *Paso Times,* June 3, 1905).

The historical Rio Grande displays a wide range of channel widths and sinuosities. We have no evidence for tectonics or climate change being the cause of variability in channel width and sinuosity, suggesting that the changes in channel character may reflect intrinsic factors, such as lateral variations in vegetation or in gradient resulting from local sedimentation or erosion. These data point to the possibility that in the rock record fluvial channel sand bodies of markedly different architecture may be stratigraphically juxtaposed without the influence of major changes in externally forced variables.

An avulsion on a smaller scale than those previously described occurred in the narrow, upper reach of the Mesilla Valley between 1892 and 1903 (site 4, Fig. 1C1). At this location three meander loops over a 4 km stretch of the 189l/92 river were abandoned in or prior to 1903. The river apparently reoccupied the meander loop of the 189l/92 river near site 2 of Fig. 1C1. Finally, an avulsion may have been responsible for the change in channel position between 1844 and 1852 below site 5 (Fig. IC.2). As discussed above, the 1852 channel belt overlapped the 1844 channel belt upstream of site 5, below which the 1852 channel shifted to the western edge of the valley, where it re-occupied the meander belt that existed prior to 1844. Although this shift may have resulted from lateral erosion, avulsion is favoured by the abruptness of the shift, by the straightness of the 1852 channel Avulsion of the Rio Grande was rapid, occurring in one flood season (a few months or less) or, at the longest, a few years. A distinctly different avulsion related package of sediment may be deposited within a semi-arid floodplain with low water table where avulsions are rapid, as was the case for the historical Rio Grande. Eyewitness accounts of Rio Grande

avulsions, particularly the 1865 event, suggest the most that might be preserved of an avulsive event In the adjacent floodplain is a thin sheet of overbank sand deposited from valley-wide flooding.

The length scale of avulsion, defined as the distance from the avulsion node to where the river reoccupies the original channel belt, is also important in alluvial stratigraphy. For the historical Rio Grande this value is 20 km for the avulsion between 1903 and 1912 in the southern Mesilla Valley, and, although not directly measurable, is estimated to be 17 km for the avulsion between 1844 and 1852 in central Mesilla Valley, and 30 km for the 1865 avulsion near Mesilla. Should avulsions occur on anything like this frequency over stratigraphically significant time scales in other rivers of Rio Grande type, then we would expect the entire floodplain to be dominated by successive channel belt deposits. In the absence of detailed subsurface data we can at present only speculate on such a possibility. However, such conditions are predicted in numerical models of half grabens in the Rio Grande system (Leeder et al., 1996a), and multistory channel sands largely devoid of overbank deposits have been observed in Plio-Pleistocene sediment deposited by the ancestral Rio Grande in the Palomas and northern Mesilla half grabens (Mack and Seager, 1990; Mack and James, 1993).

Figure 1C.1 Rio Grande migration during the period 1852 and 1889 where shows the Cordoba and Chamizal islands produced by lateral erosion. A) Is the Topo map showing location of B) Chamizal and Cordova islands in red dashed circle lines and arrow red Source: Topo-maps ESRI (2011) and (Mack and Leeder, 1998)

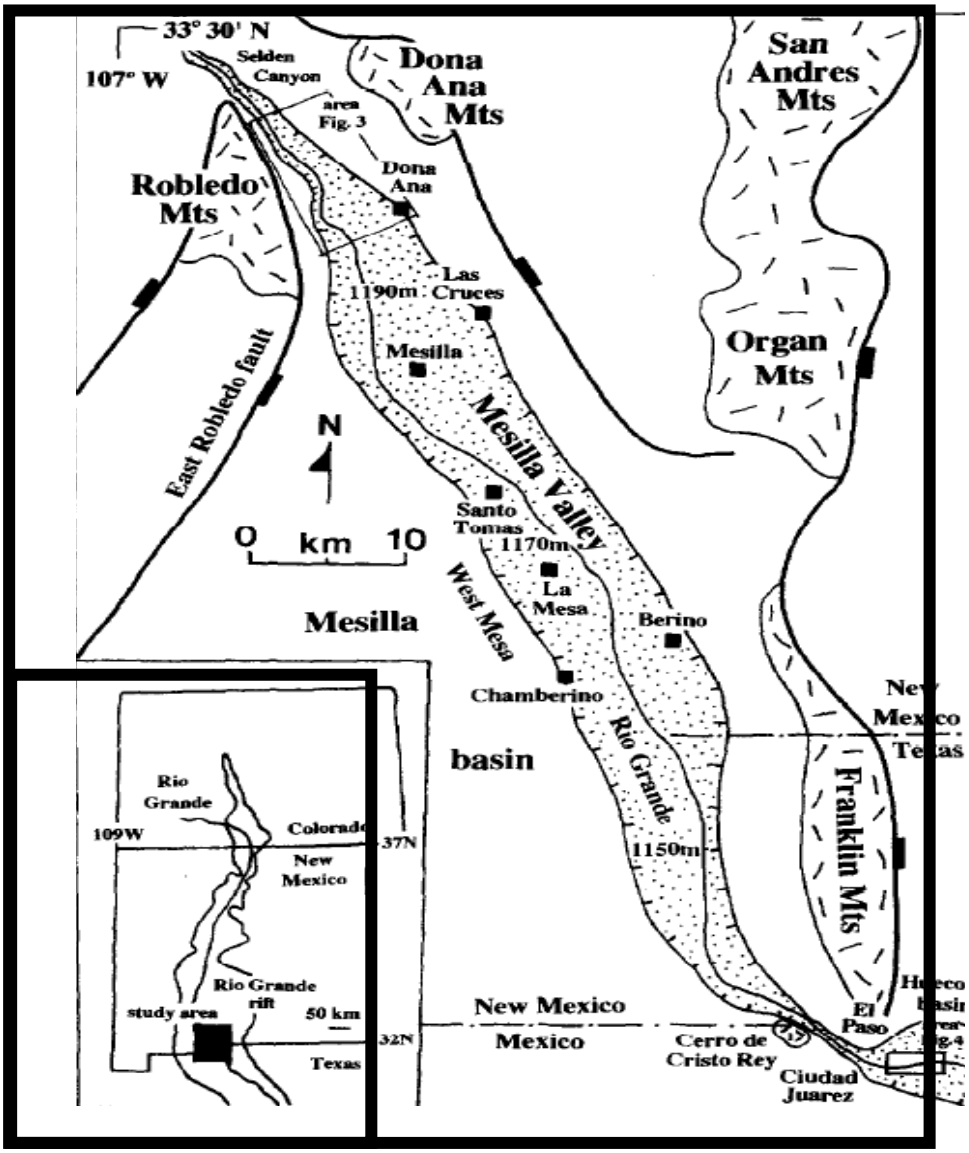

Fig.1C1. Index map of the Mesilla and northern Hueco basins in the southern Rio Grande rift of New Mexico and west Texas. Selected floodplain elevations (1190, 1170, 1150) are in meters above sea level. Source: (Mack and Leeder, 1998)

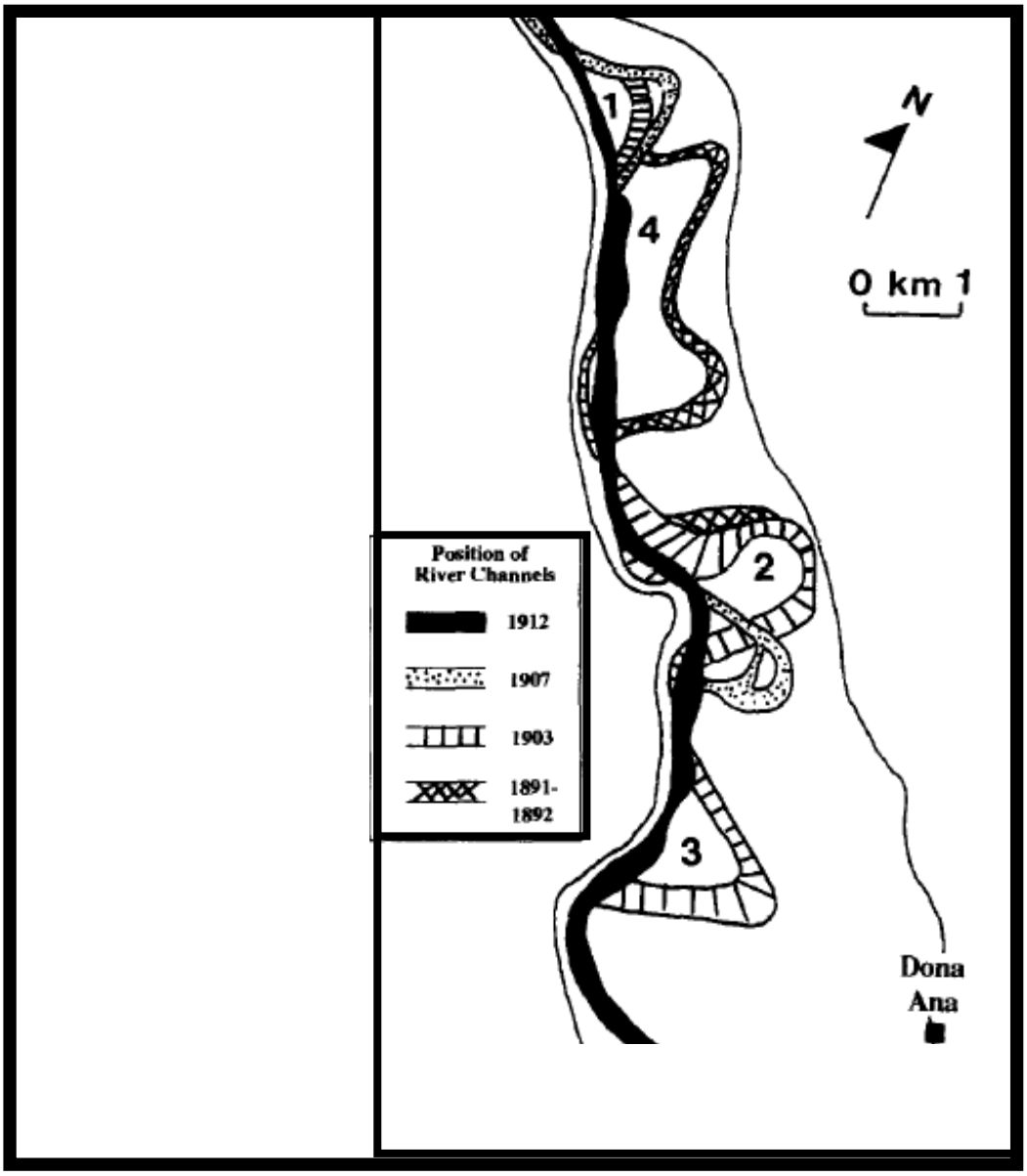

Fig.1C2. Positions of the Rio Grande channel in the northern part of the Mesilla Valley from 1891/92 to 1912. Numbers refer to specific locations discussed in the text. (Source: Mack and Leeder, 1998)

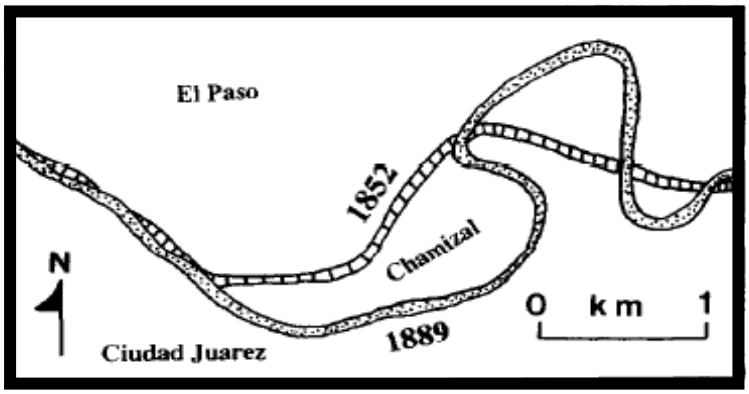

Fig. 1C3 Position of the Rio Grande in the northwestern Hueco basin in 1852 and 1889, taken from Muller (1975) in Mack et al., 1998

APPENDIX 3A

***Data sets of topography and urbanized area of the Juárez city*.**

Contour levels every 5 m (See Fig. 1); Topographic chart (See Fig. 2A); Aerial photo (See Fig. 2B); Digital Elevation Model in raster grid format (See Fig. 2C) and Finally satellite Images based on Quick Bird format (See Fig. 2D) were provided by (IMIP 2007) and constitute the support of tasks mentioned in methods chapter 3. This dataset contain fundamental information of the city such as: Different districts; Main, secondary and local streets; Urban layout of Juárez city; Location of industries as well different land uses of the city.

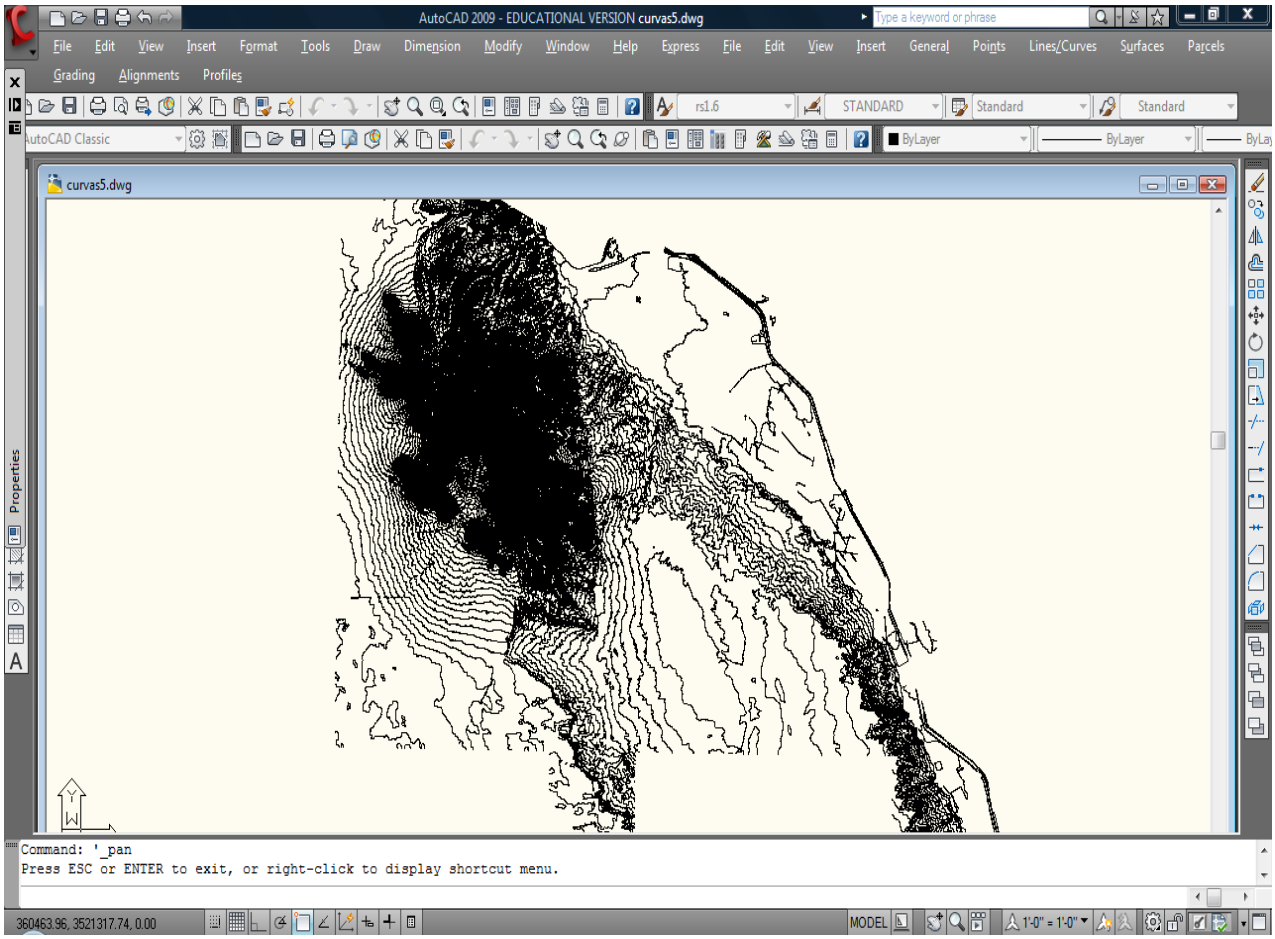

Figure 1 Contour levels dataset every 5 m. of the study area. Source: (IMIP 2007)

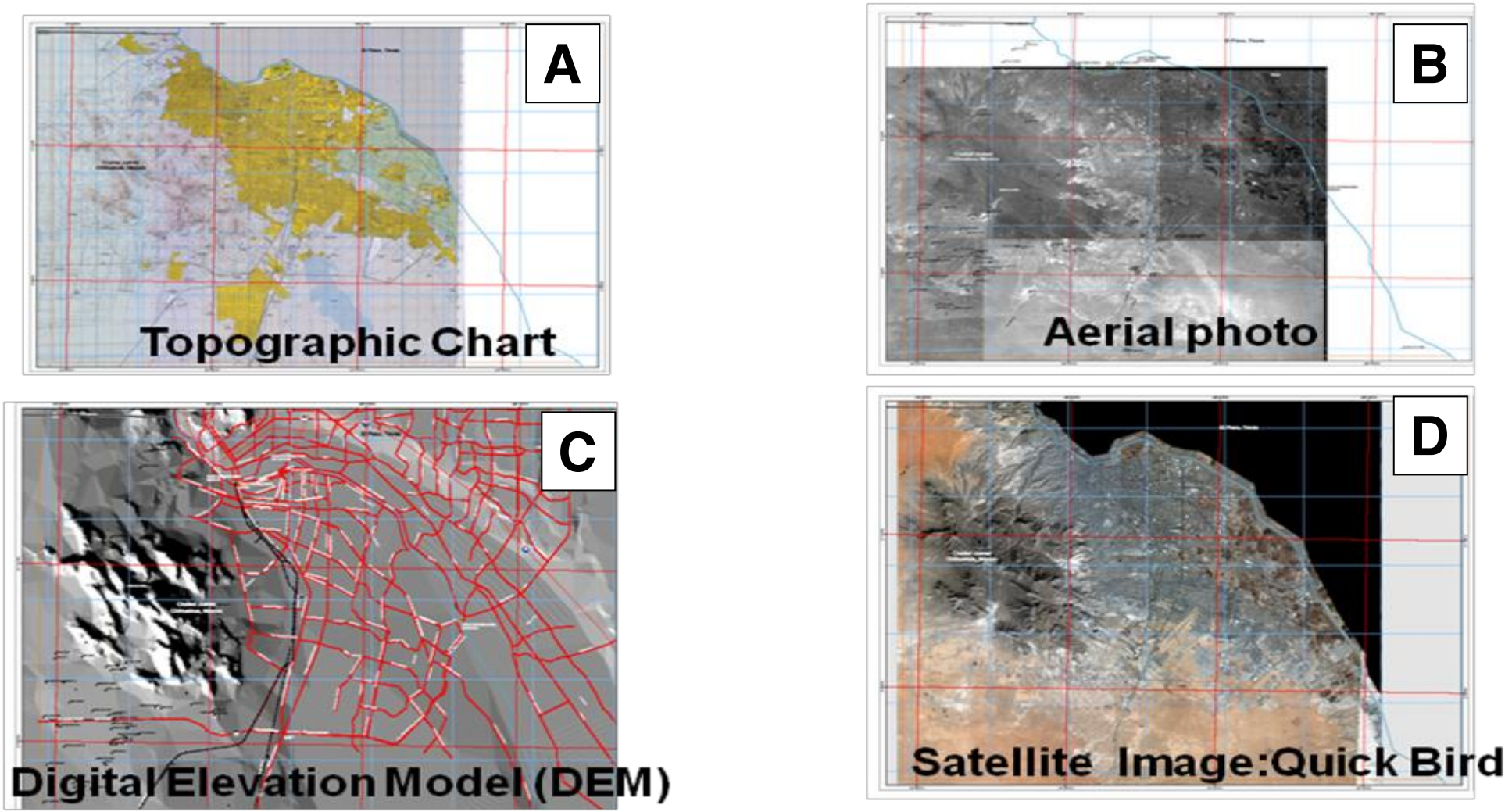

Figure 2 Topographic chart; B) Aerial photo; C) Digital Elevation Model; D) Satellite Images of the study area. Source: (IMIP 2007)

APPENDIX 3B

Creating a digital elevation model

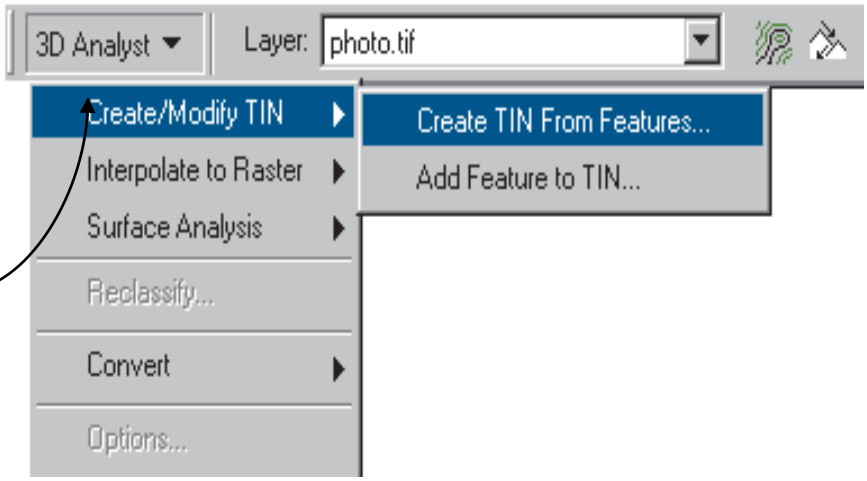

Step 1) Figure 1 Select 3D analyst and Create/Modify TIN. After that, Create TIN from features. Source: (Arc-Map 9.2, 2009)

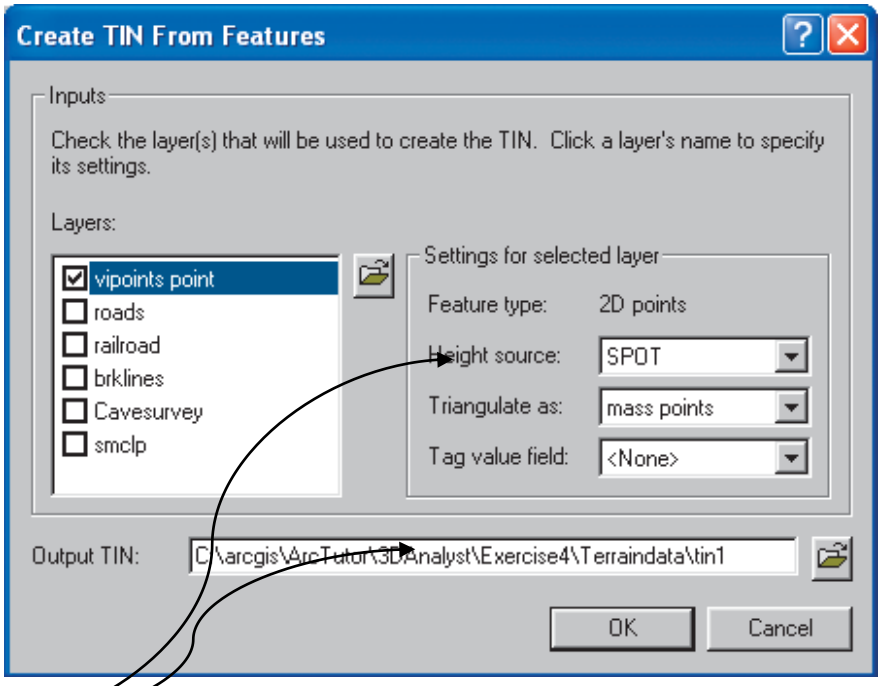

Step 2) Figure 2 Introduce the DEM (dxf Auto-Cad file) into Arc-Map program and give the output desired directory to save it. Source: (Arc-Map 9.2, 2009)

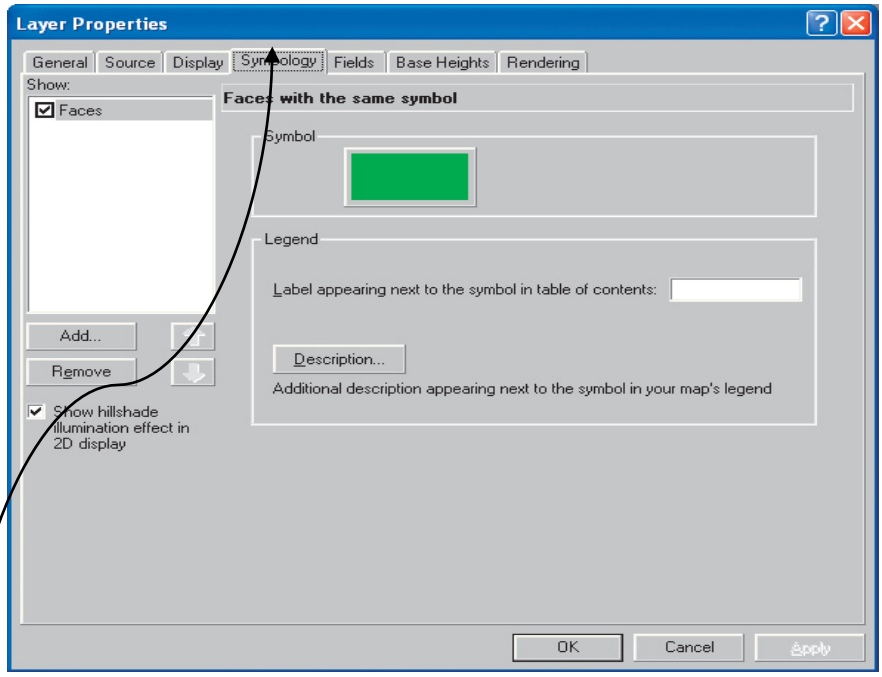

Step 3) Figure 3 Select DEM and single colour: Source: (Arc-Map 9.2, 2009)

Therefore, to complete the DEM, two more steps are needed. First, rendering tab (Fig. 4) of the properties command within the TIN feature click and a graduated color for different elevation level would performed (Fig. 5).

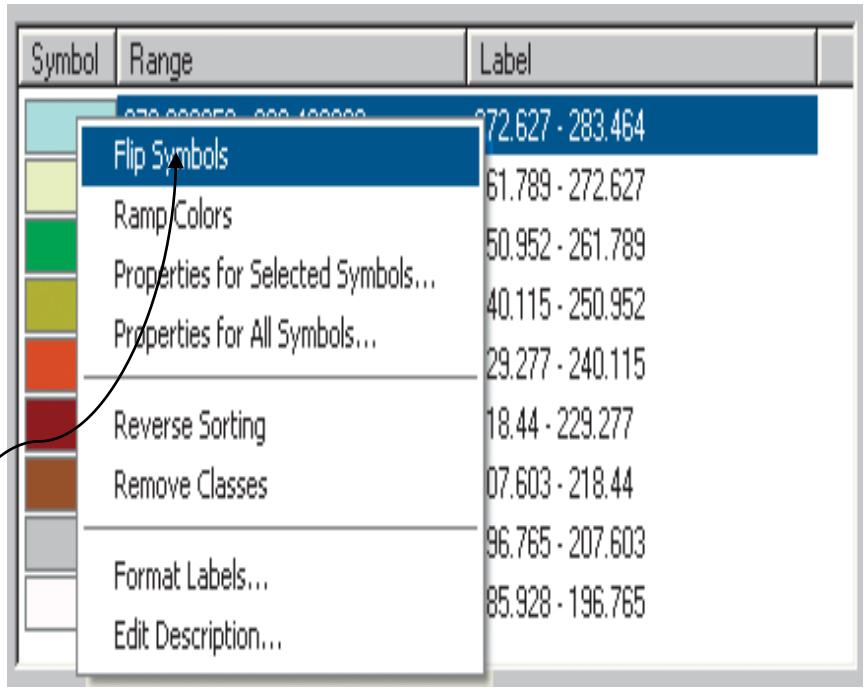

Step 4) Fig. 4 shows the DEM graduated colour for changes in elevation. Source: (Arc-Map 9.2, 2009)

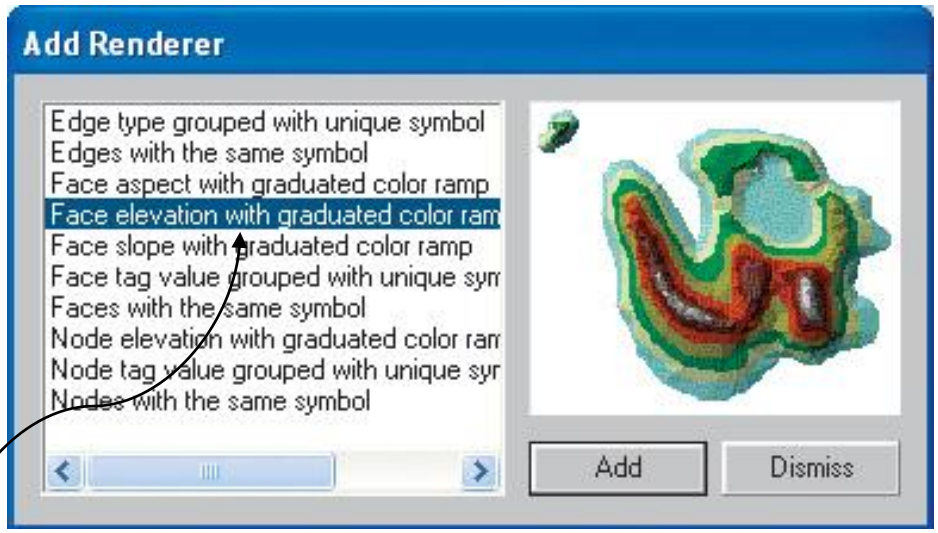

Step 5) Fig. 5 Finally the Output Digital Elevation Model is performed Source: (Arc-Map 9.2, 2009)

APPENDIX 3C

Creating a terrain profile.

This task is useful to address cross geological sections. Once activated the TIN feature or DEM, the following steps are needed and would illustrated through the steps 1 to 10 also indicated on Figs. 1 to 10.

Step1) Figure 1 Click the launch Arc-Map program and select a new empty map and the program shows a window as: (See Figure 2). Source: (Arc-Map 9.2, 2009)

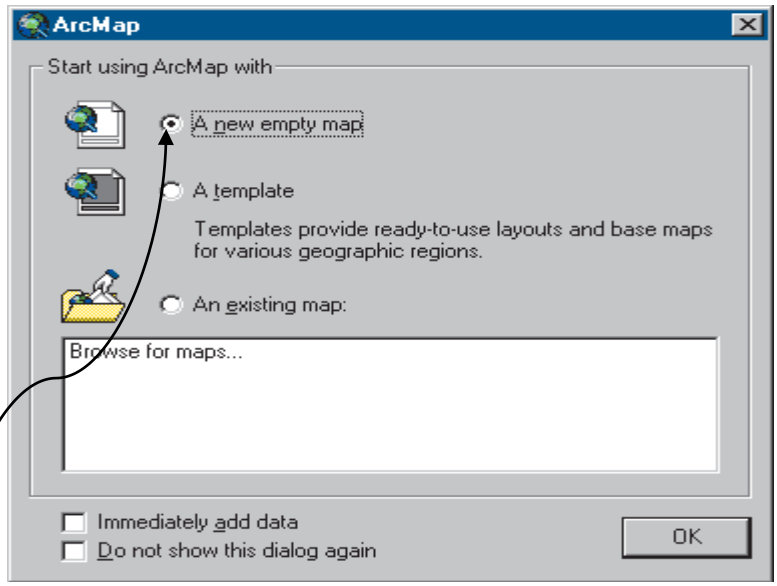

Step 2) Figure 2 Click a new empty map. Source: (Arc-Map 9.2, 2009) after that select the file and directory that contain your dataset (See Figure 3).

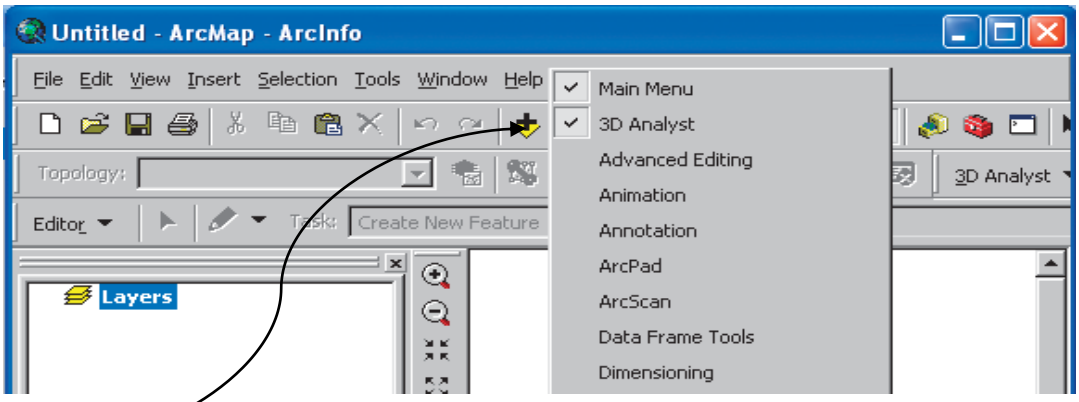

Step 3) Figure 3 From the menu select the module that contains the three dimension analysis. Click 3D analyst (Arc-Map 9.2, 2009) (See Fig. 4).

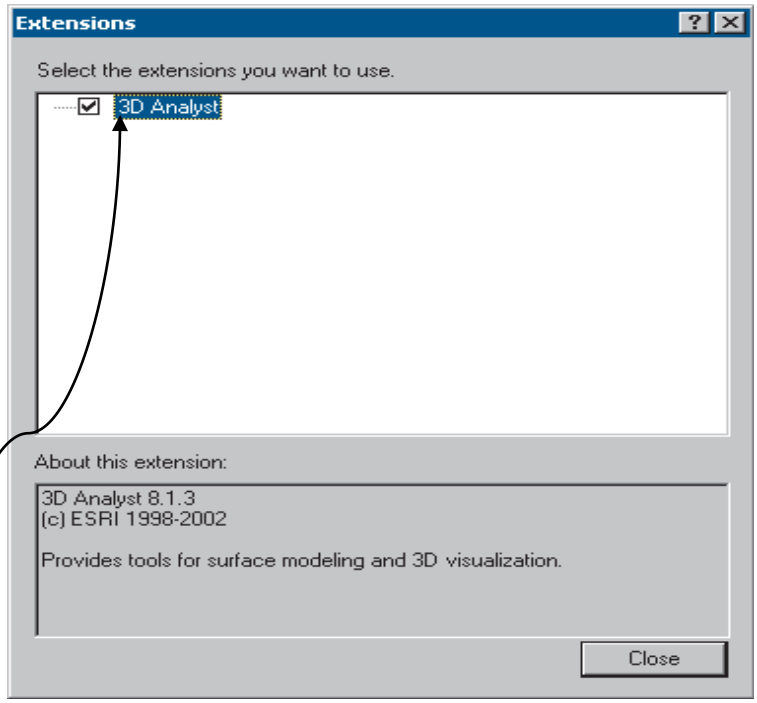

Step 4) Figure 4 Activate the 3D analyst. Source: (Arc-Map 9.2, 2009) Then select the file which contain the Triangulated Irregular Network (TIN1) of your Digital Elevation Model (DEM) (See Fig. 5).

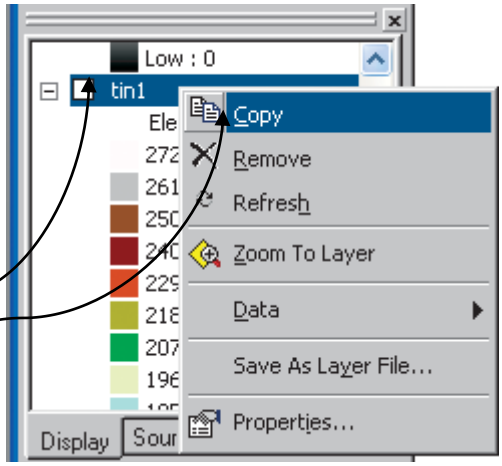

Step 5) Figure 5 Shows the graduated color of your (DEM) if you are agree with these colors click ok if not you can change graduated colours as well. (Arc-Map 9.2, 2009) (See Fig. 6).

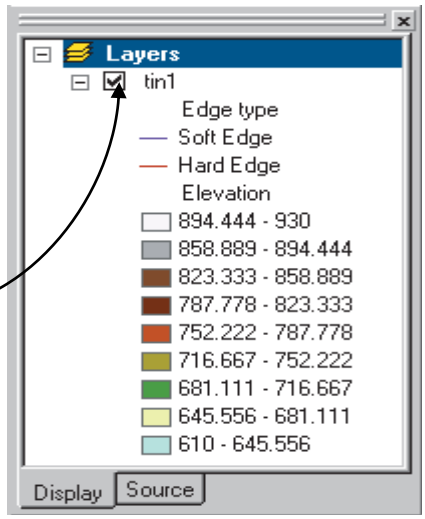

Step 6) Figure 6 Click TIN layer to view. Source: (Arc Map 9.2, 2009) (See Fig. 3.7).

Step 7) Figure 7 Click the Interpolate line. Source: (Arc-Map 9.2, 2009) (See Fig. 3.8).

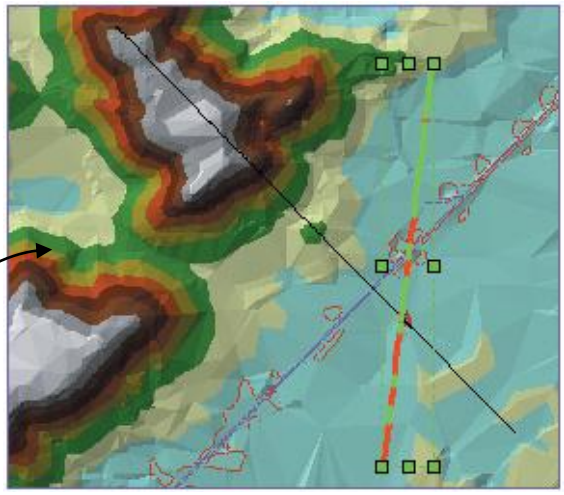

Step 8) Figure 8 Draw the line were the cross section is needed over the DEM. Source: (Arc-Map 9.2, 2009)

Step 9) Figure 9 Click in Create profile graph. Source: (Arc-Map 9.2, 2009)

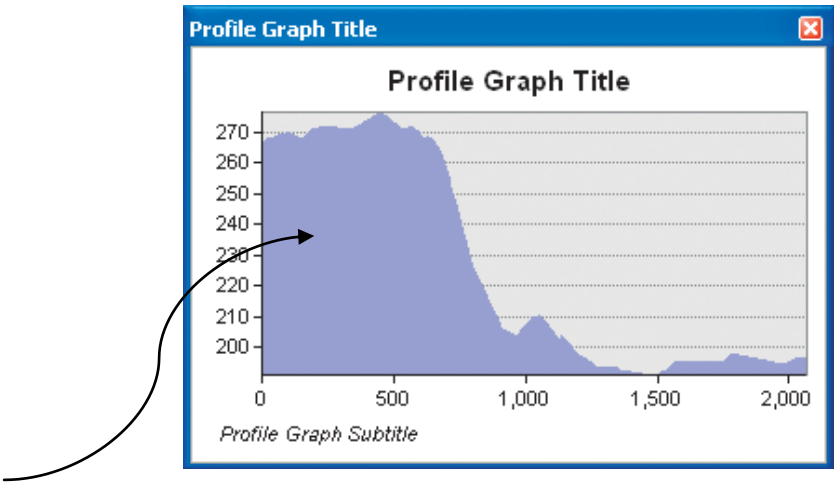

Step 10) Figure 10 Shows the graphic the profile which is created. Source: (Arc-Map 9.2, 2009)

APPENDIX 3D

Unified Soils Classification System method description.

The Unified Soil Classification System method was used in this study. This method is widely used to assess soil lithofacies (ASTM 1985). Soil parameters such as: Liquid Limit (LL); Plastic Limit (PL); size distribution; Curvature coefficient (Cc); Uniformity coefficient (Cu); Linear contraction (CL) are fundamental features to assess lithology. The method is internationally recognized and it is described in the following paragraphs. ***First***, following the next steps a representative sample of the soil is prepared: separate and eliminate fragments of rocks greater than 3 inch (76 mm). After that, separate the particles higher than 50% by weight retained on sieve No 200 (coarse-grained fraction) and those less than 50% by weight that passed the No 200 sieve as fine-grained. Also, measure the organic matter (Pt) if there is more than 50% of the sample content. ***Second.*** The coarse-grain size is sub-divided in Gravel (G) if more than 50% by weight of the fraction retained in No 200 sieve is also retained in the sieve No 4 (4.75 mm). Coarse gravel are soils between (76 mm to 19 mm); and fine gravel are soils between (19 mm to 4.75 mm). Similarly, Sands (S) are coarse-grained soils that have more than 50% by weight of soils that were retained on No 200 sieve were passed on the No 4 sieve. In addition, sands also are subdivided in coarse sands that have particles diameter between No 4 to No 10 sieve; medium sands with particles diameter between No 10 and No 40 sieve. And fine sands with particles diameter between No 40 and No 200 sieve (See Fig. 1). ***Third,*** Grading to fine soils sub-division. The mechanical behavior of the soils depends on whether it is clean or not (less than 5% by weight of fines being clean and more than 12% by weight of fines being dirty). In addition, Gravel and sands are again subdivided into well graded (W) and clean or no fines (<5% of fines); poorly graded (P) and clean no fines (<5% of fines); silt (M) dirty fine fraction behavior; clay dirty fraction behavior. ***Fourth.*** Gradation, In order to determine the grain size distribution of the sample laboratory analysis is needed. There are two methods. Firstly, by sieving analysis for the coarse fraction and wet analysis.

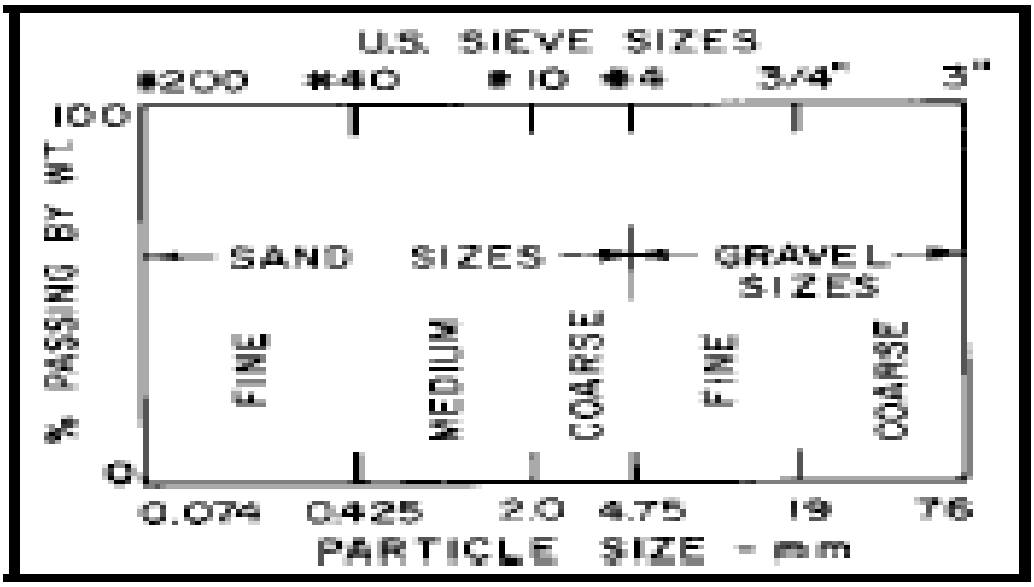

Figure 1 Ranges of diameters for coarse particle sizing. The (x) axe shows the size particles in mm and at logarithmic scale and the (y) axe shows the percent of soil passing in weight: Note also the upper axe shows the limits to classify soils as: coarse and fine Gravels fine, medium to course sands. Source: (ASTM 1985).

Process to obtain representative samples.

Firstly, extend nearly 4 kg of material on a clean flat surface and expose it to environment temperature conditions during 24 hours, after that, unbundled, extended and quartered of the sample is done. Then, select one quarter of the sample that will represent the whole sample. Finally, perform the sieve analysis to the coarse-grained and fine grained fraction of the sample as is indicated in the following paragraphs.

Process of sedimentation for the fine part of the sample.

Firstly, put the fine fraction of the sample in water during 24 hours. After that, pass the sample for the No 40 sieve manually until the sample is completely filtered. Then, the analysis of LL and PL are performed using the next process. Note that the quantity of the sample should be approximately 250 grams to perform the test. With respect to the coarse grained fraction the method used to perform the separation using several sieves from the No 200, No 40, No10, No 4, ¾ in, and 3 in.

The sieving process

This process is done through the use of an electronic apparatus that produce the vibration of the sample in vertical, horizontal as well in circular movement during a period of approximately 15 minutes. After that, the weight of the fractions of soils retained in the different sieves are recorded and the % that passes the sieve is evaluated. Then, the results were drawn in the (x) axis in logarithmic scale the grain size and in the vertical Axe (y) the accumulated (%) by weight that corresponds to the grain size were drawn. In addition, the graph of Fig. 3.7 shows expressions to evaluate (Cc) and (Cu) and the further classification as GW or SW in agree with the limits defined for (Cc and Cu) (see Fig. 2).

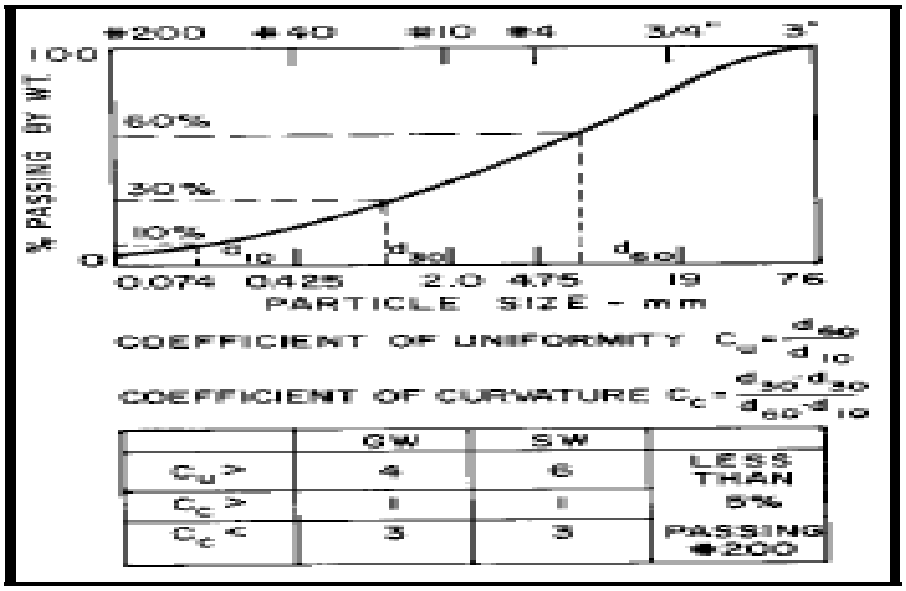

Figure 2 Definition requirements for soil to be classified as well graded. Cc and Cu in percentage define the soils gradation lower part of the Figure. The upper figure shows the curve distribution in function of size particle (x) and the percent passing the sieve (y) Source: (ASTM 1985).

In short, The classification process includes soils gradation (see Fig. 2) and two different gradation: Well graded (W), that is a soil with contains all the different diameter particles and poorly graded (P) that is soil with predominance diameter or lack of intermediate particles into the sample. Note that mixed soils occurred frequently when the % of fines are between 5% and 12%. The soil gradation can be obtained through the use of two parameters named uniformity and curvature coefficients (Cu and Cc). Where $Cu=D_{60}/D_{10}$ and $Cc = (D_{30})^2/(D_{10})(D_{60})$. Grain size curve is given by the coefficient of curvature (Cc), which is the ratio of the square of the 30% finer than size (D_{30}) divided by the product of (D_{60})(D_{10}). The definitions

used to distinguish between well graded and poorly graded gravels and sands are shown in Fig. 2.

The shape of the grains.

Influence of soils shape is very important to recognize it in the field. The identification process is described here: ***First***, Bulky or equi-dimensional grains. Shapes as: rounded, sub-rounded, sub-angular, and angular shown in Fig. 3 are characteristic of coarse grained soils. In general for the bulky type. The common mineral contained is quartz and feldspar. ***Second***. Flat, or Flaky grains also are called plate-like particles, these are presented in appreciable quantities in fine-grained soils and have width to thicknesses ratio more than 3. Mica and some clay materials have this shape that is mainly responsible of the high compressibility or plasticity. ***Third***. Elongated grains, these are long needle shaped particles and have length to width ratios more than 3. ***Fourth***. Length, width and thickness are measured between two parallel plates. Length and thickness are maximum and minimum possible distance two surface points measured by two plates. (Fig. 3)

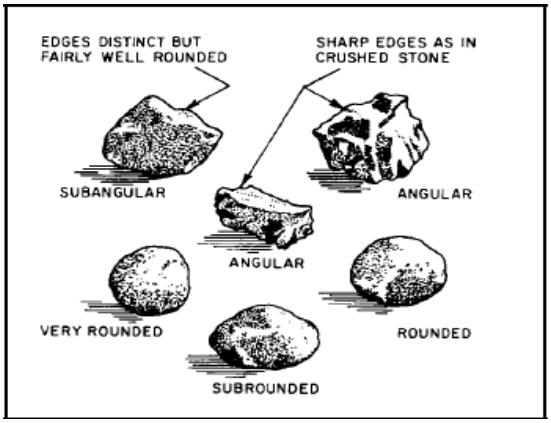

Figure 3 Typical shapes of bulky or equidimensional grains. Source: (ASTM 1985)

Determination of liquid limit (LL); plastic limit (PL) and soil classification.

This test is performed to fine-grained soil that passed the No 40 sieve. ***Firstly***. To test L.L. the apparatus named Casagrande coup is required (see Figure 3). First put into the coup a soil hand sample with a humidity closely to the L.L, after that cut the surface of the soil sample with a standard cuter device (see Figure 4) then calibrate the high between the coup base and the base plate to 1 cm and then bit the coup over the base with a speed of 1 bit per second and suspend the

operation when the two bottom sides of the sample come together. Registered the Number of bits and put in the oven a little part of this sample during 30 hours at constant temperature of 110° Celsius. Previously, this sample is weighted and registered and then when the sample is dray again is weighted. The difference between the initial and final weight divided by the initial weight gives the humidity of the sample. This task is performed for at least 5 sample fractions with different moisture content. It is recommended to add 50 mg of water at the original sample for every fraction tested. Then when all the 5 samples were tested the results of numbers of bits Axe (x) and % of humidity axe (y) are drawn in a graph. Finally, the L.L is obtained going with 25 bits in the axe (x) and in the intersection of the line going to the axe (y) there is the moisture content to L.L. (see Appendix 4B).

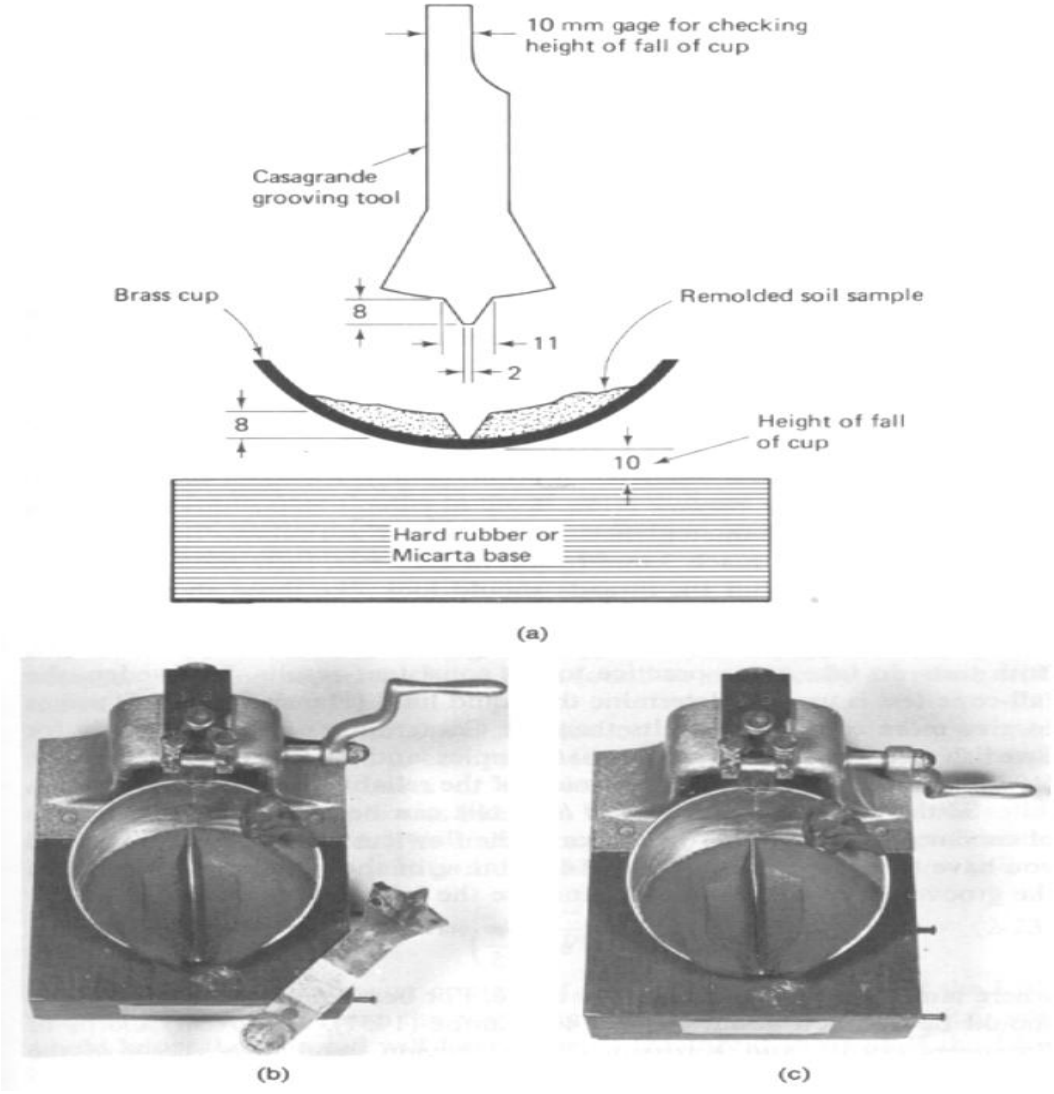

Figure 4 Liquid Limit device also named Casa Grande coup. Figure shows the devise used to perform Liquid Limit upon fine soils also see dimensions of the devise as well complementary tools. Source: (ASTM 1985)

Plastic Limit (P.L.) and Liquid Limit (L.L) were performed simultaneously and were performed over 5 little hand samples of the soil contained several humidity contents that appears to have closely the (L.L). Then, this sample is molded and rolled over a clean glass surface and stop the operation if the sample begin to fissure or break until the roll measure is approximately 9.3 cm long and 3 mm thick then, take a sample weight and put it on the oven during 24 hours at constant temperature of 110° Celsius. After that, determine the weight again and the difference between the initial weight and the final weight divided by the initial weight corresponds to (P.L).This operation is performed to five samples and the final L.P is the average of the LP of the 5 samples (See appendix 4B).

Soils Classification This process of classification consist in the use of the plasticity chart using the parameters previously obtained of LL and PL there is evaluated the Plastic Index PI that is the difference between the LL and PL with the PI and the LL and using the Plasticity chart Fig. 3.11 there is possible classify the fine grained soil.

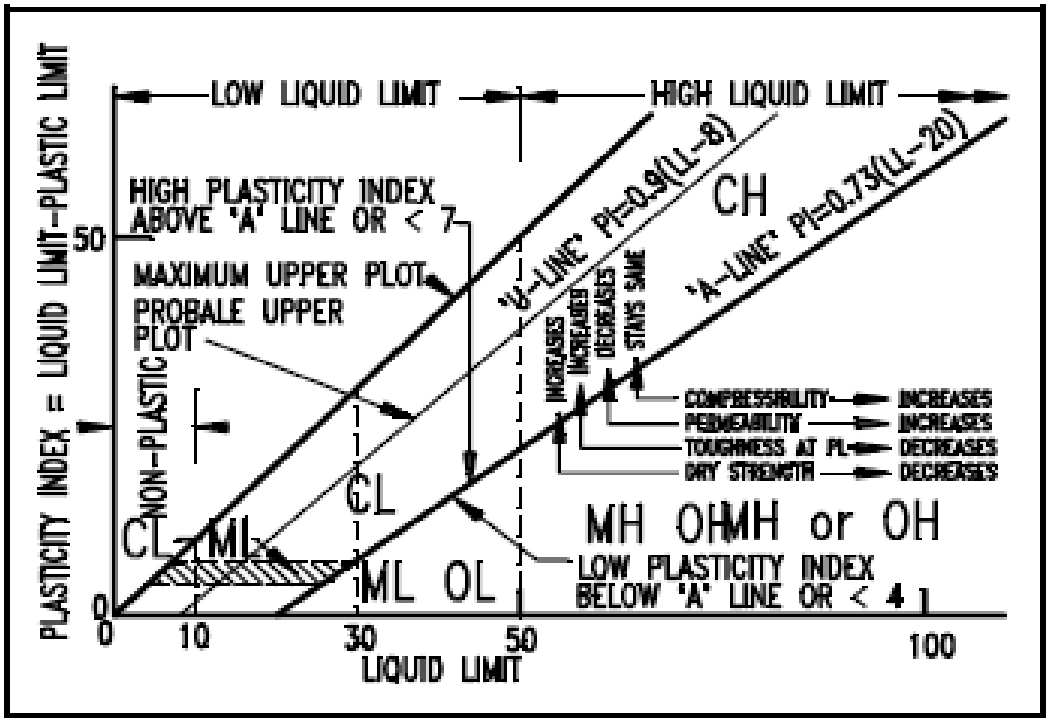

Figure 5 Plasticity chart applied to fine soils classification. Figure sows in the X axe in scale the liquid limit (LL) in (%) and in the axe (y) the plastic index (PI): Also see different lines that define the border the different kind of soils found. Source: (ASTM 1985).

In summary, regarded to soil samples analysis of Juárez City a complete report is available in (appendix 4B). The pictures shown in: (Figs. 3.9A and 3. 9B) illustrates the apparatus used and Fig. 3.11 of section 3.2.3 shows a picture of facie defined from the classification of the soils and the link with the alluvial fans soils of the study area. Fig. 3.12 also shows soils sample collection as well their transportation the Juárez University laboratory where they were tested.

APPENDIX 3E

Data sets of contour levels every 1 m using Lydar Technology

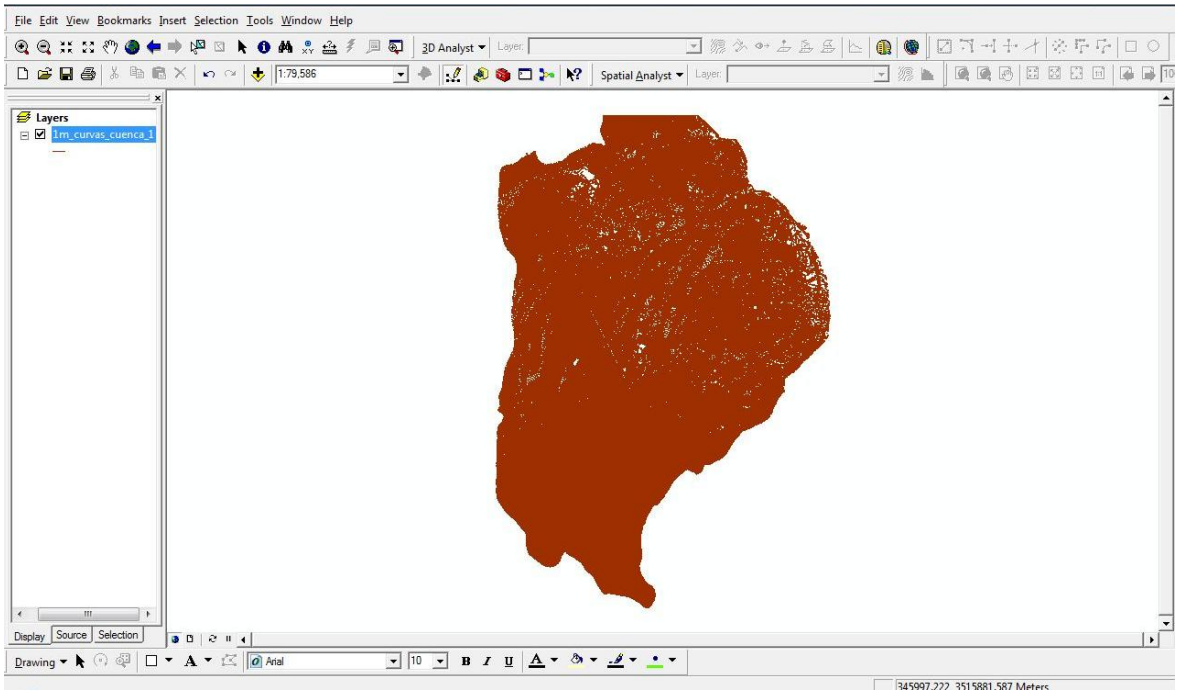

Figure 1. 1m of contour level shape file for the study area of Juarez City corresponded to the north western sector comprises Anapra sector and west and east Snake streams. Source: (UACJ 2010) derived using Lydar Technology and Arc-Map 9.3 programs.

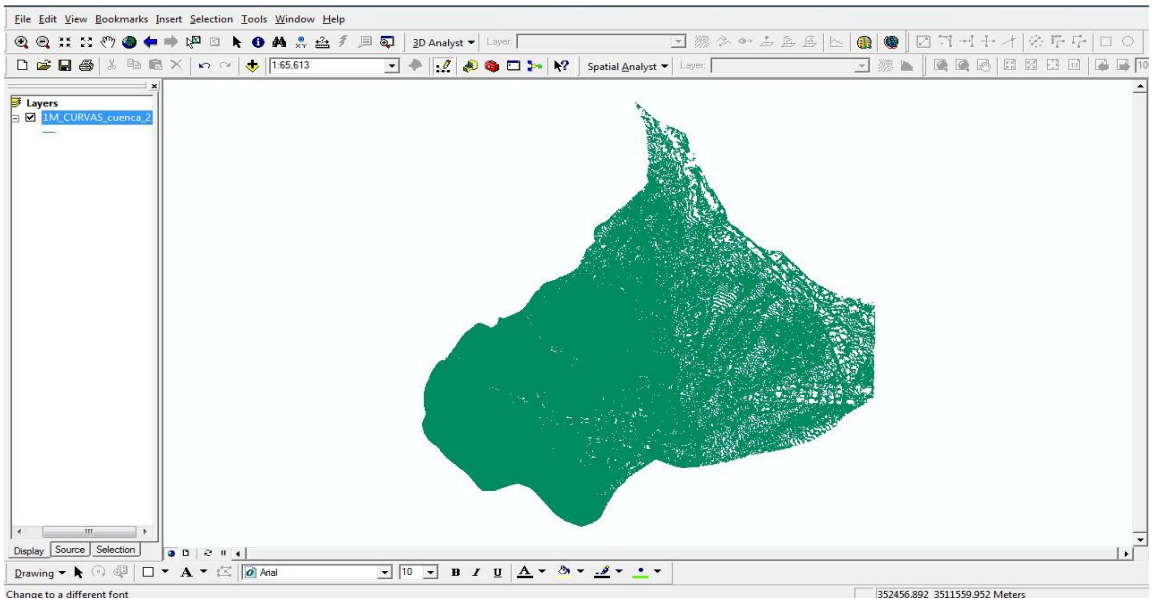

Figure 2. 1m of contour level shape file for the study area of Juarez City corresponded to the central sector comprises Colorado and Jarudo streams . Source: (UACJ 2010) derived using Lydar Technology and (Arc-Map 9.3, 2009) programs.

APPENDIX 3F

Processes to extract geometry related to streams using the HEC GeoRAS pre-processing module and the Arc view 3.2 program with , spatial and three dimension extensions included. Also the digital elevation model (DEM) which is the main datasets should be included .

During the streams centreline, left and right banks, left and right flow paths and cross section drawing, the contour levels shape file should be active instead than the DEM. The previous recommendation is needed in order to improve work velocity.

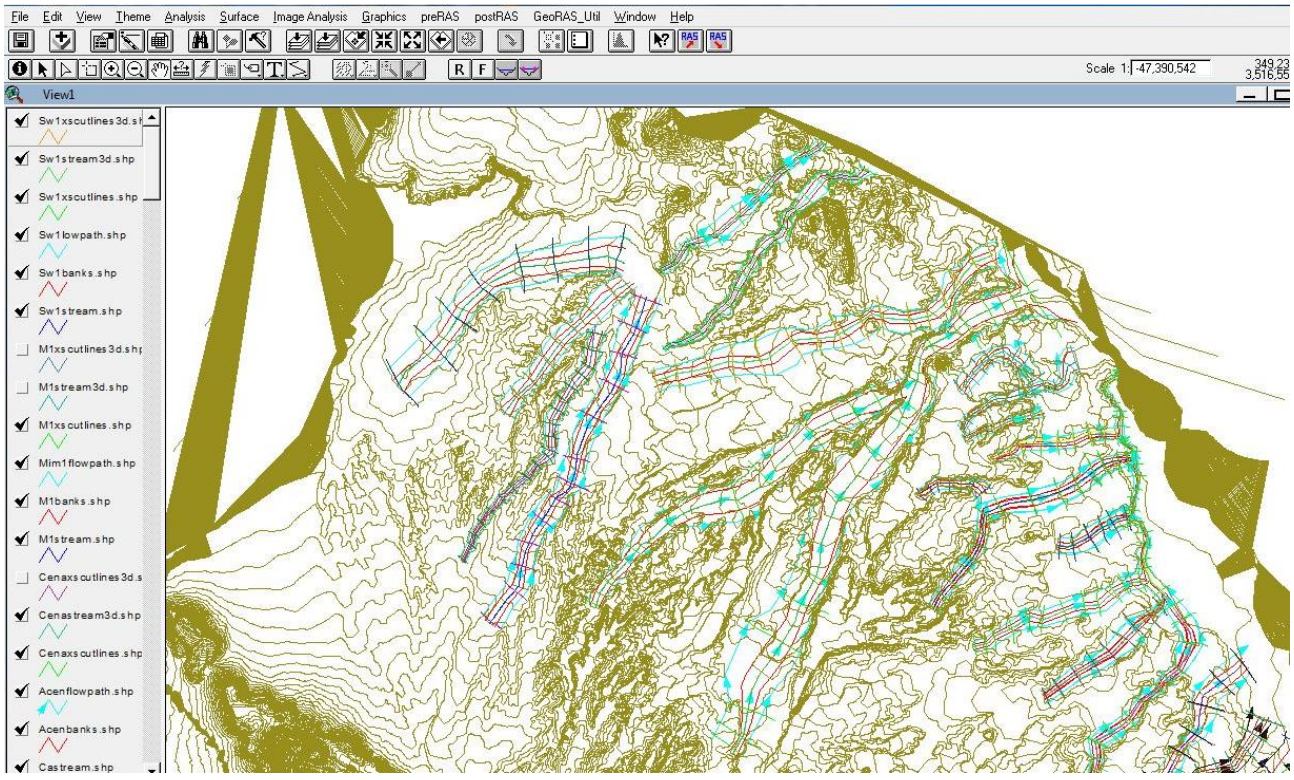

Figure 1. Shows contours levels activated but DEM not. Over them the centreline streams; cross section lines; banks; flow path and flow direction. The names registered for it are illustrated in the reference key. This sector is located in Anapra; west and east Snakes. Source: DEM 5m resolution; (Arc-View 3.2, 2002) version with Post Geo RAS and Pre GeoRAS processing modules.

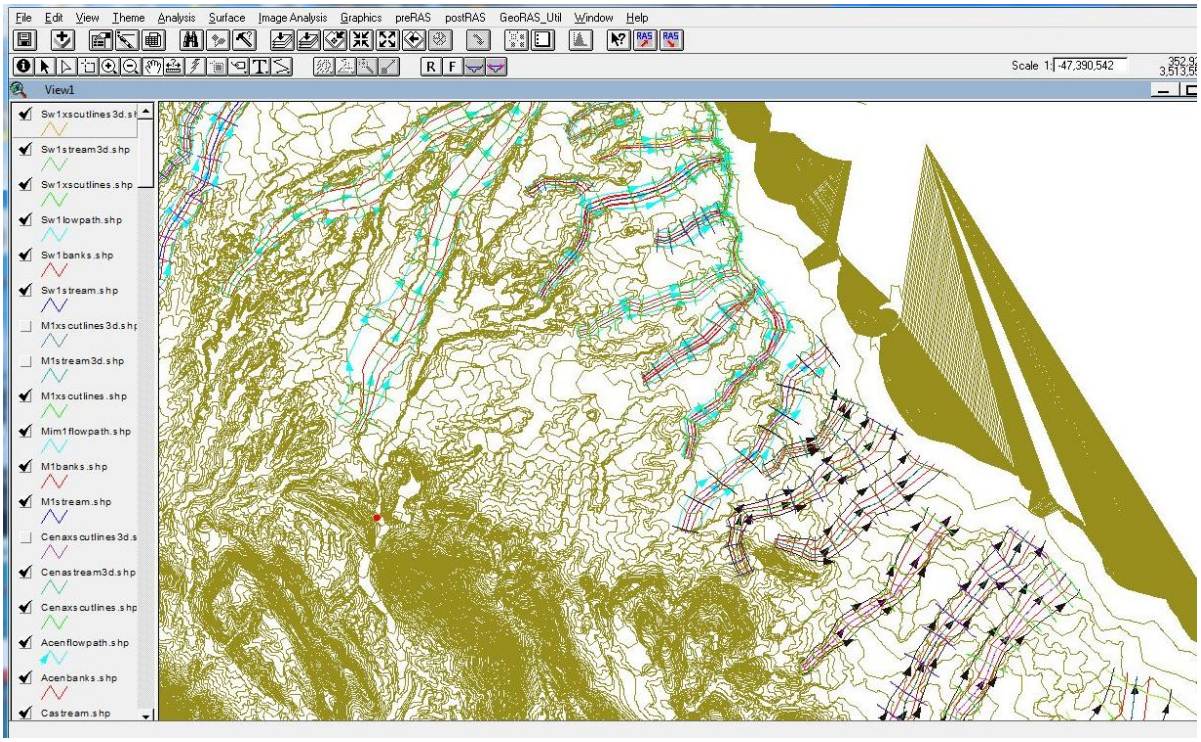

Figure 2 Shows contours levels activated but DEM not. Over them the centreline streams; cross section lines; banks; flow path and flow direction. The names registered for it are illustrated in the reference key. This sector is located in centre sector; Colorado and Viaduct streams. Source: DEM 5m resolution; (Arc-View 3.2, 2002) version with Post Geo RAS and Pre GeoRAS processing modules.

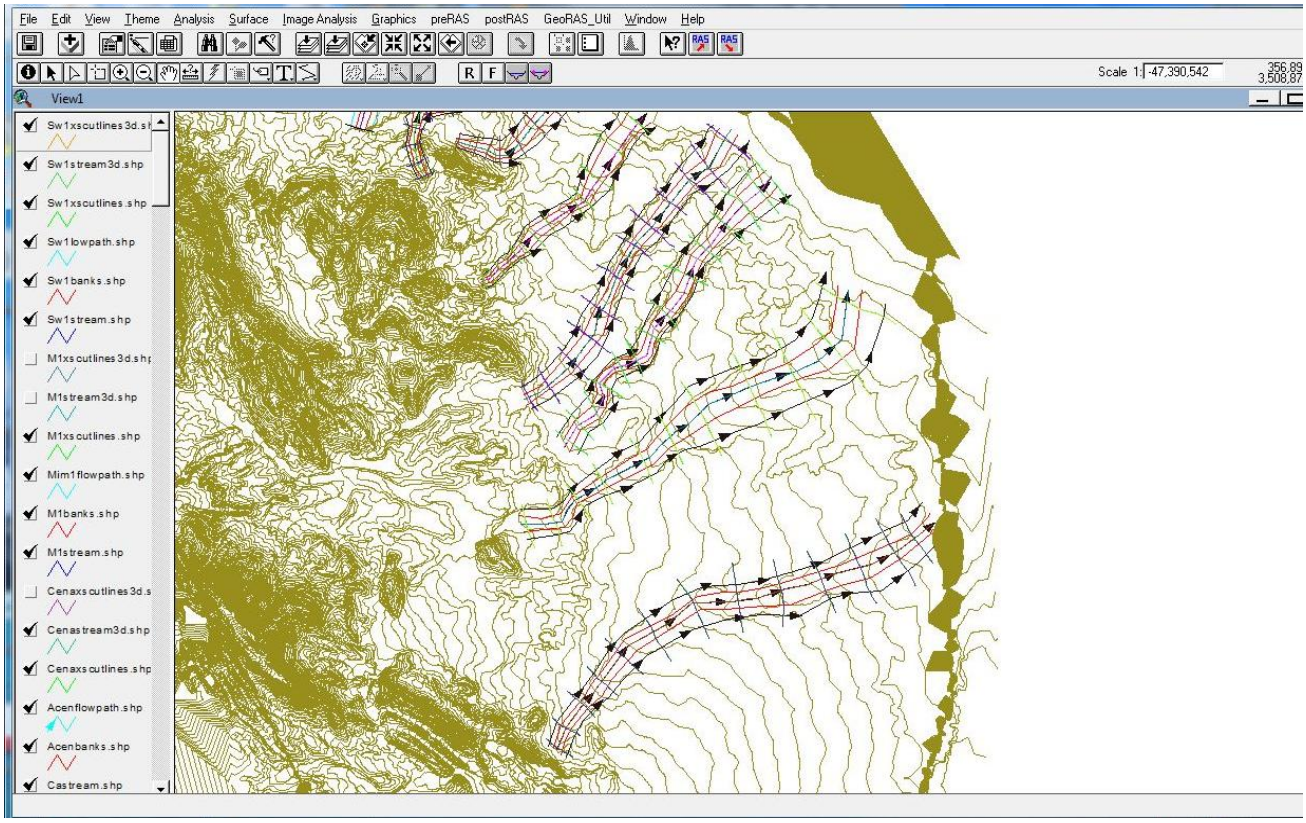

Figure 3 Shows contours levels activated but DEM not. Over them the centreline streams; cross section lines; banks; flow path and flow direction. The names registered for it are illustrated in the reference key. This sector is located in the south sector; Palo Chino and Jarudo streams. Source: DEM 5m resolution; (Arc-View 3.2, 2002) version with Post Geo RAS and Pre GeoRAS processing modules.

APPENDIX 3G

Ones performed the task defined in Appendix 3F related to streams using the HEC GeoRAS Pre-processing module and the Arc view 3.2 program then, the HEC RAS program is used to perform Hydraulic and Hydrologic calculations. Therefore, the derived (dss extension) file is opened and the hydrologic parameters related to HEC HMS Hydrographs are updated see table of Fig. 1). After that, the program perform hydraulic evaluation of the flooding see Fig. 2)

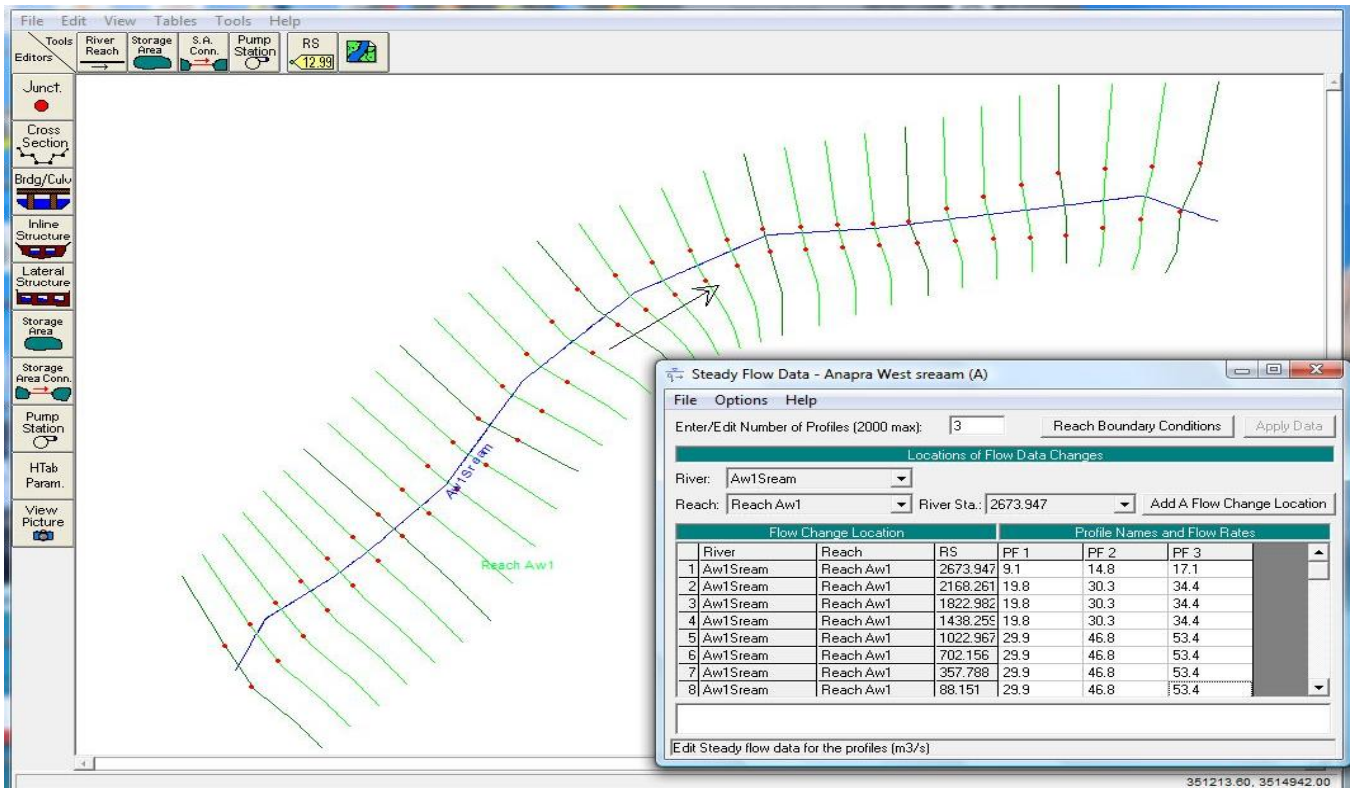

Figure 1 Association and organization of HEC-HMS flow hydrographs plans (PF1 for Tr 10 years; PF2 for Tr 50 years and PF3 for Tr 100 year) into the HEC-RAS program these stream driver corresponds to (Aw1) transference reach. Source: HEC-RAS (2002) 3.1.3 version

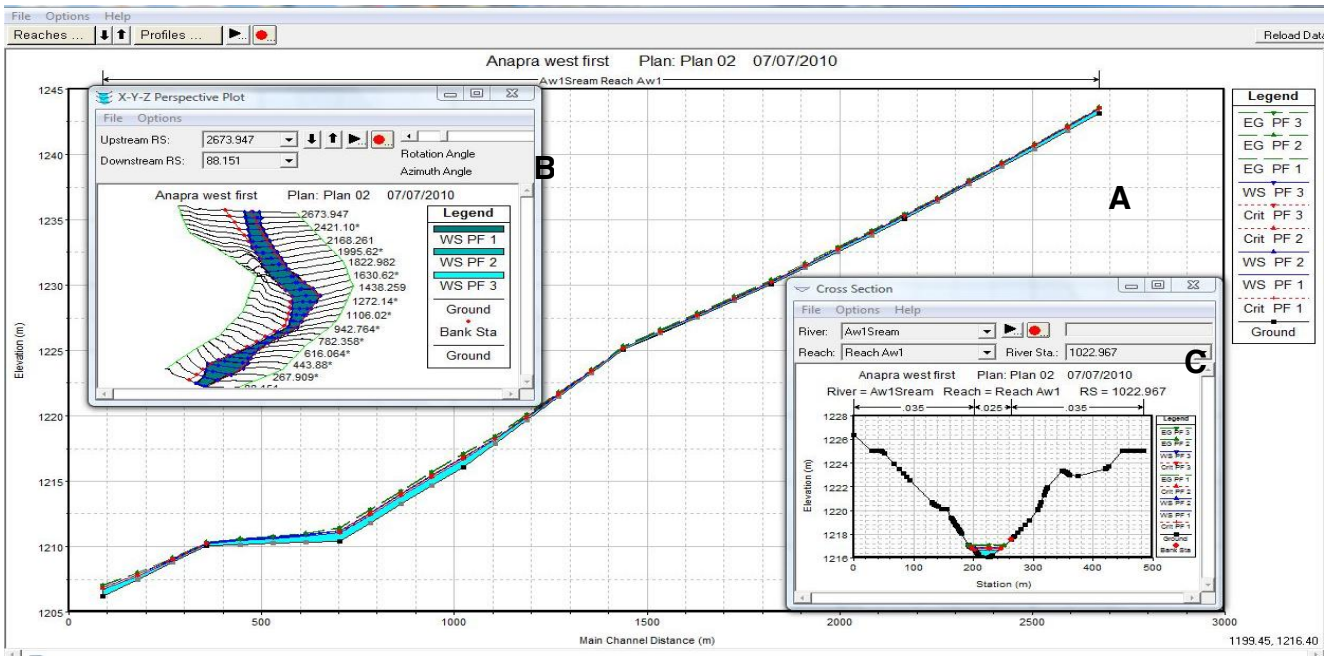

Figure 2 A) Water surface elevation of stream Aw1: 10 years (PF1); 50 years (PF2) and 100 years (PF3) return periods: B) shows a perspective view of the profile. C) Shows a cross section of the Water Surface that corresponds at station 1022.067 streams

Appendix 4A1

This appendix is integrated by complementary photoinventory and field soils collection samples of the three sectors of alluvial fans allocated on the Ciudad Juárez study area. (See Figs 4A1.1 to 4a1.5). In these 5 figures, there are illustrated the coordinate of the points as well the photos mentioned on chapter 4 also are included the soil classification assigned in agrree with Unified Soils Classification System USCS. In Figures below white dashed lines are lithological contacts and the Points visited were recorded using Manual GPS and UTM Coordinates; Source: Laboratory of soil mechanics of Juárez University UACJ (2009) and Unified Soils Classification System ASTM (1985) also for proccesing of the photos the Computer program Power Point (2007) was used. The present appendix, includes the place where smple were collected in the field and was extracted for the photography inventory done during field work on the study area during December soils exploration done from november 12 to december 18, 2009. The complete report are illustrated below in this appendix (See pages 6 to 36).

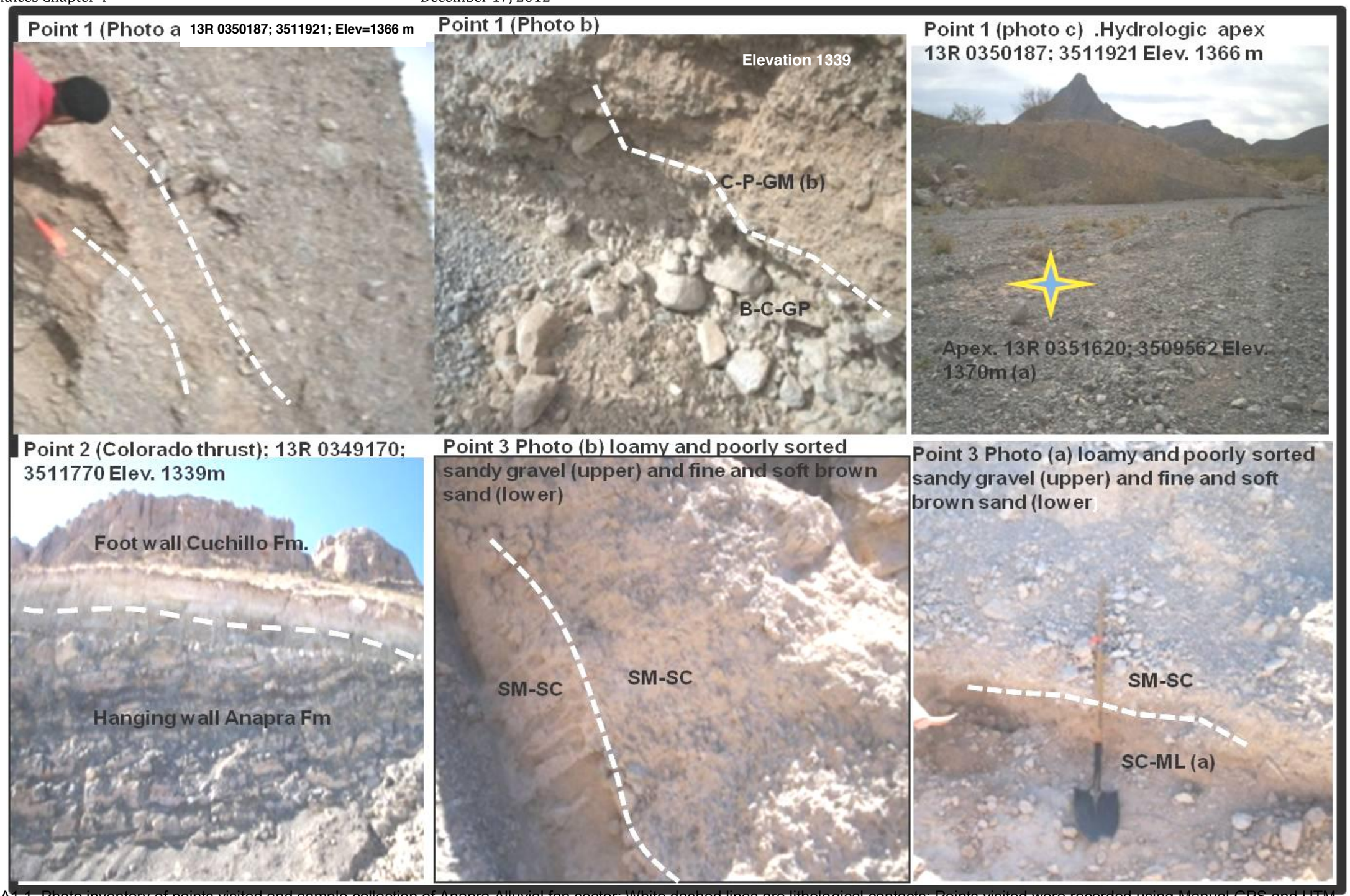

Figure 4A1.1 Photo inventory of points visited and sample collection of Anapra Alluvial fan sector. White dashed lines are lithological contacts; Points visited were recorded using Manual GPS and UTM Coordinates; Soils classification is in agree with Unified Soils Classification System USCS (2011); Yellow and blue star=Hydrological apexSource: Laboratory of soil mechanics of Juárez University UACJ (2009) and Unified Soils Classification System ASTM (1985)

Figure 4A1.2 Photo inventory of several points monitored and sample collection of Anapra Alluvial fan sector: White dashed lines are lithological contacts; Points visited were recorded using Manual GPS and UTM Coordinates. Source: Laboratory of soil mechanics of Juárez University UACJ (2009) and Unified Soils Classification System ASTM (1985); Computer program Power Point (2007).

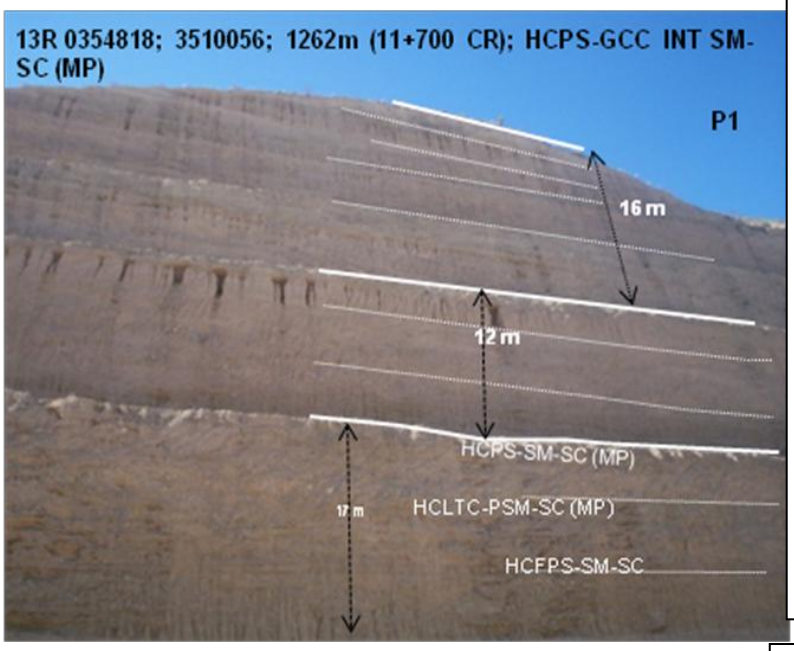

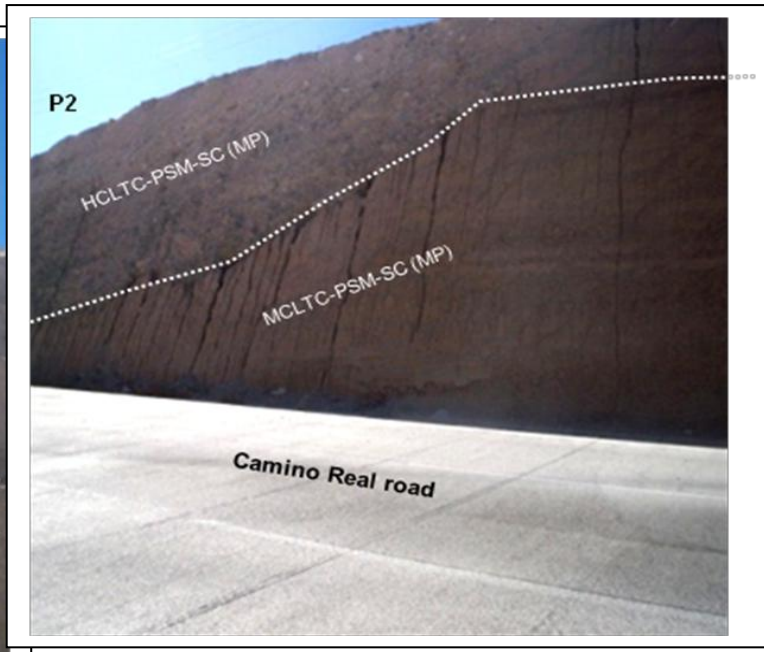

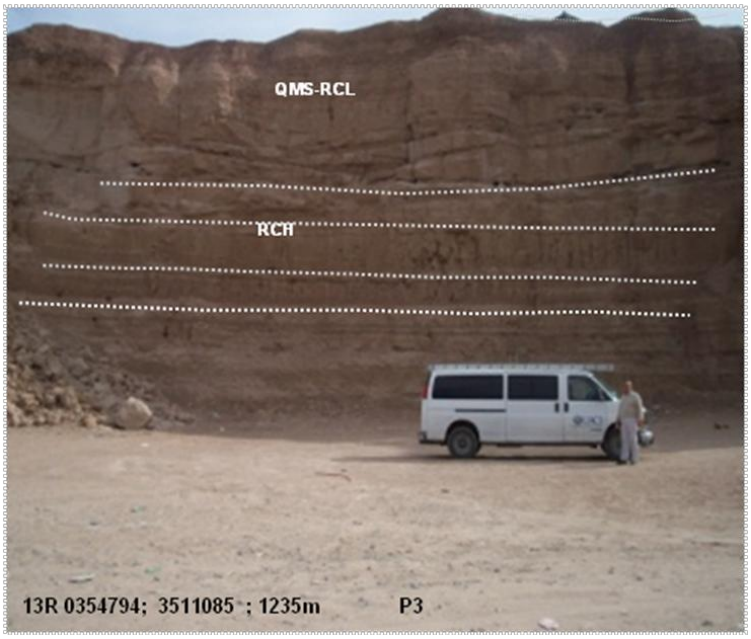

Figure 4A1.3 Photo Inventory of nine sites where soils sample collection were doneare presented in Figs 4.12A and 4.12B. In Fig. 4.12A are presented P1 to P5 on the rigth and lower side of the main Figure and the remaining points are shown in Fig. 4.14B. This figure have the 9 sites with georeferences in UTM Nad 27 geographic coordinate sistem as can see in the border of the frame.
Symbology of the main alluvial fans components as channel feder, Topographic and Hydrologic apex as well proximal, medial and distal segments of alluvil fans are also presented linked their border with dash gray and black colour lines .
(CMF) means Colorado Mountain Front; and (PCHMF) means Palo Chino Mountain Front alluvial fans. geographic location of alluvial fan Snake and Colorado is presented in : dashed white line=contact between soil facie; white words = facie abbreviation; PN= Point number collection; PNPHOTO= Photo number. Facie details and soils classification was done using the Unified Soil Classification System (USCS) ; Source: Unified Soil Classification System ASTM (1985); Laboratory of soils mechanic of Juárez University UACJ (2009).

Figure 4A1.4 Inventory of photos and soils sample collection of alluvial fan Snake and Colorado linked to Figure 4.12A: dashed white line=contact between soil facie; white text = facie abbreviation; PN= Point number collection; PNPHOTO= Photo number; Coordinate are UTM Datum elevation NAD 27; Source: Unified Soil Classification System ASTM (1985); Laboratory of soils mechanics of Juárez University UACJ (2009)

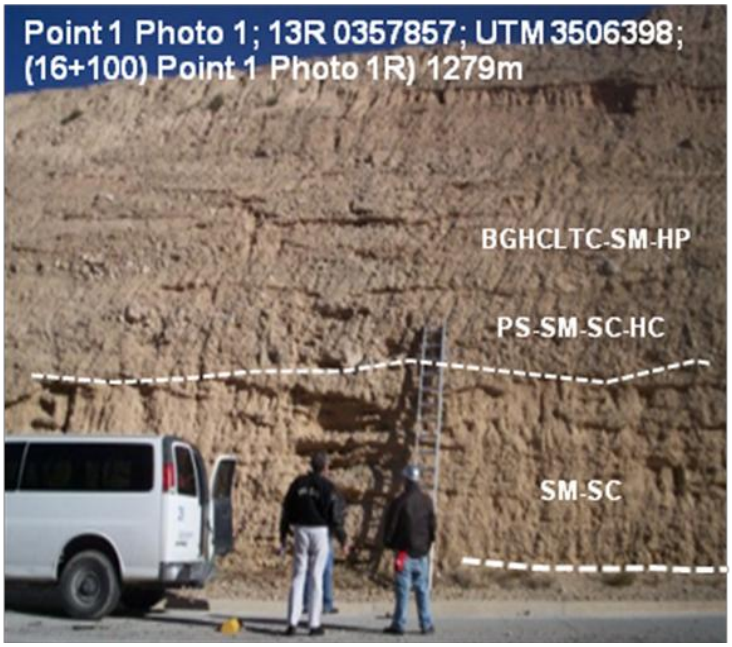

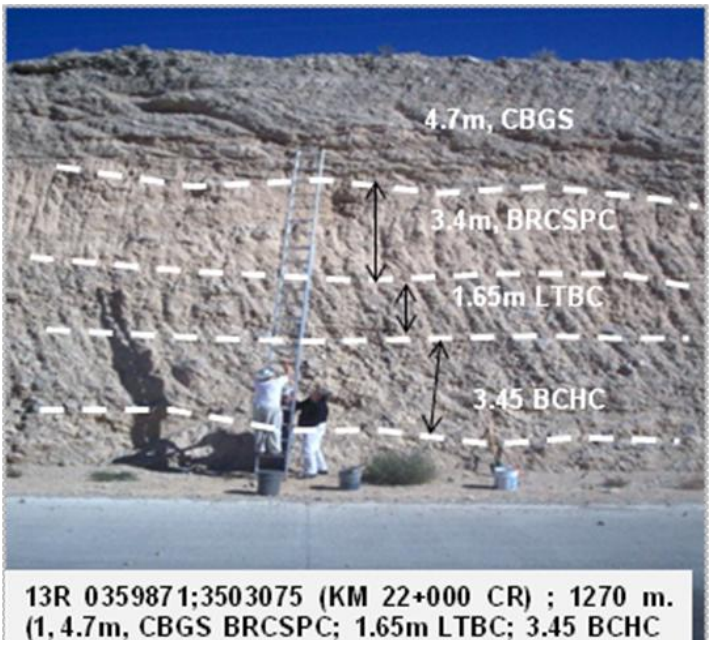

Fig. 4A1.5 Previous page shows more clear the contour levels as well the network stream system (See Figure 4.13): Figure 4.14, shows features as: Main components of the alluvial fans: Topographic Apex (5 vertexes star); Hydrologic Apex (4 vertexes star); Watershed divide; Channel Feeder; (red colour continuous line); Channel Feeder (Axe black colour line); Contour levels (green colour lines); (CR) Camino Real (blue colour line)Border lines limiting the different segments of Proximal (Qfpd), Medial (Qfmd) and Distal (Qfdd) alluvial fans are marked in dashed black lines.Points of soils sample collection and photo inventory of the Palo Chino and Jarudo fan system are shown as: Point 1 photo 1 is in the upper right sheet margin and is located at 16,100 meters from the origin of Camino real road, its elevation is 1279 masl and soils facie is Late Pleistocene Camp Rice Formation. Point 2 have two photos, Photo 1 shows three layers of soils facie described in previous paragraphs of this section and photo 2 shows the same point but in order to illustrate the tools used to collect the highly cemented limestone conglomerate. This limestone conglomerate is maybe Forthankock formation where Footwall derived deposits near Camino real (16+100=photo 1and 22+000=photo 2) Source: David Zúñiga (2011) Soils mechanics Lab of Juárez University UACJ (2009)

Appendix 4A1 SOILS EXPLORATION DONE FROM NOVEMBER 12 TO DECEMBER 18, 2009

Ciudad Juárez Chihuahua México Field work sample soils collection

Monday, November-23-2009

Point number 1 **Location: Cementera bridge 1**

Possible Fort Hancok Formation: Layer 1; Surface strata 4.70 m tick; The preliminary soil classification is Cemented Sandy Gravel of limestone origin with 1 to 3 inches rocks fragments.

Layer 2; Intermediate Strata 3.40 m tick; The preliminary soil classification is partially cemented brown red color clayed silt

Layer 3; Intermediate Strata of 1.65 m tick; The preliminary soil classification is mostly highly cemented limestone conglomerate with Limestone rocks fragments between 1 inches to 3 inches.

Layer 4; Lower Strata of 3.45 m tick there is no visible contact because floor of Camino Real was not observed. Probably Tertiary Breach composed of big rocks of Limestone fragments between (12 inches to 20 inches) highly cemented there was impossible to obtain a sample because of their hardly composition.

Coordinates: 13R 0359871 Longitude East and 3503075 Latitude North and Elevation 1270 m. Pictures taken in this point are: 168-183

Photo 1 Camino real road left cut bridge 2 Cementera ; Photo 2 similar to photo 1

Photo 3 Cementera upper Strata 1 Photo 4 sample cementera upper strata 1

Photo 5 Upper strata sample 1 Cementera

Photo 6 taken UTM coordinates sample

Photo 7 Collecting strata 2, sample 2.

Photo 8 sample 2 upper strata 1

Point Number 2 **Date November 23, 2009.**

Location; Bridge los Ojitos; Camino Real Km 16+100 near to Feldespato street.
Possible Fort Hancok Formation.
Strata number 2; Preliminary soil classification with 2.20 m depth partially cemented brown red color Clayed silt.
Strata number 3; Preliminary classification very consolidated Tertiary Limestone Breach 1.45 m depth. There not was possible to observe the contact because the floor Camino real road big limestone and sandstone fragments of 12 inches to 20 inches diameter are common.
Coordinates: Longitude East 13R 0357841; Latitude North 3506412; Elev. 1270 m
Strata number 1 taken on November 24, 2009 preliminary soil classification limestone cemented conglomerate pictures taken in this point are: 46, 48, 49, 50.
Coordinates britian gps 13R 0357857; UTM 3506398; Elevation = 1279m

Photo 3 Ojitos bridge km 16+100 Camino Real Road. Photo 4 upper strata sample strata number 1

Photo 5 Upper sample strata number 1

Photo 6 collection sample strata number 1

Photo 7 upper sample strata number 1

Photo 8 upper sample strata number 1

Photo 9 upper sample strata number 1

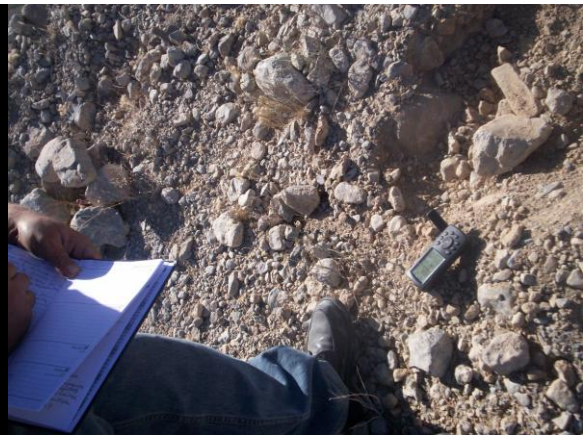

Photo 10 upper sample strata number 1

Photo 11 strata 1 point 2 Ojitos bridge

Photo 12 strata 2 point Ojitos bridge

Photo 13 strata 2 Ojitos bridge

Photo 14 strata 2 ojitos bridge

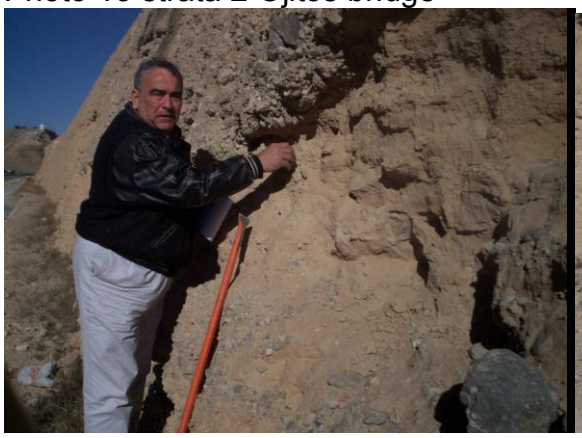

Photo 15 Strata 3 Ojitos bridge (no sample)

Photo 16 strata 2 Ojitos bridge

Point Number 3 **Date November 24, 2009.**

Camino Real road cut in at the lower level of the hidalgo viewer. Four berms of 12 m each then a total of 48 m in the right section and three more berms of 12 m each one were pictured in the left section: Strata were taken from the left cut. All the soils are very cemented and the next strata were meassured.
Strata 1: 3.45 m depth of highly cemented conglomerate with some lenses of clayed silt may be Fort Hancock Formation.
Strata 2: 1.80 m depth highly cemented clayed silt may be Fort Hancock Formation.
Strata 3: 3.00 m depth highly cemented conglomerate of limestone origen with rock limestone, sandstone and volcanic fragments of 1 to 3 inches diameter.
Strata 4: 3.20 m depth highly cemented conglomerate includes big fragments of rocks limestone, sandstone and volcanic origen visual classification. There was impossible to take sample.This strata sequence is consistent in the three berms monitored.
Coordinates 13R 0355711 UTM 3509499 Elevation 1279 or 1288 (942 waypoint).? Check with uacj gps.

Photo 1: Strata 4 Camino real road right cut, photo 2 Taking samples strata 2 and 3

Photo 3 taking strata 4 Taking strata 3 and 4

Photo 5 Strata 1 point 3

Point number 4 **(Date November 24, 2009)**

km 11+700) Camino Real road Hidalgo viewer. Left cut of camino real road there are three berms of highly cemented soils (maybe Fort Hancock formation).
Strata number 1 Upper berm 10m depth composed of high cemented sandstone and limestone (visual classification maybe tertiary breach poorly sorted)
Strata number 2 intermediate berm 12 m depth composed of similar conglomerate of limestone and sandstone white color (visual classification maybe tertiary breach poorly sorted)
berm number 3 Lower berm 17 m depth composed of highly cemented soils that include two strata
Strata number 3 highly cemented fine Sands with pebbles 16 m depth with one intermediate conglomerate layer of 2m depth in the middle.
Strata number 4 highly cemented limestone conglomerate of 1m depth in contact with andesite
Coordinates GPS Brunel 13R 0354818 UTM 3510056 Elevation 1262m (waypoint 943)

Photo 1 Tertiary conglomerate C.R road km 11+700 Photo 2 strata number 1 km 11+700 C.R road

Photo 3 taking sample strata 2

Point number 5: **(Date November 24, 2009)**

Cut in Camino Real 10+800 two windy sand strata in contact with conglomerate. Coordinates: Brunel 13R 0354160; UTM 3510359; Elevation 1281m. (waypoint 944) Strata 1 Conglomerate, strata and an upper windy sand strata of 4 m depth. strata number 1 conglomerate 2 m depth (in the middle) and lower strata number 2 windy sand 4m depth repited

Photo 1 km 10+800 Camino real strata 1 windy sand conglomerate in the middle and windy sand lower strata

Photo 3 Lower Strata 1 point 5 windy sand C.R. 10+800

Point number 6 **Date November 24, 2009**

Km 10 + 380 over cut of Camino real road two strata.
Strata number 1 cemented sandy gravel limestone conglomerate 2.50 m depth
Strata number 2 wet clayed silt with tight gravely lenses
Coordinates: Brunel GPS 13R 0353838 UTM 351105 Elevation 1254m (waypoint 945)

Photo 1 strata 10+800 Camino

Photo 2 point 6 strata 1 Camino real 10+800

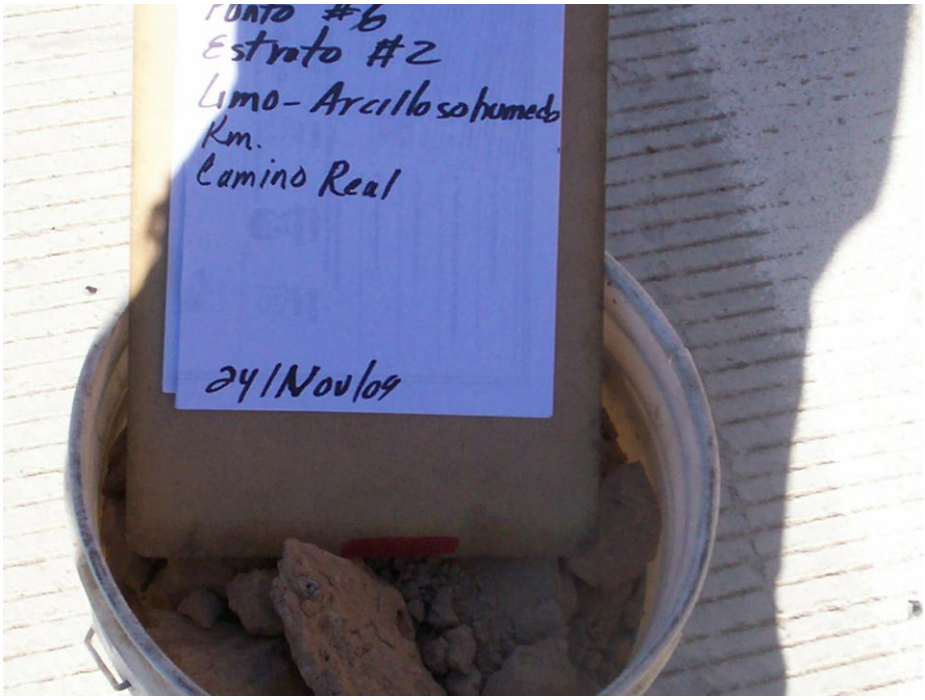

Photo 3 point 6 strata 2 Camino real 10+800

Point number 7 **Date November 24, 2009**

Located near to the Black Christ (Cristo de Curiel); Puerto la Paz Dike and Camino real road) possible geological fault. There are three strata:
Strata number 1 clayed white soil with some fossils in the upper part 1.50 m depth; (this strata is located also in the lower part maybe because a normal fault occurred and is reported in point 8).
Strata 2 clayed silt medium cemented 4.00 m depth
Strata 3 wet sand 6 m depth or more no detected visually.
Coordinates: Brunel GPS 13R 0352822 UTM 3512742 Elevation 1259m (waypoint 946)

Photo 1 Dike Panoramic Puerto la Paz dike

Photo 2 Collecting sample strata number 3 Photo 3 collecting sample number 2

Point number 8 **Date November 24, 2009**

Strata 1 Footwall of fault clayed evaporitic 1.50 m depth with fossils (dike Puerto la Paz)Coordinates: Brunel GPS; 13R 0352802 UTM 3512650 Elev 1256m (waypoint 947)

Photo 1 strata 3 Photo 2 Panoramic strata number 3

Photo 3 Collecting sample strata

Point number 9 **Date November 25, 2009**

Coordinates Brunel GPS; 13R 0354378 UTM 3510304 Elevation 1262m (waypoint 948)
Coordinates UACJ GPS; 13R 0354380 UTM 3510305 Elevation 1266m.
Plutarco Elias Calles Neighborhood back to camino real road (photos 2, 3 and 4)
Strata 1 organic clay; Strata 2 gravelly clay and strata 3 clay lenses 50 cm thickness.

Photo 1 Collecting strata number 1

Photo 2 back white home point 10 strata 3

Photo 3 Panoramic From Gasera dike to P.E.C

Point 10. Near to point 9 but in the lower part of the house (photos 6 and 7) Coordinates: Brunel gps 13R0354448 UTM 3510305 Elev. 1256 (waypoint) uacj 13R0354448 UTM 3510306 Elev. 1256
Strata 2 Gravel with flood clayey with some poorly sorted pebbles packed on a low plasticity clay.
Strata 3 Lenses of plastic and dry clay in layers of 50 cms interbedded with flow of fines and gravels debris poorly sorted. Photos 6, 7 and 8.

Photo 1 back to white home strata 3 flood of clay mixed with gravels and poor sorted pebbles of 1 inch to 3 inches diameter layer of 2.00 m.

Photo 2 Panoramic point number 10

Photo 3 white home strata number 3 point 10

Point 11 **November 25, 2009**

Alternated layers of silted clay and sandy silt the silted clay lenses decrease in thickness with depth and the sand strata begins with thick layers from 2 or 3 m and decreases with depth also the strata replies again and again. Strata 1 highly clayed silt red brown color and Strata 2 Lenses of dry clay and fine sand of 20 to 30 cm thick red brown color median hard in the upper part 3m depth, then continue strata 2 predominantly composed by fine white sands this strata is 7m thick ; Coordinates UACJ 13R 0354649 UTM 3510550 Elevation 1265m. Brunel 13R 0354649 UTM 3510545 Elevation 1244m

Photo 1 clays and sands red color
Photo 2 Alternated layers of cemented silty and sandy clay

Point 12 November 25, 2009
Left side Colorado Stream 16 de September Neighborhood Street Privada del Cerro.
Strata 1 Softy and lighty silty sand depth 7m
Strata 2 hardly and redly browm silty clay 2m thick
Strata 3 Continue Soft silty sand color red browm depth more than 2 m.
Coordinates UACJ 13R 0354794 UTM 3511085 Elevation 1235m
Brunel GPS 13R 0354796 UTM 3511086 Elev. 1231m

Point number 13 **November 26, 2009**

Located in Juan Balderas and Mariano Escobedo streets Luis Echeverria Neighborhood near to Hilario house.
Coordinates: Brunel GPS; 13R 0355722 UTM 3511681 Elevation 1235m (waypoint 952) GPS UACJ 13R 0355723 UTM 3511681 Elevation=1235m.
Four strata 1 Conglomerate 6m depth; 2 Fine sands 2m depth; 3 lent of red clay 40 cm depth and ; the lower strata 4 continue Fine sands more than 2m depth (floor of the terrain)
Strata 1=conglomerate ; strata 2 = strata 4 = Fine sands; strata 3 red clay.

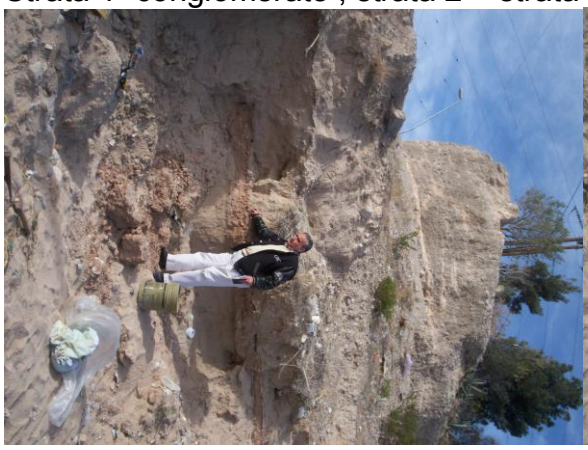

Balderas and Escobedo street Int. (Photo1, NHH) Balderas and Escobedo street Int. (Photo2,NHH)

Balderas and Escobedo street Int.(Photo3 NHH)Luis echevarria neighborhood viewing (Photo 4,NHH)

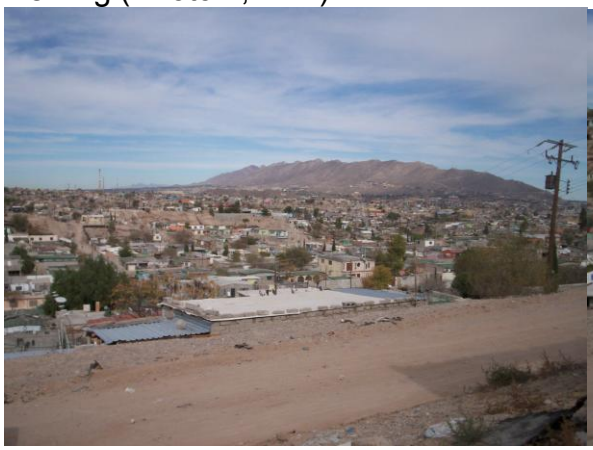

Luis echevarria neighborhood viewing (Photo 5 and 6,NHH)

Point number 14 **November 26, 2009**

Chihuahua Neighborhood Coordinates Brunel GPS 13R 0356277 UTM 3512127 Elevation=1202m GPSUACJ 13R0356277 UTM 3512122 Elevation = 1216 m.
Strata 1 similar to strata 1 in point 13 Conglomerate 4 m depth;
Strata 2 equal strata 4 = 3m depth
Strata 3 red brown dry clay 50 cm depth.

Photo 1 Chihuahua neighborhood Photo 2 Chihuahua neighborhood

Photo 3 Chihuahua neighborhood

Point number 15 **November 26, 2009**

Located in 1419 Snakes' stream street on Felipe Angeles Neighborhood at the back of house Coordinates GPS Brunel 13R 0356084 UTM 3514609 Elevation 1151m. GPS UACJ 13R 0356085 UTM 3514610 Elevation = 1161m. Strata 1; course gravelly sand white color soft in the upper part of the cerro between 6 to 10 m.Strata 2 Volcanic quartzite course sand maybe ash with some red color and very hard with depth.

Photo 1 Viboras stream street

Photo 2 Viboras stream near to sample home

Photo 3 and 4. Felipe Angeles neighborhood; viboras 1419 street, home place of sample

Photo 5. Felipe Angeles neighborhood; soils strata that were sampled

Point number 16 **November 26, 2009**

Located in Nogal street Francisco Villa Neighborhood at the back of home coordinates GPS Brunel 13R 0356405 UTM 3514674 Elev. = 1149m. GPSUACJ 13R 0356403 UTM 3514673 Elev=1148m.
Strata 1 river'white and soft gravely sand in lenses and the total depth = 10m.
Strata 2 clayed silt medium hard very depth more than 4m.

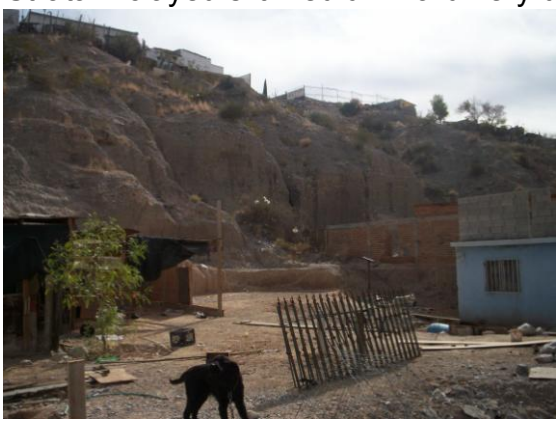

Photo 1 Fco Villa 1532 site place Photo 2 Viboras street viewing to extrusive outcrop November 27, 2009 Panoramic view at the surroundings of Pump hole of Conejos medanos water conduction line located at the west juarez mountain beginning tha Mesilla aquifer. GPS UACJ 13R 0349170 UTM 3511770 Elev. 1339m; Brunel 13R 0349169 UTM 3511769 Elev. 1337 (point 16a)

Photo 3 Pump Conejos medanos hole. Photo 4 West Juarez mountain Normal fault

Photo 5 Normal Fault west of Juarez mountains Photo 6 near of hole Pump west of Juarez mountain

Point 17 Along the Conejos medanos water conduction line: Strata 1 limestone

Sandy gravel poorly sorted 30 cm thick and Strata 2 fine sands brown color. GPS UACJ 13R 0350187 UTM 3511921 Elev. 1306m Brunel 13R 0350187 3511925 Elev. 1301m

Photos 1 and 2. Sampling strata 1 composed of limestone sandy gravel conglomerate poorly sorted

Photos 3 and 4. Sampling strata 2 composed of fine and soft brown sand

}

Point 18. Along stream, in cave 80 m left of Conejos medanos water conduction line. Strata 1; Limestone cemented conglomerate composed of poorly sorted rounded gravels ½ to 1inch thick and Strata 2 composed of cemented sandy gravel conglomerate of ¼ to ¾ thick. And Strata 3 composed of fine red-brown sand medium cemented. UACJ GPS 13R 0350369 UTM 3512163 Elev. 1293m GPS Brunel 13R 0350369 UTM 3512164 Elev. 1289m

Photo 1 viewing to N-E (Franklin mountains)

Photo 2 viewing to S-E (West of Juarez Mountain

Photo 3 sampling strata 1 point 18

Photo 4 sampling strata 2 sample 18

Photo 5 Sampling strata 1 sample 18

Photo 6 Sampling strata 2 sample 18

Photo 7 sampling strata 3 sample 18

Photo 8 hydraulic structure at the beginning of Puerto la Paz stream viewing to Juarez Mountains and Photo 9 viewing through the west along the Conejos medanos road of water conduction line

Point 18a without sample through Puerto la Paz stream and viewing to Juarez mountains . GPS UACJ 13R 0351146 UTM 3513504 Elev. 1261m. Brunel 13R 0351149 UTM 3513508 Elev. 1263m.

Photo 1 finishes of sandy strata of alluvial fan intermediate part of the alluvial fan near Puerto la Paz

Photo 2 and 3 finishes of sandy strata of alluvial fan intermediate part of the alluvial fan near Puerto la Paz

Point number 18b contact between gravelly sand poor sorted conglomerate and sandy soil Coordinates UACJ 13R 0350937 UTM 3513179 Elev. 1268m Brunel 13R 0350919 UTM 3513166 Elev. 1265m

Photo 1 contact conglomerate to sandy soil Photo 2 viewing through south the contact showed.

Point 18c Panoramic view of viboras stream viewing both sides showing poorly sorted limestone conglomerate with sands and silts. The conglomerate thickness is approximately 8m that could be appreciated in the scarp areas at both sides of the stream. Coordinates UACJ 13R0350960 UTM 3512969 Elev. 1270m Brunel 13R 0350957 UTM 3512963 Elev. 1266m

Photo 1and 2 viewing left side of Pto la Paz stream and contact between Sand and conglomerate

Photo 3 and 4 viewing to limestone conglomerate cover on both sides of Puerto la Paz stream

Photo 5 and 6 contact between sand and Conglomerate

Photo 7 and 8 scarp showing contact between layers conglomerate-sandy gravel and sandy silt

Photo 9 and 10 Puerto la Paz stream showing the contact between conglomerate and sandy gravel

Point number 18d November 23, 2009, without sample upper panoramic view of viboras stream and Puerto la Paz dike near to point sample 18 or Conejos medanos water conduction line. Coordinates UACJ 13R 0351084 UTM3512542 Elev. 1298m Brunel 13R 0351082 UTM 3512541 Elev. 1293m. Photos lower to north of the Viboras stream.

Photo 1 viewing to North of Viboras stream Photo 2 viewing to North (Franklin Mountain)

Photo 3 viewing to North (Anapra) Photo 4 viewing to North (Franklin mountain) Point number 18e November 23, 2009 without sample upper panoramic view of viboras stream and Puerto la Paz dike near to point sample 18 or Conejos medanos water conduction line. Coordinates UACJ 13R 0352308 UTM 3511374 Elev. 1304m Brunel 13R 0352301 UTM 3511378 Elev. 1300m. Photos Upper and south of the Viboras stream.

Photo 1 viewing to South (Juarez Mountains) Photo 2 to Southof (Juarez Mountains)

Photo 3 Beginning south of Puerto la Paz stream.

Point sample number 19 near to the hydrologic apex of Viboras stream (Rayito home): upper strata 1=bad sorted sandy gravel (1/4-3/4inches) 2m depth; Lower strata 2 = course gravel with redounded rock fragments bigger than 3 inches 1m depth. Packed in sandy matrix. Sample coordinates: UACJ GPS 13R 0351620;

3509562 Elev. 1370m GPS Brunel 13R 0351617; 3509571; Elev. 1369m.Photos 1 and 2.

Photo 1(Sample point 19 strata 1)

Photo 2 (Sample point 19 strata 2)

Photo 3 Viboras stream scarp near to hydrologic apex. Photo 4 Viboras stream near hydrologic apex.

Hydraulic apex Coordinates; GPS UACJ 13R 0351426; 3509443; Elev 1366m; GPS Brunel 13R 0351424; 3509447; Elev. 1363.

Photo 5 Block fault east Viboras topographic apex. Photo 6 near west Viboras stream Top. apex

Photo 7 Snake stream east view of mountain structure. Photo 8. Snake stream Top. Apex. east view

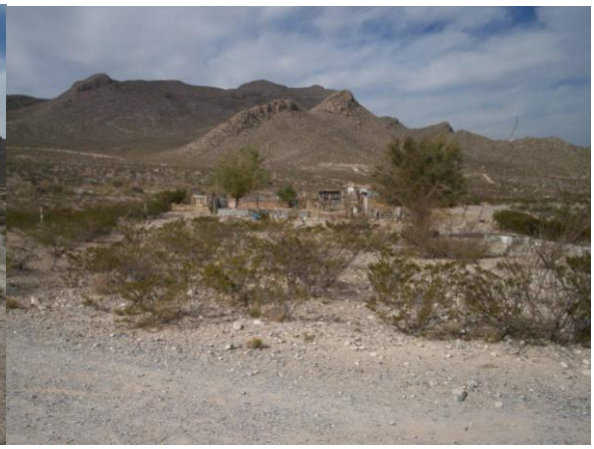

Photo 9 Proximal flow debris Alluvial fan. Photo 10 Proximal alluvial fans flow debris

Photo 11 Snake stream viewing fault structure Photo 12 Coordinate sample point 19 strata 1 and 2

Photo 13 near to east Snake stream Hydraulic Apex. Photo 14 East Snake stream near to topographic apex

Photo 15 Snake stream viewing to west Mountain.Photo 16 like Photo 15 viewing to west Mountain.

Photos taken near Hilario home (Hilario, Lalo, Villalobos, and David) at the back Juarez Mountains and it is possible to see terrain depression caused for normal faults in the Colorado stream at the bottom many neighborhoods located on this sub-basin (P.E.C; 16 DE Septiembre and Luis Etcheverria neighbours)

Point sample number 20; Anapra-Santa Teresa highway three strata Upper Strata 1= Fine soft sand light brown color 70 cm depth (Lomas de Poleo Neighborhood; intermediate strata 2 white cemented clayed evaporitic gypsum of 2 m depth; lower strata of fine and wet sand color light gray the depth was very depth more that 5

meters: GPS UACJ 13R 0349603; 3517071; Elev. 1263m. GPS Brunel 13R 0349605; 3517069; Elev. 1262m

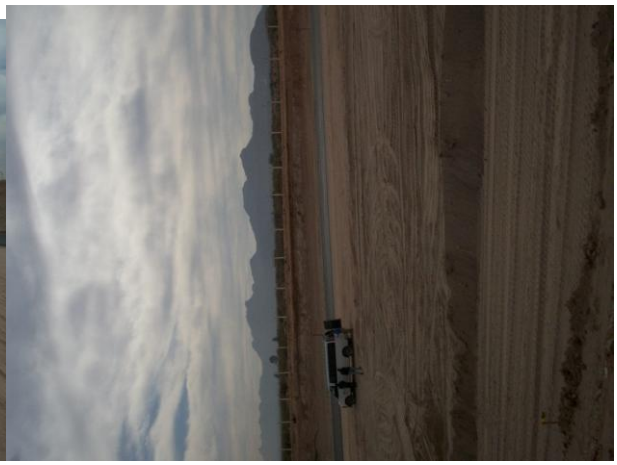

Photo number 1 and 2, Near to sample 20and 21 Strata 1and 2. Anapra-Santa Teresa highway

Photo 3 sample 21 Anapra-Sta Teresa highway Photo 4 strata 3 sample 21

Point of sample number 21; West line of Anapra-Santa Teresa Highway clean, soft, fine and wet sand Coordinates; GPS UACJ= 13R 349709; 3517036; Elev. 1256m; GPS Brunel 13R 0349707; 3517035; 1253m.

Photo 5 sample 21 strata 3 Photo 6 sample 21 strata 3

Photo 7 sample 21 strata 3

Photo 8 sample 21 strata 3

Photo 9 sample 21 strata 3

Photo 10 sample 21 strata 3

Photo 11 sample 21 strata 3

Photo 12 sample 21 strata 3

Photo 13 sample 21 strata 3

Photo 14 sample 21 strata 3

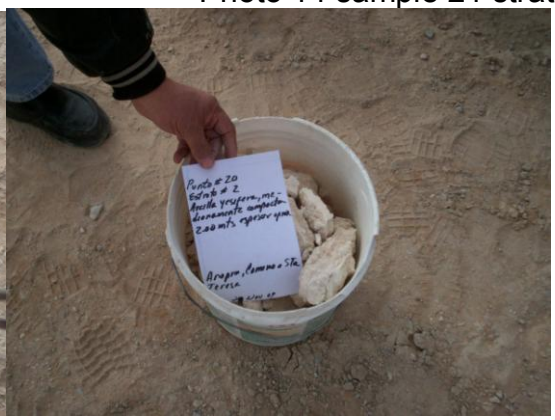

Photo 15 sample 20 strata 1

Photo 16 sample 20 strata 2

Photo 17 sample 20 strata 2

Photo 18 sample 20 strata 2

Photo 19 sample 20 strata 2

Photo 20 sample 20 strata 1

Point number 21: Panoramic Anapra photos GPS UACJ 13R 0351066; 3515296; Elev. 1265m. GPS Brunel 13R 0351063; 3515302; Elev. 1258 m (waypoint number 965)

Photo 1 Anapra to Franklin Mountains

Photo 2 Anapra to Franklin Mountains

Photo 3 Anapra to Juarez Mountains

Photo 4 Anapra to Juarez Mountains

Photo 5 Anapra To Juarez Mountains

Photo 6 Anapra to Juarez Mountains

Photo 7 Anapra

Photo 8 Anapra to Cristo Rey and Franklin Mountains

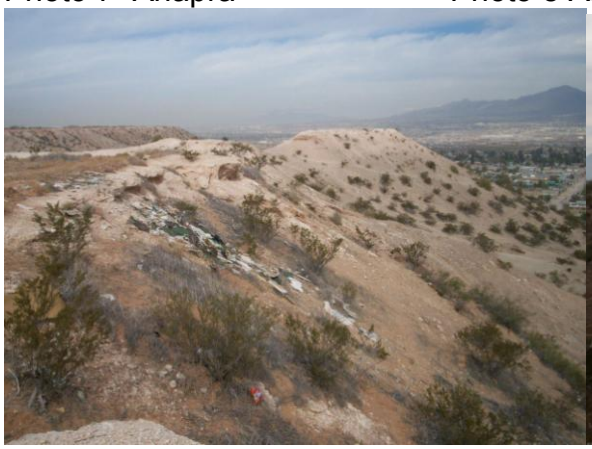

Photo 9 From Anapra to Juarez Mountains

Photo 10 Panoramic from Anapra to Juarez Mountains

Photo 11 Lomas de Poleo

Photo 12 viewing to West 0f Anapra

Photo 13 Panoramic to Cristo Rey

Photo 14 Panoramic Franklin Mountain

Photo 15 Panoramic view to the Anapra basin West to East

APPENDIX 4A2

In the tables 1 and 2 below are presented the summary of the soils sample collected during Field exploration done during June 7 to June 28 of 2012 on the study area. Summary of terraces and alluvial fan soils classification of samples is given in spanish reports (see reports 3 to 23).

ID	USCS	L.L	PI	CI	LVW	CVW	Cc	Cu	Coordinates and Elevation
1742(WH)	(SW)	29.87	6.49	4.50	1568.62	1644.77	20.95	1.14	355464.96;3515946.51 N Elev. 1147 masl
1743 (GH)	(GP)	19.62	2.65	1.70	1715.95	1757.78	66.67	4.34	356099.15E;3515159.88 N; Elev. 1160 masl (GH)
1743 (GH)	(SC) M2b	24.18	7.23	4.10	1470.17	1575.52			356099.15E;3515159.88 N; Elev. 1160 masl (GH)
1744 (Q)	(CL)	22.63	8.03	2.70	1356.29	1471.87			355969.46E;3514911.90N; Elev. 1170 masl (Q)
1744 (Q)	(GP) M3a				1935.19	2020.91	82.14	0.11	355969.46E;3514911.90N; Elev. 1170 masl (Q)
1745 (MP)	(GP)M4				1797.67	1808.37	50.91	0.05	356673.95; 3515308.83 N Elev. 1145 masl
1745(MP)	(GP)M4A				1655.86	1847.59	22.19	1.19	356673.95; 3515308.83 N Elev. 1145 masl
1746(JAC)	(SP)S1M1				1945.33	2013.42	34.44	0.20	356164.71 E;3514977.46N Elev. 1155 masl (JAM)
1747(JAM)	(GP)S2M2				1917.32	2024.71	62.31	0.53	356164.71 E;3514977.46N Elev. 1155 masl (JAM)
1748(16CR)	(SPSM)S3M3	Inap	Inap		1274.46	1386.98	2.11	0.82	
1749(16CR)	(SMSC)S4M4	23.15	5.95	3.50	1371.29	1446.30			
1750(AM)	(SP)S5M5				1775.31	1891.42	37.14	0.33	356673.95; 3515308.83 N Elev. 1145 masl
1751(CC)	(GW)S6M6	24.10	4.77	9.25	1617.36	1798.33	92.86	1.59	357159.26E; 3514609.73N Elev. 1133 masl
1752(NM)	(GP)S7M7				1678.35	IS	145.24	11.28	357448.05E; 3514394.04N Elev. 1150 masl
1753(CHICAL)	(SW)S8M8				1738.62	1814.98	7.97	1.41	
1754(CHIMIJ)	(SM)M2	20.06	0.06	0.0	1487.56	1557.45			
1756(PT)	(GP-GM)M3	18.18	1.39	1.60	1781.59	1943.72	64.29	2.57	
1756(EJG)	(SP)M4				1900.84	1980.33	25.24	0.27	
1757(16B)	(SW-SM)M1	18.75	1.39	3.00	1689.88	1764.69	23.85	1.22	357727.02E; 3512826.21N Elev. 1160 masl
1758(16S)	(GW)				1900.00	1971.76	29.20	1.78	
1759(16M)	(SP)M4				1953.89	1993.48	50.77	0.32	
1760(DNM)	(GW)				1837.97	1949.37	47.86	1.21	

Table 1. Summary of terraces and alluvial fan soils classification of samples is given in spanish reports (see reports 3 to 23). collected from field and explained in methods chapter 3. table shows soils properties obtained from different sites located along Juárez region: 1st column sample identification (ID); 2nd column soil type using Unified Soils Classification System (USCS); 3rd column Liquid Limit (LL); 4th column Plastic Limit (PL); 5th column Contraction Index (CI); 6th column loss Volumetric Weight (DVW).7th Column Curvature Coefficient; 8thColumn Uniformity Coefficient and 9thColumn UTM coordinates location.

ID	USCS	L.L(%)	P.L(%)	C.I(%)	DVW (Kg/cm^3)
100 (CR KM 14+500)	SM-SC	26.51	20.21	5.20	1607.22
101 (CR KM 14+500)	CL	24.22	17.14	3.50	1376.74
102 (CR KM 14+500)	SM	20.53	15.63	2.90	1629.69
103 (CR KM 11+700)	SM	17.46	15.05	2.41	1330.37
104 (CR KM 11+700)	SM-SC	22.82	18.18	5.90	1621.42
105 (CR KM 11+000)	GM-GC	18.53	13.04	2.70	1864.16
106 (CR KM 11+000)	SC	31.05	19.79	0.00	1297.98
107 (CR KM 10+380)	SM-SC	24.86	18.90	1.60	1228.66
108 (CM KM 11+380)	ML-OL	21.16	15.71	3.20	1354.26
109 (CR KM 9+300)	ML-OL	23.72	19.10	2.0	1303.44
110 (CR KM 9+300)	SP-SM	23.10	22.22	0.00	1373.03
111 (CR KM 9+300)	SM	18.80	13.33	2.20	1519.79
112 (Gasera)	SC	30.77	16.88	5.70	1210.00
113 (Gasera)	SC	18.72	9.70	3.20	1629.00
114 (PEC)	CL	30.03	17.78	7.90	1370.00
115 (PEC)	CH	50.95	28.81	15.10	1369.62
116 (PEC)	CH	54.64	28.30	16.40	1371.42
117 (Gasera)	CL	35.71	21.90	7.10	1250.89
118 (Col . 16 Sept)	SM	22.60	20.88	1.20	1204.77
119 (Col. 16 Sept)	CL	56.36	31.67	16.80	1318.00
120 (Col. 16 Sept)	CL	28.27	19.23	9.04	1246.42
121 (ME-JB)	SP-SM	17.42	15.89	0.00	1931.40
122 (ME-JN)	SM	22.50	21.05	0.00	1259.12
123 (COV-JB)	SM	19.03	18.35	1.20	1382.14
124 (Col. CHIH)	SM	18.07	16.13	1.94	1397.50
125 (Col. CHIH)	ML	26.16	21.31	4.50	1392.00
126 (AV-FA)	SM	17.50	16.97	0.00	1637.23
127 (AV-FA)	SC	40.06	24.69	10.50	1378.57
129 (Nogal FV)	SC	25.97	18.75	4.80	1453.00
130 (Reb-CM)	SM	23.24	16.90	0.90	1638.94
131 (Reb-CM)	SP	31.34	14.18	3.20	1667.91

Table 2. Summary of terraces and alluvial fan soils classification of samples collected from field and explained in methods chapter 3. table shows soils properties obtained from different sites located along Juárez region: 1st column sample identification (ID); 2nd column2nd column soil type using Unified Soils Classification System (USCS); 3rd column Liquid Limit (LL); 4th column Plastic Limit (PL); 5th column Contraction Index (CI); 6th column Dry Volumetric Weight (DVW).

Note: Soils classification summary given in tables 1 and 2 are presented in the following shown bellow. These reports are marked with number 2156 to 2177 (the reports are in spanish text in blue colour named Código de Control de Registro). The Soils classification used was the International Unified Soil Classification System (USCS) of the United States ASTM (1985). The soils results details are presented bellow this table.

UNIVERSIDAD AUTONOMA DE CIUDAD JUAREZ

LABORATORIO DE MATERIALES

DEPARTAMENTO DE INGENIERIA CIVIL Y AMBIENTAL

INSTITUTO DE INGENIERIA Y TECNOLOGIA

Título: **INFORME DE PRUEBAS DE SUELOS** | Coordinates: 355464.96 E; 3515946.51 N; Elev. 1147 masl (WH)

Código de Control de Registro: **2156**

OBRA :		PROCEDENCIA :	
UBICACIÓN	**Norzagaray**	LUGAR DE MUESTREO :	**Sondeo Water house**
CONSTRUCTORA :	**Dr. Zuñiga**	FECHA DE PRUEBA :	
MUESTRA Nº.:	**1742**	CANTIDAD DE MATERIAL RECIBIDO :	
FECHA DE MUESTREO :	**28-May-2012**	MATERIAL :	
		TAMAÑO MAX:	

ARENA	**59.69**	GRAVA	**36.20**	GRAVA-ARENA	**95.88**	FINOS	**4.12**

PESO INICIAL : **15,724** PESO INICIAL DE LA FRACCIÓN FINA : **200** gr

CRIBA	ABERTURA DE LA MALLA	MASA RETENIDA	RETENIDO	RETENIDO ACUMULADO	PASA	CRIBA	ABERTURA DE LA MALLA	MASA RETENIDA	RETENIDO	RETENIDO ACUMULADO	PASA
No.	mm	g	%	%	%	No.	mm	g	%	%	%
4"	100.00					No. 8	2.360			0.0	
3 1/2"	87.50					No. 10	2.000	**51.90**	16.56	16.6	47.24
3"	75.00					No. 16	1.180				
2 1/2"	62.50	**0.00**	0.00	0.00	100.00	No. 20	0.840	**60.00**	19.14	35.7	28.10
2"	50.00	**198.00**	1.26	1.26	98.74	No. 30	0.600				
1 1/2"	37.50	**219.00**	1.39	2.65	97.35	No. 40	0.420	**31.60**	10.08	45.8	18.02
1"	25.00	**1,156.00**	7.35	10.00	90.00	No. 50	0.300				
3/4"	19.00	**497.00**	3.16	13.16	86.84	No. 60	0.250	**18.30**	5.84	51.6	12.19
5/8"	16.00	**0.00**	0.00	13.16	86.84	No. 100	0.149	**11.50**	3.67	55.3	8.52
1/2"	12.50	**0.00**	0.00	13.16	86.84	No. 200	0.074	**13.80**	4.40	59.7	4.12
3/8"	9.50	**1,793.00**	11.40	24.57	75.43	PASA No. 200		**12.90**	4.12	63.8	0.00
1/4"	6.35	**0.00**	0.00	24.57	75.43	SUMA TOTAL :		**200.00**	63.80		
No. 4	4.75	**1,829.00**	11.63	36.20	63.80						
PASA No. 4		**10,032.00**	63.80			%DE MATERIAL RET. EN MALLA No.4			**36.20**		
SUMA :		**15,724**	100.00			%DE MATERIAL QUE PASA MALLA No.4			**63.80**		

PÉRDIDA POR LAVADO	
MATERIAL	RETENIDO CRIBA No. 200
PESO MATERIAL SECO, g	104.70
PESO MATERIAL SECO LAVADO, g	187.10
PESO PÉRDIDA POR LAVADO, g	-82.40
%PÉRDIDA POR LAVADO	-78.70%
%PÉRDIDA LAVADO CORREGIDO	
%PÉRDIDA LAVADO TOTAL	

OBSERVACIONES:

D10= 0.19
D30= 0.93
D60= 3.98

REFERENCIAS:	LUGAR	FECHA DE EMISION
ACI-304 **NMX C-170 - 97 ONNCCE** **NMX C-77 - 97 ONNCCE** **NMX C-84 - 90** **NMX C - 111-88**	ELABORÓ	REVISÓ
	NOMBRE Y FIRMA	NOMBRE Y FIRMA

AVENIDA DEL CHARRO 450 NORTE CD. JUAREZ CHIH.

UNIVERSIDAD AUTONOMA DE CIUDAD JUAREZ

LABORATORIO DE MATERIALES

DEPARTAMENTO DE INGENIERIA CIVIL Y AMBIENTAL

INSTITUTO DE INGENIERIA Y TECNOLOGIA

Título: INFORME DE PRUEBAS DE SUELOS

Coordinates: 356099.15 E; 3515159.88 N; Elev. 1160 masl (GH)

Código de Control de Registro: 2157

OBRA :		PROCEDENCIA :	
UBICACIÓN	Col. Felipe Ángeles	LUGAR DE MUESTREO :	calles Guadalajara y Hortencia
CONSTRUCTORA :	Dr. Zuñiga	FECHA DE PRUEBA :	29-May-2012
MUESTRA Nº.:	1743	CANTIDAD DE MATERIAL RECIBIDO :	
FECHA DE MUESTREO :	28-May-2012	MATERIAL :	Muestra 2A
		TAMAÑO MAX:	

ARENA	25.56	GRAVA	70.94	GRAVA-ARENA	96.50	FINOS	3.50

PESO INICIAL : 17,640 PESO INICIAL DE LA FRACCIÓN FINA : 200 gr

CRIBA	ABERTURA DE LA MALLA	MASA RETENIDA	RETENIDO	RETENIDO ACUMULADO	PASA	CRIBA	ABERTURA DE LA MALLA	MASA RETENIDA	RETENIDO	RETENIDO ACUMULADO	PASA
No.	mm	g	%	%	%	No.	mm	g	%	%	%
4"	100.00					No. 8	2.360			0.0	
3 1/2"	87.50					No. 10	2.000	50.80	7.38	7.4	21.68
3"	75.00					No. 16	1.180				
2 1/2"	62.50	0.00	0.00	0.00	100.00	No. 20	0.840	32.60	4.74	12.1	16.94
2"	50.00	0.00	0.00	0.00	100.00	No. 30	0.600				
1 1/2"	37.50	1,831.00	10.38	10.38	89.62	No. 40	0.420	26.90	3.91	16.0	13.04
1"	25.00	3,308.00	18.75	29.13	70.87	No. 50	0.300				
3/4"	19.00	2,083.00	11.81	40.94	59.06	No. 60	0.250	30.90	4.49	20.5	8.55
5/8"	16.00	0.00	0.00	40.94	59.06	No. 100	0.149	18.00	2.62	23.1	5.93
1/2"	12.50	0.00	0.00	40.94	59.06	No. 200	0.074	16.70	2.43	25.6	3.50
3/8"	9.50	3,203.00	18.16	59.10	40.90	PASA No. 200		24.10	3.50	29.1	0.00
1/4"	6.35	0.00	0.00	59.10	40.90	SUMA TOTAL :		200.00	29.06		
No. 4	4.75	2,088.00	11.84	70.94	29.06						
PASA No. 4		5,127.00	29.06			%DE MATERIAL RET. EN MALLA No. 4			70.94		
SUMA :		17,640	100.00			%DE MATERIAL QUE PASA MALLA No. 4			29.06		

PÉRDIDA POR LAVADO

MATERIAL	RETENIDO CRIBA No. 200
PESO MATERIAL SECO, g	104.70
PESO MATERIAL SECO LAVADO, g	175.90
PESO PÉRDIDA POR LAVADO, g	-71.20
%PÉRDIDA POR LAVADO	-68.00%
%PÉRDIDA LAVADO CORREGIDO	
%PÉRDIDA LAVADO TOTAL	

OBSERVACIONES:

D10= 0.3
D30= 5.1
D60= 20

REFERENCIAS:	LUGAR	FECHA DE EMISION
ACI-304 NMX C-170 - 97 ONNCCE NMX C-77 - 97 ONNCCE NMX C-84 - 90 NMX C - 111-88	ELABORÓ	REVISÓ
	NOMBRE Y FIRMA	NOMBRE Y FIRMA

AVENIDA DEL CHARRO 450 NORTE CD. JUAREZ CHIH.

UNIVERSIDAD AUTONOMA DE CIUDAD JUAREZ

LABORATORIO DE MATERIALES

DEPARTAMENTO DE INGENIERIA CIVIL Y AMBIENTAL

INSTITUTO DE INGENIERIA Y TECNOLOGIA

Título: **INFORME DE PRUEBAS DE SUELOS**

Coordinates: 356099.15 E; 3515159.88 N; Elev. 1160 masl (GH)

Código de Control de Registro: **2158**

OBRA :		PROCEDENCIA :	
UBICACIÓN	**Col. Felipe Ángeles**	LUGAR DE MUESTREO :	**calles Guadalajara y Hortencia**
CONSTRUCTORA :	**Dr. Zuñiga**	FECHA DE PRUEBA :	**29-May-2012**
MUESTRA Nº.:	**1743**	CANTIDAD DE MATERIAL RECIBIDO :	
FECHA DE MUESTREO :	**28-May-2012**	MATERIAL :	Muestra 2B
		TAMAÑO MAX:	

ARENA	**71.40**	GRAVA	**0.00**	GRAVA-ARENA	**71.40**	FINOS	**28.60**

PESO INICIAL : **1** PESO INICIAL DE LA FRACCIÓN FINA : **200** gr

CRIBA	ABERTURA DE LA MALLA	MASA RETENIDA	RETENIDO	RETENIDO ACUMULADO	PASA	CRIBA	ABERTURA DE LA MALLA	MASA RETENIDA	RETENIDO	RETENIDO ACUMULADO	PASA
No.	mm	g	%	%	%	No.	mm	g	%	%	%
4"	100.00					No. 8	2.360			0.0	
3 1/2"	87.50					No. 10	2.000	**22.20**	11.10	11.1	88.90
3"	75.00					No. 16	1.180				
2 1/2"	62.50	**0.00**	0.00	0.00	100.00	No. 20	0.840	**37.10**	18.55	29.7	70.35
2"	50.00	**0.00**	0.00	0.00	100.00	No. 30	0.600				
1 1/2"	37.50	**0.00**	0.00	0.00	100.00	No. 40	0.420	**26.60**	13.30	43.0	57.05
1"	25.00	**0.00**	0.00	0.00	100.00	No. 50	0.300				
3/4"	19.00	**0.00**	0.00	0.00	100.00	No. 60	0.250	**13.00**	6.50	49.5	50.55
5/8"	16.00	**0.00**	0.00	0.00	100.00	No. 100	0.149	**11.30**	5.65	55.1	44.90
1/2"	12.50	**0.00**	0.00	0.00	100.00	No. 200	0.074	**32.60**	16.30	71.4	28.60
3/8"	9.50	**0.00**	0.00	0.00	100.00	PASA No. 200		**57.20**	28.60	100.0	0.00
1/4"	6.35	**0.00**	0.00	0.00	100.00	SUMA TOTAL :		**200.00**	100.00		
No. 4	4.75	**0.00**	0.00	0.00	100.00						
PASA No. 4		**0.00**	100.00			%DE MATERIAL RET. EN MALLA No.4			**0.00**		
SUMA :		**0**	100.00			%DE MATERIAL QUE PASA MALLA No.4			**100.00**		

PÉRDIDA POR LAVADO	
MATERIAL	RETENIDO CRIBA No. 200
PESO MATERIAL SECO, g	104.70
PESO MATERIAL SECO LAVADO, g	142.80
PESO PÉRDIDA POR LAVADO, g	-38.10
%PÉRDIDA POR LAVADO	-36.39%
%PÉRDIDA LAVADO CORREGIDO	
%PÉRDIDA LAVADO TOTAL	

OBSERVACIONES:

REFERENCIAS:	LUGAR	FECHA DE EMISION
ACI-304 **NMX C-170 - 97 ONNCCE** **NMX C-77 - 97 ONNCCE** **NMX C-84 - 90** **NMX C - 111-88**	ELABORÓ	REVISÓ
	NOMBRE Y FIRMA	NOMBRE Y FIRMA

AVENIDA DEL CHARRO 450 NORTE CD. JUAREZ CHIH.

UNIVERSIDAD AUTONOMA DE CIUDAD JUAREZ

LABORATORIO DE MATERIALES

DEPARTAMENTO DE INGENIERIA CIVIL Y AMBIENTAL

INSTITUTO DE INGENIERIA Y TECNOLOGIA

Título: **INFORME DE PRUEBAS DE SUELOS**

Coordinates: 355969.46 E; 3514911.90 N; Elev. 1170 masl (Q)

Código de Control de Registro: **2159**

OBRA :		PROCEDENCIA :	
UBICACIÓN	**Col. Felipe Ángeles**	LUGAR DE MUESTREO :	**calle Quelite**
CONSTRUCTORA :	**Dr. Zuñiga**	FECHA DE PRUEBA :	**29-May-2012**
MUESTRA Nº.:	**1744**	CANTIDAD DE MATERIAL RECIBIDO :	
FECHA DE MUESTREO :	**28-May-2012**	MATERIAL :	
		TAMAÑO MAX:	

ARENA	**44.20**	GRAVA	**#DIV/0!**	GRAVA-ARENA	**#DIV/0!**	FINOS	**#####**

PESO INICIAL : **0** PESO INICIAL DE LA FRACCIÓN FINA : **200** gr

CRIBA	ABERTURA DE LA MALLA	MASA RETENIDA	RETENIDO	RETENIDO ACUMULADO	PASA	CRIBA	ABERTURA DE LA MALLA	MASA RETENIDA	RETENIDO	RETENIDO ACUMULADO	PASA
No.	mm	g	%	%	%	No.	mm	g	%	%	%
4"	100.00					No. 8	2.360			0.0	
3 1/2"	87.50					No. 10	2.000	**8.60**	4.30	4.3	95.70
3"	75.00					No. 16	1.180				
2 1/2"	62.50	**0.00**	#DIV/0!	#DIV/0!	#DIV/0!	No. 20	0.840	**6.20**	3.10	7.4	92.60
2"	50.00	**0.00**	#DIV/0!	#DIV/0!	#DIV/0!	No. 30	0.600				
1 1/2"	37.50	**0.00**	#DIV/0!	#DIV/0!	#DIV/0!	No. 40	0.420	**7.90**	3.95	11.4	88.65
1"	25.00	**0.00**	#DIV/0!	#DIV/0!	#DIV/0!	No. 50	0.300				
3/4"	19.00	**0.00**	#DIV/0!	#DIV/0!	#DIV/0!	No. 60	0.250	**6.10**	3.05	14.4	85.60
5/8"	16.00	**0.00**	#DIV/0!	#DIV/0!	#DIV/0!	No. 100	0.149	**13.80**	6.90	21.3	78.70
1/2"	12.50	**0.00**	#DIV/0!	#DIV/0!	#DIV/0!	No. 200	0.074	**45.80**	22.90	44.2	55.80
3/8"	9.50	**0.00**	#DIV/0!	#DIV/0!	#DIV/0!	PASA No. 200		**111.60**	55.80	100.0	0.00
1/4"	6.35	**0.00**	#DIV/0!	#DIV/0!	#DIV/0!	SUMA TOTAL :		**200.00**	100.00		
No. 4	4.75	**0.00**	#DIV/0!	#DIV/0!	100.00						
PASA No. 4		**0.00**	100.00			% DE MATERIAL RET. EN MALLA No. 4			**#DIV/0!**		
SUMA :		**0**	0.00			% DE MATERIAL QUE PASA MALLA No. 4			**100.00**		

PÉRDIDA POR LAVADO	
MATERIAL	RETENIDO CRIBA No. 200
PESO MATERIAL SECO, g	104.70
PESO MATERIAL SECO LAVADO, g	88.40
PESO PÉRDIDA POR LAVADO, g	16.30
%PÉRDIDA POR LAVADO	15.57%
%PÉRDIDA LAVADO CORREGIDO	
%PÉRDIDA LAVADO TOTAL	

OBSERVACIONES:

REFERENCIAS:	LUGAR	FECHA DE EMISION
ACI-304 **NMX C-170 - 97 ONNCCE** **NMX C-77 - 97 ONNCCE** **NMX C-84 - 90** **NMX C - 111-88**	ELABORÓ	REVISÓ
	NOMBRE Y FIRMA	NOMBRE Y FIRMA

AVENIDA DEL CHARRO 450 NORTE CD. JUAREZ CHIH.

UNIVERSIDAD AUTONOMA DE CIUDAD JUAREZ

LABORATORIO DE MATERIALES

DEPARTAMENTO DE INGENIERIA CIVIL Y AMBIENTAL

INSTITUTO DE INGENIERIA Y TECNOLOGIA

Título: INFORME DE PRUEBAS DE SUELOS

Coordinates: 355969.46 E; 3514911.90 N; Elev. 1170 masl (Q)

Código de Control de Registro: 2160

OBRA :		PROCEDENCIA :	
UBICACIÓN	Col. Felipe Àngeles	LUGAR DE MUESTREO :	calle Quelite
CONSTRUCTORA :	Dr. Zuñiga	FECHA DE PRUEBA :	29-May-2012
MUESTRA Nº.:	1744	CANTIDAD DE MATERIAL RECIBIDO :	
FECHA DE MUESTREO :	28-May-2012	MATERIAL :	
		TAMAÑO MAX:	

ARENA	33.61	GRAVA	64.32	GRAVA-ARENA	97.93	FINOS	2.07

PESO INICIAL : 19,332 PESO INICIAL DE LA FRACCIÓN FINA : 200 gr

CRIBA	ABERTURA DE LA MALLA	MASA RETENIDA	RETENIDO	RETENIDO ACUMULADO	PASA	CRIBA	ABERTURA DE LA MALLA	MASA RETENIDA	RETENIDO	RETENIDO ACUMULADO	PASA
No.	mm	g	%	%	%	No.	mm	g	%	%	%
4"	100.00					No. 8	2.360			0.0	
3 1/2"	87.50					No. 10	2.000	21.60	3.85	3.9	31.82
3"	75.00					No. 16	1.180				
2 1/2"	62.50	0.00	0.00	0.00	100.00	No. 20	0.840	10.10	1.80	5.7	30.02
2"	50.00	2,704.00	13.99	13.99	86.01	No. 30	0.600				
1 1/2"	37.50	900.00	4.66	18.64	81.36	No. 40	0.420	31.40	5.60	11.3	24.42
1"	25.00	3,629.00	18.77	37.41	62.59	No. 50	0.300				
3/4"	19.00	1,818.00	9.40	46.82	53.18	No. 60	0.250	103.10	18.39	29.6	6.03
5/8"	16.00	0.00	0.00	46.82	53.18	No. 100	0.149	15.30	2.73	32.4	3.30
1/2"	12.50	1,450.00	7.50	54.32	45.68	No. 200	0.074	6.90	1.23	33.6	2.07
3/8"	9.50	616.00	3.19	57.51	42.49	PASA No. 200		11.60	2.07	35.7	0.00
1/4"	6.35	861.00	4.45	61.96	38.04	SUMA TOTAL :		200.00	35.68		
No. 4	4.75	457.00	2.36	64.32	35.68						
PASA No. 4		6,897.00	35.68			%DE MATERIAL RET. EN MALLA No. 4			64.32		
SUMA :		19,332	100.00			%DE MATERIAL QUE PASA MALLA No. 4			35.68		

PÉRDIDA POR LAVADO	
MATERIAL	RETENIDO CRIBA No. 200
PESO MATERIAL SECO, g	104.70
PESO MATERIAL SECO LAVADO, g	188.40
PESO PÉRDIDA POR LAVADO, g	-83.70
%PÉRDIDA POR LAVADO	-79.94%
%PÉRDIDA LAVADO CORREGIDO	
%PÉRDIDA LAVADO TOTAL	

OBSERVACIONES:

D10= 0.28
D30= 0.85
D60= 23

REFERENCIAS:

ACI-304
NMX C-170 - 97 ONNCCE
NMX C-77 - 97 ONNCCE
NMX C-84 - 90
NMX C - 111-88

LUGAR	FECHA DE EMISION
ELABORÓ	REVISÓ
NOMBRE Y FIRMA	NOMBRE Y FIRMA

AVENIDA DEL CHARRO 450 NORTE CD. JUAREZ CHIH.

UNIVERSIDAD AUTONOMA DE CIUDAD JUAREZ

LABORATORIO DE MATERIALES

DEPARTAMENTO DE INGENIERIA CIVIL Y AMBIENTAL

INSTITUTO DE INGENIERIA Y TECNOLOGIA

Título: INFORME DE PRUEBAS DE SUELOS

Coordinates: 356164.71 E; 3514977.46N; Elev. 1155 masl (JAM)

Código de Control de Registro: 2163

OBRA :		PROCEDENCIA :	
UBICACIÓN	Río	LUGAR DE MUESTREO :	calle Jacintos
CONSTRUCTORA :	Dr. Zuñiga	FECHA DE PRUEBA :	5-Jun-2012
MUESTRA Nº.:	1746	CANTIDAD DE MATERIAL RECIBIDO :	
FECHA DE MUESTREO :	4-Jun-2012	MATERIAL :	
		TAMAÑO MAX:	

ARENA	49.49	GRAVA	48.98	GRAVA-ARENA	98.47	FINOS	1.53

PESO INICIAL : 20,698 PESO INICIAL DE LA FRACCIÓN FINA : 200 gr

CRIBA	ABERTURA DE LA MALLA	MASA RETENIDA	RETENIDO	RETENIDO ACUMULADO	PASA	CRIBA	ABERTURA DE LA MALLA	MASA RETENIDA	RETENIDO	RETENIDO ACUMULADO	PASA
No.	mm	g	%	%	%	No.	mm	g	%	%	%
4"	100.00					No. 8	2.360			0.0	
3 1/2"	87.50					No. 10	2.000	37.90	9.67	9.7	41.36
3"	75.00					No. 16	1.180				
2 1/2"	62.50	0.00	0.00	0.00	100.00	No. 20	0.840	34.20	8.73	18.4	32.63
2"	50.00	1,415.00	6.84	6.84	93.16	No. 30	0.600				
1 1/2"	37.50	2,278.00	11.01	17.84	82.16	No. 40	0.420	45.10	11.51	29.9	21.12
1"	25.00	1,683.00	8.13	25.97	74.03	No. 50	0.300				
3/4"	19.00	778.00	3.76	29.73	70.27	No. 60	0.250	49.70	12.68	42.6	8.44
5/8"	16.00	0.00	0.00	29.73	70.27	No. 100	0.149	11.60	2.96	45.5	5.49
1/2"	12.50	0.00	0.00	29.73	70.27	No. 200	0.074	15.50	3.95	49.5	1.53
3/8"	9.50	2,051.00	9.91	39.64	60.36	PASA No. 200		6.00	1.53	51.0	0.00
1/4"	6.35	0.00	0.00	39.64	60.36	SUMA TOTAL :		200.00	51.02		
No. 4	4.75	1,932.00	9.33	48.98	51.02						
PASA No. 4		7,752.00	51.02			%DE MATERIAL RET. EN MALLA No.4			48.98		
SUMA :		17,889	100.00			%DE MATERIAL QUE PASA MALLA No.4			51.02		

PÉRDIDA POR LAVADO	
MATERIAL	RETENIDO CRIBA No. 200
PESO MATERIAL SECO, g	104.70
PESO MATERIAL SECO LAVADO, g	194.00
PESO PÉRDIDA POR LAVADO, g	-89.30
%PÉRDIDA POR LAVADO	-85.29%
%PÉRDIDA LAVADO CORREGIDO	
%PÉRDIDA LAVADO TOTAL	

OBSERVACIONES:

D10= 0.27
D30= 0.7
D60= 9.3

REFERENCIAS:

ACI-304
NMX C-170 - 97 ONNCCE
NMX C-77 - 97 ONNCCE
NMX C-84 - 90
NMX C - 111-88

LUGAR	FECHA DE EMISION
ELABORÓ	REVISÓ
NOMBRE Y FIRMA	NOMBRE Y FIRMA

AVENIDA DEL CHARRO 450 NORTE CD. JUAREZ CHIH.

UNIVERSIDAD AUTONOMA DE CIUDAD JUAREZ

LABORATORIO DE MATERIALES

DEPARTAMENTO DE INGENIERIA CIVIL Y AMBIENTAL

INSTITUTO DE INGENIERIA Y TECNOLOGIA

Título: **INFORME DE PRUEBAS DE SUELOS** Coordinates: 356164.71 E; 3514977.46N; Elev. 1155 masl (JAM)

Código de Control de Registro: **2164**

OBRA :		PROCEDENCIA :	
UBICACIÓN	**Abánico**	LUGAR DE MUESTREO :	**calles Jacintos y Michoacán**
CONSTRUCTORA :	**Dr. Zuñiga**	FECHA DE PRUEBA :	**5-Jun-2012**
MUESTRA Nº.:	**1747**	CANTIDAD DE MATERIAL RECIBIDO :	
FECHA DE MUESTREO :	**4-Jun-2012**	MATERIAL :	
		TAMAÑO MAX:	

ARENA	**48.29**	GRAVA	**48.98**	GRAVA-ARENA	**97.27**	FINOS	**2.73**

PESO INICIAL : **20,814** PESO INICIAL DE LA FRACCIÓN FINA : **200** gr

CRIBA	ABERTURA DE LA MALLA	MASA RETENIDA	RETENIDO	RETENIDO ACUMULADO	PASA	CRIBA	ABERTURA DE LA MALLA	MASA RETENIDA	RETENIDO	RETENIDO ACUMULADO	PASA
No.	mm	g	%	%	%	No.	mm	g	%	%	%
4"	100.00					No. 8	2.360			0.0	
3 1/2"	87.50					No. 10	2.000	**56.70**	14.46	14.5	36.55
3"	75.00					No. 16	1.180				
2 1/2"	62.50	**0.00**	0.00	0.00	100.00	No. 20	0.840	**24.20**	6.17	20.6	30.38
2"	50.00	**198.00**	0.95	0.95	99.05	No. 30	0.600				
1 1/2"	37.50	**1,130.00**	5.43	6.38	93.62	No. 40	0.420	**11.70**	2.98	23.6	27.40
1"	25.00	**1,768.00**	8.49	14.87	85.13	No. 50	0.300				
3/4"	19.00	**1,343.00**	6.45	21.33	78.67	No. 60	0.250	**22.60**	5.77	29.4	21.63
5/8"	16.00	**0.00**	0.00	21.33	78.67	No. 100	0.149	**29.50**	7.53	36.9	14.11
1/2"	12.50	**0.00**	0.00	21.33	78.67	No. 200	0.074	**44.60**	11.38	48.3	2.73
3/8"	9.50	**3,268.00**	15.70	37.03	62.97	PASA No. 200		**10.70**	2.73	51.0	0.00
1/4"	6.35	**0.00**	0.00	37.03	62.97	SUMA TOTAL :		**200.00**	51.02		
No. 4	4.75	**2,488.00**	11.95	48.98	51.02						
PASA No. 4		**10,619.00**	51.02			%DE MATERIAL RET. EN MALLA No. 4			**48.98**		
SUMA :		**20,814**	100.00			%DE MATERIAL QUE PASA MALLA No. 4			**51.02**		

PÉRDIDA POR LAVADO

MATERIAL	RETENIDO CRIBA No. 200
PESO MATERIAL SECO, g	104.70
PESO MATERIAL SECO LAVADO, g	189.30
PESO PÉRDIDA POR LAVADO, g	-84.60
%PÉRDIDA POR LAVADO	-80.80%
%PÉRDIDA LAVADO CORREGIDO	
%PÉRDIDA LAVADO TOTAL	

OBSERVACIONES:

D10= 0.13
D30= 0.8
D60= 8.1

REFERENCIAS:	LUGAR	FECHA DE EMISION
ACI-304 **NMX C-170 - 97 ONNCCE** **NMX C-77 - 97 ONNCCE** **NMX C-84 - 90** **NMX C - 111-88**	ELABORÓ	REVISÓ
	NOMBRE Y FIRMA	NOMBRE Y FIRMA

AVENIDA DEL CHARRO 450 NORTE CD. JUAREZ CHIH.

UNIVERSIDAD AUTONOMA DE CIUDAD JUAREZ

LABORATORIO DE MATERIALES

DEPARTAMENTO DE INGENIERIA CIVIL Y AMBIENTAL

INSTITUTO DE INGENIERIA Y TECNOLOGIA

Título: INFORME DE PRUEBAS DE SUELOS

Código de Control de Registro: 2165

OBRA :		PROCEDENCIA :	
UBICACIÓN	13R0354531 355411	LUGAR DE MUESTREO :	16 de septiembre y Camino Real
CONSTRUCTORA :	Dr. Zuñiga	FECHA DE PRUEBA :	5-Jun-2012
MUESTRA Nº.:	1748	CANTIDAD DE MATERIAL RECIBIDO :	
FECHA DE MUESTREO :	4-Jun-2012	MATERIAL :	
		TAMAÑO MAX:	

ARENA	93.65	GRAVA	0.00	GRAVA-ARENA	93.65	FINOS	6.35

PESO INICIAL : 1 PESO INICIAL DE LA FRACCIÓN FINA : 200 gr

CRIBA	ABERTURA DE LA MALLA	MASA RETENIDA	RETENIDO	RETENIDO ACUMULADO	PASA	CRIBA	ABERTURA DE LA MALLA	MASA RETENIDA	RETENIDO	RETENIDO ACUMULADO	PASA
No.	mm	g	%	%	%	No.	mm	g	%	%	%
4"	100.00					No. 8	2.360			0.0	
3 1/2"	87.50					No. 10	2.000	0.00	0.00	0.0	100.00
3"	75.00					No. 16	1.180				
2 1/2"	62.50	0.00	0.00	0.00	100.00	No. 20	0.840	0.10	0.05	0.1	99.95
2"	50.00	0.00	0.00	0.00	100.00	No. 30	0.600				
1 1/2"	37.50	0.00	0.00	0.00	100.00	No. 40	0.420	1.20	0.60	0.7	99.35
1"	25.00	0.00	0.00	0.00	100.00	No. 50	0.300				
3/4"	19.00	0.00	0.00	0.00	100.00	No. 60	0.250	25.10	12.55	13.2	86.80
5/8"	16.00	0.00	0.00	0.00	100.00	No. 100	0.149	56.40	28.20	41.4	58.60
1/2"	12.50	0.00	0.00	0.00	100.00	No. 200	0.074	104.50	52.25	93.7	6.35
3/8"	9.50	0.00	0.00	0.00	100.00	PASA No. 200		12.70	6.35	100.0	0.00
1/4"	6.35	0.00	0.00	0.00	100.00	SUMA TOTAL :		200.00	100.00		
No. 4	4.75	0.00	0.00	0.00	100.00						
PASA No. 4		7,752.00	100.00			%DE MATERIAL RET. EN MALLA No. 4			0.00		
SUMA :		7,752	100.00			%DE MATERIAL QUE PASA MALLA No. 4			100.00		

PÉRDIDA POR LAVADO	
MATERIAL	RETENIDO CRIBA No. 200
PESO MATERIAL SECO, g	104.70
PESO MATERIAL SECO LAVADO, g	187.30
PESO PÉRDIDA POR LAVADO, g	-82.60
%PÉRDIDA POR LAVADO	-78.89%
%PÉRDIDA LAVADO CORREGIDO	
%PÉRDIDA LAVADO TOTAL	

OBSERVACIONES:

D10= 0.076
D30= 0.1
D60= 0.16

REFERENCIAS:	LUGAR	FECHA DE EMISION
ACI-304 NMX C-170 - 97 ONNCCE NMX C-77 - 97 ONNCCE NMX C-84 - 90 NMX C - 111-88	ELABORÓ	REVISÓ
	NOMBRE Y FIRMA	NOMBRE Y FIRMA

AVENIDA DEL CHARRO 450 NORTE CD. JUAREZ CHIH.

UNIVERSIDAD AUTONOMA DE CIUDAD JUAREZ

LABORATORIO DE MATERIALES

DEPARTAMENTO DE INGENIERIA CIVIL Y AMBIENTAL

INSTITUTO DE INGENIERIA Y TECNOLOGIA

Título: **INFORME DE PRUEBAS DE SUELOS**

Código de Control de Registro: **2166**

OBRA :		PROCEDENCIA :	
UBICACIÓN	13R0354531 355411	LUGAR DE MUESTREO :	16 de septiembre y Camino Real
CONSTRUCTORA :	Dr. Zuñiga	FECHA DE PRUEBA :	
MUESTRA Nº.:	1749	CANTIDAD DE MATERIAL RECIBIDO :	
FECHA DE MUESTREO :	4-Jun-2012	MATERIAL :	
		TAMAÑO MAX:	

ARENA	73.20	GRAVA	0.00	GRAVA-ARENA	73.20	FINOS	26.80

PESO INICIAL : 1 PESO INICIAL DE LA FRACCIÓN FINA : 200 gr

CRIBA	ABERTURA DE LA MALLA	MASA RETENIDA	RETENIDO	RETENIDO ACUMULADO	PASA	CRIBA	ABERTURA DE LA MALLA	MASA RETENIDA	RETENIDO	RETENIDO ACUMULADO	PASA
No.	mm	g	%	%	%	No.	mm	g	%	%	%
4"	100.00					No. 8	2.360			0.0	
3 1/2"	87.50					No. 10	2.000	0.00	0.00	0.0	100.00
3"	75.00					No. 16	1.180				
2 1/2"	62.50	0.00	0.00	0.00	100.00	No. 20	0.840	0.10	0.05	0.1	99.95
2"	50.00	0.00	0.00	0.00	100.00	No. 30	0.600				
1 1/2"	37.50	0.00	0.00	0.00	100.00	No. 40	0.420	4.20	2.10	2.2	97.85
1"	25.00	0.00	0.00	0.00	100.00	No. 50	0.300				
3/4"	19.00	0.00	0.00	0.00	100.00	No. 60	0.250	39.90	19.95	22.1	77.90
5/8"	16.00	0.00	0.00	0.00	100.00	No. 100	0.149	56.20	28.10	50.2	49.80
1/2"	12.50	0.00	0.00	0.00	100.00	No. 200	0.074	46.00	23.00	73.2	26.80
3/8"	9.50	0.00	0.00	0.00	100.00	PASA No. 200		53.60	26.80	100.0	0.00
1/4"	6.35	0.00	0.00	0.00	100.00	SUMA TOTAL :		200.00	100.00		
No. 4	4.75	0.00	0.00	0.00	100.00						
PASA No. 4		7,752.00	100.00			%DE MATERIAL RET. EN MALLA No.4			0.00		
SUMA :		7,752	100.00			%DE MATERIAL QUE PASA MALLA No.4			100.00		

PÉRDIDA POR LAVADO

MATERIAL	RETENIDO CRIBA No. 200
PESO MATERIAL SECO, g	104.70
PESO MATERIAL SECO LAVADO, g	146.40
PESO PÉRDIDA POR LAVADO, g	-41.70
%PÉRDIDA POR LAVADO	-39.83%
%PÉRDIDA LAVADO CORREGIDO	
%PÉRDIDA LAVADO TOTAL	

OBSERVACIONES:

REFERENCIAS:

ACI-304
NMX C-170 - 97 ONNCCE
NMX C-77 - 97 ONNCCE
NMX C-84 - 90
NMX C - 111-88

LUGAR	FECHA DE EMISION
ELABORÓ	REVISÓ
NOMBRE Y FIRMA	NOMBRE Y FIRMA

AVENIDA DEL CHARRO 450 NORTE CD. JUAREZ CHIH.

UNIVERSIDAD AUTONOMA DE CIUDAD JUAREZ

LABORATORIO DE MATERIALES

DEPARTAMENTO DE INGENIERIA CIVIL Y AMBIENTAL

INSTITUTO DE INGENIERIA Y TECNOLOGIA

Título: **INFORME DE PRUEBAS DE SUELOS** Coordinates: 356673.95 E;3515308.83; Elev. 1145 masl (AM)

Código de Control de Registro: **2167**

OBRA :		PROCEDENCIA :	**Déposito grava-arena de río**
UBICACIÓN	**Col. Ampliación Felipe Ángeles**	LUGAR DE MUESTREO :	**Arroyo del Mimbre**
CONSTRUCTORA :	**Dr. Zuñiga**	FECHA DE PRUEBA :	
MUESTRA Nº.:	**1750**	CANTIDAD DE MATERIAL RECIBIDO :	
FECHA DE MUESTREO :	**4-Jun-2012**	MATERIAL :	
		TAMAÑO MAX:	

ARENA	**54.21**	GRAVA	**41.99**	GRAVA-ARENA	**96.20**	FINOS	**3.80**

PESO INICIAL : **18,082** PESO INICIAL DE LA FRACCIÓN FINA : **200** gr

CRIBA	ABERTURA DE LA MALLA	MASA RETENIDA	RETENIDO	RETENIDO ACUMULADO	PASA	CRIBA	ABERTURA DE LA MALLA	MASA RETENIDA	RETENIDO	RETENIDO ACUMULADO	PASA
No.	mm	g	%	%	%	No.	mm	g	%	%	%
4"	100.00					No. 8	2.360			0.0	
3 1/2"	87.50					No. 10	2.000	**28.90**	8.38	8.4	49.63
3"	75.00					No. 16	1.180				
2 1/2"	62.50	**0.00**	0.00	0.00	100.00	No. 20	0.840	**39.80**	11.54	19.9	38.09
2"	50.00	**0.00**	0.00	0.00	100.00	No. 30	0.600				
1 1/2"	37.50	**400.00**	2.21	2.21	97.79	No. 40	0.420	**36.10**	10.47	30.4	27.61
1"	25.00	**496.00**	2.74	4.96	95.04	No. 50	0.300				
3/4"	19.00	**1,010.00**	5.59	10.54	89.46	No. 60	0.250	**29.80**	8.64	39.0	18.97
5/8"	16.00	**0.00**	0.00	10.54	89.46	No. 100	0.149	**27.30**	7.92	47.0	11.05
1/2"	12.50	**0.00**	0.00	10.54	89.46	No. 200	0.074	**25.00**	7.25	54.2	3.80
3/8"	9.50	**2,819.00**	15.59	26.13	73.87	PASA No. 200		**13.10**	3.80	58.0	0.00
1/4"	6.35	**0.00**	0.00	26.13	73.87	SUMA TOTAL :		**200.00**	58.01		
No. 4	4.75	**2,867.00**	15.86	41.99	58.01						
PASA No. 4		**10,490.00**	58.01			%DE MATERIAL RET. EN MALLA No.4			**41.99**		
SUMA :		**18,082**	100.00			%DE MATERIAL QUE PASA MALLA No.4			**58.01**		

PÉRDIDA POR LAVADO	
MATERIAL	RETENIDO CRIBA No. 200
PESO MATERIAL SECO, g	104.70
PESO MATERIAL SECO LAVADO, g	186.90
PESO PÉRDIDA POR LAVADO, g	-82.20
%PÉRDIDA POR LAVADO	-78.51%
%PÉRDIDA LAVADO CORREGIDO	
%PÉRDIDA LAVADO TOTAL	

OBSERVACIONES:

D10= 0.14
D30= 0.49
D60= 5.2

REFERENCIAS:	LUGAR	FECHA DE EMISION
ACI-304 **NMX C-170 - 97 ONNCCE** **NMX C-77 - 97 ONNCCE** **NMX C-84 - 90** **NMX C - 111-88**	ELABORÓ	REVISÓ
	NOMBRE Y FIRMA	NOMBRE Y FIRMA

AVENIDA DEL CHARRO 450 NORTE CD. JUAREZ CHIH.

UNIVERSIDAD AUTONOMA DE CIUDAD JUAREZ

LABORATORIO DE MATERIALES

DEPARTAMENTO DE INGENIERIA CIVIL Y AMBIENTAL

INSTITUTO DE INGENIERIA Y TECNOLOGIA

Título: **INFORME DE PRUEBAS DE SUELOS** Coordinates: 357159.26 E;3514609.73 Elev. 1133 masl (CC)

Código de Control de Registro: **2168**

OBRA :		PROCEDENCIA :	
UBICACIÓN	**Blvrd. Fronterizo**	LUGAR DE MUESTREO :	**Coffee cake**
CONSTRUCTORA :	**Dr. Zuñiga**	FECHA DE PRUEBA :	
MUESTRA Nº.:	**1751**	CANTIDAD DE MATERIAL RECIBIDO :	
FECHA DE MUESTREO :	**4-Jun-2012**	MATERIAL :	
		TAMAÑO MAX:	

ARENA	**37.72**	GRAVA	**58.09**	GRAVA-ARENA	**95.81**	FINOS	**4.19**

PESO INICIAL : **17,192** PESO INICIAL DE LA FRACCIÓN FINA : **200** gr

CRIBA	ABERTURA DE LA MALLA	MASA RETENIDA	RETENIDO	RETENIDO ACUMULADO	PASA	CRIBA	ABERTURA DE LA MALLA	MASA RETENIDA	RETENIDO	RETENIDO ACUMULADO	PASA
No.	mm	g	%	%	%	No.	mm	g	%	%	%
4"	100.00					No. 8	2.360			0.0	
3 1/2"	87.50					No. 10	2.000	**50.00**	10.48	10.5	31.44
3"	75.00					No. 16	1.180				
2 1/2"	62.50	**0.00**	0.00	0.00	100.00	No. 20	0.840	**50.80**	10.65	21.1	20.79
2"	50.00	**1,108.00**	6.44	6.44	93.56	No. 30	0.600				
1 1/2"	37.50	**1,643.00**	9.56	16.00	84.00	No. 40	0.420	**30.00**	6.29	27.4	14.50
1"	25.00	**1,639.00**	9.53	25.54	74.46	No. 50	0.300				
3/4"	19.00	**1,184.00**	6.89	32.42	67.58	No. 60	0.250	**10.10**	2.12	29.5	12.39
5/8"	16.00	**0.00**	0.00	32.42	67.58	No. 100	0.149	**8.60**	1.80	31.3	10.58
1/2"	12.50	**0.00**	0.00	32.42	67.58	No. 200	0.074	**30.50**	6.39	37.7	4.19
3/8"	9.50	**2,391.00**	13.91	46.33	53.67	PASA No. 200		**20.00**	4.19	41.9	0.00
1/4"	6.35	**0.00**	0.00	46.33	53.67	SUMA TOTAL :		**200.00**	41.91		
No. 4	4.75	**2,021.00**	11.76	58.09	41.91						
PASA No. 4		**7,206.00**	41.91			%DE MATERIAL RET. EN MALLA No.4			**58.09**		
SUMA :		**17,192**	100.00			%DE MATERIAL QUE PASA MALLA No.4			**41.91**		

PÉRDIDA POR LAVADO	
MATERIAL	RETENIDO CRIBA No. 200
PESO MATERIAL SECO, g	104.70
PESO MATERIAL SECO LAVADO, g	180.00
PESO PÉRDIDA POR LAVADO, g	-75.30
%PÉRDIDA POR LAVADO	-71.92%
%PÉRDIDA LAVADO CORREGIDO	
%PÉRDIDA LAVADO TOTAL	

OBSERVACIONES:

D10= 0.14
D30= 1.7
D60= 13

REFERENCIAS:	LUGAR	FECHA DE EMISION
ACI-304 **NMX C-170 - 97 ONNCCE** **NMX C-77 - 97 ONNCCE** **NMX C-84 - 90** **NMX C - 111-88**	ELABORÓ	REVISÓ
	NOMBRE Y FIRMA	NOMBRE Y FIRMA

AVENIDA DEL CHARRO 450 NORTE CD. JUAREZ CHIH.

UNIVERSIDAD AUTONOMA DE CIUDAD JUAREZ

LABORATORIO DE MATERIALES

DEPARTAMENTO DE INGENIERIA CIVIL Y AMBIENTAL

INSTITUTO DE INGENIERIA Y TECNOLOGIA

Título: **INFORME DE PRUEBAS DE SUELOS** Elev. 1150 masl (NM)

Código de Control de Registro: **2169**

OBRA :		PROCEDENCIA :	
UBICACIÓN	**13R0357501 3514560**	LUGAR DE MUESTREO :	**calles Nardo y Magnesio**
CONSTRUCTORA :	**Dr. Zuñiga**	FECHA DE PRUEBA :	
MUESTRA Nº.:	**1752**	CANTIDAD DE MATERIAL RECIBIDO :	
FECHA DE MUESTREO :	**4-Jun-2012**	MATERIAL :	
		TAMAÑO MAX:	

ARENA	**21.06**	GRAVA	**77.65**	GRAVA-ARENA	**98.71**	FINOS	**1.29**

PESO INICIAL : **16,045** PESO INICIAL DE LA FRACCIÓN FINA : **200** gr

CRIBA	ABERTURA DE LA MALLA	MASA RETENIDA	RETENIDO	RETENIDO ACUMULADO	PASA	CRIBA	ABERTURA DE LA MALLA	MASA RETENIDA	RETENIDO	RETENIDO ACUMULADO	PASA
No.	mm	g	%	%	%	No.	mm	g	%	%	%
4"	100.00					No. 8	2.360			0.0	
3 1/2"	87.50					No. 10	2.000	**35.90**	4.01	4.0	18.34
3"	75.00					No. 16	1.180				
2 1/2"	62.50	**0.00**	0.00	0.00	100.00	No. 20	0.840	**23.50**	2.63	6.6	15.71
2"	50.00	**2,773.00**	17.28	17.28	82.72	No. 30	0.600				
1 1/2"	37.50	**1,776.00**	11.07	28.35	71.65	No. 40	0.420	**16.10**	1.80	8.4	13.91
1"	25.00	**3,180.00**	19.82	48.17	51.83	No. 50	0.300				
3/4"	19.00	**1,097.00**	6.84	55.01	44.99	No. 60	0.250	**23.20**	2.59	11.0	11.32
5/8"	16.00	**0.00**	0.00	55.01	44.99	No. 100	0.149	**35.10**	3.92	15.0	7.40
1/2"	12.50	**0.00**	0.00	55.01	44.99	No. 200	0.074	**54.70**	6.11	21.1	1.29
3/8"	9.50	**2,094.00**	13.05	68.06	31.94	PASA No. 200		**11.50**	1.29	22.3	0.00
1/4"	6.35	**0.00**	0.00	68.06	31.94	SUMA TOTAL :		**200.00**	22.35		
No. 4	4.75	**1,539.00**	9.59	77.65	22.35						
PASA No. 4		**3,586.00**	22.35			%DE MATERIAL RET. EN MALLA No.4			**77.65**		
SUMA :		**16,045**	100.00			%DE MATERIAL QUE PASA MALLA No.4			**22.35**		

PÉRDIDA POR LAVADO	
MATERIAL	RETENIDO CRIBA No. 200
PESO MATERIAL SECO, g	104.70
PESO MATERIAL SECO LAVADO, g	188.50
PESO PÉRDIDA POR LAVADO, g	-83.80
%PÉRDIDA POR LAVADO	-80.04%
%PÉRDIDA LAVADO CORREGIDO	
%PÉRDIDA LAVADO TOTAL	

OBSERVACIONES:

D10= 0.21
D30= 8.5
D60= 30.5

REFERENCIAS:	LUGAR	FECHA DE EMISION
ACI-304 NMX C-170 - 97 ONNCCE NMX C-77 - 97 ONNCCE NMX C-84 - 90 NMX C - 111-88	ELABORÓ	REVISÓ
	NOMBRE Y FIRMA	NOMBRE Y FIRMA

AVENIDA DEL CHARRO 450 NORTE CD. JUAREZ CHIH.

UNIVERSIDAD AUTONOMA DE CIUDAD JUAREZ

LABORATORIO DE MATERIALES

DEPARTAMENTO DE INGENIERIA CIVIL Y AMBIENTAL

INSTITUTO DE INGENIERIA Y TECNOLOGIA

Título: INFORME DE PRUEBAS DE SUELOS

Código de Control de Registro: 2170

OBRA :		PROCEDENCIA :	
UBICACIÓN	13R0361594 3508041	LUGAR DE MUESTREO :	Chichimecas y Calchaquies
CONSTRUCTORA :	Dr. Zuñiga	FECHA DE PRUEBA :	
MUESTRA Nº.:	1753	CANTIDAD DE MATERIAL RECIBIDO :	
FECHA DE MUESTREO :	5-Jun-2012	MATERIAL :	
		TAMAÑO MAX:	

ARENA	57.65	GRAVA	39.95	GRAVA-ARENA	97.60	FINOS	2.40

PESO INICIAL : 18,658

PESO INICIAL DE LA FRACCIÓN FINA : 200 gr

CRIBA	ABERTURA DE LA MALLA	MASA RETENIDA	RETENIDO	RETENIDO ACUMULADO	PASA	CRIBA	ABERTURA DE LA MALLA	MASA RETENIDA	RETENIDO	RETENIDO ACUMULADO	PASA
No.	mm	g	%	%	%	No.	mm	g	%	%	%
4"	100.00					No. 8	2.360			0.0	
3 1/2"	87.50					No. 10	2.000	97.80	29.36	29.4	30.69
3"	75.00					No. 16	1.180				
2 1/2"	62.50	0.00	0.00	0.00	100.00	No. 20	0.840	60.80	18.25	47.6	12.43
2"	50.00	189.00	1.01	1.01	98.99	No. 30	0.600				
1 1/2"	37.50	93.00	0.50	1.51	98.49	No. 40	0.420	19.20	5.76	53.4	6.67
1"	25.00	295.00	1.58	3.09	96.91	No. 50	0.300				
3/4"	19.00	428.00	2.29	5.39	94.61	No. 60	0.250	7.30	2.19	55.6	4.47
5/8"	16.00	0.00	0.00	5.39	94.61	No. 100	0.149	2.60	0.78	56.4	3.69
1/2"	12.50	0.00	0.00	5.39	94.61	No. 200	0.074	4.30	1.29	57.6	2.40
3/8"	9.50	2,261.00	12.12	17.50	82.50	PASA No. 200		8.00	2.40	60.0	0.00
1/4"	6.35	0.00	0.00	17.50	82.50	SUMA TOTAL :		200.00	60.05		
No. 4	4.75	4,188.00	22.45	39.95	60.05						
PASA No. 4		11,204.00	60.05			%DE MATERIAL RET. EN MALLA No.4			39.95		
SUMA :		18,658	100.00			%DE MATERIAL QUE PASA MALLA No.4			60.05		

PÉRDIDA POR LAVADO	
MATERIAL	RETENIDO CRIBA No. 200
PESO MATERIAL SECO, g	104.70
PESO MATERIAL SECO LAVADO, g	192.00
PESO PÉRDIDA POR LAVADO, g	-87.30
%PÉRDIDA POR LAVADO	-83.38%
%PÉRDIDA LAVADO CORREGIDO	
%PÉRDIDA LAVADO TOTAL	

OBSERVACIONES:

D10= 0.59

D30= 1.98

D60= 4.7

REFERENCIAS:	LUGAR	FECHA DE EMISION
ACI-304 NMX C-170 - 97 ONNCCE NMX C-77 - 97 ONNCCE NMX C-84 - 90 NMX C - 111-88	ELABORÓ	REVISÓ
	NOMBRE Y FIRMA	NOMBRE Y FIRMA

AVENIDA DEL CHARRO 450 NORTE CD. JUAREZ CHIH.

UNIVERSIDAD AUTONOMA DE CIUDAD JUAREZ

LABORATORIO DE MATERIALES

DEPARTAMENTO DE INGENIERIA CIVIL Y AMBIENTAL

INSTITUTO DE INGENIERIA Y TECNOLOGIA

Título: INFORME DE PRUEBAS DE SUELOS

Código de Control de Registro: 2171

OBRA :		PROCEDENCIA :	
UBICACIÓN	13R0361414 35007831	LUGAR DE MUESTREO :	Mijes y Calchaquies
CONSTRUCTORA :	Dr. Zuñiga	FECHA DE PRUEBA :	
MUESTRA Nº.:	1754	CANTIDAD DE MATERIAL RECIBIDO :	
FECHA DE MUESTREO :	5-Jun-2012	MATERIAL :	
		TAMAÑO MAX:	

ARENA	73.75	GRAVA	0.00	GRAVA-ARENA	73.75	FINOS	26.25

PESO INICIAL : 1 PESO INICIAL DE LA FRACCIÓN FINA : 200 gr

CRIBA	ABERTURA DE LA MALLA	MASA RETENIDA	RETENIDO	RETENIDO ACUMULADO	PASA	CRIBA	ABERTURA DE LA MALLA	MASA RETENIDA	RETENIDO	RETENIDO ACUMULADO	PASA
No.	mm	g	%	%	%	No.	mm	g	%	%	%
4"	100.00					No. 8	2.360			0.0	
3 1/2"	87.50					No. 10	2.000	1.40	0.70	0.7	99.30
3"	75.00					No. 16	1.180				
2 1/2"	62.50	0.00	0.00	0.00	100.00	No. 20	0.840	4.20	2.10	2.8	97.20
2"	50.00	0.00	0.00	0.00	100.00	No. 30	0.600				
1 1/2"	37.50	0.00	0.00	0.00	100.00	No. 40	0.420	9.70	4.85	7.7	92.35
1"	25.00	0.00	0.00	0.00	100.00	No. 50	0.300				
3/4"	19.00	0.00	0.00	0.00	100.00	No. 60	0.250	15.60	7.80	15.5	84.55
5/8"	16.00	0.00	0.00	0.00	100.00	No. 100	0.149	15.20	7.60	23.1	76.95
1/2"	12.50	0.00	0.00	0.00	100.00	No. 200	0.074	101.40	50.70	73.8	26.25
3/8"	9.50	0.00	0.00	0.00	100.00	PASA No. 200		52.50	26.25	100.0	0.00
1/4"	6.35	0.00	0.00	0.00	100.00	SUMA TOTAL :		200.00	100.00		
No. 4	4.75	0.00	0.00	0.00	100.00						
PASA No. 4		7,752.00	100.00			%DE MATERIAL RET. EN MALLA No. 4			0.00		
SUMA :		7,752	100.00			%DE MATERIAL QUE PASA MALLA No. 4			100.00		

PÉRDIDA POR LAVADO	
MATERIAL	RETENIDO CRIBA No. 200
PESO MATERIAL SECO, g	104.70
PESO MATERIAL SECO LAVADO, g	147.50
PESO PÉRDIDA POR LAVADO, g	-42.80
%PÉRDIDA POR LAVADO	-40.88%
%PÉRDIDA LAVADO CORREGIDO	
%PÉRDIDA LAVADO TOTAL	

OBSERVACIONES:

D10= 0.27
D30= 0.7
D60= 9.3

REFERENCIAS:	LUGAR	FECHA DE EMISION
ACI-304 NMX C-170 - 97 ONNCCE NMX C-77 - 97 ONNCCE NMX C-84 - 90 NMX C - 111-88	ELABORÓ	REVISÓ
	NOMBRE Y FIRMA	NOMBRE Y FIRMA

AVENIDA DEL CHARRO 450 NORTE CD. JUAREZ CHIH.

UNIVERSIDAD AUTONOMA DE CIUDAD JUAREZ

LABORATORIO DE MATERIALES

DEPARTAMENTO DE INGENIERIA CIVIL Y AMBIENTAL

INSTITUTO DE INGENIERIA Y TECNOLOGIA

Título: INFORME DE PRUEBAS DE SUELOS

Código de Control de Registro: 2172

OBRA :		PROCEDENCIA :	
UBICACIÓN	13R0359960 3509093	LUGAR DE MUESTREO :	Panteón Tepeyac
CONSTRUCTORA :	Dr. Zuñiga	FECHA DE PRUEBA :	
MUESTRA Nº.:	1756	CANTIDAD DE MATERIAL RECIBIDO :	
FECHA DE MUESTREO :	5-Jun-2012	MATERIAL :	
		TAMAÑO MAX:	

ARENA	36.19	GRAVA	58.55	GRAVA-ARENA	94.74	FINOS	5.26

PESO INICIAL : 18,582 PESO INICIAL DE LA FRACCIÓN FINA : 200 gr

CRIBA	ABERTURA DE LA MALLA	MASA RETENIDA	RETENIDO	RETENIDO ACUMULADO	PASA	CRIBA	ABERTURA DE LA MALLA	MASA RETENIDA	RETENIDO	RETENIDO ACUMULADO	PASA
No.	mm	g	%	%	%	No.	mm	g	%	%	%
4"	100.00					No. 8	2.360			0.0	
3 1/2"	87.50					No. 10	2.000	49.80	10.32	10.3	31.13
3"	75.00					No. 16	1.180				
2 1/2"	62.50	0.00	0.00	0.00	100.00	No. 20	0.840	46.40	9.62	19.9	21.51
2"	50.00	926.00	4.98	4.98	95.02	No. 30	0.600				
1 1/2"	37.50	219.00	1.18	6.16	93.84	No. 40	0.420	22.80	4.73	24.7	16.79
1"	25.00	451.00	2.43	8.59	91.41	No. 50	0.300				
3/4"	19.00	1,764.00	9.49	18.08	81.92	No. 60	0.250	15.40	3.19	27.9	13.60
5/8"	16.00	0.00	0.00	18.08	81.92	No. 100	0.149	11.90	2.47	30.3	11.13
1/2"	12.50	0.00	0.00	18.08	81.92	No. 200	0.074	28.30	5.87	36.2	5.26
3/8"	9.50	3,718.00	20.01	38.09	61.91	PASA No. 200		25.40	5.26	41.5	0.00
1/4"	6.35	0.00	0.00	38.09	61.91	SUMA TOTAL :		200.00	41.45		
No. 4	4.75	3,801.00	20.46	58.55	41.45						
PASA No. 4		7,703.00	41.45			%DE MATERIAL RET. EN MALLA No.4			58.55		
SUMA :		18,582	100.00			%DE MATERIAL QUE PASA MALLA No.4			41.45		

PÉRDIDA POR LAVADO	
MATERIAL	RETENIDO CRIBA No. 200
PESO MATERIAL SECO, g	104.70
PESO MATERIAL SECO LAVADO, g	174.60
PESO PÉRDIDA POR LAVADO, g	-69.90
%PÉRDIDA POR LAVADO	-66.76%
%PÉRDIDA LAVADO CORREGIDO	
%PÉRDIDA LAVADO TOTAL	

OBSERVACIONES:

D10= 0.14
D30= 1.8
D60= 9

REFERENCIAS:	LUGAR	FECHA DE EMISION
ACI-304 NMX C-170 - 97 ONNCCE NMX C-77 - 97 ONNCCE NMX C-84 - 90 NMX C - 111-88	ELABORÓ	REVISÓ
	NOMBRE Y FIRMA	NOMBRE Y FIRMA

AVENIDA DEL CHARRO 450 NORTE CD. JUAREZ CHIH.

UNIVERSIDAD AUTONOMA DE CIUDAD JUAREZ

LABORATORIO DE MATERIALES

DEPARTAMENTO DE INGENIERIA CIVIL Y AMBIENTAL

INSTITUTO DE INGENIERIA Y TECNOLOGIA

Título: **INFORME DE PRUEBAS DE SUELOS**

Código de Control de Registro: **2173**

OBRA :		PROCEDENCIA :	
UBICACIÓN	13R0362368 3508689	LUGAR DE MUESTREO :	Eje vial Juan Gabriel
CONSTRUCTORA :	Dr. Zuñiga	FECHA DE PRUEBA :	
MUESTRA Nº.:	1756	CANTIDAD DE MATERIAL RECIBIDO :	
FECHA DE MUESTREO :	5-Jun-2012	MATERIAL :	
		TAMAÑO MAX:	

ARENA	55.76	GRAVA	41.64	GRAVA-ARENA	97.40	FINOS	2.60

PESO INICIAL : 18,932 PESO INICIAL DE LA FRACCIÓN FINA : 200 gr

CRIBA	ABERTURA DE LA MALLA	MASA RETENIDA	RETENIDO	RETENIDO ACUMULADO	PASA	CRIBA	ABERTURA DE LA MALLA	MASA RETENIDA	RETENIDO	RETENIDO ACUMULADO	PASA
No.	mm	g	%	%	%	No.	mm	g	%	%	%
4"	100.00					No. 8	2.360			0.0	
3 1/2"	87.50					No. 10	2.000	39.50	11.53	11.5	46.84
3"	75.00					No. 16	1.180				
2 1/2"	62.50	0.00	0.00	0.00	100.00	No. 20	0.840	33.90	9.89	21.4	36.94
2"	50.00	436.00	2.30	2.30	97.70	No. 30	0.600				
1 1/2"	37.50	645.00	3.41	5.71	94.29	No. 40	0.420	40.50	11.82	33.2	25.12
1"	25.00	1,145.00	6.05	11.76	88.24	No. 50	0.300				
3/4"	19.00	902.00	4.76	16.52	83.48	No. 60	0.250	43.20	12.61	45.8	12.52
5/8"	16.00	0.00	0.00	16.52	83.48	No. 100	0.149	18.20	5.31	51.2	7.21
1/2"	12.50	0.00	0.00	16.52	83.48	No. 200	0.074	15.80	4.61	55.8	2.60
3/8"	9.50	2,542.00	13.43	29.95	70.05	PASA No. 200		8.90	2.60	58.4	0.00
1/4"	6.35	0.00	0.00	29.95	70.05	SUMA TOTAL :		200.00	58.36		
No. 4	4.75	2,213.00	11.69	41.64	58.36						
PASA No. 4		11,049.00	58.36			%DE MATERIAL RET. EN MALLA No. 4			41.64		
SUMA :		18,932	100.00			%DE MATERIAL QUE PASA MALLA No. 4			58.36		

PÉRDIDA POR LAVADO	
MATERIAL	RETENIDO CRIBA No. 200
PESO MATERIAL SECO, g	104.70
PESO MATERIAL SECO LAVADO, g	191.10
PESO PÉRDIDA POR LAVADO, g	-86.40
%PÉRDIDA POR LAVADO	-82.52%
%PÉRDIDA LAVADO CORREGIDO	
%PÉRDIDA LAVADO TOTAL	

OBSERVACIONES:

D10= 0.21
D30= 0.55
D60= 5.3

REFERENCIAS:	LUGAR	FECHA DE EMISION
ACI-304 NMX C-170 - 97 ONNCCE NMX C-77 - 97 ONNCCE NMX C-84 - 90 NMX C - 111-88	ELABORÓ NOMBRE Y FIRMA	REVISÓ NOMBRE Y FIRMA

AVENIDA DEL CHARRO 450 NORTE CD. JUAREZ CHIH.

UNIVERSIDAD AUTONOMA DE CD JUAREZ

LABORATORIO DE MATERIALES

DEPARTAMENTO DE INGENIERIA CIVIL Y AMBIENTAL

ASEGURAMIENTO DE CALIDAD

Título: REPORTE DE PRUEBAS DE SUELOS

Coordinates: 356673.95 E;3515308.83; Elev. 1145 masl (PM)

Código de control de registro: 2174

OBRA :	0	PROCEDENCIA:	
UBICACIÓN :	0	LUGAR DE MUESTREO:	Calles Parral y Arroyo del Mimbre
CONSTRUCTORA:	Dr. Zuñiga	CANTIDAD DE MATERIAL RECIBIDO :	0
MUESTRA Nº.:	1757	MATERIAL:	0
FECHA DE MUESTREO.:	0706/2012	TAMAÑO:	0

PRUEBA	MÉTODO ASTM	VALORES OBTENIDOS	LÍMITES ESPECIFICADOS	PRUEBA		MÉTODO ASTM	VALORES OBTENIDOS	LÍMITES ESPECIFICADOS
GRAVEDAD ESPECÍFICA (SSS)	C-127	---	-----	INTEMPERISMO ACELERADO EN ARENA %		C-88	--	10 MAX.
ABSORCIÓN %	C-127	----	-----	PARTÍCULAS	CARBÓN Y LIGNITO %	C-123	---	1 MÁX
PESO UNITARIO SUELTO kg / m³	C-29	1,690	-----	LIGERAS	PEDERNAL %	C-123	---	5 MÁX
PESO UNITARIO VARILLADO kg / m³	C-29	1,765	-----	PARTÍCULAS FRIABLES Y TERRONES DE ARCILLA %		C-142	---	5 MÁX
VACÍOS %	C-29	---	-----	INTEMPERISMO ACELERADO EN GRAVA %		C-88	---	12 MÁX
MATERIAL MENOR A 0.075 mm %	C-117	5.6	15 MÁX	COEFICIENTE VOLUMÉTRICO		NF	---	0.20 MÍN
ARENA EN LA GRAVA %	C-136	45.74%	MÁX	DESGASTE DE LOS ÁNGELES %		C-131	----	50 MÁX
GRAVA EN LA GRAVA %	C-136	48.64%	MÍN	EQUIVALENTE DE ARENA %		-----	----	80 MÍN

GRAVA 45.74
ARENA 48.64
GRAVA ARENA 94.38
FINOS 5.62

GRANULOMETRÍA

% RETENIDOS

CRIBA	LÍM. ACUM. MÍN.	LÍM. ACUM. MÁX.	MATERIAL RET.	MATERIAL ACUM.	MATERIAL PASA
4"			0.00	0.0	0.0
3 1/2"			0.00	0.0	0.0
3"			0.00	0.0	0.0
2 1/2"			0.00	0.00	100.0
2"			0.84	0.84	99.2
1 1/2"			6.60	7.45	92.6
1"			6.63	14.08	85.9
3/4"			5.44	19.51	80.5
1/2"			7.55	27.07	72.9
3/8"			4.54	3160	68.4
1/4"			7.83	39.43	60.6
No. 4			6.31	45.74	54.3
No. 10			15.84	6159	38.4
No. 16					
No. 20			16.49	78.08	219
No. 30					
No. 40			8.36	86.44	13.6
No. 50					
No. 60			3.80	90.23	9.8
No. 100			149	9173	8.3
No. 200			2.66	94.38	5.6
CHAROLA			5.62	100.00	

OBSERVACIONES:

CRIBAS

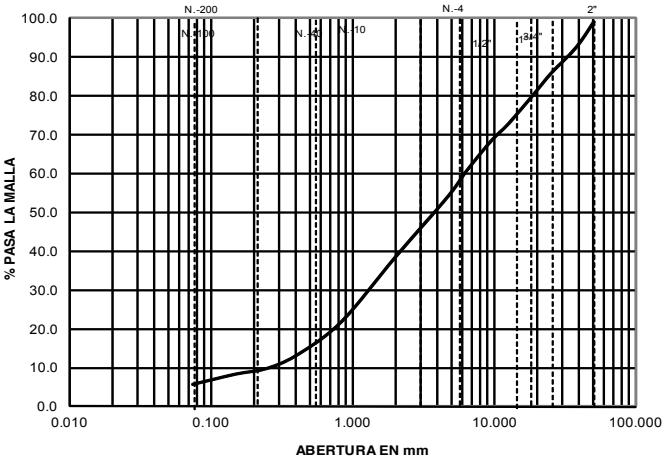

MALLAS	mm	SUP	INF	REAL
2"	50.800	0	0	99.2
1 1/2"	38.100	0	0	92.6
1"	25.400	0	0	85.9
3/4"	19.100	0	0	80.5
1/2"	12.700	0	0	72.9
3/8"	9.520			68.4
1/4"	6.350			60.6
No. 4	4.760			54.3
No. 10	2.000			38.4
No. 20	0.840			21.9
No. 40	0.420			13.6
No. 60	0.250			9.8
No. 100	0.149			8.3
No. 200	0.074			5.6

Fecha: 4 DE SEPTIEMBRE DEL 20003 **Lugar:** UACJ, LABORATORIO DE MATERIALES

REFERENCIAS:	REVISÓ	RECIBIÓ
ASTM -C-33		
ACI-304		
NMX C-170 - 97 ONNCCE		
NMX C-77 - 97 ONNCCE		
NMX C-84 - 90	0	
NMX C - 111-88	NOMBRE Y FIRMA	NOMBRE Y FIRMA

UNIVERSIDAD AUTONOMA DE CIUDAD JUAREZ

LABORATORIO DE MATERIALES

DEPARTAMENTO DE INGENIERIA CIVIL Y AMBIENTAL

INSTITUTO DE INGENIERIA Y TECNOLOGIA

Título: INFORME DE PRUEBAS DE SUELOS

Código de Control de Registro: 2175

OBRA :		PROCEDENCIA :	Arroyo de las víboras oeste
UBICACIÓN	13R0355474 3513776	LUGAR DE MUESTREO :	16 de septiembre y Sinaloa
CONSTRUCTORA :	Dr. Zuñiga	FECHA DE PRUEBA :	
MUESTRA Nº.:	1758	CANTIDAD DE MATERIAL RECIBIDO :	
FECHA DE MUESTREO :	7-Jun-2012	MATERIAL :	
		TAMAÑO MAX:	

ARENA	48.75	GRAVA	50.00	GRAVA-ARENA	98.75	FINOS	1.25

PESO INICIAL : 18,850 PESO INICIAL DE LA FRACCIÓN FINA : 200 gr

CRIBA	ABERTURA DE LA MALLA	MASA RETENIDA	RETENIDO	RETENIDO ACUMULADO	PASA	CRIBA	ABERTURA DE LA MALLA	MASA RETENIDA	RETENIDO	RETENIDO ACUMULADO	PASA
No.	mm	g	%	%	%	No.	mm	g	%	%	%
4"	100.00					No. 8	2.360			0.0	
3 1/2"	87.50					No. 10	2.000	74.10	18.53	18.5	31.48
3"	75.00					No. 16	1.180				
2 1/2"	62.50	0.00	0.00	0.00	100.00	No. 20	0.840	29.60	7.40	25.9	24.08
2"	50.00	0.00	0.00	0.00	100.00	No. 30	0.600				
1 1/2"	37.50	540.00	2.86	2.86	97.14	No. 40	0.420	14.40	3.60	29.5	20.48
1"	25.00	1,058.00	5.61	8.48	91.52	No. 50	0.300				
3/4"	19.00	1,236.00	6.56	15.03	84.97	No. 60	0.250	40.90	10.23	39.8	10.25
5/8"	16.00	0.00	0.00	15.03	84.97	No. 100	0.149	24.80	6.20	46.0	4.05
1/2"	12.50	2,115.00	11.22	26.25	73.75	No. 200	0.074	11.20	2.80	48.8	1.25
3/8"	9.50	1,382.00	7.33	33.59	66.41	PASA No. 200		5.00	1.25	50.0	0.00
1/4"	6.35	1,879.00	9.97	43.55	56.45	SUMA TOTAL :		200.00	50.00		
No. 4	4.75	1,215.00	6.45	50.00	50.00						
PASA No. 4		11,049.00	50.00			%DE MATERIAL RET. EN MALLA No. 4			50.00		
SUMA :		20,474	100.00			%DE MATERIAL QUE PASA MALLA No. 4			50.00		

PÉRDIDA POR LAVADO	
MATERIAL	RETENIDO CRIBA No. 200
PESO MATERIAL SECO, g	104.70
PESO MATERIAL SECO LAVADO, g	195.00
PESO PÉRDIDA POR LAVADO, g	-90.30
%PÉRDIDA POR LAVADO	-86.25%
%PÉRDIDA LAVADO CORREGIDO	
%PÉRDIDA LAVADO TOTAL	

OBSERVACIONES:

D10= 0.25
D30= 1.8
D60= 7.3

REFERENCIAS:	LUGAR	FECHA DE EMISION
ACI-304 NMX C-170 - 97 ONNCCE NMX C-77 - 97 ONNCCE NMX C-84 - 90 NMX C - 111-88	ELABORÓ	REVISÓ
	NOMBRE Y FIRMA	NOMBRE Y FIRMA

AVENIDA DEL CHARRO 450 NORTE CD. JUAREZ CHIH.

UNIVERSIDAD AUTONOMA DE CIUDAD JUAREZ

LABORATORIO DE MATERIALES

DEPARTAMENTO DE INGENIERIA CIVIL Y AMBIENTAL

INSTITUTO DE INGENIERIA Y TECNOLOGIA

Título: INFORME DE PRUEBAS DE SUELOS

Código de Control de Registro: 2176

OBRA :		PROCEDENCIA :	
UBICACIÓN	13R0354923 3514284	LUGAR DE MUESTREO :	16 de septiembre y Musita
CONSTRUCTORA :	Dr. Zuñiga	FECHA DE PRUEBA :	
MUESTRA Nº.:	1759	CANTIDAD DE MATERIAL RECIBIDO :	
FECHA DE MUESTREO :	7-Jun-2012	MATERIAL :	
		TAMAÑO MAX:	

ARENA	48.38	GRAVA	46.75	GRAVA-ARENA	95.13	FINOS	4.87

PESO INICIAL : 20,493 PESO INICIAL DE LA FRACCIÓN FINA : 200 gr

CRIBA	ABERTURA DE LA MALLA	MASA RETENIDA	RETENIDO	RETENIDO ACUMULADO	PASA	CRIBA	ABERTURA DE LA MALLA	MASA RETENIDA	RETENIDO	RETENIDO ACUMULADO	PASA
No.	mm	g	%	%	%	No.	mm	g	%	%	%
4"	100.00					No. 8	2.360			0.0	
3 1/2"	87.50					No. 10	2.000	37.50	9.98	10.0	43.27
3"	75.00					No. 16	1.180				
2 1/2"	62.50	0.00	0.00	0.00	100.00	No. 20	0.840	29.00	7.72	17.7	35.55
2"	50.00	0.00	0.00	0.00	100.00	No. 30	0.600				
1 1/2"	37.50	636.00	3.10	3.10	96.90	No. 40	0.420	32.10	8.55	26.3	27.00
1"	25.00	1,042.00	5.08	8.19	91.81	No. 50	0.300				
3/4"	19.00	1,192.00	5.82	14.00	86.00	No. 60	0.250	30.80	8.20	34.5	18.80
5/8"	16.00	0.00	0.00	14.00	86.00	No. 100	0.149	25.30	6.74	41.2	12.06
1/2"	12.50	2,201.00	10.74	24.75	75.25	No. 200	0.074	27.00	7.19	48.4	4.87
3/8"	9.50	1,335.00	6.51	31.26	68.74	PASA No. 200		18.30	4.87	53.3	0.00
1/4"	6.35	1,973.00	9.63	40.89	59.11	SUMA TOTAL :		200.00	53.25		
No. 4	4.75	1,201.00	5.86	46.75	53.25						
PASA No. 4		10,913.00	53.25			%DE MATERIAL RET. EN MALLA No. 4			46.75		
SUMA :		20,493	100.00			%DE MATERIAL QUE PASA MALLA No. 4			53.25		

PÉRDIDA POR LAVADO	
MATERIAL	RETENIDO CRIBA No. 200
PESO MATERIAL SECO, g	104.70
PESO MATERIAL SECO LAVADO, g	181.70
PESO PÉRDIDA POR LAVADO, g	-77.00
%PÉRDIDA POR LAVADO	-73.54%
%PÉRDIDA LAVADO CORREGIDO	
%PÉRDIDA LAVADO TOTAL	

OBSERVACIONES:

D10= 0.13
D30= 0.52
D60= 6.6

REFERENCIAS:	LUGAR	FECHA DE EMISION
ACI-304 NMX C-170 - 97 ONNCCE NMX C-77 - 97 ONNCCE NMX C-84 - 90 NMX C - 111-88	ELABORÓ	REVISÓ
	NOMBRE Y FIRMA	NOMBRE Y FIRMA

AVENIDA DEL CHARRO 450 NORTE CD. JUAREZ CHIH.

UNIVERSIDAD AUTONOMA DE CIUDAD JUAREZ

LABORATORIO DE MATERIALES

DEPARTAMENTO DE INGENIERIA CIVIL Y AMBIENTAL

INSTITUTO DE INGENIERIA Y TECNOLOGIA

Título: **INFORME DE PRUEBAS DE SUELOS**

Código de Control de Registro: 2177

OBRA :		PROCEDENCIA :	
UBICACIÓN	P4 M4	LUGAR DE MUESTREO :	División del norte y Mariscal
CONSTRUCTORA :	Dr. Zuñiga	FECHA DE PRUEBA :	
MUESTRA Nº.:	1760	CANTIDAD DE MATERIAL RECIBIDO :	
FECHA DE MUESTREO :	7-Jun-2012	MATERIAL :	
		TAMAÑO MAX:	

ARENA	39.89	GRAVA	56.95	GRAVA-ARENA	96.84	FINOS	3.16

PESO INICIAL : 18,636

PESO INICIAL DE LA FRACCIÓN FINA : 200 gr

CRIBA	ABERTURA DE LA MALLA	MASA RETENIDA	RETENIDO	RETENIDO ACUMULADO	PASA
No.	mm	g	%	%	%
4"	100.00				
3 1/2"	87.50				
3"	75.00				
2 1/2"	62.50	0.00	0.00	0.00	100.00
2"	50.00	0.00	0.00	0.00	100.00
1 1/2"	37.50	449.00	2.41	2.41	97.59
1"	25.00	1,861.00	9.99	12.40	87.60
3/4"	19.00	1,738.00	9.33	21.72	78.28
5/8"	16.00	0.00	0.00	21.72	78.28
1/2"	12.50	1,920.00	10.30	32.02	67.98
3/8"	9.50	1,832.00	9.83	41.85	58.15
1/4"	6.35	1,854.00	9.95	51.80	48.20
No. 4	4.75	959.00	5.15	56.95	43.05
PASA No. 4		8,023.00	43.05		
SUMA :		18,636	100.00		

CRIBA	ABERTURA DE LA MALLA	MASA RETENIDA	RETENIDO	RETENIDO ACUMULADO	PASA
No.	mm	g	%	%	%
No. 8	2.360			0.0	
No. 10	2.000	46.30	9.97	10.0	33.08
No. 16	1.180				
No. 20	0.840	43.50	9.36	19.3	23.72
No. 30	0.600				
No. 40	0.420	32.60	7.02	26.3	16.70
No. 50	0.300				
No. 60	0.250	23.30	5.02	31.4	11.69
No. 100	0.149	20.60	4.43	35.8	7.25
No. 200	0.074	19.00	4.09	39.9	3.16
PASA No. 200		14.70	3.16	43.1	0.00
SUMA TOTAL :		200.00	43.05		
% DE MATERIAL RET. EN MALLA No. 4			56.95		
% DE MATERIAL QUE PASA MALLA No. 4			43.05		

PÉRDIDA POR LAVADO	
MATERIAL	RETENIDO CRIBA No. 200
PESO MATERIAL SECO, g	104.70
PESO MATERIAL SECO LAVADO, g	185.30
PESO PÉRDIDA POR LAVADO, g	-80.60
% PÉRDIDA POR LAVADO	-76.98%
% PÉRDIDA LAVADO CORREGIDO	
% PÉRDIDA LAVADO TOTAL	

OBSERVACIONES:

D10= 0.21

D30= 1.6

D60= 10.05

REFERENCIAS:

ACI-304

NMX C-170 - 97 ONNCCE

NMX C-77 - 97 ONNCCE

NMX C-84 - 90

NMX C - 111-88

LUGAR	FECHA DE EMISION
ELABORÓ	REVISÓ
NOMBRE Y FIRMA	NOMBRE Y FIRMA

AVENIDA DEL CHARRO 450 NORTE CD. JUAREZ CHIH.

Appendix 4A3

The purpose of this appendix is to complement and illustrate the sites of samples collection and the petrographic analysis explained in the in methods chapter 3 and the results chapter 4. The majority part of the present analysis is mostly related to terraces and fluvial deposits which were illustradted in previous tables given in appendix 4A2 tables 2 and 3 as well in the following Figures 1 to 10. Shorytly; Some sedimentary fluvial deposits derived from older and younger tributaries of the Bravo River such as: Smart Supermarked Anapra (SSA) which is given Figure 2 ; Water House (WH) that is given in Figure 3; Coffe Cake (CC) given in Figure 4; and all the Terraces systems allocated in the study area and described in tables 1 and 2 of appendix 4A2.(See Figures from 1 to 10 and Fig 10 shows pictures of soils petrographic analysis and soils classification results.

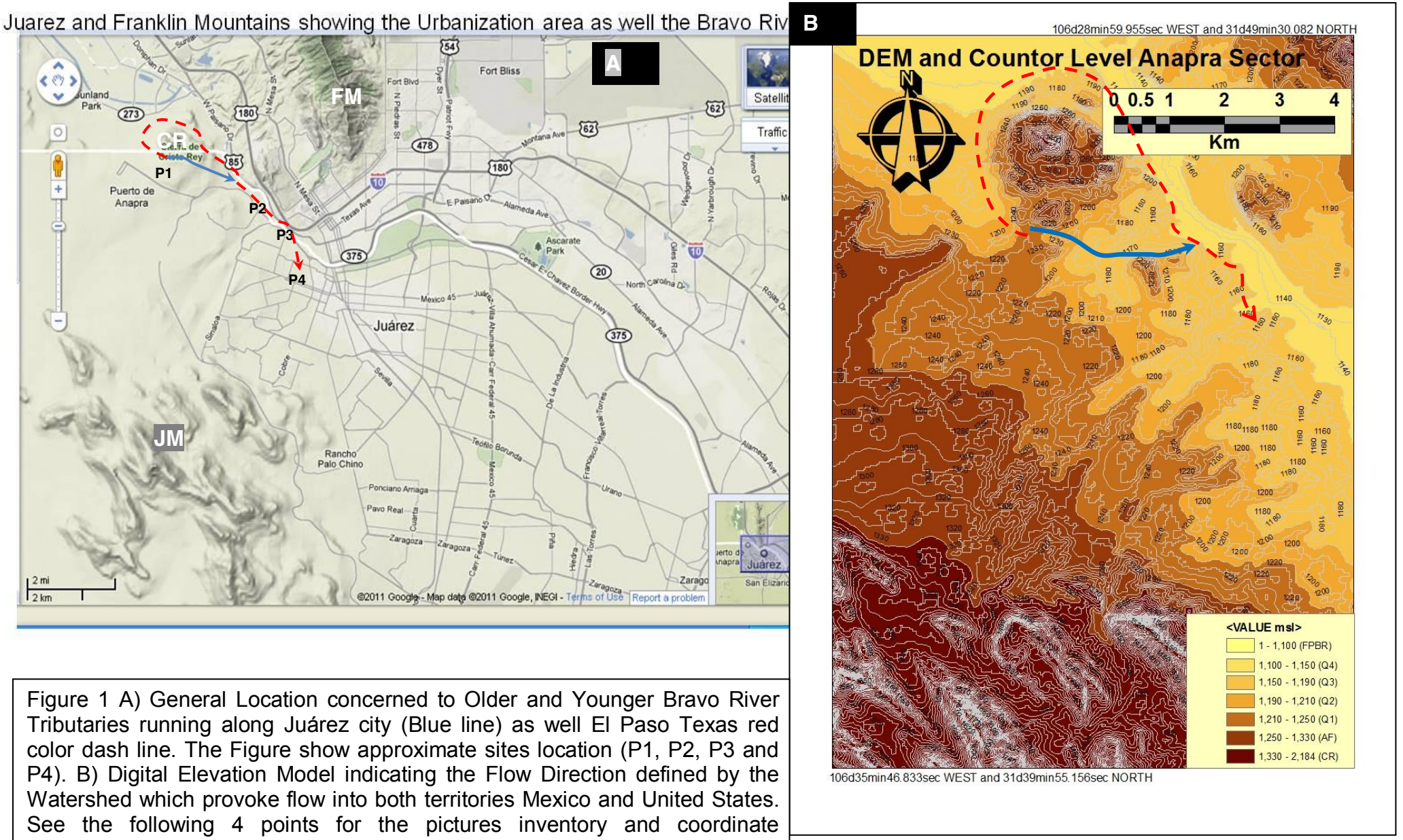

Figure 1 A) General Location concerned to Older and Younger Bravo River Tributaries running along Juárez city (Blue line) as well El Paso Texas red color dash line. The Figure show approximate sites location (P1, P2, P3 and P4). B) Digital Elevation Model indicating the Flow Direction defined by the Watershed which provoke flow into both territories Mexico and United States. See the following 4 points for the pictures inventory and coordinate location.Source: Google map 2011 and Arc-Map 2011.

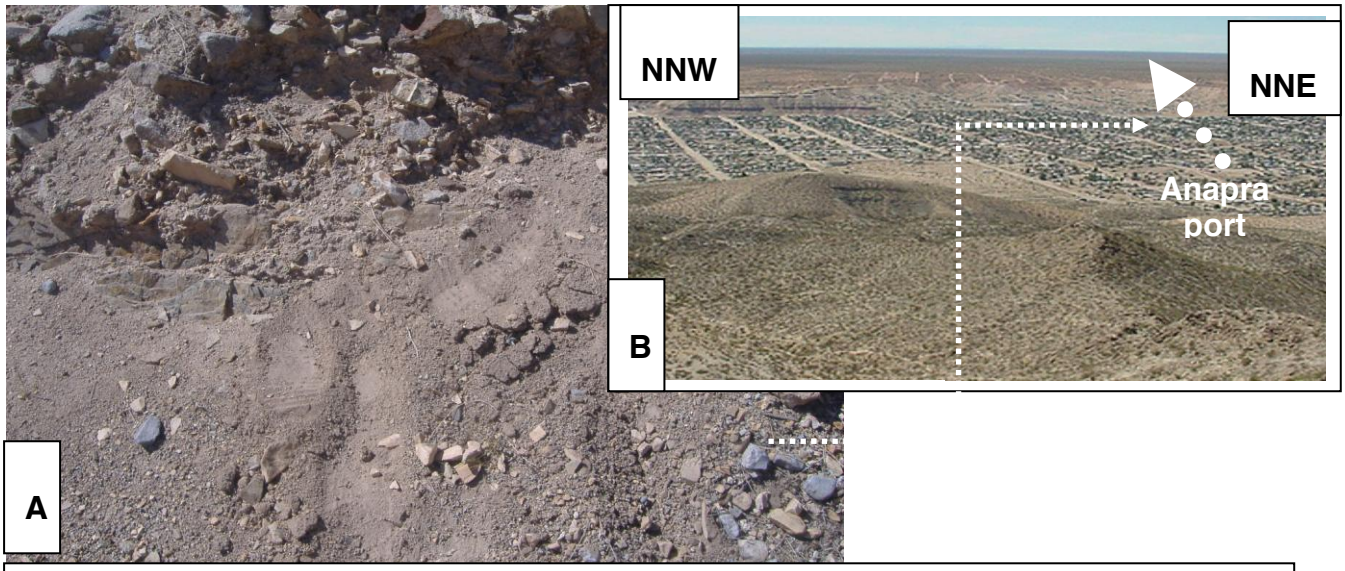

Figure 2 Point 1 of BRT. Smart Anapra outcrop of older BRT deposits (probably footwall block of A) Fragments mostly andesitic and felsitic origen derived for Cristo Rey mountains note bellow the deposits a probable Lava volcanic eruption Note the angular and sub-angular shape of andesitic and felsites fragments flow direction would be (SSE). B) Panoramic view showing Coordinates of the site location UTM 352555.83 E; 3516878.36 N; Elev. 1170 masl white arrow shows flow direction to El Paso Texas consistent with DEM showed in Fig. 1 related to location.

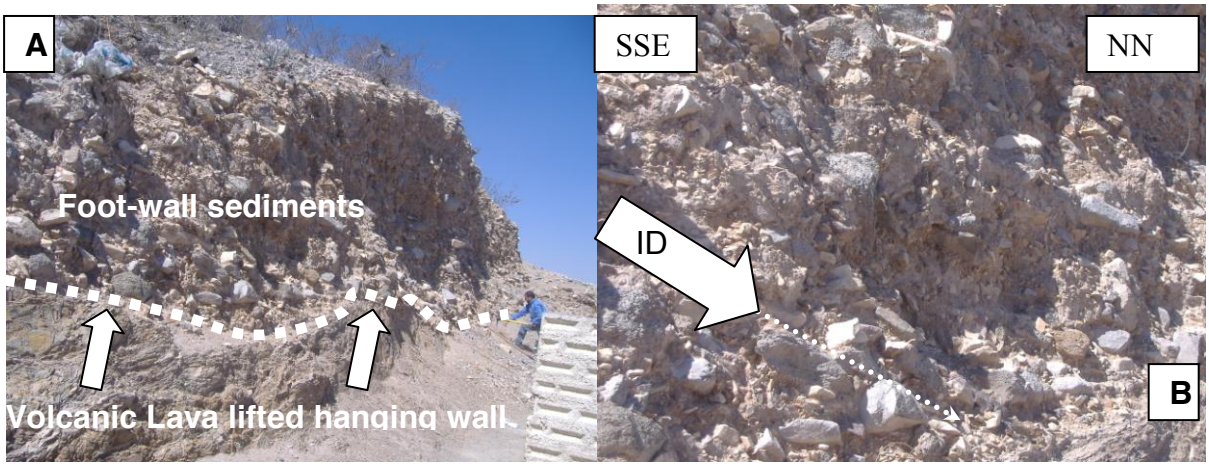

Figure 3 Point 2 of BRT. Water House outcrop of older BRT Deposits above volcanic rock (probably footwall block of Pleistocene normal fault). A) Contact between volcanic rocks and Older tributary fragments mostly Andesitic and felsites. B) Note the angular and sub-angular shape of big andesitic and felsites fragments and the Imbrication Direction ID flow direction would be (SSE) Note matrix support predominates over clast support and big fragment insert into the matrix. Coordinates UTM with nad 27 datum: measured were: 355464.96 E; 3515966.51N; Elev. 1147 masl.

Figure 4 Point 3 of BRT. A) Coffee Cake outcrop of older BRT. Note the angular and sub-angular shape of big andesitic and felsites fragments and the Imbrication Direction ID flow direction would be (SSE) Note matrix support predominates over clast support and big fragment insert into the matrix. Coordinates UTM with nad 27 datum: 357159.26E; 3514609.73N; Elev. 1133: Point 4. B) Crossing of 16 de Septiembre and Bario streets. Coordinates: 357727.02E; 3512826.21N; Elev. 1160m, this outcrop contains many small sub angular gravels of andesitic, felsites as well Bravo River fragments mixed together probably deposited during younger avulsion of Bravo River.As a result, the recent bed of Bravo River is approximately located below elevation 1160 masl.

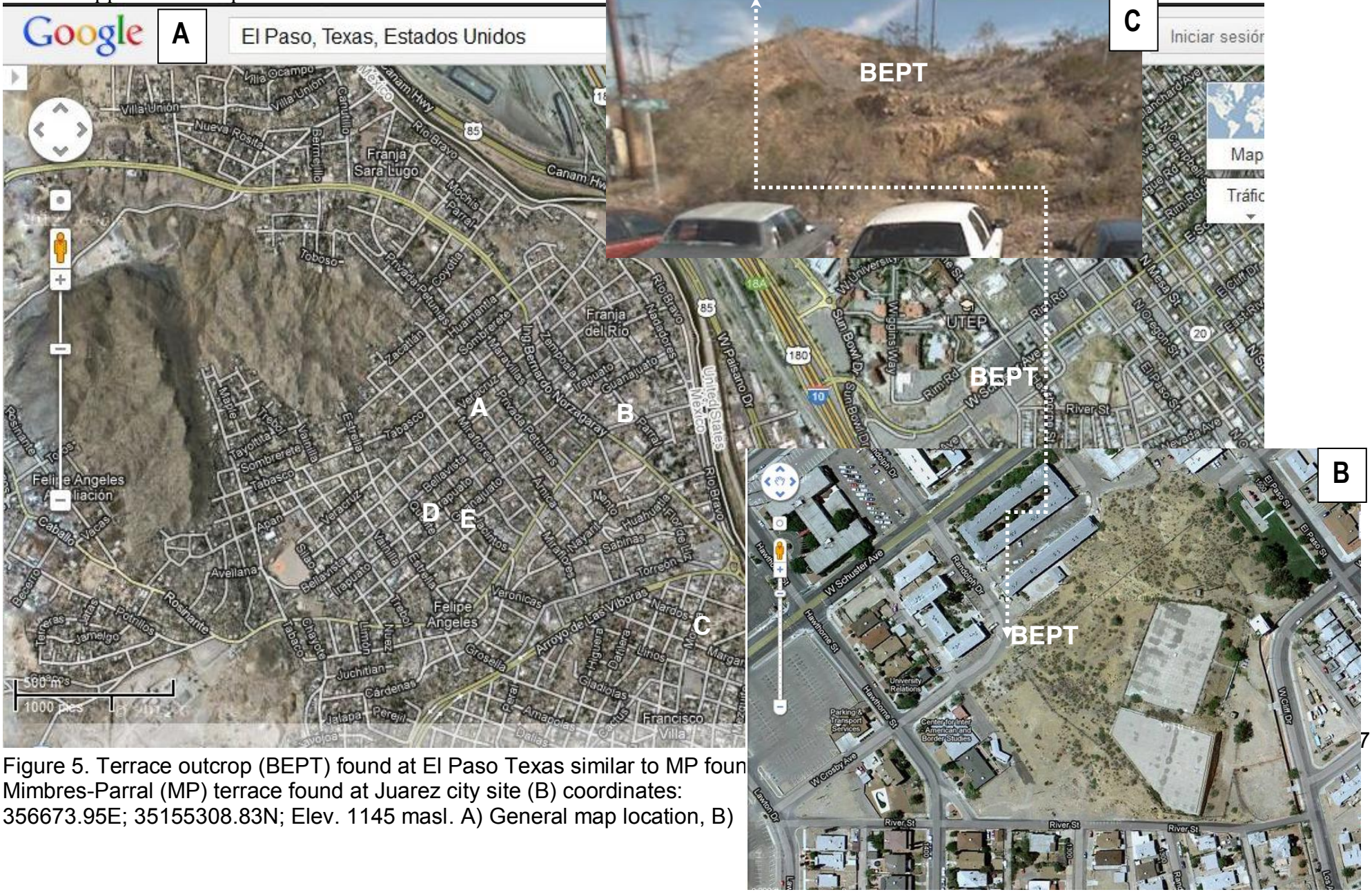

Figure 5. Terrace outcrop (BEPT) found at El Paso Texas similar to MP foun
Mimbres-Parral (MP) terrace found at Juarez city site (B) coordinates:
356673.95E; 35155308.83N; Elev. 1145 masl. A) General map location, B)

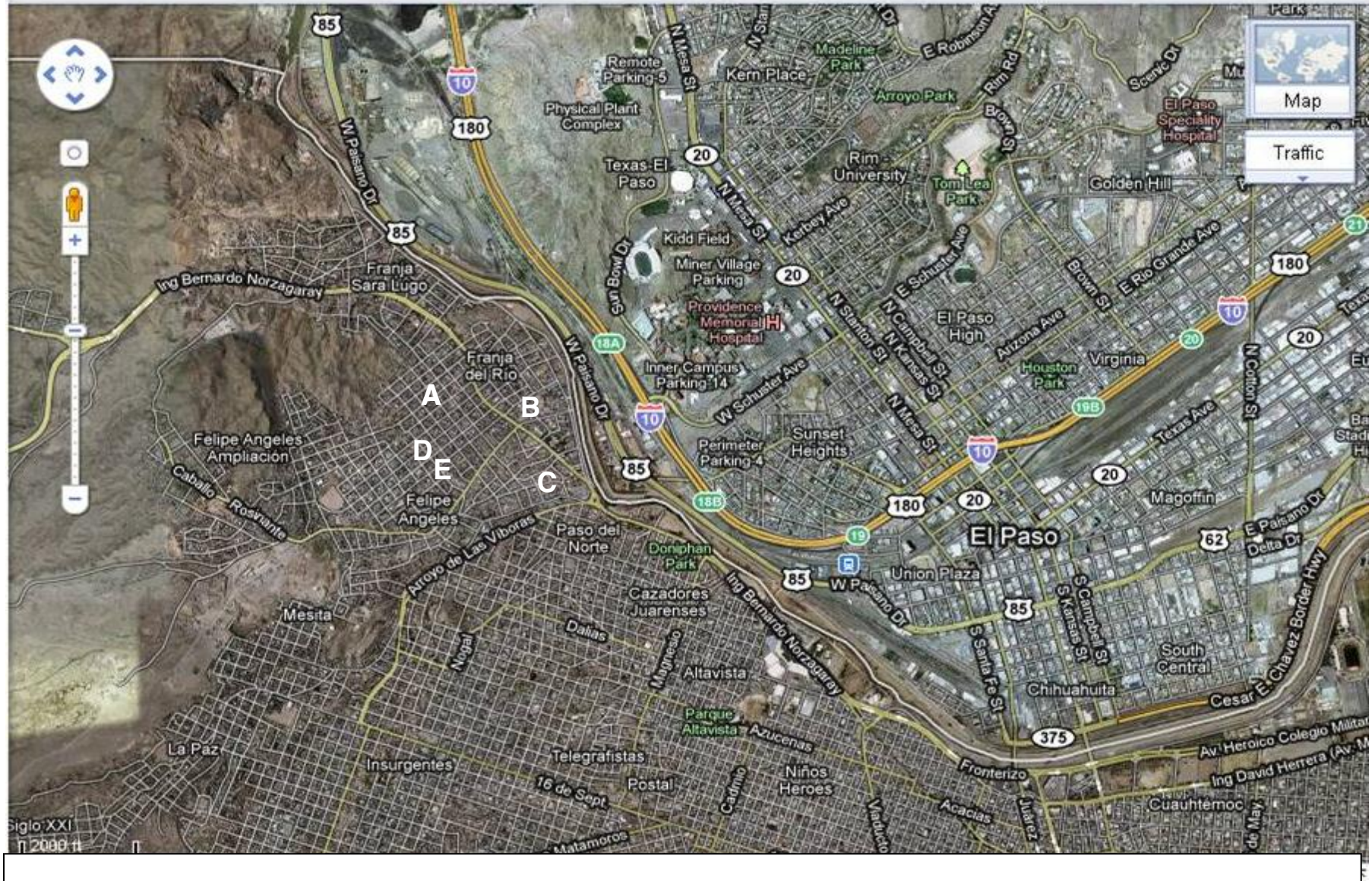

Figure 6 Location of Terraces outcropped in Felipe Angeles Neigbourhood: A) GH Terrace Coordinates: 356099.15E; 3515159.88N Elev; 1160 masl. B)MP Terrace Coordinates. 356673.95E; 35155308.83N; Elev. 1145 masl C) NM Terrace 357448.05;; 3514394.04N; Elev. 1150 masl. D) JAM Terrace Coordinates 356164.71E; 3514977.46N Elev. 1155 masl; E) Q Terrace Coordinates 355969.46E; 3514911.90N; Elev. 1170 masl. Source: Google maps (2011)

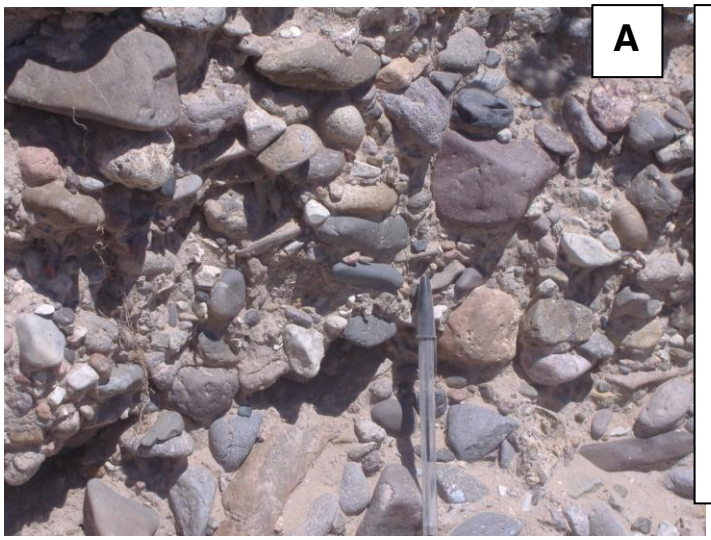

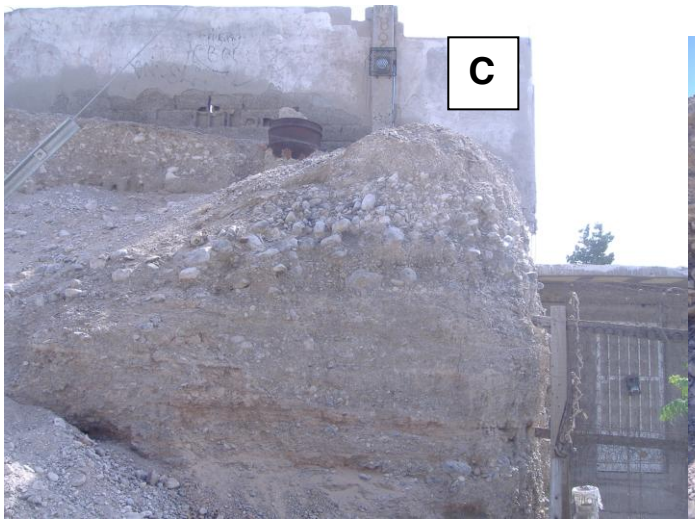

Figure 7 Sector Terraces in Felipe Angeles Neigbourhood: A) GH Terrace Coordinates: 356099.15E; 3515159.88N Elev; 1160 masl. B)MP Terrace Coordinates. 356673.95E; 35155308.83N; Elev. 1145 masl C) NM Terrace 357448.05;; 3514394.04N; Elev. 1150 masl. D) JAM Terrace Coordinates 356164.71E; 3514977.46N Elev. 1155 masl; E) Q Terrace Coordinates 355969.46E; 3514911.90N; Elev. 1170 masl;

Figure 8 A) Bravo River terraces Barrio Azul “CEISAME” located in the proximity of Zaragoza Boulevard and Juarez Porvenir Higway. B) Panoramic view toward the Juarez valley and El Paso Texas. B) Outcrop zoom of the Terrace deposits Coordinates 372187.35 E; 3501260.75 Elev. 1135 masl C) Another outcrop near to the showing in picture B but maybe is contaminated for loose deposits.

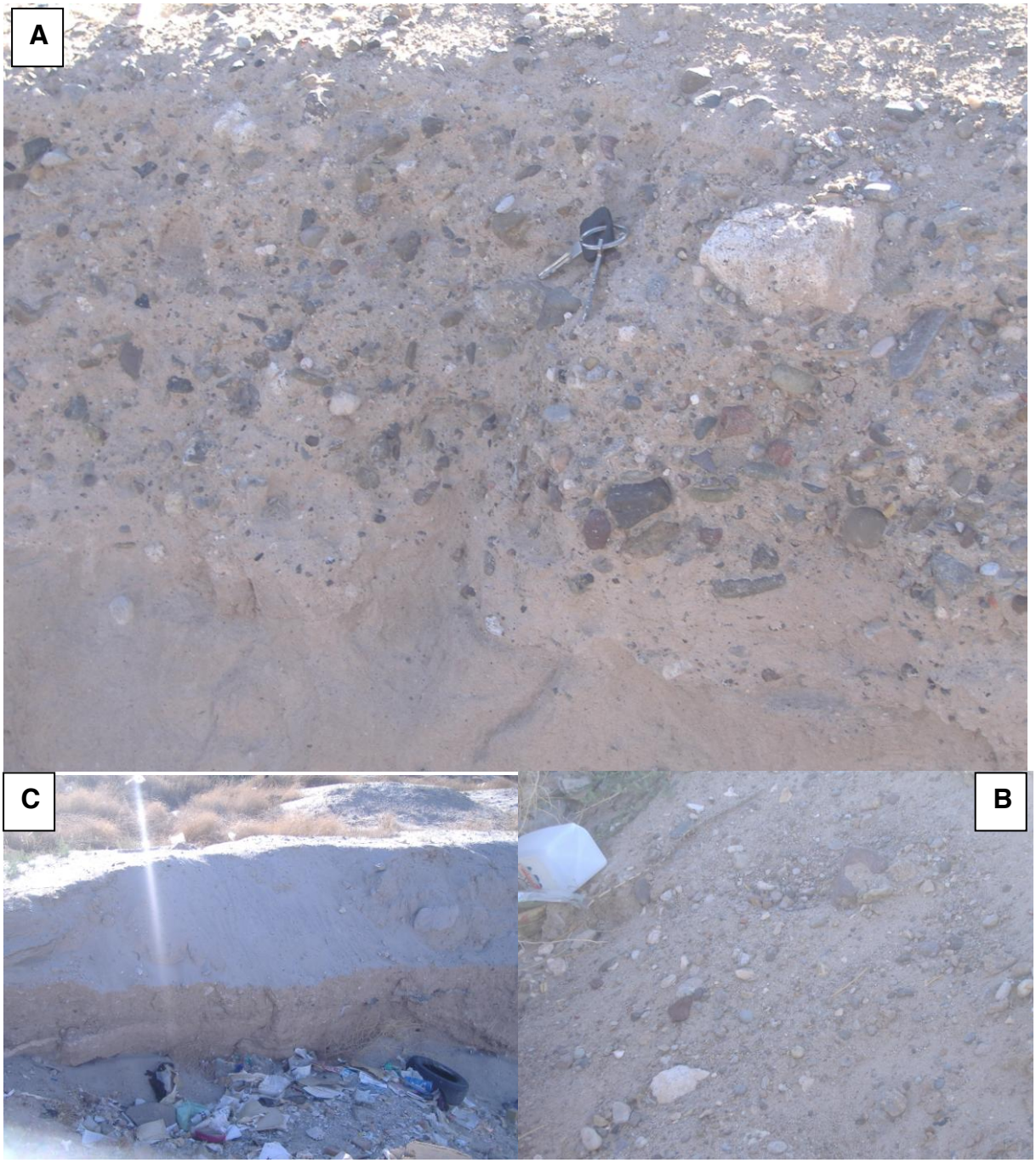

Figure 9 Bravo River terrace Sectors Aguilas de Zaragoza and Riveras del Bravo. A) Outcrop located in Aguilas de Zaragoza Coordinates 375069.21E; 3495491.16N; Elev. 1135 masl. B) Outcrop located at the intersection of Puerto Dunkerque and Nacaxoc streets. C) Outcrop showing contact between old Bravo River channel bed and Bravo River eroded recent deposits which are common in all the surrounded area.

Figure 10. Bravo River terraces petrographic analysis in the laboratory of the samples collected and listed in tables 1 and 2 of Appendix A2.

M-1151
E-2168

M-1196 E-2163

M-1196 E-2163

M-1151
E-2168

Complementary draft information of alluvial fills underlying terraces deposits

Three fluvial terraces deposits derived from the Bravo River are overlying by alluvial fills derived from the Juárez mountains. These alluvial fills terraces are outcropping in sites knowed like Astecas San Antonio Neigbourhoods (ASA); Tepeyac Cementery (TC) and Municipal Cementery (MC) and were explained in results chapter 4 Maps 4.1B and 4.1C. In the following illustrations are presented somes pictures using Google maps geographic coordinates and sample collection and resuls of soils classificasion is presented in appendix 4.A1 to 4.A3.. These deposits are in contact with fluvial deposits Points were referred to Geographic Coordinates given in google maps (2011)

Figure 4.1 Tepeyac Cementery (TC) alluvial fills in plan view. See the flat shape adopted for these alluvial fills deposits. In Figures 4.2 to 4.5 are presented presented the texture of this alluvial fills derived Juárez mountains.

Figure 4.2. Shows the conglomerate deposits derived from Juárez mountains

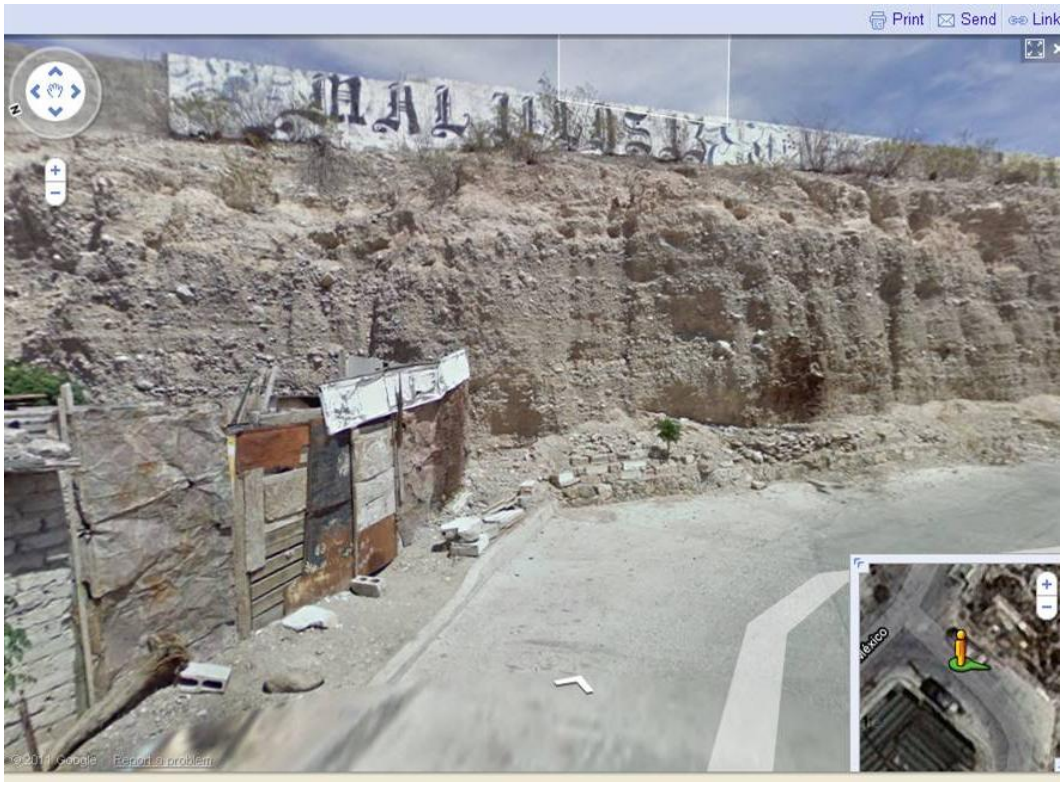

Figure 4.3 Shows the conglomerate deposits derived from Juárez mountains

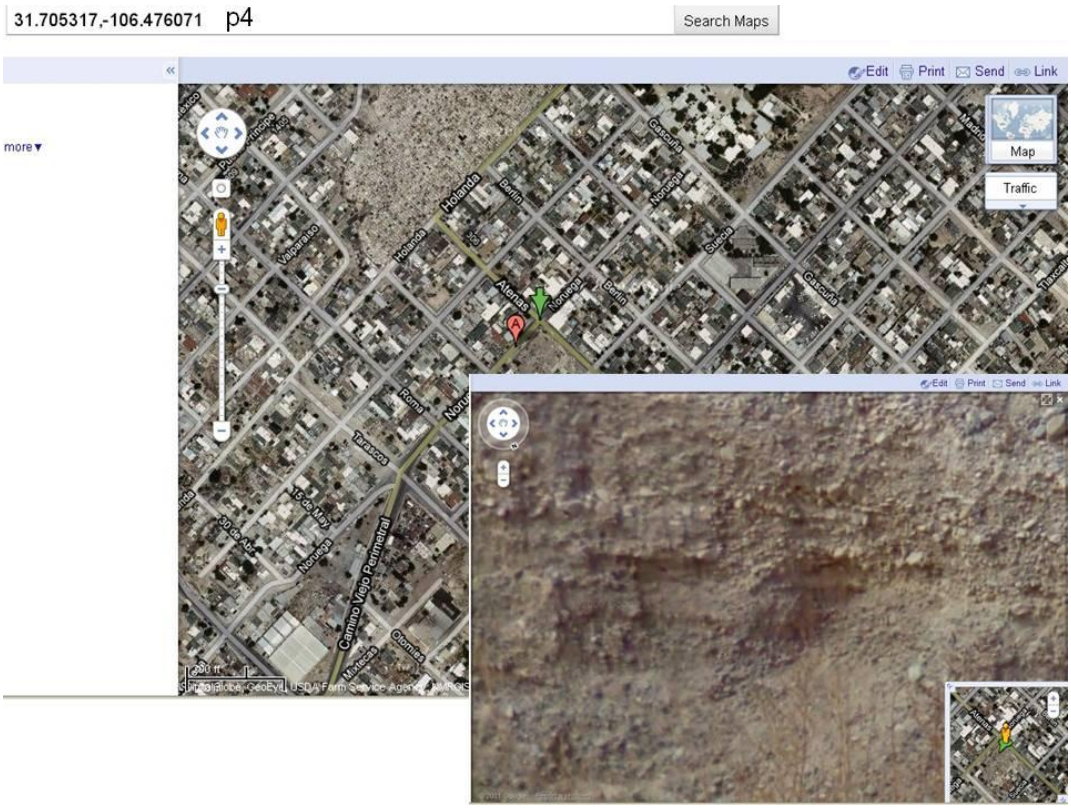

Figure 4.4 Shows the conglomerate deposits derived from Juárez mountains

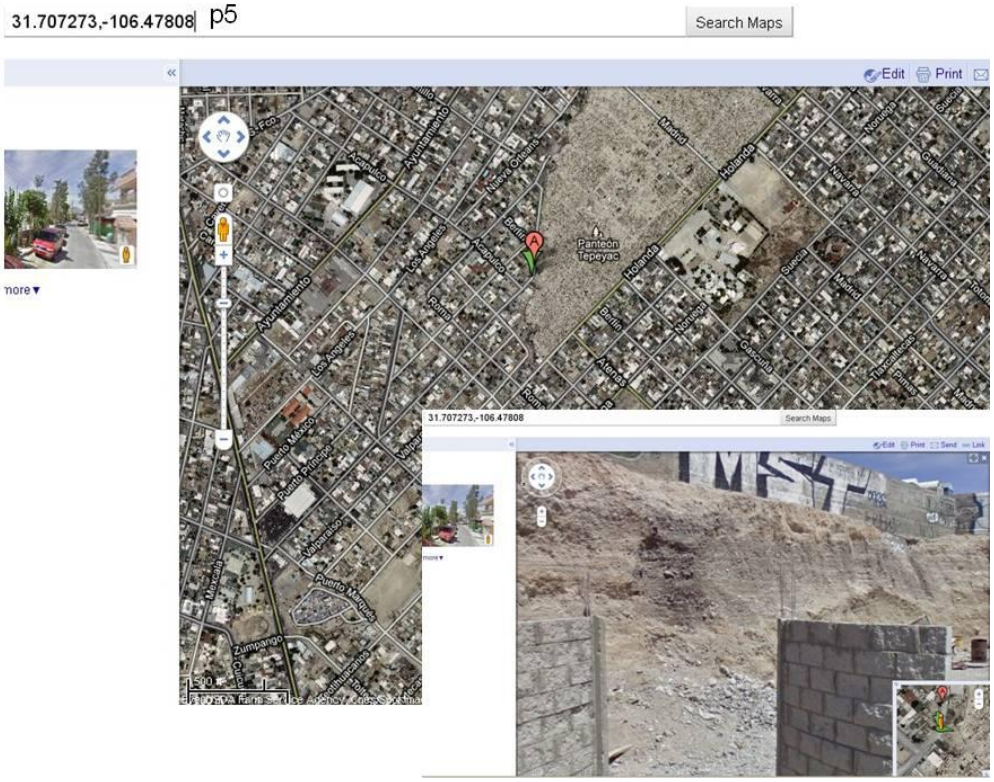

Figure 4.5 Shows the conglomerate deposits derived from Juárez mountains

Figure 4.6 Municipal Cementery (MC) alluvial fills in plan view. See the flat shape adopted for these alluvial fills deposits. In the upper right corner of the figure is shown the alluvial fill outcropping the Municipal Cementery area.

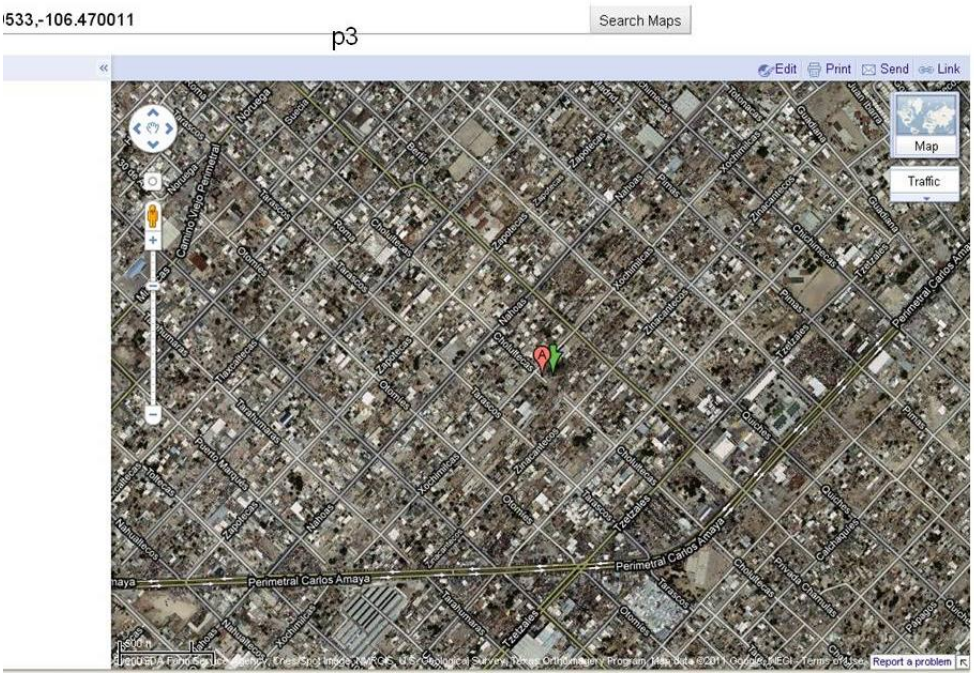

Figure 4.7Aztecas San Antonio Neighbourhoods (ASA) alluvial fills in plan view. See the flat shape adopted for these alluvial fills deposits. In Figures 4.2 to 4.5 are presented presented the texture of this alluvial fills derived Juárez mountains.

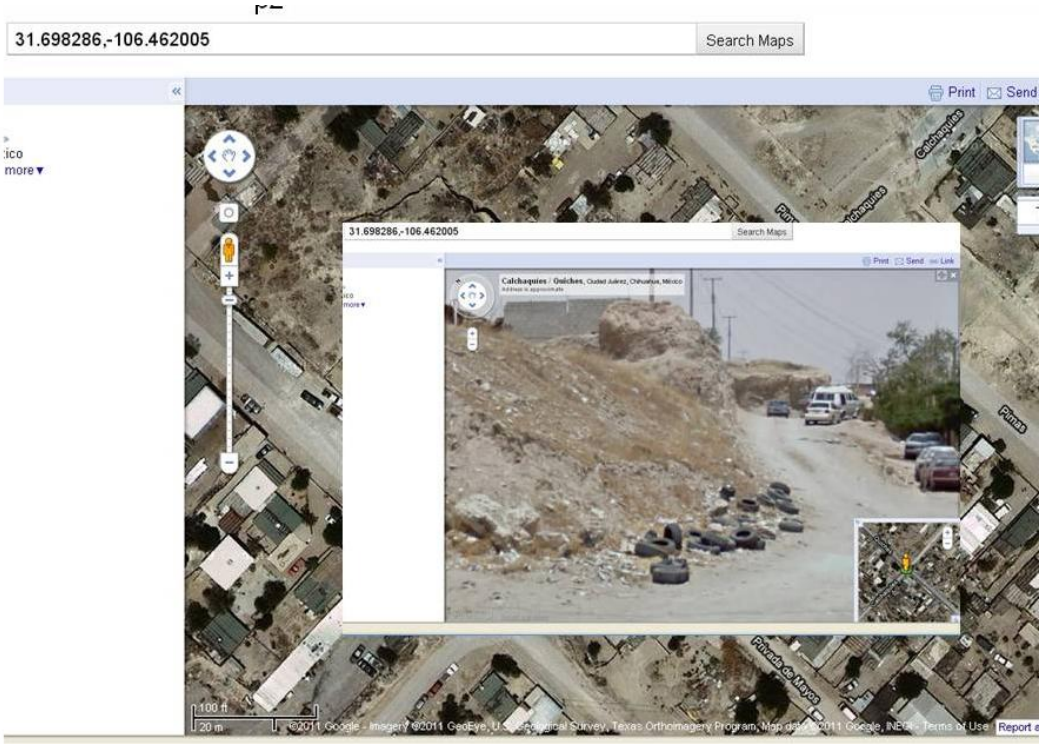

Figure 4.8 Aztecas San Antonio Neighbourhoods (ASA) alluvial fills in plan view. See the flat shape adopted for these alluvial fills deposits. In Figures 4.2 to 4.5 are presented presented the texture of this alluvial fills derived Juárez mountains.

Appendix 4A4

.

Fan system history of the study area through boreholes evidence is the first part of the task oriented to assess the dynamic of the active alluvial fan system that is threatening the Ciudad Juárez area. For this reason the present Chapter is dedicated to analyze and discuss the results obtained during collection data that were provided and actually performed by the Sanitation and Water Municipal Meeting (JMAS). This Municipal Government organization is responsible to provide water to Juárez city population which principal source of water is constituted by the aquifer El Hueco basin.

People who live in the study area use water from the Hueco basin intramontane aquifer originated due to normal faults occurred basically during two geologic events. These events can be separated in two principal types. Firstly, the Basin and Range geological province that produced a sequence of gravens, half gravens and horsts during Eocene to Miocene time as a consequence of the Farallon plate subduction. Secondly, the continuation of many intrabasinal normal faults that were active during Pliocene to Quaternary time (Rio Bravo rift system). These extension events provided accommodation space for sediments that were derived from the rocks outcrops fragmentation and erosion of the footwall and transported and deposited in the hanging wall during a long periods of time that finally produced the actual intramontane characteristic landform of the Hueco basin.

The information regarded to boreholes lithology is mostly located in the Hueco aquifer basin area that corresponds to the centre of the urbanized area of Ciudad Juárez area (Figure 1).This information provided by (JMAS) that is integrated by 59 boreholes that were drawn in terms of the type of soil in order to construct the holes lithology illustrated in (Figures 2 to 60). As shown in Figures 2 to 60 some boreholes lithological units are typical of some areas. Therefore, it is important to distinguish them attending not only to the operation mode but also to the geomorphological expression that is present in the terrain surface.

The association between geomorphology and mode of operation could be done in terms of the surface landscape and the two big drivers that control the operation mode of fan formation tectonic or climate or both. Additionally, it is necessary to consider if aggradation or incision were operated during some periods

of time in order to distinguish between the energy of soils deposition such as sheetflow, flowdebris, channel flow, or fluvial soils. Finally, could be possible to correlate the soils facies actually recorded on the boreholes lithology with the deposition environment that were active. In short these analysis suggests five principal groups of holes with similar characteristics of soils.

Group 1. Soils types of this group are basically (clay, clayey sand, sandy clay, and fine, medium, coarse and mixed sand mostly of eolic origin) and their geographic distribution are presented in yellow colour (Figure 1) there are: 7R, 16, 19, 42, 46, 50, 61, 94, 146, 156, 170, 176, 193, 194, 196, and 197. The principal characteristic of these units is the absence of conglomeratic soils that suggest that among the depth explored not important faults were occurred. Contrary, the presence of eolic sands as well as clay soils indicates that climatic mode alone were present during these boreholes that maybe corresponds to periods of climatic changes during the glacial interglacial epochs of recent Quaternary time.

The boreholes of group 1 are divided in three subgroups with different geographic location, One subgroup, and the more important have a explored depth variable between 300 m to 400 m, is located on the southeastern area of the city and is represented by the following holes: 197 (Free municipe neighborhood); 196 (Oasis neighborhood); 194 (Independence boulevard); 193 (Praderas del Sur neighborhood); 176 (Independence and Panamerican highway); 170 (Lazaro Cardenas Airport); 156 (Henequen Industrial park); 46 (Zaragoza boulevard); 146 (Jarudo Infonavit unit). The principal characteristic of these boreholes are that the soils behavior on the surface layers are represented by eolic fine to coarse sands intercalated with thin layers of clay and sandy clay but for more depth layers the thickness of the clay soils increases instead the sand soils thickness reduces. These soils borehole behavior suggest and justify the formation of the Barreal basin approximately during Pleistocene time and confirm that the operation mode active were climate.

The boreholes that constitute the second subgroup located on the southeastern but more central area of the city are the following: 61 (Benito Juarez habitational unit); 42 (Cuernavaca Neighborhood); 16 (Miguel Hidalgo market) and 7R (Grande river Park). The soils behavior of these units are more sandy that the first subgroup maybe because the borehole of this subgroup have a depth of 250

meters that represents the beginning of formation of relevant layers of clay instead of the subgroup one that have a explored depth of 300m to 400 meters..

Finally, the last group is represented by the following boreholes: 94 (Casa de Janos neighborhood) 19 (Ave Ejercito Pradera dorada); 50 (Andres Figueroa Neighborhood) and basically represent an important thickness of clayey soils of lacustrine origen approximately to 150 meters depth. In addition these boreholes were explored only to 250 meters. In short is possible to consider that these three subgroup could be grouped into the group 1.

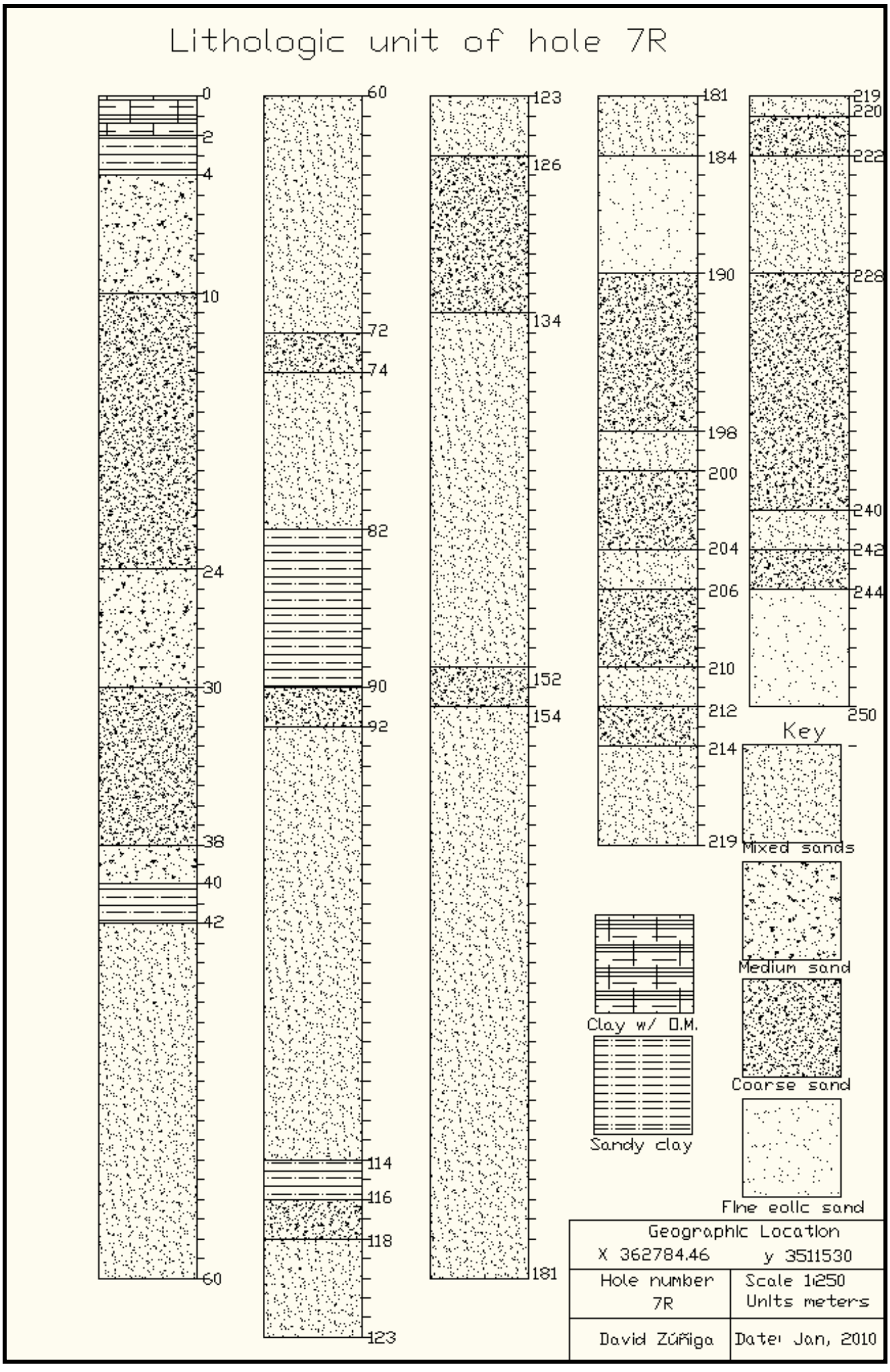
Lithologic unit of hole 7R
0
2
4
10
24
30
38
40
42
60
60
72
74
82
90
92
114
116
118
123
123
126
134
152
154
181
181
184
190
198
200
204
206
210
212
214
219
219
220
222
228
240
242
244
250
Key
Mixed sands
Medium sand
Coarse sand
Fine eolic sand
Clay w/ O.M.
Sandy clay
Geographic Location
X 362784.46 y 3511530
Hole number 7R
Scale 1:250 Units meters
David Zúñiga
Date: Jan, 2010

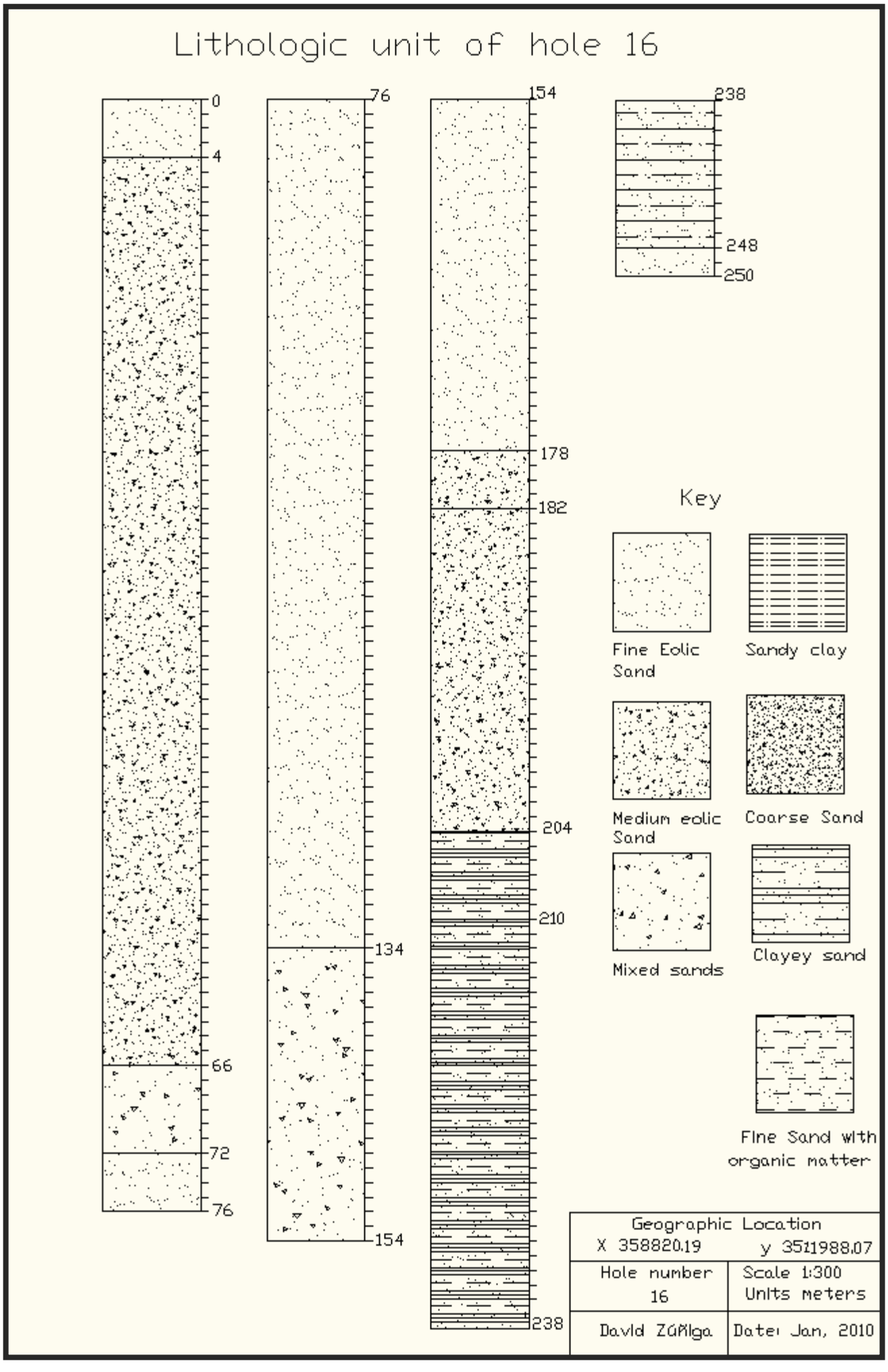
Lithologic unit of hole 16
0
4
66
72
76
76
134
154
154
178
182
204
210
238
238
248
250
Key
Fine Eolic Sand
Sandy clay
Medium eolic Sand
Coarse Sand
Mixed sands
Clayey sand
Fine Sand with organic matter
Geographic Location
X 358820.19
y 3511988.07
Hole number 16
Scale 1:300 Units meters
David Zúñiga
Date: Jan, 2010

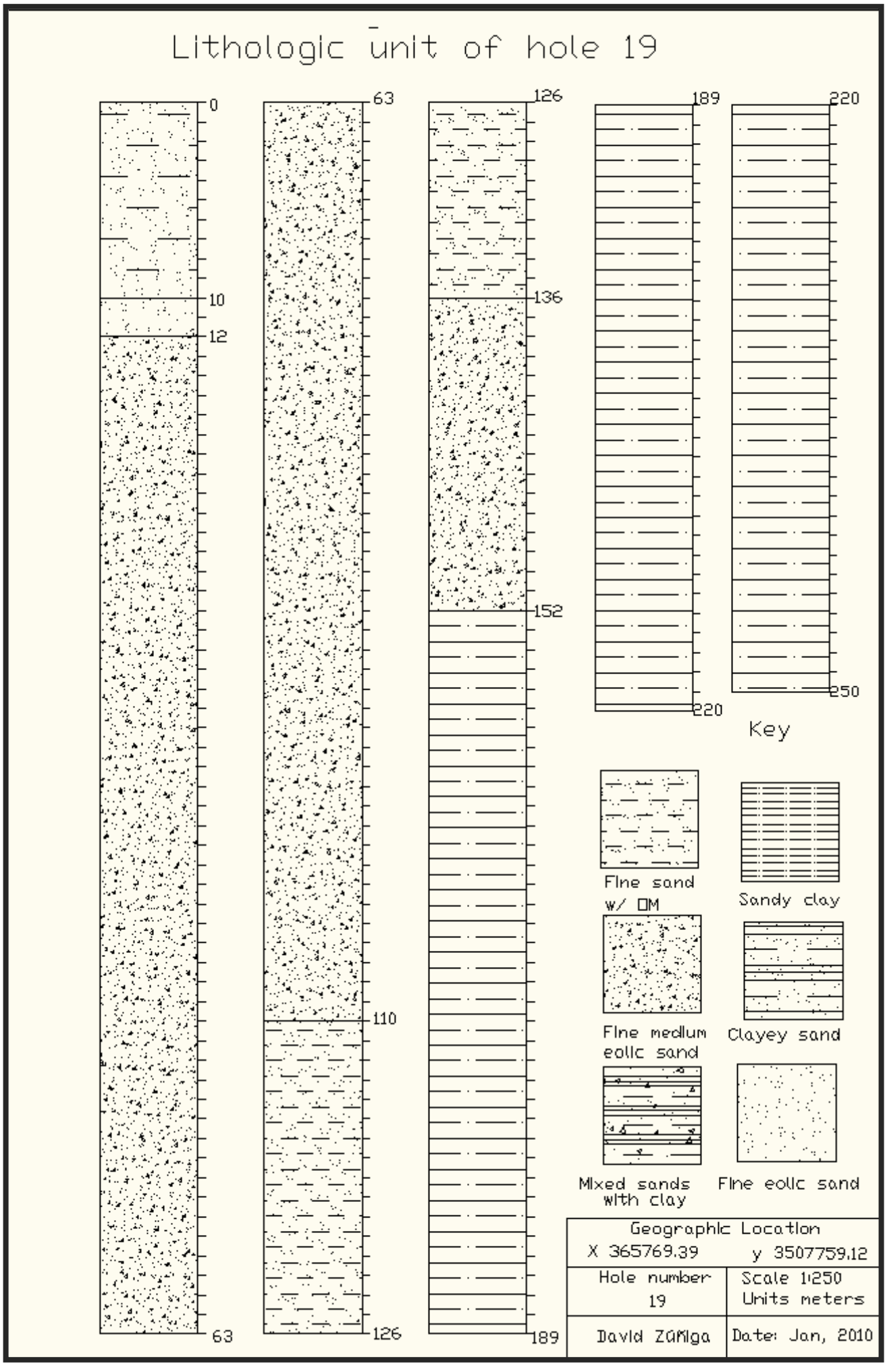
Lithologic unit of hole 19
0
10
12
63
63
110
126
126
136
152
189
189
220
220
250
Key
Fine sand w/ OM
Sandy clay
Fine medium eolic sand
Clayey sand
Mixed sands with clay
Fine eolic sand
Geographic Location
X 365769.39
y 3507759.12
Hole number 19
Scale 1:250 Units meters
David Zúñiga
Date: Jan, 2010

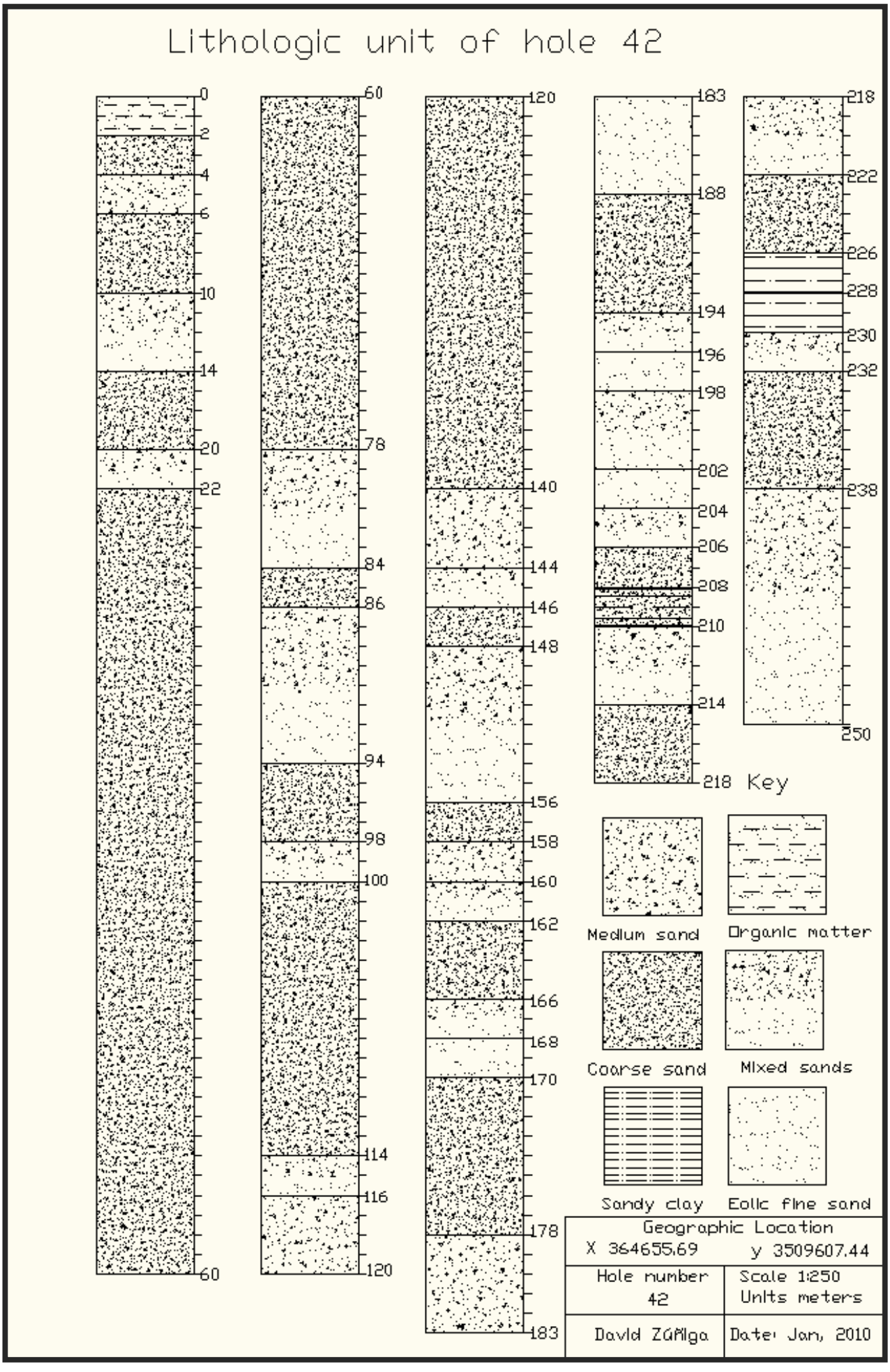
Lithologic unit of hole 42
0
2
4
6
10
14
20
22
60
60
78
84
86
94
98
100
114
116
120
120
140
144
146
148
156
158
160
162
166
168
170
178
183
183
188
194
196
198
202
204
206
208
210
214
218
218
222
226
228
230
232
238
250
Key
Medium sand
Organic matter
Coarse sand
Mixed sands
Sandy clay
Eolic fine sand
Geographic Location
X 364655.69
y 3509607.44
Hole number
42
Scale 1:250
Units meters
David ZÁÑiga
Date: Jan, 2010

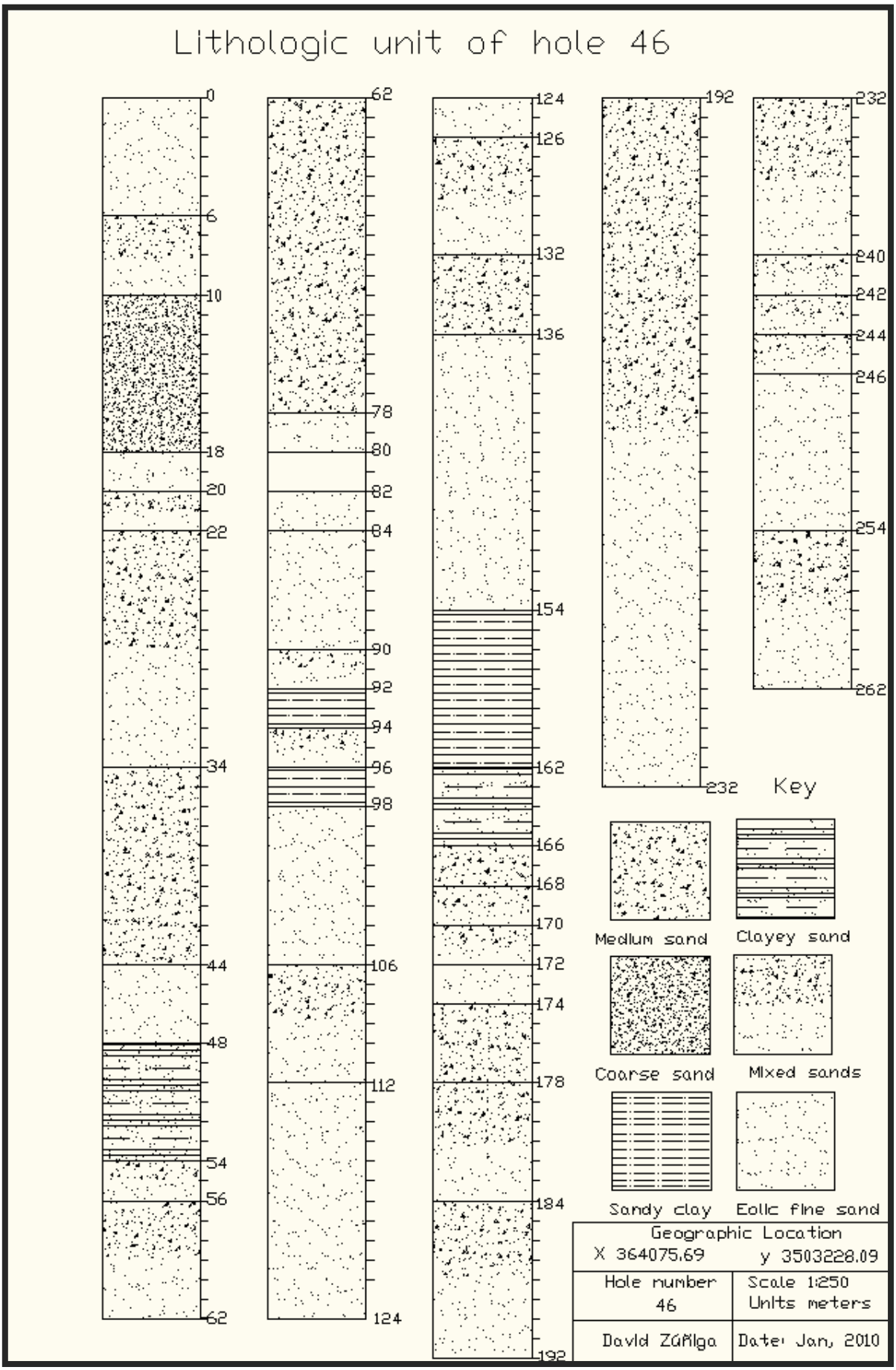
Lithologic unit of hole 46
0
6
10
18
20
22
34
44
48
54
56
62
62
78
80
82
84
90
92
94
96
98
106
112
124
124
126
132
136
154
162
166
168
170
172
174
178
184
192
192
232
240
242
244
246
254
262
Key
Medium sand
Clayey sand
Coarse sand
Mixed sands
Sandy clay
Eolic fine sand
Geographic Location
X 364075.69 y 3503228.09
Hole number 46
Scale 1:250 Units meters
David ZúÑiga
Date: Jan, 2010

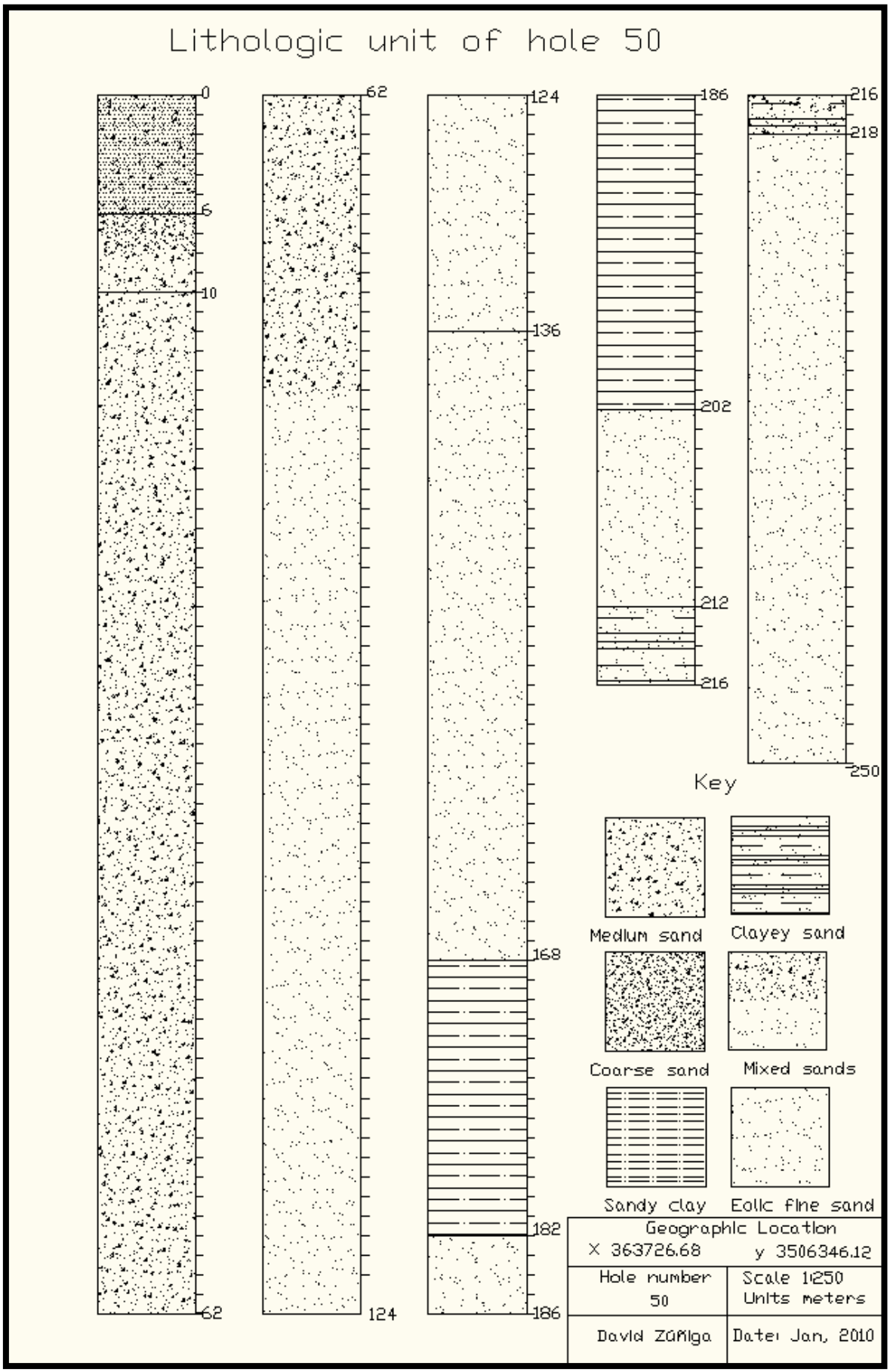
Lithologic unit of hole 50
0
6
10
62
62
124
124
136
168
182
186
186
202
212
216
216
218
250
Key
Medium sand
Clayey sand
Coarse sand
Mixed sands
Sandy clay
Eolic fine sand
Geographic Location
X 363726.68
y 3506346.12
Hole number
50
Scale 1:250
Units meters
David ZAMiga
Date: Jan, 2010

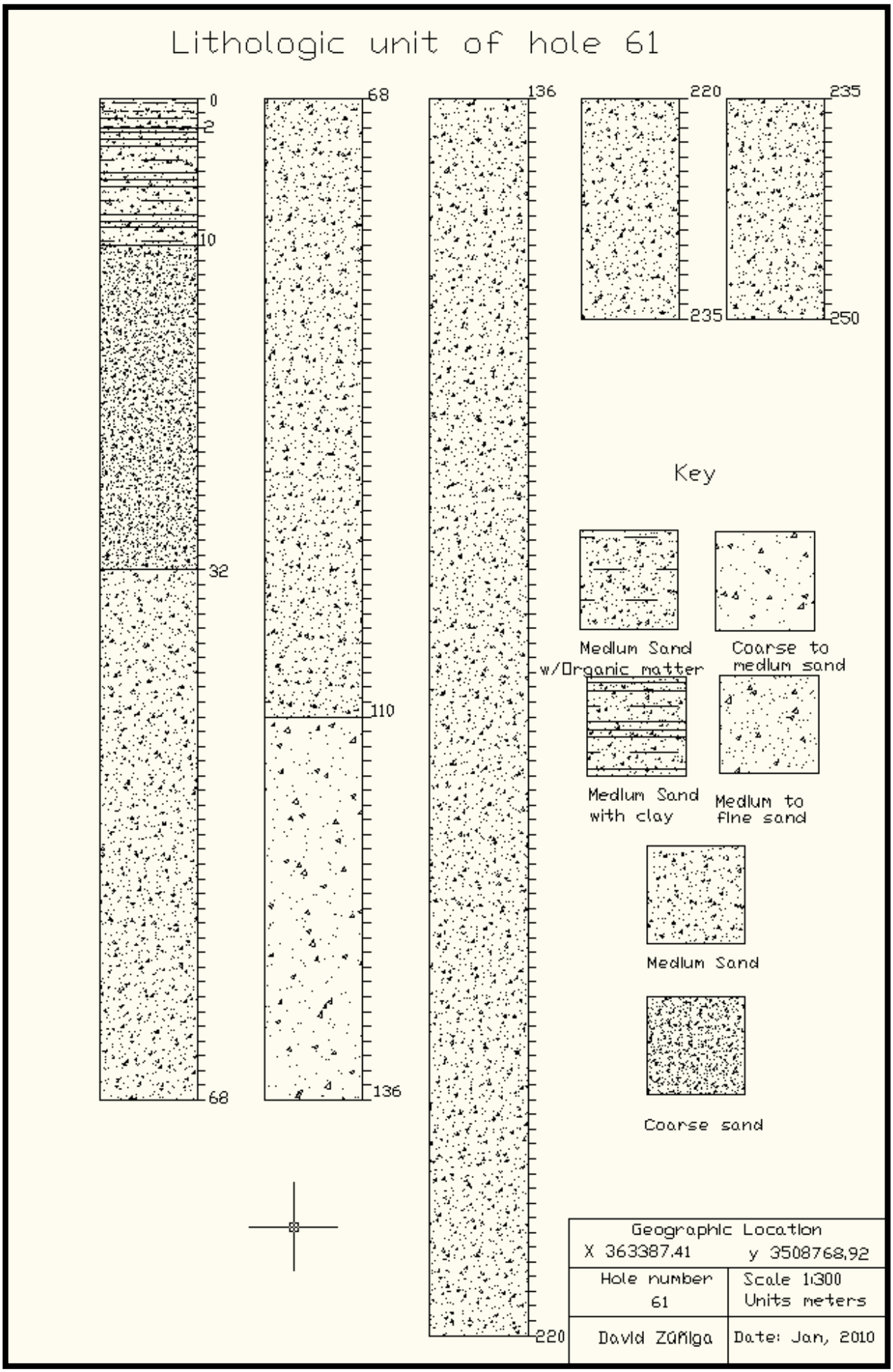
Lithologic unit of hole 61
0
2
10
32
68
68
110
136
136
220
220
235
235
250
Key
Medium Sand w/Organic matter
Coarse to medium sand
Medium Sand with clay
Medium to fine sand
Medium Sand
Coarse sand
Geographic Location
X 363387.41
y 3508768.92
Hole number 61
Scale 1:300
Units meters
David Zúñiga
Date: Jan, 2010

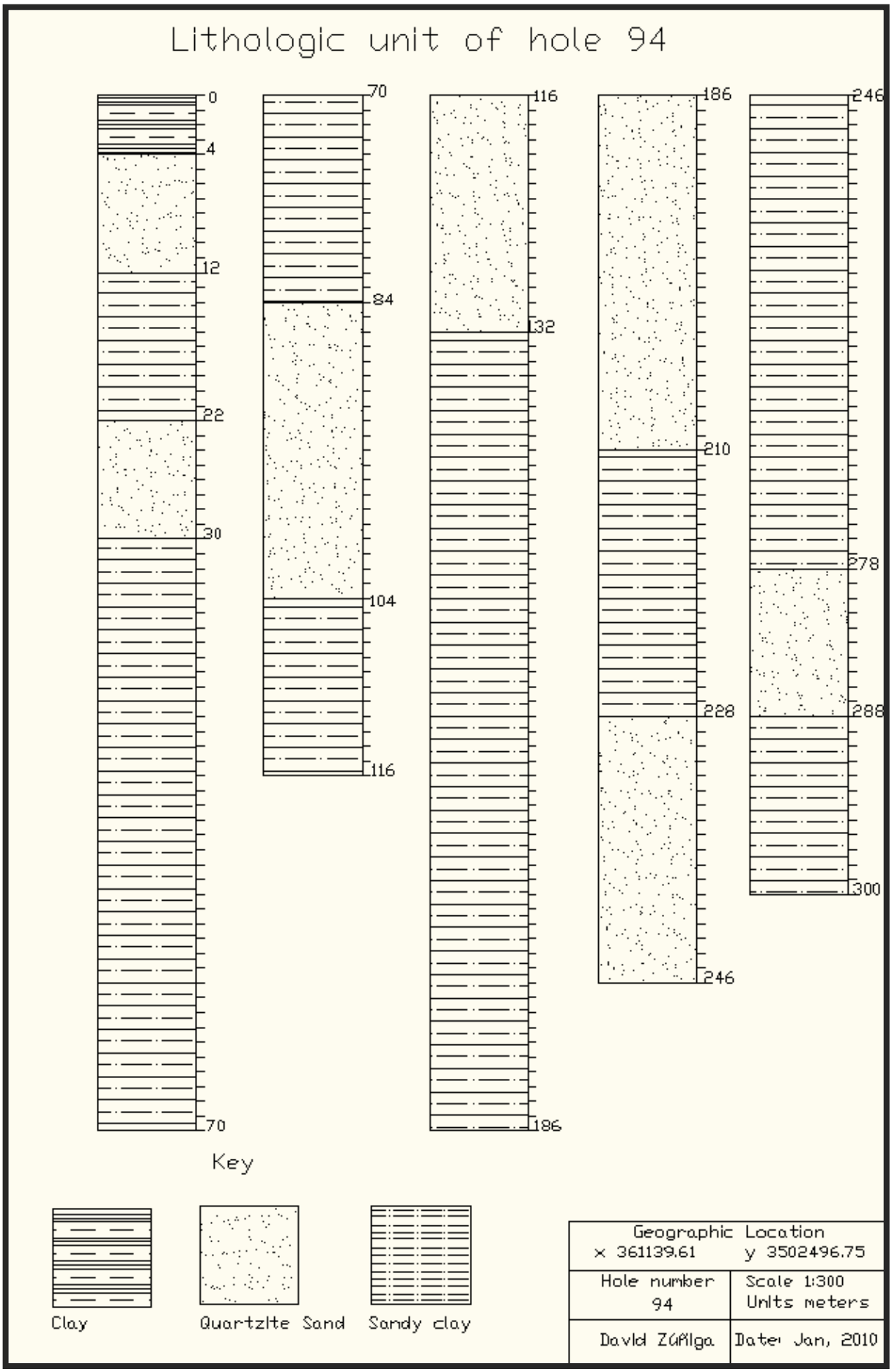
Lithologic unit of hole 94
0
4
12
22
30
70
70
84
104
116
116
32
186
186
210
228
246
246
278
288
300
Key
Clay
Quartzite Sand
Sandy clay
Geographic Location
x 361139.61 y 3502496.75
Hole number
94
Scale 1:300
Units meters
David ZÚÑiga
Date: Jan, 2010

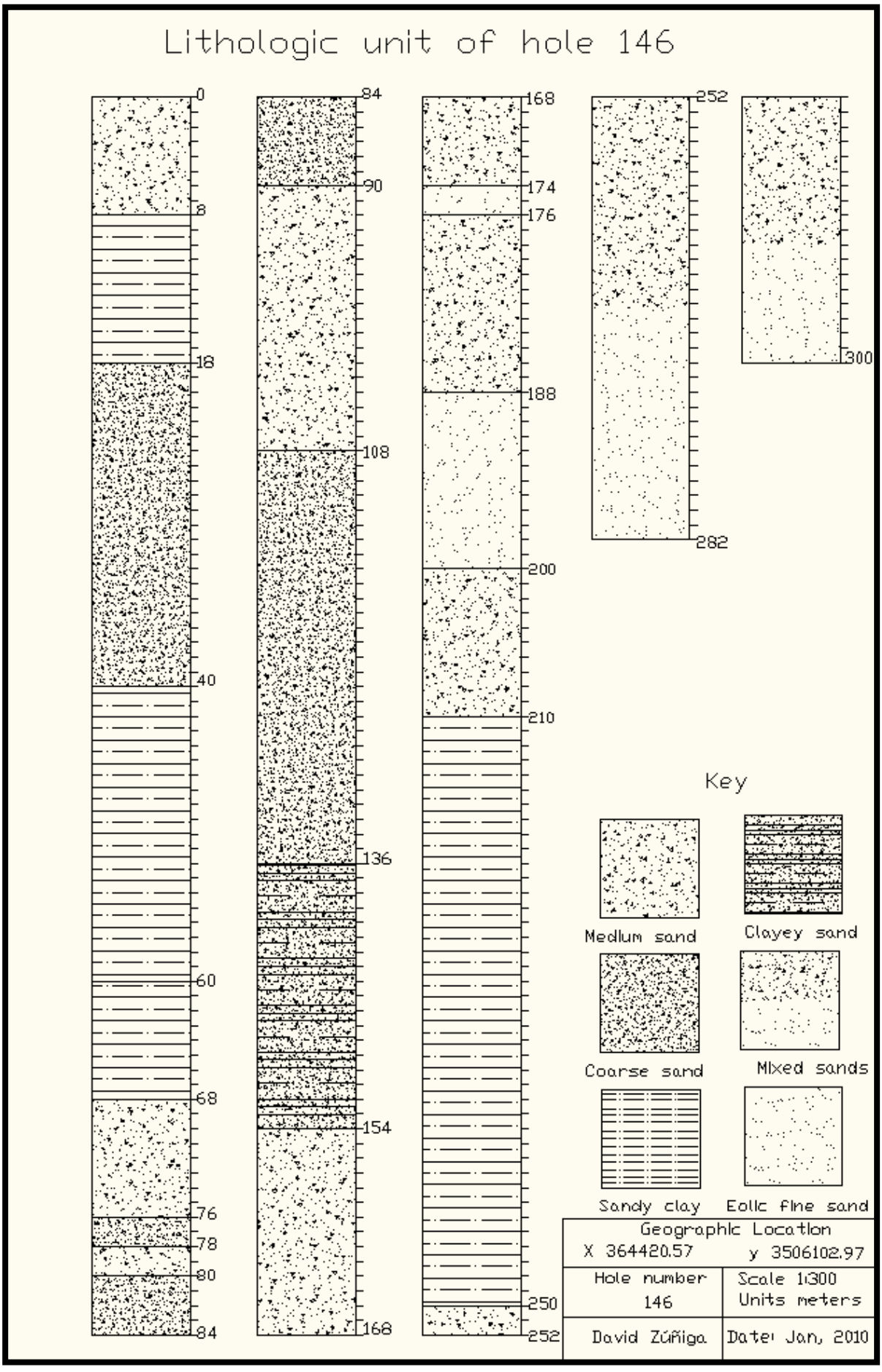
Lithologic unit of hole 146
0
8
18
40
60
68
76
78
80
84
84
90
108
136
154
168
168
174
176
188
200
210
250
252
252
282
300
Key
Medium sand
Clayey sand
Coarse sand
Mixed sands
Sandy clay
Eolic fine sand
Geographic Location
X 364420.57
y 3506102.97
Hole number
146
Scale 1:300
Units meters
David Zúñiga
Date: Jan, 2010

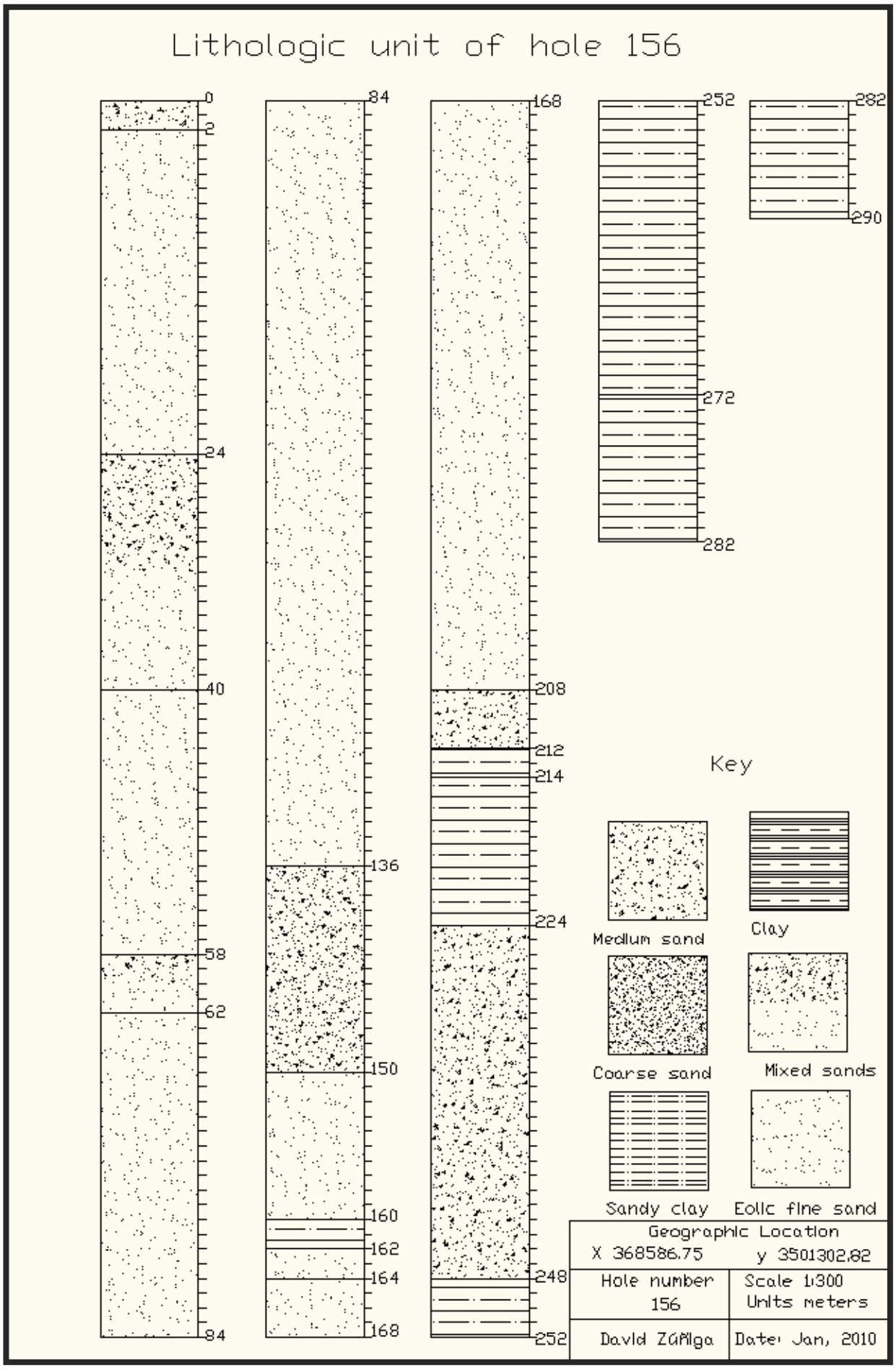
Lithologic unit of hole 156
0
2
24
40
58
62
84
84
136
150
160
162
164
168
168
208
212
214
224
248
252
252
272
282
282
290
Key
Medium sand
Clay
Coarse sand
Mixed sands
Sandy clay
Eolic fine sand
Geographic Location
X 368586.75
y 3501302.82
Hole number
156
Scale 1:300
Units meters
David ZÁÑiga
Date: Jan, 2010

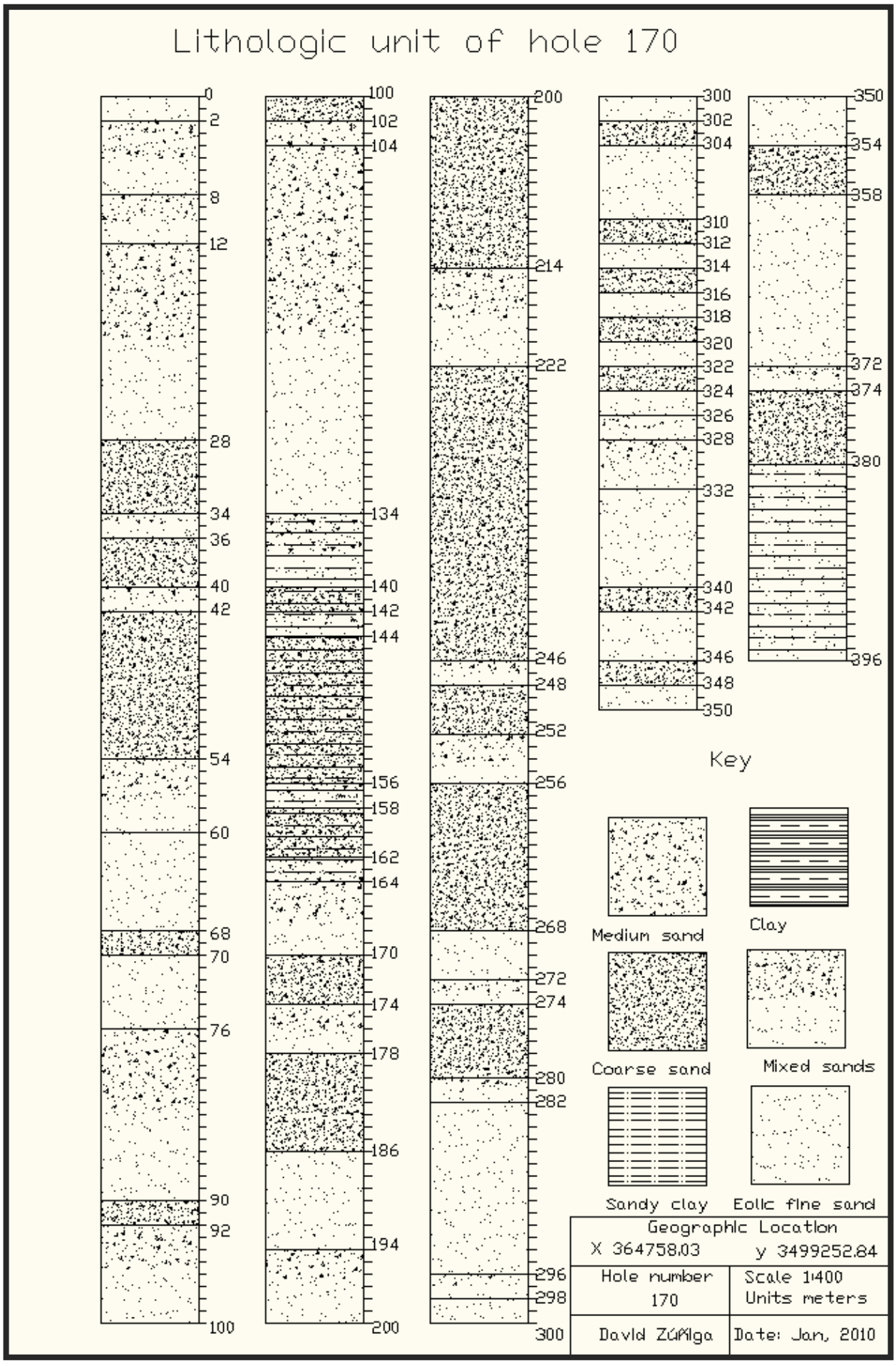
Lithologic unit of hole 170
0
2
8
12
28
34
36
40
42
54
60
68
70
76
90
92
100
100
102
104
134
140
142
144
156
158
162
164
170
174
178
186
194
200
200
214
222
246
248
252
256
268
272
274
280
282
296
298
300
300
302
304
310
312
314
316
318
320
322
324
326
328
332
340
342
346
348
350
350
354
358
372
374
380
396
Key
Medium sand
Clay
Coarse sand
Mixed sands
Sandy clay
Eolic fine sand
Geographic Location
X 364758.03
y 3499252.84
Hole number
170
Scale 1:400
Units meters
David Zúñiga
Date: Jan, 2010

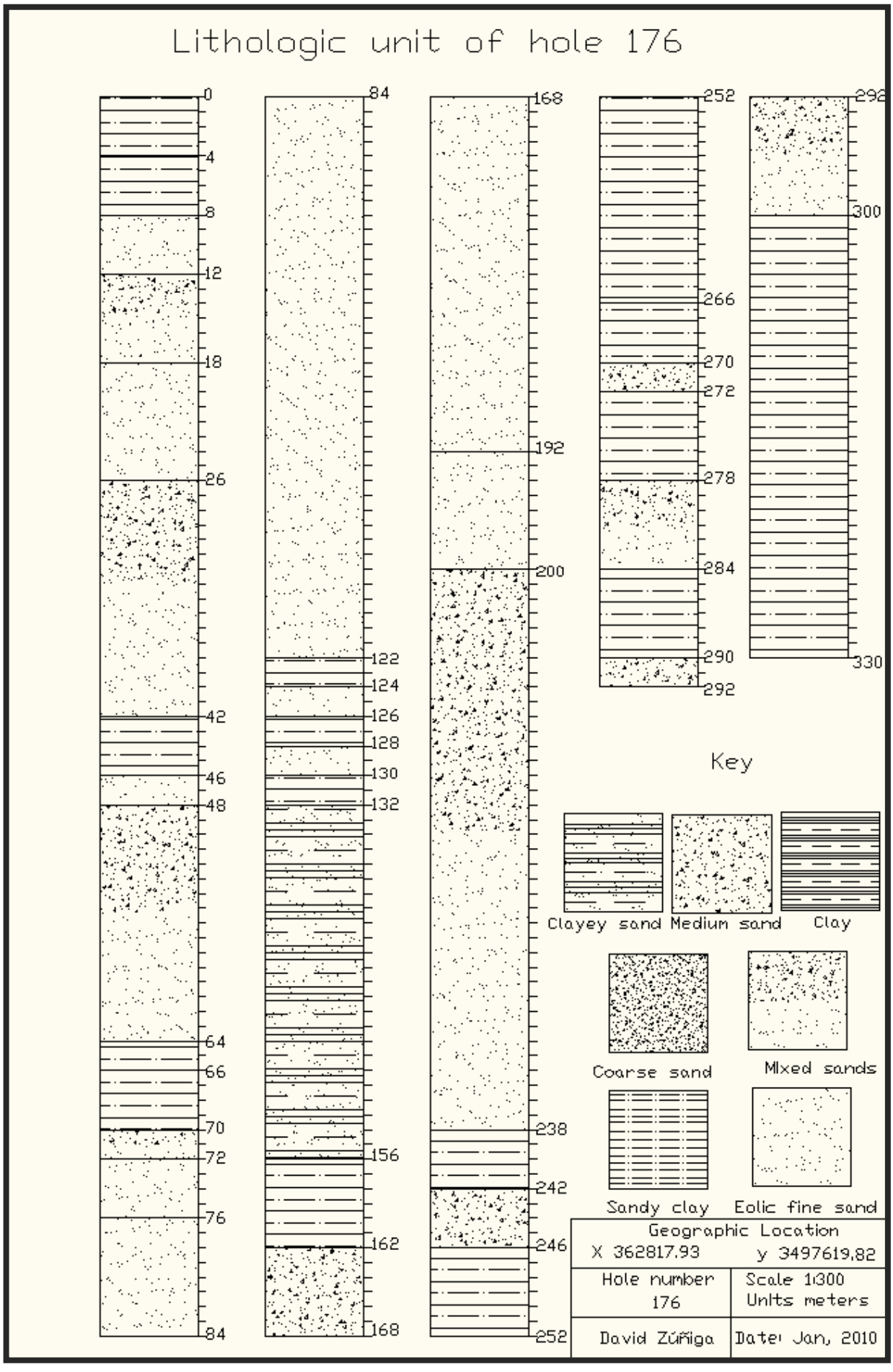
Lithologic unit of hole 176
0
4
8
12
18
26
42
46
48
64
66
70
72
76
84
84
122
124
126
128
130
132
156
162
168
168
192
200
238
242
246
252
252
266
270
272
278
284
290
292
292
300
330
Key
Clayey sand
Medium sand
Clay
Coarse sand
Mixed sands
Sandy clay
Eolic fine sand
Geographic Location
X 362817.93
y 3497619.82
Hole number
176
Scale 1:300
Units meters
David Zúñiga
Date: Jan, 2010

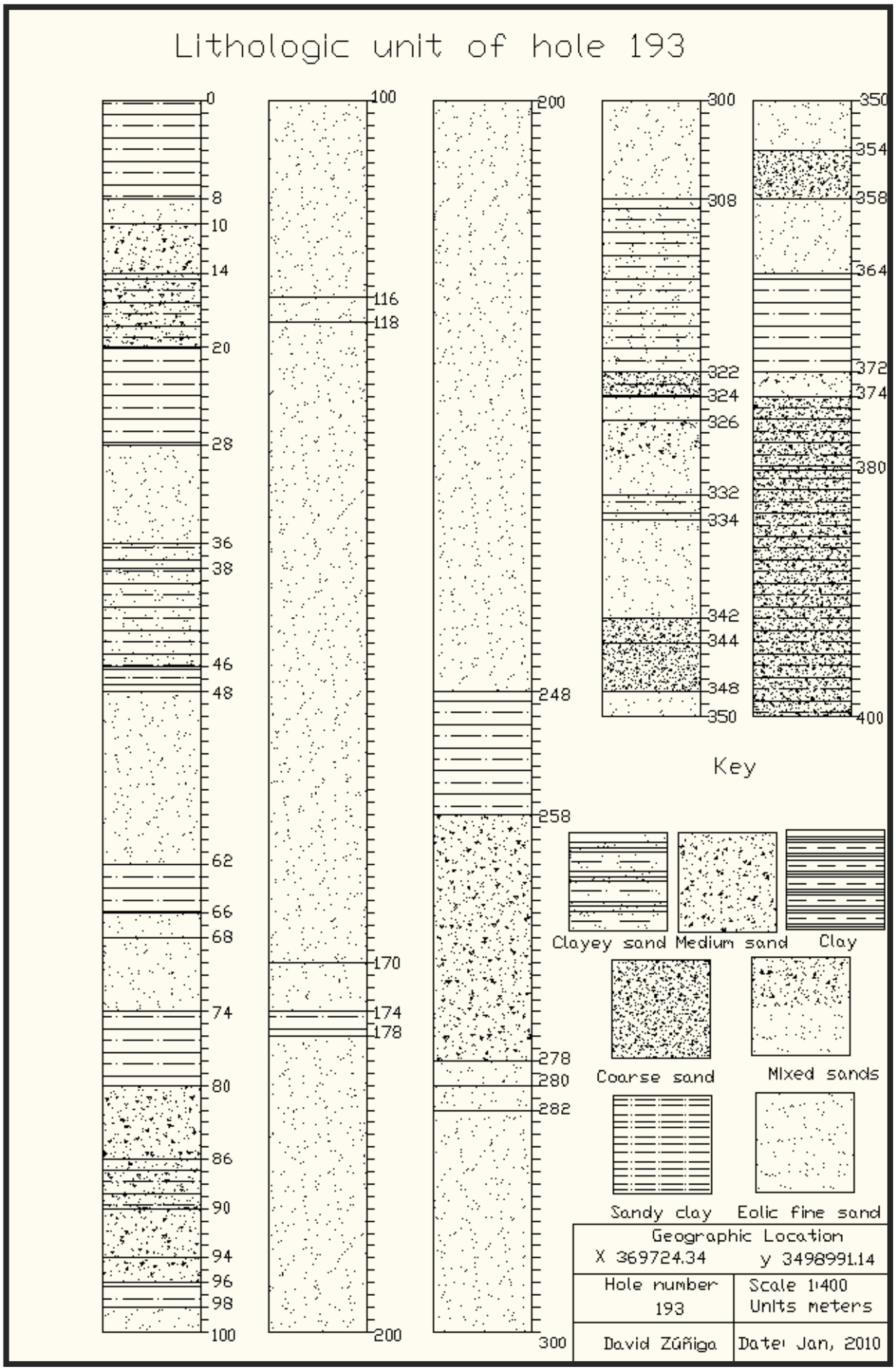
Lithologic unit of hole 193
0
8
10
14
20
28
36
38
46
48
62
66
68
74
80
86
90
94
96
98
100
100
116
118
170
174
178
200
200
248
258
278
280
282
300
300
308
322
324
326
332
334
342
344
348
350
350
354
358
364
372
374
380
400
Key
Clayey sand
Medium sand
Clay
Coarse sand
Mixed sands
Sandy clay
Eolic fine sand
Geographic Location
X 369724.34
y 3498991.14
Hole number
193
Scale 1:400
Units meters
David Zúñiga
Date: Jan, 2010

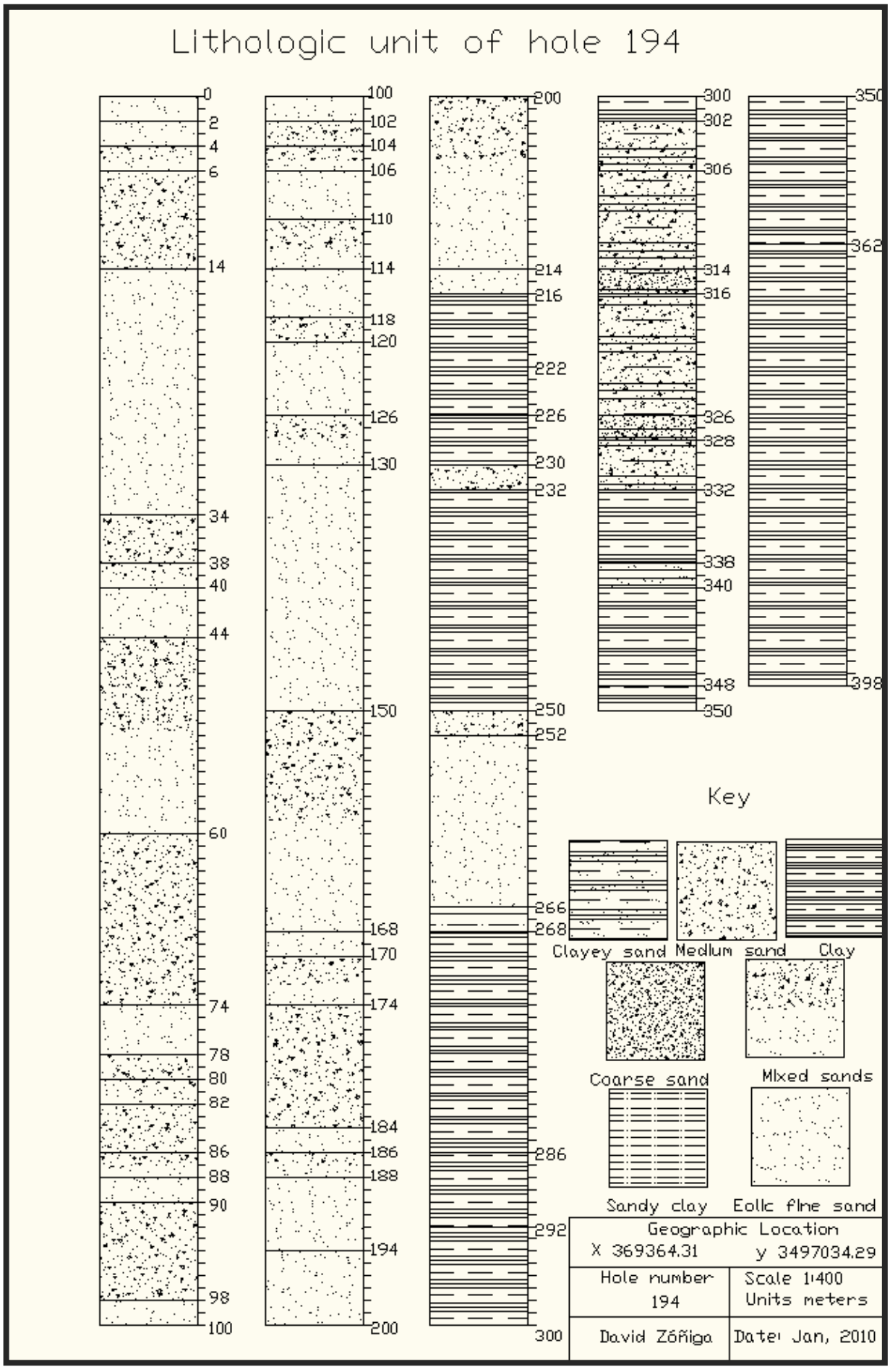
Lithologic unit of hole 194
0
2
4
6
14
34
38
40
44
60
74
78
80
82
86
88
90
98
100
100
102
104
106
110
114
118
120
126
130
150
168
170
174
184
186
188
194
200
200
214
216
222
226
230
232
250
252
266
268
286
292
300
300
302
306
314
316
326
328
332
338
340
348
350
350
362
398
Key
Clayey sand
Medium sand
Clay
Coarse sand
Mixed sands
Sandy clay
Eolic fine sand
Geographic Location
X 369364.31
y 3497034.29
Hole number
194
Scale 1:400
Units meters
David Zúñiga
Date: Jan, 2010

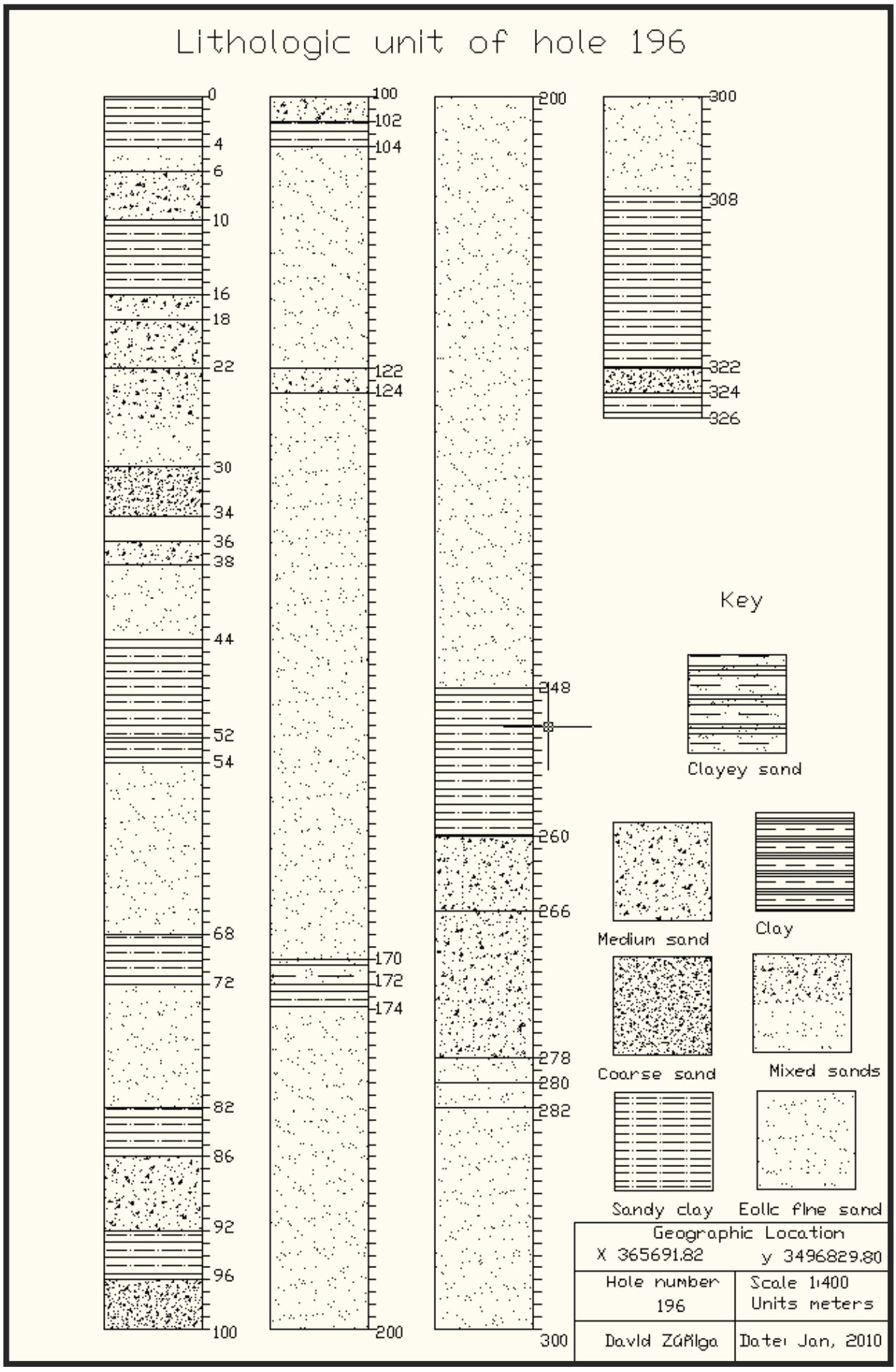
Lithologic unit of hole 196
0
4
6
10
16
18
22
30
34
36
38
44
52
54
68
72
82
86
92
96
100
100
102
104
122
124
170
172
174
200
200
248
260
266
278
280
282
300
300
308
322
324
326
Key
Clayey sand
Medium sand
Clay
Coarse sand
Mixed sands
Sandy clay
Eolic fine sand
Geographic Location
X 365691.82
y 3496829.80
Hole number
196
Scale 1:400
Units meters
David ZARIga
Date: Jan, 2010

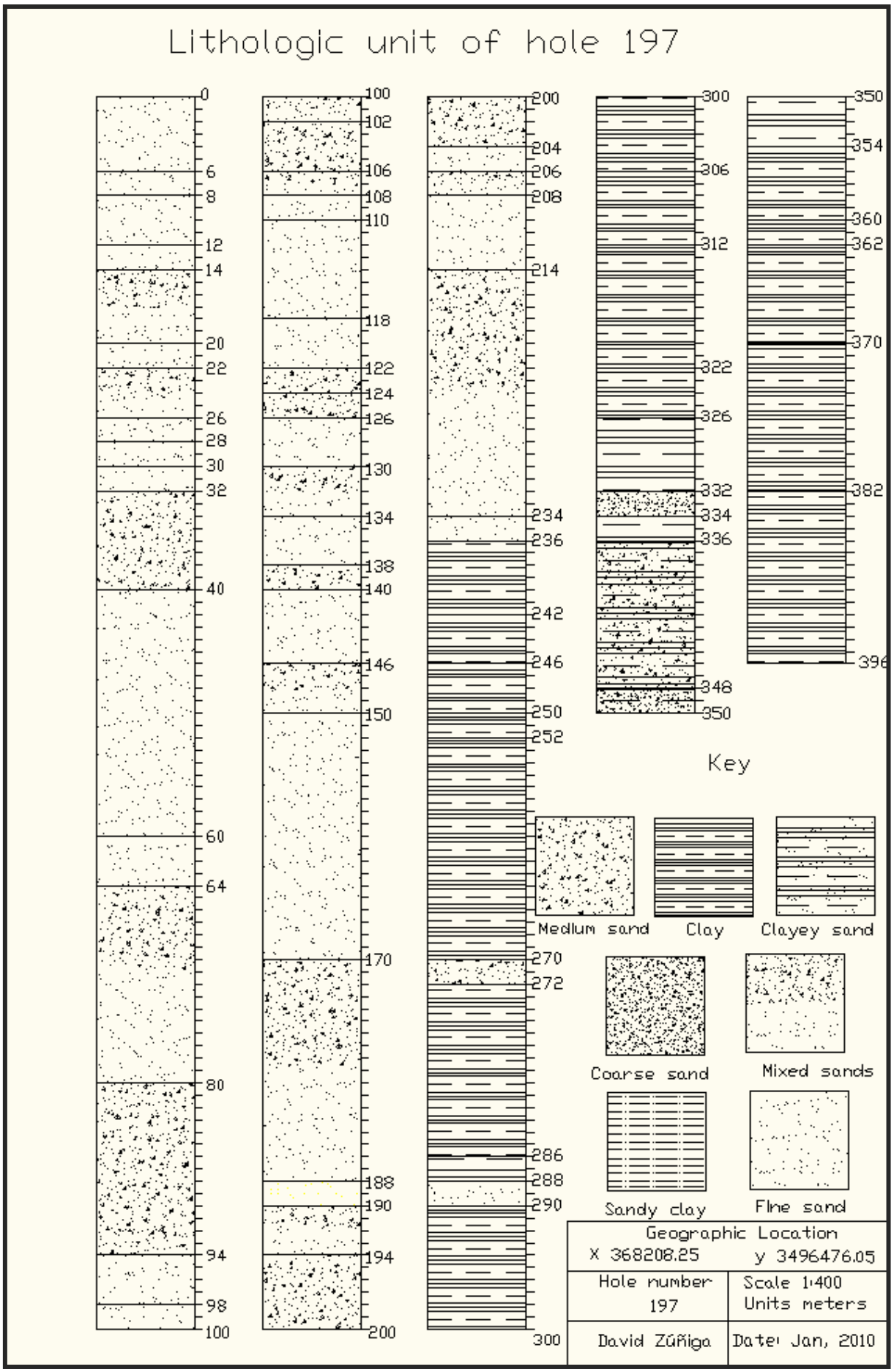
Lithologic unit of hole 197
0
6
8
12
14
20
22
26
28
30
32
40
60
64
80
94
98
100
100
102
106
108
110
118
122
124
126
130
134
138
140
146
150
170
188
190
194
200
200
204
206
208
214
234
236
242
246
250
252
270
272
286
288
290
300
300
306
312
322
326
332
334
336
348
350
350
354
360
362
370
382
396
Key
Medium sand
Clay
Clayey sand
Coarse sand
Mixed sands
Sandy clay
Fine sand
Geographic Location
X 368208.25
y 3496476.05
Hole number
197
Scale 1:400
Units meters
David Zúñiga
Date: Jan, 2010

Group 2. The soils of this borehole group are composed of (organic matter, clayey sand, sandy clay, clayey sand, and fine, medium, coarse and mixed sands predominantly sandy clay). The holes of this group are: 96, 161, 162, 167 and are illustrated in blue colour (Figure1). Note that in this group the predominant characteristic is the sandy clay type of soil and the only difference with respect of soils of group 1 is that in this soil group the upper layer is formed of organic matter. This, obviously suggest similarly that in group 1 a period of recent deposition that originated the lacustrine deposit that dominate the barreal basin. In addition these soils facies are strongly influenced by low gradient stream flow developed under closed or endorreic environment maybe during Quaternary to Pleistocene time and the climatic mode of operation instead of the tectonic operation mode.

The geographical location of group 2 boreholes are the following: 161 (Pablo Gomez neighborhood). The explored depth of this borehole was 400 m mostly composed by thick layers of clay as well sandy clay. The soils distribution of this borehohe is described in the following paragraphs: In the first (14 m to 116 m) there was found an important layer of clay as well sandy clay soils. Then, an intermediate layer of sands as well clays between 116 m to 226 m and finally another thick layer of Clay from 226 m to 400 m. Similarly, with respect to the soils found on borehole 162 in the first 106 meters the presence of a competent layer of clay were found, and another sandy soil intermediate layer from 106 m to 188 m finally the last layer of clay from 188 m to 390 meters. This borehole named the Granjas Santa Elena neighborhood located in the deposition centre of the barreal basin suggest the influence of low gradient streams that concentrated its sediments discharge following the behavior of a closed basin. For this reason, the high concentration of fine clays soils are allocated in the depositional centre.

The borehole 167 (Airport neighborhood); presents a little differences with respect to boreholes Santa Elena Granjas as well Pablo Gomez neighborhood, these differences in soils facies are regarded to reduction in the thick of clay layers and an increase in the sandy layers maybe because are located in the perimetral area of the Barreal basin. The depth explored for this borehole was 384 meters. Finally the borehole 96 located in (Praderas de los Oasis neighborhood) is very similar to the Airport neighborhood and the explored depth of this borehole was only 272 m where the first 68 m are mostly composed by clay and sandy clay, in the middle (68 m to 144 m) there are fine to coarse sands then another clay layer

between (144 m to 166 m) and finally, the lower part of the borehole (166 m to 272 m) there are fine to coarse sands. The previous boreholes (167 and 96) are located in the perimetral area of the barreal basin therefore the facies soils distribution showed in the boreholes mentioned suggest the variability of the sedimentation energy of the differnts stream sourronding the barreal basin

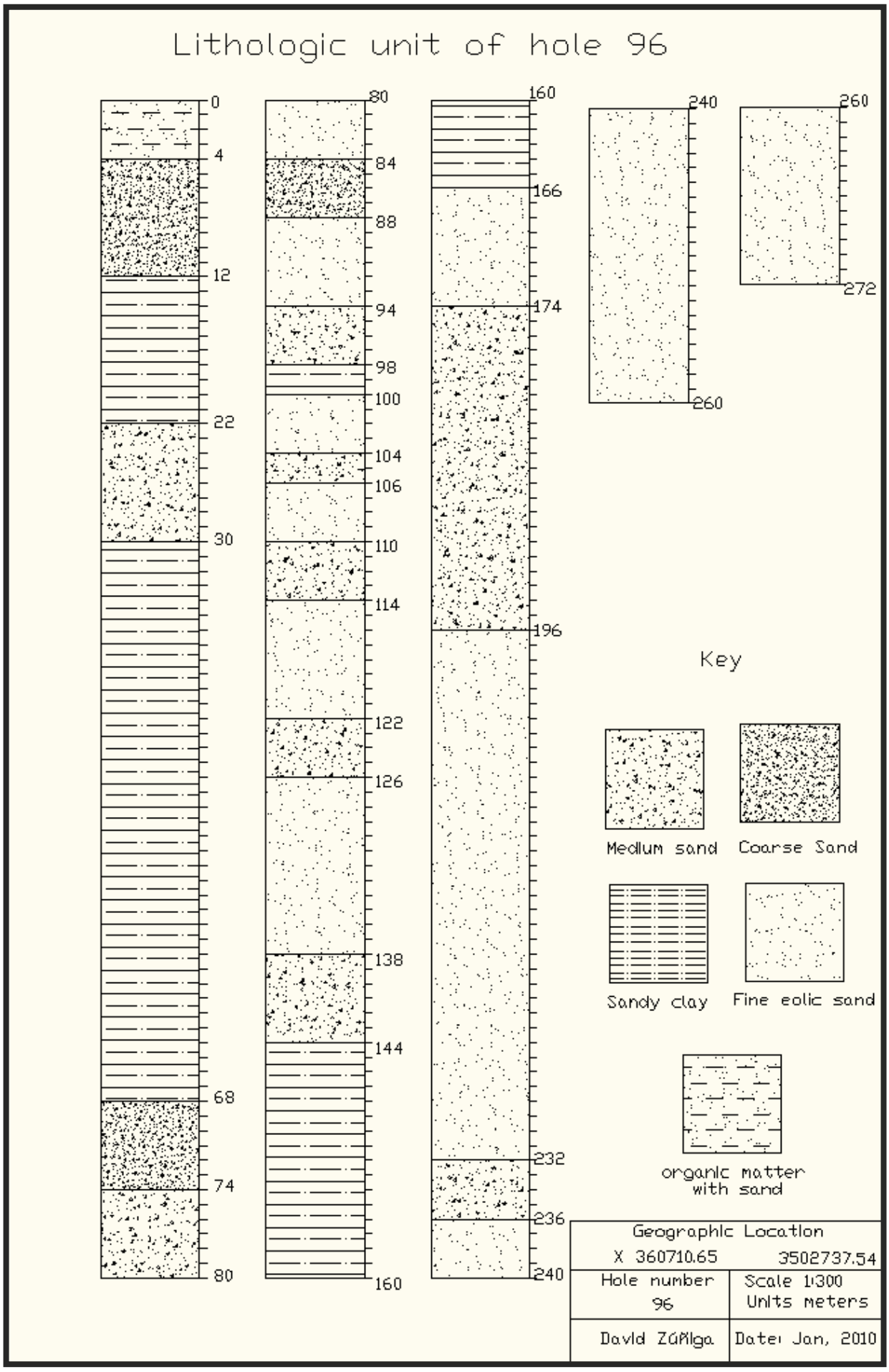
Lithologic unit of hole 96
0
4
12
22
30
68
74
80
80
84
88
94
98
100
104
106
110
114
122
126
138
144
160
160
166
174
196
232
236
240
240
260
260
272
Key
Medium sand
Coarse Sand
Sandy clay
Fine eolic sand
organic matter with sand
Geographic Location
X 360710.65
3502737.54
Hole number 96
Scale 1:300 Units meters
David ZúÑiga
Date: Jan, 2010

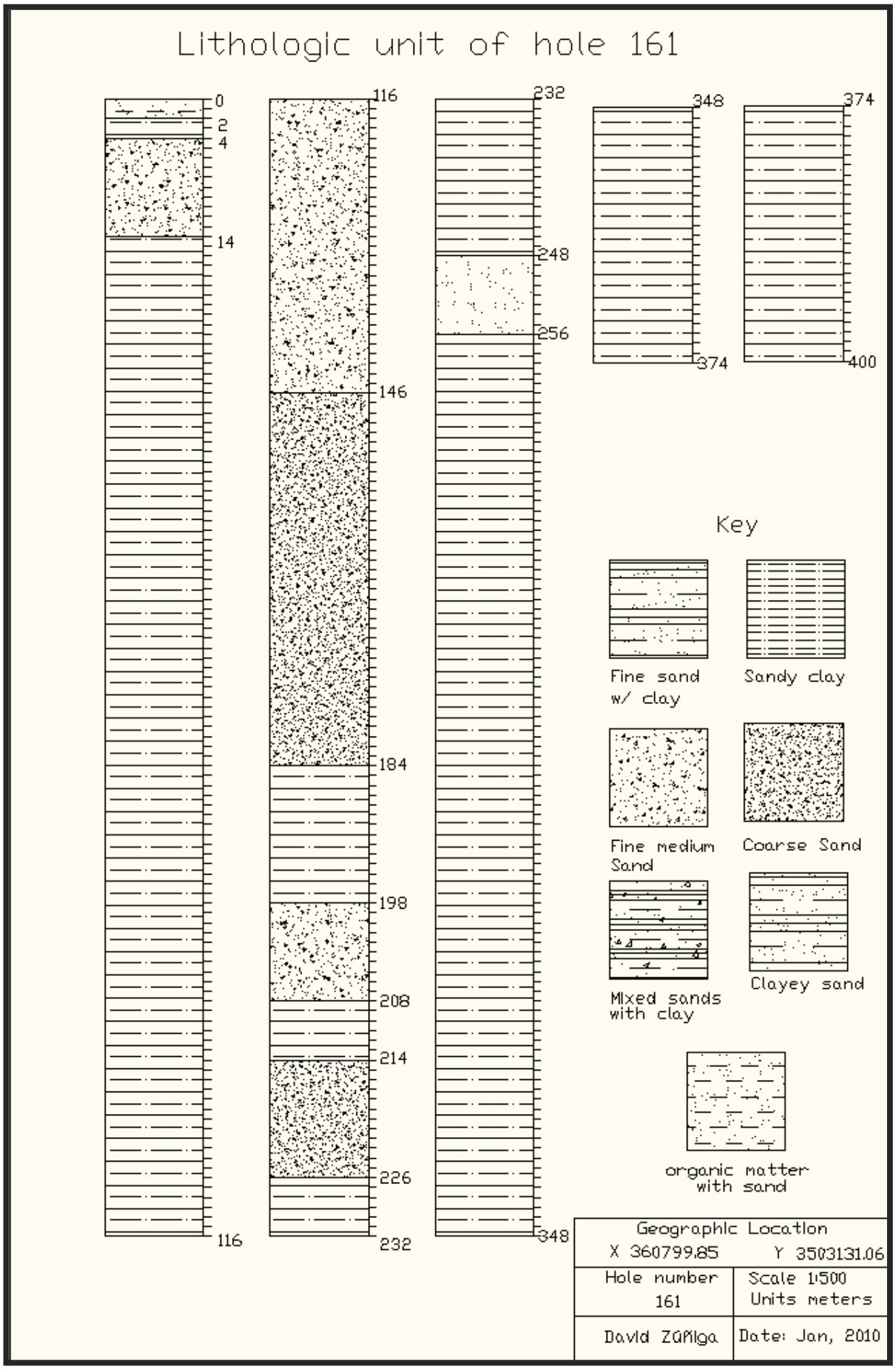
Lithologic unit of hole 161
0
2
4
14
116
116
146
184
198
208
214
226
232
232
248
256
348
348
374
374
400
Key
Fine sand w/ clay
Sandy clay
Fine medium Sand
Coarse Sand
Mixed sands with clay
Clayey sand
organic matter with sand
Geographic Location
X 360799.85
Y 3503131.06
Hole number 161
Scale 1:500 Units meters
David ZAMIga
Date: Jan, 2010

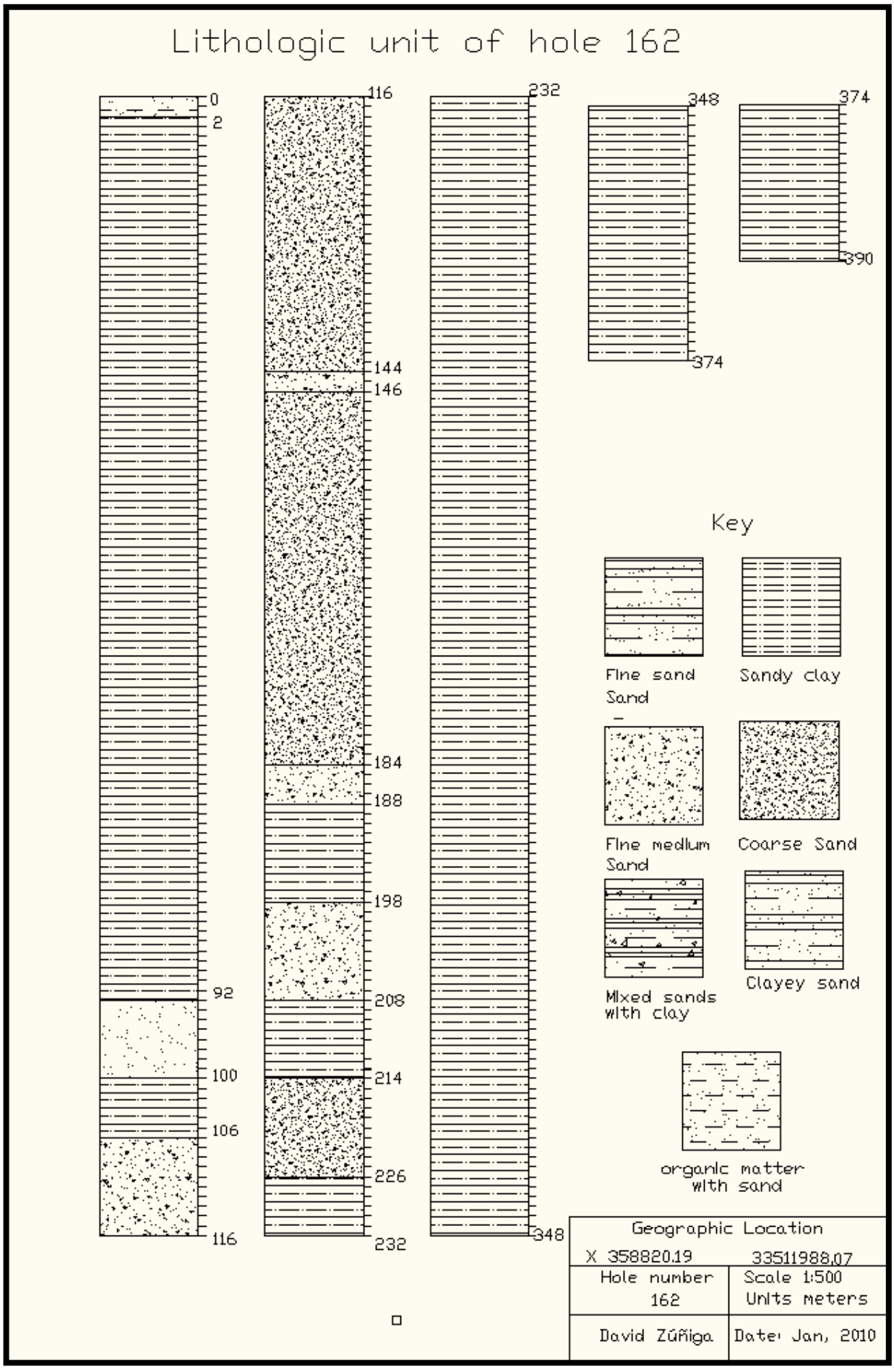
Lithologic unit of hole 162
0
2
92
100
106
116
116
144
146
184
188
198
208
214
226
232
232
348
348
374
374
390
Key
Fine sand
Sandy clay
Sand
Fine medium Sand
Coarse Sand
Mixed sands with clay
Clayey sand
organic matter with sand
Geographic Location
X 358820.19
33511988.07
Hole number 162
Scale 1:500
Units meters
David Zúñiga
Date: Jan, 2010

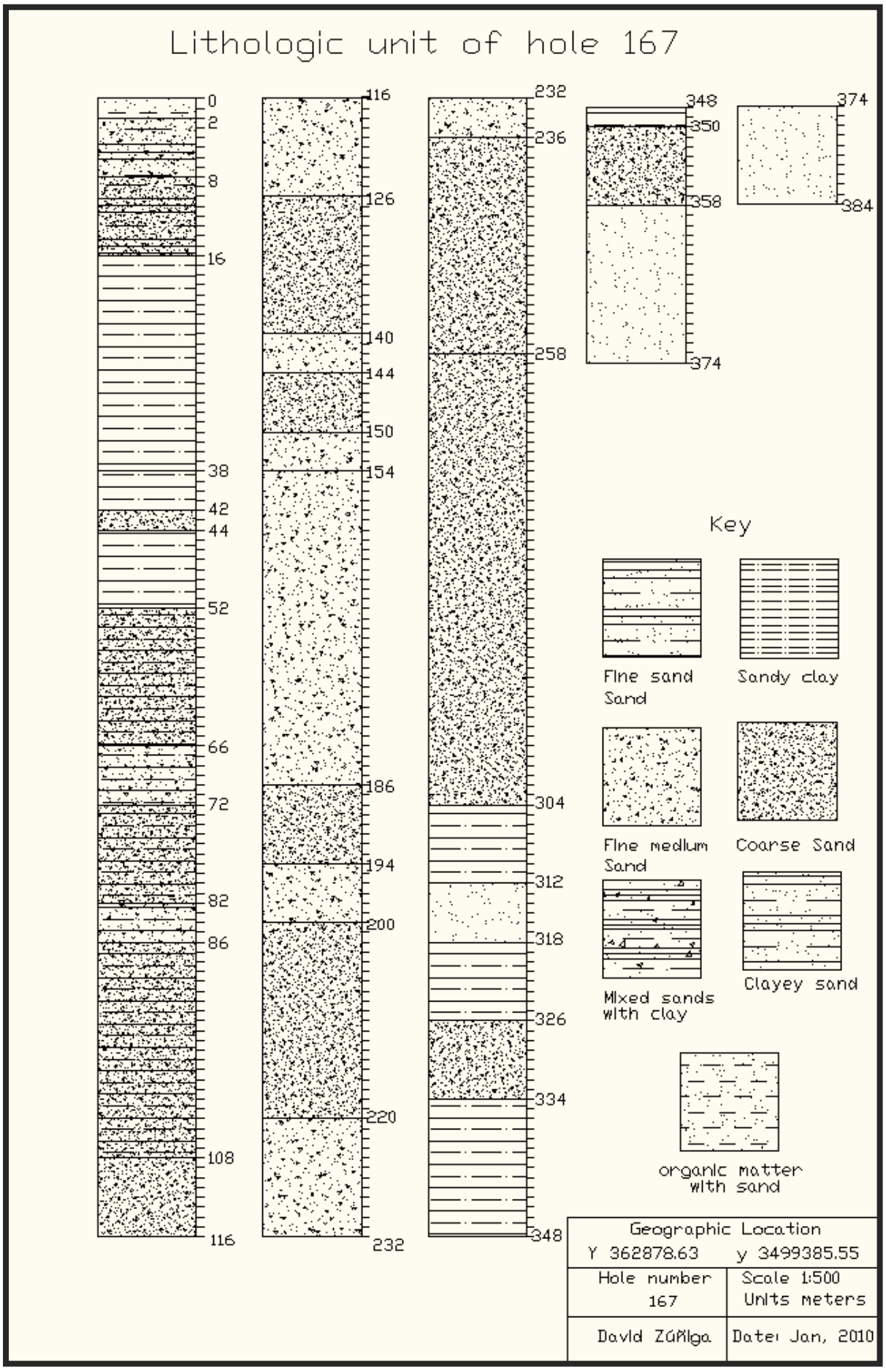
Lithologic unit of hole 167
0
2
8
16
38
42
44
52
66
72
82
86
108
116
116
126
140
144
150
154
186
194
200
220
232
232
236
258
304
312
318
326
334
348
348
350
358
374
374
384
Key
Fine sand
Sand
Sandy clay
Fine medium
Sand
Coarse Sand
Mixed sands
with clay
Clayey sand
organic matter
with sand
Geographic Location
Y 362878.63 y 3499385.55
Hole number
167
Scale 1:500
Units meters
David ZAMIga
Date: Jan, 2010

Group 3. This group presents soils like fine, medium, coarse and mixed eolic sands with Little conglomerate. The boreholes representative of this group are: 1RR, 47, 63, 145, 147, 148, 149, 150, 178 and 221 and are represented in colour gray (Figure 1). Note, in this group the portion of conglomeratic soil is not relevant maybe because was due by an event of channel deposit that occurred in one isolated high energy sheetflood instead of a tension normal fault that could provided the enough topography for accommodation space for this reason the deposition environment of this soils maybe corresponds of an agggradation climatic mode of operation occurred during the last Pleistocene time.

The geographic distribution of these boreholes are: 1RR (Magnaflex Industrial Park near to Bravo river); 47 (Satellite neighborhood); 63 (Fernandes Industrial Park); 145 (San Marcos Campestre neighborhood); 147 (Oasis Neighborhood); 148 (Colinas del desierto neighborhood); 149 (Infonavit Solidaridad); 150 (Infonavit Juarez Nuevo); 178 (El Papalote Zaragoza neighborhood); 221 (Colinas del Norte neighborhood near to Eje Juan Gabriel Boulevard). All the units that formed the previous boreholes are located in areas that were subjected to deposition of fine, medium, coarse as well mixed and in some areas little layers of conglomerate. Therefore, the geomorphology of the study area suggest the probability that some streams with high capacity and competence were active in the recent time and deposited these conglomeratic soils.

In order to consider the more relevant soil characteristic associated with facies presented on group 3 it is important to mention that holes located near to the inundation area of the Bravo river like 1RR, 47, 145, 149, are composed of important layers of clay soils intercalated with sand soils and also little conglomerate. Additionaly the quantity of clay layers decreases and the sands layers increases as the location of the boreholes are far away from the inundation area of the bravo river like boreholes 147, 148, 150, 178, 221. These situation is more likely on the surface layers of the terrain and the tendency to have more sandy soils are to the distal areas of the river. This behavior is persistent through the different urbanized area of the city.

In order to understand the existence of little conglomerate layers into the sandy and clayey soils it is important to mention in the possibility of occurrence of some inundation events maybe occurred as a consequence of climatic change conditions. For instance, that occurred during the last Pleistocene glacial maximum.

In short, the region situated between the bravo river center line and approximately 5 km west represent a typical variation like that described for this group.

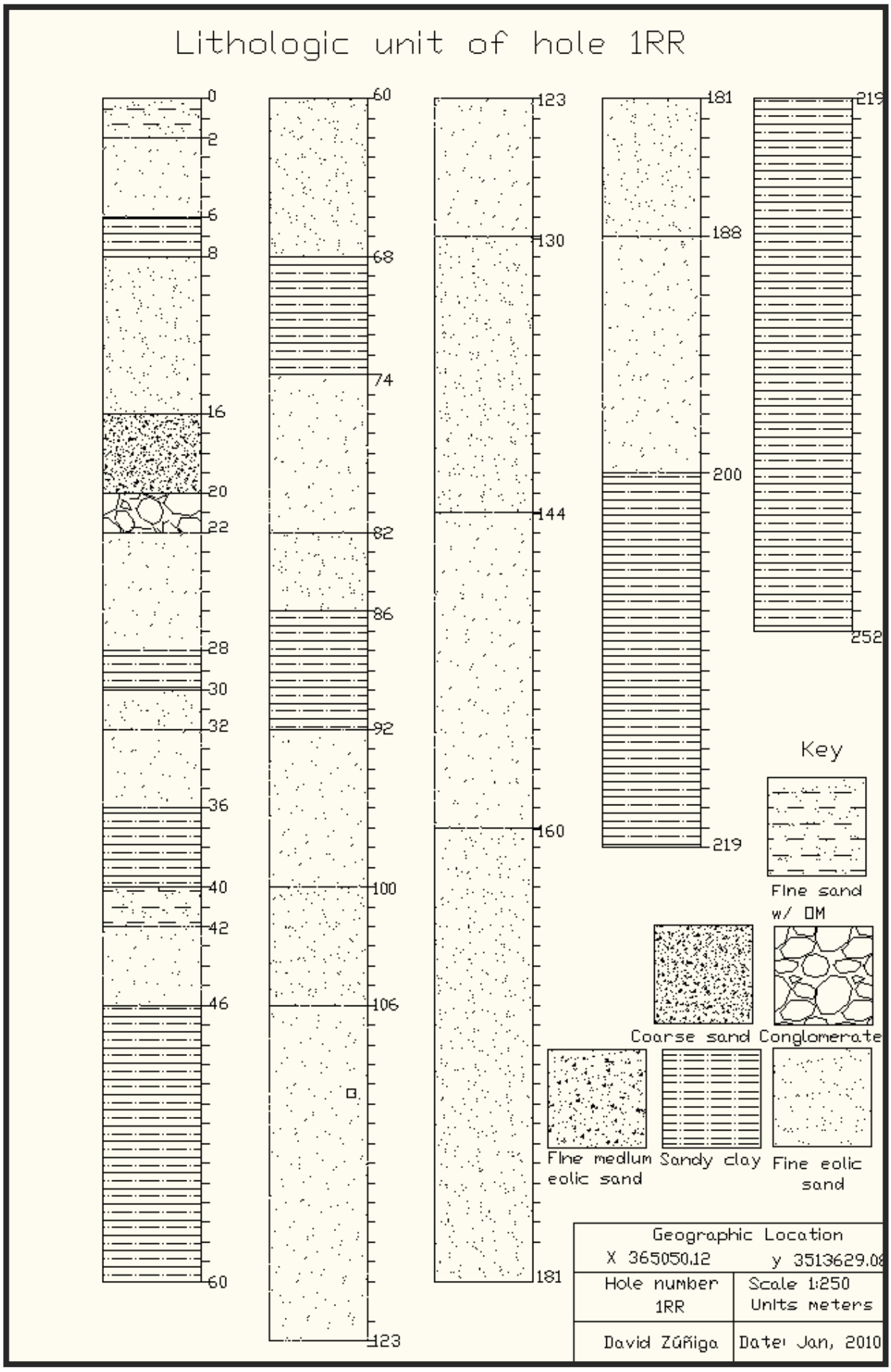
Lithologic unit of hole 1RR
0
2
6
8
16
20
22
28
30
32
36
40
42
46
60
60
68
74
82
86
92
100
106
123
123
130
144
160
181
181
188
200
219
219
252
Key
Fine sand w/ OM
Coarse sand
Conglomerate
Fine medium eolic sand
Sandy clay
Fine eolic sand
Geographic Location
X 365050.12
y 3513629.08
Hole number 1RR
Scale 1:250
Units meters
David Zúñiga
Date: Jan, 2010

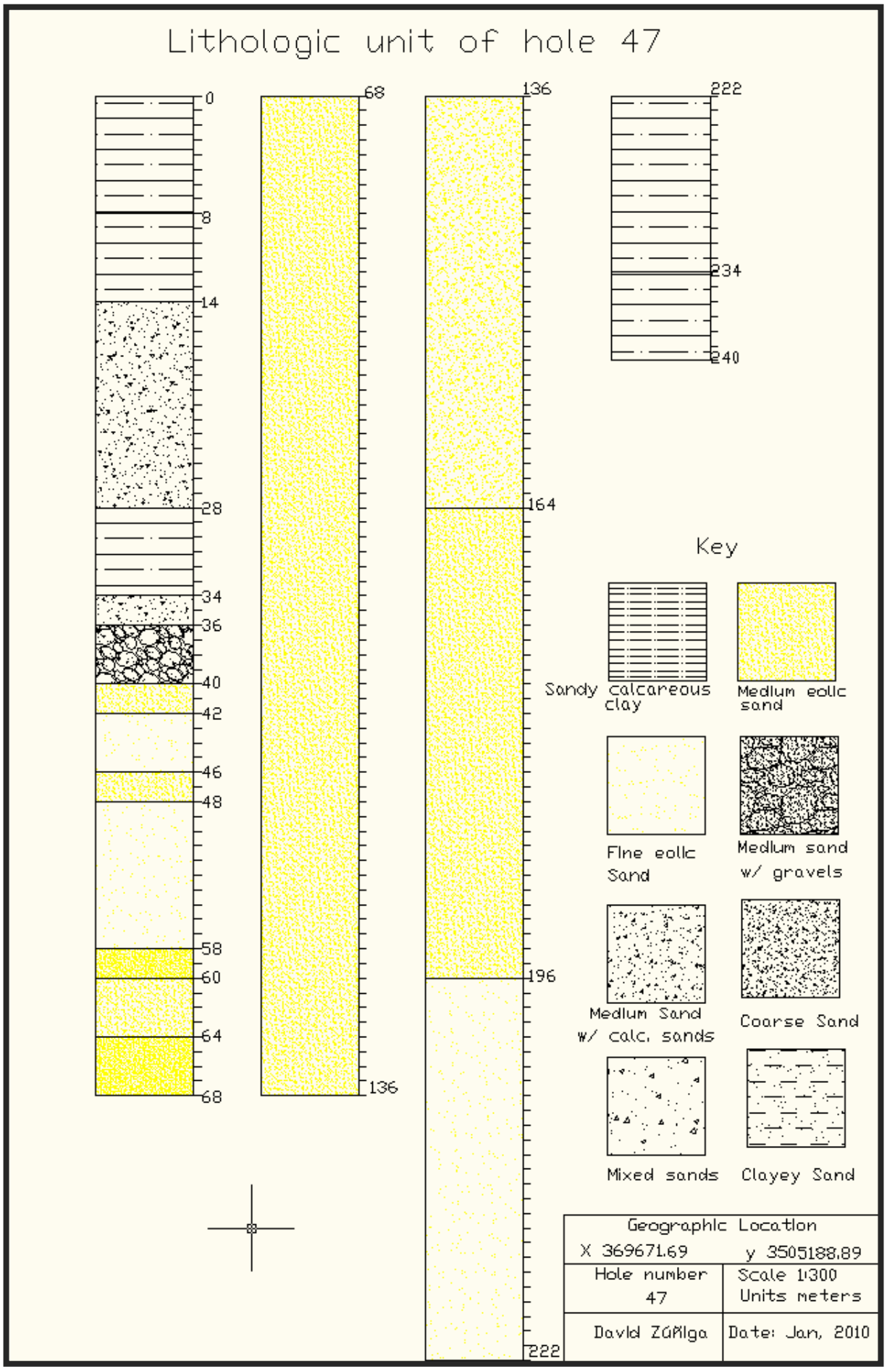
Lithologic unit of hole 47
0
8
14
28
34
36
40
42
46
48
58
60
64
68
68
136
136
164
196
222
222
234
240
Key
Sandy calcareous clay
Medium eolic sand
Fine eolic Sand
Medium sand w/ gravels
Medium Sand w/ calc. sands
Coarse Sand
Mixed sands
Clayey Sand
Geographic Location
X 369671.69
y 3505188.89
Hole number 47
Scale 1:300
Units meters
David Zúñiga
Date: Jan, 2010

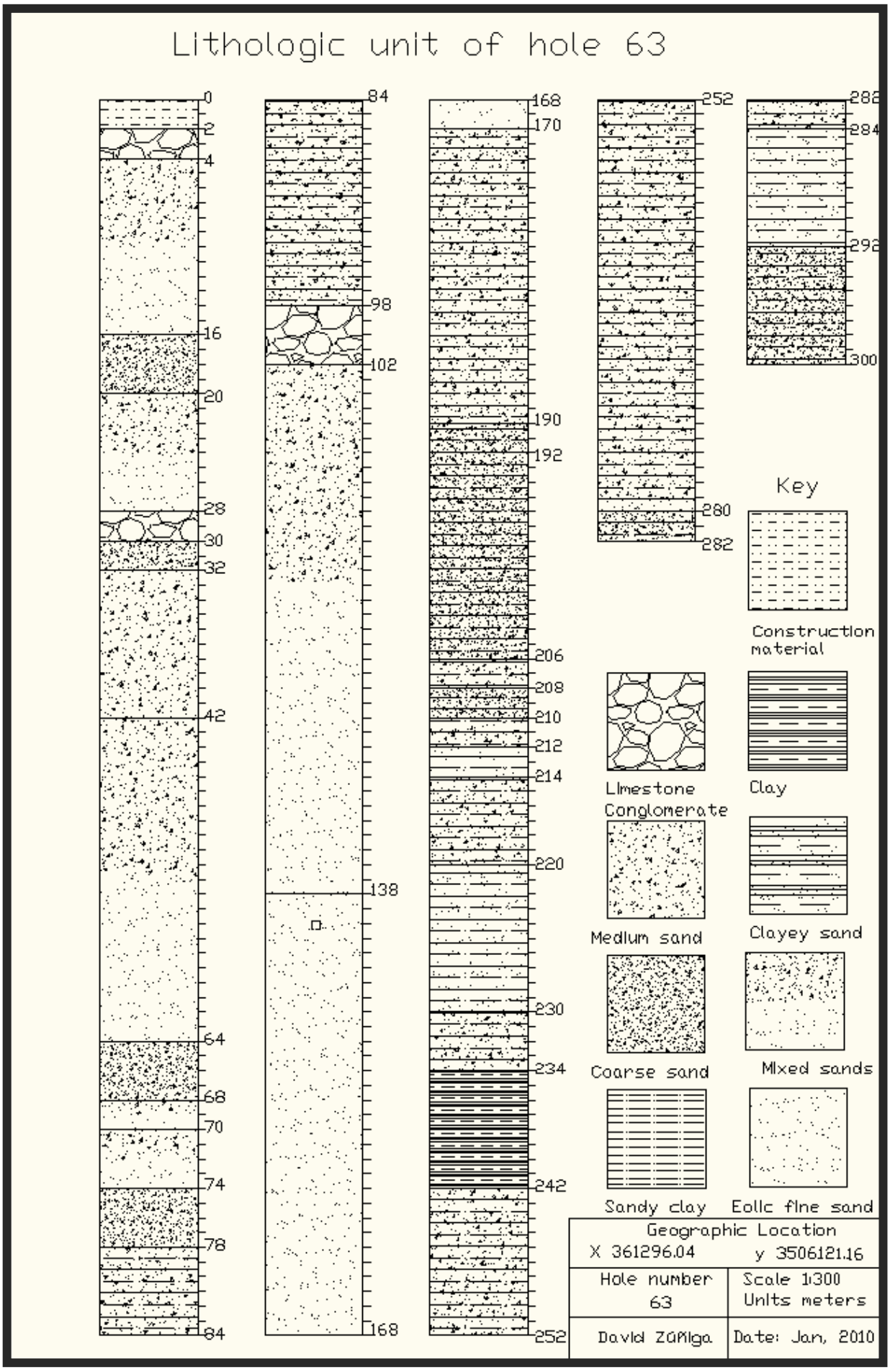
Lithologic unit of hole 63
0
2
4
16
20
28
30
32
42
64
68
70
74
78
84
84
98
102
138
168
168
170
190
192
206
208
210
212
214
220
230
234
242
252
252
280
282
288
284
298
300
Key
Construction material
Limestone Conglomerate
Clay
Medium sand
Clayey sand
Coarse sand
Mixed sands
Sandy clay
Eolic fine sand
Geographic Location
X 361296.04
y 3506121.16
Hole number
63
Scale 1:300
Units meters
David ZAMiga
Date: Jan, 2010

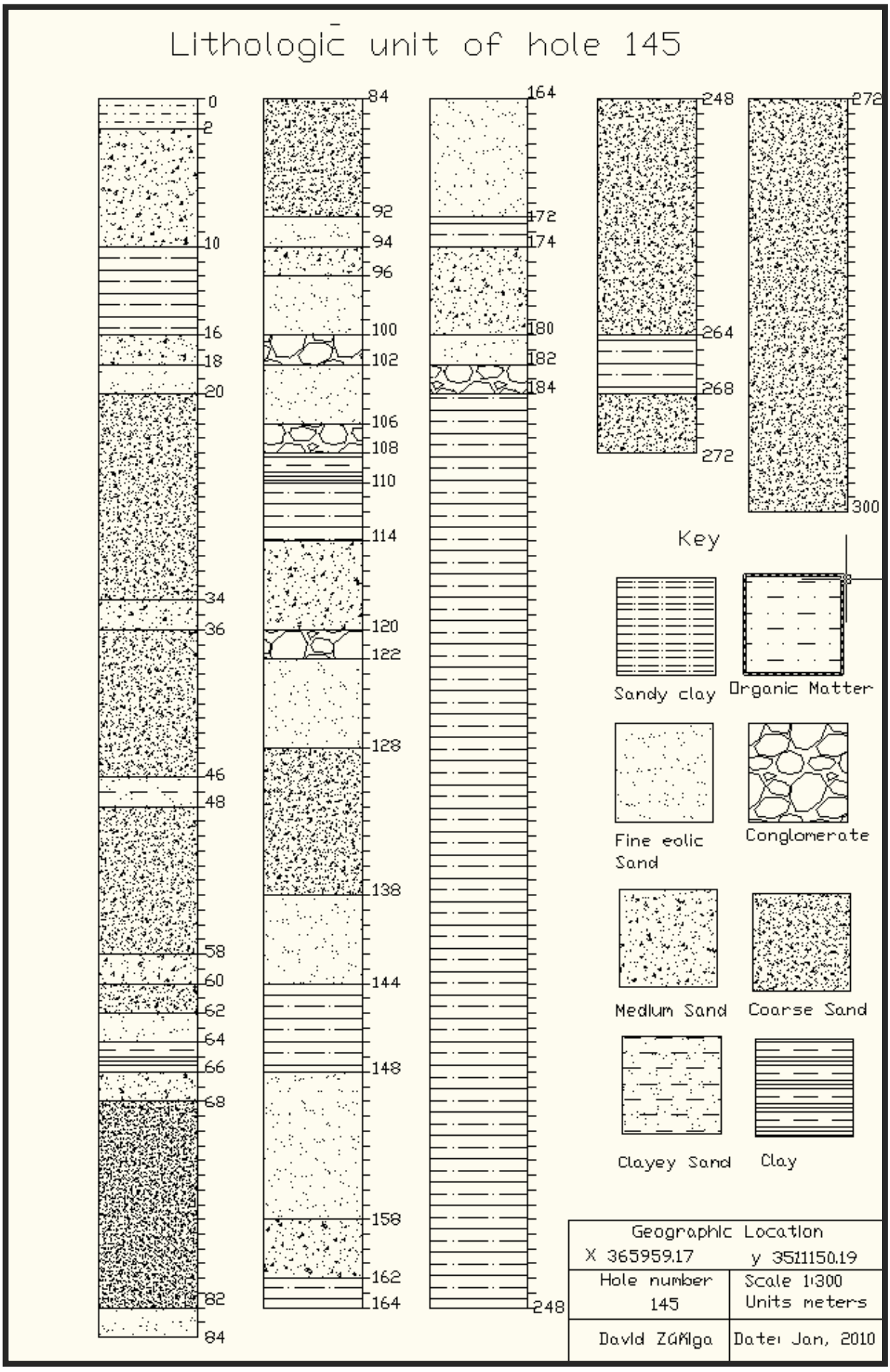
Lithologic unit of hole 145
0
2
10
16
18
20
34
36
46
48
58
60
62
64
66
68
82
84
84
92
94
96
100
102
106
108
110
114
120
122
128
138
144
148
158
162
164
164
172
174
180
182
184
248
248
264
268
272
272
300
Key
Sandy clay
Organic Matter
Fine eolic Sand
Conglomerate
Medium Sand
Coarse Sand
Clayey Sand
Clay
Geographic Location
X 365959.17
y 3511150.19
Hole number 145
Scale 1:300
Units meters
David ZAMIga
Date: Jan, 2010

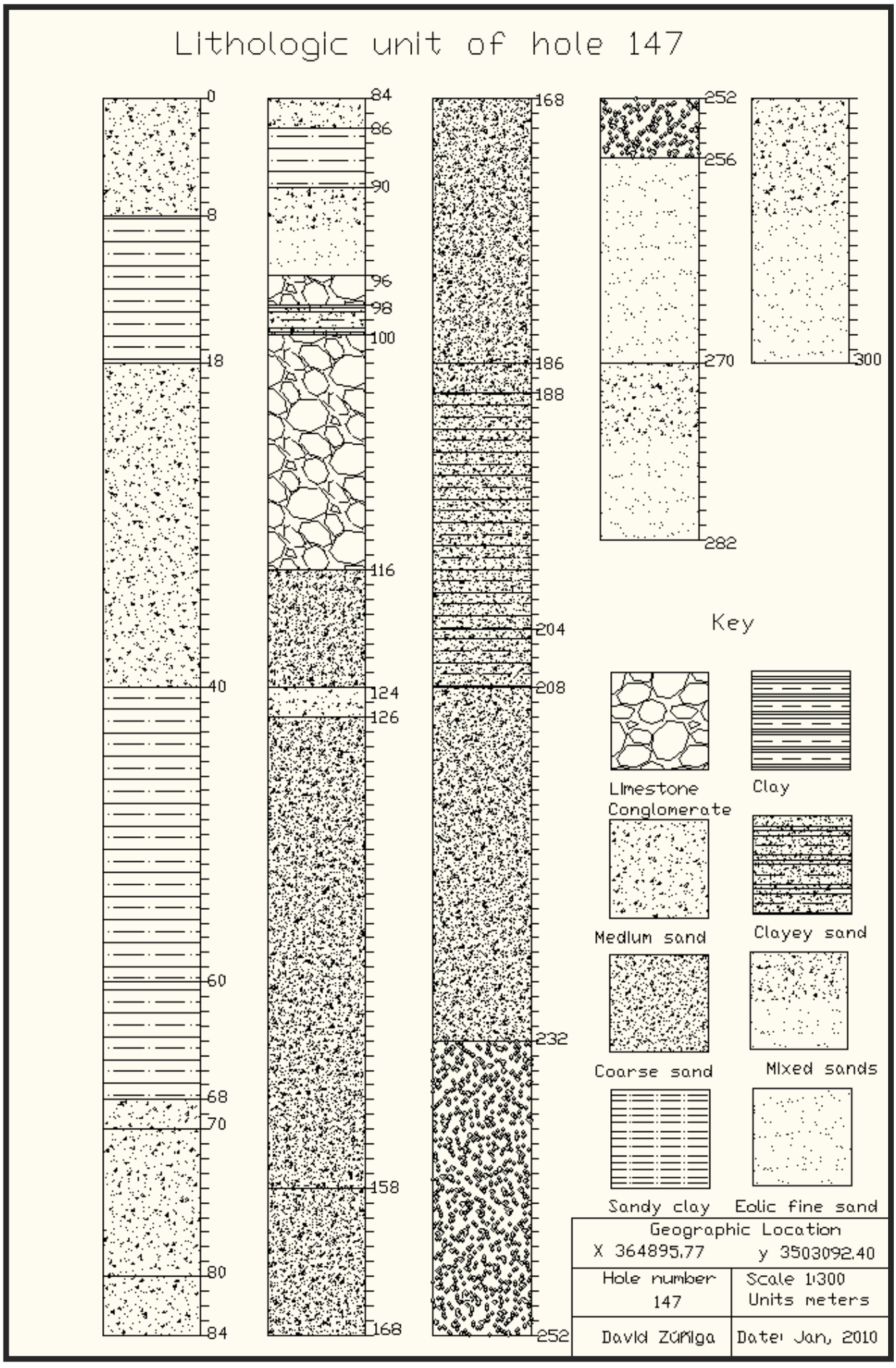
Lithologic unit of hole 147
0
8
18
40
60
68
70
80
84
84
86
90
96
98
100
116
124
126
158
168
168
186
188
204
208
232
252
252
256
270
282
300
Key
Limestone Conglomerate
Clay
Medium sand
Clayey sand
Coarse sand
Mixed sands
Sandy clay
Eolic fine sand
Geographic Location
X 364895.77
y 3503092.40
Hole number 147
Scale 1:300
Units meters
David Zúñiga
Date: Jan, 2010

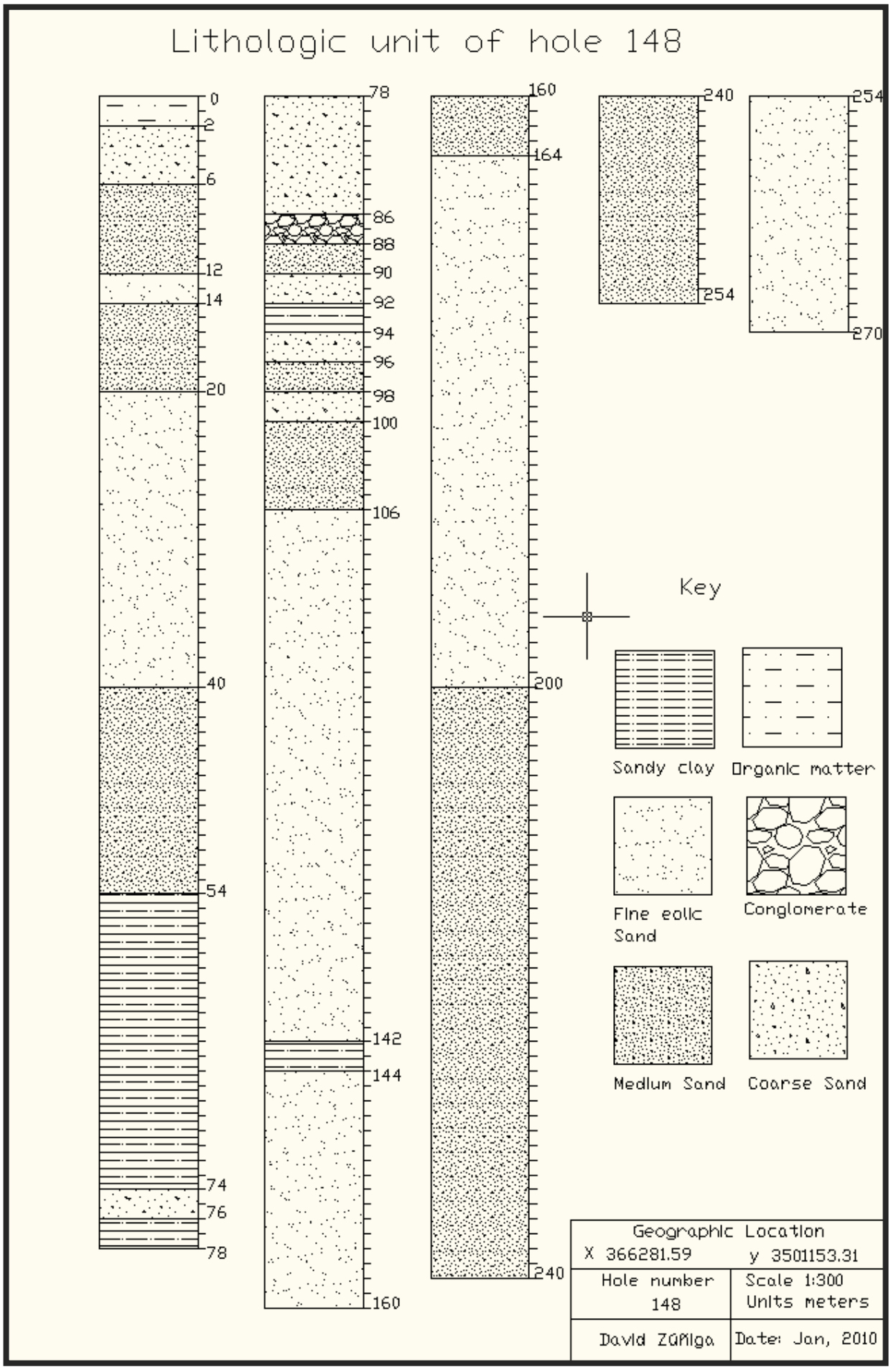
Lithologic unit of hole 148
0
2
6
12
14
20
40
54
74
76
78
78
86
88
90
92
94
96
98
100
106
142
144
160
160
164
200
240
240
254
254
270
Key
Sandy clay
Organic matter
Fine eolic Sand
Conglomerate
Medium Sand
Coarse Sand
Geographic Location
X 366281.59
y 3501153.31
Hole number 148
Scale 1:300
Units meters
David ZÚñiga
Date: Jan, 2010

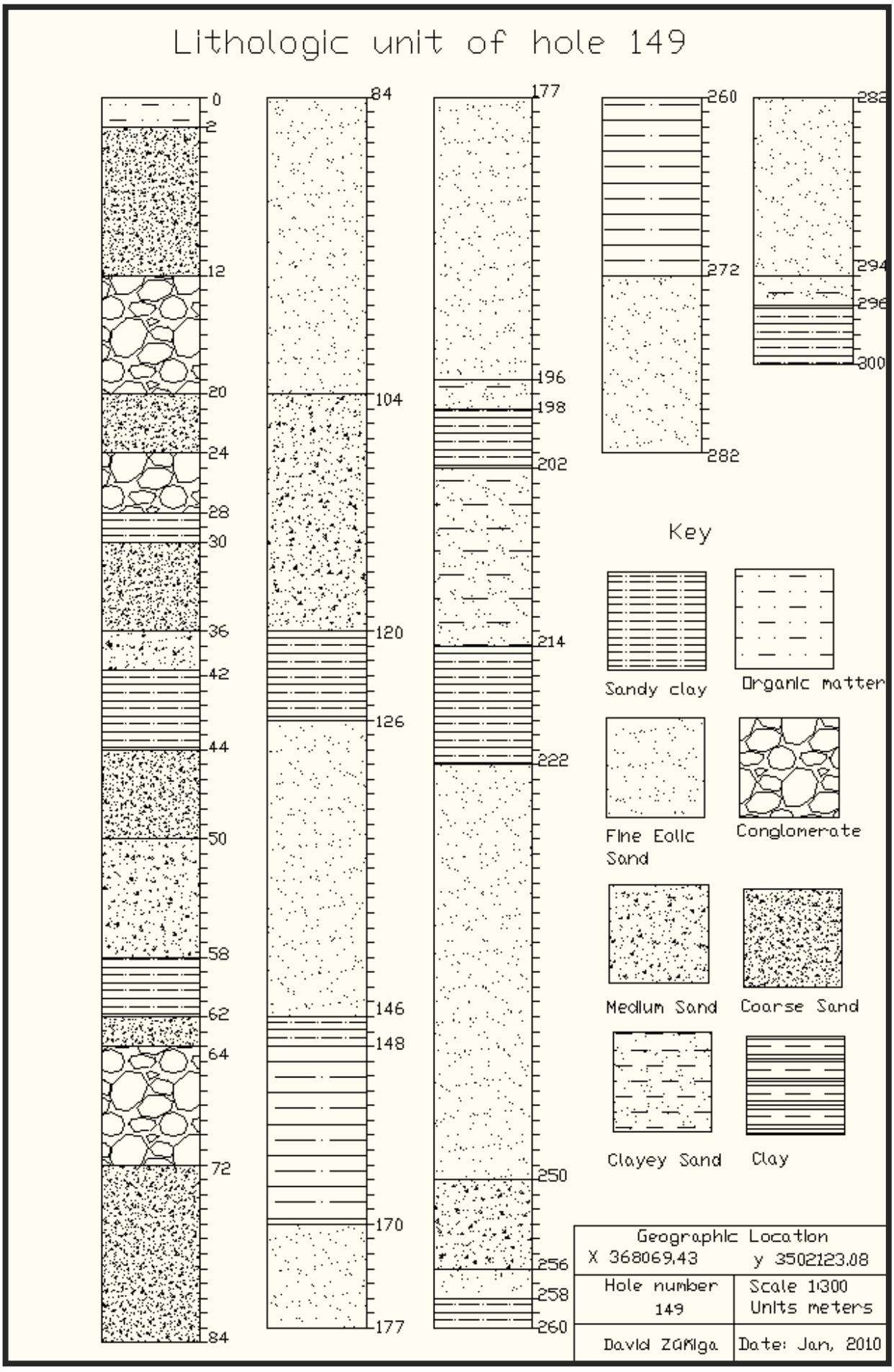
Lithologic unit of hole 149
0
2
12
20
24
28
30
36
42
44
50
58
62
64
72
84
84
104
120
126
146
148
170
177
177
196
198
202
214
222
250
256
258
260
260
272
282
282
294
296
300
Key
Sandy clay
Organic matter
Fine Eolic Sand
Conglomerate
Medium Sand
Coarse Sand
Clayey Sand
Clay
Geographic Location
X 368069.43
y 3502123.08
Hole number 149
Scale 1:300
Units meters
David ZAMIga
Date: Jan, 2010

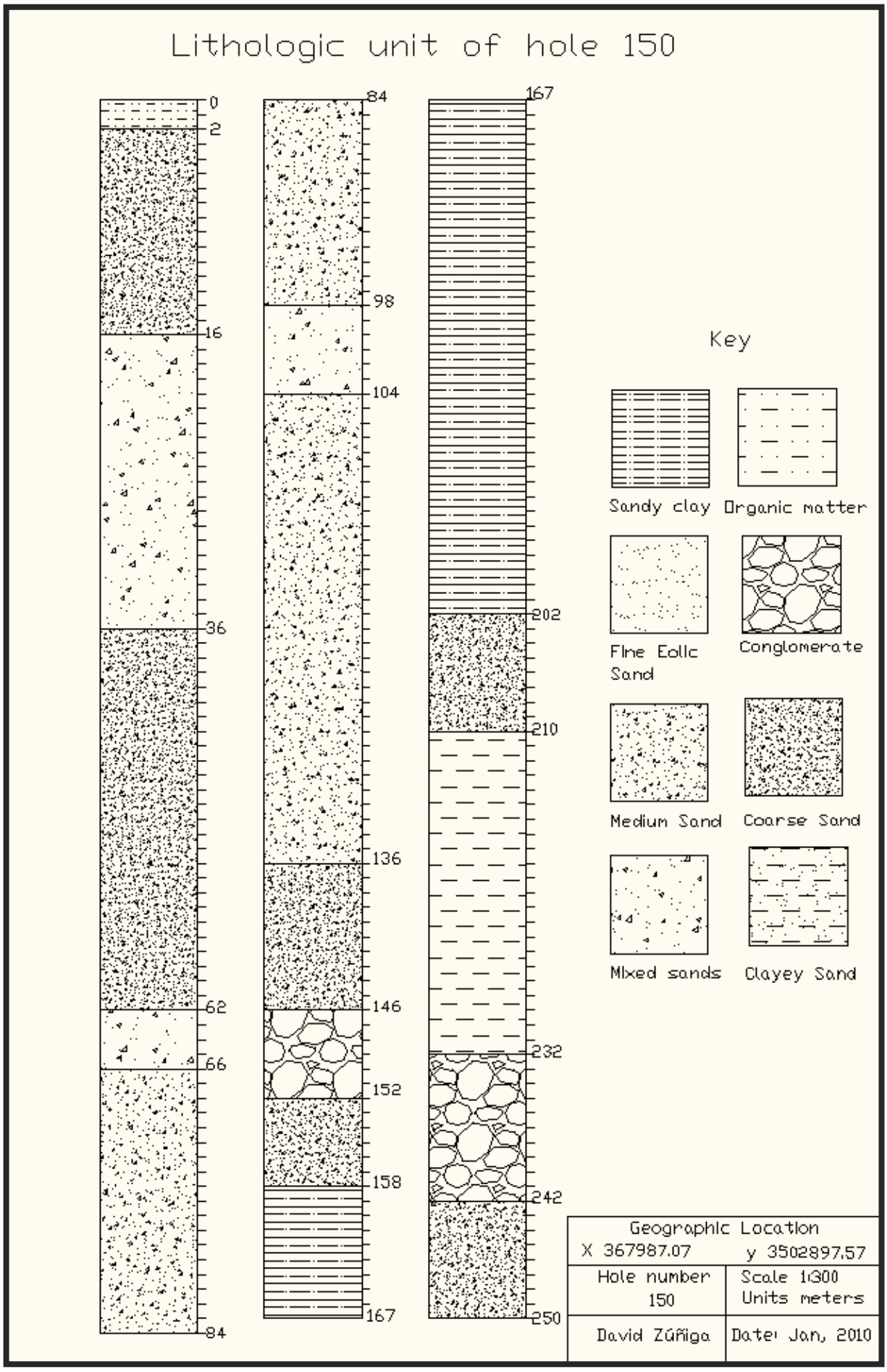
Lithologic unit of hole 150
0
2
16
36
62
66
84
84
98
104
136
146
152
158
167
167
202
210
232
242
250
Key
Sandy clay
Organic matter
Fine Eolic Sand
Conglomerate
Medium Sand
Coarse Sand
Mixed sands
Clayey Sand
Geographic Location
X 367987.07
y 3502897.57
Hole number 150
Scale 1:300
Units meters
David Zúñiga
Date: Jan, 2010

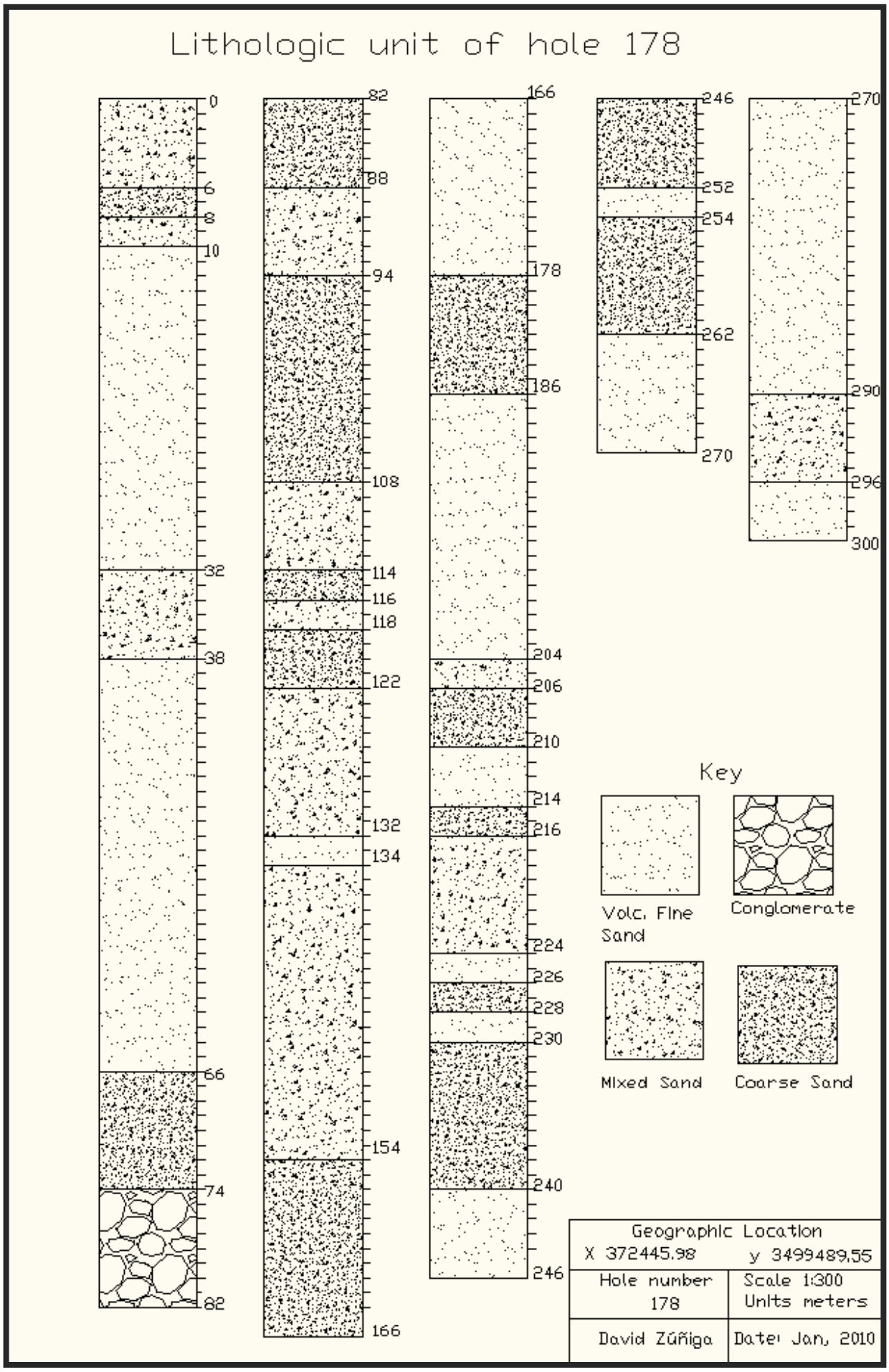
Lithologic unit of hole 178
0
6
8
10
32
38
66
74
82
82
88
94
108
114
116
118
122
132
134
154
166
166
178
186
204
206
210
214
216
224
226
228
230
240
246
246
252
254
262
270
270
290
296
300
Key
Volc. Fine Sand
Conglomerate
Mixed Sand
Coarse Sand
Geographic Location
X 372445.98 y 3499489.55
Hole number 178
Scale 1:300 Units meters
David Zúñiga
Date: Jan, 2010

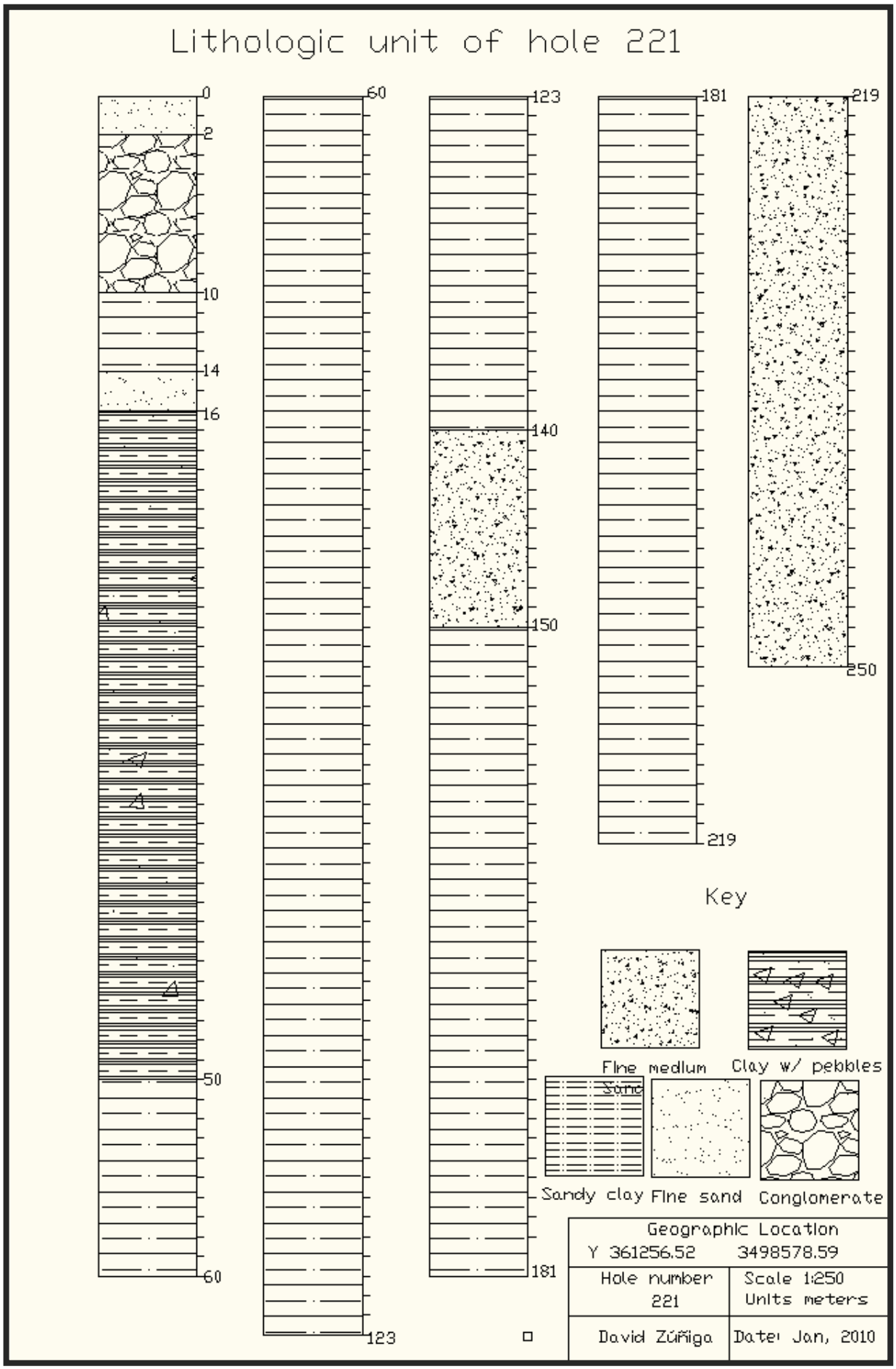
Lithologic unit of hole 221
0
2
10
14
16
50
60
60
123
123
140
150
181
181
219
219
250
Key
Fine medium Sand
Clay w/ pebbles
Sandy clay
Fine sand
Conglomerate
Geographic Location
Y 361256.52 3498578.59
Hole number 221
Scale 1:250
Units meters
David Zúñiga
Date: Jan, 2010

Group 4. This group is integrated predominantly by (enough conglomerate, quartzite sand, plastic clay, sandstone, shale, silts, ash) the holes that are included in this group are: 13, 57 and 114 and are shown in green colour (Figure 1). Note that in these holes the Cretaceous units sandstone and shale and are located at 145 meters bellow the surface in addition the thickness of conglomerate layers are relevant in the order of 20 meters for these reasons a region of extensive normal faults existed on these area and obviously the boreholes lithology suggests a tectonic mode.

The boreholes of this units are the following: 13 (Carlos Amaya and Division del Norte streets); 57 (Ignacio Manuel Altamirano street) and 114 (Mision de los Lagos neighborhood). The previous boreholes represent the geologic indicators that will help to understand that the northwest and southwest of the Juarez city was constructed and populated over a recent active alluvial fan system. This asseveration is done because in hole 13 the Cretaceous layers is located at 166 meters as well as in hole 157 that has this layer at a depth of 145 meters. In addition, in the surface layers of these holes there are a lot and thicker layers of conglomerate that suggest the intense period of extensive normal intrabasinal faults occurred during Pliocene to Pleistocene time as a consequence of the Bravo river rift system. In addition, in the mentioned boreholes the presence of sands as well as clay are also present but the principal difference is that the type of matrix that is mostly of quartzite composition in the case of sandy as well conglomeratic soils and in the case of clays basically it is of high plasticity as well red colour.

The previous consideration already done reinforce the idea concerned that in the area located near to the east flank of the Juarez mountains there are a great zone that was dominated by many normal faults. Obviously the geomorphology of the study area strongly suggest the previous comment. For this reason the contact between the tectonic mode and the climatic mode that is producing the actual alluvial fan system is located to the west of the city

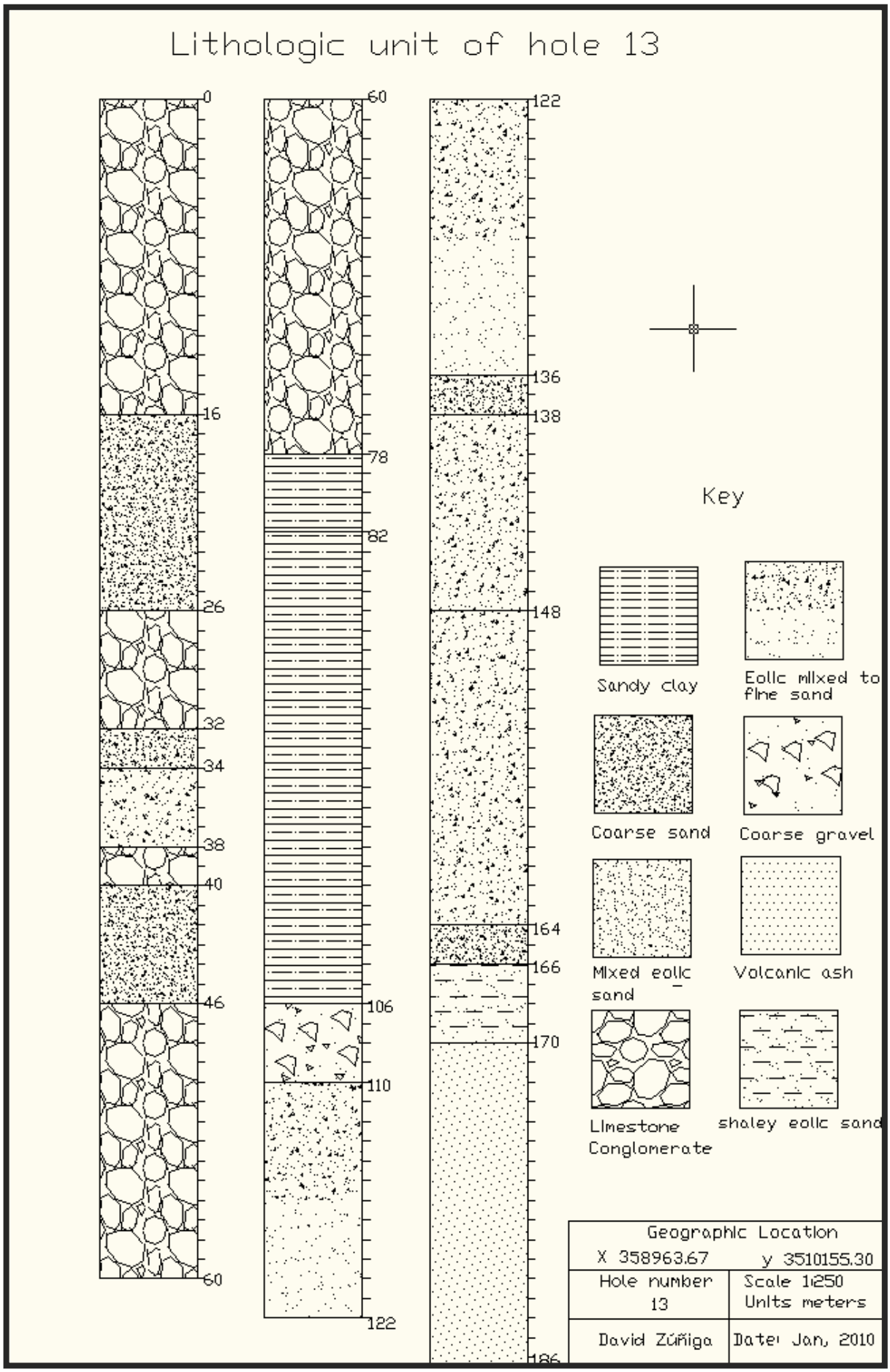
Lithologic unit of hole 13
0
16
26
32
34
38
40
46
60
60
78
82
106
110
122
122
136
138
148
164
166
170
186
Key
Sandy clay
Eolic mlxed to fine sand
Coarse sand
Coarse gravel
Mlxed eolic sand
Volcanic ash
Llmestone Conglomerate
shaley eolic sand
Geographic Location
X 358963.67
y 3510155.30
Hole number 13
Scale 1:250
Units meters
David Zúñiga
Date: Jan, 2010

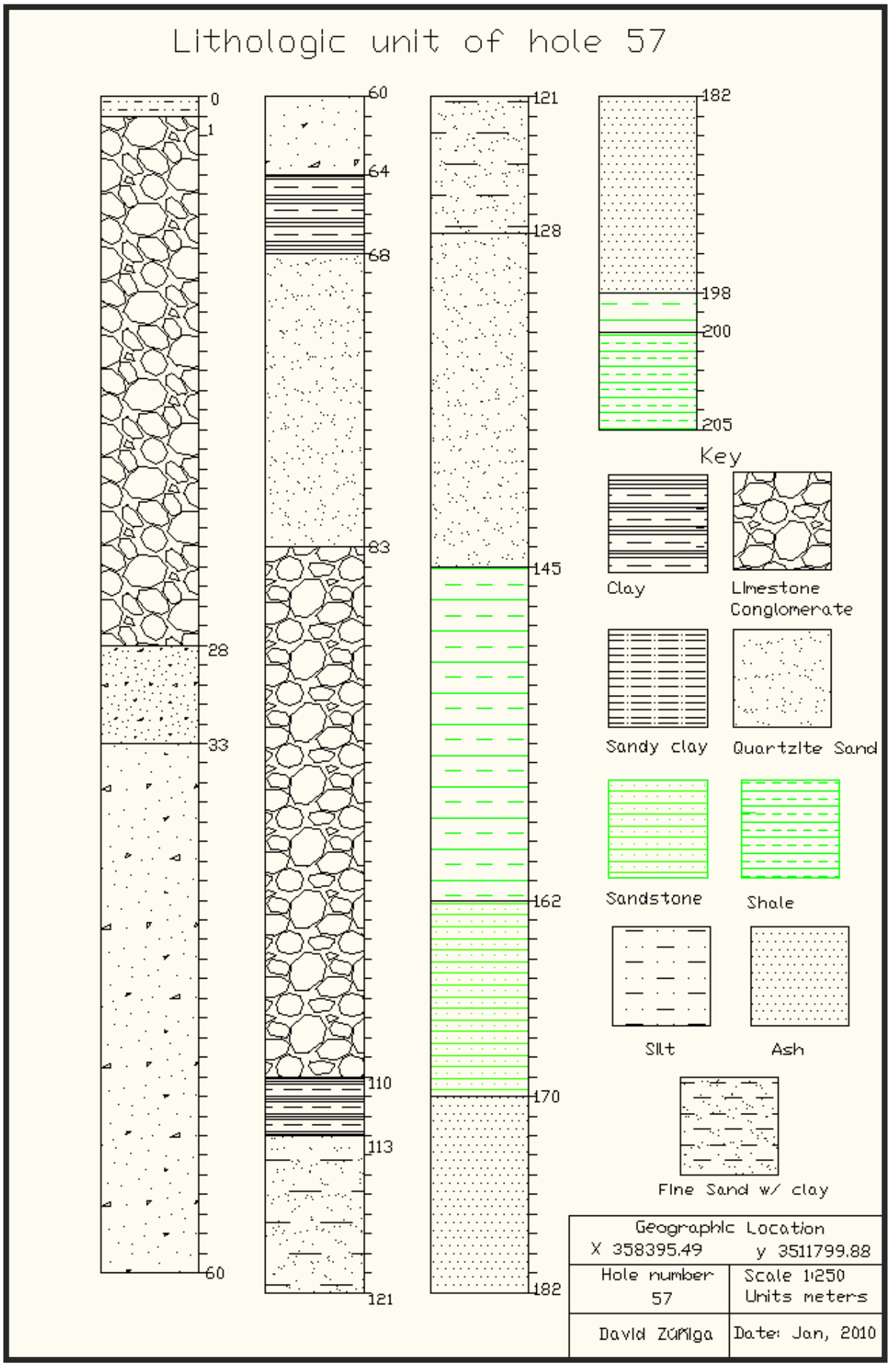
Lithologic unit of hole 57
0
1
28
33
60
64
68
83
110
113
121
128
145
162
170
182
198
200
205
Key
Clay
Limestone Conglomerate
Sandy clay
Quartzite Sand
Sandstone
Shale
Silt
Ash
Fine Sand w/ clay
Geographic Location
X 358395.49
y 3511799.88
Hole number 57
Scale 1:250 Units meters
David Zúñiga
Date: Jan, 2010

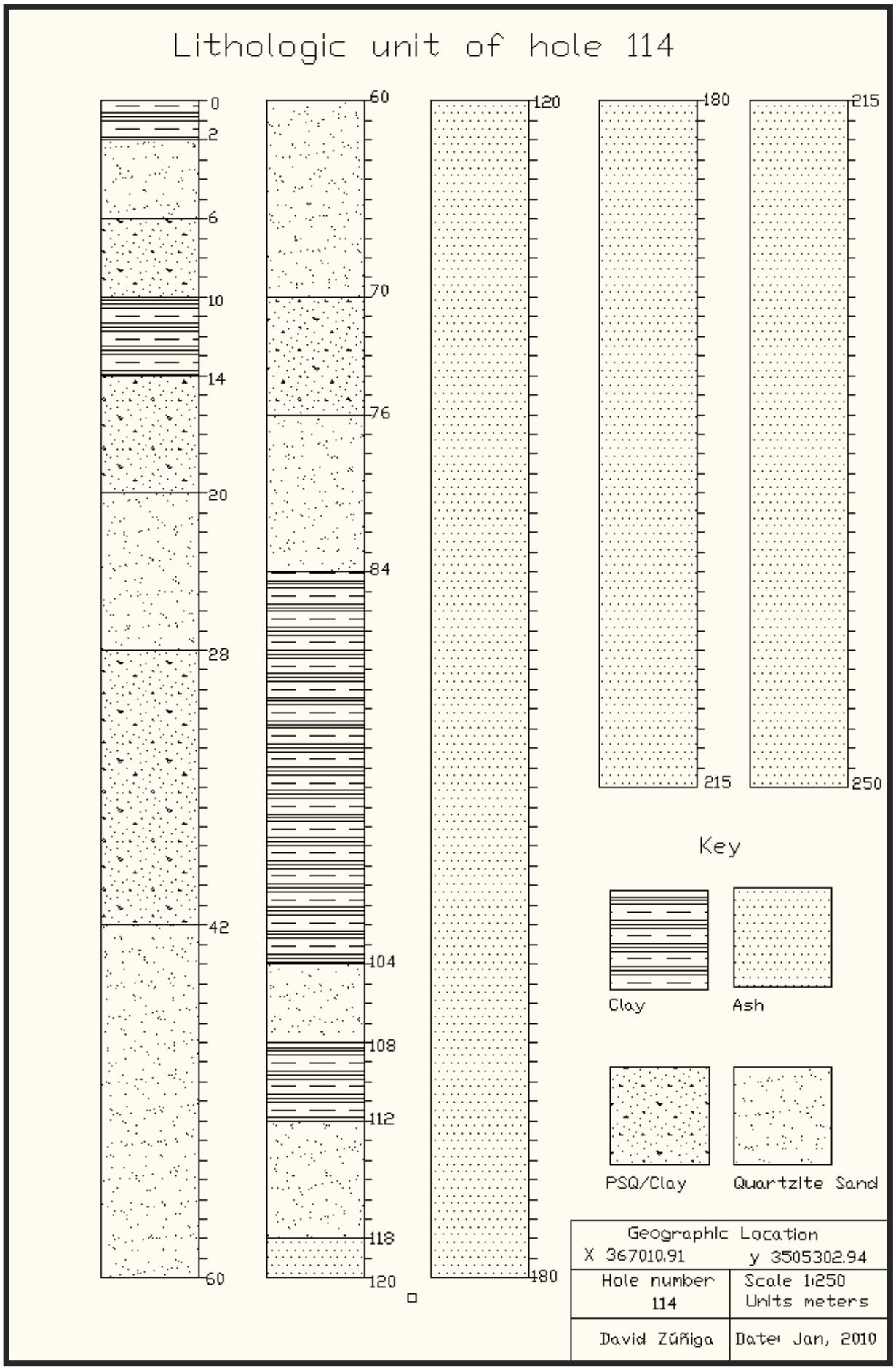
Lithologic unit of hole 114
0
2
6
10
14
20
28
42
60
60
70
76
84
104
108
112
118
120
120
180
180
215
215
250
Key
Clay
Ash
PSQ/Clay
Quartzite Sand
Geographic Location
X 367010.91
y 3505302.94
Hole number
114
Scale 1:250
Units meters
David Zúñiga
Date: Jan, 2010

Group 5. This group is composed of relevant thickness of conglomeratic soils layers as well as pebbles, quartzite sand, plastic clay and also, fine, medium, coarse and mixed sands. All these facies represented by the next holes: 9R, 11, 15, 59, 72, 86, 88, 92, 93, 95, 97, 100, 111, 115, 116, 122, 123, 124, 128, 129, 130, 131, 133, 141 and 142 and are represented in colour red (Figure 1). Note, the persistence and constant intercalation of thick layers of conglomeratic soils suggest that this area was subjected to tensive normal faults during Miocene to Plio-Pleistocene time because that happened as a result of the Bravo river rift system mode tectonic operation.

The geographic distribution of these boreholes are: 9R (Bellavista neighborhood); 11 (Del Charro and Rafael Perez Serna streets); 15 (Ave Insurgentes and Constitution streests); 57 (Ignacio Manuel Altamirano street); 59 (Azteca neighborhood); 72 (Jilotepec street); 86 (Aztecas neighborhood); 88 (Francisco Villa neighborhood near Oscar Flores boulevard); 92 (uuuuuu); 93 (Division del Norte neighborhood); 95 (Boulevard Zaragoza and Juan Gabriel street); 97 (Eje Juan Gabriel and Barranco Azul streets); 100 (Colinas de Juarez neighborhood and Panamericana streets); 111 (Hermanos Escobar and esteros streets near to Bravo River); 115 (Misiones de los Lagos neighborhood); 116 (Jardines de San Carlos neighborhood); 122 (Residential Bugambilias neighborhood); 123 (Partido Iglesias neighborhood); 124 (Jardines del Bosque neighborhood); 128 (La Joya Continental neighborhood); 129 (near to Teofilo Borunda street); 130 (Lucio Cabañas neighborhood); 131 (near to pradera Dorada neighborhood); 133 (Central de Abastos de Ciudad Juarez); 141 (Campestre Virreyes and Panamericana Highway) and 142 (Colinas del Sur Neighborhood near to Cementera).

Soils facies of this group have the peculiar characteristic that the conglomeratic soils are present in all the holes. However, the quartzite sand facies as well the eolic fine, medium, coarse and mixed sands are also present. The boreholes located near to the mountains such as boreholes: 9R, 11, 15, 59, 133, 142, 97, 86, 88, 92, 95 and 97 are more conglomeratic maybe because the presence of normal faults (tectonic mode). This situation persisted but in less quantity through the distance from the mountains and the soils facies of the sands are more eolic when the distance from the mountains increases. These boreholes are: 100, 111, 115, 116, 122, 123, 124, 129, 130, 131, 133 and 141. The interpretation of the

previous soils facies borehole group 5 is strongly associated with two principal environment of deposition: The first is regarded to some events of flooding through streams located on the mountains that transported the conglomeratic soils like sheetflood along high energy of deposition. The other may be was due as a result of some inundation events of the bravo river that undertook many changes in the trajectory of the river and the logical high energy of deposition associated

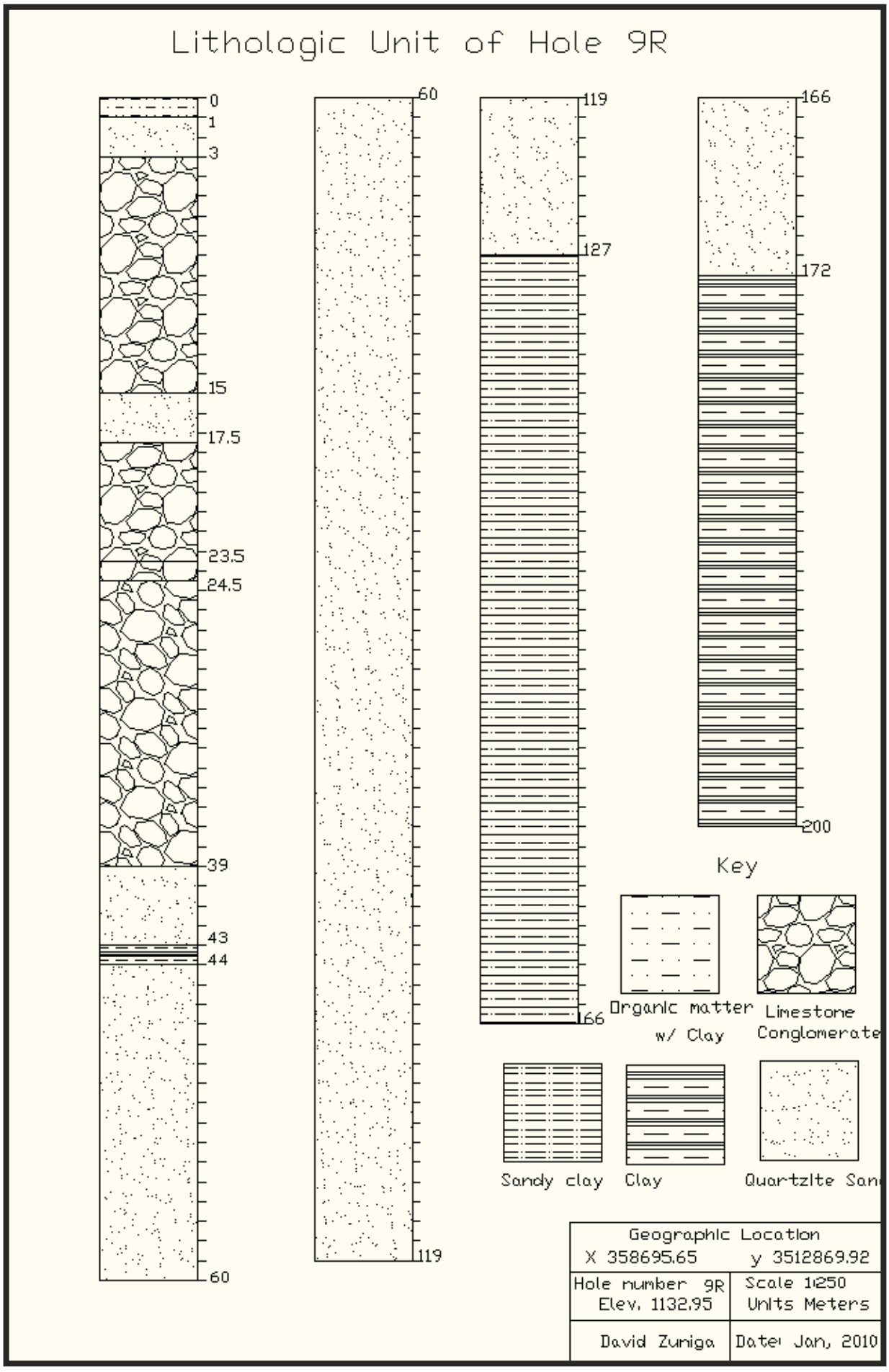
Lithologic Unit of Hole 9R
0
1
3
15
17.5
23.5
24.5
39
43
44
60
60
119
119
127
166
172
200
Key
Organic matter w/ Clay
Limestone Conglomerate
Sandy clay
Clay
Quartzite San
Geographic Location
X 358695.65
y 3512869.92
Hole number 9R
Elev. 1132.95
Scale 1:250
Units Meters
David Zuniga
Date: Jan, 2010

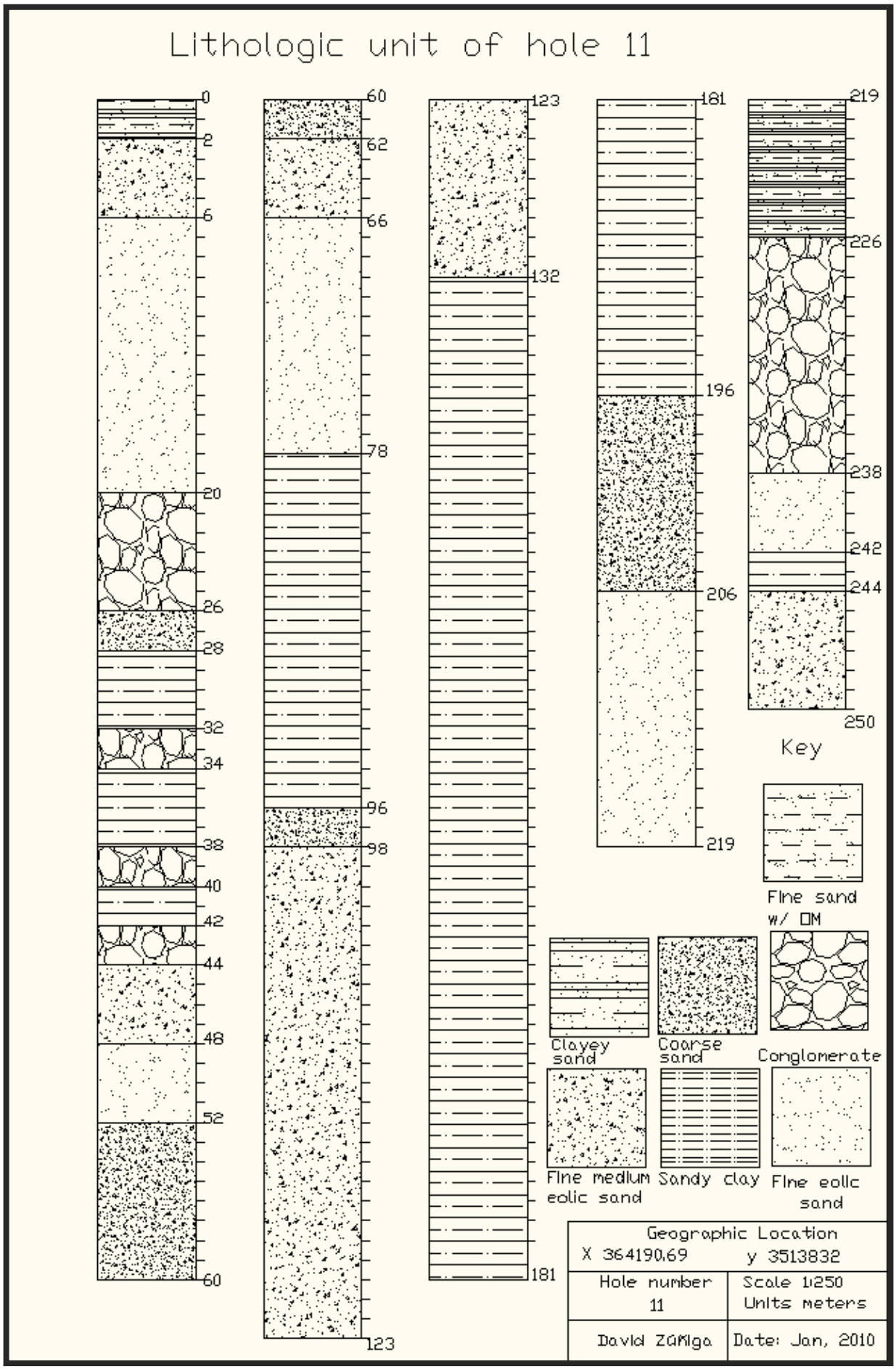
Lithologic unit of hole 11
0
2
6
20
26
28
32
34
38
40
42
44
48
52
60
60
62
66
78
96
98
123
123
132
181
181
196
206
219
219
226
238
242
244
250
Key
Fine sand
w/ OM
Clayey sand
Coarse sand
Conglomerate
Fine medium eolic sand
Sandy clay
Fine eolic sand
Geographic Location
X 364190.69 y 3513832
Hole number 11
Scale 1:250
Units meters
David ZAMIga
Date: Jan, 2010

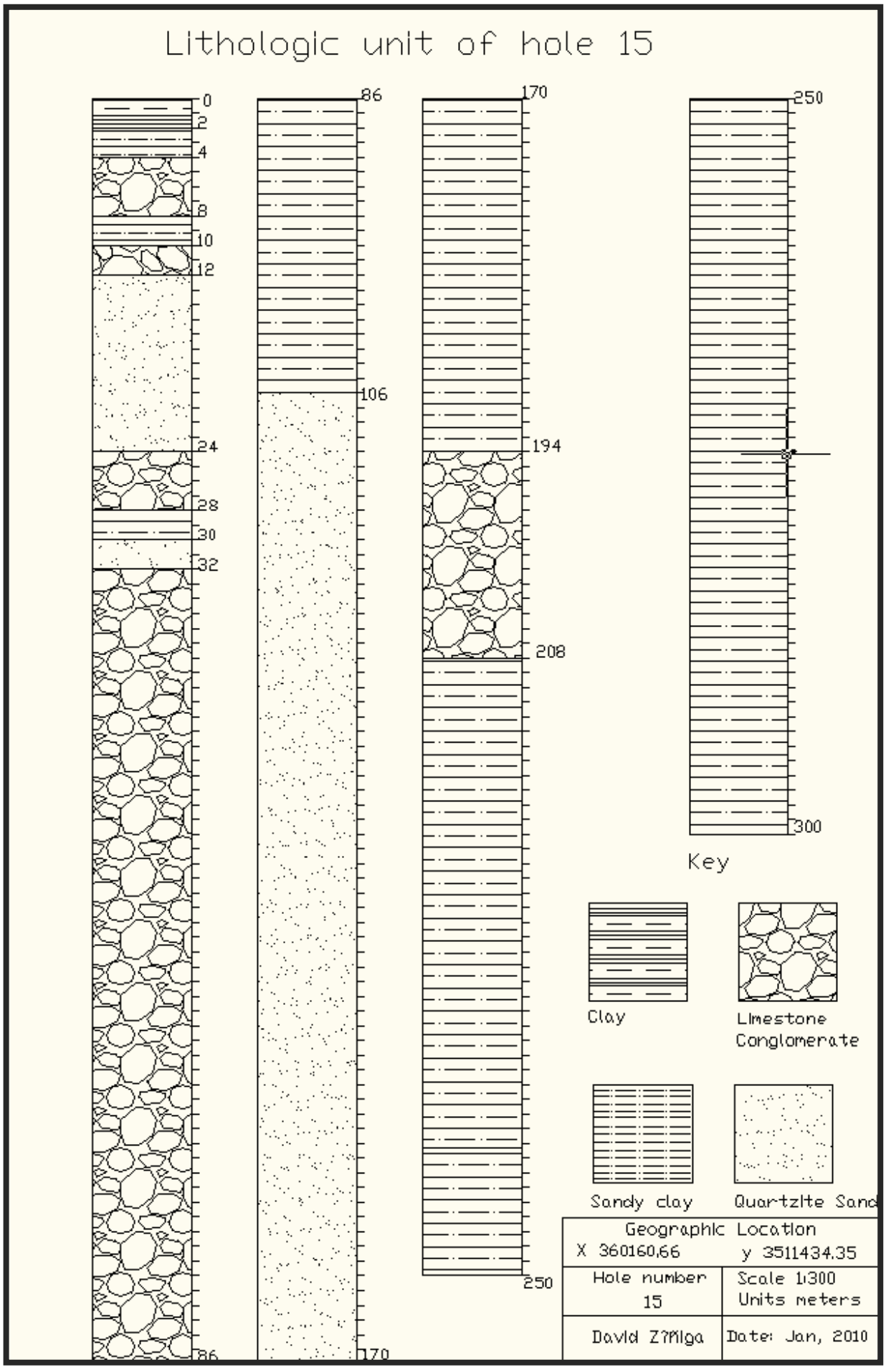
Lithologic unit of hole 15
0
2
4
8
10
12
24
28
30
32
86
106
170
194
208
250
300
Key
Clay
Limestone
Conglomerate
Sandy clay
Quartzite Sand
Geographic Location
X 360160,66
y 3511434,35
Hole number
15
Scale 1:300
Units meters
David Zúñiga
Date: Jan, 2010

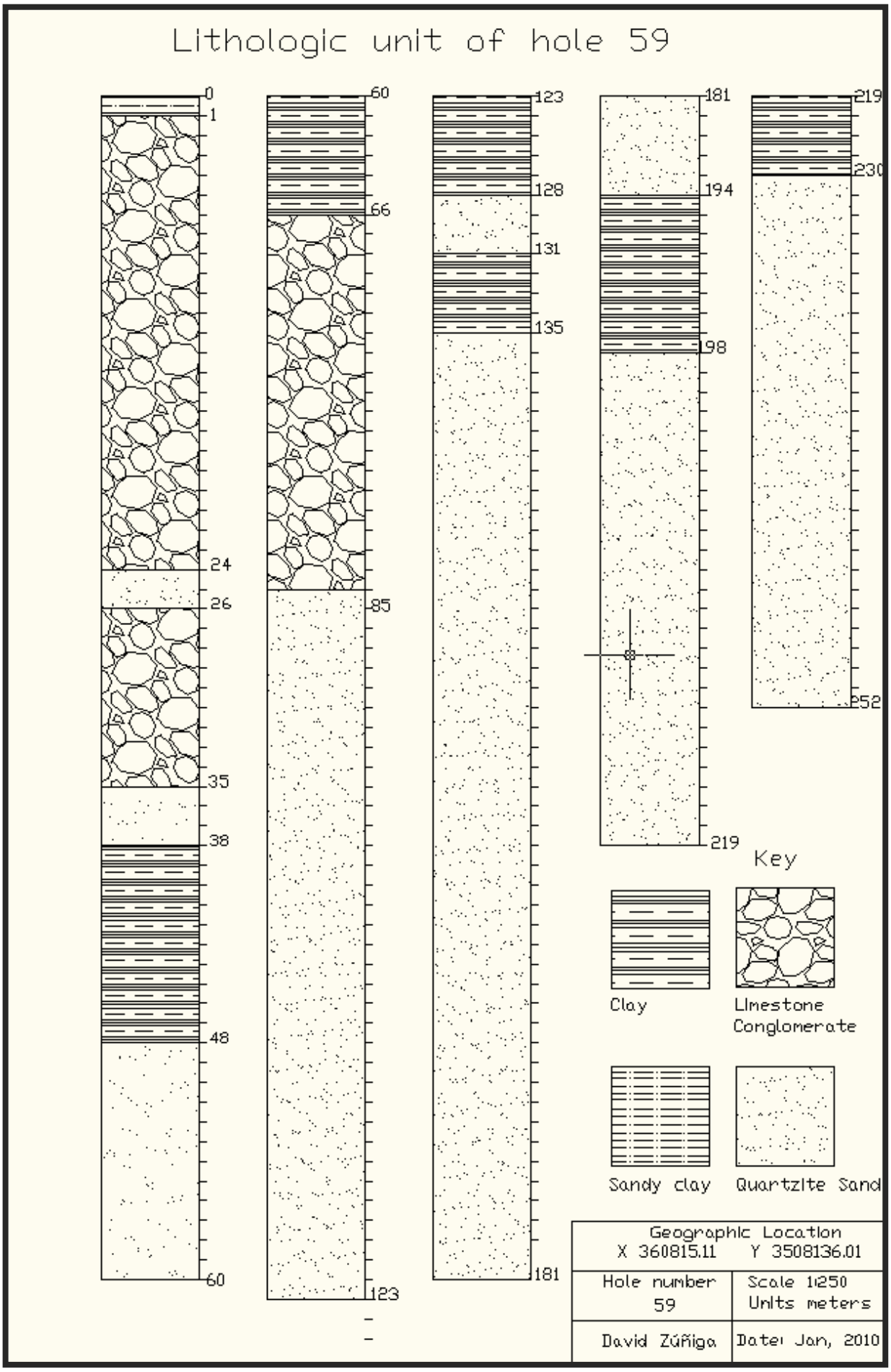
Lithologic unit of hole 59
0
1
24
26
35
38
48
60
60
66
85
123
123
128
131
135
181
181
194
198
219
219
230
252
Key
Clay
Limestone
Conglomerate
Sandy clay
Quartzite Sand
Geographic Location
X 360815.11 Y 3508136.01
Hole number
59
Scale 1:250
Units meters
David Zúñiga
Date: Jan, 2010

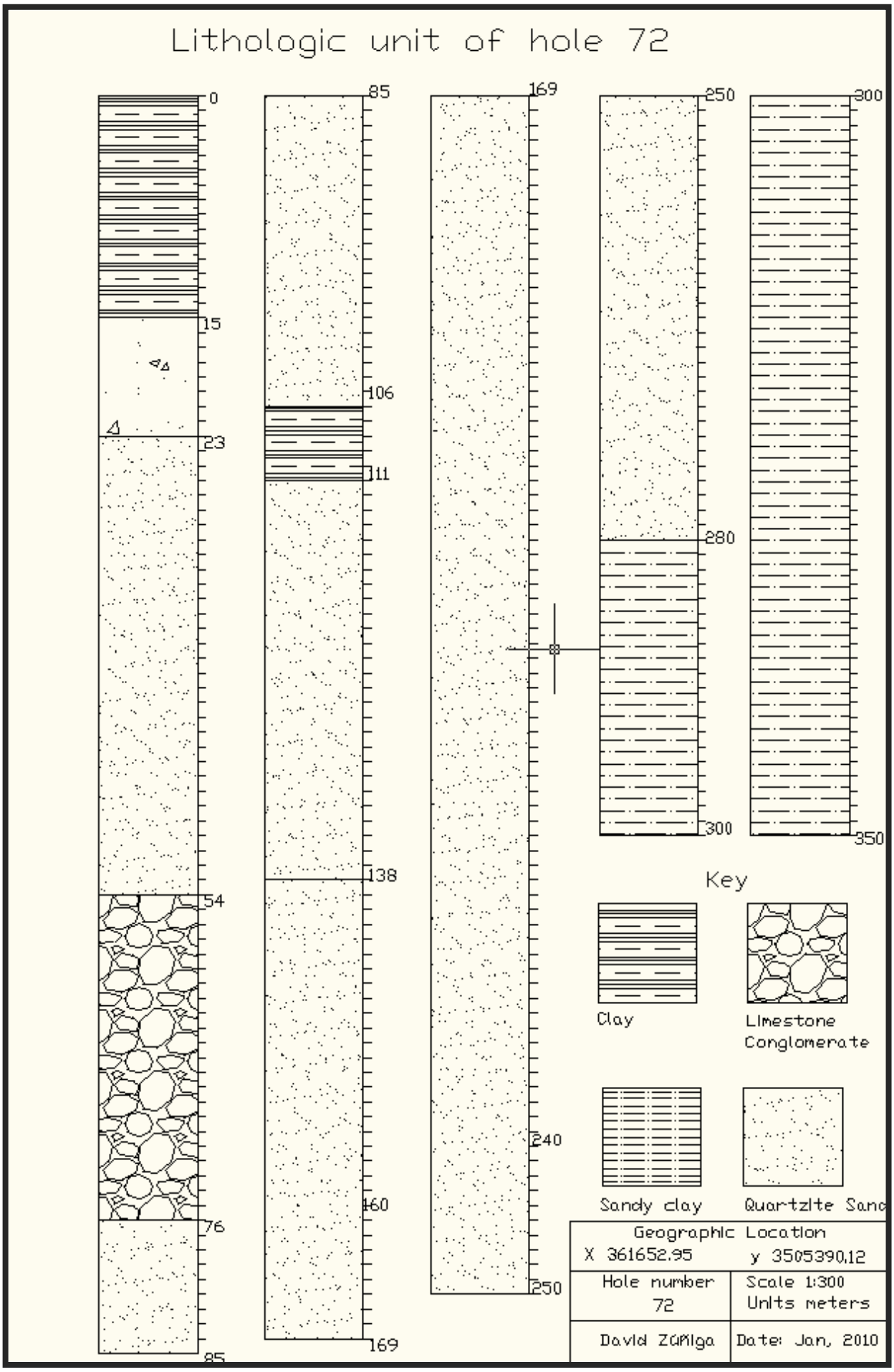
Lithologic unit of hole 72
0
15
23
54
76
85
85
106
111
138
169
169
240
250
250
280
300
300
350
Key
Clay
Limestone
Conglomerate
Sandy clay
Quartzite Sand
Geographic Location
X 361652.95
y 3505390.12
Hole number
72
Scale 1:300
Units meters
David ZAMiga
Date: Jan, 2010

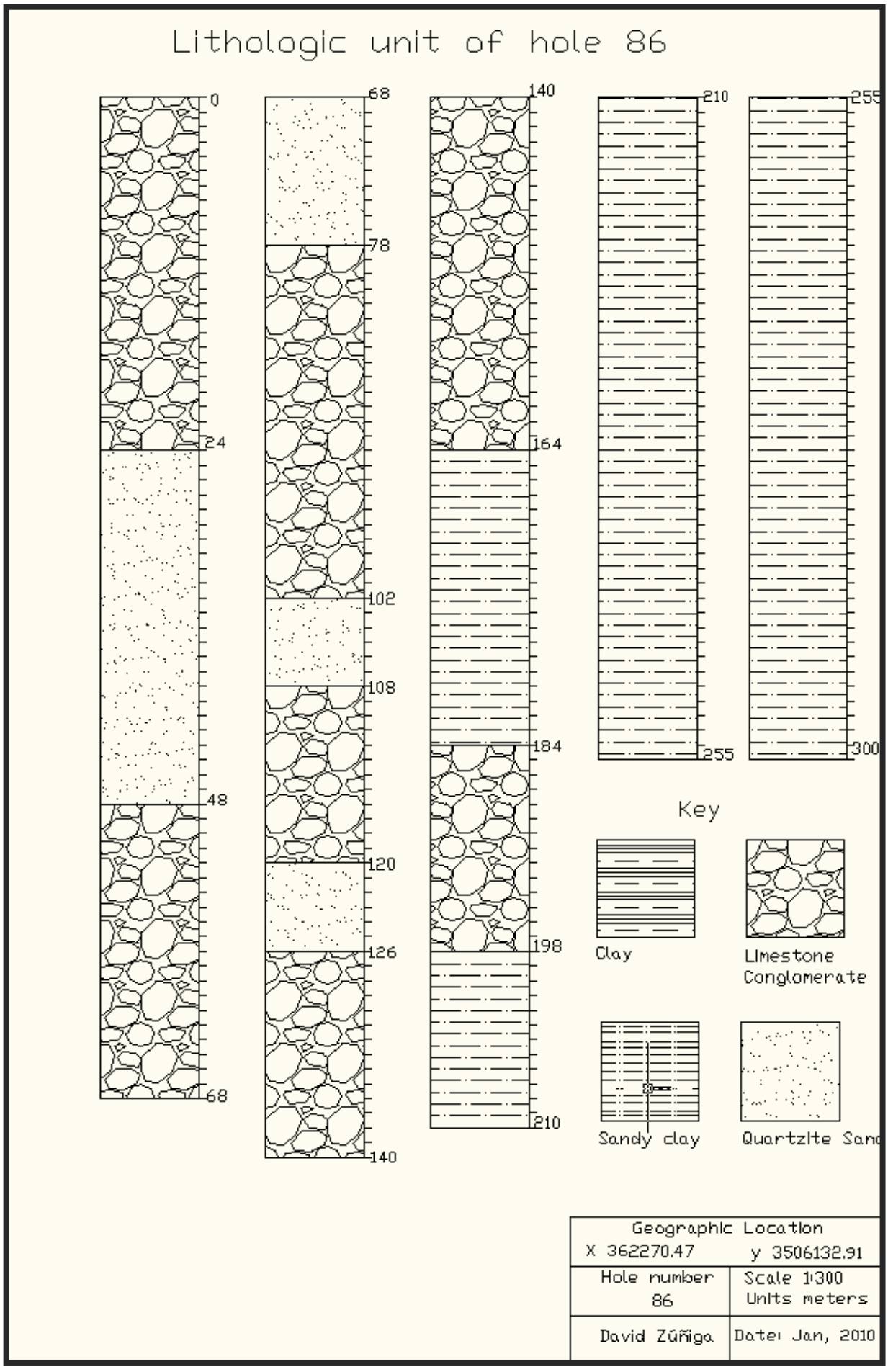
Lithologic unit of hole 86
0
24
48
68
68
78
102
108
120
126
140
140
164
184
198
210
210
255
255
300
Key
Clay
Limestone
Conglomerate
Sandy clay
Quartzite Sand
Geographic Location
X 362270.47
y 3506132.91
Hole number
86
Scale 1:300
Units meters
David Zúñiga
Date: Jan, 2010

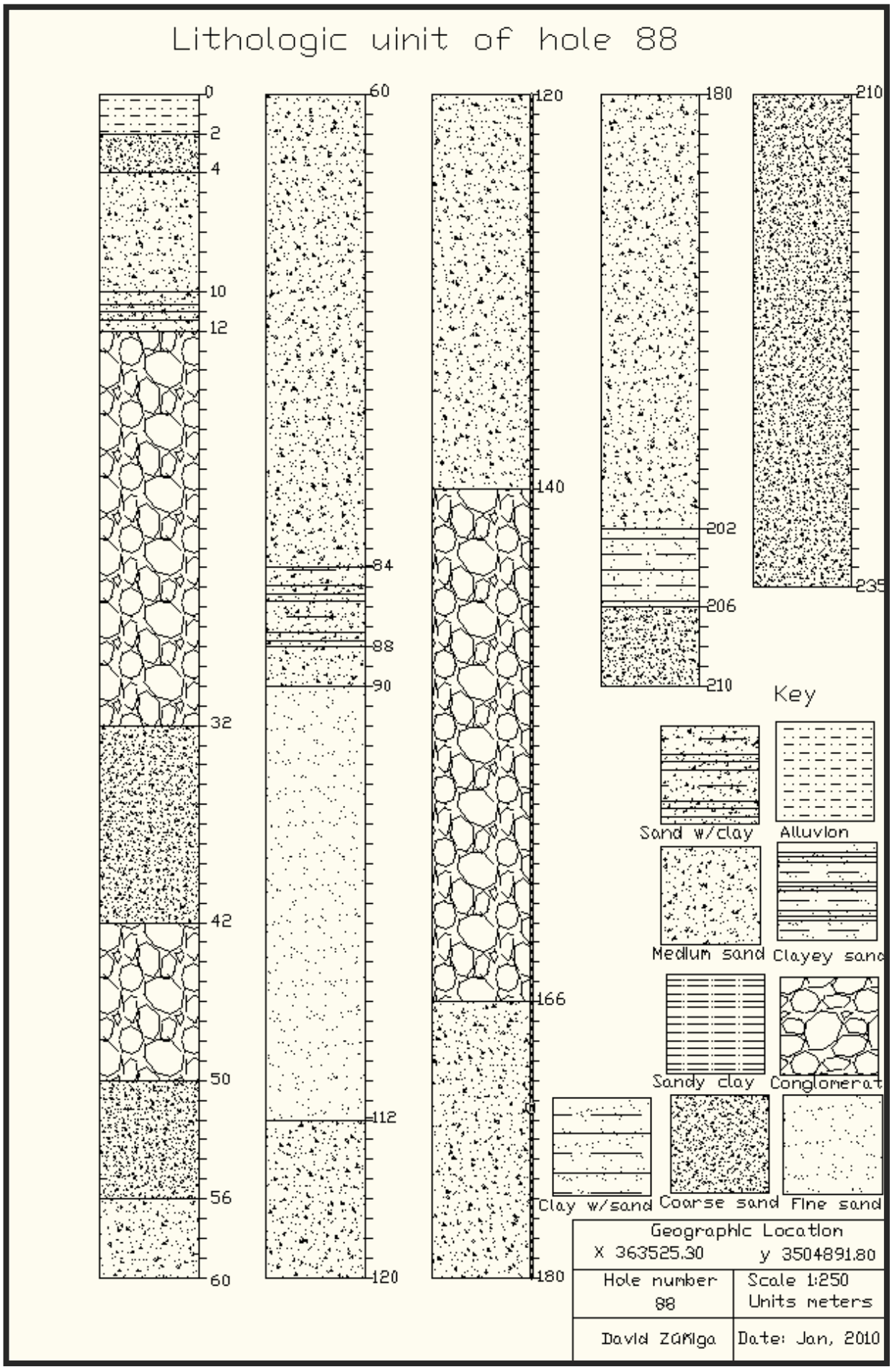
Lithologic uinit of hole 88
0
2
4
10
12
32
42
50
56
60
60
84
88
90
112
120
120
140
166
180
180
202
206
210
210
235
Key
Sand w/clay
Alluvion
Medium sand
Clayey sand
Sandy clay
Conglomerat
Clay w/sand
Coarse sand
Fine sand
Geographic Location
X 363525.30
y 3504891.80
Hole number
88
Scale 1:250
Units meters
David Zúñiga
Date: Jan, 2010

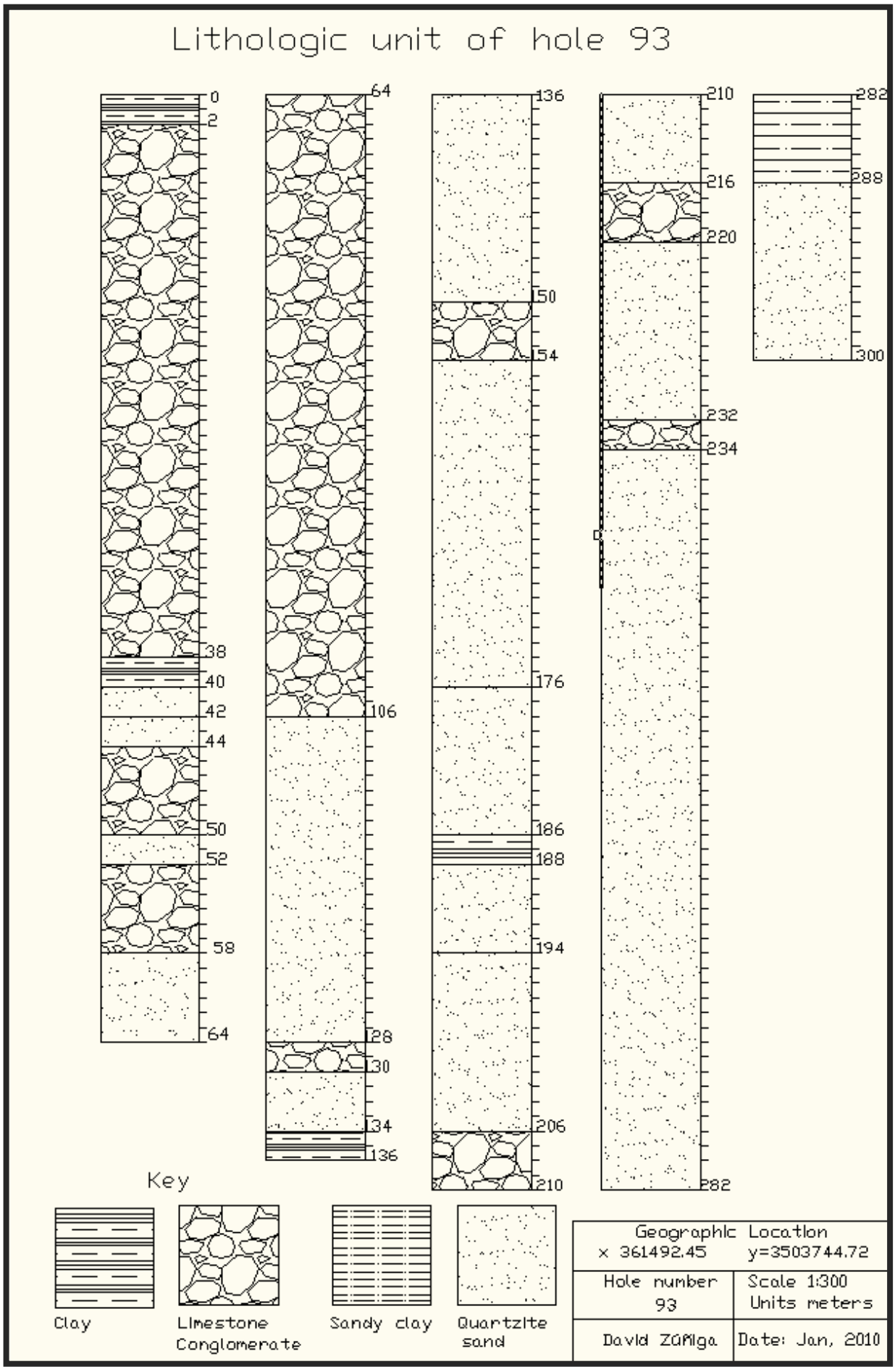
Lithologic unit of hole 93
0
2
38
40
42
44
50
52
58
64
64
106
28
30
34
136
136
50
54
176
186
188
194
206
210
210
216
220
232
234
282
282
288
300
Key
Clay
Limestone Conglomerate
Sandy clay
Quartzite sand
Geographic Location
x 361492.45 y=3503744.72
Hole number 93
Scale 1:300 Units meters
David ZAMiga
Date: Jan, 2010

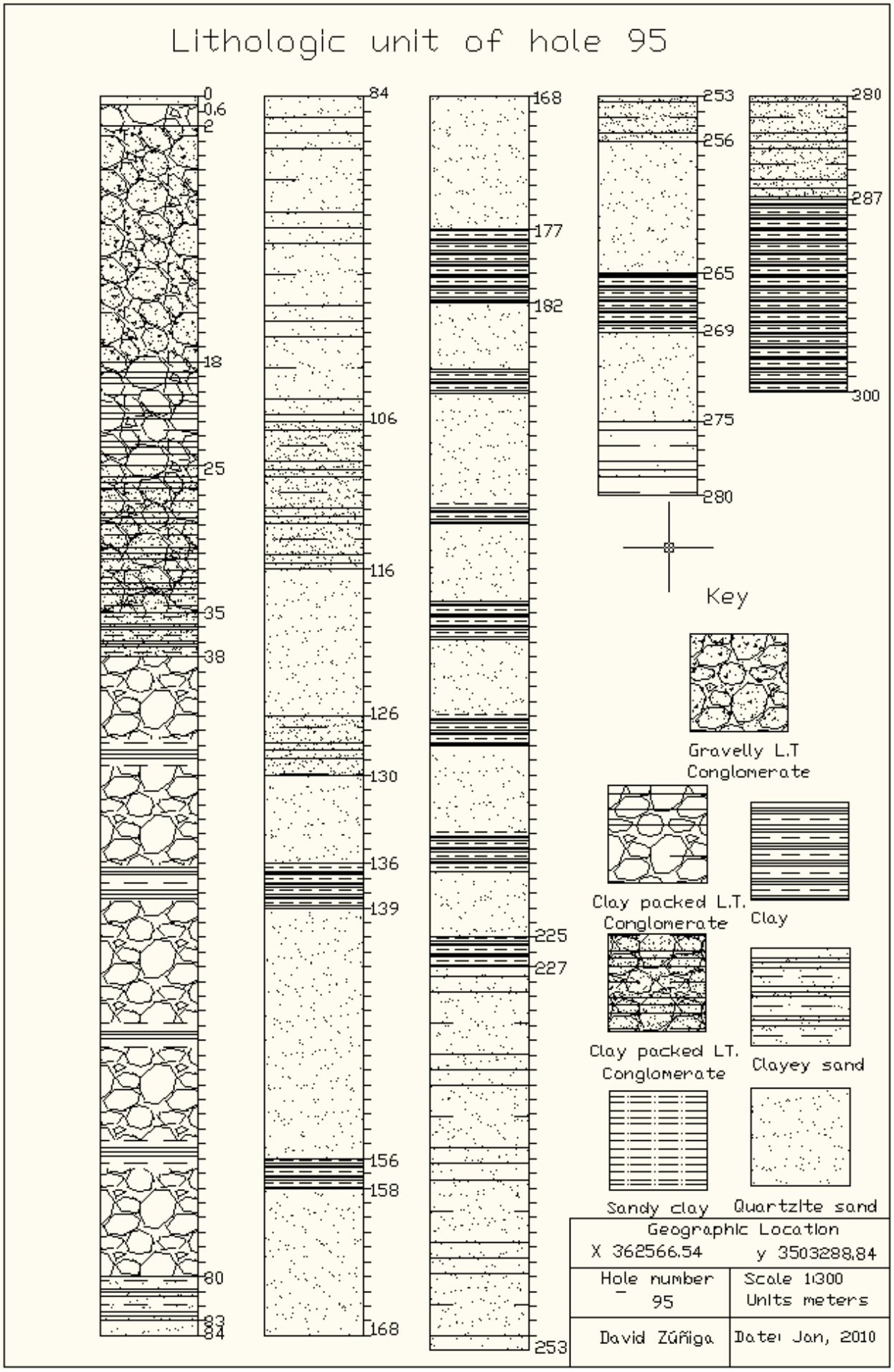
Lithologic unit of hole 95
0
0.6
2
18
25
35
38
80
83
84
84
106
116
126
130
136
139
156
158
168
168
177
182
225
227
253
253
256
265
269
275
280
280
287
300
Key
Gravelly L.T Conglomerate
Clay packed L.T. Conglomerate
Clay
Clay packed LT. Conglomerate
Clayey sand
Sandy clay
Quartzite sand
Geographic Location
X 362566.54 y 3503288.84
Hole number 95
Scale 1:300
Units meters
David Zúñiga
Date: Jan, 2010

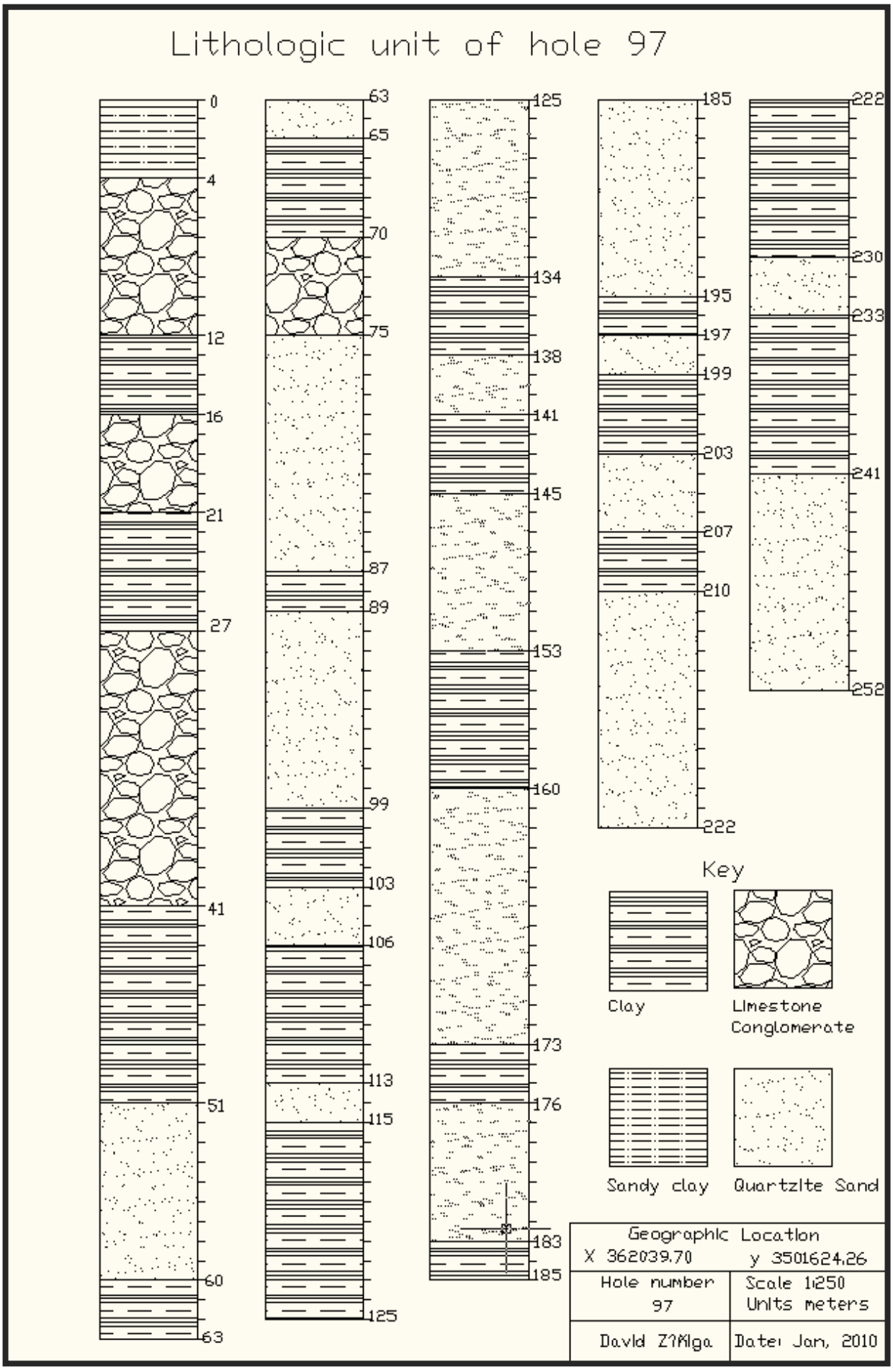
Lithologic unit of hole 97
0
4
12
16
21
27
41
51
60
63
63
65
70
75
87
89
99
103
106
113
115
125
125
134
138
141
145
153
160
173
176
183
185
185
195
197
199
203
207
210
222
222
230
233
241
252
Key
Clay
Limestone Conglomerate
Sandy clay
Quartzite Sand
Geographic Location
X 362039.70
y 3501624.26
Hole number 97
Scale 1:250
Units meters
David Z?Alga
Date: Jan, 2010

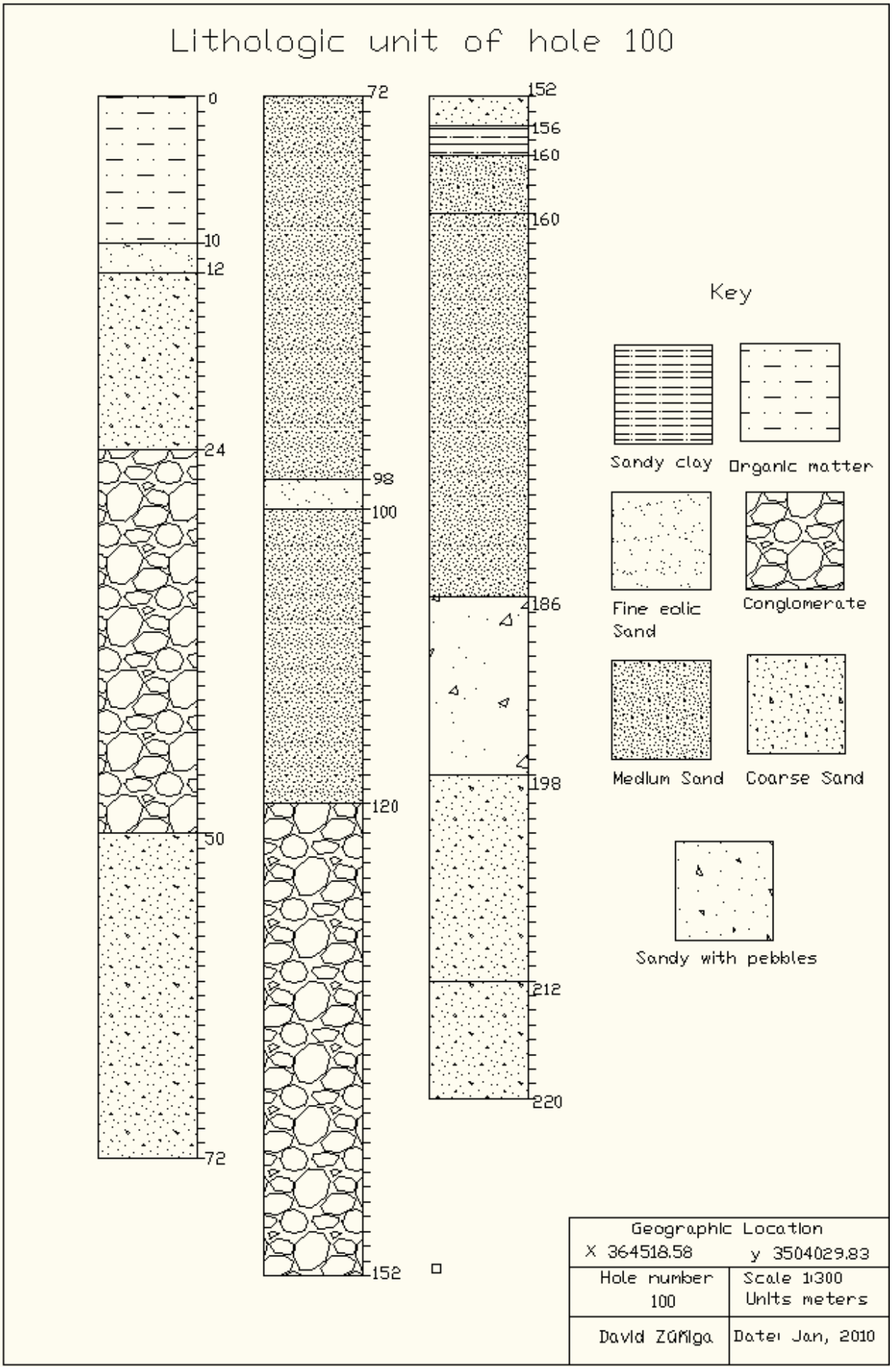
Lithologic unit of hole 100
0
10
12
24
50
72
72
98
100
120
152
152
156
160
160
186
198
212
220
Key
Sandy clay
Organic matter
Fine eolic Sand
Conglomerate
Medium Sand
Coarse Sand
Sandy with pebbles
Geographic Location
X 364518.58
y 3504029.83
Hole number 100
Scale 1:300 Units meters
David ZAMIga
Date: Jan, 2010

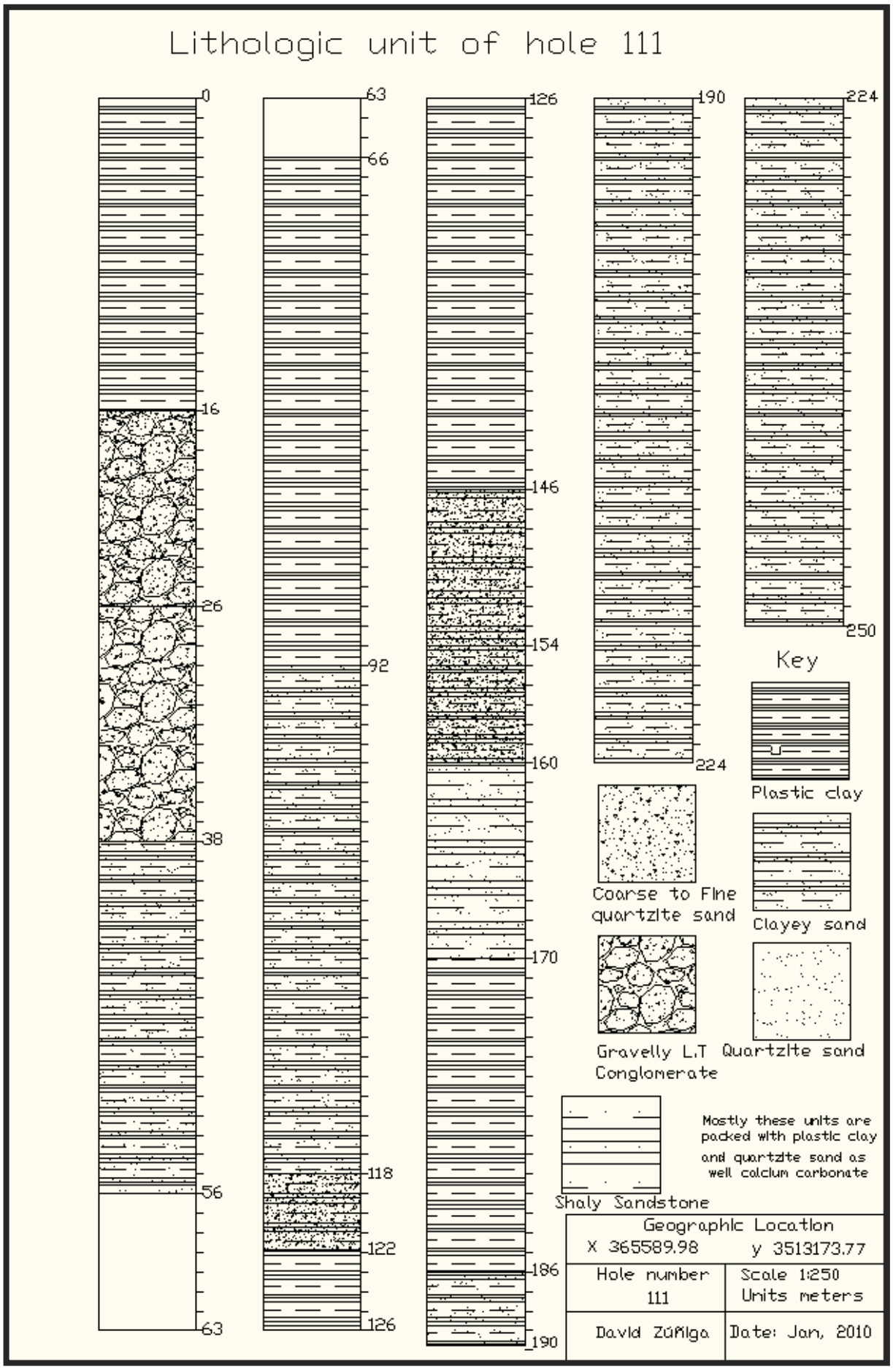
Lithologic unit of hole 111
0
16
26
38
56
63
63
66
92
118
122
126
126
146
154
160
170
186
190
190
224
224
250
Key
Plastic clay
Coarse to Fine quartzite sand
Clayey sand
Gravelly L.T Conglomerate
Quartzite sand
Shaly Sandstone
Mostly these units are packed with plastic clay and quartzite sand as well calcium carbonate
Geographic Location
X 365589.98
y 3513173.77
Hole number 111
Scale 1:250
Units meters
David Zúñiga
Date: Jan, 2010

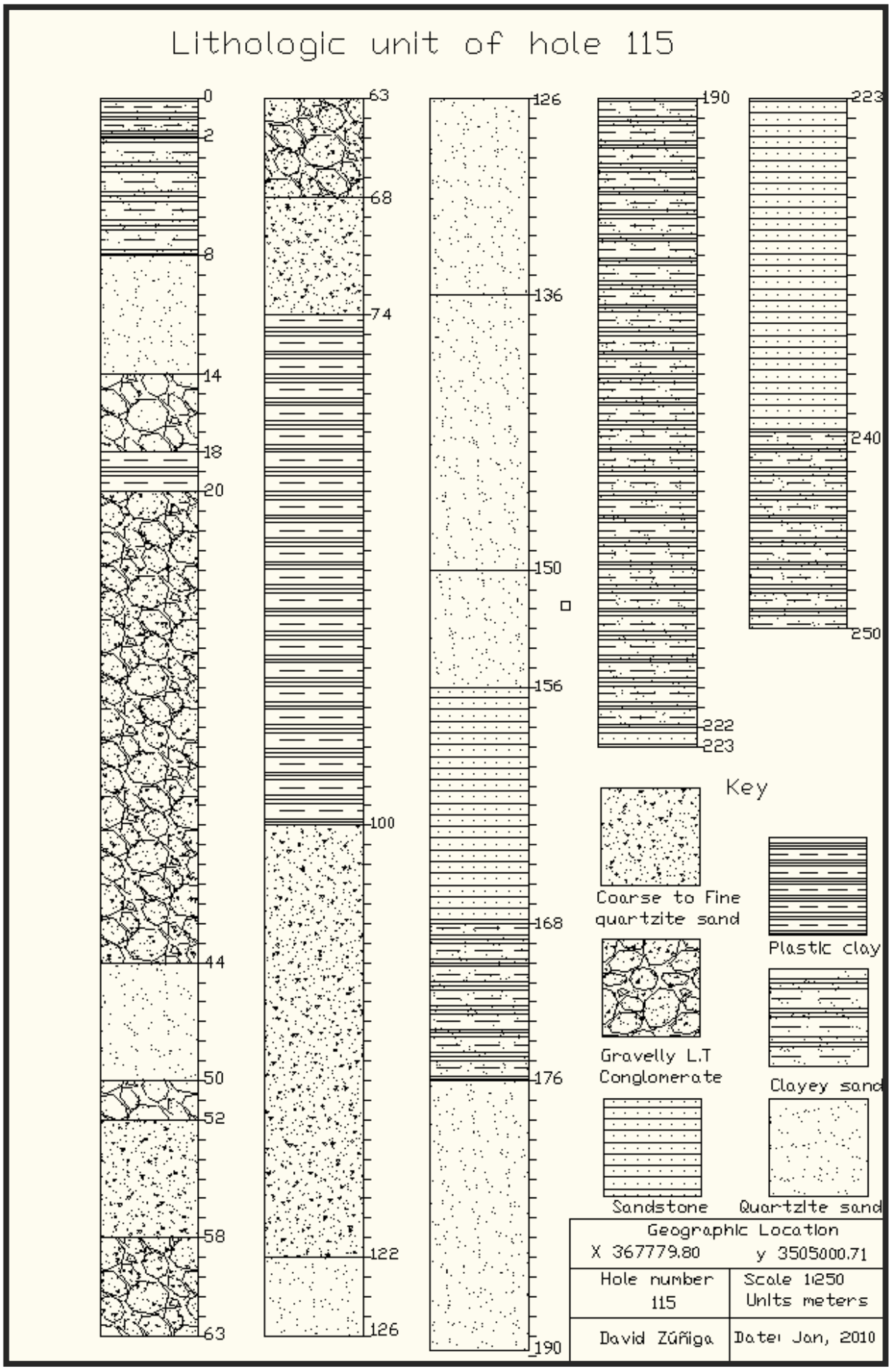
Lithologic unit of hole 115
0
2
8
14
18
20
44
50
52
58
63
63
68
74
100
122
126
126
136
150
156
168
176
190
190
222
223
223
240
250
Key
Coarse to Fine quartzite sand
Plastic clay
Gravelly L.T Conglomerate
Clayey sand
Sandstone
Quartzite sand
Geographic Location
X 367779.80
y 3505000.71
Hole number 115
Scale 1:250
Units meters
David Zúñiga
Date: Jan, 2010

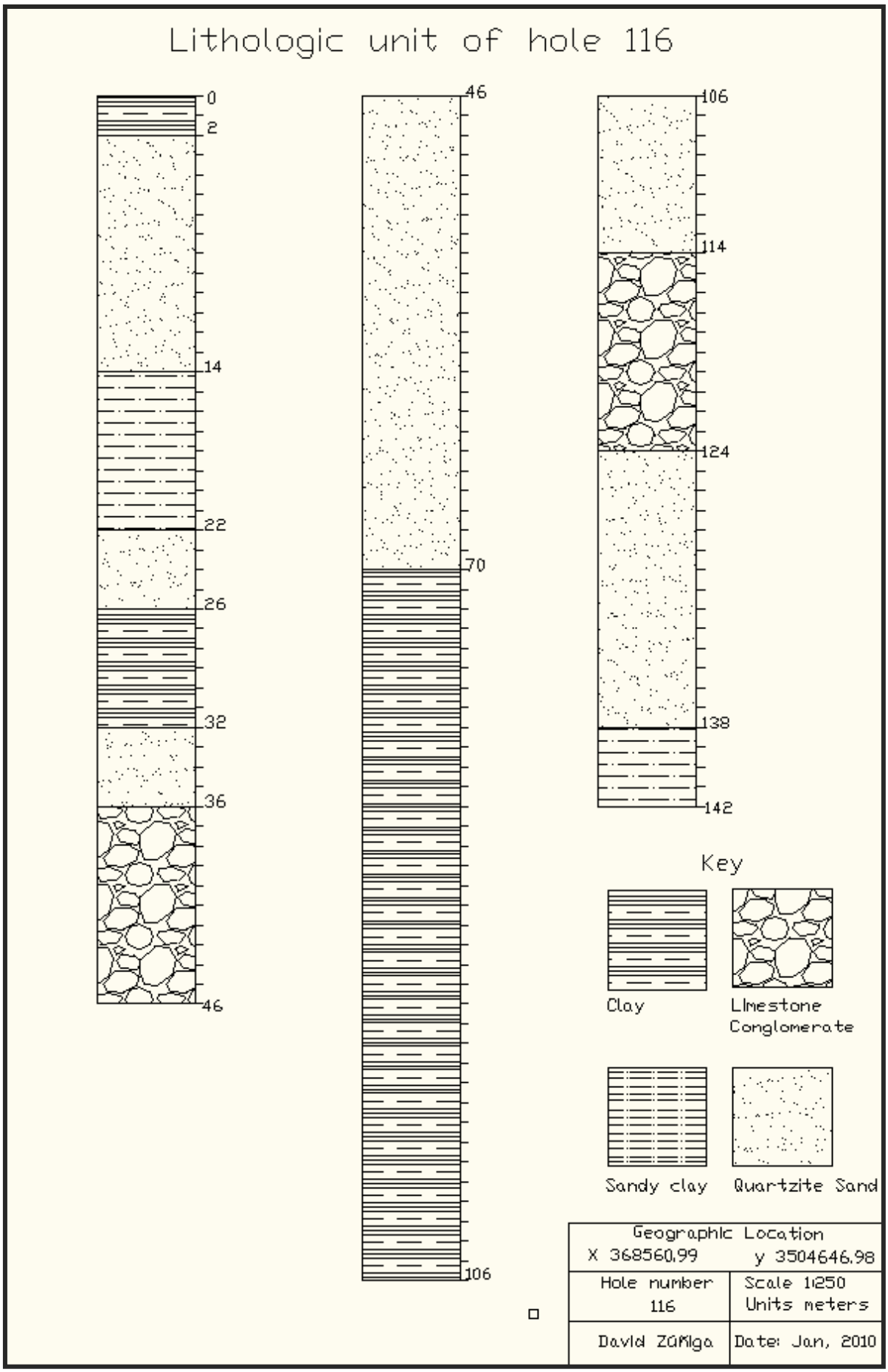
Lithologic unit of hole 116
0
2
14
22
26
32
36
46
46
70
106
106
114
124
138
142
Key
Clay
Limestone
Conglomerate
Sandy clay
Quartzite Sand
Geographic Location
X 368560.99
y 3504646.98
Hole number
116
Scale 1:250
Units meters
David Zúñiga
Date: Jan, 2010

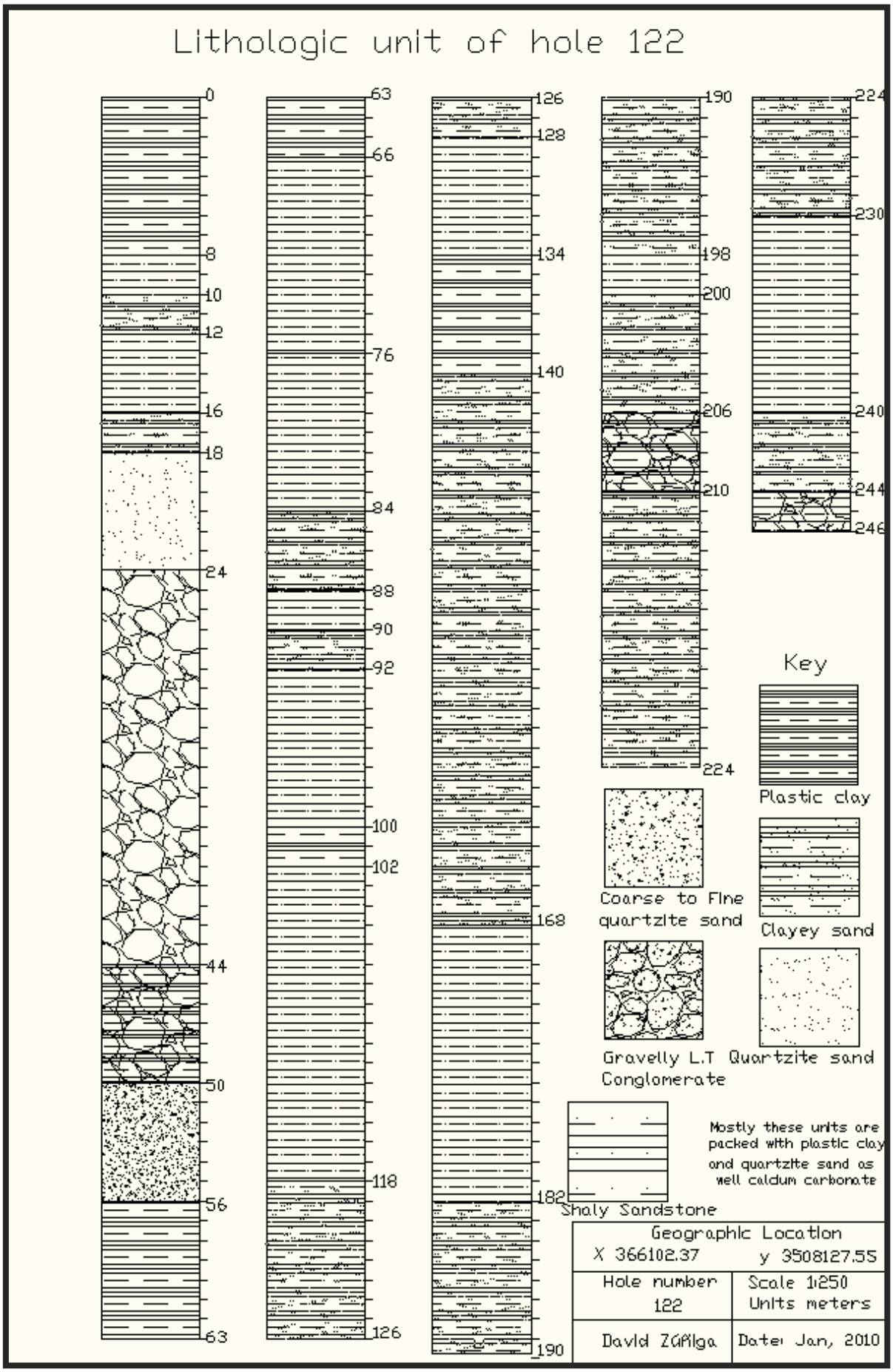
Lithologic unit of hole 122
0
8
10
12
16
18
24
44
50
56
63
63
66
76
84
88
90
92
100
102
118
126
126
128
134
140
168
182
190
190
198
200
206
210
224
224
230
240
244
246
Key
Plastic clay
Clayey sand
Coarse to Fine quartzite sand
Quartzite sand
Gravelly L.T Conglomerate
Shaly Sandstone
Mostly these units are packed with plastic clay and quartzite sand as well caldum carbonate
Geographic Location
X 366102.37
y 3508127.55
Hole number 122
Scale 1:250
Units meters
David ZAMlga
Date: Jan, 2010

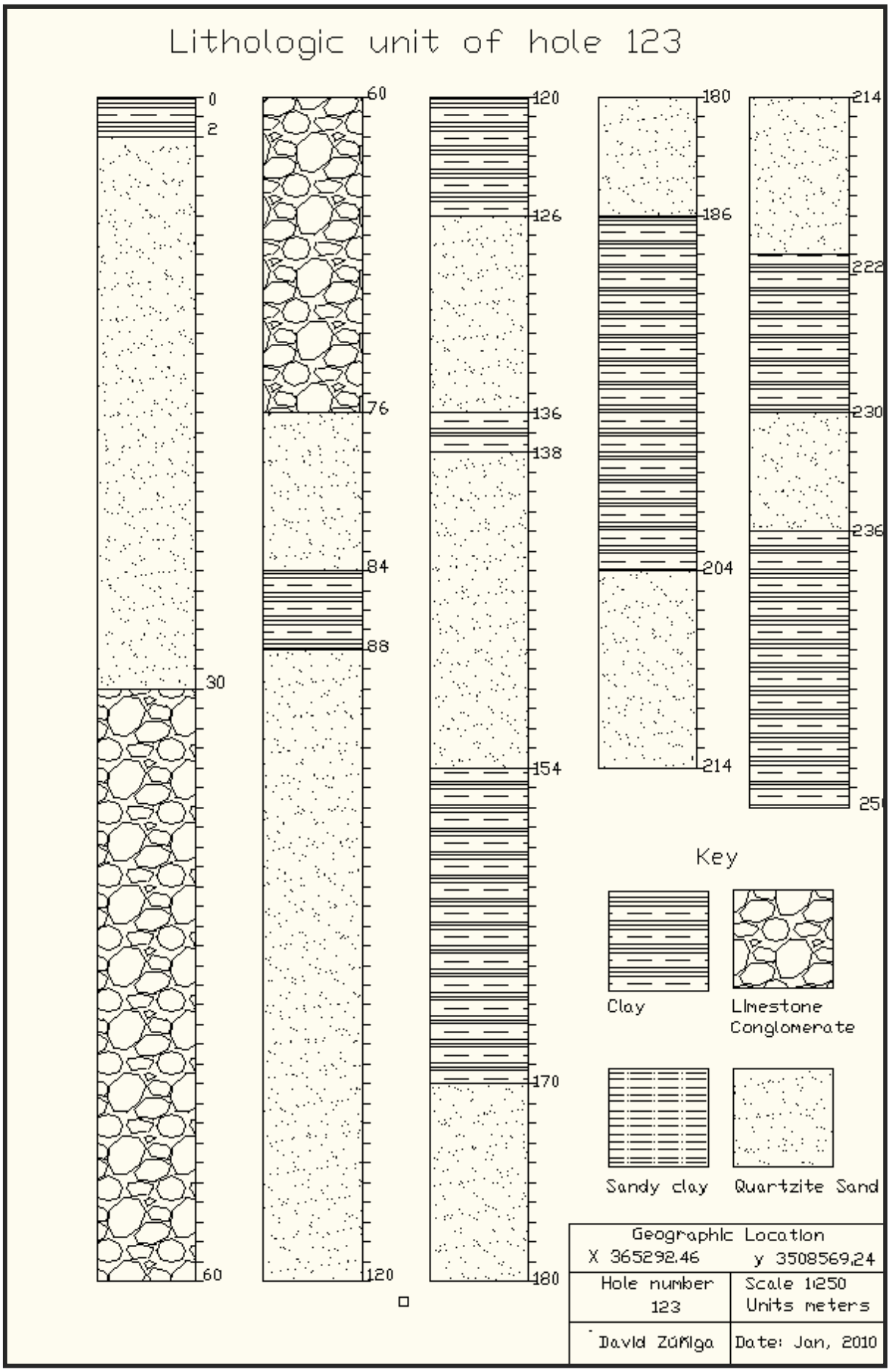
Lithologic unit of hole 123
0
2
30
60
60
76
84
88
120
120
126
136
138
154
170
180
180
186
204
214
214
222
230
236
250
Key
Clay
Limestone Conglomerate
Sandy clay
Quartzite Sand
Geographic Location
X 365292.46
y 3508569.24
Hole number 123
Scale 1:250 Units meters
David Zúñiga
Date: Jan, 2010

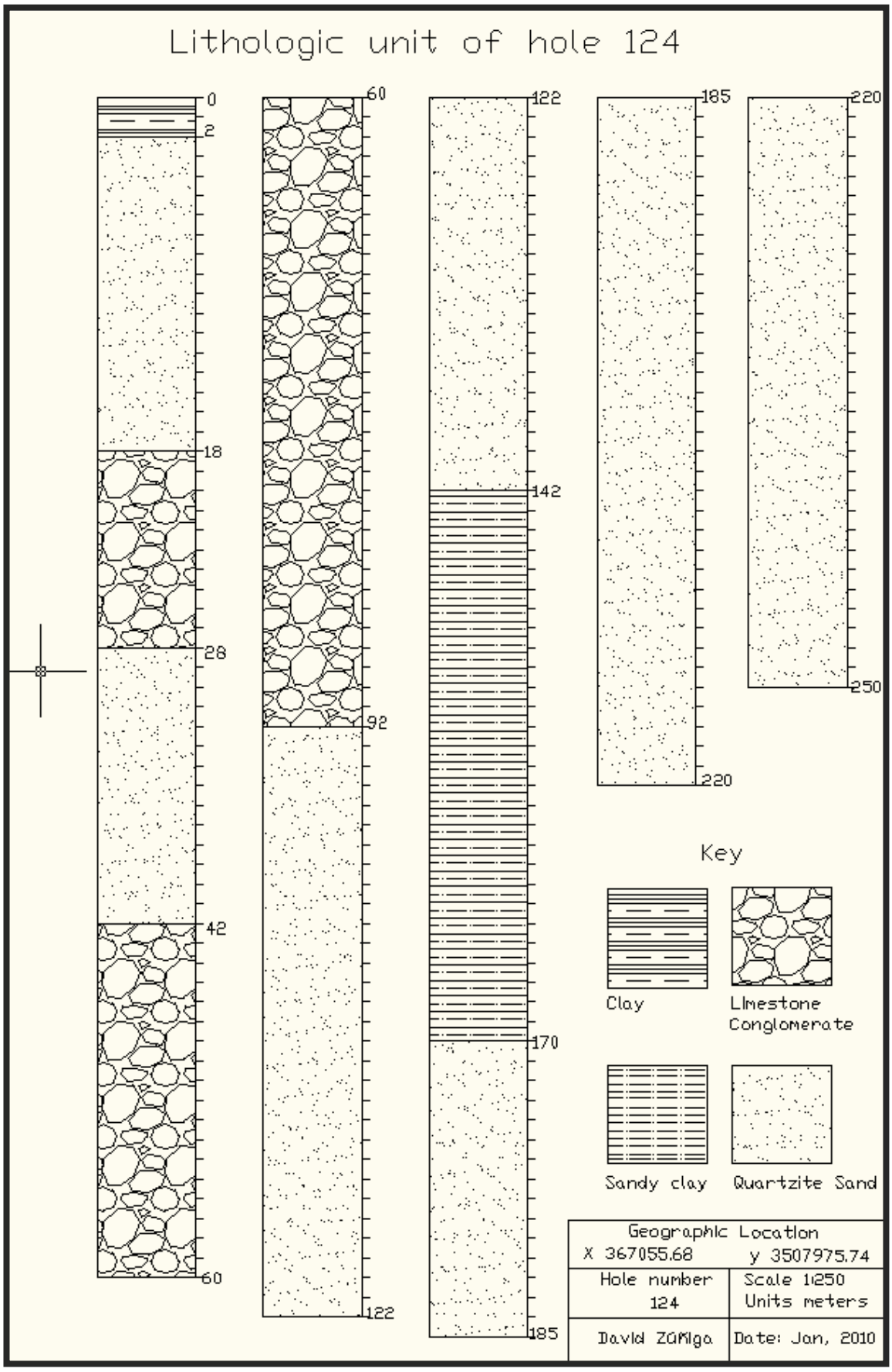
Lithologic unit of hole 124
0
2
18
28
42
60
60
92
122
122
142
170
185
185
220
220
250
Key
Clay
Limestone
Conglomerate
Sandy clay
Quartzite Sand
Geographic Location
X 367055.68
y 3507975.74
Hole number
124
Scale 1:250
Units meters
David ZAMIga
Date: Jan, 2010

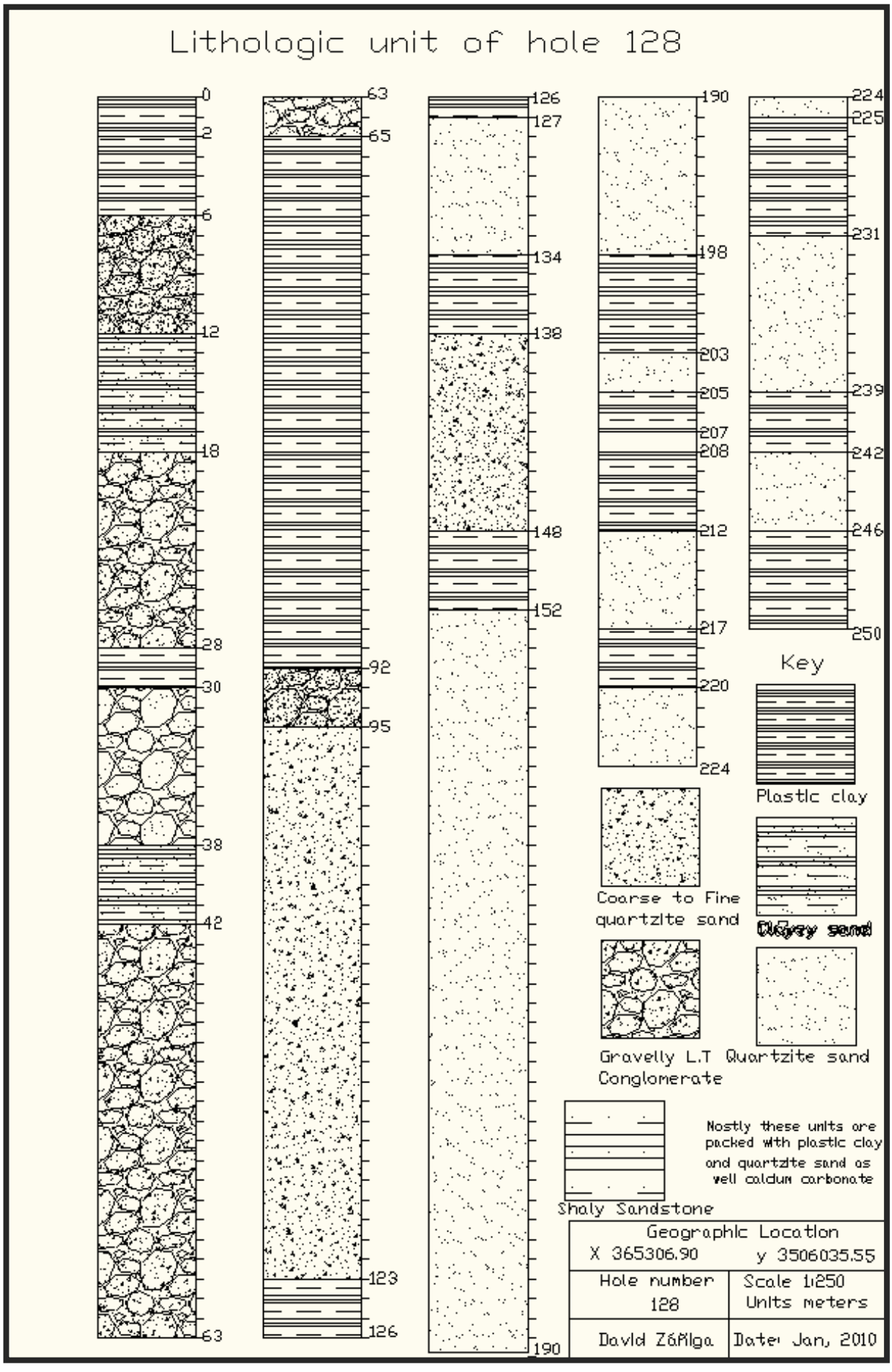
Lithologic unit of hole 128
0
2
6
12
18
28
30
38
42
63
63
65
92
95
123
126
126
127
134
138
148
152
190
190
198
203
205
207
208
212
217
220
224
224
225
231
239
242
246
250
Key
Plastic clay
Clayey sand
Coarse to Fine quartzite sand
Gravelly L.T Conglomerate
Quartzite sand
Shaly Sandstone
Nostly these units are packed with plastic clay and quartzite sand as well caldum carbonate
Geographic Location
X 365306.90
y 3506035.55
Hole number 128
Scale 1:250
Units meters
David ZáRiga
Date: Jan, 2010

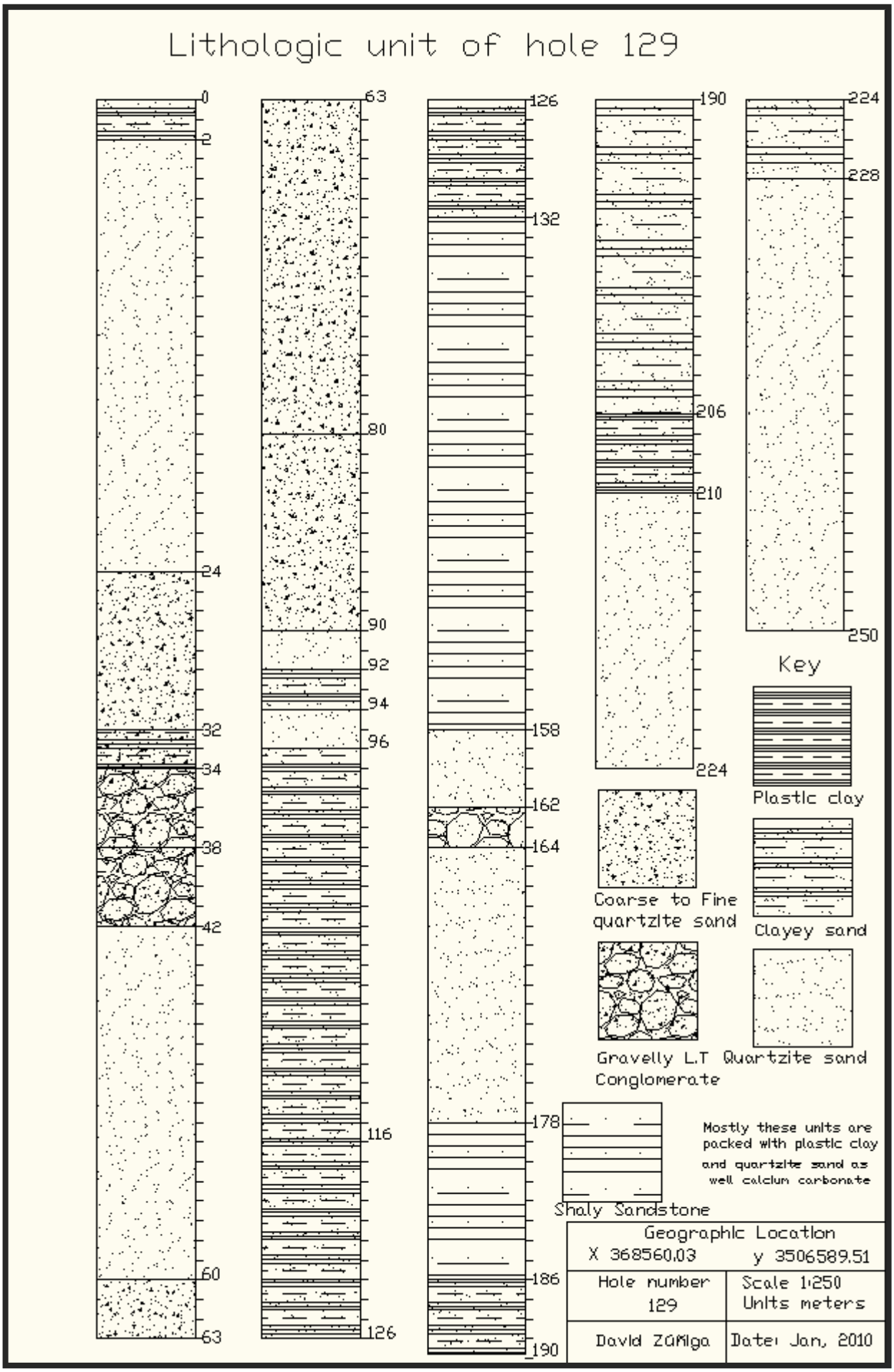
Lithologic unit of hole 129
0
2
24
32
34
38
42
60
63
63
80
90
92
94
96
116
126
126
132
158
162
164
178
186
190
190
206
210
224
224
228
250
Key
Plastic clay
Coarse to Fine quartzite sand
Clayey sand
Gravelly L.T Conglomerate
Quartzite sand
Shaly Sandstone
Mostly these units are packed with plastic clay and quartzite sand as well calcium carbonate
Geographic Location
X 368560.03
y 3506589.51
Hole number 129
Scale 1:250 Units meters
David Zúñiga
Date: Jan, 2010

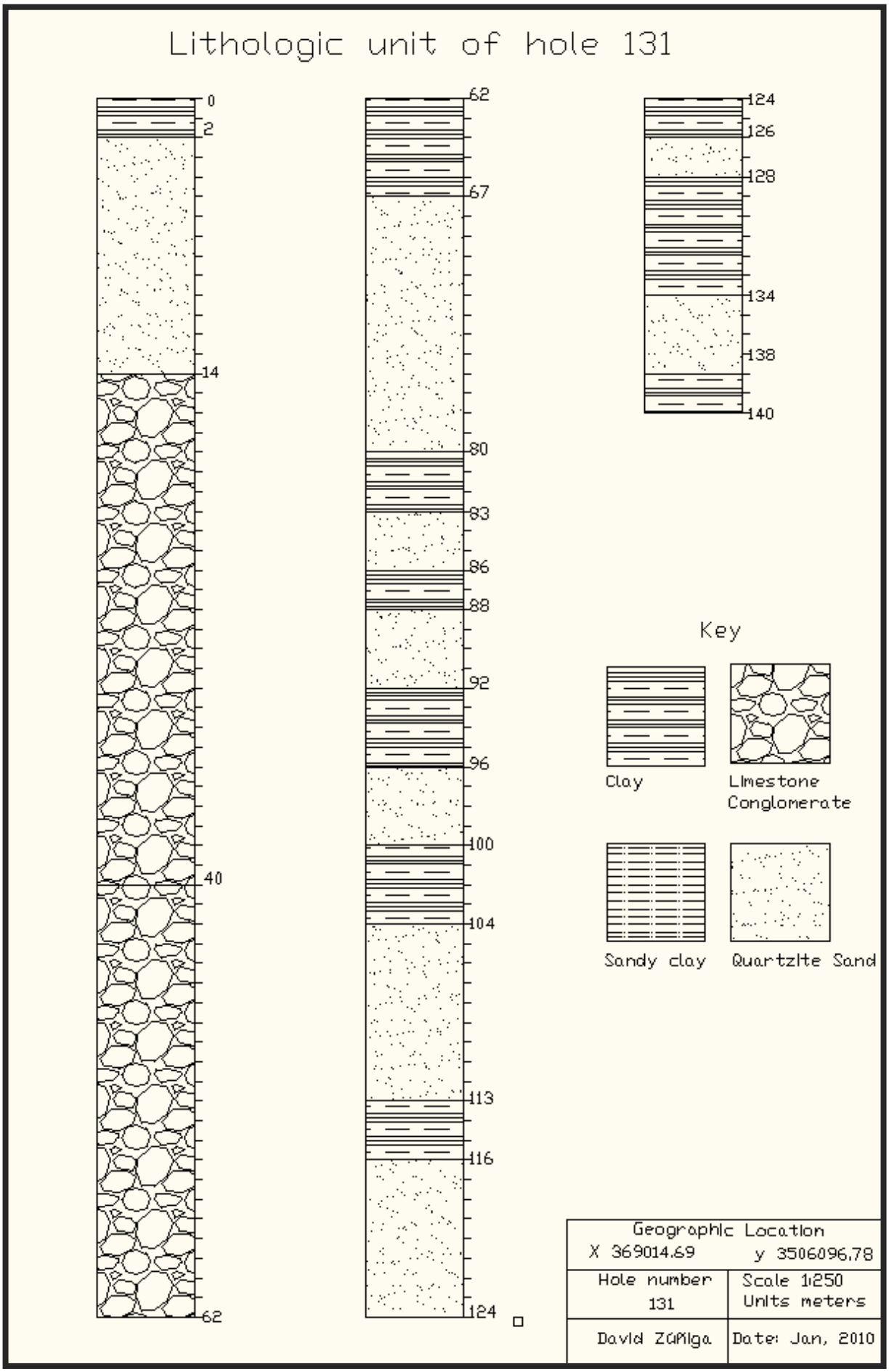
Lithologic unit of hole 131
0
2
14
40
62
62
67
80
83
86
88
92
96
100
104
113
116
124
124
126
128
134
138
140
Key
Clay
Limestone
Conglomerate
Sandy clay
Quartzite Sand
Geographic Location
X 369014.69
y 3506096.78
Hole number
131
Scale 1:250
Units meters
David Zúñiga
Date: Jan, 2010

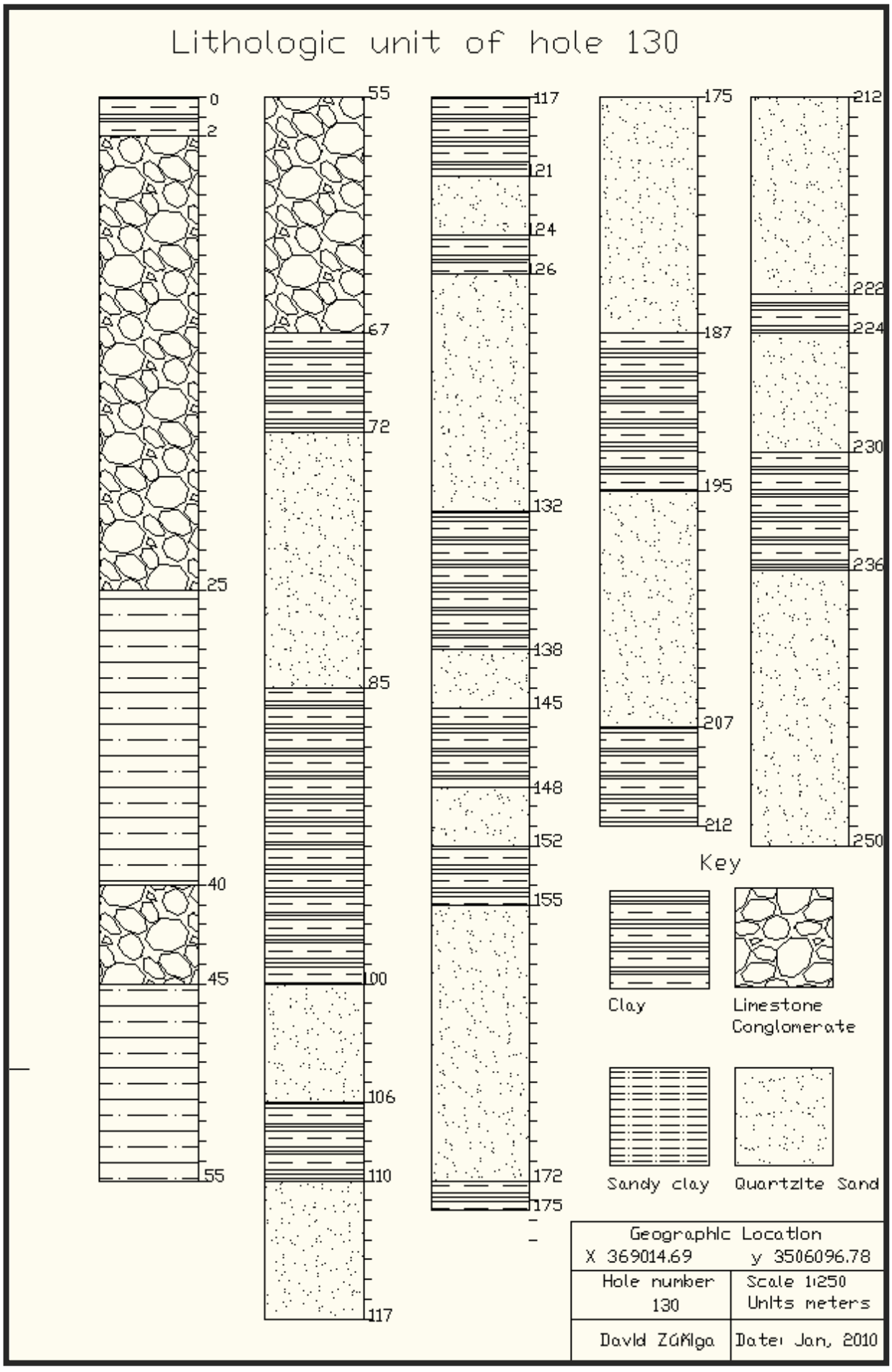
Lithologic unit of hole 130
0
2
25
40
45
55
55
67
72
85
100
106
110
117
117
121
124
126
132
138
145
148
152
155
172
175
175
187
195
207
212
212
222
224
230
236
250
Key
Clay
Limestone
Conglomerate
Sandy clay
Quartzite Sand
Geographic Location
X 369014.69 y 3506096.78
Hole number
130
Scale 1:250
Units meters
David Zúñiga
Date: Jan, 2010

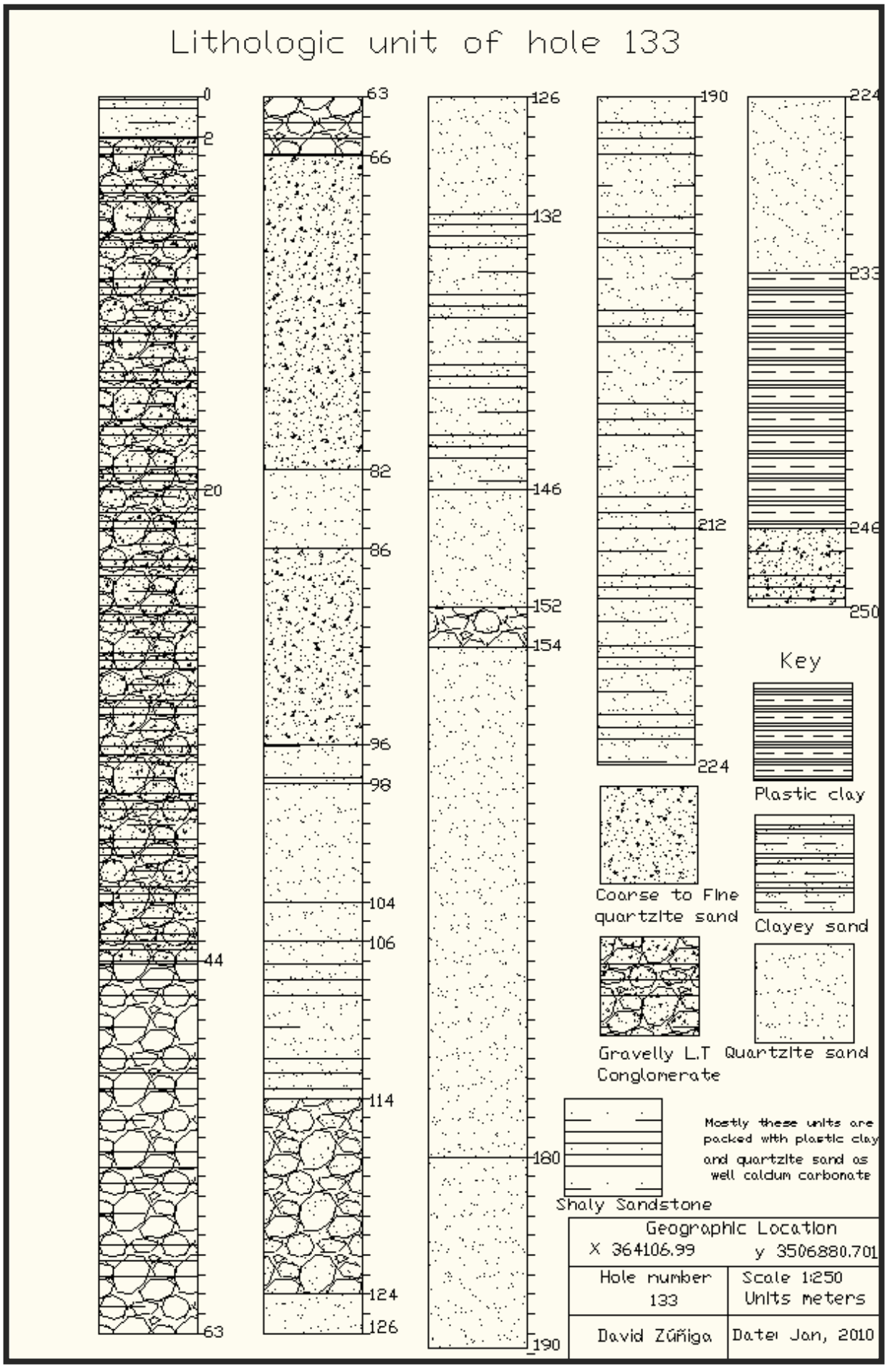
Lithologic unit of hole 133
0
2
20
44
63
63
66
82
86
96
98
104
106
114
124
126
126
132
146
152
154
180
190
190
212
224
224
233
246
250
Key
Plastic clay
Coarse to Fine quartzite sand
Clayey sand
Gravelly L.T Conglomerate
Quartzite sand
Mostly these units are packed with plastic clay and quartzite sand as well caldum carbonate
Shaly Sandstone
Geographic Location
X 364106.99
y 3506880.701
Hole number 133
Scale 1:250 Units meters
David Zúñiga
Date: Jan, 2010

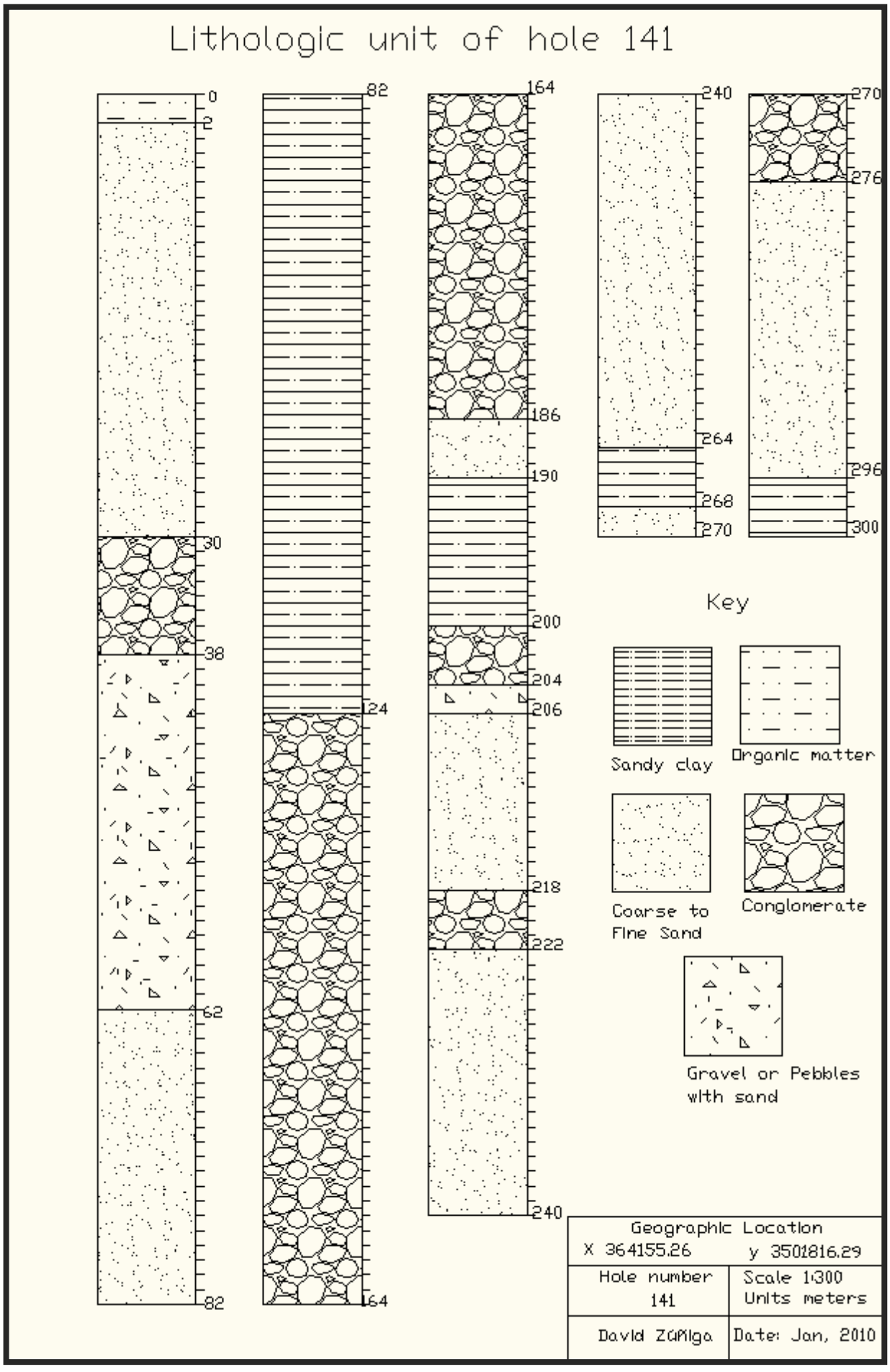
Lithologic unit of hole 141
0
2
30
38
62
82
82
124
164
164
186
190
200
204
206
218
222
240
240
264
268
270
270
276
296
300
Key
Sandy clay
Organic matter
Coarse to Fine Sand
Conglomerate
Gravel or Pebbles with sand
Geographic Location
X 364155.26
y 3501816.29
Hole number 141
Scale 1:300 Units meters
David ZAMIga
Date: Jan, 2010

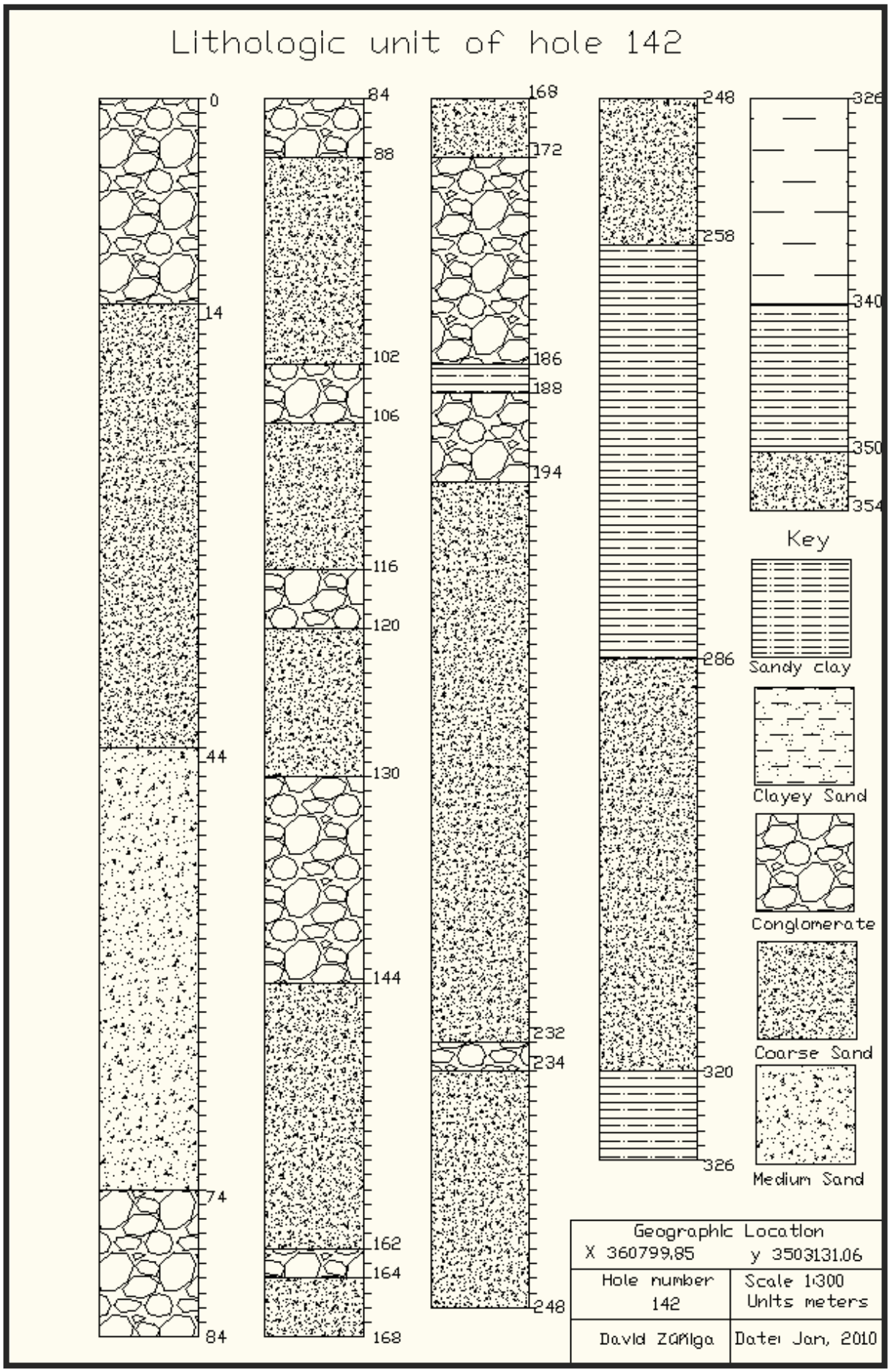
Lithologic unit of hole 142
0
14
44
74
84
84
88
102
106
116
120
130
144
162
164
168
168
172
186
188
194
232
234
248
248
258
286
320
326
326
340
350
354
Key
Sandy clay
Clayey Sand
Conglomerate
Coarse Sand
Medium Sand
Geographic Location
X 360799.85
y 3503131.06
Hole number
142
Scale 1:300
Units meters
David ZAMIga
Date: Jan, 2010

Appendix 4B

Boreholes of the study area were provided by JMAS (2009) Junta Municipal de Aguas y Saneamiento Ciudad Juárez Chihuahua Mexico. (See lithological columns of all the boreholes availlable in appendix 4A4 above). However, in order to build the Three representative cross sections of the study area, only those including in red colour stars (sectio A-A'), blue colour stars (section B-B') and yellow colour stars (section C-C') are shown (See Fig. 1 below) and in Figs 2 to 4 are illustrated the stratigraphic profile derived from these boreholes. Note that the number of figures for practical reasons is the same of that given to the first version of the present thesis.

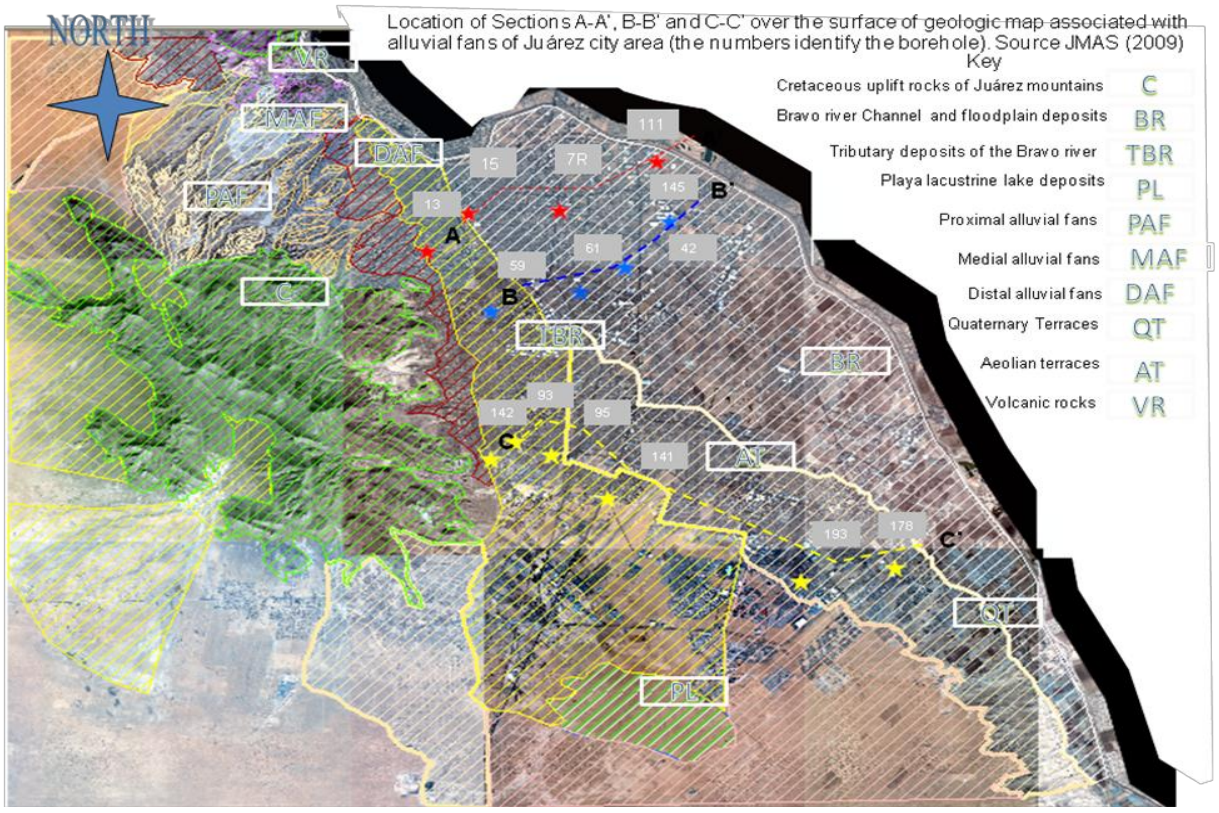

` Figure 1 Cross sections A-A'; B-B' and C-C' performed in the area of Hueco aquifer center of Juárez city; Red stars=Section A-A'=holes 13, 15, 7R and 111; Blue stars=Section B-B'=holes 59, 61, 42, 145; Yellow stars=Section C-C' holes 142, 93, 95, 141, 193 and 178; additional Key is showed in the upper part of Figure and refers to the different soils derived from the Pliocene – Holocene of Rio Grande Formation: Adapted from (Hawley and Kernodle, 2000) and Satellite Images worked with GIS (Arc-Map 9.2, 2009)

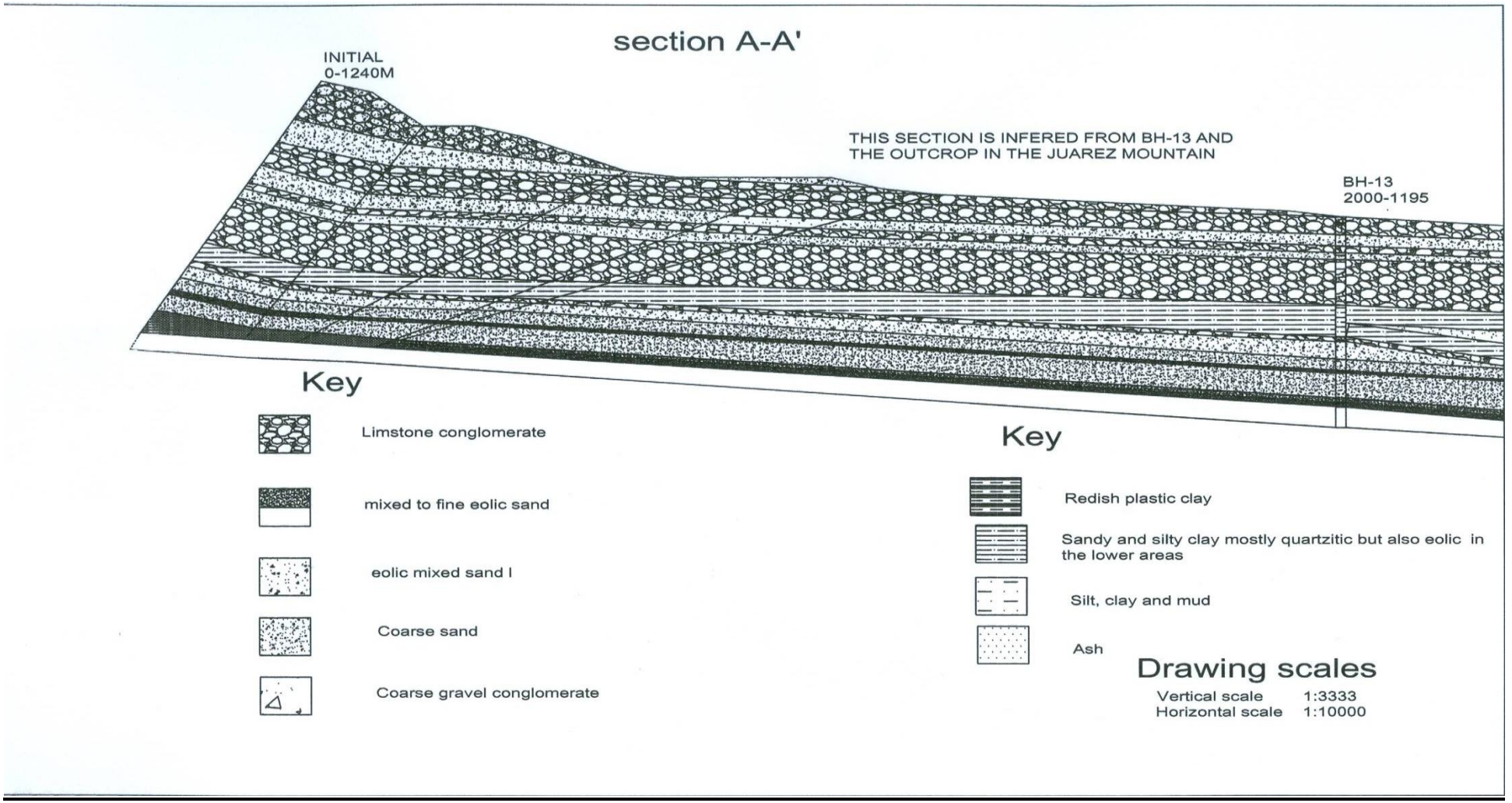

Figure 2 Cross section A-A'; boreholes that integrates this section are: 13, 15, 7R and 111: Source: Autocad (2009) imported in wmf extension into Power Point 2009; Key of Lithology is shown in the lower part of the Figure; Horizontal scale=1:10000; verticalscale=1:3333

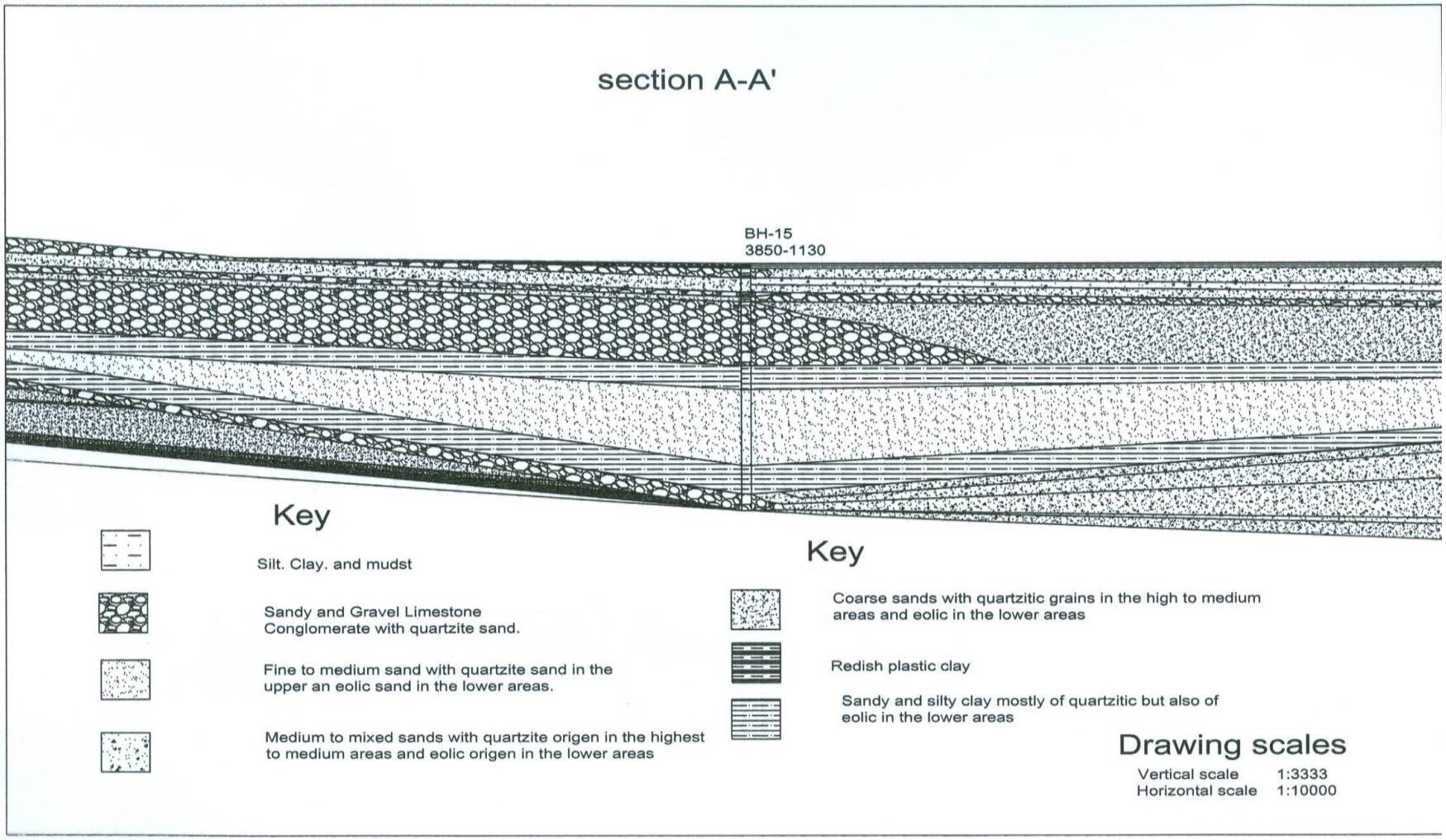

Figure 2 Cross section A-A'; boreholes that integrates this section are: 13, 15, 7R and 111: Source: Autocad (2009) imported inwmfextension into Power Point 2009; Key of Lithology is shown in the lower part of the Figure; Horizontal scale=1:10000; verticalscale=1:3333

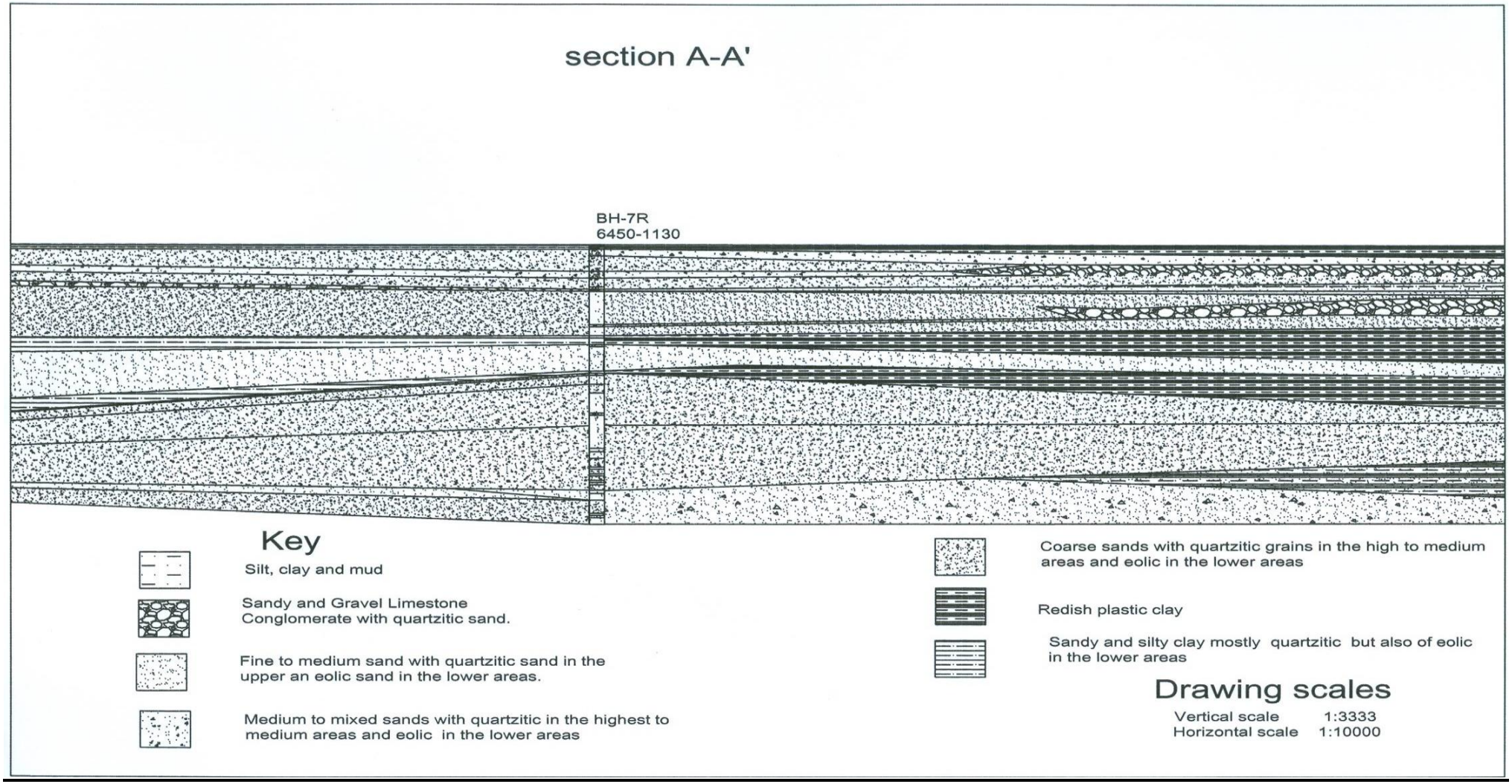

Figure 2 Cross section A-A'; boreholes that integrates this section are: 13, 15, 7R and 111: Source: Autocad (2009) imported in wmf extension into Power Point 2009; Key of Lithology is shown in the lower part of the Figure; Horizontal scale=1:10000; verticalscale=1:3333

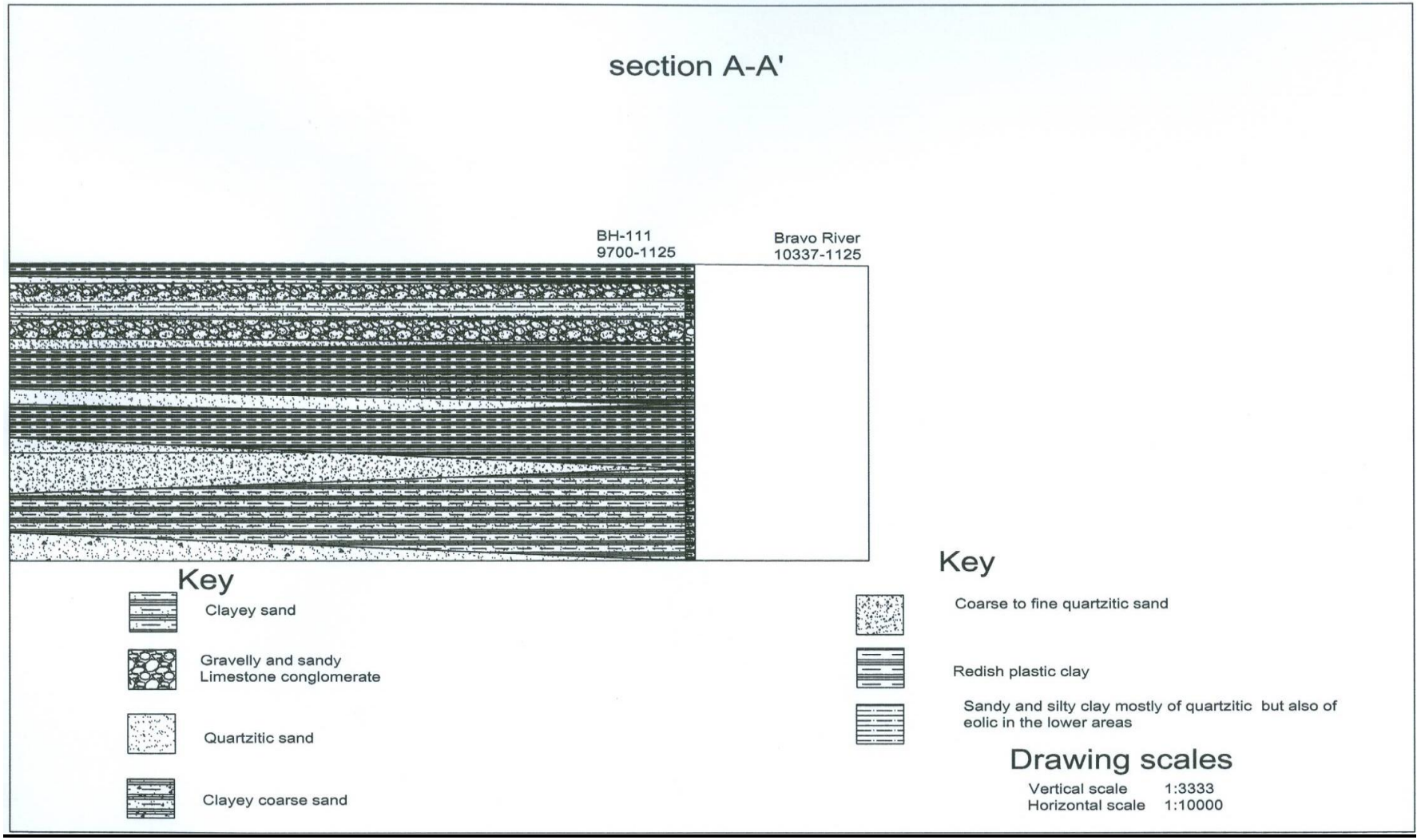

Figure 2 Cross section A-A'; boreholes that integrates this section are: 13, 15, 7R and 111: Source: Autocad (2009) imported in wmf extension into Power Point 2009; Key of Lithology is shown in the lower part of the Figure; Horizontal scale=1:10000; verticalscale=1:3333

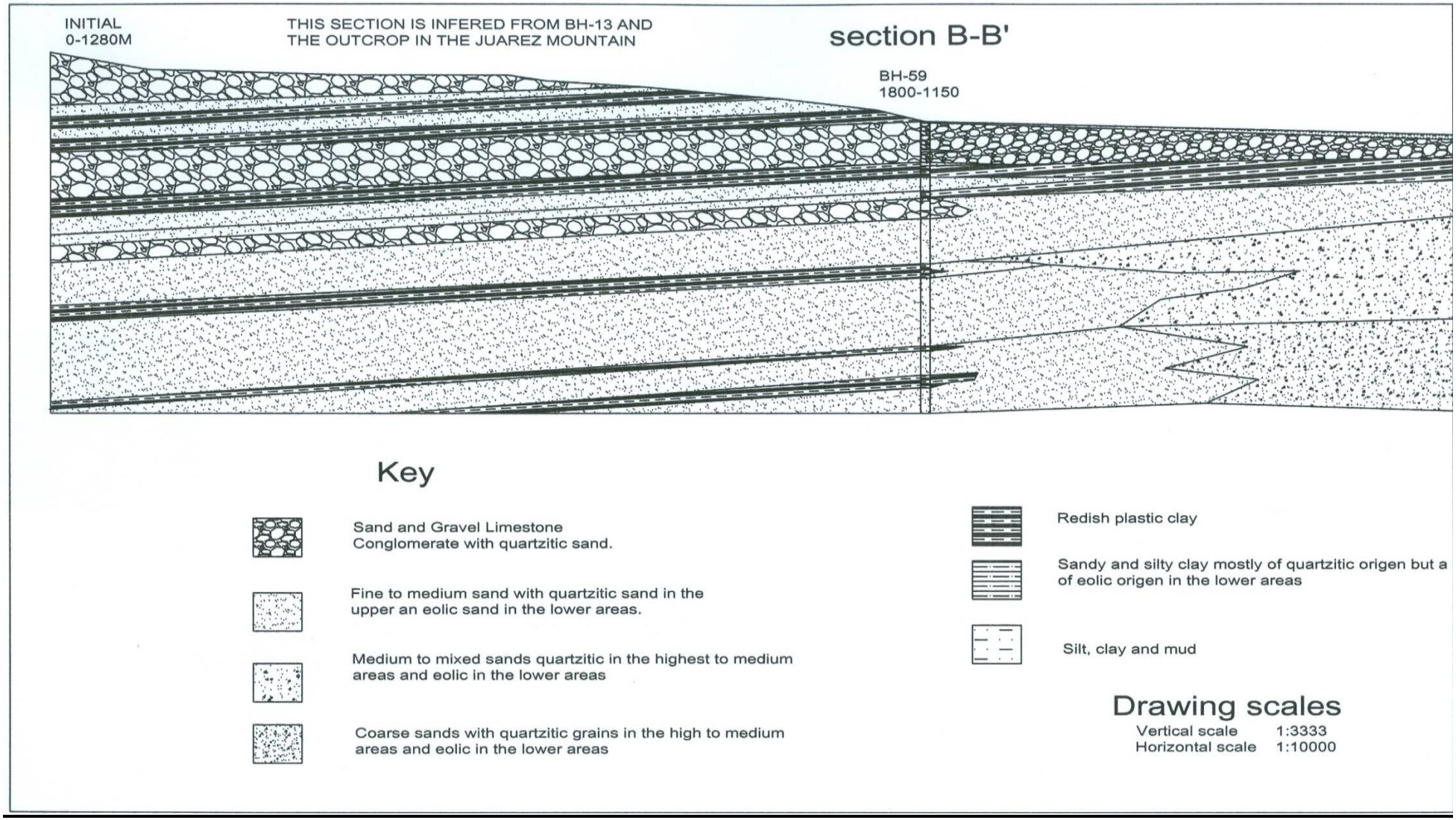

Figure 3 Cross section B-B'; boreholes that integrates this section are:59, 61, 42: Source: Autocad (2009) imported in wmf extension into Power Point 2009; Key of Lithology is shown in the lower part of the Figure; Horizontal scale=1:10000; verticalscale=1:3333

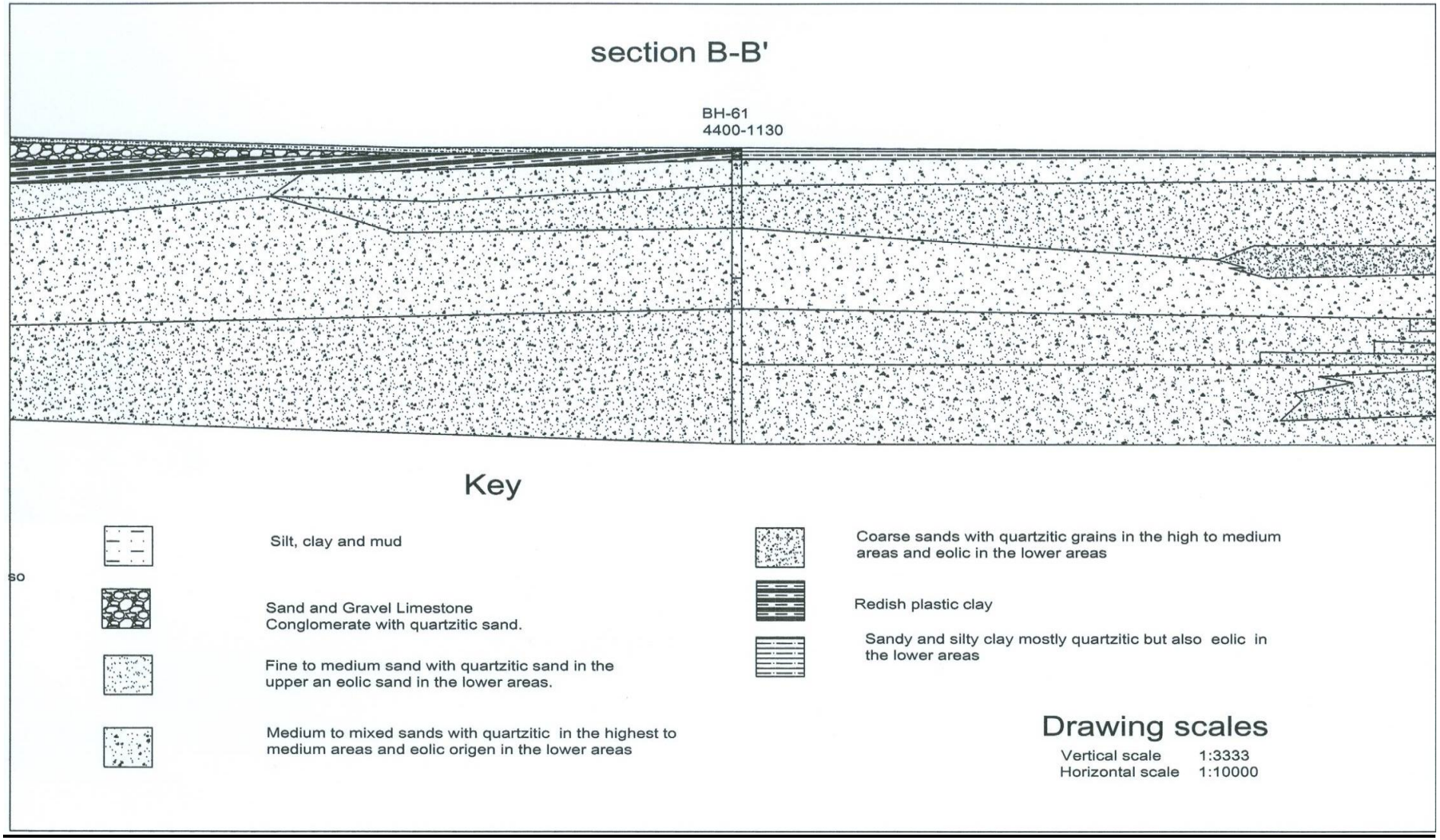

Figure 3 Cross section B-B'; boreholes that integrates this section are: 59, 61 and 42: Source: Autocad (2009) imported in wmf extension into Power Point 2009; Key of Lithology is shown in the lower part of the Figure; Horizontal scale=1:10000; verticalscale=1:3333

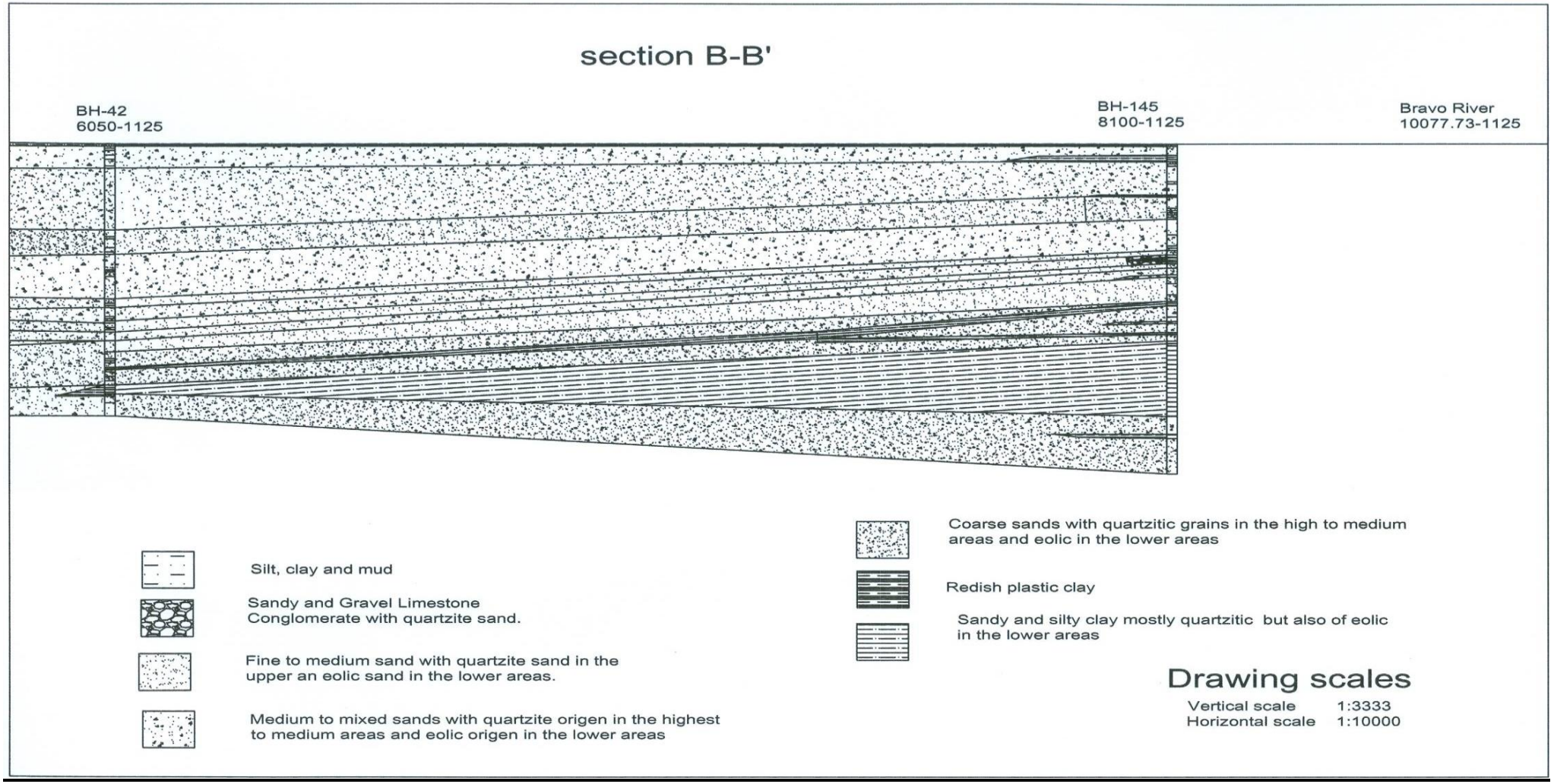

Figure 3 Cross section B-B'; boreholes that integrates this section are: 13, 15, 7R and 111: Source: Autocad (2009) imported in wmf extension into Power Point 2009; Key of Lithology is shown in the lower part of the Figure; Horizontal scale=1:10000; verticalscale=1:3333

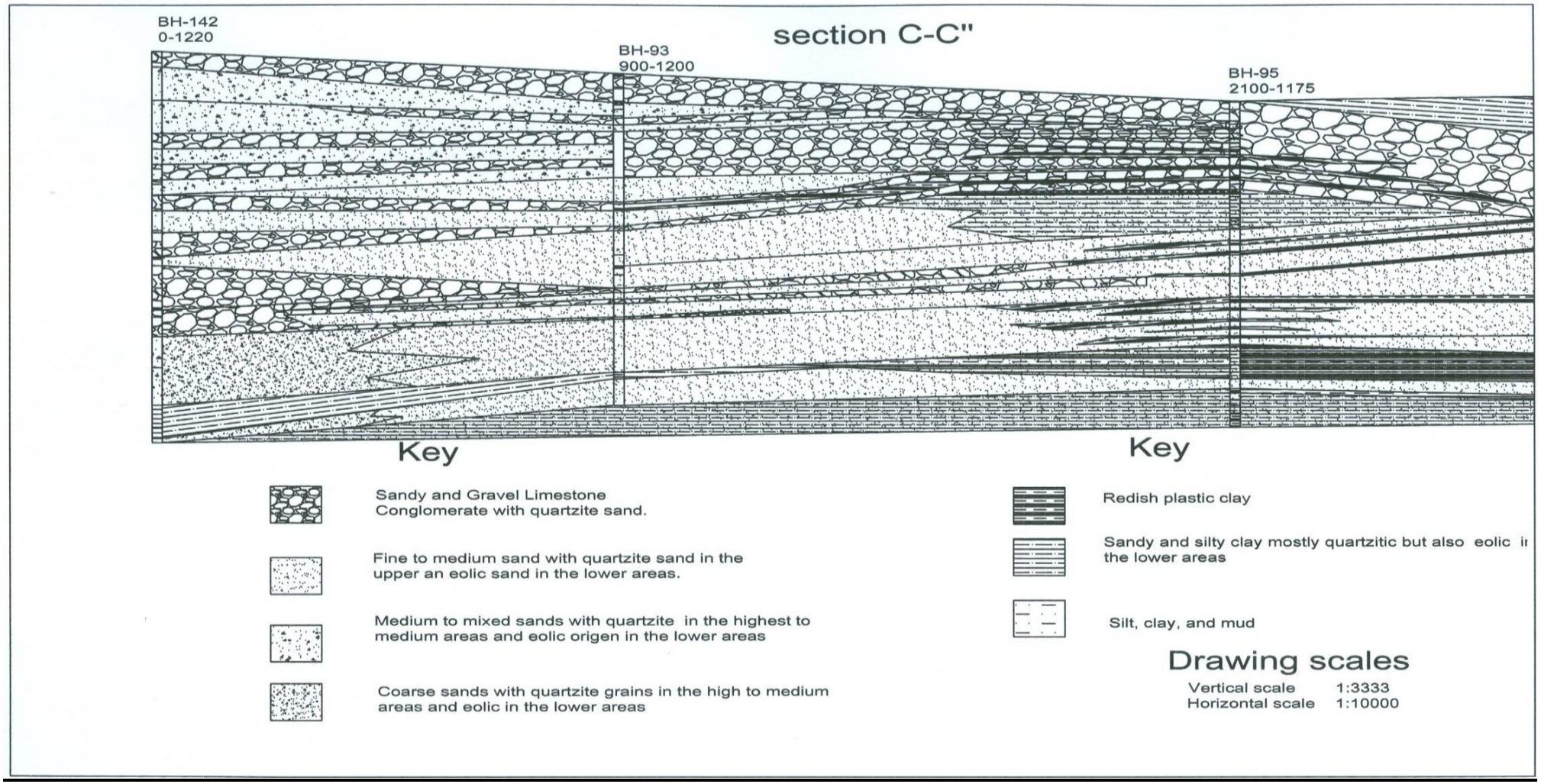

Figure 4 Cross sections C-C' which is composed of boreholes142, 93, 95,141, 193 and 178: Diagram was constructed in and Autocad 2009 exported into Power point 2007 in format WMF; Key of lithology in indicated in the lower part of Fig.; Horizontal scale=1:10000; Vertical scale = 1:3333

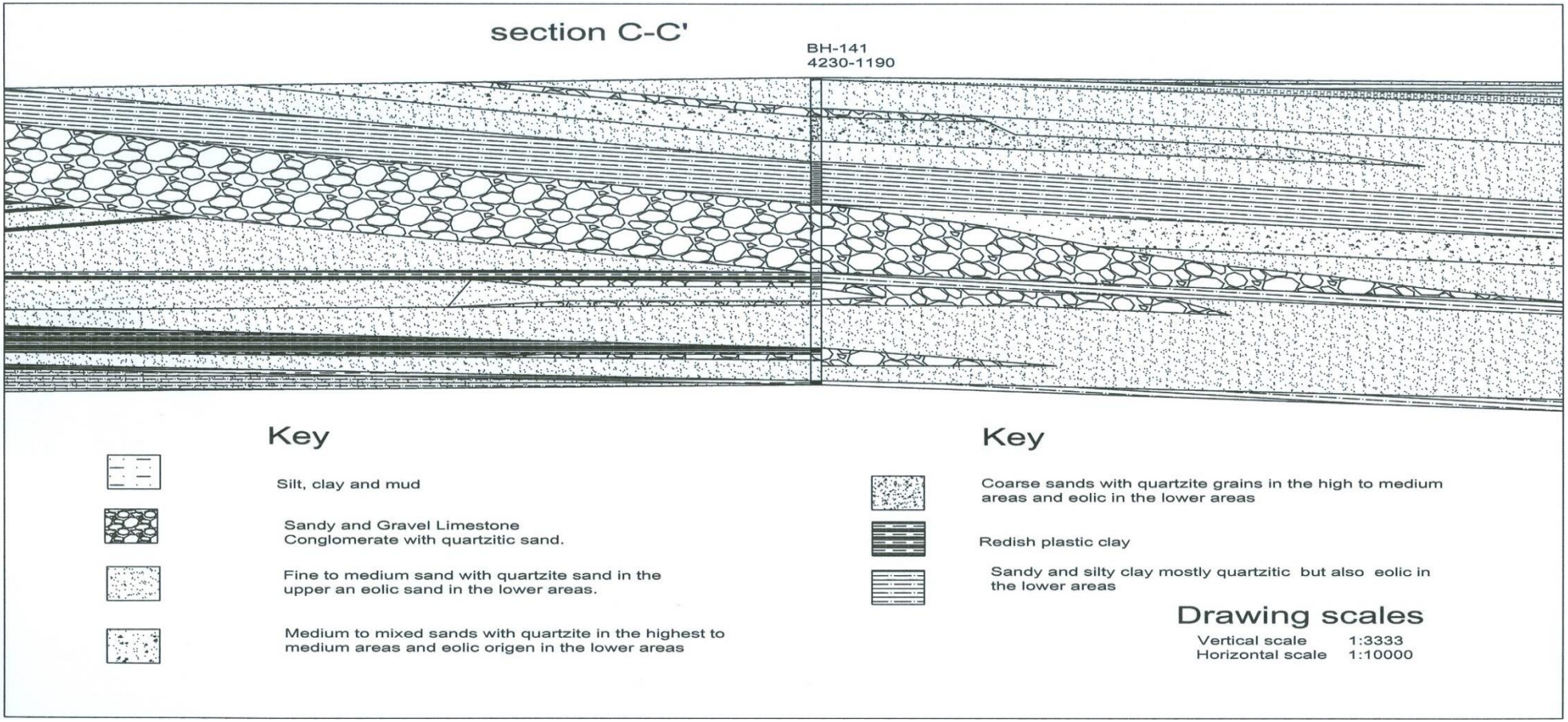

Figure 4 Cross sections C-C' which is composed of boreholes142, 93, 95,141, 193 and 178: Diagram was constructed in and Autocad 2009 exported into Power point 2007 in format WMF; Key of lithology in indicated in the lower part of Fig.; Horizontal scale=1:10000; Vertical scale = 1:3333

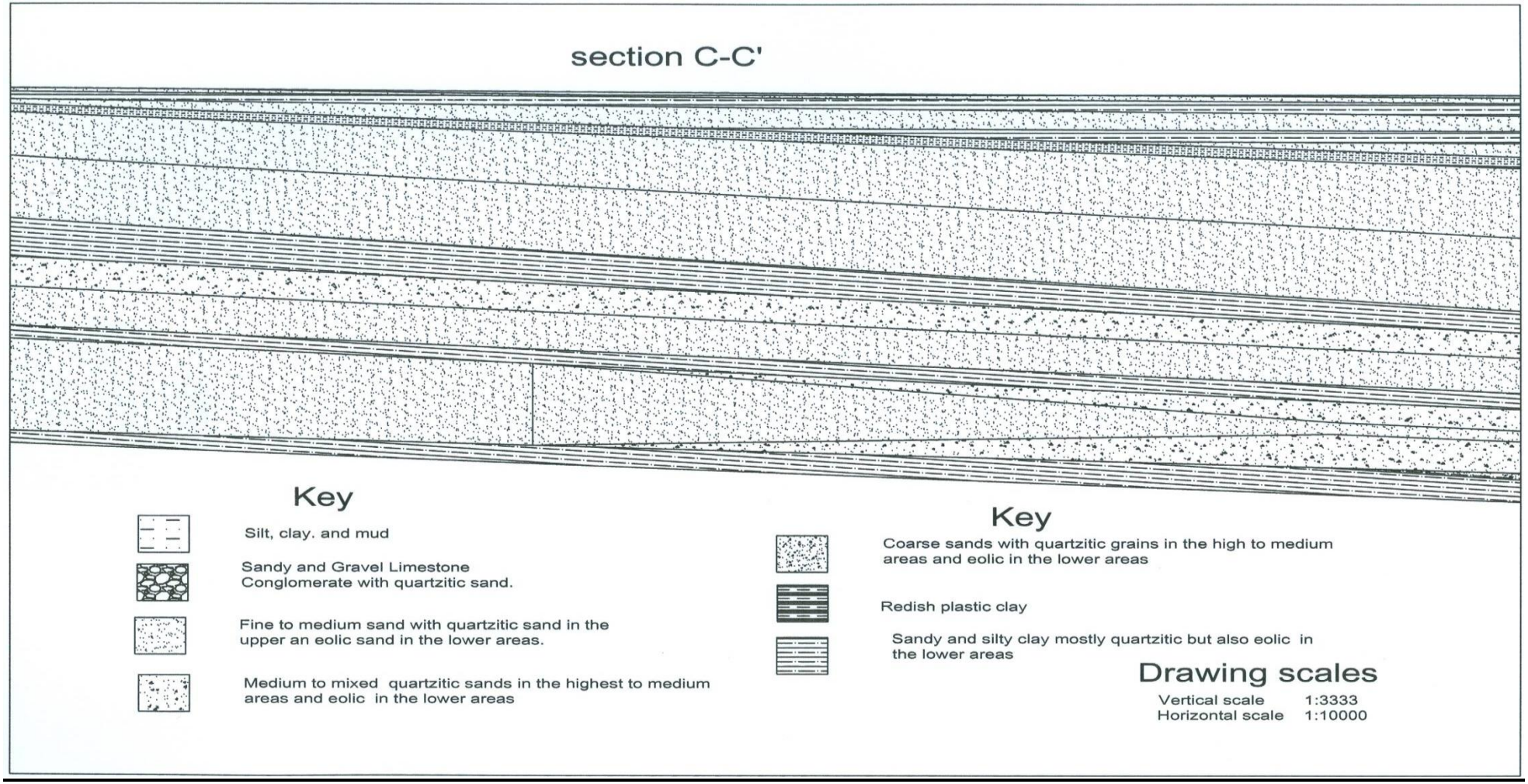

Figure 4 Cross sections C-C' which is composed of boreholes142, 93, 95,141, 193 and 178: Diagram was constructed in and Autocad 2009 exported into Power point 2007 in format WMF; Key of lithology in indicated in the lower part of Fig.; Horizontal scale=1:10000; Vertical scale = 1:3333

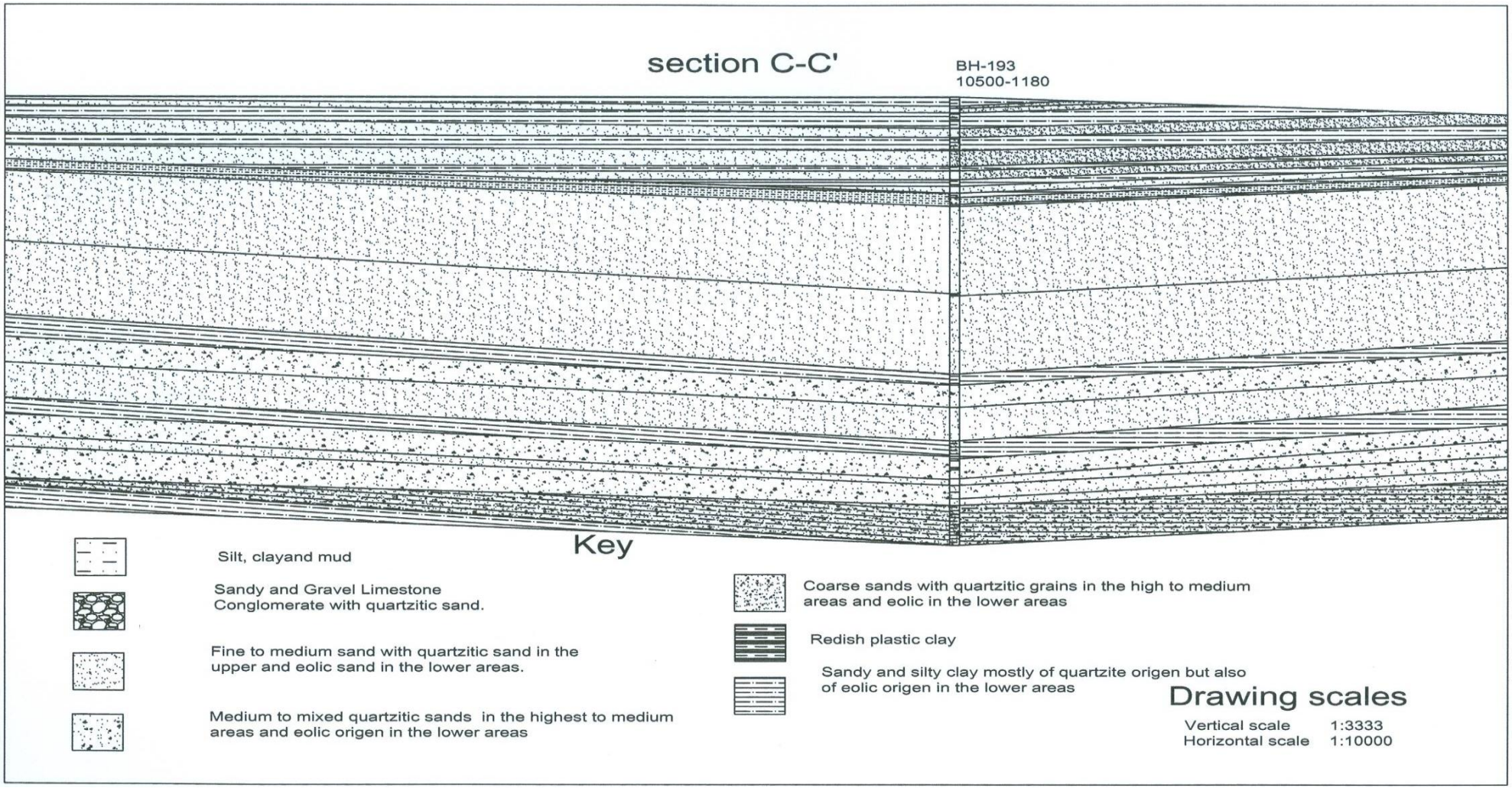

Figure 4 Cross sections C-C' which is composed of boreholes142, 93, 95,141, 193 and 178: Diagram was constructed in and Autocad 2009 exported into Power point 2007 in format WMF; Key of lithology in indicated in the lower part of Fig.; Horizontal scale=1:10000; Vertical scale = 1:3333

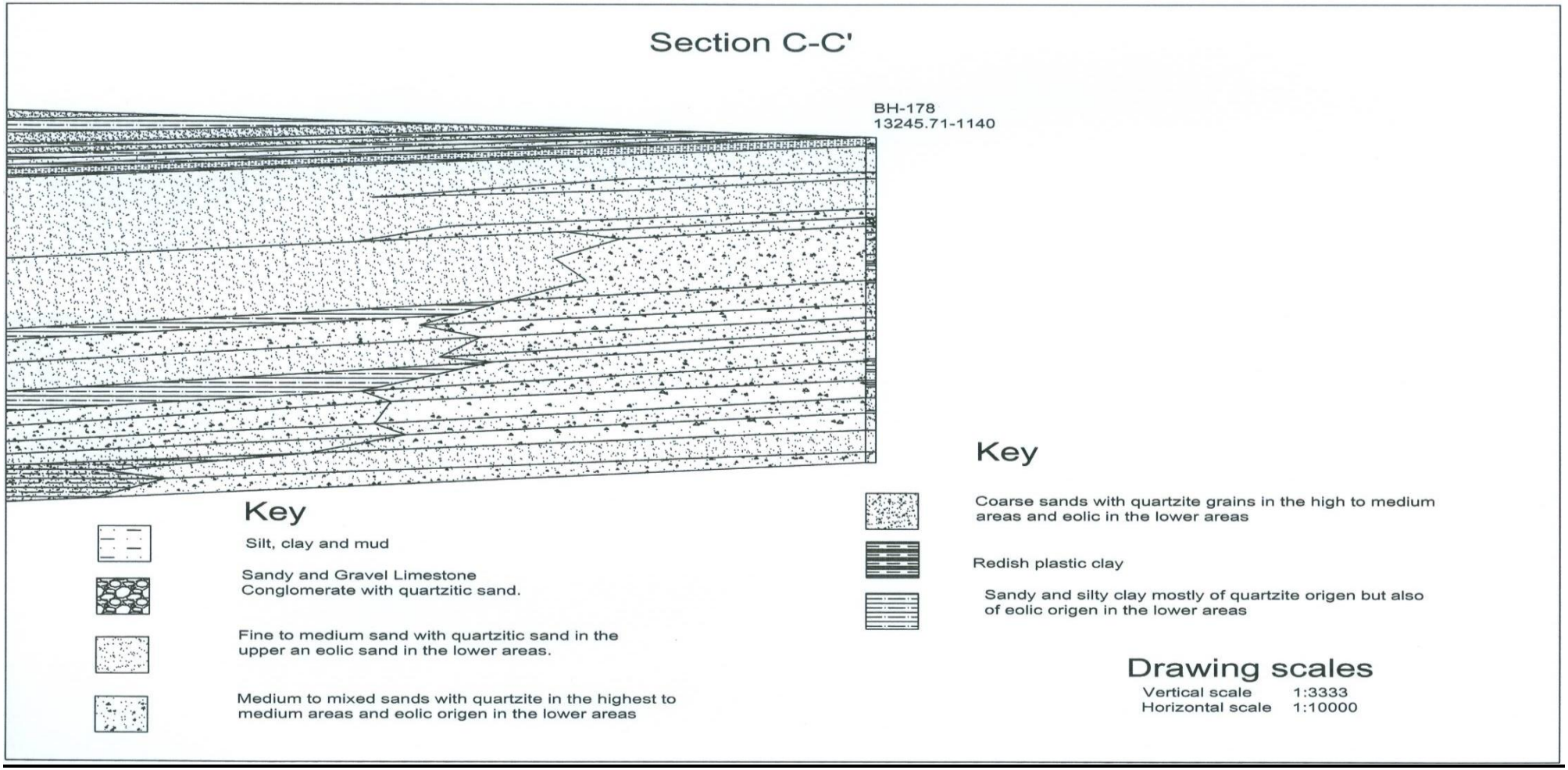

Figure 4 Cross sections C-C' which is composed of boreholes142, 93, 95,141, 193 and 178: Diagram was constructed in and Autocad 2009 exported into Power point 2007 in format WMF; Key of lithology in indicated in the lower part of Fig.; Horizontal scale=1:10000; Vertical scale = 1:333

Appendix 4C

ALBUQUERQUE MODEL GEOLOGICAL SETTINGS RESULTS OF BRAVO RIVER FLUVIAL

Introduction. The present appendix is needed in order to simplify and to reduce the size of the original thesis version. Therefore, for clarity and for practical reasons the number of figures given in the following paragraphs correspond with those given to the first version of the thesis.

Channel strath and tread deposits derived from the Bravo River and its tributaries have been impacted the landscape of the study area through geologic time. Therefore, a depth understanding of the work performed by this River is needed mostly regarded to Pleistocene-Holocene when the river was operating in climatic mode. The Bravo River path begins in the Colorado Rocky Mountains northern to the study area and finishes in the Gulf of México (southeastern). However, in the study area the River shifted many times forced by the big drivers tectonic and climate and was discontinued by an upper sector located north and another lower at the south. Therefore in the northwest and southeast sectors the influence of these deposits is less than at the central sector (Snake Colorado and Palo Chino big drivers of Juárez mountains). In this sector the model suggest that the end of the segment that define: (Qfpa and Qfpb (See Fig. 4.7 Chapter 4), are in contact with older Snake fluvial deposits; Qfda; Qfdb,Qdfb1 and Qfdc (See Figs. 4.8, Chapter 4) are in contact with younger deposits of Bravo River; Qfpb, Qfpc are in contact with fluvial Municipal and Tepeyac Pantheons terraces; Qfpd that is in contact with Aztecas terraces). In the following paragraphs is explained the evolution of fluvial Bravo River deposits.

Bravo River spatial and temporal distribution.

Addressing the spatial and temporal distribution of the alluvial fan and fluvial systems requires a key feature. This feature records the contact between these systems. Moreover, an analysis of Bravo River components behaviour is needed. These components as capacity and competence are associated with gravity and energy law linked with hydrological and hydraulic subjects as capacity and competence as well discharge distribution. In the preceding sections of this chapter were delimited the contact between Alluvial fan and fluvial Bravo River tributaries

deposits. Therefore, here is summarized their spatial and temporal distribution using a prototype model located in Albuquerque New México. The lithologic column adopted for the study area was taken for that located in Albuquerque New México. Lithology of these soils contains fluvial deposits. Then, for clarity these five formations are here repeated from older to younger: Lomatas Negras (Qrl), Edith (Qe, Qre), Menaul (Qpm1, Qrm, Qpm2), Los Duranes (Qrd), Arenal (Qra, Qay) and finally Los Padillas Formation (Qrp) brief comments of the fluvial facie inset in the previous five prototype formations are remarked basically because are the key to understand their actual spatial and temporal distribution on the study area (See Fig.1 below) lithologic column for the prototype Terrace Albuquerque model)

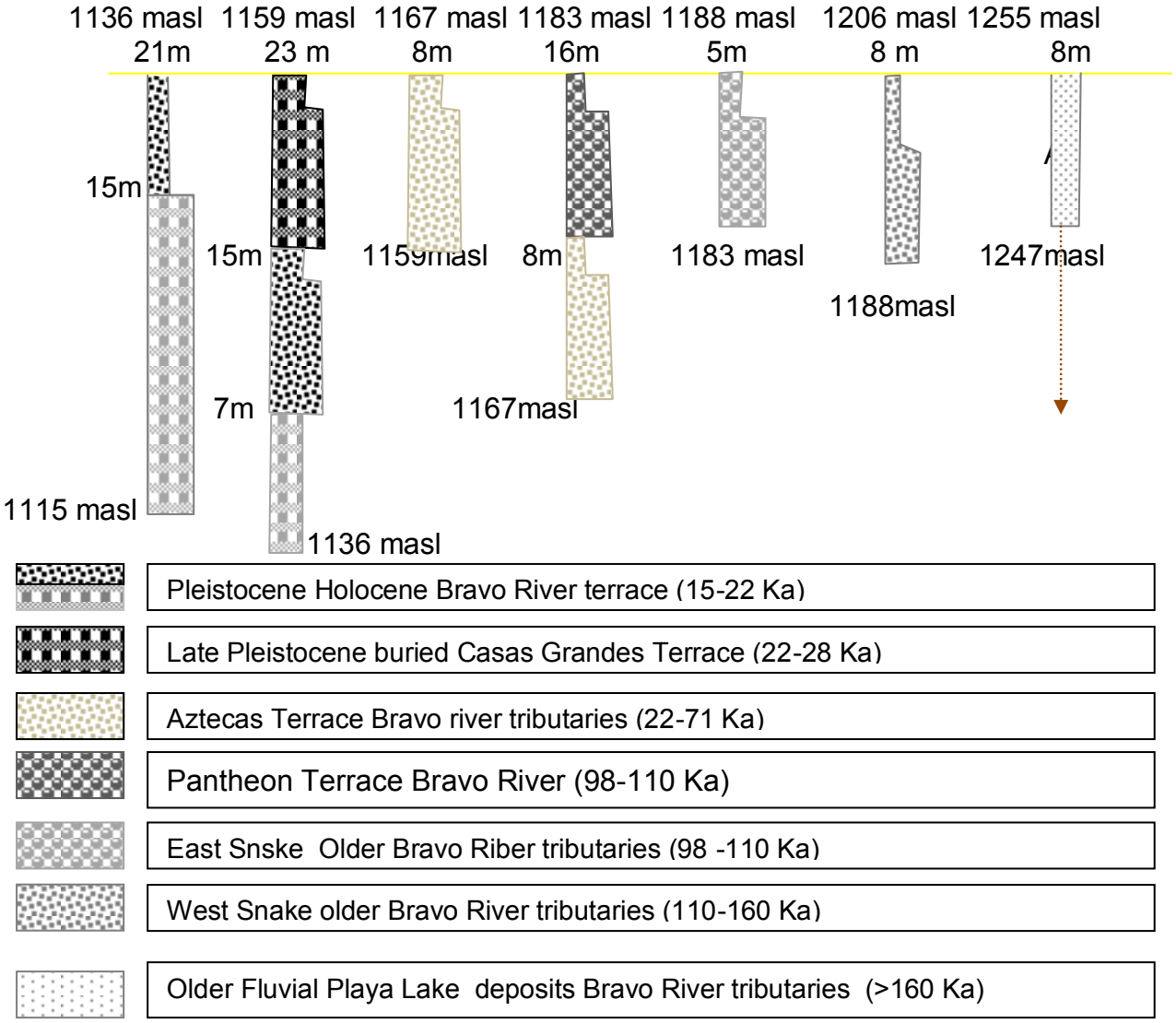

Figure 1 Contact with alluvial fan and terrace deposits of Bravo River during the geologic period (Pleistocene-Holocene). Legend is indicated in the lower part of the Figure. The fluvial deposits are indicated in agree with their temporal deposition. Number in the upper and lower part of the lithological column means elevation in meters above sea level and is not at scale. The value in the lower part means elevation at the base of fluvial strath or tread deposition. Source: Lambert (1968); (Machette et al., 1997)

The model proposed here for the Bravo River path is based in the prototype model of Albuquerque New Mexico previously described. Therefore, five Bravo River

It is important to say that the model proposed is only a pioneer proposal for the study area based on the prototype lithological as well as to many insights derived from many authors mentioned in literature review chapter. Firstly, the Lacustrine Cabeza de Vaca Lake of Plio-Pleistocene time (>2.5 Ma). Secondly, The ancestral Bravo River trajectory during middle to Late Pleistocene (0.66 Ma to 0.16Ma) was running through the path marked in blue color ink this proposed Bravo River path basically was linked the well preserved terrace named (Tepeyac and Municipal pantheons). Thirdly, the older Bravo River tributaries has built a dissected terrace located in the neighborhood that is also marked with blue colour Late Pleistocene time (0.16 to 0.10 Ma). Fourthly, another terrace was constructed during approximately Late Pleistocene time (78 to 28 Ka) when the Bravo River was running along the same path marked in blue color. Fifthly, during Holocene (15 to 22 Ka) another Bravo River shift was occurred and is marked with café colour. Also during this period of time the younger tributaries of the Bravo River were acting. Finally, in recent time 15 ka to the present the last shift of the Bravo River has occurred the actual path is marked with red colour. (Fig. 2) illustrates the paths followed by the Bravo River over recent geological history which were simulated using a comparative analysis between the soils facie previously described in the five formations identified. In addition, (Fig. 2) also shows the spatial distribution actually covered by older buried lacustrine deposits of Cabeza de Baca Lake but, the Barreal basin lacustrine deposits which outcrops on the study area was the center of deposition of this Playa-lake (See chapter 2). The red stars indicated in Fig. 2 represents points location detected using google maps in order to link the preliminarily link of the prototype model with that proposed in the study area. Once this proposed model was done a field work was performed on the study area and basically a five sectors were detected each sector with their owns lithological and facie characteristics and would briefly described in the following paragraphs.

The more extensive manifestation of terrace deposits on the study area is located in the Aztecas Neighborhood as well Tepeyac and Municipal pantheons. These deposits correspond to the Duranes formation with the more prominent terrace deposits of the Bravo River and its tributaries. Basically it is formed for 42 m to 48 m of tread terrace consisting of poorly to consolidated deposits of light reddish-

brown to yellowish-brown gravel, sand and minor sandy clay derived from the ancestral Bravo River and its tributaries. The terrace tread of the Duranes formation named Meanul Formation of Lambert (1968) is composed of less than 3m thick and overlies piedmont deposits of yellowish-brown pebble-gravel and pebbly sand derived from the ancestral Bravo River and its tributaries, rounded quartzite pebbles that are generally smaller in size than pebbles and cobbles of the Edith Formation. In addition, its basal contact is 31 m above the Bravo river (1136+31=1167 masl see Fig. 1). Is conformably and overlain by younger margin piedmont alluvium exhibiting stage II+ carbonate morphology and is inset by younger stream alluvium that exhibits weakly developed soils suggesting a late Pleistocene deposition. (42-48m above the actual Bravo river (1136+45=1181 masl see Fig. 1) and is locally named the Segundo alto surface in the Albuquerque area Lambert, (1968); Hawley (1996). The Duranes Formation represents the major aggradation episode that may have locally buried the Edith Formation and the age is (98-110 Ka). Fig. 1 shows the spatial and temporal association in the sector showing the model emerged as well facie observed for this terraces. In addition to Aztecas and Pantheon terraces, another fluvial contemporaneous deposits above the elevation 1167 was found. This deposits are interpreted like fluvial soils derived from older tributaries of Bravo River as Snake terrace at elevation 1183 masl (period of 98-110 Ka) (see Fig. 1). These deposits are associated with East as well West Snake fluvial deposits of older Bravo river. The elevation marked by East Snake terrace 1188 m corresponds to the Lowest and Younger deposits of Bravo river tributaries. Instead the fluvial deposits found in the west Snake stream corresponds with the oldest tributaries of the Bravo River elevation (1201 m) and are interpreted by the prototype alike with the upper layer Meanul Formation that is temporally distributed over 110 -160 ka and topographically corresponds with (1136+52=1188 masl see Fig. 1). On the other hand the west Snake stream fluvial deposits of Bravo River corresponds with that marked by Lomatas Negras Formation (156+/- 20 Ka, Peate et al., 1996) which is located topographically with (1136+65m = 1201m). (see Fig. 1).

Finally, Oldest preserved and highest fluvial deposits outcropped the study area. This deposits located in a flat area between (Elevation 1255 m asl) perhaps were deposited in an environment of low energy interpreted as a lake deposits this deposits would be assigned inset into the upper layer of the oldest prototype model Formation (Lomatas Negras) which in the base and is composed by 5m of

moderately consolidated and weakly cemented sandy pebble to cobble gravel primarily composed of sub-rounded to rounded quartzite, volcanic units and is located approx. 75m above Bravo river floodplain.(1136+74=1210m asl (see Fig. 1). In short the contact between alluvial fan and fluvial deposits is located above this elevation. In the west side of the study area. Fig. 4.18 shows the spatial distribution of Bravo River deposits proposed for the study area derived from the prototype Albuquerque terrace model already explained.

Alternated layers of silted clay and sandy silt where silted clay lenses decrease in thickness with depth and the sandy silt strata begins with thick layers from 2 or 3 m and decreases with depth also the strata repeats again and again. Strata 1; highly clayed silt red brown colour strata 2, Lenses of dry clay and fine sand of 20 to 30 cm thick interbedded with red brown color in the upper part 3m depth, then continue strata 2 predominantly composed by fine white sands this strata is 7m thick Coordinates UACJ 13R 0354649 UTM 3510550 Elevation 1255 masl)

RESULTS FLUVIAL DEPOSITS FROM BRAVO RIVER (ASA, MP and PT)

Introduction.

Channel strath and tread deposits derived from the Bravo River and its tributaries have been impacted the landscape of the study area through the recent geologic time. Therefore, a depth understanding of the work performed by this River is needed mostly regarded to Pleistocene-Holocene time when the river was operating in climatic mode. During its geological history the Bravo River have been followed an inherited path derived from ancestral continental drift discussed in introduction and geological settings of the study area (section 4.2.1). Bravo River path begins in the Colorado Mountains at north of the study area and finishes in the Gulf of México (southeast). However, in the study area the River shifted many times forced by the big drivers tectonic and climate and was discontinued by an upper sector located north and another lower at the south. Therefore in the northwest and southeast sectors the influence of these deposits is minor than at the central sector (Snake Colorado and Palo Chino big drivers of the Juárez mountains). In this sector the model suggest that the end of the segment that define: (Qfpa and Qfpb (see Fig. 4.7 section 4.4), are in contact with older Snake fluvial deposits; Qfda; Qfdb,Qdfb1

and Qfdc (see Figs 4.8) are in contact with younger deposits of Bravo River; Qfpb, Qfpc are in contact with fluvial Municipal and Tepeyac Pantheons terraces; Qfpd that is in contact with Aztecas terraces). In the following paragraphs is explained the evolution of fluvial Bravo River deposits.

In order to address the spatial and temporal distribution of the alluvial fan system a key feature is needed. This feature is like a thermometer that detect the contact between the alluvial fan and fluvial deposits. Therefore, to understand the alluvial fan evolution depth analysis of Bravo River components behaviour are needed. These components as capacity and competence are associated with gravity and energy laws fundaments linked with hydrological and hydraulic subjects. The sort of deposits actually exhibited in areas of Albuquerque New México have very similar facie and were printed by the Bravo River with the same hydrological and hydraulics principle which undergone similarities in capacity and competence as well discharge distribution. In the preceding sections of this chapter were assessed the contact between Alluvial fan and fluvial Bravo River tributaries deposits. Therefore, here is summarized their spatial and temporal distribution using a prototype model located in Albuquerque New México. The lithologic column adopted for the study area was taken for that located in Albuquerque New México. Lithology of these soils contains fluvial deposits. Then, for clarity these five formations are here repeated from older to younger: Lomatas Negras (Qrl), Edith (Qe, Qre), Menaul (Qpm1, Qrm, Qpm2), Los Duranes (Qrd), Arenal (Qra, Qay) and finally Los Padillas Formation (Qrp) (see chapter 2). A brief discussion of the fluvial facie inset in the previous five prototype formations are remarked basically because are the key to understand their actual spatial and temporal distribution on the study area.

The model proposed here for the Bravo River path is based in the prototype model of Albuquerque New Mexico previously described. Therefore, five Bravo River events during Pleistocene-Holocene time are suggested. However, it is important to say that the model proposed is only a pioneer proposal for the study area based on the prototype lithological as well as to many insights derived from many authors mentioned in literature review chapter as model. Firstly, the Lacustrine Cabeza de Vaca Lake of Plio-Pleistocene time (>2.5 Ma) (see Fig. 2). Secondly, The ancestral Bravo River trajectory during middle to Late Pleistocene (see Fig. 2) (0.66 Ma to 0.16Ma) was running through the path marked in blue color ink (see Fig. 2 personal interpretation) this proposed Bravo River path basically was linked the well

preserved terrace named (Tepeyac and Municipal pantheons). Thirdly, the older Bravo River tributaries has built a dissected terrace located in the neighborhood that is also marked with blue colour Late Pleistocene time (see section 2.5.12) (0.16 to 0.10 Ma). Fourthly, another terrace was constructed during approximately Late Pleistocene time (78 to 28 Ka) when the Bravo River was running along the same path marked in blue color. Fifthly, during Holocene time (15 to 22 Ka) another Bravo River shift was occurred and is marked with café colour. Also during this period of time the younger tributaries of the Bravo River were acting. Finally, in recent time 15 ka to the present the last shift of the Bravo River has occurred the actual path is marked with red colour. (Fig. 2) illustrates the paths followed by the Bravo River over recent geological history which were simulated using a comparative analysis between the soils facie previously described in the five formations identified. In addition, (Fig. 2) also shows the spatial distribution actually covered by older buried lacustrine deposits of Cabeza de Baca Lake but, the Barreal basin lacustrine deposits which outcrops on the study area was the center of deposition of this Playa-lake soils (see chapter 2). The red stars indicated in Fig. 2 represents points location detected using google maps in order to link the preliminarily link of the prototype model with that proposed in the study area (Proposed model based in model of Albuquerque). Once this proposed model was done a field work was performed on the study area and basically a five sectors were detected each sector with their owns lithological and facie characteristics and would briefly described in the following paragraphs.

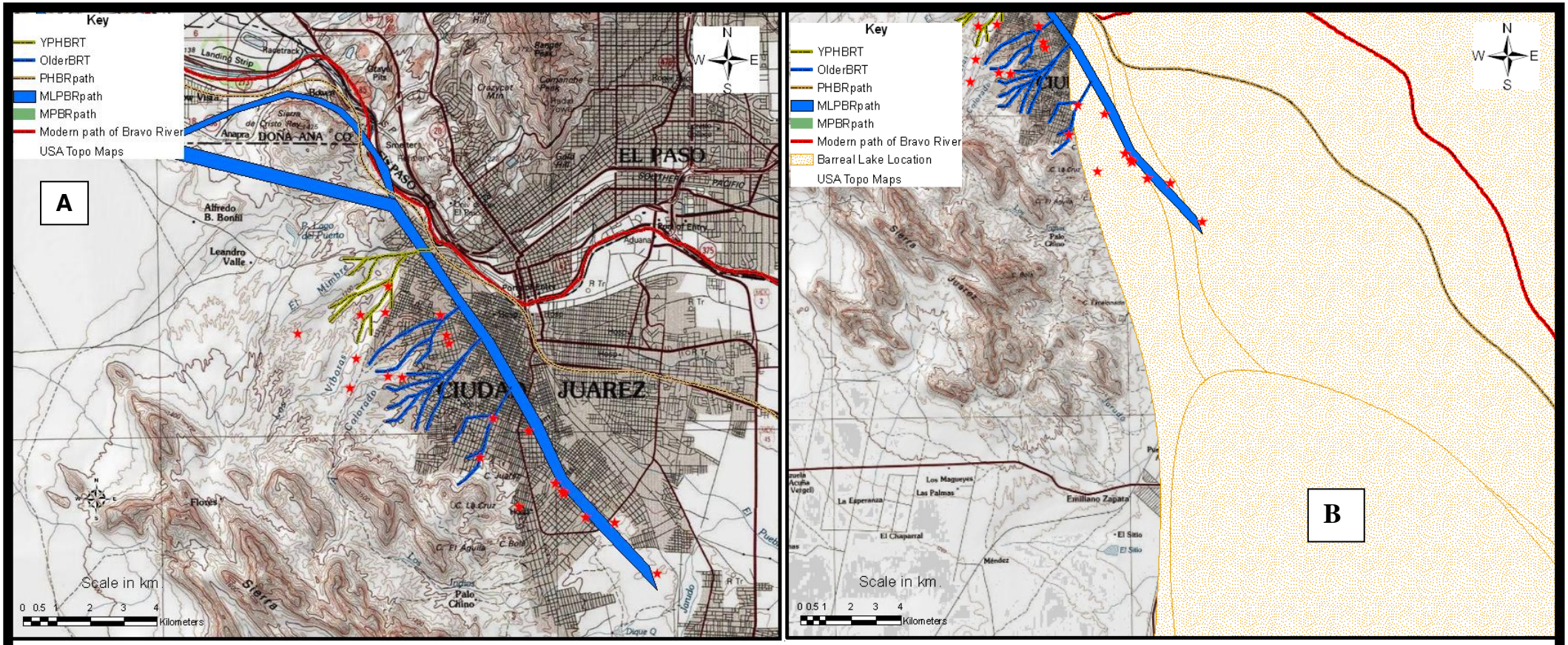

Figure 2 Different pathways followed by the Bravo River over recent geological historybased in the terrace model of Albuquerque New México (see section 2.5.12 in Literature review chapter 2) **A**) Shows Bravo river paths; Juarez City and El Paso Texas urbanized areas; red stars are geographical points where evidence of fluvial deposits were found see appendix 4.1 for the complete information of points monitored with google maps 2011. **B)** Shows location of Barreal Basin which overly Cabeza de Vaca Playa Lake deposits BB=Barreal Basin; YPHBRT=Younger path Holocene Bravo River Tributaries; OlderBRT; PHBRpath=Pleistocene Holocene Bravo River path; MLPBRP= Middle Late Pleistocene Bravo River Path; Modern Path Bravo River. Source: ESRI (2011)Topo maps and (Arc-Map 9.3, 2009).

The following paragraphs summarize the work done in this research. Previous works about evidence of paired or unpaired terraces on the study area are not available at the moment then in the present work an extension of the terrace model available in New Mexico is applied. Based on lithological and topographic position similarities then the model for Albuquerque New México would be adopted to the study area.

The model type stated that the Padillas Formation underlain the Bravo River Valley and is linked with the latest incision-Aggradational phase (Pleistocene-Holocene time <15 Ka). This unit is composed by (15–25 m) of no consolidated an poorly consolidated, pale-brown fine coarse-grained sand and rounded gravel with inter-bedded lenses of fine grained sand, silt and clay derived from the Bravo River. The previous evidence in the study area was found in the boreholes presented in Appendix 4A4 and its geographical location is shown in: (see Fig. 3 boreholes for detailed appreciation). (9R, 11, 15, 72, 59, 86, 88, 142, 141, 133, 130, 131, 129, 128, 123, 124, 116, 122, 115, 111, 100, 97, 95, 93) the previous boreholes clearly shown how the base of Padillas Formation is formed by gravelly cross bedding fluvial sands soils. Lithological column of the model Type. The link of this formation with the average elevation on the study area is (1136 + 21=1157 masl (see Fig. 1). Above this formation lays Arenal formation which is a 3 to 6 m thick composed by poorly consolidated deposits of very pale-brown to yellow sandy pebble to cobble gravel. Gravel grains are primarily rounded quartzite and sub-rounded volcanic rocks (welded tuff and rare pumice). Soils developments are very weak, with stage I to II+ carbonate morphology the upper part of Arenal formation is Primero Alto surface of Lambert (1968) also is buried and doesn't outcrop the study area. Basically is located in the sector assured in Fig. 1. Therefore, elevation of this buried terrace is (1136 m +23m 1159 m see Fig. 1). The temporal distribution given a these layers corresponds to Pleistocene-Holocene time (71-28 Ka) and are deposited along the line marked in café color (see Figs. 4 and 5). In the study area some not well preserved top deposits were found in the Casas Grandes neighborhood and are presented in (Fig. 4) corresponded to the Digital Elevation model (DEM) performed in the study area.

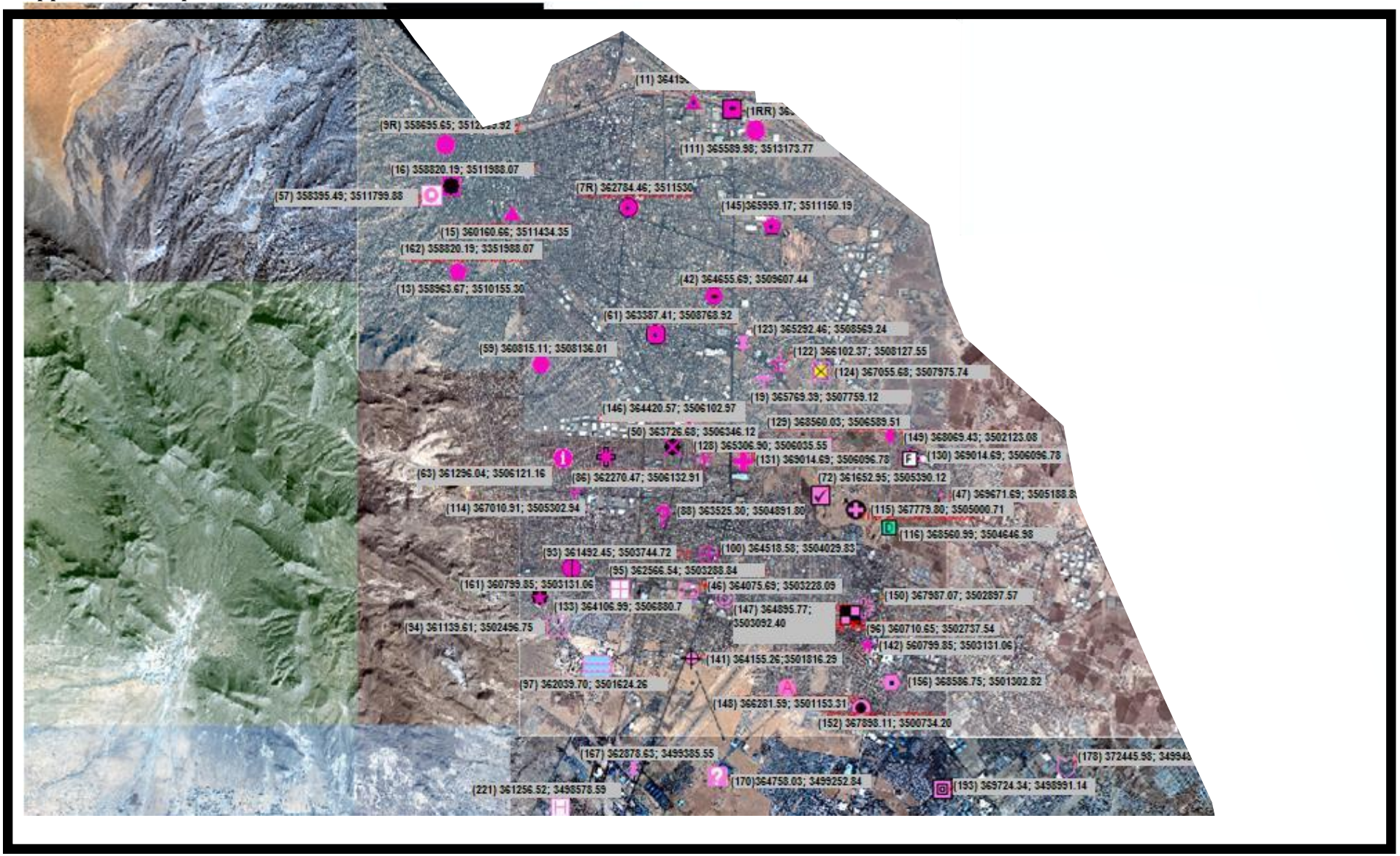

Figure 3 Boreholes distribution and Location of the study area: Source: Junta Municipal de Aguas y Saneamiento Ciudad Juárez Chihuahua Mexico. (see lithological column in appendix 4A4 of Chapter 4)

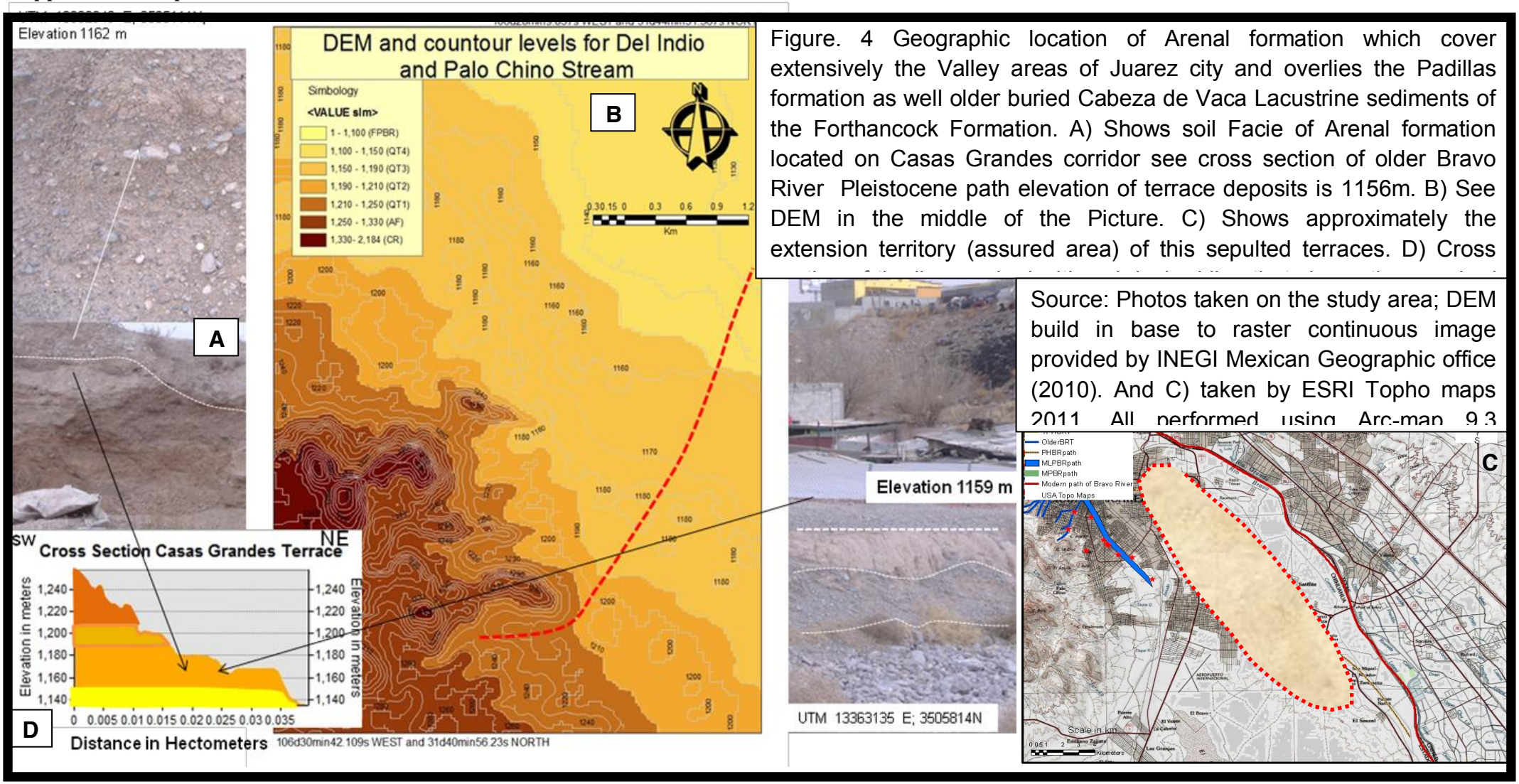

Figure. 4 Geographic location of Arenal formation which cover extensively the Valley areas of Juarez city and overlies the Padillas formation as well older buried Cabeza de Vaca Lacustrine sediments of the Forthancock Formation. A) Shows soil Facie of Arenal formation located on Casas Grandes corridor see cross section of older Bravo River Pleistocene path elevation of terrace deposits is 1156m. B) See DEM in the middle of the Picture. C) Shows approximately the extension territory (assured area) of this sepulted terraces. D) Cross

Source: Photos taken on the study area; DEM build in base to raster continuous image provided by INEGI Mexican Geographic office (2010). And C) taken by ESRI Topho maps 2011. All performed using Arc-map 9.3

The more extensive manifestation of terrace deposits on the study area is located in the Aztecas Neighborhood as well Tepeyac and Municipal pantheons. These deposits correspond to the Duranes formation with the more prominent terrace deposits of the Bravo River and its tributaries. Basically it is formed for 42 m to 48 m of tread terrace consisting of poorly to consolidated deposits of light reddish-brown to yellowish-brown gravel, sand and minor sandy clay derived from the ancestral Bravo River and its tributaries. The terrace tread of the Duranes formation named Meanul Formation of Lambert (1968) is composed of less than 3m thick and overlies piedmont deposits of yellowish-brown pebble-gravel and pebbly sand derived from the ancestral Bravo River and its tributaries, rounded quartzite pebbles that are generally smaller in size than pebbles and cobbles of the Edith Formation. In addition, its basal contact is 31 m above the Bravo river (1136+31=1167 masl see Fig. 6). Is conformably and overlain by younger margin piedmont alluvium exhibiting stage II+ carbonate morphology and is inset by younger stream alluvium that exhibits weakly developed soils suggesting a late Pleistocene deposition. (42-48m above the actual Bravo river (1136+45=1181 masl see Fig. 6) and is locally named the Segundo alto surface in the Albuquerque area Lambert, (1968); Hawley (1996). The Duranes Formation represents the major aggradation episode that may have locally buried the Edith Formation and the age is (98-110 Ka). Fig. 6 shows the spatial and temporal association in the sector showing the model emerged as well facie observed for this terraces. In addition to Aztecas and Pantheon terraces, another fluvial contemporaneous deposits above the elevation 1167 was found. This deposits are interpreted like fluvial soils derived from older tributaries of Bravo River as Snake terrace at elevation 1183 masl (period of 98-110 Ka) (see Fig. 6). These deposits are associated with East as well West Snake fluvial deposits of older Bravo river. The elevation marked by East Snake terrace 1188 m corresponds to the Lowest and Younger deposits of Bravo river tributaries. Instead the fluvial deposits found in the west Snake stream corresponds with the oldest tributaries of the Bravo River elevation (1201 m) and are interpreted by the prototype alike with the upper layer Meanul Formation that is temporally distributed over 110 -160 ka and topographically corresponds with (1136+52=1188 masl see Fig. 6). On the other hand the west Snake stream fluvial deposits of Bravo River corresponds with that marked by

Lomatas Negras Formation (156+/- 20 Ka, Peate et al., 1996) which is located topographically with (1136+65m = 1201m). (see Fig. 6).

Finally, Oldest preserved and highest fluvial deposits outcropped the study area. This deposits located in a flat area between (Elevation 1255 m asl) perhaps were deposited in an environment of low energy interpreted as a lake deposits this deposits would be assigned inset into the upper layer of the oldest prototype model Formation (Lomatas Negras) which in the base and is composed by 5m of moderately consolidated and weakly cemented sandy pebble to cobble gravel primarily composed of sub-rounded to rounded quartzite, volcanic units and is located approx. 75m above Bravo river floodplain.(1136+74=1210m asl (see Fig. 6). In short the contact between alluvial fan and fluvial deposits is located above this elevation. In the west side of the study area. Fig. 5 shows the spatial distribution of Bravo River deposits proposed for the study area derived from the prototype Albuquerque terrace model already explained.

Alternated layers of silted clay and sandy silt where silted clay lenses decrease in thickness with depth and the sandy silt strata begins with thick layers from 2 or 3 m and decreases with depth also the strata repeats again and again. Strata 1; highly clayed silt red brown colour strata 2, Lenses of dry clay and fine sand of 20 to 30 cm thick interbedded with red brown color in the upper part 3m depth, then continue strata 2 predominantly composed by fine white sands this strata is 7m thick Coordinates UACJ 13R 0354649 UTM 3510550 Elevation 1255 m.

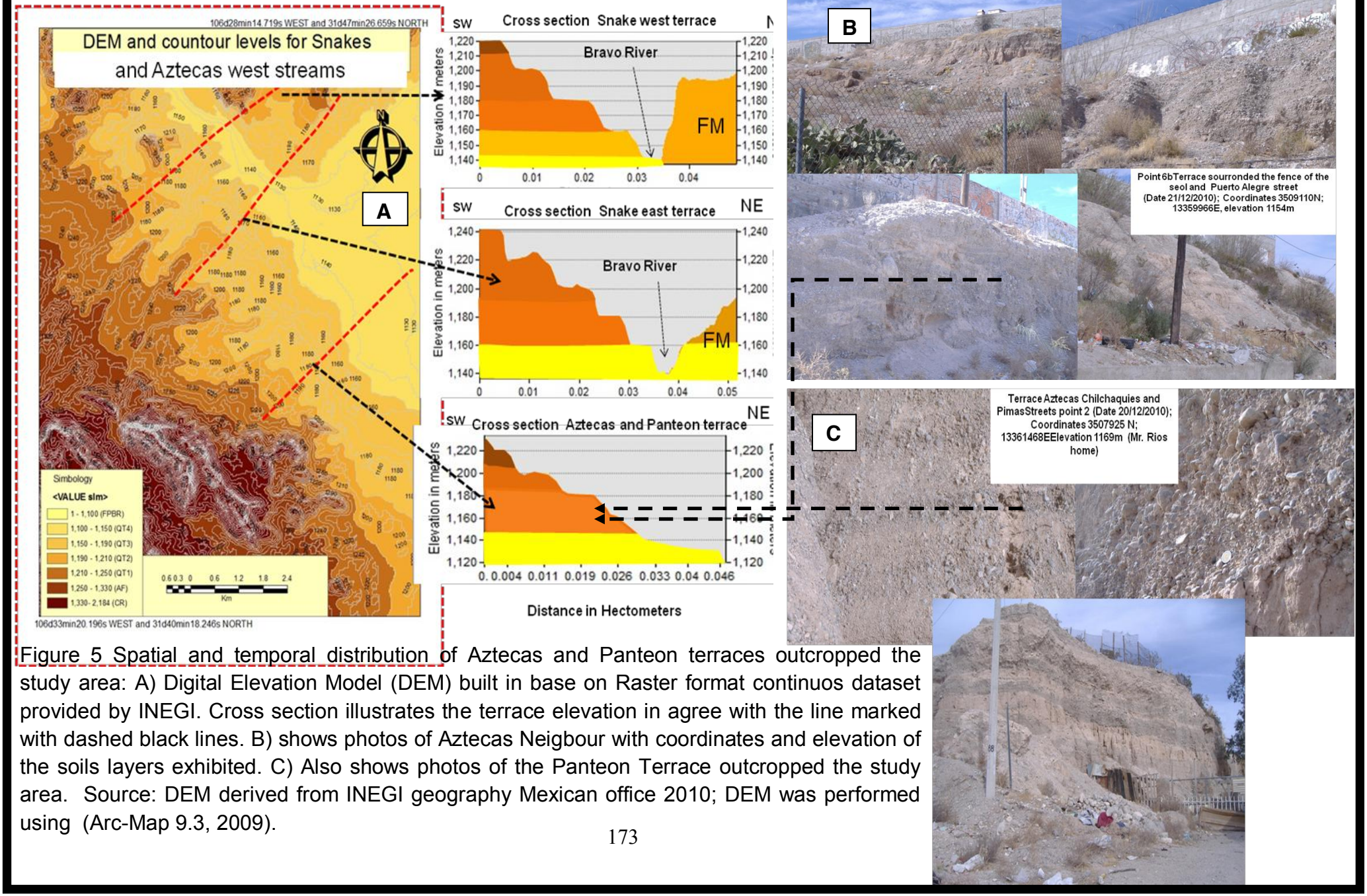

Figure 5 Spatial and temporal distribution of Aztecas and Panteon terraces outcropped the study area: A) Digital Elevation Model (DEM) built in base on Raster format continuos dataset provided by INEGI. Cross section illustrates the terrace elevation in agree with the line marked with dashed black lines. B) shows photos of Aztecas Neigbour with coordinates and elevation of the soils layers exhibited. C) Also shows photos of the Panteon Terrace outcropped the study area. Source: DEM derived from INEGI geography Mexican office 2010; DEM was performed using (Arc-Map 9.3, 2009).

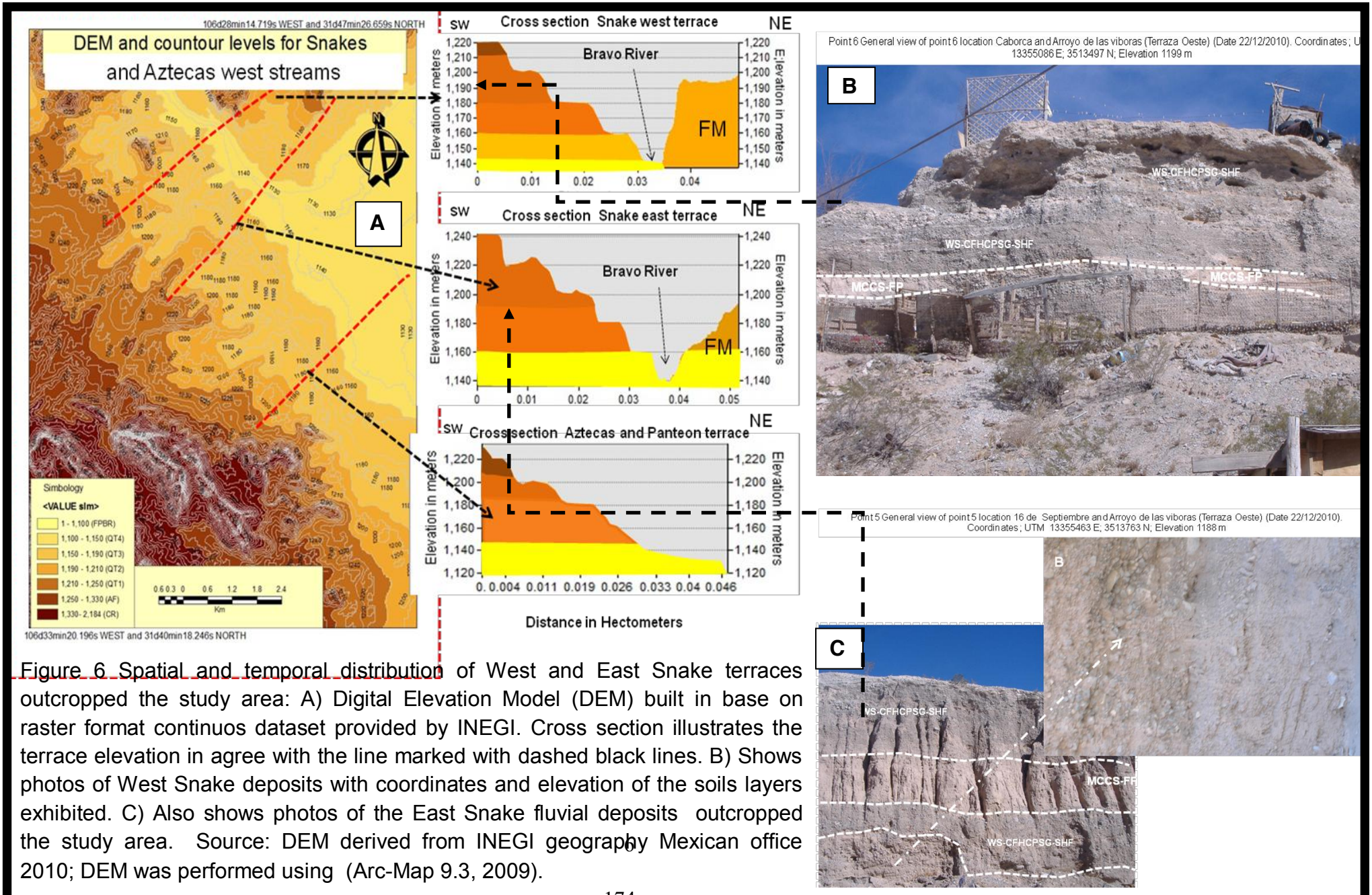

Figure 6 Spatial and temporal distribution of West and East Snake terraces outcropped the study area: A) Digital Elevation Model (DEM) built in base on raster format continuos dataset provided by INEGI. Cross section illustrates the terrace elevation in agree with the line marked with dashed black lines. B) Shows photos of West Snake deposits with coordinates and elevation of the soils layers exhibited. C) Also shows photos of the East Snake fluvial deposits outcropped the study area. Source: DEM derived from INEGI geography Mexican office 2010; DEM was performed using (Arc-Map 9.3, 2009).

APPENDIX 5.1

The HEC-HMS program uses the CN method established by the Soil Conservation Service SCS (1986). Also, HEC-HMS uses hyetographs to produce hydrographs. Hyetographs are rainfall charts, which record the rainfall in mm over time. Instead, Hydrographs are water runoff graphics, which record the pattern of runoff from rainfall. Both parameters are measurable features of rainfall events. When rain falls, the hyetograph begins, but there is a time-lag before the associated hydrograph starts. Because of the nature of the ground surface, including surface roughness, ground porosity, permeability, and vegetation, there is normally a build-up period called the concentration time, as the rainfall develops, leading to sudden flooding, and the key feature of which is the peak discharge. Furthermore, the hyetograph is a chart of rainfall often called a design rainfall graph, particularly applicable to this study; because the study deals with rapid rainfall events, the terms “Design storm” and “Design hyetograph” are commonly used, noting that these terms refer to modelled rainfall patterns. Thus, hyetographs and hydrographs are widely and effectively applied to solve many hydrologic problems particularly those associated with flooding. These hydrographs are produced by the HEC-HMS software and in the present work they are applied for a design rainfall event of one hour of duration because a one-hour rainfall episode approximates the rainstorms threatening the study area.

APPENDIX 5.2

Gumbel Extreme Value type 1 probability distribution function (GEV1).

With regard to the statistical approach named (GEV1) a brief explanation of its methodology ispresented below. Firstly, the Cummulative density function F(x) of the Gumbel method is the double exponential expression:

$$F(x) = (e^{-e^{-y}}) \quad .....(a)$$

where: F(x) is probability of no exceedence of the random variable (24HMR); but, in rainfall frequency analysis, the concern is the exceeded probability then, a complementary function is needed, then we have:

$$G(x)= 1-F(x)...(b).$$

On the other hand, the return period (Tr) is the inverse of the exceeded probability regarded to the random variable (24HMR). Then expressing formula (a) in terms of (Tr) we have:

$$I/Tr= 1- (e^{-e^{-y}})...(c).$$

As a result applying natural logarithms an equivalent equation (d) emerges:

$$y=-LnLn(Tr/Tr-1)..(d).$$

In the Gumbel method, values of storm design are obtained from the frequency expression:

$$x=Xm+Ks)...(e). \qquad y=\bar{Y}n+K\sigma_n....(f)$$

In which (x) is the random variable (24HMR) and (y) is the Gumbel reduced variate in function of the return period (Tr). Moreover, the frequency factor $K=(y-\bar{Y}n)/\sigma_n$) emerges from the simple mathematical equality equations (e) and (f). Additionally, ($\bar{Y}n$) and (σ_n) are the mean and standard deviation of the Gumbel variate determined in function of the length recorded (n) see (Fig. A5.2.1).

TABLE A-8 MEAN $\bar{y}_n$ AND STANDARD DEVIATION σ_n OF GUMBEL VARIATE (y) VERSUS RECORD LENGTH (n)

n	$\bar{y}_n$	σ_n	n	$\bar{y}_n$	σ_n	n	$\bar{y}_n$	σ_n
8	0.4843	0.9043	35	0.5403	1.1285	64	0.5533	1.1793
9	0.4902	0.9288	36	0.5410	1.1313	66	0.5538	1.1814
10	0.4952	0.9497	37	0.5418	1.1339	68	0.5543	1.1834
11	0.4996	0.9676	38	0.5424	1.1363	70	0.5548	1.1854
12	0.5035	0.9833	39	0.5430	1.1388	72	0.5552	1.1873
13	0.5070	0.9972	40	0.5436	1.1413	74	0.5557	1.1890
14	0.5100	1.0095	41	0.5442	1.1436	76	0.5561	1.1906
15	0.5128	1.0206	42	0.5448	1.1458	78	0.5565	1.1923
16	0.5157	1.0316	43	0.5453	1.1480	80	0.5569	1.1938
17	0.5181	1.0411	44	0.5458	1.1499	82	0.5572	1.1953
18	0.5202	1.0493	45	0.5463	1.1519	84	0.5576	1.1967
19	0.5220	1.0566	46	0.5468	1.1538	86	0.5580	1.1980
20	0.5236	1.0628	47	0.5473	1.1557	88	0.5583	1.1994
21	0.5252	1.0696	48	0.5477	1.1574	90	0.5586	1.2007
22	0.5268	1.0754	49	0.5481	1.1590	92	0.5589	1.2020
23	0.5283	1.0811	50	0.5485	1.1607	94	0.5592	1.2032
24	0.5296	1.0864	51	0.5489	1.1623	96	0.5595	1.2044
25	0.5309	1.0915	52	0.5493	1.1638	98	0.5598	1.2055
26	0.5320	1.0961	53	0.5497	1.1653	100	0.5600	1.2065
27	0.5332	1.1004	54	0.5501	1.1667	150	0.5646	1.2253
28	0.5343	1.1047	55	0.5504	1.1681	200	0.5672	1.2360
29	0.5353	1.1086	56	0.5508	1.1696	250	0.5688	1.2429
30	0.5362	1.1124	57	0.5511	1.1708	300	0.5699	1.2479
31	0.5371	1.1159	58	0.5515	1.1721	400	0.5714	1.2545
32	0.5380	1.1193	59	0.5518	1.1734	500	0.5724	1.2588
33	0.5388	1.1226	60	0.5521	1.1747	750	0.5738	1.2651
34	0.5396	1.1255	62	0.5527	1.1770	1000	0.5745	1.2685

Source: Gumbel, E. J. (1958). *Statistics of Extremes.* Irvington, New York: Columbia University Press.

Figure A5.2.1. mean and Standard Deviation of the Gumbel variate (y) for different record length (n). Source: Gumbel (1958). Statistics of Extremes. Irvington. New York: Columbia University Press given in: Ponce (1994). In the dataset of this study, n=37, since there are 37 years of 24HMR data (See Figure 5.2.2 of chapter 5)

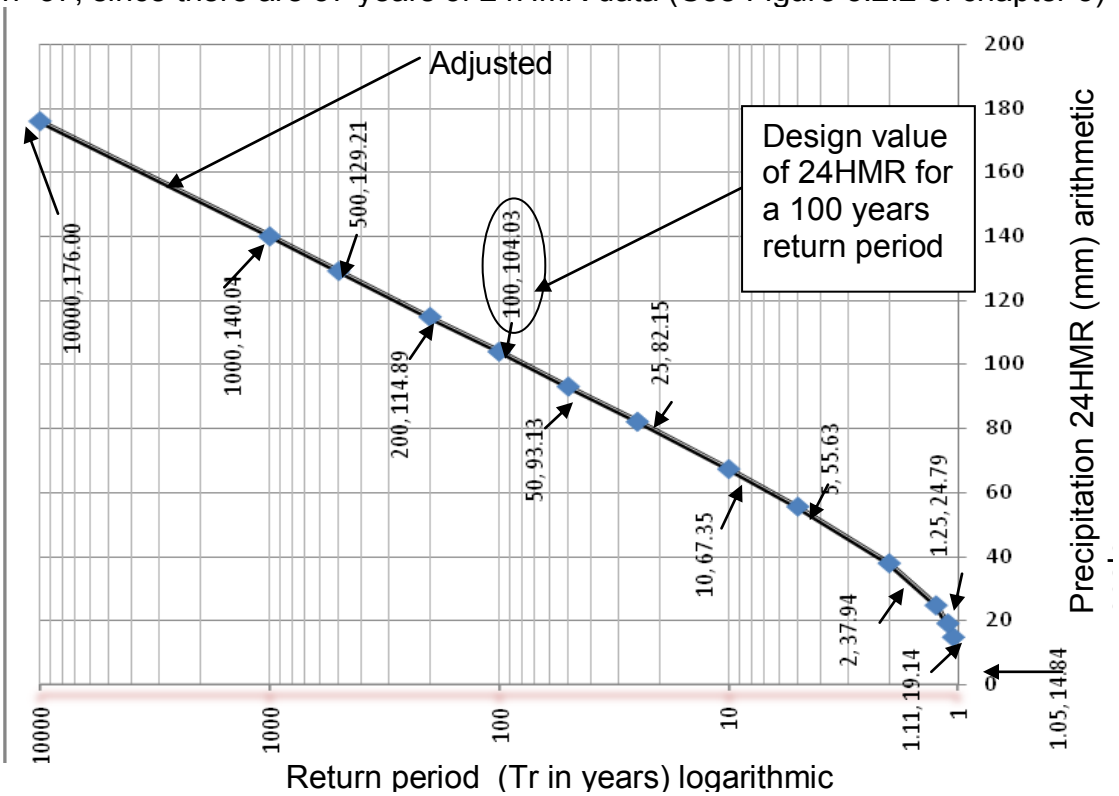

Figure A5.2.2 The results predicted graphic of Gumbel EV1 method linked several return periods to the random variable (24HMR). Source of method for this plot : Ponce (1994).

The values shown in chapter 5 Fig. 5.3 were previously calculated analytically and are indicated in Col. 7. However, a brief explanation of the construction of this graph is presented in the following paragraphs: Firstly, as a result of the equality of the adjusted double logarithmic cumulative density function given $F(x) = (e^{-e^{-y}})$ .....(a)

. The elementary function G(x)= 1-F(x)...(b) enables calculation of $1/Tr = 1 - (e^{-e^{-y}})$...(c). that is expressed in terms of the return period. Consequently, the Gumbel variate emerges; y=-LnLn(Tr/Tr-1)...(d). In the Gumbel method, values of storm design are obtained from the frequency formulae (x=Xm+Ks)...(e) and formulae: $y=\bar{Y}n+K\sigma_n$..(f). Thus, values obtained for the random variable (24HMR) in (mm) are on the Y axis, whereas values of the return period (Tr) in years were drawn on the X axis in logarithmic scale. The line derived is the adjusted function of Gumbel method and contains the values of the random variable (24HMR) for several return periods (Tr).

APPENDIX 5.3 (Log Pearson III Method detailed results table)

Col.1 col.2 col.3 col. 4 col.5 col.6 col.7 col.8 col.9 col.10

Year	(24HMR)	(X-M)^3	(X-M)^2	n+1	p=m/n+1	Log10(x)	(log(x)-log M)	(log(x)-log M)^2	(log(x)-log M)^3
1973	80.20	61724	1561.8	38	41.1008	1.90417	0.3328	0.11073878	0.03685103
1987	70.50	26517	889.23	38	23.4009	1.84819	0.2768	0.07661222	0.02120543
2000	66.80	17820	682.25	38	17.9541	1.82478	0.2768	0.07661222	0.02120543
1975	63.00	11119	498.18	38	13.1101	1.79934	0.2534	0.06419963	0.01626668
1978	62.50	10389	476.11	38	12.5293	1.79588	0.2279	0.05195689	0.01184308
1990	62.00	9690.8	454.54	38	11.9616	1.79239	0.2245	0.05039128	0.01131184
2006	59.00	6148.6	335.62	38	8.83217	1.77085	0.221	0.04883733	0.01079264
1984	58.40	5564.1	314	38	8.26312	1.76641	0.1995	0.0397811	0.00793442
1982	56.10	3666.5	237.78	38	6.25727	1.74896	0.195	0.03803001	0.00741634
1971	55.50	3255	219.63	38	5.7798	1.74429	0.1776	0.03152857	0.0055983
1974	52.70	1736.7	144.48	38	3.80212	1.72181	0.1729	0.02989198	0.00516811
1976	51.10	1131.4	108.58	38	2.85727	1.70842	0.1504	0.02262335	0.00340279
1981	46.50	197.14	33.872	38	0.89138	1.66745	0.137	0.01877473	0.00257253
1992	44.00	36.594	11.022	38	0.29006	1.64345	0.0961	0.00922617	0.0008862
1972	41.90	1.8158	1.4884	38	0.03917	1.62221	0.0721	0.00519159	0.00037407
1991	40.00	-0.314	0.4624	38	0.01217	1.60206	0.0508	0.00258206	0.00013121
1986	39.60	-1.26	1.1664	38	0.03069	1.5977	0.0307	0.00094004	2.8821E-05
1983	38.70	-7.762	3.9204	38	0.10317	1.58771	0.0263	0.00069144	1.8181E-05
1989	37.30	-38.61	11.424	38	0.30064	1.57171	0.0163	0.00026605	4.3395E-06
1970	36.20	-89.92	20.07	38	0.52817	1.55871	0.0003	9.5377E-08	2.9455E-11
2007	36.00	-102.5	21.902	38	0.57638	1.5563	-0.0127	0.00016107	-2.044E-06
1988	35.60	-131.1	25.806	38	0.67912	1.55145	-0.0151	0.00022793	-3.441E-06
1980	33.00	-453	58.982	38	1.55217	1.51851	-0.02	0.000398	-7.94E-06
2005	32.00	-654	75.342	38	1.98269	1.50515	-0.0529	0.00279694	-0.0001479
1985	30.50	-1055	103.63	38	2.72717	1.4843	-0.0663	0.00438907	-0.0002908
1977	28.70	-1719	143.52	38	3.77685	1.45788	-0.0871	0.00758644	-0.0006608
2004	28.00	-2039	160.78	38	4.23112	1.44716	-0.1135	0.01288636	-0.0014628
1993	27.40	-2342	176.36	38	4.64101	1.43775	-0.1242	0.01543607	-0.0019178
1979	26.50	-2851	201.07	38	5.29138	1.42325	-0.1336	0.01786217	-0.0023873
2003	25.00	-3855	245.86	38	6.47006	1.39794	-0.1482	0.02194965	-0.0032519
1996	24.00	-4641	278.22	38	7.32164	1.38021	-0.1735	0.03008837	-0.0052191
1969	22.80	-5716	319.69	38	8.41301	1.35793	-0.1912	0.03655314	-0.0069885
1999	22.00	-6518	348.94	38	9.18269	1.34242	-0.2135	0.04556737	-0.009727
1997	19.00	-10190	470.02	38	12.369	1.27875	-0.229	0.05243061	-0.0120054
2002	18.50	-10912	491.95	38	12.9461	1.26717	-0.2926	0.08564191	-0.0250628
2001	18.00	-11666	514.38	38	13.5364	1.25527	-0.3042	0.09255484	-0.0281578
1998	16.00	-15033	609.1	38	16.029	1.20412	-0.3161	0.09993659	-0.0315927
Total		78982	10251		M	1.57141		1.20534206	0.03412525
M	40.68					Sd^3	0.0061		
S	16.8747					S	0.183		
CV	0.41486					CV =	0.1164		
S^2	284.757	284.76				a	0.001		
N	37					Cy=	0.1639		
N-1	36								
N-2	35								

This values enable to evaluate Cy and formulas are indicated in the lower Note of this table

Figure A5.3.1 Worksheet to assess the skew coefficient (Cy) needed to evaluate the factor (K). ol.1 observation year; Col.2 random variable (24HMR); Cols. 3 and 4, 3rd and 2nd power of (X-M) where X is the random variable (24HMR) and M is the mean value of it; col. 5, (n+1), number of trials plus 1; Col. 6 (Pexc) for the random variable; col. 7, logarithm of col.2; col. 8, 9 and 10, 1st, 2nd and 3rd power of (log(x)-log M) where M is the mean value of the random variable given in col.7. Note: formulae used: Cy=a/Sd^3..(3), where a=(N/(N-1)*(N-2))*[Σ(Log P(24HMR)i-Ym)^3)..(4) and Sy=Σ(Log P(24HMR)i- Ym)^2)/ (N-1)^2.(5), and Ym =Σ(log P(24HMR)i)/N...(6). N=number of historical P(24HMR). M; is the mean value of the random variable (24HMR).

TABLE A-6 FREQUENCY FACTORS K FOR PEARSON TYPE III DISTRIBUTIONS VERSUS SKEW COEFFICIENT C_s AND RETURN PERIOD T (OR PROBABILITY OF EXCEEDENCE P)

	Return Period T (y)									
	1.05	1.11	1.25	2	5	10	25	50	100	200
Skew Coefficient C_s	Probability of Exceedence P (percent)									
	95	90	80	50	20	10	4	2	1	0.5
3.0	−0.665	−0.660	−0.636	−0.396	0.420	1.180	2.278	3.152	4.051	4.97
2.8	−0.711	−0.702	−0.666	−0.384	0.460	1.210	2.275	3.114	3.973	4.84
2.6	−0.762	−0.747	−0.696	−0.368	0.499	1.238	2.267	3.071	3.889	4.71
2.4	−0.819	−0.795	−0.725	−0.351	0.537	1.262	2.256	3.023	3.800	4.58
2.2	−0.882	−0.844	−0.752	−0.330	0.574	1.284	2.240	2.970	3.075	4.44
2.0	−0.949	−0.895	−0.777	−0.307	0.609	1.302	2.219	2.912	3.605	4.39
1.8	−1.020	−0.945	−0.799	−0.282	0.643	1.318	2.193	2.848	3.499	4.14
1.6	−1.093	−0.994	−0.817	−0.254	0.675	1.329	2.163	2.780	3.388	3.99
1.4	−1.168	−1.041	−0.832	−0.225	0.705	1.337	2.128	2.706	3.271	3.82
1.2	−1.243	−1.086	−0.844	−0.195	0.732	1.340	2.087	2.626	3.149	3.66
1.0	−1.317	−1.128	−0.852	−0.164	0.758	1.340	2.043	2.542	3.022	3.48
0.8	−1.388	−1.166	−0.856	−0.132	0.780	1.336	1.993	2.453	2.891	3.31
0.6	−1.458	−1.200	−0.857	−0.099	0.800	1.328	1.939	2.359	2.755	3.13
0.4	−1.524	−1.231	−0.855	−0.066	0.816	1.317	1.880	2.261	2.615	2.94
0.2	−1.586	−1.258	−0.850	−0.033	0.830	1.301	1.818	2.159	2.472	2.76
0.0	−1.645	−1.282	−0.842	0.000	0.842	1.282	1.751	2.054	2.326	2.57
−0.2	−1.700	−1.301	−0.830	0.033	0.850	1.258	1.680	1.945	2.178	2.38
−0.4	−1.750	−1.317	−0.816	0.066	0.855	1.231	1.606	1.834	2.029	2.20
−0.6	−1.797	−1.328	−0.800	0.099	0.857	1.200	1.528	1.720	1.880	2.01
−0.8	−1.839	−1.336	−0.780	0.132	0.856	1.166	1.448	1.606	1.733	1.83
−1.0	−1.877	−1.340	−0.758	0.164	0.852	1.128	1.366	1.492	1.588	1.66
−1.2	−1.910	−1.340	−0.732	0.195	0.844	1.086	1.282	1.379	1.449	1.50
−1.4	−1.938	−1.337	−0.705	0.225	0.832	1.041	1.198	1.270	1.318	1.35
−1.6	−1.962	−1.329	−0.675	0.254	0.817	0.994	1.116	1.166	1.197	1.21
−1.8	−1.981	−1.318	−0.643	0.282	0.799	0.945	1.035	1.069	1.087	1.09
−2.0	−1.996	−1.302	−0.609	0.307	0.777	0.895	0.959	0.980	0.990	0.99
−2.2	−2.006	−1.284	−0.574	0.330	0.752	0.844	0.888	0.900	0.905	0.90
−2.4	−2.011	−1.262	−0.537	0.351	0.725	0.795	0.823	0.830	0.832	0.83
−2.6	−2.013	−1.238	−0.499	0.368	0.696	0.747	0.764	0.768	0.769	0.76
−2.8	−2.010	−1.210	−0.460	0.384	0.666	0.702	0.712	0.714	0.714	0.71
−3.0	−2.003	−1.180	−0.420	0.393	0.636	0.660	0.666	0.666	0.667	0.66

Source: U.S. Interagency Advisory Committee on Water Data, Hydrology Subcommittee (1983). "Guidelines for Determining Flood Flow Frequency," *Bulletin No.* 17B, issued 1981, revised 1983.

Figure A5.3.2 illustrates a table that gives the frequency factors (K) of Log Pearsson type III distribution in function of skew coefficients Cy, and return period Tr or probability of exceedence P(exc). Source: Ponce (1994). Note: Once obtained the parameter Cy= 0.1639 showed in Figure 5.9 and with the probability of exceedence P(exc) or return period (Tr) it is possible to find the values of frequency factor (K) extreme values are indicated in the red square. A simple linear interpolation allows assessment of K in col. 3 of Figure 5.7.

APPENDIX 5.3A

Design storm for the study area using Cheng-Lung-Chen approach.

Once derived the 24HMR rainfall design, another probabilistic approach was used in order to assess the design storm that would be applied to build the hyetograph required. Studies performed by Cheng (1983) contain statistical approaches for design rainfall formulae for many countries of the United States including Arizona, New Mexico and El Paso Texas. El Paso Texas and Juárez city have practically the same climatic and regional conditions. Therefore, the climatic information available in El Paso Texas for the main components that define the rainfall behaviour would be adopted for the study area. These components named Intensity Duration and Frequency (IDF) are given in the following reference: Isopluvial curves of the Technical Paper 40 *National Weather Service. (U.S. Department of Commerce, Washington, DC) given in:* NOAA (1961) were used. Moreover Cheng (1983) formulas were used to predict the storm design for the study area. Bell (1969) stated a generalized IDF formula using 1 hour-10 years rainfall depth; (P_1^{10}) as an index. $R_1^{10} = (0.35 x Ln(T_r) + 0.76) x (0.54 x (t)^{0.25} - 0.50) x (R_1^2)$...(1). In this formula, the rainfall depth for 1 hour duration and 2 years return period (R_1^2) is obtained from graph given in (Fig. A5.3A.1) In this Figure (t) is the storm duration in minutes (60 min.) and (Tr) is the return period (Tr=10 years). Formula (1) allows evaluation of the design storm for 1 hour duration and 10 years return period (R_1^{10}) in function of the rainfall for 1 hour duration and 2 years return period given by the Isopluvial curves of the Technical Paper 40 *National Weather Service* (NOAA 1961)

Cheng (1983) further developed a generalized IDF formula for any location of the United States using regional constants such as: $f = (R_{24}^{100}/R_{24}^{10})$ and $Fr = (R_1^2/R_{24}^2)$. The values R_{24}^2; R_{24}^{10} and R_{24}^{100} were obtained through the use of Gumbel EV1 in the previous section; and R_1^2 was obtained from (Fig. A5.3A.1) of this section. The formula derived from Cheng (1983) in combination with Bell (1969) formula are here reproduced: $R_1^{100} = a_* R_1^{10} Log(10^{2-f} x T^{f-1})/(t+d)^n$ ...(2). in this formula; a, d and n are regional parameters obtained from the graph given in (Fig. A5.3A.2) in function of the regional factor $Fr = (R_1^2/R_{24}^2)$; T_r, is the return period adopted; R_1^{10}, is the rainfall depth predicted by Bell (1969) formula for 10 years return period. And

finally the coefficient f= (R_{24}^{100}/R_{24}^{10}).The following paragraphs describe the process to assess the design storm basically derived by the combined method of Bell (1969) and Cheng (1983):

Firstly, with the values of rainfall depth for 24HMR predicted for GEV1 for return periods of 100 and 10 years; (R_{24}^{100} ; R_{24}^{10} and R_{24}^{2}) it is possible to evaluate the factor (f) that considers the regional extension of rainfall patterns: f=(R_{24}^{100}/R_{24}^{10})=(104.13mm/67.35mm)=1.54. Secondly, using Bell (1969) formula (1) to estimate the rainfall depth for 1 hour duration and 10 years of return period (R_1^{10}) where rainfall depth for 1 hour duration and 2 years return period (R_1^{2}=23.62 mm=0.93) given in curve (i-d-f) illustrated in (Fig. 1) given by NOAA (1961). The rainfall depth derived using Bell formula was 37.0 mm:

R_1^{10} = (0.35xLn(T_r) + 0.76)x(0.54x(t)$^{0.25}$ – 0.50)x(R_1^{2}) = 37.0 mm; Bell formula. Once the rainfall depth for 1 hour duration and 10 years return period is evaluated using the Bell (1969)- formula (1), then Cheng (1983) formula (2) was applied but before the regional ratio given by Fr=(R_1^{2}/R_{24}^{2})=(23.62/37.94)=0.622 and the factor f= (R_{24}^{100}/R_{24}^{10})=(104.13 mm/67.35 mm)=1.54 were evaluated. Finally, the design storm derived from Cheng (1983) model for 100 years and 50 years of return period were evaluated and mentioned in the following paragraphs.

R_1^{100} = a* R_1^{10}Log(10^{2-f}xT^{f-1})/$(t+d)^{n}$= 55.5mm; Cheng (1983) formulae was R_1^{100} = 55.5 mm. Cheng regional constants (a_1=39.4; d=11.3; and n=0.865) were found using (Fig. A5.3A.2) B with Rr=0.6 and are given in the following page. Summarising, in the present research the flooding model would be performed for three different return periods: 10 years, 50 years and 100 years. Therefore, the following storm design were obtained: 37 mm; 50.5 mm and 55.5 mm respectively.

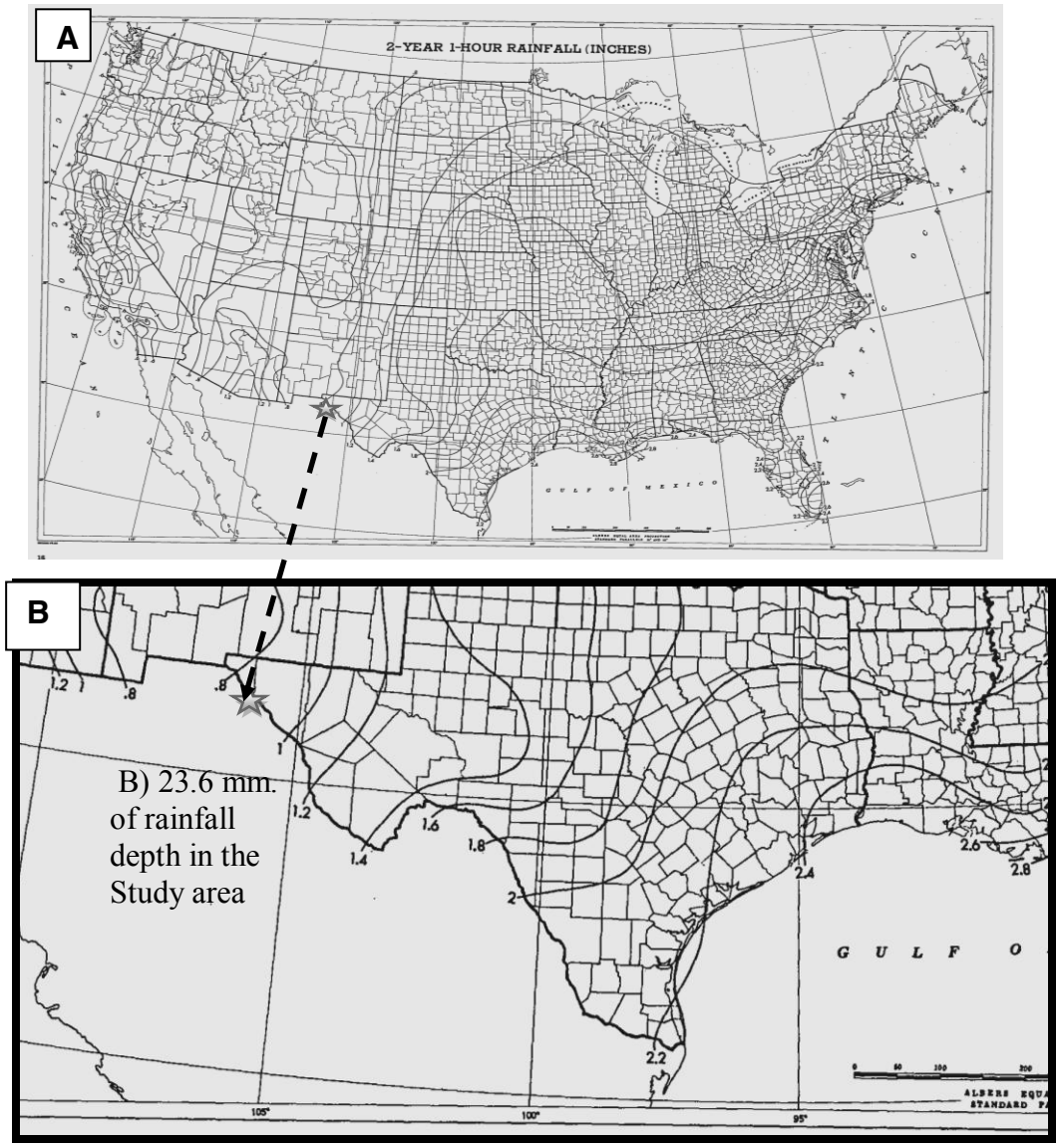

Figure A5.3A.1 Curve of Intensity Duration Frequency for a storm of 1hr duration and 2 years of return period from USA**. A)** The graph shows in inch the rainfall depth contour for different regions of USA. As can be seen the limit sector bordered between El Paso Texas and Juárez city is illustrated by the gray star**. B)** For the study area; R_1^2 = 23.6 mm that corresponds to (0.93 in). Source: NOAA (1961).

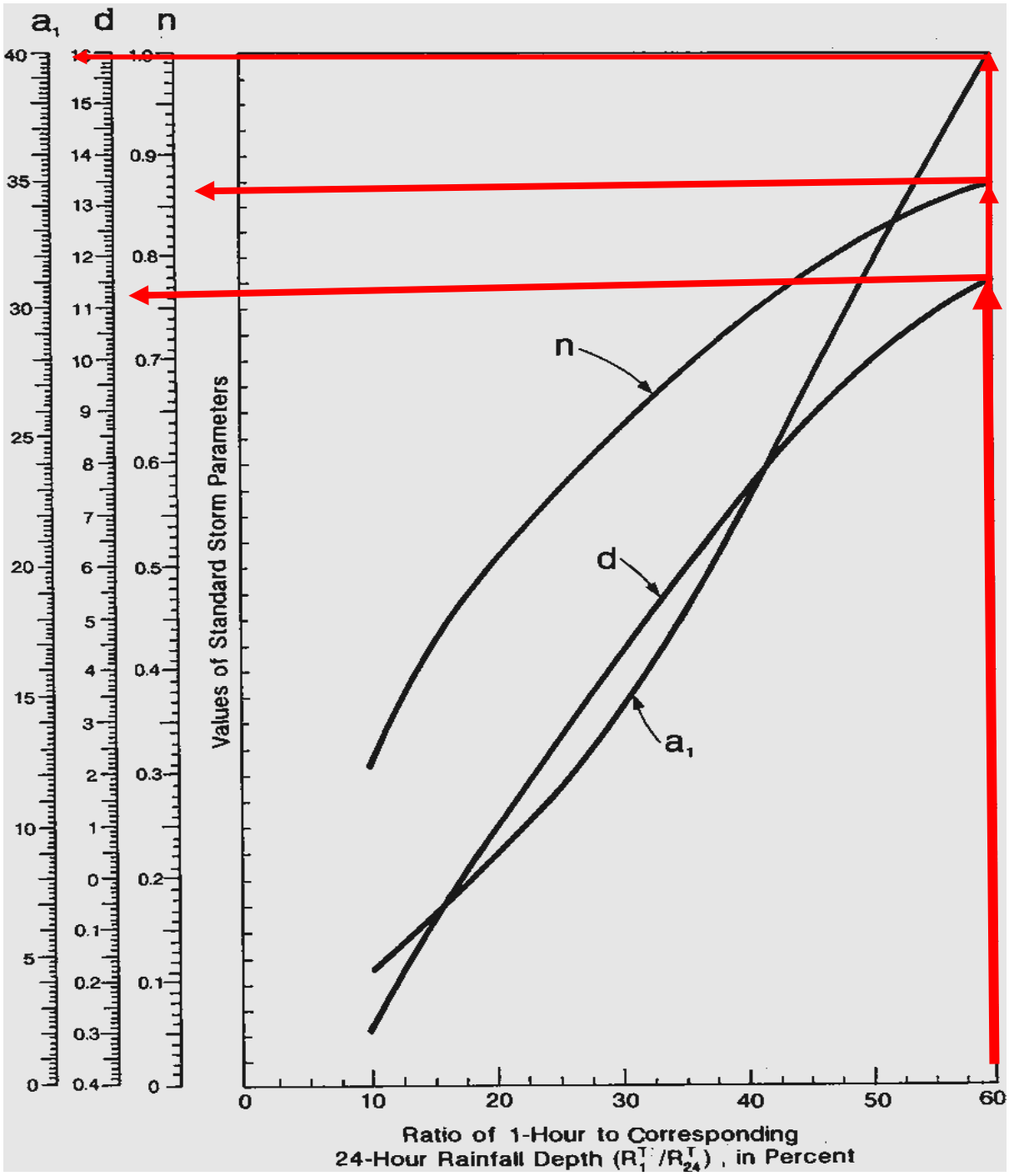

Figure A5.3A.2 Graphic used to find the coefficients a_1; d and n, needed to evaluate the design storm predicted for any return period and 1 hour duration given by Cheng (1983). The process to find its coefficients starts locating the value of regional factor (R_1^2/R_{24}^2) = 0.6 in the horizontal axis, then ascending until the intersection with curves a_1; d and n we find the values in the scaled rule located in the left vertical axe: a_1=39.4; d=11.3 and n= 0.865: Note that arrows illustrate the values near to the ruled vertical scale. Source: Cheng (1983).

APPENDIX 5.4

(CN) Method description.

This section describes the empiric methodology involved in the method. This empirical method was derived from the simulation of many Land-use terrains and soil types against a predicted runoff (Fig. A5.4.1A). In addition, this method can be assessed using the widely known HEC-HMS computer programme capable to simulate long urbanized areas like that of the study area. On the other hand, the Rainfall-Runoff simulation is expressed as $Q=(P-I_a)^2/(Q-I_a)+S...(1)$ where: Q is volume of accumulated runoff (in); P is the total rainfall or potential maximum runoff in (in); S, potential maximum retention storm of the watershed at the beginning of the storm (in). In addition, $I_a=0,2S..(2)$ is the initial retention including, surface storage, interception and evaporation (in). Equation (3) emerges by replacing equation (2) $I_a=0.2S$ into equation (1) then eq. (1) become; $Q=(P-0.2S)^2/(Q+0.8S)..(3)$; where, S is related to the soil and cover condition of the watershed through the CN (curve number parameter). This factor varies from 0 to 100 and S is linked to CN by $S=(100/CN)-10..(4)$, Optionally $S=(25400/CN)-254$ where S is expressing in (mm). Pitt (1994) stated a method to address CN using equation (4) which allows to find the rainfall-runoff response resulted from any rainfall falling over a different cover surfaces and soils types. Finally, this method provides CN values stated by: 2C-5-NRCS TR-55 and are presented in the model method. In short, In order to consider the effect of soil properties into the rainfall-runoff behaviour SCS (1986) method considers the following four groups (See Fig.Fig. A5.4.1A):

1. Group A, soils with low runoff potential due to high infiltration rates mainly deep and well drained sands and gravels.
2. Group B, soils with moderately low runoff potential due to moderate infiltration rates primarily moderately deep to deep, moderately well to well drained soils with moderately fine to moderately coarse textures.
3. Group C, soils that have a moderately high runoff potential due to slow infiltration rates these soils consists principally of soils in which a layer exists near the surface that impedes the downward movement of water of soils with moderately fine to fine texture.

4. Group D Soils, have a high runoff potential due to very slow infiltration rates. These soils consists mostly of clays with high swelling potential, soils with permanently water table, soils with a pan clay or a clay layer at or near the surface and shallow near or over the surface soils over nearly impervious parent material. 2C-5-NRCS TR-55

The Fig. 1 shows table of CN coefficients. This values are explained in the next paragraphs Firstly, CN in no paved areas (pervious areas) with poor grass cover condition and soil (group D) has the highest CN value (89), whereas good grass cover condition soil (group A) has the lowest CN value (39). Therefore, intermediate CN values are directly proportional with good to poor grass cover condition but inversely proportional with soil group, thus group D to group A. Secondly, On the other hand, Impervious areas like paved streets, roads, parking lots, roofs, curbs and storm sewers have the maximum value of CN (98) independently of their hydrologic soil group (see Fig. Fig. A5.4.1A). However, paved open ditches, gravel and dust are impervious areas and gives lower values of CN. Thus, vary inversely with the quality of impervious material paved to dust but directly proportional with the hydrologic soil group. Thirdly, the third Group is regarded to western desert urban areas with natural desert landscaping (pervious areas only) values of CN are 63, 77, 85 and 88 for groups A, B, C, and D respectively (see Fig. 5.8). The fourth group refers to artificial desert landscaping (impervious weed barrier, desert shrub with 1-2 inch sand or gravel mulch and basin borders) has a CN of 96 for all hydrologic soil group. and for commercial and business (85% impervious area) as well Industrial (72% of impervious areas) Land uses, CN values varies directly proportional with soil group but their values are lower for industrial Land use. Group 5 is integrated for residential districts by average lots size 1/8, 1/4, 1/3, 1/2, 1 and 2 acres and an average impervious surfaces area of 65, 38, 30, 25, 20 and 12. The CN values assigned to this group varies directly proportional with the soil group from A to D, but inversely proportional with the lot size from 1/8 acres to 2 acres. Finally, group 6 registered on the table has CN values of 77, 86, 91, 94 for the hydrologic soil group A, B, C and D

Cover description		Curve Number for Hydrologic soil group			
Cover type and hydrologic condition	Average Impervious	A	B	C	D
Fully developed urban areas (vegetation established) Open space (lawns, parks, golf courses, cementeries)					
Poor condition (grass cover <50%)		68	79	86	89
Fair condition (grass cover 50% to 75%)		49	69	79	84
Good condition (grass cover > 75%)		39	61	74	80
Impervious Areas:					
Paved parking lots, roofs, driveways, etc (excluding ROW) street and roads:		98	98	98	98
Paved: curbs and storm sewers (excluding ROW)		98	98	98	98
Paved: open ditches (including ROW)		83	89	92	93
Gravel (including ROW)		76	85	89	91
Dust (including ROW)		72	82	87	89
Western desert urban areas:					
Natural desert landscaping (pervious areas only)		63	77	85	88
Artificial desert landscaping (Impervious weed barrier, desert shrub with 1-2 inch sand or gravel mulch and basin borders.		96	96	96	96
Industrial districts:					
Commercial and business	85	89	92	94	95
Industrial	72	81	88	91	93
Residential districts by average lots size:					
1/8 acre or less (town houses)	65	77	85	90	92
1/4 acre	38	61	75	83	87
1/3 acre	30	57	72	81	86
1/2 acre	25	54	70	80	85
1 acre	20	51	68	79	84
2 acres	12	46	65	77	82
Developing urban areas Newly graded (pervious areas only, no vegetation)		77	86	91	94

Figure A5.4.1A Curve numbers (CN) for selected urban land use and soil type of watersheds located in dessert urbanized areas. Source: SCS (1986).

Appendix 5.4.1 CN and physiographic parameters of Jarudo Basin

(CN) Curve Number coefficient determination method for Jarudo basin The CN parameter was estimated using CN values given in Fig. A5.4.1A and reproduced in Fig. Fig. A5.4.1.1 below. The terms involved as well the process to obtain the CN coefficients are explained in the following paragraphs. The first part in the process is to divide into homogeneous areas with similar land-use the sub-basin.

Sub-basin	I.S.T. L.U	(dimensionless)	P.S.T.L.U.	(dimensionless)	(dimensionless)
name	I.S. (%)	C.N.	P.S (%)	C.N.	C.C.N.
Sb 4a	80	72	20	68	71
Sb 4b	90	76	10	68	75
Sb 4c	90	76	10	68	75
Sb 3a	70	76	30	49	68
Sub-basin 1	100	85	0	0	85
Sb 2b	25	82	75	69	72
Sb 3b	40	82	60	65	72
Sb 1a	10	98	90	65	68
Sb 1b	25	85	75	62	68
Sb 1c	25	82	75	69	72
Sb 1d	40	82	60	69	74
		(dimensionless)		(dimensionless)	(dimensionless)
Sub-basin	%A (S.T. B	(C.N.S.T.A)	%B (S.T A)	(C.N.S.T.B)	(C.C.N.)
Sb 2a	85	77	15	63	75

Figure A5.4.1.1. CN parameters for all the sub-basins that formed the Jarudo basin (CN). This parameter is used to convert the design rainfall (hyetograph) into runoff or precipitation excess that produce runoff (Pe). Results of Curve Number (CN) Fig. Fig. A5.4.1.1 CN parameters were addressed. and results are shown of the table on Fig. Fig. A5.4.1A above.

I.S.T.L.U Impervious Surface for specific type of land-use in (%) of the total area and the soil type (e.g. for sub-basin 4a (80% of I.S., dust cover, and soil type A, gives a CN=72 (Fig. A5.4.1A), instead for sub-basins 4b (90% I.S), 4c(90% I.S) ,and 3a (70% I.S) for gravel land use surface, and soil type A, gives a CN=76 (Fig. A5.4.1A). **P.S.T.L.U** Pervious Surface for specific land-use type in % of the total area and the soil type (e.g. for sub-basins 4a (20% of P.S, poor condition grass cover and soil type A, gives a CN=68 (Fig. 1A). For sub-basin 4b and 4c (10% of P.S, poor condition grass cover and soil type A, gives a CN=68 (Fig. A5.4.1A) instead in Sub-basin 3a (30% of P.S, fair condition grass cover and soil type A, gives a CN =49 (Fig. A5.4.1A). The (C.C.N) Composite curve number is the simple multiplication of the two values of CN for (I.S) as well (P.S) and are indicated in column 6 of (Fig. A5.4.1A). **C.N.S.T.A** and **C.N.S.T.B** Curve number value in agree with the soil type A and B with only pervious surface. (e.g. In the sub-basin 2a all the surface is Impervious (100%) but, there are two soil types A with 15 % and B with 85%. The land-use corresponds to western desert urban areas gives values for CN = 63% and 77% respectively (Fig. A5.4.1.1) **%A (S.T.A)** and **%B (S.T.B**) = % of area cover by soil type A and soil type B respectively.

Concentration time and Lag-time evaluation for Jarudo basin.

HEC-HMS computer program performs hydrologic and hydraulic calculation such as hydrographs and storage volume for the sub-basins allocated within the basins of the study area. However, Concentration time and Lag-time are fundamental features and were evaluated with the simple application of Kiprich's equation: $Tc= 0.000325[L/Ss^{0.5}]^{0.77}$ where Tc=concentration time in hours; L=length of the stream in meters; Ss=gradient of the main stream. Main stream length was evaluated with Auto-Cad and Arc-Map programs. Physiographic and hydrologic parameters as: (A) area; (Is) Impervious surface; (Ia) Initial abstraction are parameters also needed for HEC-HMS flooding simulation and are presented in Fig. A5.4.2. In relation to (Anapra, Center, Barreal, Airport, Bravo River, Acequias and Chamizal basins), the same method was used, therefore the previous paragraph would be omitted and only the results are presented. The same process would applied for CN parameter as well discharge evaluation for the rest of the basins.

Sub-basin	Length (meters)	Slope (%)	Tc (minutes)	Lag-time (minutes)
Sb 4a	1122	0.0767	11.99163167	7.194979
Sb 4b	1026	0.0133	21.97508591	13.18505
Sb 4c	2750	0.0132	47.08636951	28.25182
Sb 3a	3755	0.0951	27.98209015	16.78925
Sub-basin 1	5720	0.0028	150.3381133	90.20287
Sb 2b	3250	0.0105	58.48201172	35.08921
Sb 3b	1780	0.0087	39.54927123	23.72956
Sb 1a	6950	0.0106	104.6201979	62.77212
Sb 1b	5860	0.0176	75.47250813	45.2835
Sb 1c	1780	0.01	37.48464459	22.49079
Sb 1d	3755	0.00167	132.6581111	79.59487
Sb2a	2650	0.014	44.73732627	26.8424

Figure. A5.4.2 Concentration time and lag-time using Kirpich formulae for the Jarudo Basin. Source of method for these calculations: Kirpich (1940 in: Loukas and Quick, 1995).

Sub-basin	Physiographic and hydrologic parameters					
Name	**Area km^2**	**CN**	**I.S (%)**	**(Ia)**	**(Tc) (min.)**	**Lag-time 0.6*Tc (min.)**
Sb4a	1.8100	71.5	80	0.2	12.0	7.0
Sb4b	3.5500	75.0	90	0.2	22.0	13.0
Sb4c	2.1620	75.0	90	0.2	47.0	28.0
Sb3a	6.0790	68.0	70	0.2	28.0	17.0
Sub-basin-1	4.5400	85.0	100	0.2	150.0	90.0
Sb2a	2.0630	75.0	0	0.2	45.0	27.0
Sb2b	3.3617	72.0	25	0.2	58.0	35.0
Sb3b	1.4658	72.0	40	0.2	40.0	24.0
Sb1a	7.7230	68.0	10	0.2	105.0	63.0
Sb1b	5.5647	68.0	25	0.2	75.0	45.0
Sb1c	1.3563	72.3	25	0.2	37.0	22.0
Sb1d	1.5959	74.0	40	0.2	133.0	80.0

Figure A5.4.3 Physiographic and hydrologic parameters used in the application of the CN of the SCS (1986) of USA method for Jarudo basin. Source of method for these calculations: SCS (1986).

IS = Impervious surface or surface treated with some type of material or substance in order to modify land use properties (in percentage); **Ia** = Initial abstraction refers to water losses by evaporation, transpiration, and water retained on little terrain depressions, the method considers 20% of the (hyetograph) rainfall model; **Tc** = Concentration time in minutes or time from beginning of runoff and the concentration of this water in the inundation area of interest); **Lag-time** = time between centroid of rainfall excess and the centroid of direct runoff = 60% of the concentration time in minutes; lag time is evaluated by Kirpich formulae; **CN** = Curve number as defined by SCS (1986) method.

APPENDIX 5.4.2

(CN) Curve Number coefficient determination method for Anapra basin

Regarded to CN parameters of Anapra sub-basins a brief explanation is given in the lower part of Fig. A5.4.1A for all the sub-basins which integrates the Anapra basin.

Asb1a[5]	Asb5[7]	Sb1CB[6]	Sb4CC[6]	Sb5C2Ca	Sb7C[5]
Asb1b[5]	AsbC[4]	Sb8ES[5]	Sb4WS[1]	Sb5C2CD	Sb8aES
Asb1c[5]	AsbE[4]	Sb2C[6]	Sb5C11[6]	Sb5C2Cl[1]	Sb8bES
Asb1d[7]	CRSb[1a]	Sb3C[6]	Sb5C1C[2]	Sb5WS[7]	Sb8C[5]
ASb1e[4]	CSb[6]	Sb3S[3]	Sb5C1N[1a]	Sb6C[6]	Sb8cES
ASb2[4]	LSb[1a]	Sb3V1[5]	Sb5C1S[4]	Sb6Ca[7]	SbFV1[6]
Asb3[4]	Msb1[6a]	Sb4ACOL[6]	Sb5C2C1a	Sb6ColB[5]	SbFV2[6]
Asb4W[4]	Sb1CC[6]	Sb4BC[6]	Sb5C2C1b	Sb6Cb[7]	SbMbN[1]
	SbMsbS[1a]	SbS1[1a]	SbS2[1a]	TSb[1a]	Sb8ES[2]

Figure A5.4.2.1 Curve Number parameters for all the sub-basins that formed the Anapra basin (CN).

CN *= Curve number as defined by S.C.S (1986) method.*

(1)CN=73 derived from Fig. A5.4.1A *for two types of hydrologic soils group A and B and fully developed urban areas with poor condition (grass cover <50%)* Fig. A5.4.1A*; A=55% (0.55x68=37.4) + B=45% (0.45x79=35.55).*

(1a)CN=73 derived from Fig. A5.4.1A *for two types of hydrologic soils group A and C and fully developed residential districts 1000 m^2* Fig. A5.4.1A*; C=55% (0.55X83=45.65) + A=45% (0.45x61=27.45)*

(1b)CN=73 derived from Fig. A5.4.1A *for two types of hydrologic soils group A and B and fully developed impervious areas with dust* Fig. A5.4.1A*; A=90% (0.9x72=64.8) + B=10% (0.1x82=8.2)*

(2) CN=75 derived from Fig. A5.4.1A*; for two types of hydrologic soils group A and B and fully developed urban areas with poor condition (grass cover <50%). A=35% (0.35x68=23.80) + B=65%(0.65x79=51.35).*

3) CN=71 derived from Fig. A5.4.1A *two types of hydrologic soils group A and B and fully developed urban areas with poor condition (grass cover <50%). A=75% (0.75x68=51) + B=25%(0.25x79=19.75).*

4) CN=70 derived from Fig. 1A *for two types of hydrologic soils group A and B and Western desert urban areas natural landscaping (pervious areas) A=50 (0.80x68=54.4) + B=0.20%(0.20x79=15.8).*

5) CN=68 derived from Fig. A5.4.1A *for hydrologic soil group A and fully developed urban areas with poor condition (grass cover <50%). A=100%.*

6a) CN=85; derived from Fig. A5.4.1A *hydrologic for soil group B=100% and for residential districts with 500 m^2 or less with an impervious area of 65 %.*

6) CN=85 derived from Fig. A5.4.1A *for Impervious paved areas two types of hydrologic soils group A=60% and B=40% CN = 0.6X83 + 0.4X89=49.8 +35.6*

7) CN=69 derived from Fig. A5.4.1A *for hydrologic soils group A=90% and B=10% fully developed areas and poor condition (grass cover less than 50%) 0.9x68+0.1x79=61.2+7.9=69.1*

8) CN=80 derived from Fig. A5.4.1A *for Impervious dust surface areas and two types of hydrologic soils group A=60% and B=40% CN = 0.60X77 + 0.40X85=46.2 +34=80*

Concentration time and Lag-time evaluation for the Anapra basin.

Figs. A5.4.2.2 and A5.4.2.3 show the Concentration time (Tc) for the sub-basins which integrates the Anapra basin and the Physiographic parameters as: (A) area; (Is) Impervious surface; (Ia) Initial abstraction also needed for HEC-HMS flooding simulation

Sub-basin	Length (meters)	Slope (%)	Tc (minutes)	Lag-time (minutes)
Sb8ES	873	0,0325	32.00	19
Asb1a	3855	0.0208	50.00	30
Asb1b	1746	0.004267	50.00	30
Asb1c	2108	0.006219	50.00	30
Asb1d	4144	0.022066	51.67	31
ASb1e	1804	0.004555	50.00	30
ASb2	3362	0.015816	50.00	30
Asb3	3106	0.038692	33.33	20
Asb4W	4262	0.072846	33.33	20
Asb5	4357	0.076129	33.33	20
AsbC	4235	0.071926	33.33	20
AsbE	3245	0.042232	33.33	20
CRSb	3470	0.147819	21.67	13
CSb	1258	0.023925	20.00	12
LSb	2360	0.068383	21.67	13
Msb1	2137	0.011409	40.00	24
Sb1C	1624	0.022333	25.00	15
Sb1CB	1807	0.033074	23.33	14
Sb1CC	2493	0.013964	41.67	25
Sb2C	1906	0.030761	25.00	15
Sb3C	1501	0.019079	25.00	15
Sb3S	3164	0.009387	58.33	35
Sb3V1	1256	0.144291	10.00	6
Sb4ACOL	716	0.004342	25.00	15
Sb4BC	983	0.004429	31.67	19
Sb4CC	873	0.011523	20.00	12
Sb4WS	3100	0.009716	56.67	34
Sb5C11	1900	0.008112	41.67	25
Sb5C1C	1273	0.016416	23.33	14
Sb5C1N	1334	0.043194	16.67	10
Sb5C1S	1622	0.016096	28.33	17
Sb5C2C1a	1247	0.023508	20.00	12
Sb5C2C1b	1951	0.03223	25.00	15
Sb5C2Ca	1995	0.0285	26.67	16
Sb5C2CD	2157	0.039395	25.00	15
Sb5C2CI	1596	0.048267	18.33	11
Sb5WS	2490	0.005033	61.67	37
Sb6C	2964	0.010396	53.33	32
Sb6Ca	873	0.033027	13.33	8
Sb6ColB	1026	0.00336	15.00	9
Sb6Cb	997	0.043074	13.33	8
Sb7C	657	0.113184	6.67	4
Sb8aES	2220	0.041729	25.00	15
Sb8bES	1664	0.01269	31.67	19
Sb8C	873	0.024324	15.00	9
Sb8cES	1626	0.007378	38.33	23
SbFV1	2010	0.076551	18.33	11
SbFV2	1700	0.043686	20.00	12

SbMbN	2332	0.013586	40.00	24
SbMsbS	3335	0.006495	70.00	42
SbS1	1230	0.001653	55.00	33
SbS2	899	0.000612	63.33	38
TSb	1280	0.038535	16.67	10
R4c	987	0.009869	23.33	14

Figure A5.4.2.2 Show the results of the Concentration time as well as the Lag-time for the sub-basin located within the Anapra Basin. Source of method for calculations: Kirpich (1940 in: Loukas and Quick, 1995).

Sub-basin	Area km^2	CN	IS	(Ia)	Tc(min)	LT= 0.6*Tc
Asb1a[5]	2.5030	68	0	0.2	50.00	30
Asb1b[5]	1.5400	68	0	0.2	50.00	30
Asb1c[5]	1.4100	68	0	0.2	51.00	30
Asb1d[7]	2.2900	69	0	0.2	51.5	31
ASb1e[4]	0.6720	70	0	0.2	50.00	30
ASb2[4]	1.7470	70	0	0.2	50.00	30
Asb3[4]	1.7000	70	0	0.2	33.33	20
Asb4W[4]	2.3980	70	0	0.2	33.33	20
Asb5[7]	4.9730	69	0	0.2	33.33	20
AsbC[4]	2.6640	70	0	0.2	33.33	20
AsbE[4]	1.6880	70	25	0.2	33.33	20
CRSb[1a]	1.5700	73	10	0.2	21.67	13
CSb[6]	1.0200	85	80	0.2	20.00	12
LSb[1a]	1.4700	73	10	0.2	21.67	13
Msb1[6a]	2.3000	85	40	0.2	40.00	24
Sb1CC[6]	1.5355	85	95	0.2	42	25
Sb1CB[6]	1.5813	85	85	0.2	23.33	14
Sb8ES[5]	3.1200	68	0	0.2	32	19
Sb2C[6]	0.7319	85	90	0.2	25.00	15
Sb3C[6]	0.3593	85	95	0.2	25.00	15
Sb3S[3]	2.7805	71	10	0.2	58.33	35
Sb3V1[5]	0.3428	68	5	0.2	10.00	6
Sb4ACOL[6]	0.3586	85	90	0.2	25.00	15
Sb4BC[6]	0.5526	85	95	0.2	31.67	19
Sb4CC[6]	0.5033	85	85	0.2	20.00	12
Sb4WS[1]	1.9495	73	15	0.2	56.67	34
Sb5C11[6]	1.0530	85	90	0.2	41.67	25
Sb5C1C[2]	0.3275	75	20	0.2	23.33	14
Sb5C1N[1a]	0.3250	73	10	0.2	16.67	10
Sb5C1S[4]	0.4090	70	10	0.2	28.33	17
Sb5C2C1a[2]	0.3560	75	60	0.2	20.00	12
Sb5C2C1b[8]	0.9080	80	70	0.2	25.00	15
Sb5C2Ca[1a]	1.4920	73	10	0.2	26.67	16
Sb5C2CD[8]	0.9250	80	60	0.2	25.00	15
Sb5C2CI[1]	0.6540	73	60	0.2	18.33	11
Sb5WS[7]	1.0500	69	0	0.2	61.67	37
Sb6C[6]	1.2460	85	60	0.2	53.33	32
Sb6Ca[7]	0.2400	69	10	0.2	13.33	8
Sb6ColB[5]	0.3740	68	10	0.2	15.00	9
Sb6Cb[7]	0.2000	69	5	0.2	13.33	8
Sb7C[5]	0.0900	68	0	0.2	6.67	4
Sb8aES[5]	1.2600	68	0	0.2	25.00	15
Sb8bES[5]	1.0270	68	0	0.2	31.67	19

Sb8C[5]	0.3500	68	0	0.2	15.00	9
Sb8cES[5]	0.6400	68	0	0.2	38.33	23
SbFV1[6a]	1.0000	85	75	0.2	18.33	11
SbFV2[6a]	0.8000	85	70	0.2	20.00	12
SbMbN[1a]	0.8130	73	50	0.2	40.00	24
SbMsbS[1a]	1.7470	73	60	0.2	70.00	42
SbS1[1a]	0.7020	73	75	0.2	55.00	33
SbS2[1a]	1.5900	73	40	0.2	63.33	38
TSb[1a]	1.1400	73	20	0.2	16.67	10
Sb8ES[2]	3.12	68	0	0.2	23.33	14

Figure A5.4.2.3 Hydrologic parameters used in the application of the CN of the SCS (1986) of USA method for Jarudo basin. Source: SCS (1986).

***IS** = Impervious surface or surface treated with some type of material or substance in order to modify land use properties (in percentage); **Ia** = Initial abstraction refers to water losses by evaporation, transpiration, and water retained on little terrain depressions, the method considers 20% of the (hyetograph) rainfall model; **Tc** = Concentration time in minutes or time from beginning of runoff and the interest area); **Lag-time** = time between centroid of rainfall excess and the centroid of direct runoff = 60% of the concentration time in minutes; lag time is evaluated by Kirpich formulae; **CN** = Curve number as defined by S.C.S (1986) method.*

[9)] The evaluation of concentration time is indicated in Figure A5.4.2.2

[10)] The evaluation of Lag-time is indicated in Figure A5.4.2.2

APPENDIX 5.4.3

(CN) Curve Number coefficient determination method for Center basin.

The CN parameters were estimated using the same methodology as Jarudo and Anapra basins previously described and the general explanation given in section 5.2.3 using the model table given in Fig. A5.4.1A. The results of CN and the physiographic and hydrologic parameters for the sub-basins comprised Centre Basin are presented in Fig. A5.4.3.1

Physiographic and hydrologic parameters for Center basin.

HEC-HMS computer program performs hydrologic calculation such as hydrographs and storage volume for the sub-basins allocated within the different basins of the study area. However, before use it physiographic and hydrologic parameters are needed. Such parameters as: (A) area; (Is) Impervious surface; (Ia) Initial abstraction; (Tc) Concentration time and (Lag-time). For this reason in the lower part of the table of Fig. 1 is again explained. In relation to the (A) area, Length and slope of the streams of the sub-basins were evaluated using Auto-Cad Programs, the landuse was identified using Satellite Images and the spatial module of program Arc-Map 9.2 GIS for their interpretation

	Physiographic and hydrologic Parameters					
Sub-basin Name	**Area km^2**	**CN**	**IS (%)**	**(Ia)**	**(Tc) min**	**Lag-time min**
Sbla[1)]	0.3962	85.0	100	0.2	*42.0*	25.0
Sbl4a[1)]	0.2080	85.0	80	0.2	7.0	4.0
Sbl3a[1)]	0.3100	85.0	90	0.2	7.0	4.0
Sbl2a[1)]	0.1240	85.0	80	0.2	5.0	3.0
Sbl1a[1)]	1.7560	85.0	100	0.2	42.0	25.0
Sb2a[1)]	1.4568	85.0	100	0.2	38.0	27.0
Sb31a[2)]	0.5540	68.0	50	0.2	20.0	12.0
Sb31b[1]	0.5380	85.0	80	0.2	5.0	3.0
Sb31c[4]	0.2420	70.0	50	0.2	10.0	6.0
Sb31d[6)]	1.2020	80.0	50	0.2	23.0	14.0
Sb31e[1)]	0.1710	85.0	95	0.2	3.0	2.0
Sb31f[1)]	0.1300	85.0	100	0.2	15.0	9.0
Sb31g[1)]	0.3410	85.0	95	0.2	33.0	20.0
Sb31h[1)]	0.6590	85.0	100	0.2	23.0	14.0
Sb31i[1)]	0.2480	85.0	100	0.2	3.0	2.0

Sb41a[2)]	0.5760	68.0	60	0.2	42.0	25.0
Sb41b[6]	0.6638	75.0	85	0.2	45.0	27.0
Sb51a[2)]	0.6944	68.0	50	0.2	30.0	18.0
Sb51b[2)]	1.4111	68.0	40	0.2	23.0	14.0
Sb51c[3)]	0.4123	73.0	60	0.2	33.0	20.0
Sb51d[3)]	0.2232	73.0	80	0.2	25.0	15.0
Sb51e[1)]	1.0000	85.0	75	0.2	33.0	20.0
Sb61a[2)]	2.6511	68.0	0	0.2	28.0	17.0
Sb61b[5)]	1.8700	6.5	50	0.2	75.0	45.0
Sb62a[3)]	0.4244	73.0	40	0.2	50.0	30.0
sb62b[3)]	0.4305	73.0	50	0.2	43.0	26.0
Sb71a[4)]	1.2894	72.0	40	0.2	35.0	21.0
Sb71b[4)]	1.5978	72.0	60	0.2	42.0	25.0
Sb81b[2)]	5.8616	68.0	10	0.2	33.0	20.0
Sb81a[2)]	2.2961	68.0	25	0.2	37.0	22.0
Sb81c[2)]	2.3697	68.0	25	0.2	50.0	30.0
Sb81d[1)]	0.5616	85.0	50	0.2	32.0	19.0
Sb81e[1)]	2.9689	85.0	80	0.2	20.0	12.0
Sb91a[1)]	4.1590	85.0	100	0.2	62.0	37.0
Sb101a[1)]	2.5700	85.0	90	0.2	42.0	25.0

Figure A5.4.3.1 hydrologic parameters used in the application of the CN of the SCS (1986) of USA method for Center basin. Source: SCS (1986).

I.S *= Impervious surface or surface treated with some type of material or substance in order to modify land use properties (in percentage);* ***Ia*** *= Initial abstraction refers to water losses by evaporation, transpiration, and water retained on little terrain depressions, the method considers 20% of the (hyetograph) rainfall model;* ***Tc*** *= Concentration time in minutes or time from beginning of runoff and the interest area);* ***Lag-time*** *= time between centroid of rainfall excess and the centroid of direct runoff = 60% of the concentration time in minutes; lag time is evaluated by Kirpich formulae;* ***CN*** *= Curve number as defined by S.C.S (1983) method.*

[2)] CN=68 derived from Fig. A5.4.1A *for hydrologic soil group A and fully developed urban areas with poor condition (grass cover <50%). A=100%.*

[1)] CN=85 derived from Fig. A5.4.1A *for Impervious gravel areas type of hydrologic soil group B=100% and districts with 500 lots size town houses (50%) CN = 0.50X85+ + 0.50X85=42.5+42.5*

[3)] CN=73 derived from Fig. A5.4.1A *for Impervious paved areas (28%) type of hydrologic soils group A=50% and B=50% districts with 500 lots size town houses (72%) CN = 0.28X0.5X83+0.28X0.5X89 + 0.72X0.5X61+0.72X0.5X75=11.62+12.46+21.96+27.00*

[4)] CN=72 derived from Fig. A5.4.1A *for Impervious paved areas (22%) type of hydrologic soils group A=50% and B=50% districts with 500 lots size town houses (78%) CN = 0.22X0.5X83+0.22X0.5X89 + 0.78X0.5X61+0.78X0.5X75=9.13+9.79+23.79+29.25*

[5)] CN=76.5 derived from Fig. A5.4.1A *for Impervious paved areas (20%) type of hydrologic soils group A=30% and B=70% districts with 500 lots size town houses (80%); CN=0.20X0.30X83+0.20X0.70X89 0.80X0.30X61+0.80X0.70X80=4.98+12.46+14.64+44.80*

[6)] CN=80 derived from Fig. A5.4.1A *for Impervious dust surface areas and two types of hydrologic soils group A=60% and B=40% CN = 0.60X77 + 0.40X85=46.2 +34=80*

Concentration time and Lag-time evaluation for the Center basin.

Concentration time and Lag-time are presented in Fig. A5.4.3.2

Subbasin	Length (m)	Slope (%)	Tc (min)	Lag-time (min)
Sbla	500.0	0.00055	42.0	25.0
Sbl4a	567.0	0.07427	7.0	4.0
Sbl3a	765.0	0.13519	7.0	4.0
Sbl2a	450.0	0.11210	5.0	3.0
Sbl1a	2,125.0	0.00994	42.0	25.0
Sb2a	1,887.0	0.01016	38.0	27.0
Sb31a	956.0	0.01382	20.0	12.0
Sb31b	754.0	0.31466	5.0	3.0
Sb31c	712.0	0.04638	10.0	6.0
Sb31d	1,567.0	0.02582	23.0	14.0
Sb31e	278.0	0.16124	3.0	2.0
Sb31f	453.0	0.00655	15.0	9.0
Sb31g	765.0	0.00241	33.0	20.0
Sb31h	876.0	0.00807	23.0	14.0
Sb31i	387.0	0.31243	3.0	2.0
Sb41a	934.0	0.00192	42.0	25.0
Sb41b	887.0	0.00145	45.0	27.0
Sb51a	934.0	0.00460	30.0	18.0
Sb51b	1,732.0	0.03154	23.0	14.0
Sb51c	813.0	0.00272	33.0	20.0
Sb51d	734.0	0.00456	25.0	15.0
Sb51e	1,412.0	0.00821	33.0	20.0
Sb61a	3,546.0	0.07931	28.0	17.0
Sb61b	2,312.0	0.00261	75.0	45.0
Sb62a	986.0	0.00136	50.0	30.0
sb62b	765.0	0.00121	43.0	26.0
Sb71a	1,654.0	0.00967	35.0	21.0
Sb71b	2,134.0	0.01002	42.0	25.0
Sb81b	6,756.0	0.18786	33.0	20.0
Sb81a	2,345.0	0.01682	37.0	22.0
Sb81c	2,867.0	0.01150	50.0	30.0
Sb81d	976.0	0.00425	32.0	19.0
Sb81e	3,245.0	0.15914	20.0	12.0
Sb91a	5,321.0	0.02266	62.0	37.0
Sb101a	3,423.0	0.02578	42.0	25.0

Figure A5.4.3.2 Concentation time and lag-time using Kirpich formulae for the Center basin. Source of method for these calculations: Kirpich (1940 in: Loukas and Quick, 1995).

APPENDIX 5.4.4

(CN) Curve Number coefficient determination method for Barreal basin.

The CN parameters were estimated using model table given in A5.4.1A in similar form as the precedent basins. On the other hand, physiographic and hydrologic parameters involved are gathered together in Fig. A5.4.4.1 These parameters are for all the sub-basins which integrate the Barreal basin.

Physiographic and hydrologic parameters for Barreal Basin.

HEC-HMS computer program performs hydrologic calculation such as hydrographs and storage volume for the sub-basins allocated within the different basins of the study area. However, before use it physiographic and hydrologic parameters are needed. Such parameters as: (A) area; (Is) Impervious surface; (Ia) Initial abstraction; (Tc) Concentration time and (Lag-time). For this reason in the lower part of the table of Fig. A5.4.4.1. This terms are explained. In relation to the (A) area, Length and slope of the streams of the sub-basins were evaluated using Auto-Cad Programs, the landuse was identified using Satellite Images and the spatial module of program Arc-Map 9.2 GIS for their interpretation.

Barreal Basin							
Basin	Sub-basin	Physiographic and hydrologic Parameters					
Num.	**Name**	**Area km^2**	**CN**	**I.S(%)**	**(Ia)**	**(Tc) min**	**L. T min**
5.5.1	SbCLA2[2)]	6.4700	78.2	40	0.2	62.0	37.0
5.5.2	SbCLA1[1)]	14.9600	79.9	60	0.2	102.0	61.0
5.5.3	SbCL3a[3)]	8.2440	70	10	0.2	87.0	52.0
5.5.3	SbCL3b[5)]	5.2730	68.0	0	0.2	85.0	57.0
5.5.3	SbCL3c[3)]	2.4930	70	0	0.2	47.0	28.0
5.5.4	SbCL2[3)]	2.2600	70	10	0.2	100.0	60.0
5.5.4	SbCL1[3)]	3.7100	70	30	0.2	90.0	54.0
5.5.4	SbCL4[5)]	7.5400	68	0	0.2	120.0	72.0
5.5.5	SbCLBW[3)]	6.3400	70	0	0.2	80.0	48.0
5.5.5	SbCLBE[4)]	3.1700	71.4	30	0.2	100.0	60.0
5.5.6	SbCLCW[3)]	9.6200	70	20	0.2	82.0	49.0
5.5.6	SbCLCE[3)]	0.6000	70	10	0.2	22.0	13.0
5.5.7	SbCLDW[5)]	4.9000	68.0	0	0.2	67.0	40.0
5.5.7	SbCLDE[6)]	2.8900	70.5	15	0.2	95.0	57.0
5.5.8	SbCL5[5)]	5.8500	68.0	0	0.2	123.0	74.0
5.5.8	SbCLFW[5)]	16.3800	68.0	0	0.2	100.0	60.0
5.5.8	SbCLEW[5)]	3.3800	68.0	0	0.2	83.0	50.0
5.5.8	SbCLEE[3]	4.2900	70	10	0.2	107.0	64.0
5.5.9	SbCLGW[5)]	16.3800	68.0	0	0.2	62.0	37.0
5.5.9	SbCLG1[5)]	12.5900	68.0	0	0.2	100.0	60.0
5.5.9	SbCLGE[5)]	6.5900	68.0	0	0.2	100.0	60.0
5.5.10	SbCLH2[5)]	13.9700	68.0	0	0.2	113.0	68.0
5.5.10	SbCLH1[5)]	20.7200	68.0	0	0.2	72.0	43.0

Figure A5.4.4.1 hydrologic parameters used in the application of the CN of the SCS (1986) of USA method for Barreal basin. Source: SCS (1986).

I.S *= Impervious surface or surface treated with some type of material or substance in order to modify land use properties (in percentage);* ***Ia*** *= Initial abstraction refers to water losses by evaporation, transpiration, and water retained on little terrain depressions, the method considers 20% of the (hyetograph) rainfall model;* ***Tc*** *= Concentration time in minutes or time from beginning of runoff and the interest area);* ***Lag-time*** *= time between centroid of rainfall excess and the centroid of direct runoff = 60% of the concentration time in minutes; lag time is evaluated by Kirpich formulae;* ***CN*** *= Curve number as defined by S.C.S (1986) method.*

[1)] CN=79.9 derived from Fig. A5.4.1A *for hydrologic soils groups B=17% and C=83% districts 1333m^2 lots size 0.17x72 +.83x81=12.24+67.23*

[2] CN=78.2 derived from Fig. A5.4.1A *for hydrologic soils groups B=25% and C=75% districts 1333m^2 lots size 0.25x72+.75x81=18+60.75*

[3)] CN=70 derived from Fig. A5.4.1A *for hydrologic soils groups B=90% and C=10% and fair condition of grass cover 0.90x69+.10x79=62.1+7.9*

[4)] CN=71.4 derived from Fig. A5.4.1A *for hydrologic soils groups B=75% and C=25% and fair condition of grass cover 0.75x69+.25x79=51.75+19.75*

[5)]CN=68 derived from Fig. A5.4.1A *for hydrologic soils groups B=45% and C=55% and good condition of grass cover 0.45x61+.55x74=27.45+40.7*

[6)] CN=70.5 derived from Fig. A5.4.1A *for hydrologic soils groups B=85% and C=15% and fair condition of grass cover 0.85x69+.15x79=58.65+11.85*

Concentration time and Lag-time evaluation for Barreal basin.

Concentration time and Lag-time results are presented below (See A5.4.4.2)

Sub-basin	Length (meters)	Slope (%)	Tc (min)	Lag-time (minutes)
SbCLA2	2636	0.005	62.0	37.0
SbCLA1	5495	0.005	102.0	61.0
SbCL3a	4469	0.006	87.0	52.0
SbCL3b	4056	0.0105	85.0	57.0
SbCL3c	6219	0.0068	47.0	28.0
SbCL2	6219	0.0068	100.0	60.0
SbCL1	6869	0.0124	90.0	54.0
SbCL4	8364	0.0096	120.0	72.0
SbCLBW	4031	0.006	80.0	48.0
SbCLBE	3877	0.0036	100.0	60.0
SbCLCW	4671	0.0075	82.0	49.0
SbCLCE	593	0.0034	22.0	13.0
SbCLDW	3669	0.006	67.0	40.0
SbCLDE	2311	0.0035	95.0	57.0
SbCL5	8809	0.0091	123.0	74.0
SbCLFW	6219	0.0068	100.0	60.0
SbCLEW	3360	0.0036	83.0	50.0
SbCLEE	3925	0.0025	107.0	64.0
SbCLGW	7121	0.0105	62.0	37.0
SbCLG1	7030	0.0102	100.0	60.0
SbCLGE	4031	0.006	100.0	60.0
SbCLH2	8120	0.01	113.0	68.0
SbCLH1	4510	0.01	72.0	43.0

Figure A5.4.4.2 Shows the results of the Concentration time as well as the Lag-time for the sub-basin located within the Barreal basin. Source of method for these calculations: Kirpich (1940 in: Loukas and Quick, 1995).

APPENDIX 5.4.5

(CN) Curve Number and Hydrologic parameters of Airport basin.

Values of CN for Airport basin were evaluated following similar methodology to the previous Basins allocated on the study area that was defined by SCS (1986) method (*Fig.* A5.4.1A) of this chapter. However, CN values are integrated together with the Physiographic and hydrologic parameters associated with Airport Basin and in the lower part of the Figure are explained (See Fig. A5.4.5.1)

Basin	Sub-basin	Physiographic and hydrologic Parameters						Results	
Num.	Name	Area km^2	CN	I.S (%)	(Ia)	(Tc) min	L.T 0.6*Tc min	Peak Disch. m^3s^{-1}	Storage Volume m^3
5.4.1 *1)*	Sb1a	6.1611	83.3	90	0.2	58.0	35.0	88.9	303,100
5.4.2 *1)*	SB2a	0.6760	83.3	90	0.2	33.0	20.0	13.1	35,500
5.4.3 *1)*	Sb2b	5.9500	83.3	90	0.2	85.0	51.0	66.0	246,600
5.4.4 *1)*	Sb3a	3.1205	83.3	90	0.2	33.0	20.0	60.4	164,000
5.4.5 *3)*	Sb4a	4.9080	79.9	70	0.2	43.0	26.0	73.4	223,600
5.4.5 *3)*	Sb4b	1.9580	79.9	80	0.2	22.0	13.0	41.3	97,000
5.4.6 *1)*	Sb4c	0.5260	81.6	80	0.2	27.0	16.0	10.5	26,200
5.4.6 *1)*	Sb4d	1.9250	83.3	90	0.2	42.0	25.0	33.5	99,900
5.4.6 *2)*	Sb4e	4.3710	81.6	80	0.2	40.0	24.0	73.4	214,700
5.4.6 *2)*	Sb4f	0.8640	81.6	80	0.2	12.0	7.0	21.3	43,100
5.4.3 *2)*	Sb5a	1.8130	81.6	80	0.2	25.0	15.0	37.1	90,300
5.4.8 *3)*	Sb6a	4.9080	79.9	60	0.2	47.0	28.0	71.2	221,700
5.4.9 *4)*	Sb7a	0.5430	78.2	60	0.2	17.0	10.0	10.9	23,300
5.4.10 *5)*	Sb8a	0.6180	76.5	50	0.2	13.0	8.0	11.8	24,200
5.4.11 *6)*	Sb9a	1.7970	74.8	40	0.2	47.0	28.0	19.8	61,300
5.4.12 *6)*	Sb10a	4.0000	74.8	40	0.2	57.0	34.0	39.3	131,500
5.4.13 *7)*	Sb11a	0.4890	73.1	30	0.2	82.0	49.0	3.3	12,000
5.4.14 *7)*	Sb12a	5.7130	73.1	30	0.2	67.0	40.0	44.8	156,600
5.4.15 *8)*	Sb13a	1.7890	71.4	20	0.2	37.0	22.0	17.0	47,200
5.4.16 *8)*	Sb14a	2.0000	71.4	20	0.2	45.0	27.0	17.2	51,900
5.4.17 *8)*	Sb15a	3.1640	71.4	80	0.2	43.0	26.0	49.1	149,600

Figure A5.4.5.1 CN Curve Number and; Physiographic and Hydrologic Parameters used in the application of the CN SCS (1986) also results of peak discharge and storage volume (Airport basin)

I.S *= Impervious surface or surface treated with some type of material or substance in order to modify land use properties (in percentage);* ***Ia*** *= Initial abstraction refers to water losses by evaporation, transpiration, and water retained on little terrain depressions, the method considers 20% of the (hyetograph) rainfall model;* ***Tc*** *= Concentration time in minutes or time from beginning of runoff and the interest area);* ***Lag-time*** *= time between centroid of rainfall excess and the centroid of direct runoff = 60% of the concentration time in minutes; lag time is evaluated by Kirpich formulae;* ***CN*** *= Curve number as defined by S.C.S (1986) method.*

[1] CN=83.3 derived from Fig. A5.4.1A *for of hydrologic soil group C=100% and districts lots size 1000 m^2 (85%) and dust pervious areas 15% = 0.85x83 +0.15X87 =70.55+13.05*
[2] CN=81.6 derived from Fig. A5.4.1A *for of hydrologic soil group C=100% and districts lots size 1333 m^2 (90%) and dust pervious areas 10% = 0.90x81 +0.10X87 =72.9+8.7*
[3] CN=79.9 derived from Fig. A5.4.1A *for hydrologic soil groups B=42% and C=58% and districts lots size 1000 m^2 = 0.42x75 +0.58X83 =31.5+48.14*
[4] CN=78.2 derived from Fig. A5.4.1A *for hydrologic soil groups B=60% and C=40% and districts lots size 1000 m^2 = 0.60x75 +0.40X83 =45+33.2*
[5] CN=76.5 derived from Fig. A5.4.1A *for hydrologic soil groups B=70% and C=30% and districts lots size 1000 m^2 = 0.75x75 +0.25X83 =56.25+20.75*
[6] CN=74.8 derived from Fig. A5.4.1A *for hydrologic soil group B=100% and districts lots size 1000 m^2*
[7] CN=73.1 derived from Fig. A5.4.1A *for hydrologic soil groups B=87% and C=13% and districts lots size 1333 m^2 = 0.87x72+0.13X81 =62.64+10.53*
[8] CN=71.4 derived from Fig. A5.4.1A *for hydrologic soil group B=100 and districts lots size 1333 m^2 (90%)and lots size 2000 m^2 (10%) 0.95x72+0.05X70 =68.4+3.5*

5.3.4.5 Concentration time and Lag-time evaluation for Airport basin.

Concentration time and Lag-time and were assessed with the Kiprich's equation: $Tc= 0.000325[L/Ss^{0.5}]^{0.77}$ where Tc=concentration time in hours; L=length of the stream in meters; Ss=gradient of the main stream. Main stream length was evaluated with Auto-Cad and Arc-Map programs. (see results in Fig. A5.4.5.2). Physiographic and hydrologic parameters as: (A) area; (Is) Impervious surface; (Ia) Initial abstraction are parameters also needed for HEC-HMS flooding simulation and are presented in (Fig. A5.4.5.2).

Sub-basin	Length (meters)	Slope (%)	Tc (min)	Lag-time (minutes)
Sb1a	4,058.0	0.0136	58.0	35.0
SB2a	1,496.0	0.0103	33.0	20.0
Sb2b	5,650.0	0.0103	85.0	51.0
Sb3a	1,880.0	0.0128	33.0	20.0
Sb4a	1,450.0	0.0083	43.0	26.0
Sb4b	1,000.0	0.0104	22.0	13.0
Sb4c	2,500.0	0.0118	27.0	16.0
Sb4d	3,000.0	0.0212	42.0	25.0
Sb4e	700.0	0.0029	40.0	24.0

Sb4f	600.0	0.0200	12.0	7.0
Sb5a	1,550.0	0.0016	25.0	15.0
Sb6a	4,100.0	0.0256	47.0	28.0
Sb7a	900.0	0.0175	17.0	10.0
Sb8a	600.0	0.0150	13.0	8.0
Sb9a	3,000.0	0.0136	47.0	28.0
Sb10a	4,000.0	0.0146	57.0	34.0
Sb11a	4,500.0	0.0135	82.0	49.0
Sb12a	4,714.0	0.0135	67.0	40.0
Sb13a	2,255.0	0.0135	37.0	22.0
Sb14a	3,062.0	0.0135	45.0	27.0
Sb15a	2,825.0	0.0135	43.0	26.0

Figure. A5.4.5.2 Concentation time and lag-time using Kirpich formulae for the Airport Basin. Source of the method for calculations: Kirpich (1940 in: Loukas and Quick, 1995)

APPENDIX 5.4.6

(CN) Curve Number and hydrologic parameters Bravo River basin.

Values of CN for Airport basin were evaluated following similar methodology to the previous Basins allocated on the study area that was defined by SCS (1986) method (Fig. A5.4.1A) of this chapter. However, in Fig. A5.4.6.1 are given the CN values are integrated together with the Physiographic and hydrologic parameters associated with Airport Basin and in the lower part of the Figure are explained.

Basin	Sub-basin	Physiographic and hydrologic Parameters						Results	
Num.	Name	Area km^2	CN	I.S.(%)	(Ia)	(Tc) min	L.T= 0.6*Tc min	P.D. m^3s^{-1}	Storage Volume m^3
5.8.1 1)	SbBR.1	5.5000	85.0	100	0.2	85.0	51.0	64.1	295,000
5.8.2 1)	SbBR.2	2.5600	85.0	100	0.2	85.0	51.0	29.9	137,300
5.8.3 1)	SbBR.3	2.7900	85.0	100	0.2	75.0	45.0	35.8	152,000
5.8.4 1)	SbBR.4	2.2400	85.0	100	0.2	37.0	22.0	43.2	124,300
5.8.5 2)	SbBR.5	6.6480	81.6	90	0.2	65.0	38.0	90.9	347,600
5.8.6 2)	SbBR.6	6.6500	81.6	80	0.2	65.0	38.0	86.1	329,000
5.8.7 3)	SbBR.7	3.2600	79.9	90	0.2	49.0	29.0	52.3	171,700
5.8.9 4)	SbBR.8	3.6800	74.8	80	0.2	52.0	31.0	52.4	179,100
5.8.8 5)	SbBR.9	5.0200	76.5	76.5	0.2	82.0	49.0	52.2	233,400
5.8.10 4)	SbBR.10	20.6700	74.8	50	0.2	85.0	51.0	168.5	770,000

Figure A5.4.6.1 Physiographic and Hydrologic Parameters used in the application of CN method SCS (1986) of USA also results of peak discharge and storage water of the Bravo River basin

1) CN=85 derived from Fig. 1A for Impervious paved areas two types of hydrologic soils group B=30% and C=70% and districts 1000 m2 soil type C CN = 0.7X83 + 0.3X89= 58.1+26.7

2) CN=81.6 derived from Fig. A5.4.1A for type of hydrologic soil group C=100% fair condition grass cover (50% to 75%) and Industrial landuse 20 % CN = 0.80X79 + 0.20x91 =63.2+18.2

3) CN=79.9 derived from A5.4.1A for type of hydrologic soil group C=100% fair condition grass cover (50% to 75%) and Industrial landuse 25 % CN = 0.85X79 + 0.15x91 =67.15+13.65

4) CN=74.8 derived from A5.4.1A for type of hydrologic soil group C=100% good condition grass cover (>75%) and Industrial landuse 10 % CN = 0.95X74 + 0.05x91 =70.3+4.5

5) CN=76.5 derived from A5.4.1A for type of hydrologic soil group C=100% good condition grass cover (>75%) dust impervious areas 20 % CN = 0.8X74 + 0.105) x87 =59.2+8.7

Concentration time and Lag-time evaluation for Bravo River basin.

Concentration time and Lag-time were assessed using the Kiprich's equation: $Tc= 0.000325[L/Ss^{0.5}]^{0.77}$ where Tc=concentration time in hours; L=length of the stream in meters; Ss=gradient of the main stream. Main stream length was evaluated with Auto-Cad and Arc-Map programs. (See Fig. A5.4.1.1). Physiographic and hydrologic parameters as: (A) area; (Is) Impervious surface; (Ia) Initial abstraction are parameters also needed for HEC-HMS flooding simulation and are presented in Fig. A5.4.6.2

Sub-basin	Length (meters)	Slope (%)	Tc (min)	Lag-time (minutes)
SbBR.1	,393.0	0.0040	85.0	51.0
SbBR.2	2,592.0	0.0025	85.0	51.0
SbBR.3	2,533.0	0.0030	75.0	45.0
SbBR.4	1,133.0	0.0035	37.0	22.0
SbBR.5	2,320.0	0.0035	65.0	38.0
SbBR.6	1,625.0	0.0018	65.0	38.0
SbBR.7	10,3000	0.0005	49.0	29.0
SbBR.8	2,280.0	0.0070	52.0	31.0
SbBR.9	1,860.0	0.0013	82.0	49.0
SbBR.10	3,425.0	0.0045	85.0	51.0

Figure A5.4.6.2 Shows the results of the Concentration time as well as the Lag-time for the sub-basin located within the Bravo River basin. Source of the method for calculations: Kirpich (1940 in: Loukas and Quick, 1995)

APPENDIX 5.4.7

(CN) Curve Number and hydrologic parameters for Acequias basin.

Values of CN for Acequias basin were evaluated following similar methodology to the previous basins allocated on the study area that was defined by SCS (1986) method and illustrated in (Fig. A5.4.1A). However, in Fig. A5.4.7.1are given the CN values are integrated together with the Physiographic and hydrologic parameters associated with Airport basin and in the lower part of the Figure are explained.

Acequias Basin									
Basin	**Sub-basin**	**Physiographic and hydrologic Parameters**						**Results**	
Num.	**Name**	**Area km^2**	**CN**	**I.S (%)**	**(Ia)**	**(Tc) min**	**L. T 0.6*Tc min**	**Peak Disch m^{3}s^{-1}**	**Storage Volume m^3**
5.6.1[1)]	SbAE1	3.8810	85.0	90	0.2	85.0	51.0	43.2	198,800
5.6.2[1)]	SbAE2	4.0120	85.0	100	0.2	140.0	84.0	30.9	179,400
5.6.3[1)]	SbAE3	3.858	85.0	90	0.2	112	67.0	34.5	184500
5.6.4[1)]	SbAE4	6.9410	85.0	90	0.2	138	83	51.6	298,500
5.6.5[2)]	SbAE5	2.1090	81.6	90	0.2	82.0	49.0	24.1	108,000
5.6.6[3)]	SbAE6	4.8230	76.5	75	0.2	103.0	62.0	34.5	211300
		28.7070							

Figure A5.4.7.1. Physiographic and Hydrologic Parameters used in the application of the CN of tne NRCS of USA Method also results of peak discharge and storage volume obtained

[1)] CN=85 derived from Fig. A5.4.1A *for hydrologic soil group B=100% and residential districts with less than 500 m^2 lote size; CN = 85*
[2)] CN=81.6 derived from Fig. A5.4.1A *for hydrologic soil type C=100%, residential districts from 500 m^2 (60%) and residential districts from 1000 m^2 (40%) 0.45x83 +0.55x81 = 37.35+44.55*
[3)] CN=76.5 derived from Fig. A5.4.1A *for hydrologic soil type C=100%, residential districts from 500 m^2 (60%) and residential districts from 1000 m^2 (40%) 0.40x83 +0.60x81 = 33.2+48.*

Concentration time and Lag-time evaluation for Acequias basin.

Concentration time and Lag-time were assessed with the Kiprich's equation: $Tc= 0.000325[L/Ss^{0.5}]^{0.77}$ where Tc=concentration time in hours; L=length of the stream in meters; Ss=gradient of the main stream. Main stream length was evaluated with Auto-Cad and Arc-Map programs. Physiographic and hydrologic parameters as: (A) area; (Is) Impervious surface; (Ia) Initial abstraction are parameters also needed for HEC-HMS flooding simulation and are presented in Fig. A5.4.7.2

Sub-basin	Length (meters)	Slope (%)	Tc (min)	Lag-time (minutes)
SbAE1	2,750.0	0.0025	85.0	51.0
SbAE2	3,100.0	0.0009	140.0	84.0
SbAE3	2,876.0	0.0012	112.0	67.0
SbAE4	2,876.0	0.0013	112.0	67.0
SbAE5	2,600.0	0.0026	82.0	49.0
SbAE6	2,910.0	0.0065	103.0	2.0

Figure A5.4.7.2. Shows the results of the Concentration time as well as the Lag-time for the sub-basin located within the Acequias Basin.

APPENDIX 5.4.8

(CN) Curve Number and Hydrologyc parameters Chamizal basin.

Values of CN for Chamizal basin were evaluated following similar methodology to the previous basins allocated on the study area that was defined by SCS (1986) model method (Fig. A5.4.1A) of this chapter. However, in Fig. A5.4.8.1 are given the CN values are integrated together with the Physiographic and hydrologic parameters associated with Airport basin and in the lower part of the Figure are explained.

Figure 1 Physiographic and Hydrologic Parameters used in the application of the SCS (1986) of USA method also results of peak discharge and storage (Chamizal basin)

Basin	**Sub-basin**	**Physiographic and hydrologic Parameters**						**Results**	
Num.	**Name**	**Area km^2**	**CN**	**I.S (%)**	**(Ia)**	**(Tc) min**	**L. T 0.6*Tc min**	**Peak Disch m^{3}s^{-1}**	**Storage Volume m^3**
5.7.1[1]	SbBRAM1	1.1940	81.6	90	0.2	73.0	44.0	14.8	53,800
5.7.2[2]	SbBRAM2	3.6730	76.5	50	0.2	73.0	44.0	33.9	122,400
5.7.3[3]	SbBRAM3	1.1910	73.1	50	0.2	57.0	34.0	12.6	42,300

6.0580

[3)]CN=73.1 derived from Fig. 1A two conditions parks areas (45%) with good condition (grass cover >75%) soil B and soil C (55%) and districts 1000 m^2 (0.45x61=27.45) + (0.55x83=45.65)

[1)] CN=81.6 derived from Fig. A5.4.1A for two conditions parks (30%) with grass cover (more 50%) and soil C and residential districts (70%) more than 1000 m^2 CN = 0.3X79+ 0.7X83=23.7+58.1

[2)] CN=76.5 derived from Fig. A5.4.1A two conditions parks areas (30%) with good condition (grass cover >75%) soil B and soil C (70%) and districts 1000 m^2 (0.30x61=18.3) + (0.70x83=58.1)

Figure A5.4.8.1. Physiographic and Hydrologic Parameters used in the application of the SCS (1986) of USA method also results of peak discharge and storage (Chamizal basin).

Concentration time and Lag-time evaluation for the Chamizal basin.

Concentration time and Lag-time were assessed using Kiprich's equation: $Tc= 0.000325[L/Ss^{0.5}]^{0.77}$ where Tc=concentration time in hours; L=length of the stream in meters; Ss=gradient of the main stream. Main stream length was evaluated with Auto-Cad and Arc-Map programs. Physiographic and hydrologic parameters as: (A) area; (Is) Impervious surface; (Ia) Initial abstraction are parameters also needed for HEC-HMS flooding model and are presented in (Fig. A5.4.8.2.).

Sub-basin	Length (m.)	Slope (%)	Tc (min)	Lag-time (minutes)
SbBRAM1	2,272.0	0.0022	73.0	44.0
SbBRAM2	2,380.0	0.0027	73.0	44.0
SbBRAM3	1,800.0	0.0030	7.0	34.0

Figure A5.4.8.2. Shows the results of the Concentration time as well as the Lag-time

APPENDIX 6A

Chapter 6 section 6.3.2 details the HEC-RAS flooding hazard model which requires transference zones where discharges must be routed along many sub-basins and reaches. Then, due to the extensive descriptions required to explain the resulted stream models the present appendix is needed. Thus, the purpose of this appendix is to simplify the chapter 6.

The first sector 1 or transference zone which corresponds to Anapra was already explained in chapter 6 (See Fig. 6.5). The remaining transference zones are presented in the following paragraphs.

Firstly, three main streams which integrate transference zones of Anapra basin are formed by: (M1, Fig. 6A.1; SW1, Fig 6A.2 and Snakes, Fig. 6A.3) and the discharges assigned to these transference reach zones derived from HEC-HMS (See Figs. 6.3 to 6.5 of results Chapter 6)

Transference reach zones for sector 1 of Center Basin (See Fig. 6A.4) were defined similarly to Anapra Basin as: (FV1, Fig. 6A.4; FV2, Fig. 6A.5; Sb1C, Fig. 6A.6; Firstone test, Fig. 6A.7; Sb3C, Fig. 6A.8; 4BC, Fig. 6A.9; 5C11, Fig. 6A.10; Sb8C,Fig. 6A.11; Jc8, Fig. 6A.12 and GI, Fig. 6A.13). The discharge values assigned to these transference reaches were derived by HEC-HMS (See points green colour of Fig. 6.1 and green colour box of Fig. 6.3, Chapter 6).

Transference reach zones of sector 2 of Center Basin were defined similarly Anapra Basin (See Fig. 6A.15). This transference zone has eight streams: (CS, Fig. 6A.16; S^{nd}, Fig. 6A.17; Three, Fig. 6A.18; Four, Fig. 6A.19; Five CS, Fig. 6A.20; Six CS, Fig. 6A.21; Seven CS, Fig. 6A.22 and Eigth CS, Fig. 6A.23). The discharge values assigned to these transference reaches zones was derived by HEC-HMS (See blue colour points of Fig. 6.2 and blue colour box of Fig. 6.4 chapter 6). In order to connect these sub-basins with the main reach drivers from upstream to downstream areas a fundamental and logic course along the stream should be defined to route the peak discharge obtained by HEC-HMS (2002) computer programs.

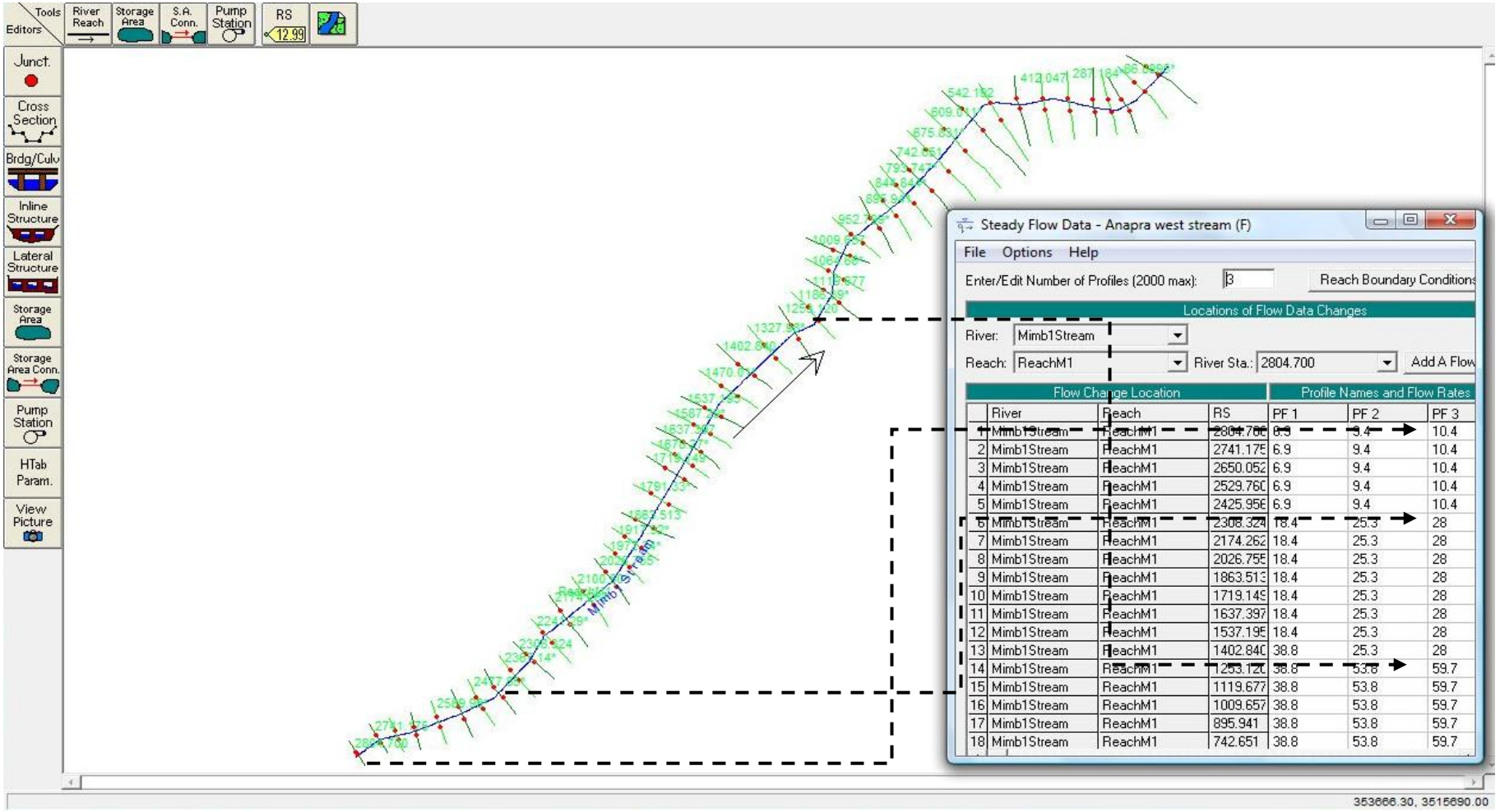

Figure 6A.1. Association and organization of HEC-HMS hydrographs for plans: PF1 to Tr 10 years; PF2 for Tr 50 years and PF3 to Tr 100 years into the HEC-RAS program. This stream driver corresponds to M1 transference reach. Note the dash black line indicate the site of reach location in relation to discharge values given in upper left table Source: Created by David Zúñiga (2012) using HEC-RAS (2002) version 3.1.3.

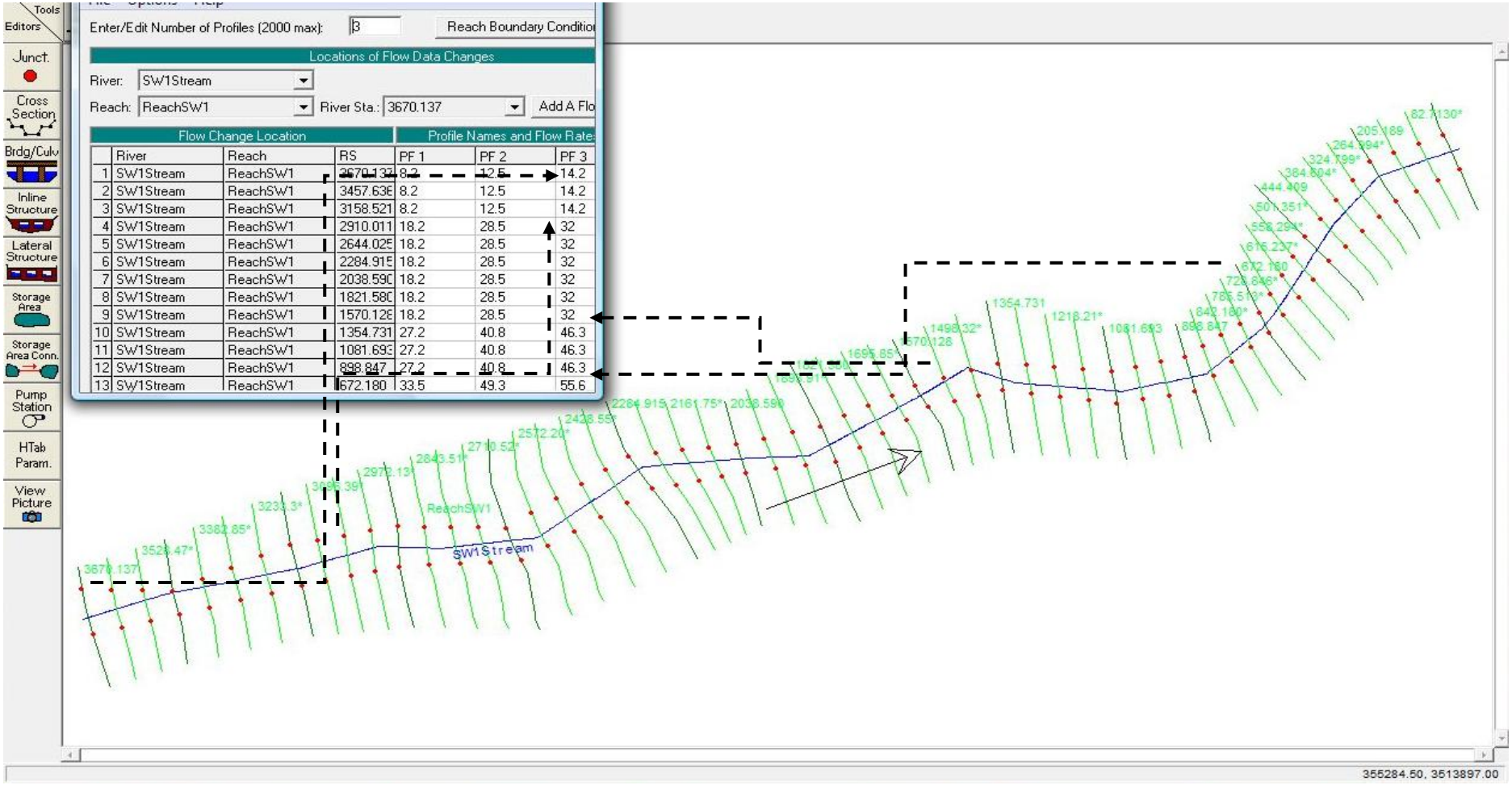

Figure 6A.2. Association and organization of HEC-HMS hydrographs for plans: PF1 to Tr 10 years; PF2 to Tr 50 years and PF3 to Tr 100 years into the HEC-RAS program. Note the dash black line indicate the site of reach location in relation to discharge values given in upper left table This stream driver corresponds to SW1 transference reach. Source: Created by David Zúñiga (2012) using HEC-RAS (2002) version 3.1.3.

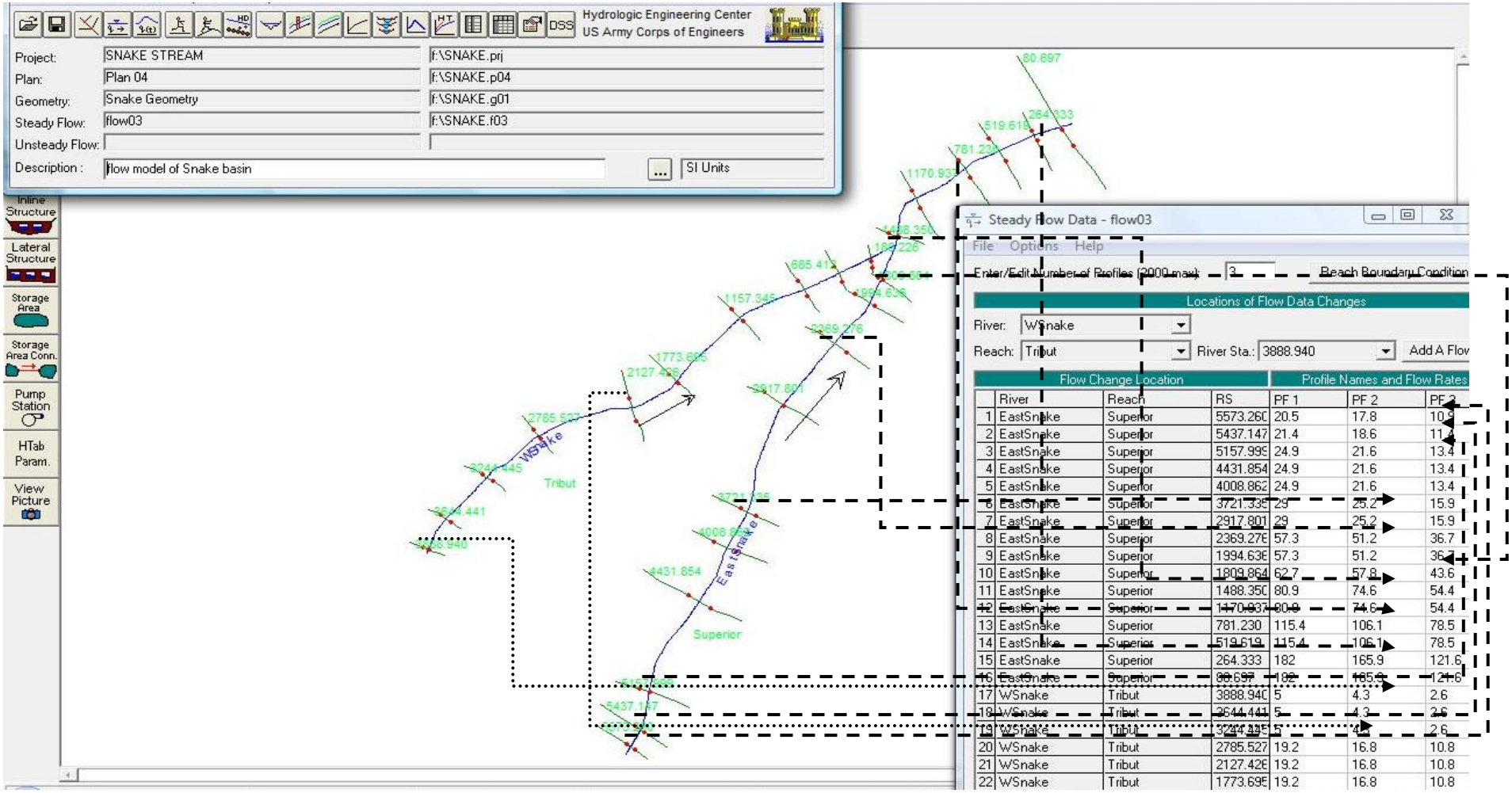

	River	Reach	RS	PF 1	PF 2	PF 3
1	EastSnake	Superior	5573.260	20.5	17.8	10.9
2	EastSnake	Superior	5437.147	21.4	18.6	11.4
3	EastSnake	Superior	5157.999	24.9	21.6	13.4
4	EastSnake	Superior	4431.854	24.9	21.6	13.4
5	EastSnake	Superior	4008.862	24.9	21.6	13.4
6	EastSnake	Superior	3721.335	29	25.2	15.9
7	EastSnake	Superior	2917.801	29	25.2	15.9
8	EastSnake	Superior	2369.276	57.3	51.2	36.7
9	EastSnake	Superior	1994.638	57.3	51.2	36.7
10	EastSnake	Superior	1809.864	62.7	57.8	43.6
11	EastSnake	Superior	1488.350	80.9	74.6	54.4
12	EastSnake	Superior	1470.937	80.9	74.6	54.4
13	EastSnake	Superior	781.230	115.4	106.1	78.5
14	EastSnake	Superior	519.619	115.4	106.1	78.5
15	EastSnake	Superior	264.333	182	165.9	121.6
16	EastSnake	Superior	80.697	182	165.9	121.6
17	WSnake	Tribut	3888.940	5	4.3	2.6
18	WSnake	Tribut	3644.441	5	4.3	2.6
19	WSnake	Tribut	3244.445	5	4.3	2.6
20	WSnake	Tribut	2785.527	19.2	16.8	10.8
21	WSnake	Tribut	2127.426	19.2	16.8	10.8
22	WSnake	Tribut	1773.695	19.2	16.8	10.8

Figure 6A.3. Association and organization of HEC-HMS hydrographs plans PF1 for Tr 10 years; PF2 for Tr 50 years and PF3 for Tr 100 years into the HEC-RAS program. Note the dash black line indicate the site of reach location in relation to discharge values given in upper left table This stream driver corresponds to Snake stream transference reach. Source: Created by David Zúñiga (2012) using HEC-RAS (2002) version 3.1.3.

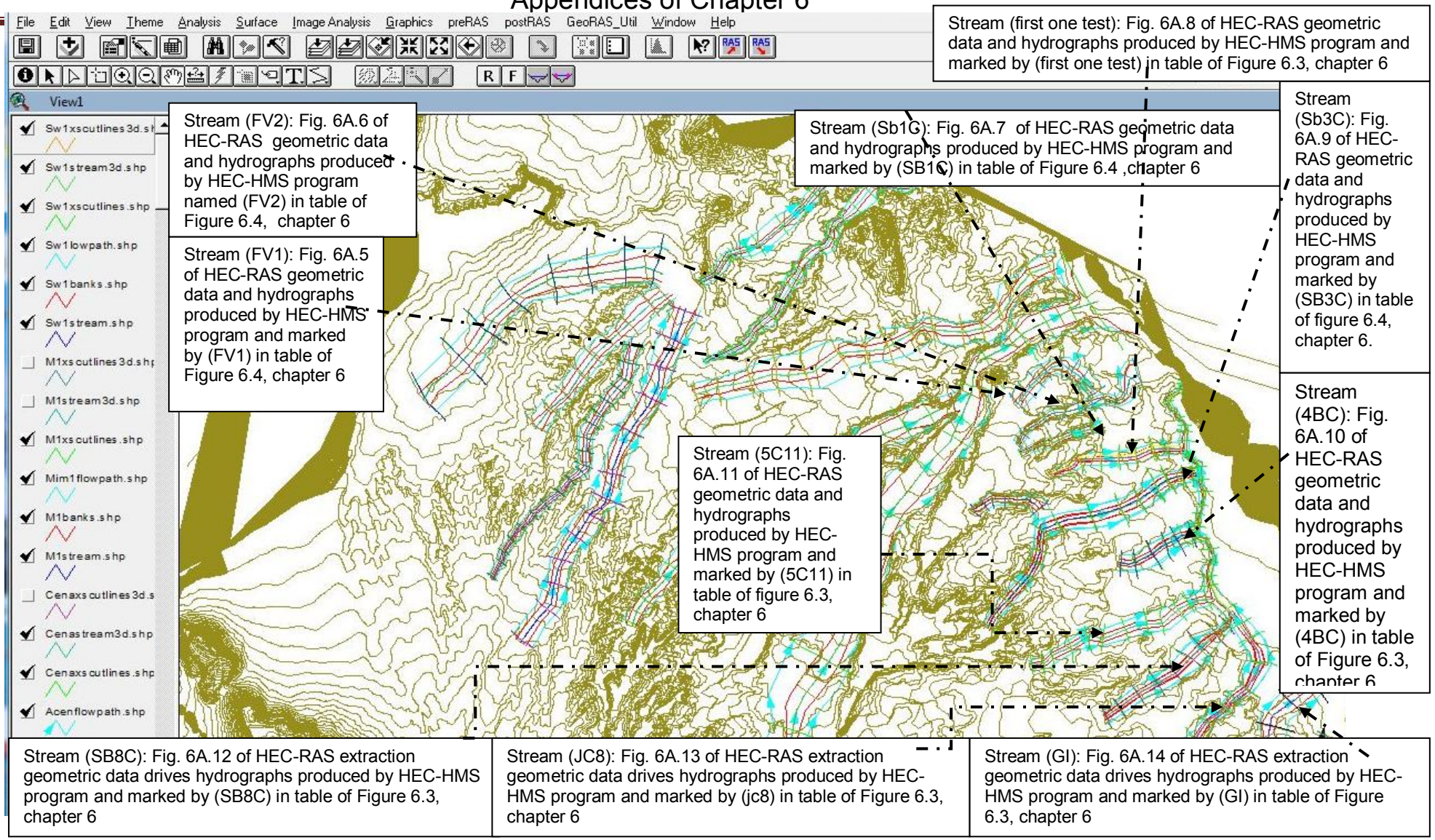

Figure 6A.4 Link between the different transference reaches performed over the DEM during Pre-GeoRAS processor associated flooding profile derived from HEC-HMS (2002) hydrographs and the reaches which would routed the hydrographs (Center sector 1). Source: Created by David Zúñiga using Arc-view 3.2 with HEC-GeoRAS pre-processor and post-processor included as well 3D and spatial extensions.

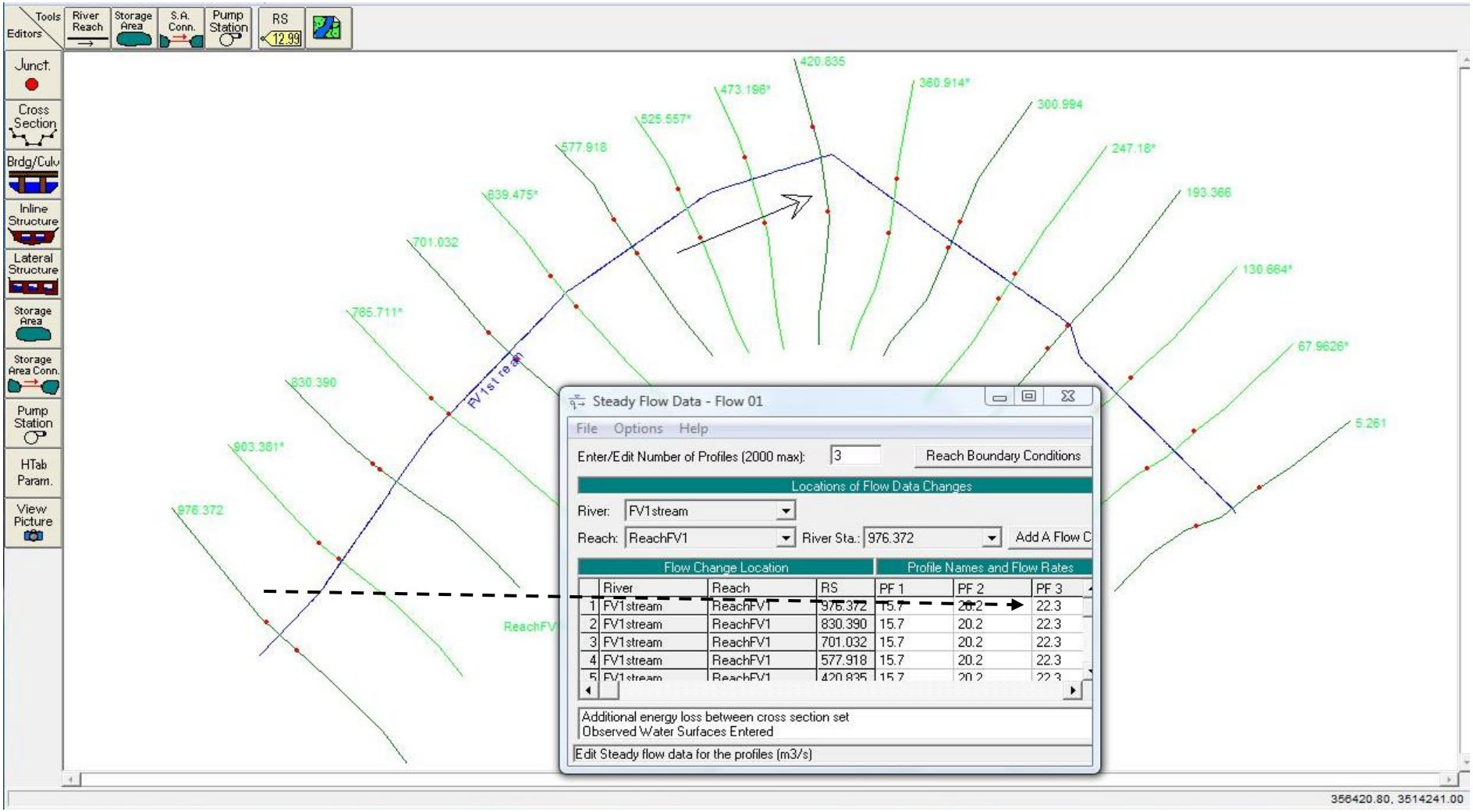

Figure 6A.5. Association and organization of HEC-HMS hydrographs plans. PF1 to Tr 10 years; PF2 to Tr 50 years and PF3 to Tr 100 years into the HEC-RAS program. Note the dash black line indicate the site of reach location in relation to discharge valuesgiven in upper left table these stream drivers correspond to FV1 transference reaches. Source: Created by David Zúñiga using HEC-RAS (2002) version 3.1.3.

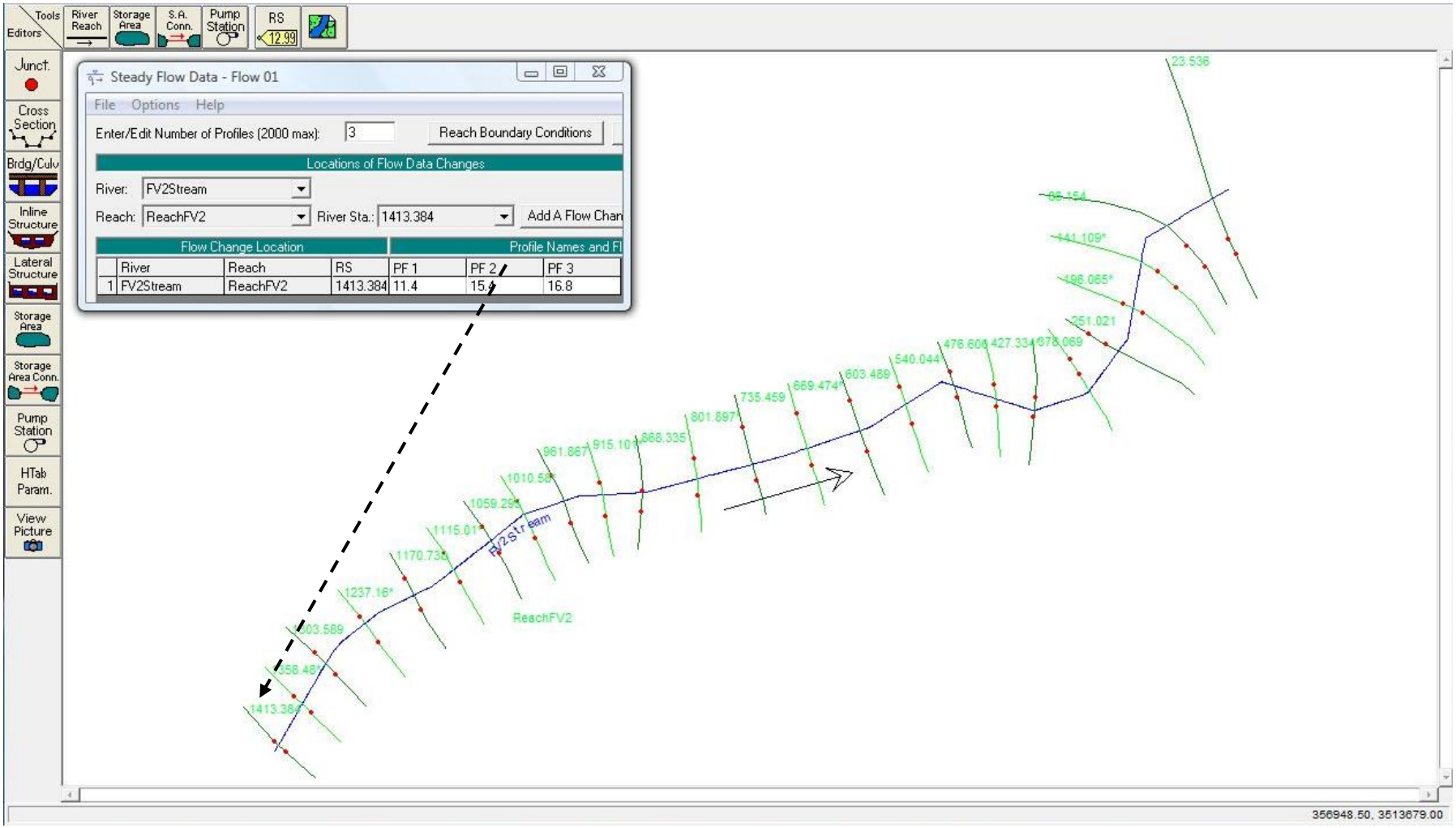

Figure 6A.6. Association and organization of HEC-HMS hydrographs plans: PF1 to Tr 10 years; PF2 to Tr 50 years and PF3 to Tr 100 years into the HEC-RAS program. Note the dash black line indicate the site of reach location in relation to discharge values given in upper left table This stream driver corresponds to FV2 transference reach. Source:Created by David Zúñiga using HEC-RAS (2002) version 3.1.3.

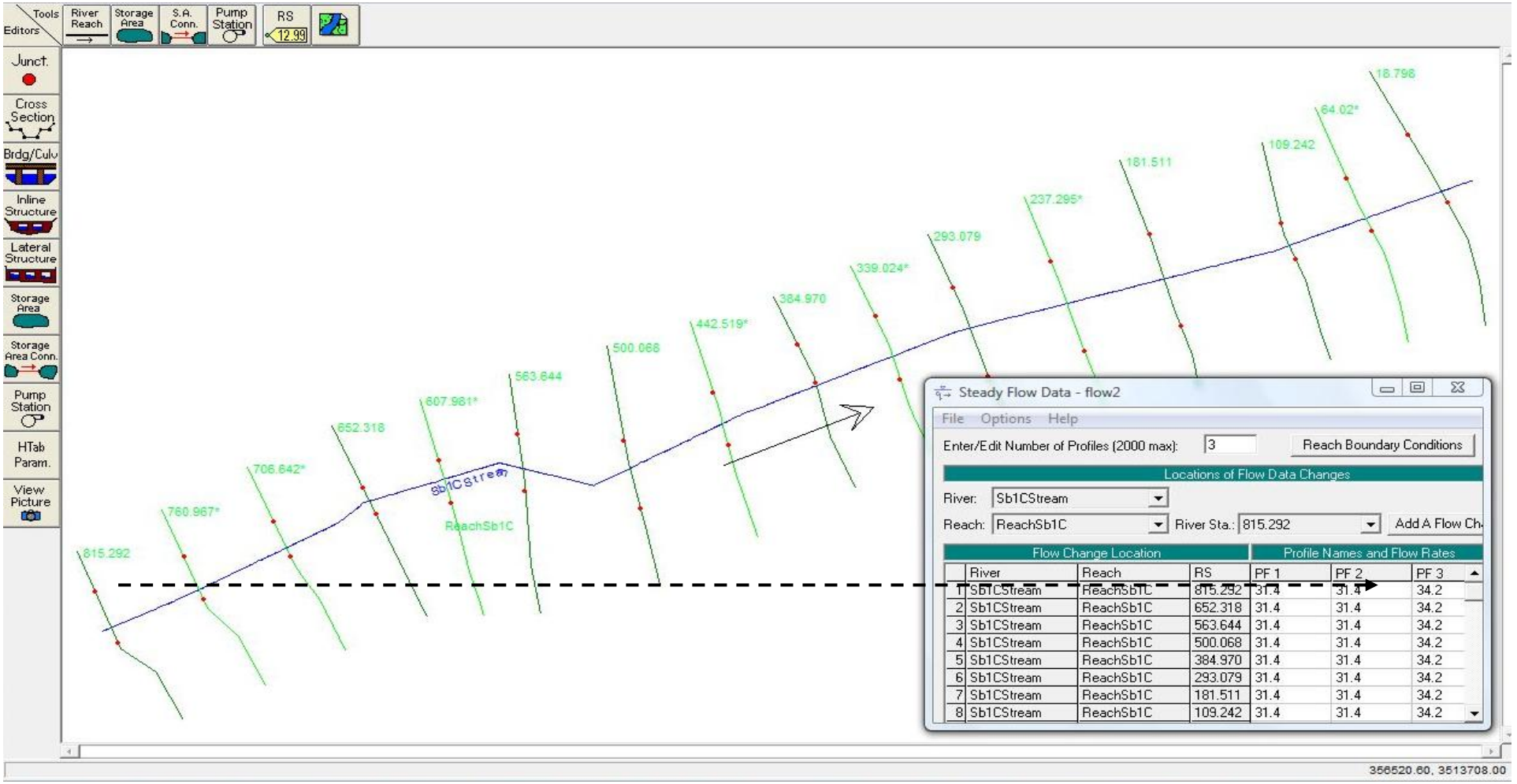

Figure 6A.7. Association and organization of HEC-HM hydrographs plans: PF1 to Tr 10 years; PF2 for Tr 50 years and PF3 to Tr 100 years into the HEC-RAS program. Note the dash black line indicate the site of reach location inrelation to discharge values given in upper left table This stream driver corresponds to Sb1C transference reach. Source: Created by David Zúñiga (2012) using HEC-RAS (2002) version 3.1.3.

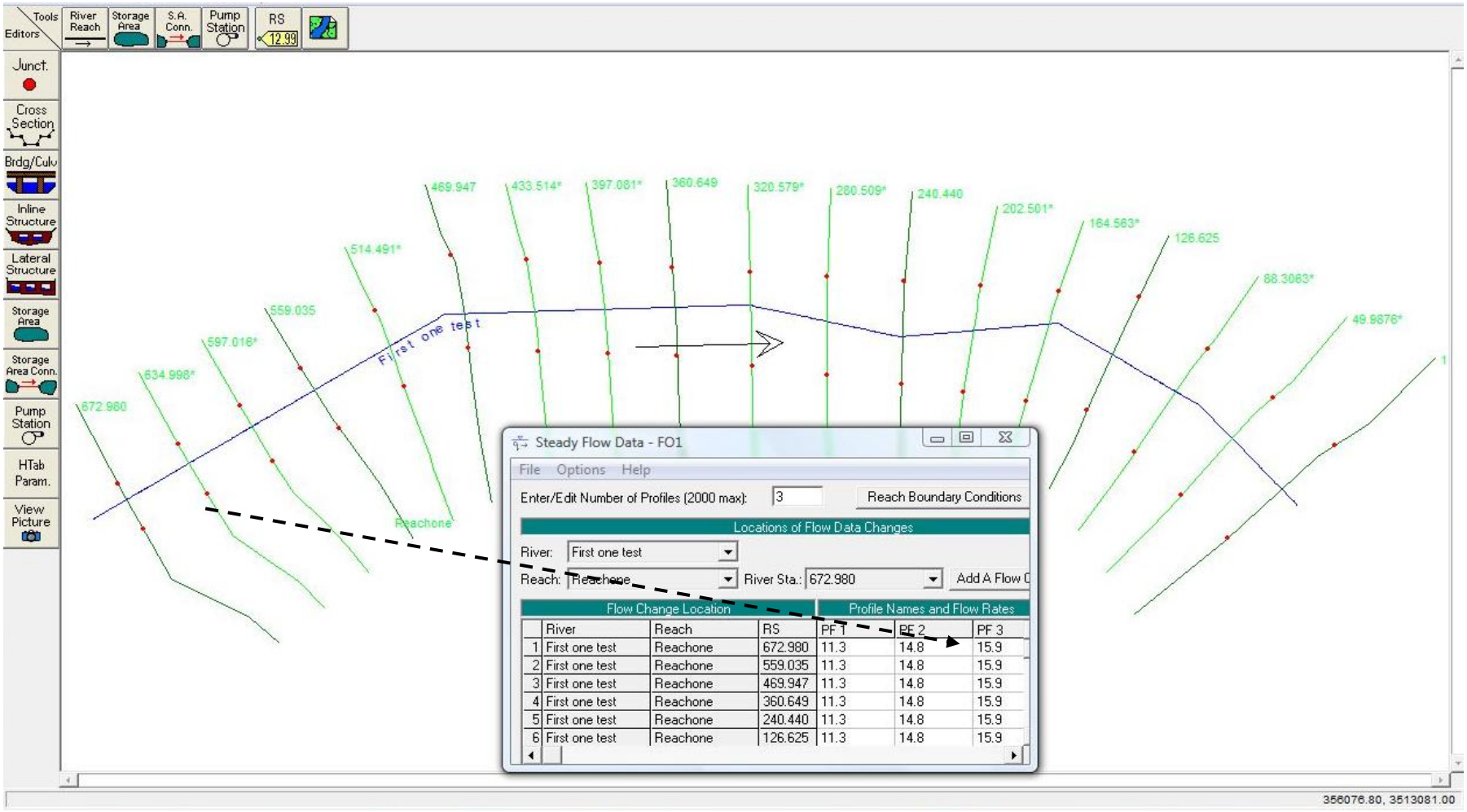

Figure 6A.8. Association and organization of HEC-HMS hydrographs plans: PF1 to Tr 10 years; PF2 toTr 50 years and PF3 to Tr 100 years into the HEC-RAS program. Note the dash black line indicate the site of reach location in relation to discharge values given in upper left table Stream driver corresponds to firstone test transference reach. Source:Created by David Zúñiga (2012) using HEC-RAS (2002) version 3.1.3.

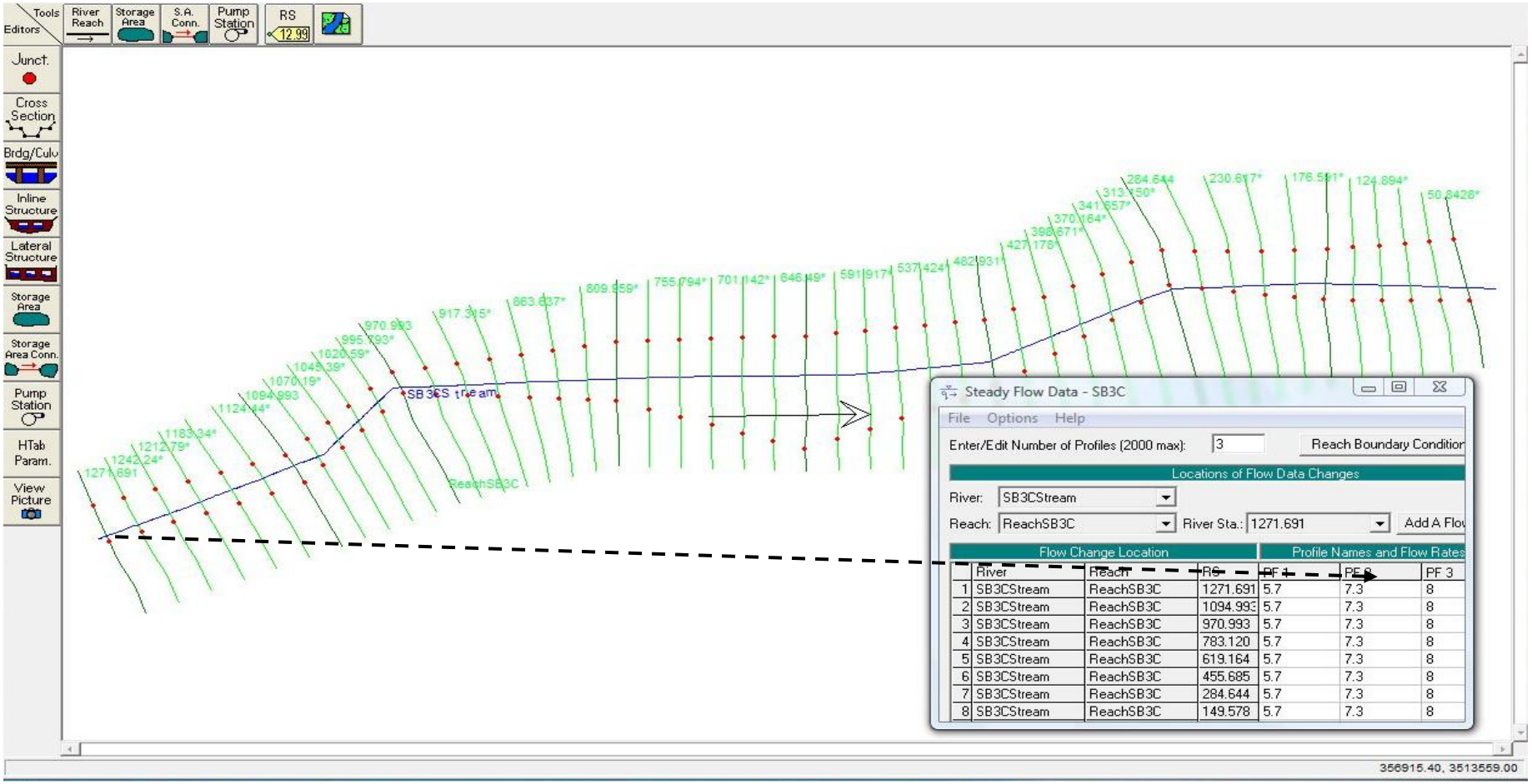

Figure 6A.9. Association and organization of HEC-HMS hydrographs plans: PF1 to Tr 10 years; PF2 to Tr 50 years and PF3 to Tr 100 years into the HEC-RAS program. Note the dash black line indicate the site of reach location in relation to discharge values given in upper left table This stream driver corresponds to SB3C transference reach. Source: Created by David Zúñiga (2012) using HEC-RAS (2002) version 3.1.3.

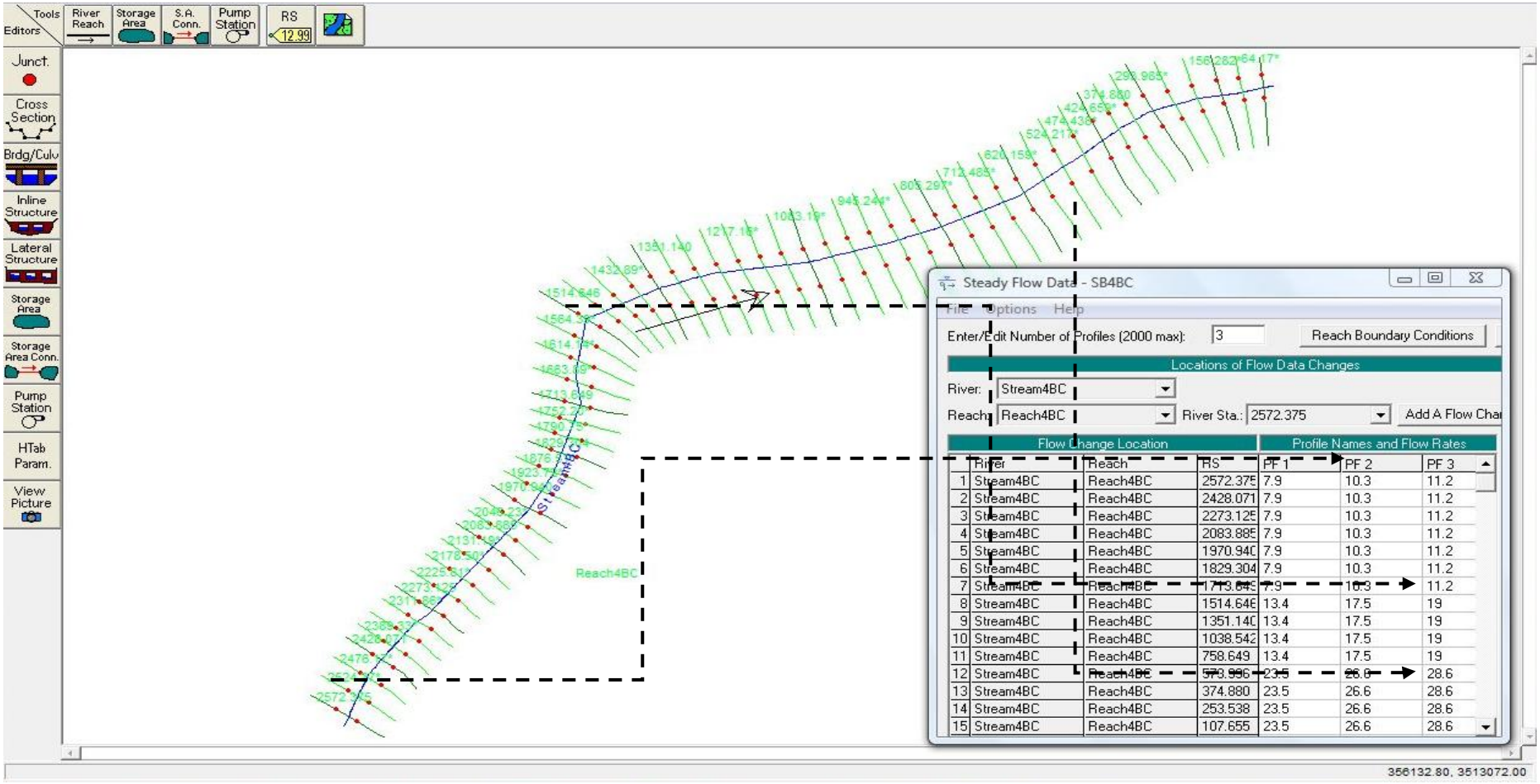

Figure 6A.10. Association and organization of HEC-HMS hydrographs plans: PF1 to Tr 10 years; PF2 to Tr 50 years and PF3 to Tr 100 years into the HEC-RAS program. Note the dash black line indicate the site of reach location in relation to discharge values given in upper left table This stream driver corresponds to 4BC transference reach. Source: Created by David Zúñiga (2012) using HEC-RAS (2002) version 3.1.3.

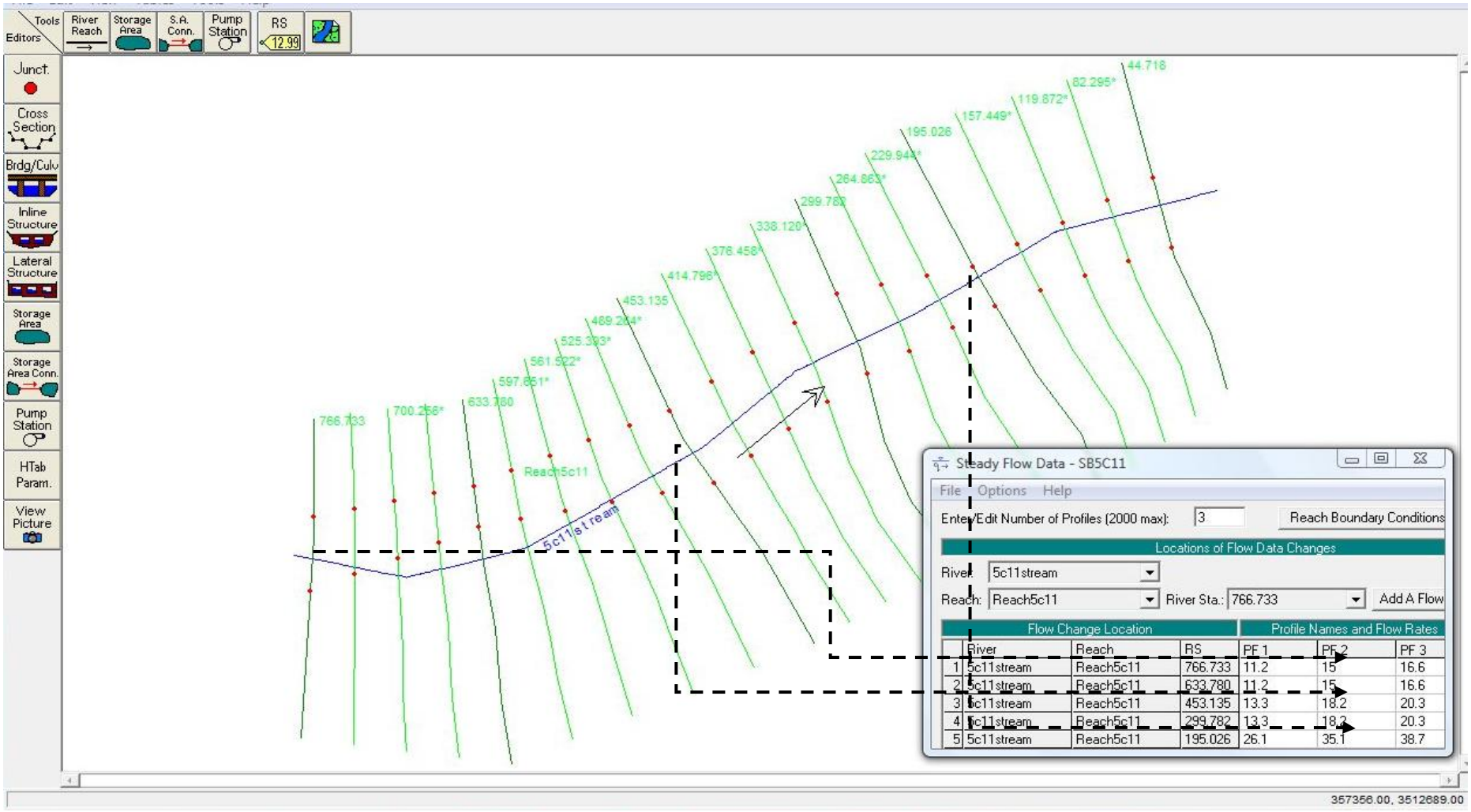

Figure 6A.11. Association and organization of HEC-HMS hydrographs plans: PF1 to Tr 10 years; PF2 to Tr 50 years and PF3 to Tr 100 years into the HEC-RAS program. Note the dash black line indicate the site of reach location in relation to discharge values given in upper left table This stream driver corresponds to 5C11 transference reach. Source: Created by David Zúñiga (2012) using HEC-RAS (2002) version 3.1.3.

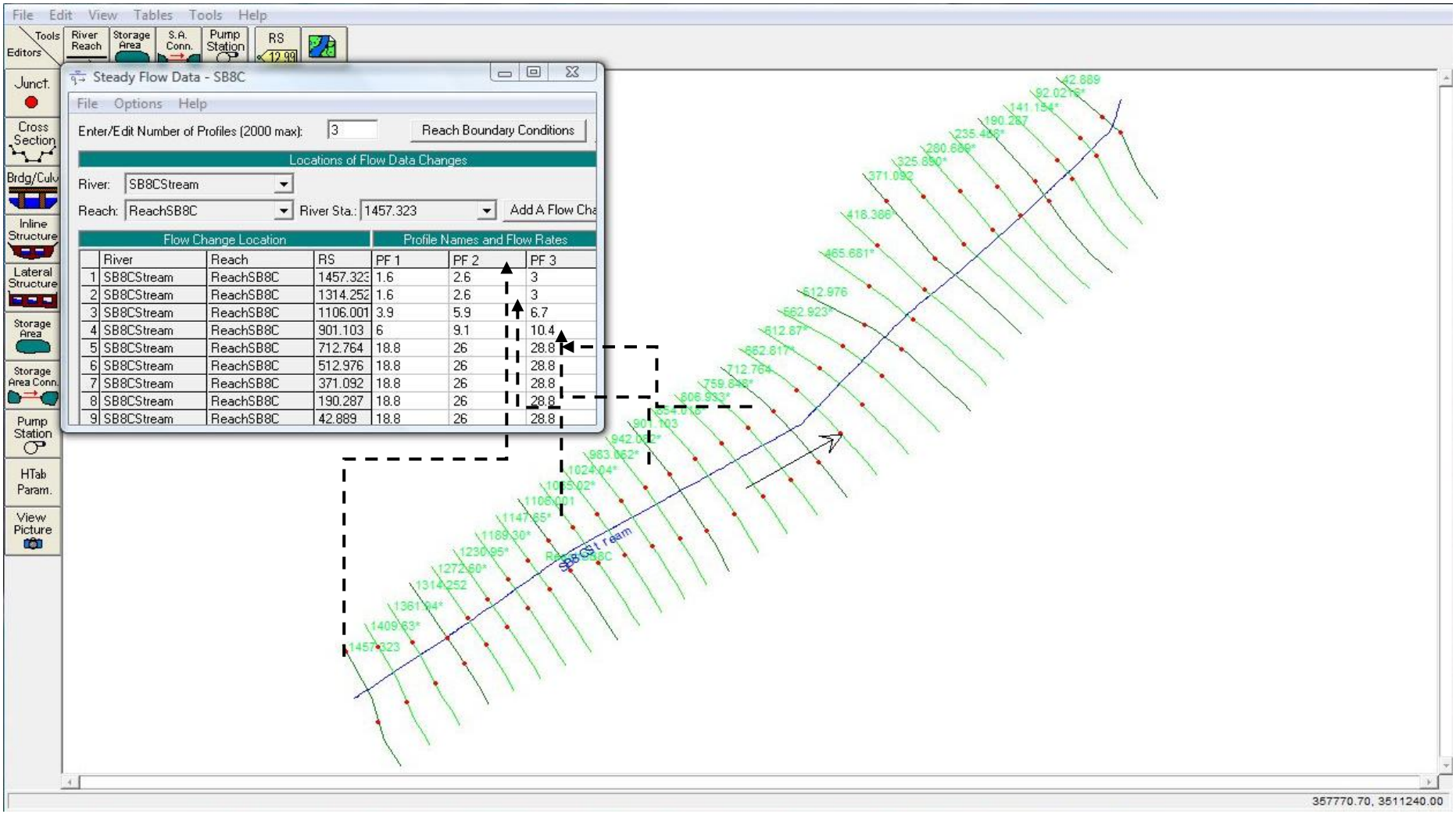

Figure 6A.12. Association and organization of HEC-HMS hydrographs plans: PF1 to Tr 10 years; PF2 to Tr 50 years and PF3 to Tr 100 years into the HEC-RAS program. Note the dash black line indicate the site of reach location in relation to discharge values given in upper left table This stream driver corresponds to SB8C transference reach. Source Created by David Zúñiga (2012) HEC-RAS (2002) version 3.1.3.

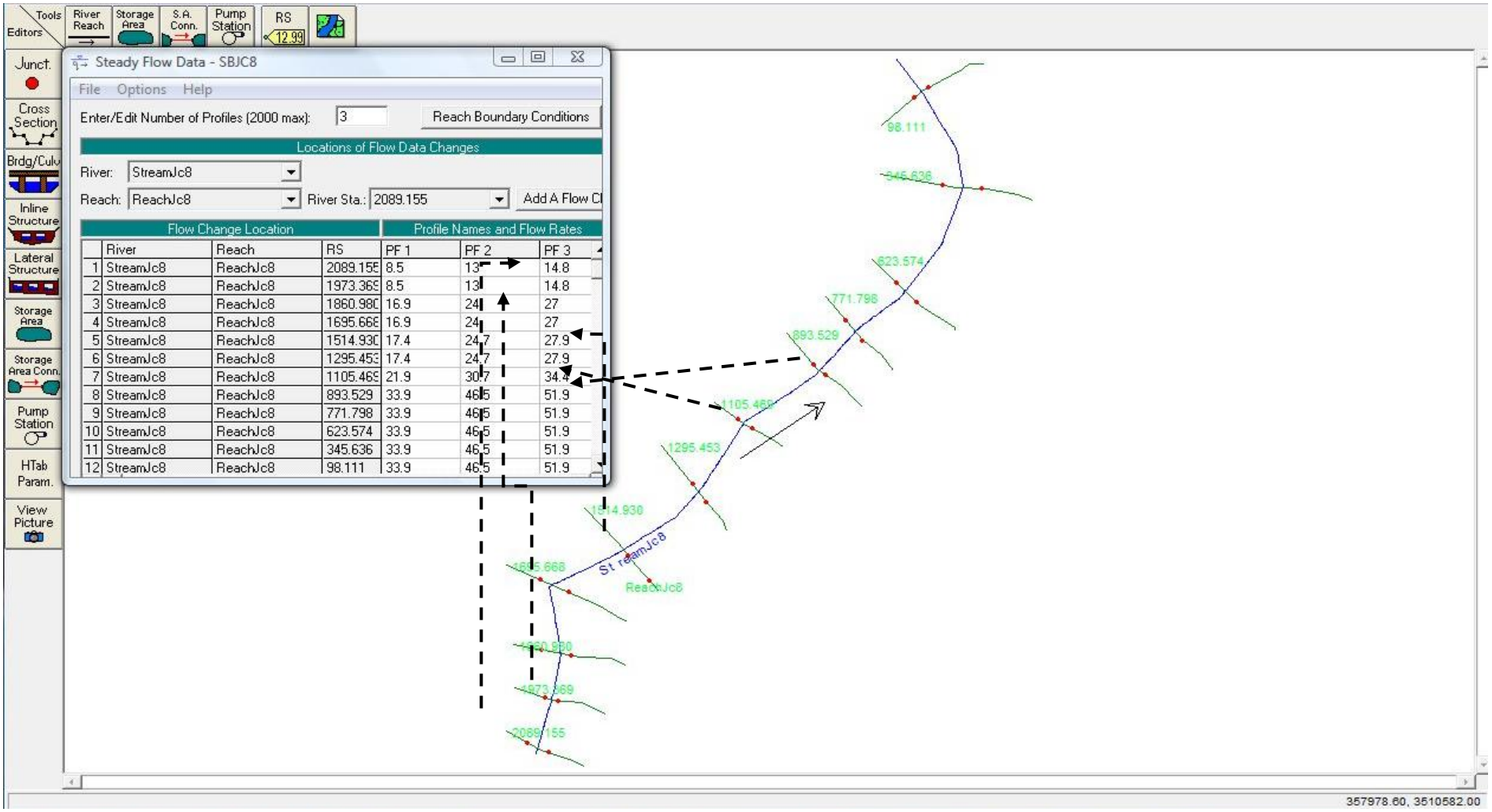

Figure 6A.13. Association and organization of HEC-HMS hydrographs plans: PF1 to Tr 10 years; PF2 to Tr 50 years and PF3 to Tr 100 years into the HEC-RAS program. Note the dash black line indicate the site of reach location in relation to discharge values given in upper left table This stream driver corresponds to Jc8 transference reach. Source: Created by David Zúñiga (2012) using HEC-RAS (2002) version3.1.3.

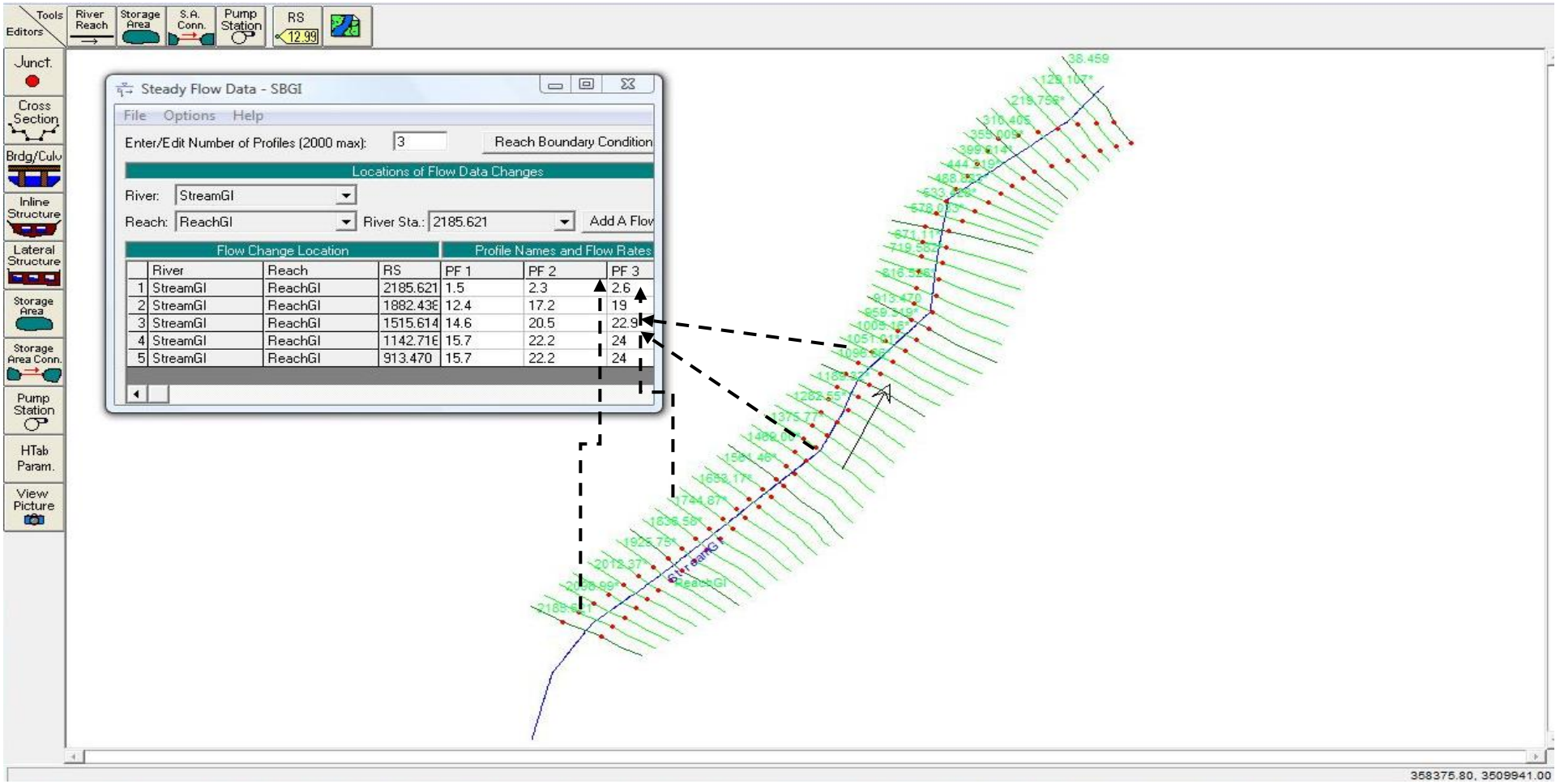

Figure 6A.14. Association and organization of HEC-HMS hydrographs plans: PF1 to Tr 10 years; PF2 to Tr 50 years and PF3 to Tr 100 years into the HEC-RAS program. Note the dash black line indicate the site of reach location in relation to discharge values given in upper left table This stream driver corresponds to GI transference reach. Source: Created by David Zúñiga (2012) using HEC-RAS (2002) version3.1.3.

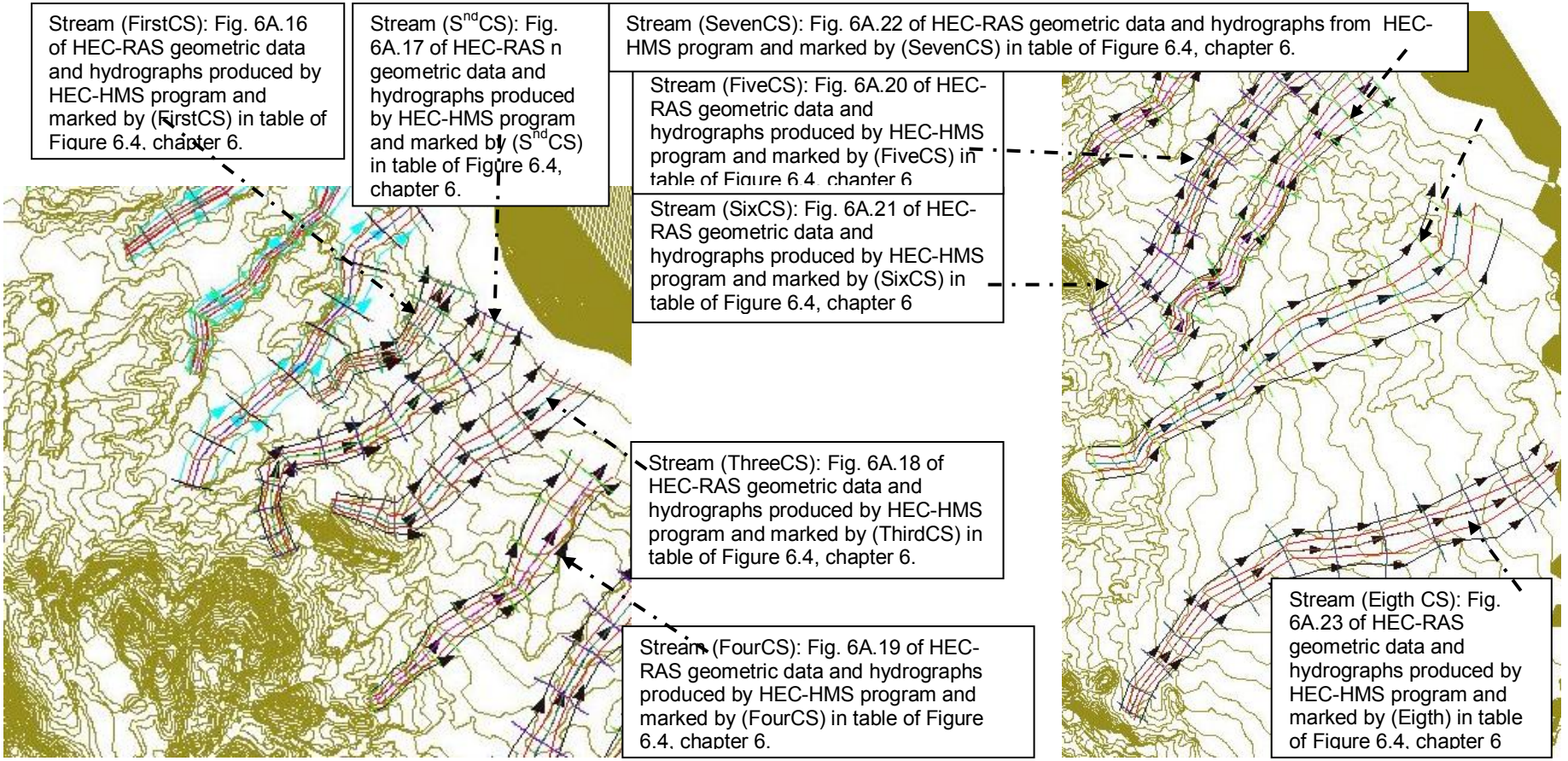

Figure 6A.15. Link between the different transference reaches performed over the DEM during Pre-GeoRAS processor and the associated flooding profile given in previous association between HEC-HMS (2002) hydrographs and the reaches that would routing the HEC-HMS hydrographs Source: Created by David Zúñiga (2012) using Arc-view 3.2 with HEC-GeoRAS pre and Post processor; 3D and spatial extensions.

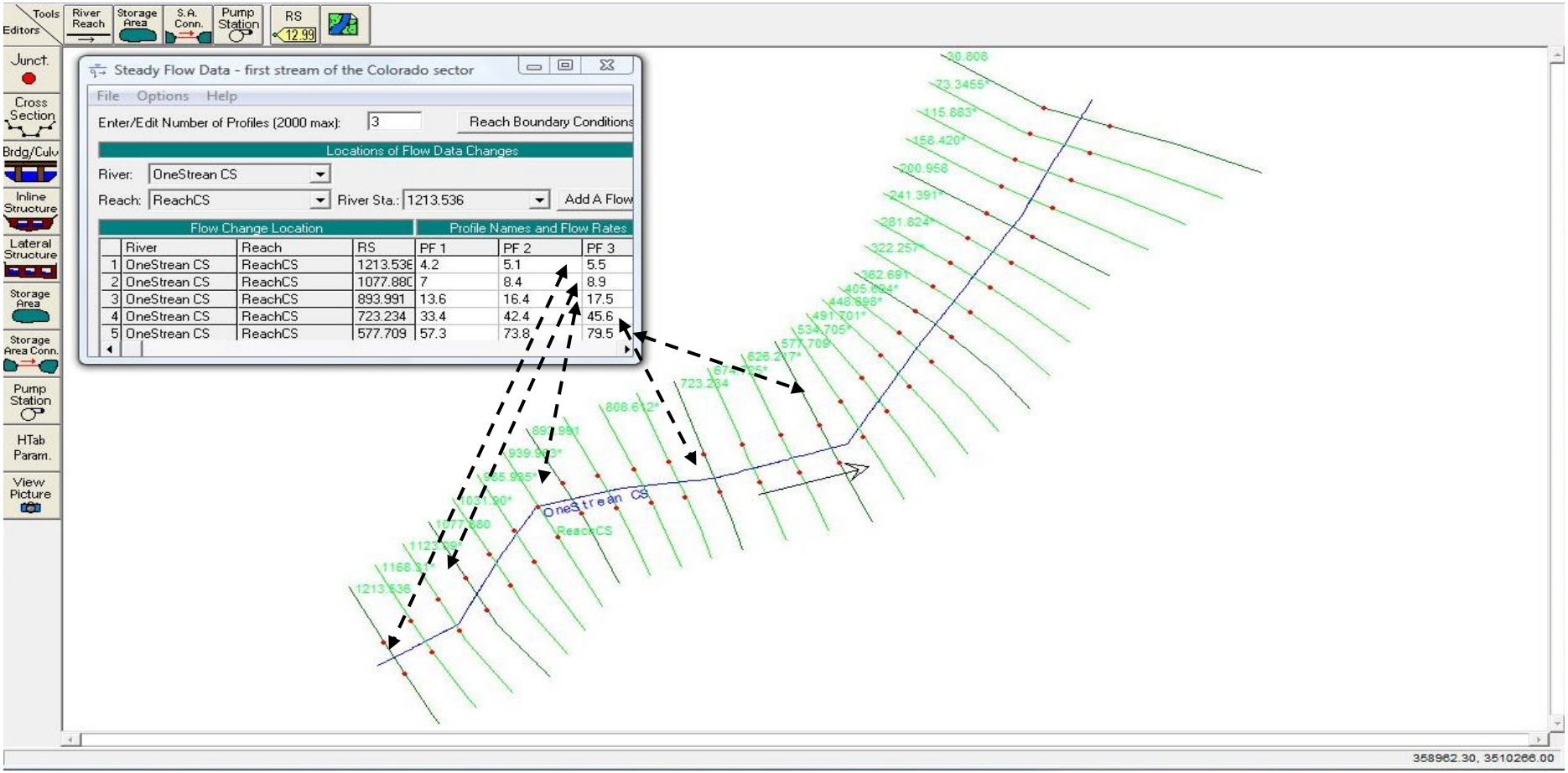

Figure 6A.16. Association and organization of HEC-HMS hydrographs plans: PF1 to Tr 10 years; PF2 to Tr 50 years and PF3 to Tr 100 years into the HEC-RAS program. Note the dash black line indicate the site of reach location in relation to discharge values given in upper left table This stream driver corresponds to FirstCS transference reach. Source: Created by David Zúñiga (2012) using HEC-RAS (2002) version 3.1.3.

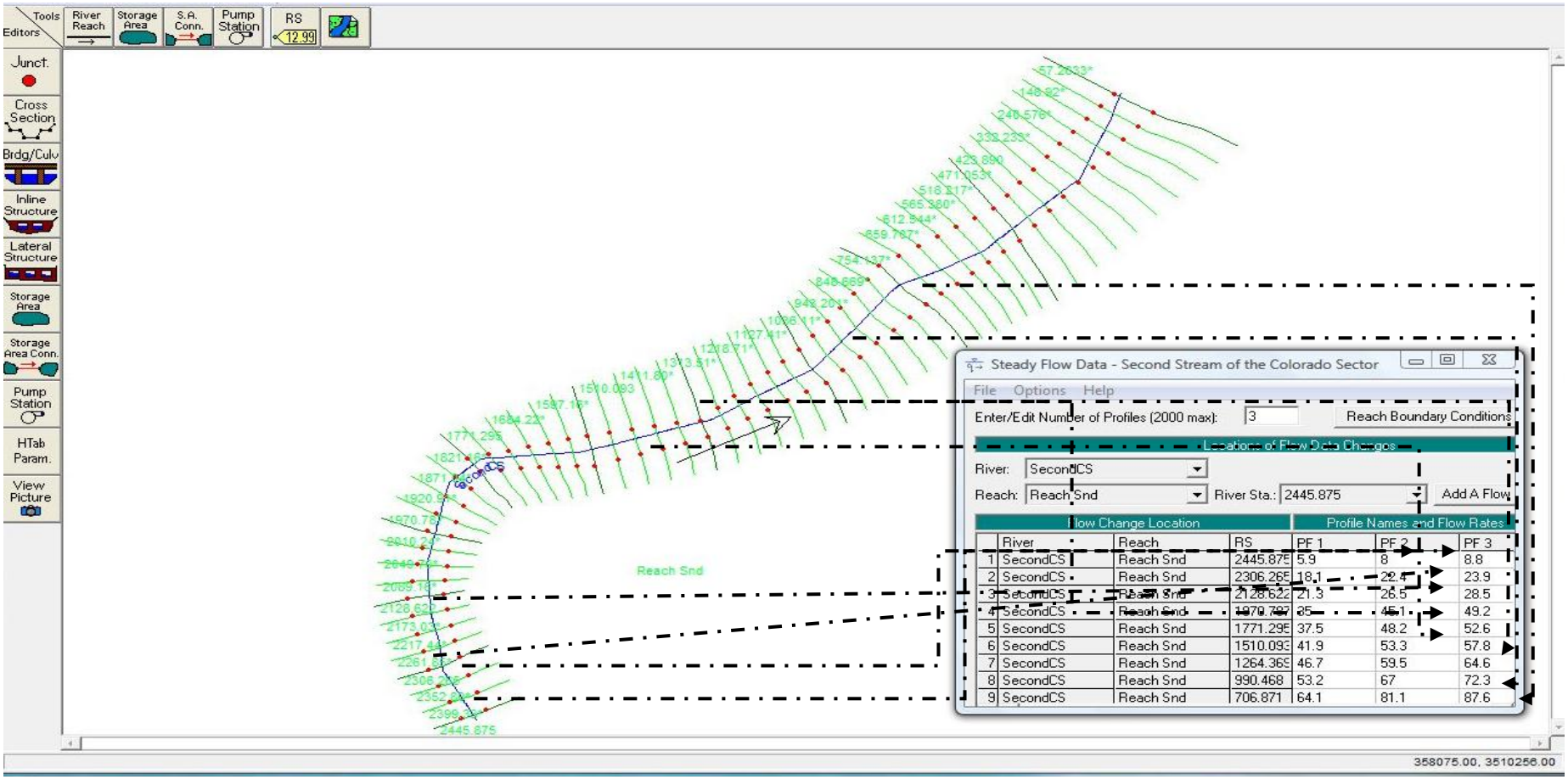

Figure 6A.17. Association and organization of HEC-HMS hydrographs plans: PF1 to Tr 10 years; PF2 to Tr 50 years and PF3 to Tr 100 years into the HEC-RAS program. Note the dash black line indicate the site of reach location in relation to discharge values given in upper left table This stream driver corresponds to SndCS transference reach. Source: Created by David Zúñiga (2012) using HEC-RAS (2002) version 3.1.3.

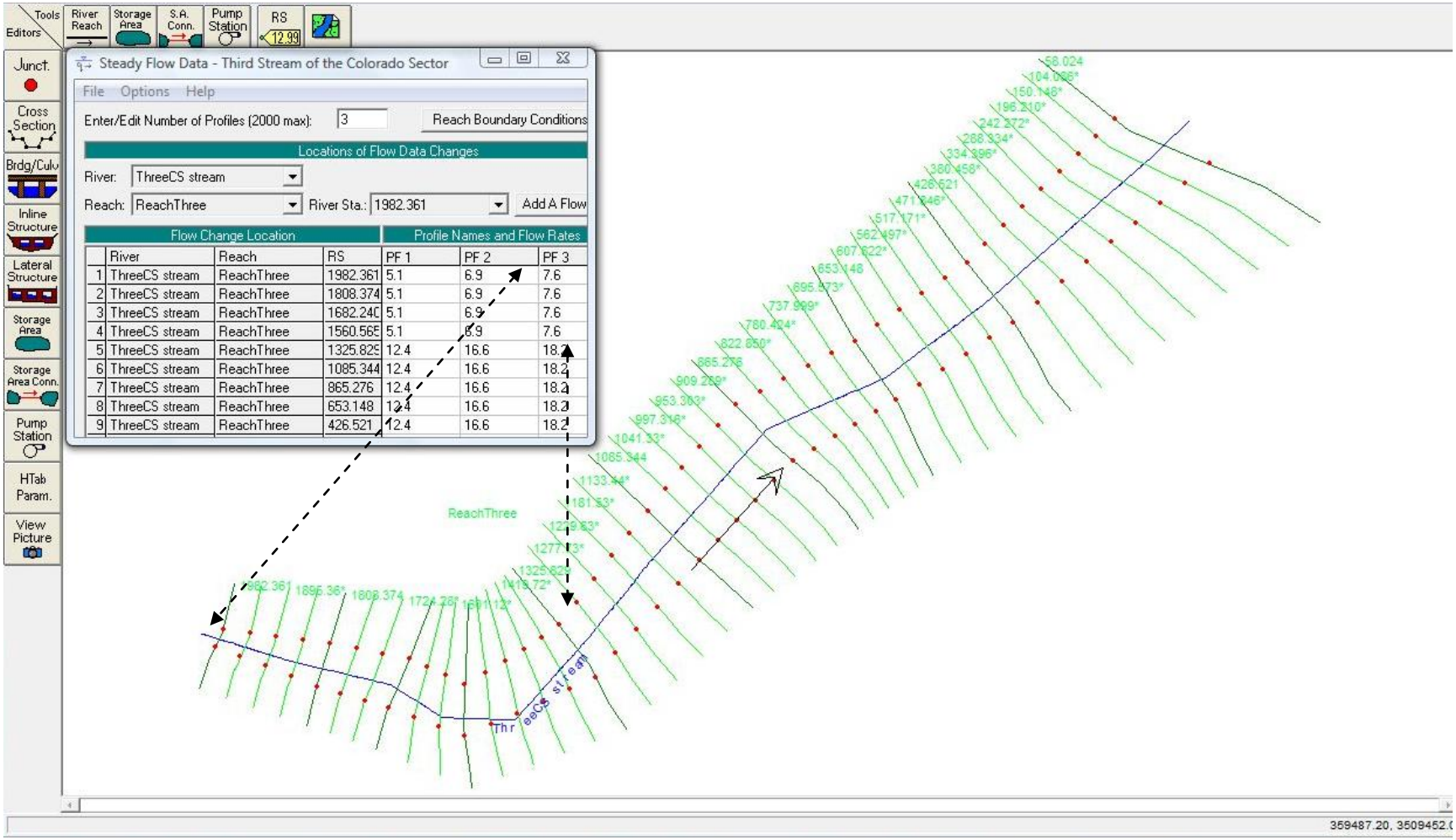

Figure 6A.18. Association and organization of HEC-HMS hydrographs plans: PF1 to Tr 10 years; PF2 to Tr 50 years and PF3 to Tr 100 years into the HEC-RAS program. Note the dash black line indicate the site of reach location in relation to discharge values given in upper left table This stream driver corresponds to ThirdCS transference reach. Source: Created by David Zúñiga (2012) using HEC-RAS (2002) version 3.1.3.

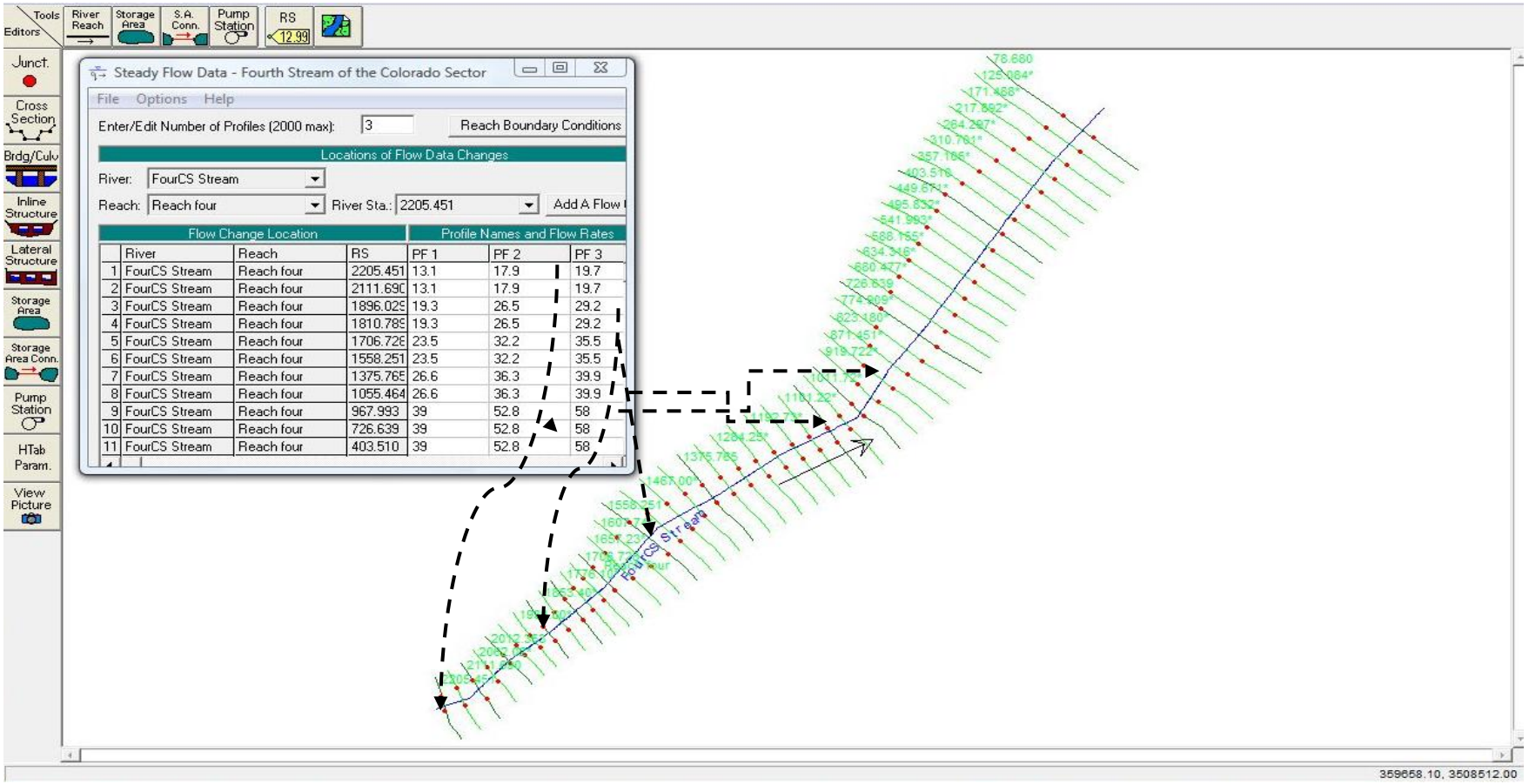

Figure 6A.19. Association and organization of HEC-HMS hydrographs plans: PF1 to Tr 10 years; PF2 to Tr 50 years and PF3 to Tr 100 years into the HEC-RAS program. Note the dash black line indicate the site of reach location inrelation to discharge values given in upper left table This stream driver corresponds to fourCS transference reach. Source: Created by David Zúñiga (2012) using HEC-RAS (2002) version 3.1.3.

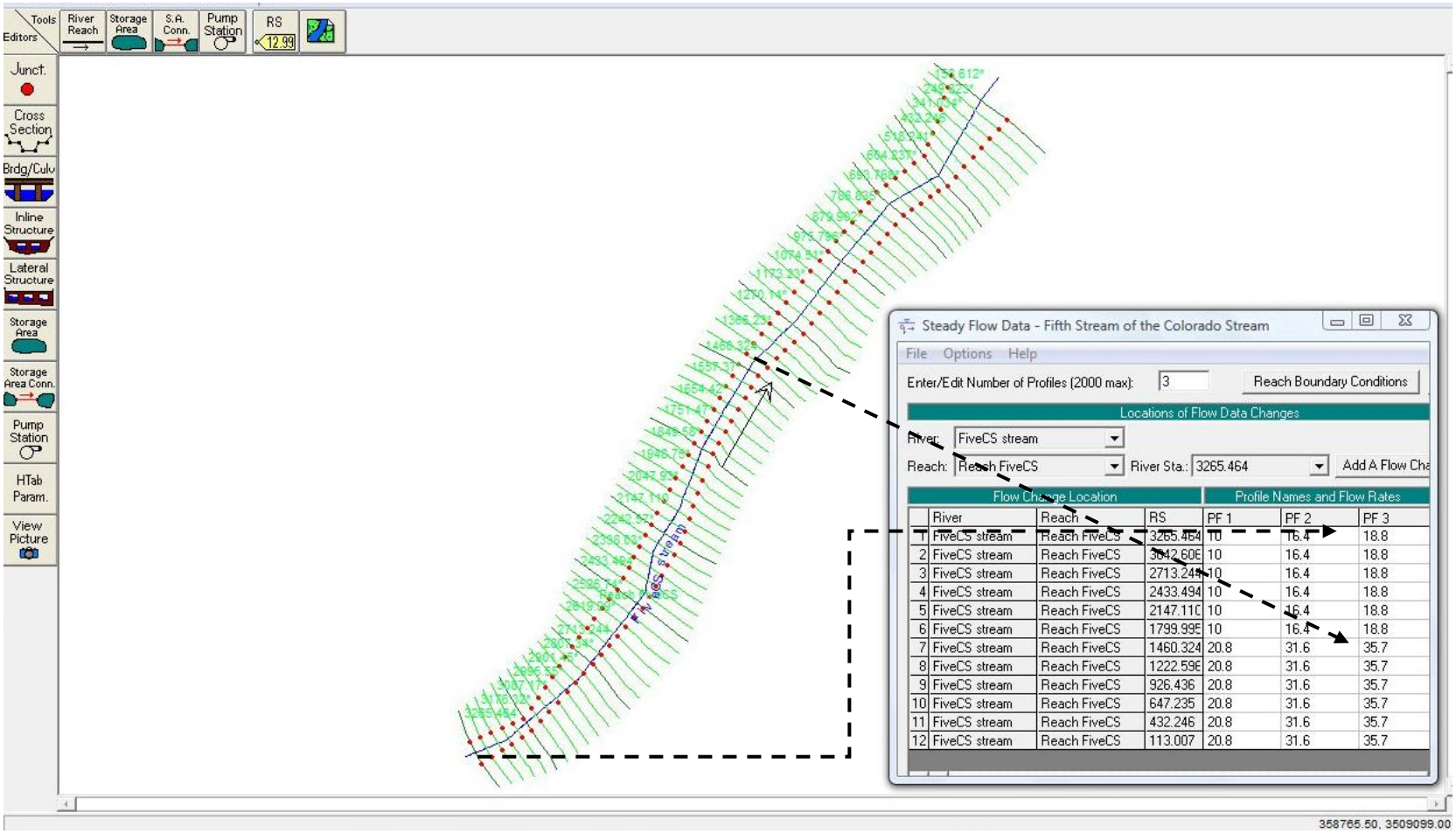

Figure 6A.20. Association and organization of HEC-HMS hydrographs plans: PF1 to Tr 10 years; PF2 to Tr 50 years and PF3 to Tr 100 years into the HEC-RAS program. Note the dash black line indicate the site of reach location inrelation to discharge values given in upper left table This stream driver corresponds to FiveCS transference reach. Source: Created by David Zúñiga (2012) using HEC-RAS (2002) version 3.1.3.

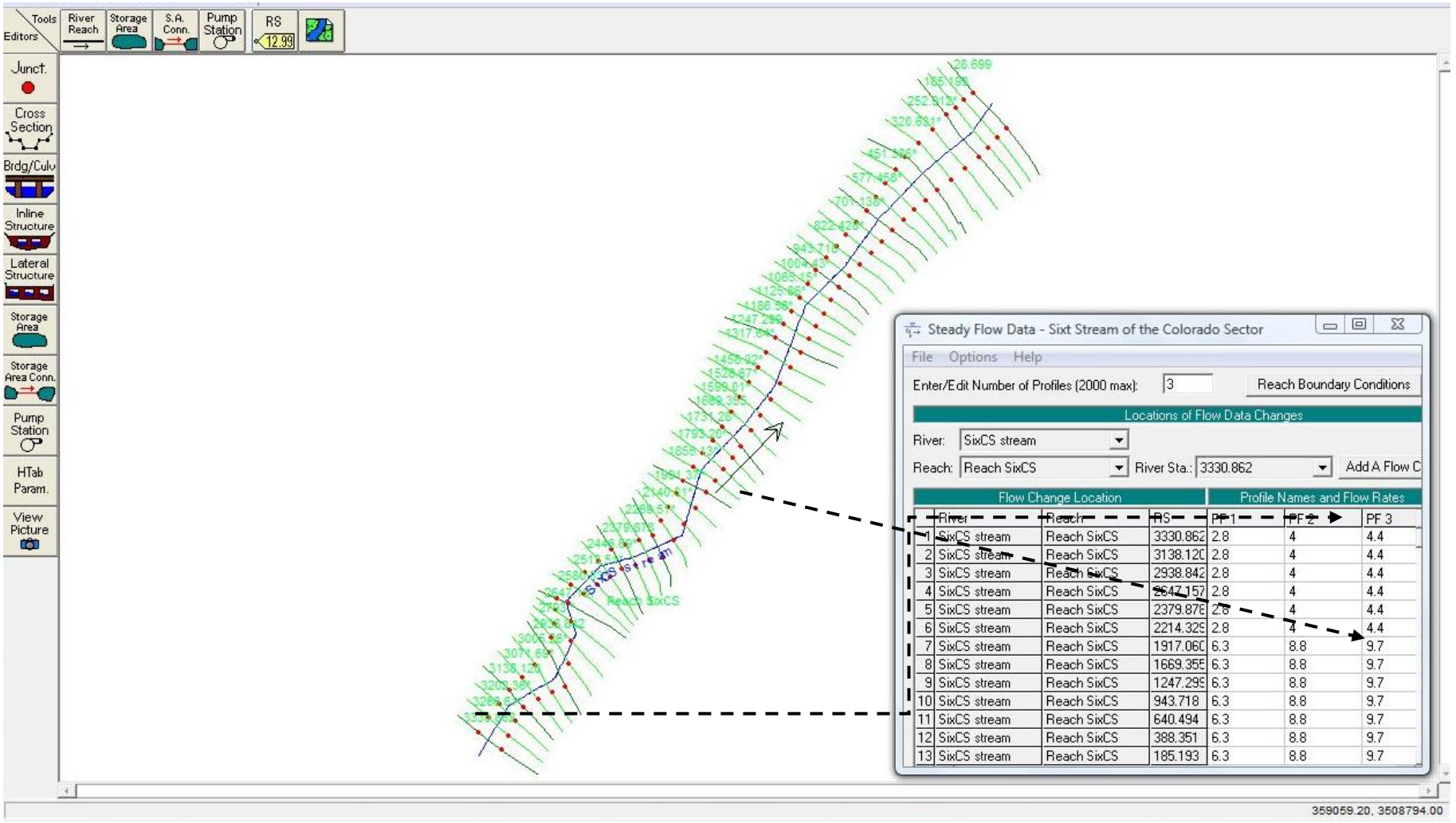

Figure 6A.21. Association and organization of HEC-HMS hydrographs plans: PF1 to Tr 10 years; PF2 to Tr 50 years and PF3 to Tr 100 years into the HEC-RAS program. Note the dash black line indicate the site of reach location in relation to discharge values given in upper left table This stream driver corresponds to SixCS transference reach. Source: Created by David Zúñiga (2012) using HEC-RAS (2002) version 3.1.3.

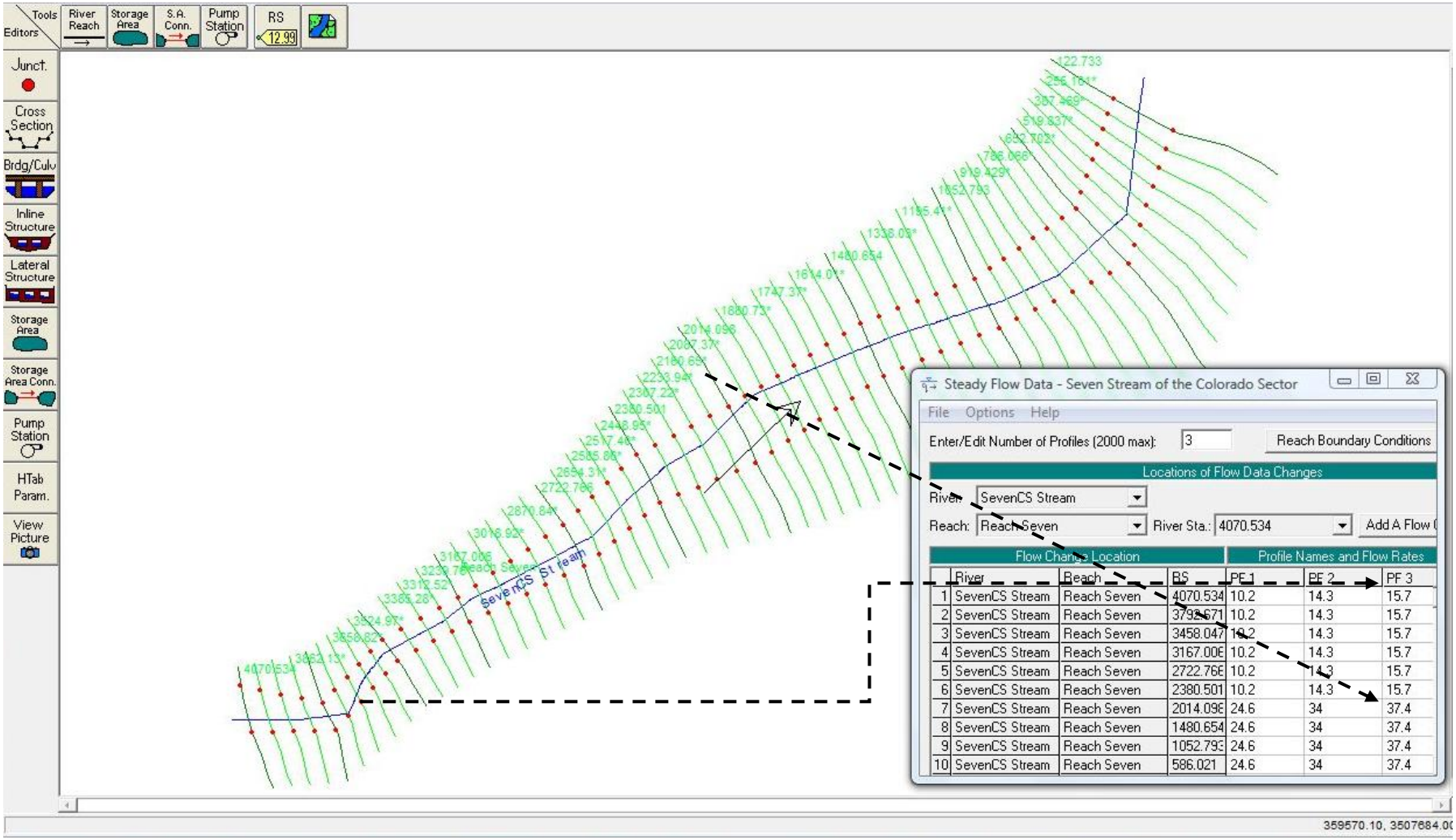

Figure 6A.22. Association and organization of HEC-HMS hydrographs plans: PF1 to Tr 10 years; PF2 to Tr 50 years and PF3 to Tr 100 years into the HEC-RAS program. Note the dash black line indicate the site of reach location in relation to discharge values given in upper left table This stream driver corresponds to SevenCS transference reach. Source:Created by David Zúñiga (2012) using HEC-RAS (2002) version 3.1.3.

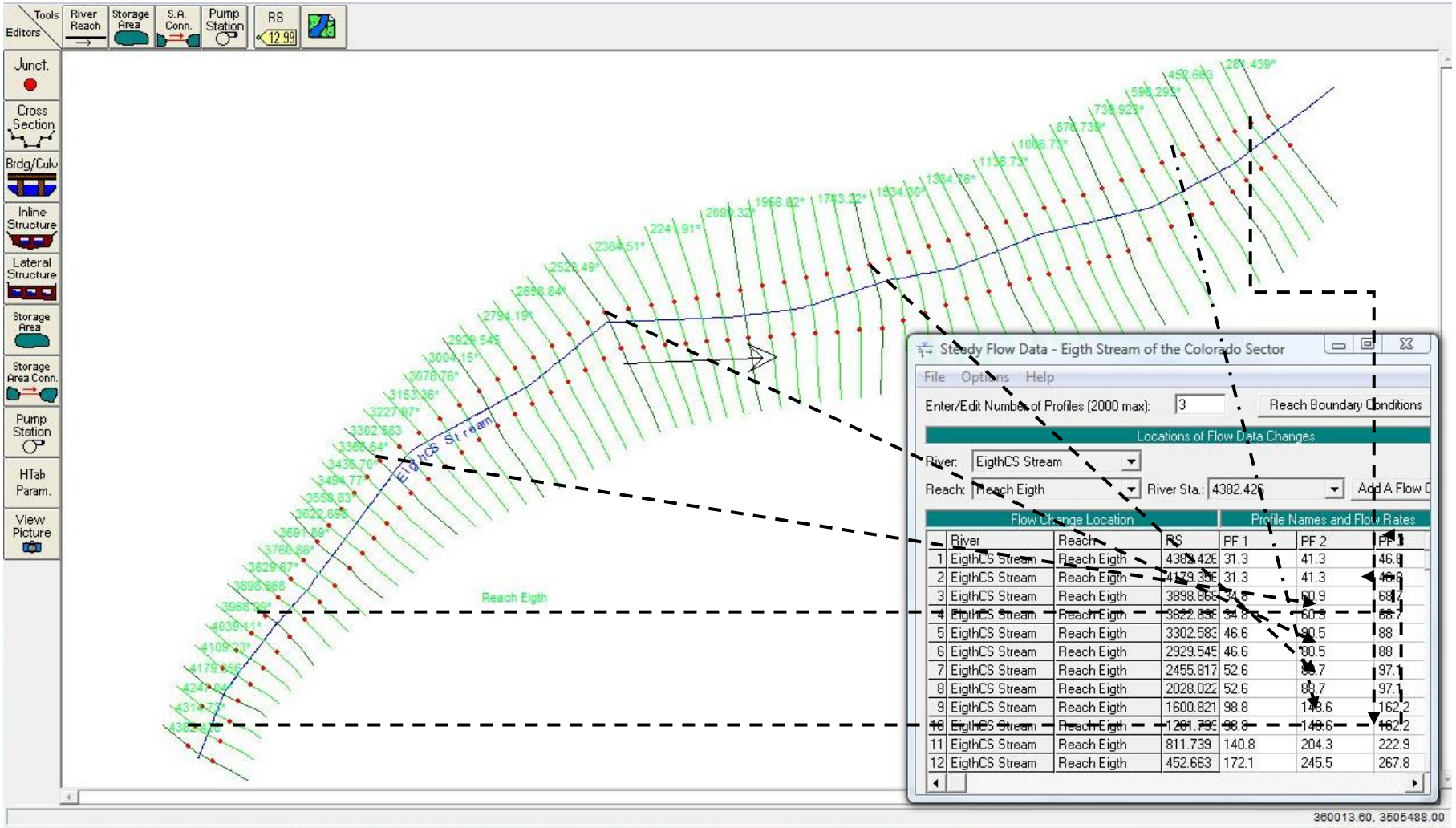

Figure 6A.23. Association and organization of HEC-HMS hydrographs plans: PF1 to Tr 10 years; PF2 to Tr 50 years and PF3 to Tr 100 years into the HEC-RAS program. Note the dash black line indicate the site of reach location in relation to discharge values given in upper left table This stream driver corresponds to EigthCS transference reach. Source:Created by David Zúñiga (2012) using HEC-RAS (2002) version 3.1.3.

APPENDIX 6B

The flooding results using HEC-RAS.

Modelling of a steady flow regime mentioned in Chapter 6 was performed using the HEC-RAS computer program to simulate the flooding hazard. Water stream surface elevation of the Anapra sector AW1; AW2; AW3; AW4; AC; M1; SW1west and SW1 east for 10 years (PF1); 50 years (PF2) and 100 years (PF3) return periods were evaluated and are presented in Figs. 6B.1 to 6B.23 below. These figures show the location of cross sections corresponding to the major streams draining watersheds in Anapra and Center basin areas. In addition, figures show the water elevation flow limits in both profile and cross sections profile. WS1 PF1; WS2 PF2 and WS3 PF3 referred to water surface elevation from different flow plans as: P1 to 10 years return period; P2 to 50 years return period and P3 to 100 years of return period of the design storm. Watersurface elevation of stream: 10 years (PF1); 50 years (PF2) and 100 years (PF3) return periods: A perspective view of the profile and all the cross sections and water surface for all the sub-basins are shown in the figures below.

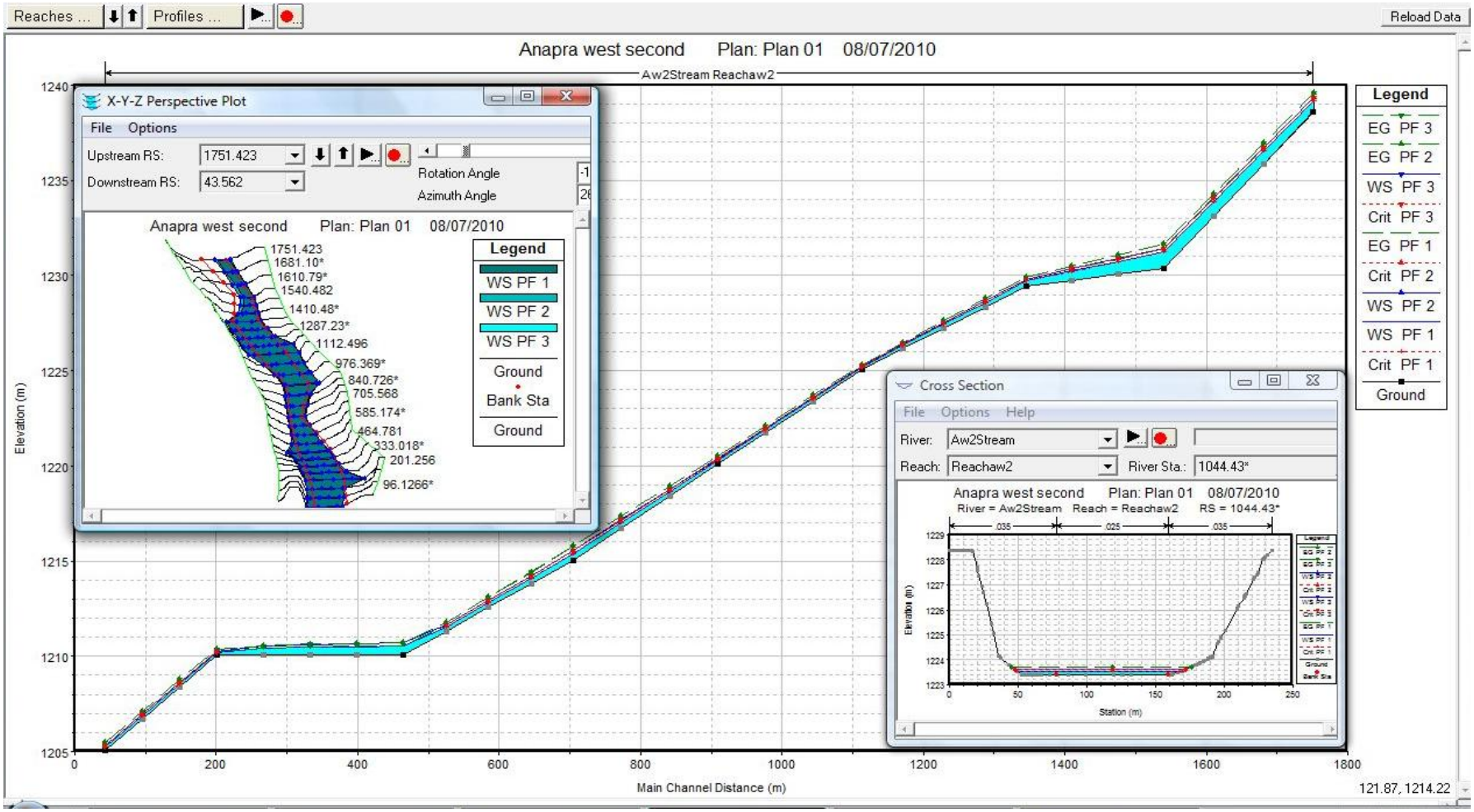

Figure 6B.1. Water surface elevation of stream AW2: 10 years (PF1); 50 years (PF2) and 100 years (PF3) return periods: A) shows a perspective view of the profile. B) shows a cross section of the Water Surface that corresponds at station 1044.43 of the stream. (See map location in figure 6.6 Chapter 6). Source: Created by David Zúñiga (2012) using HEC-RAS (2002) version 3.1.3.

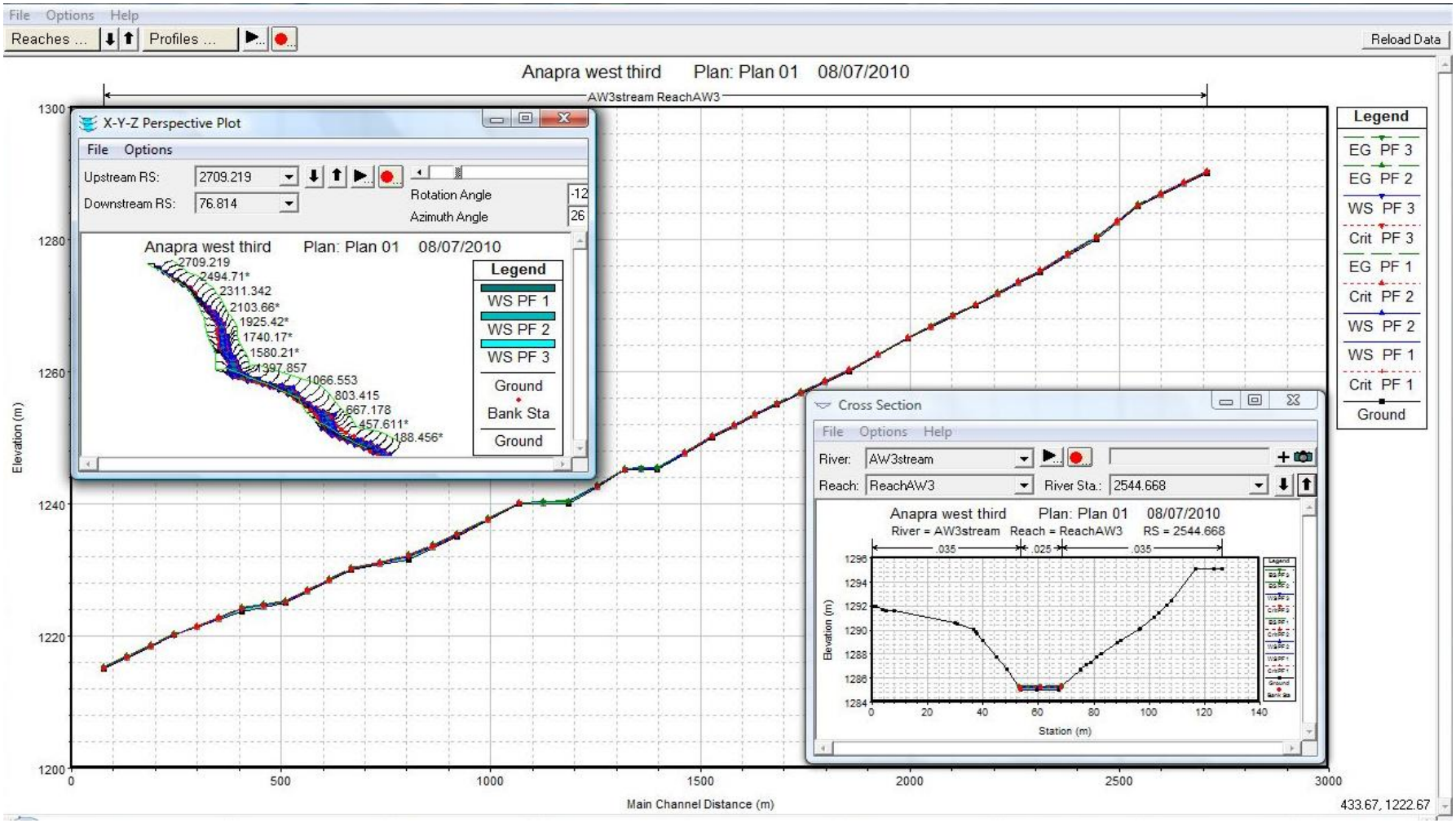

Figure 6B.2. Water surface elevation of stream AW3: 10 years (PF1); 50 years (PF2) and 100 years (PF3) return periods: A) shows a perspective view of the profile. B) shows a cross section of the Water Surface that corresponds at station 2544.668 of the stream. (See map location in figure 6.6 Chapter 6) Source:Created by David Zúñiga (2012) using HEC-RAS (2002) version 3.1.3.

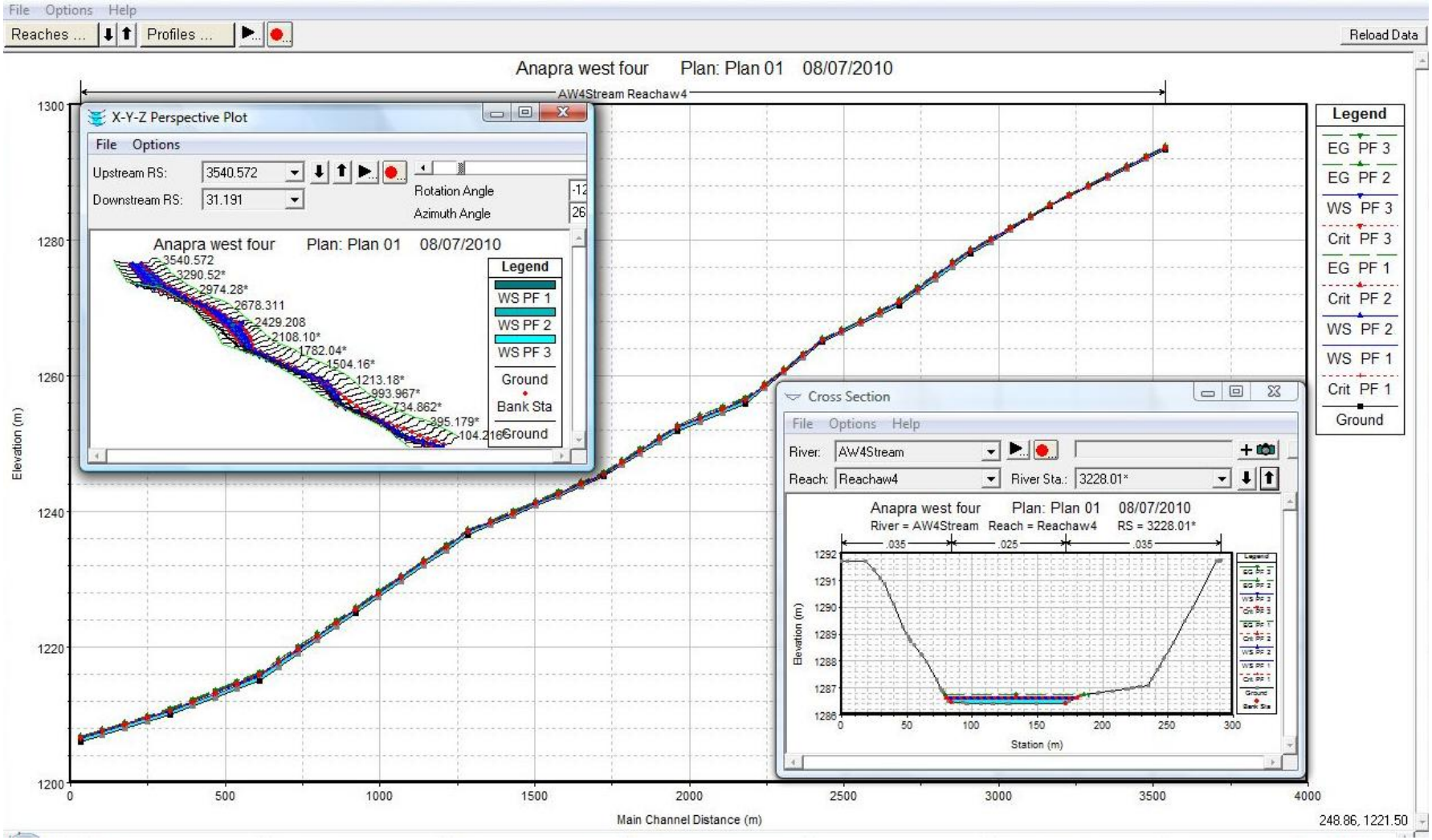

Figure 6B.3. Water surface elevation of stream AW4: 10 years (PF1); 50 years (PF2) and 100 years (PF3) return periods: A) shows a perspective view of the profile. B) shows a cross section of the Water Surface that corresponds at station 3228.01 of the stream. (See map location in figure 6.6 Chapter 6) Source: Created by David Zúñiga (2012) using HEC-RAS (2002) version 3.1.3.

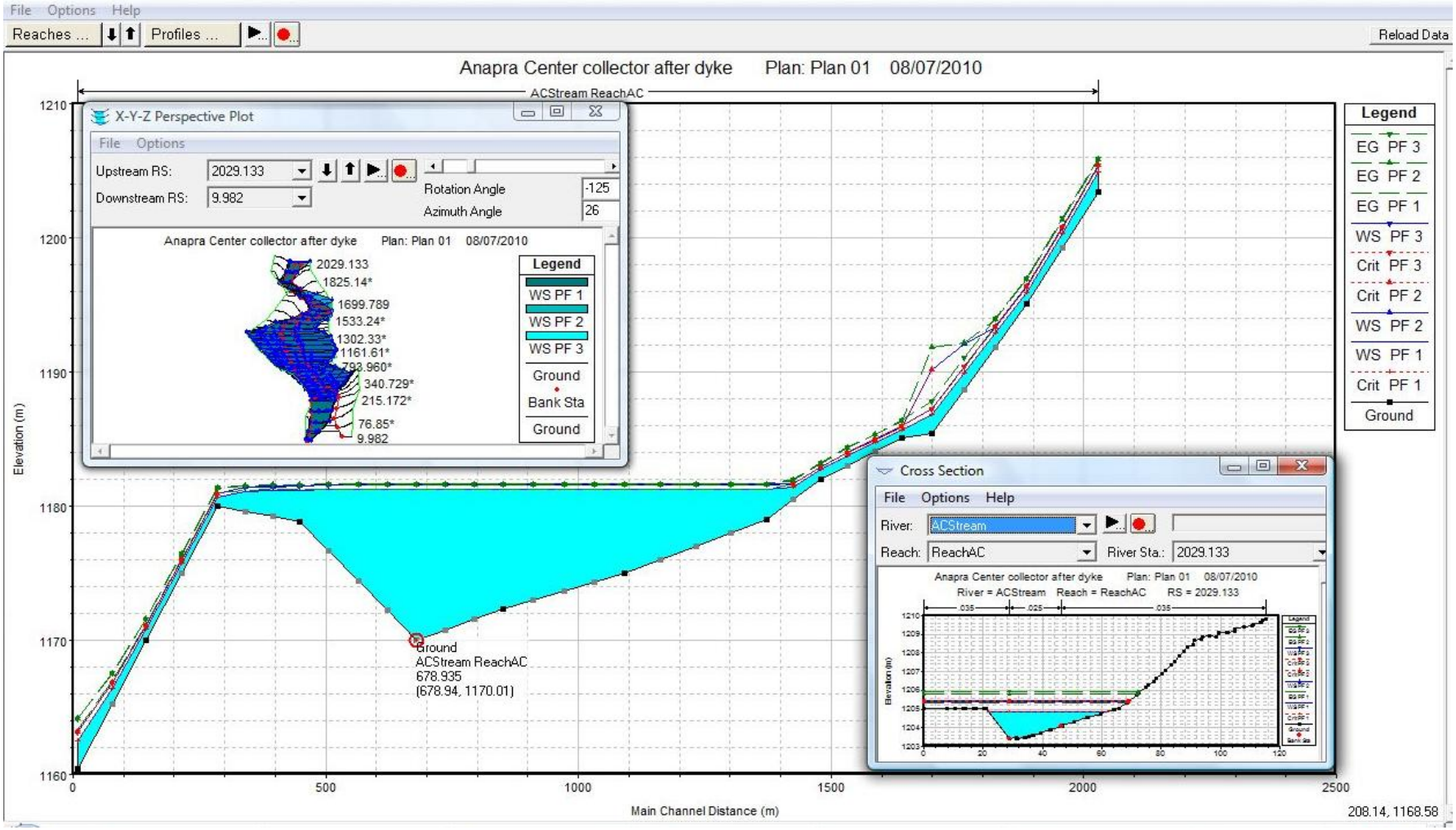

Figure 6B.4. Water surface elevation of stream AC: 10 years (PF1); 50 years (PF2) and 100 years (PF3) return periods: A) shows a perspective view of the profile. B) shows a cross section of the Water Surface that corresponds at station 2029.133 of the stream. (See map location in figure 6.6 Chapter 6) Source: Created by David Zúñiga (2012) using HEC-RAS (2002) version 3.1.3.

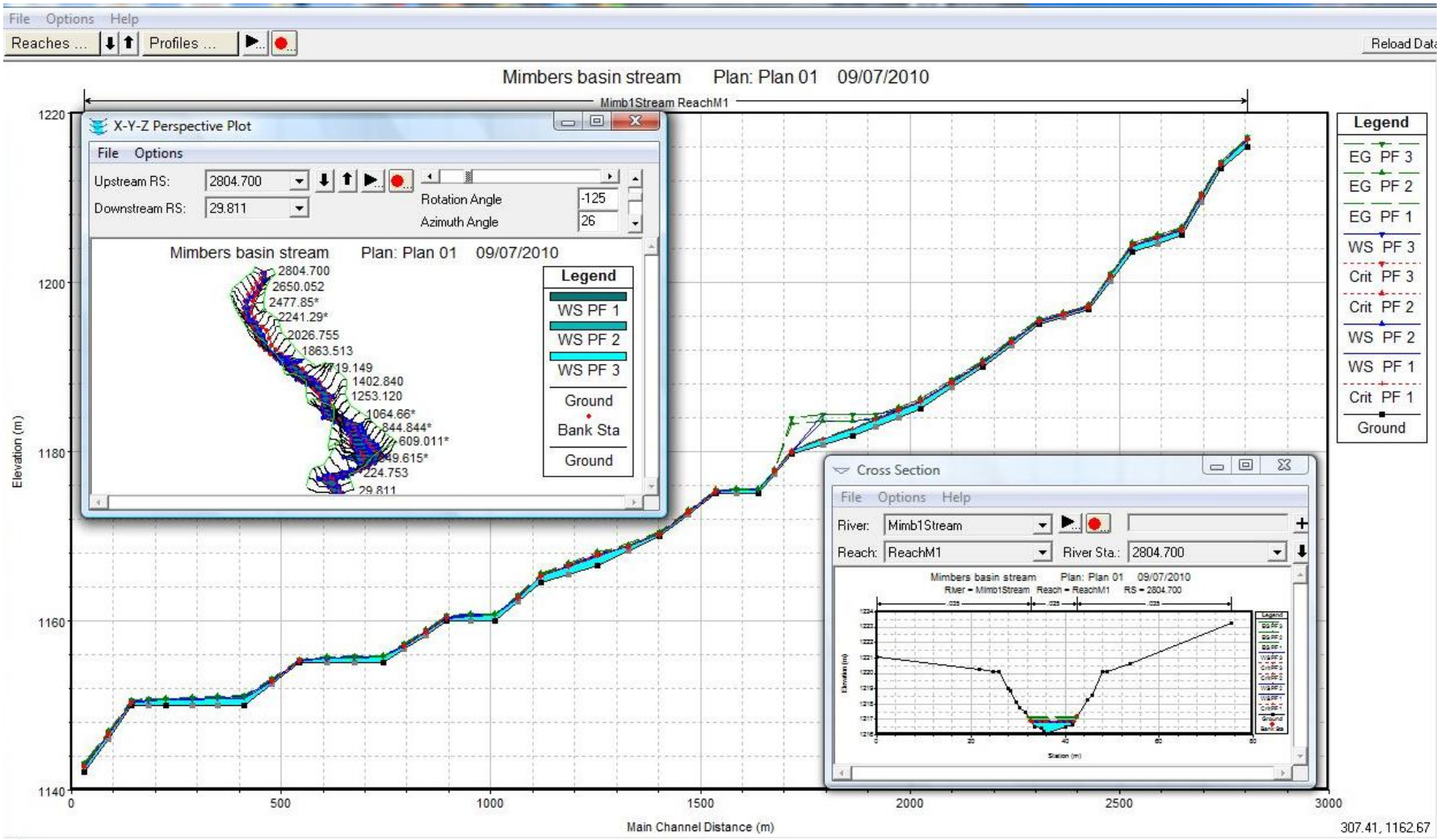

Figure 6B.5. Water surface elevation of stream M1: 10 years (PF1); 50 years (PF2) and 100 years (PF3) return periods: A) shows a perspective view of the profile. B) shows a cross section of the Water Surface that corresponds at station 2804.700 of the stream. (See map location in figure 6.6 Chapter 6) Source:Created by David Zúñiga (2012) using HEC-RAS (2002) version 3.1.3.

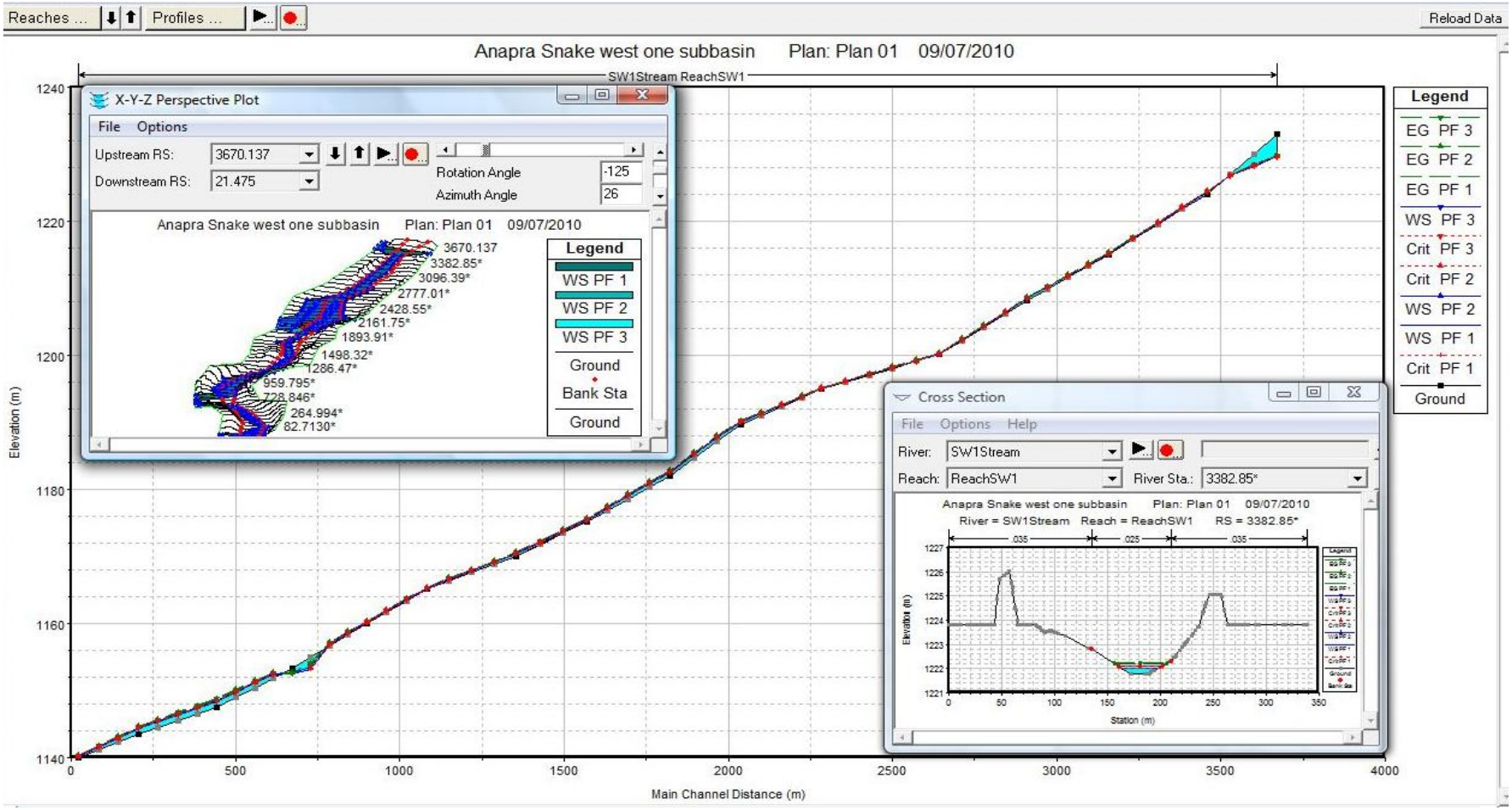

Figure 6B.6. Water surface elevation of stream SW1: 10 years (PF1); 50 years (PF2) and 100 years (PF3) return periods: A) shows a perspective view of the profile. B) shows a cross section of the Water Surface that corresponds at station 2804.700 of the stream. (See map location in figure 6.6 Chapter 6) Source: Created by David Zúñiga (2012) using HEC-RAS (2002) version 3.1.3.

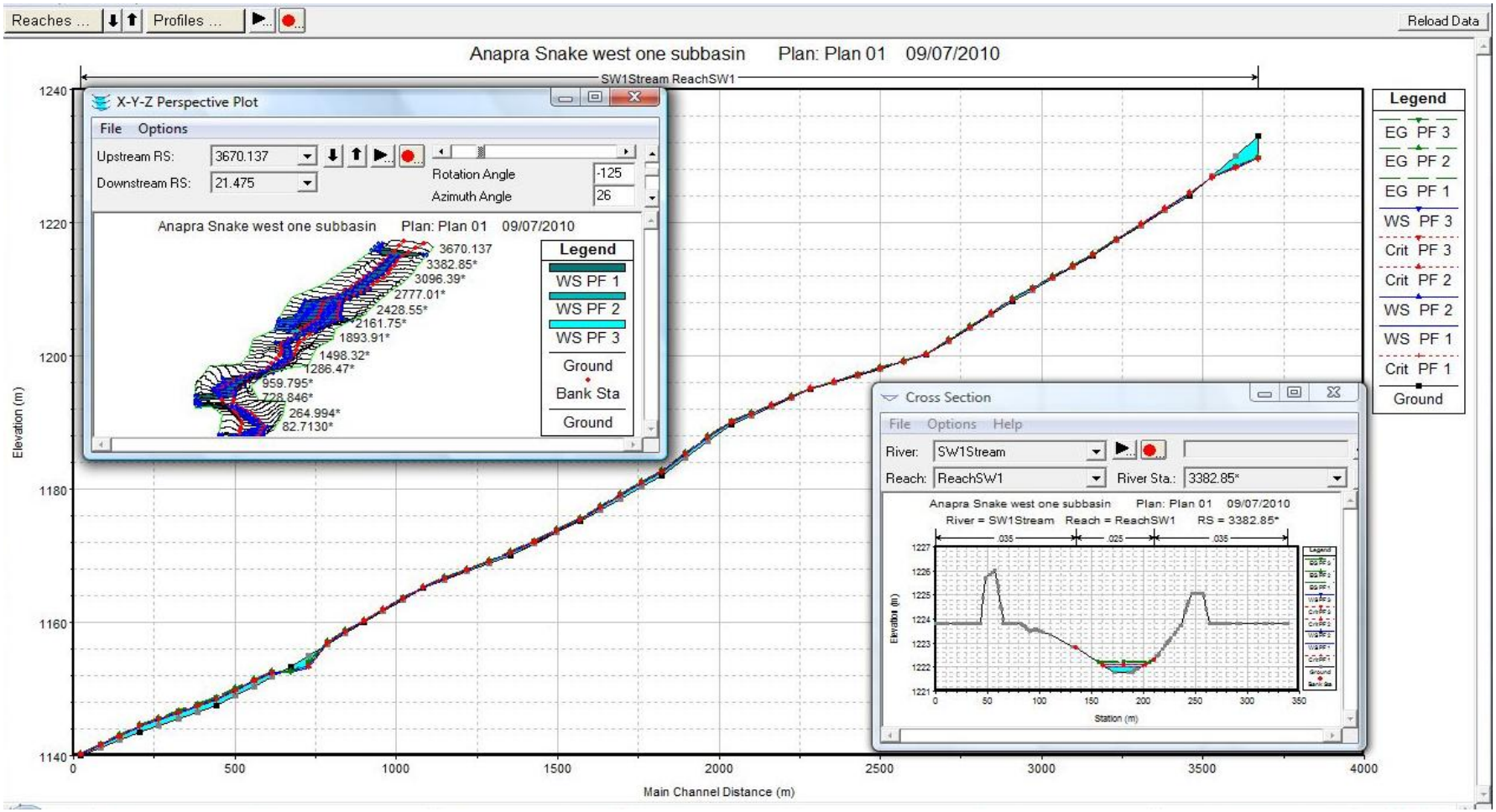

Figure 6B.7. Water surface elevation of stream SW1: 10 years (PF1); 50 years (PF2) and 100 years (PF3) return periods: A) shows a perspective view of the profile. B) shows a cross section of the Water Surface that corresponds at station 3382.85 of the stream. (See map location in figure 6.6 Chapter 6) Source:Created by David Zúñiga (2012) using HEC-RAS (2002) version 3.1.3.

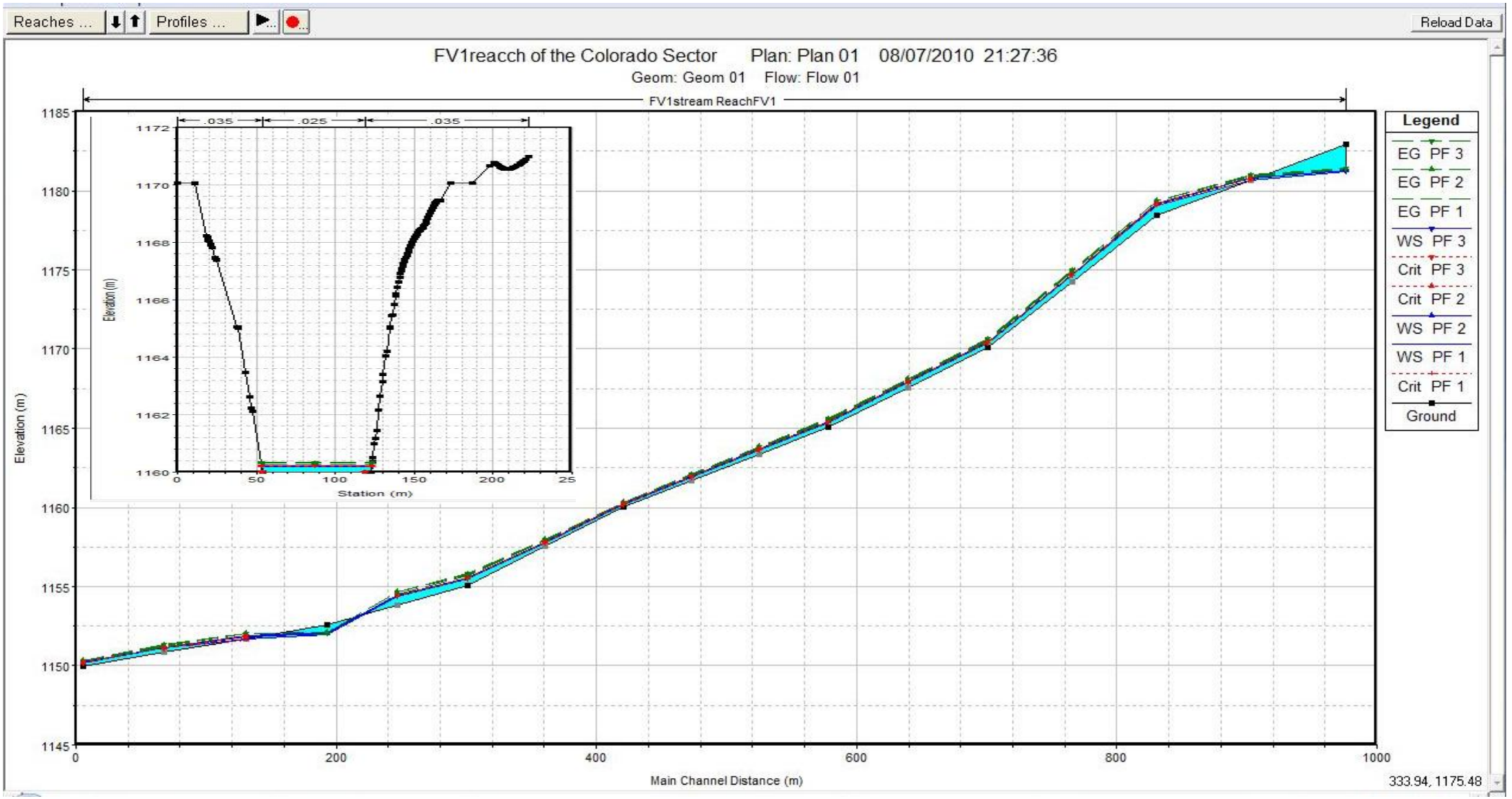

Figure 6B.8. Water surface elevation of stream FV1: 10 Yr. (PF1); 50 Yr. (PF2); and 100 Yr. (PF3); Shows profile and cross section of water surface level during flooding (See map location in figure 6A.4 Appendix 6A). Source: Created by David Zúñiga (2012) using HEC-RAS (2002) version 3.1.3.

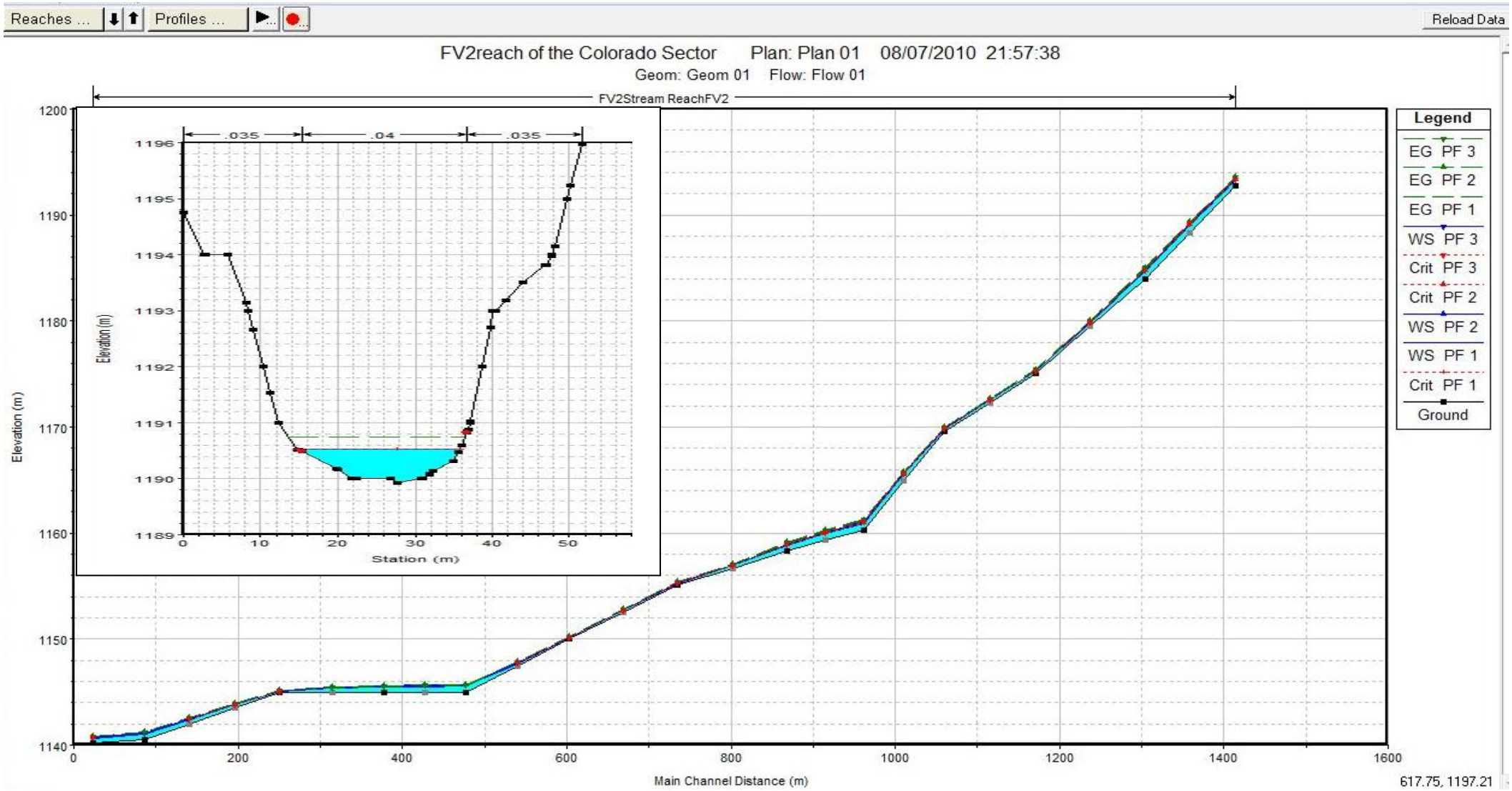

Figure 6B.9. Water surface elevation of stream FV2: 10 Yr. (PF1); 50 Yr. (PF2); and 100 Yr. (PF3); Shows profile and cross section of water surface level during flooding (See map location in figure 6A.4 Appendix 6A) Source: Created by David Zúñiga (2012) using HEC-RAS (2002) version 3.1.3.

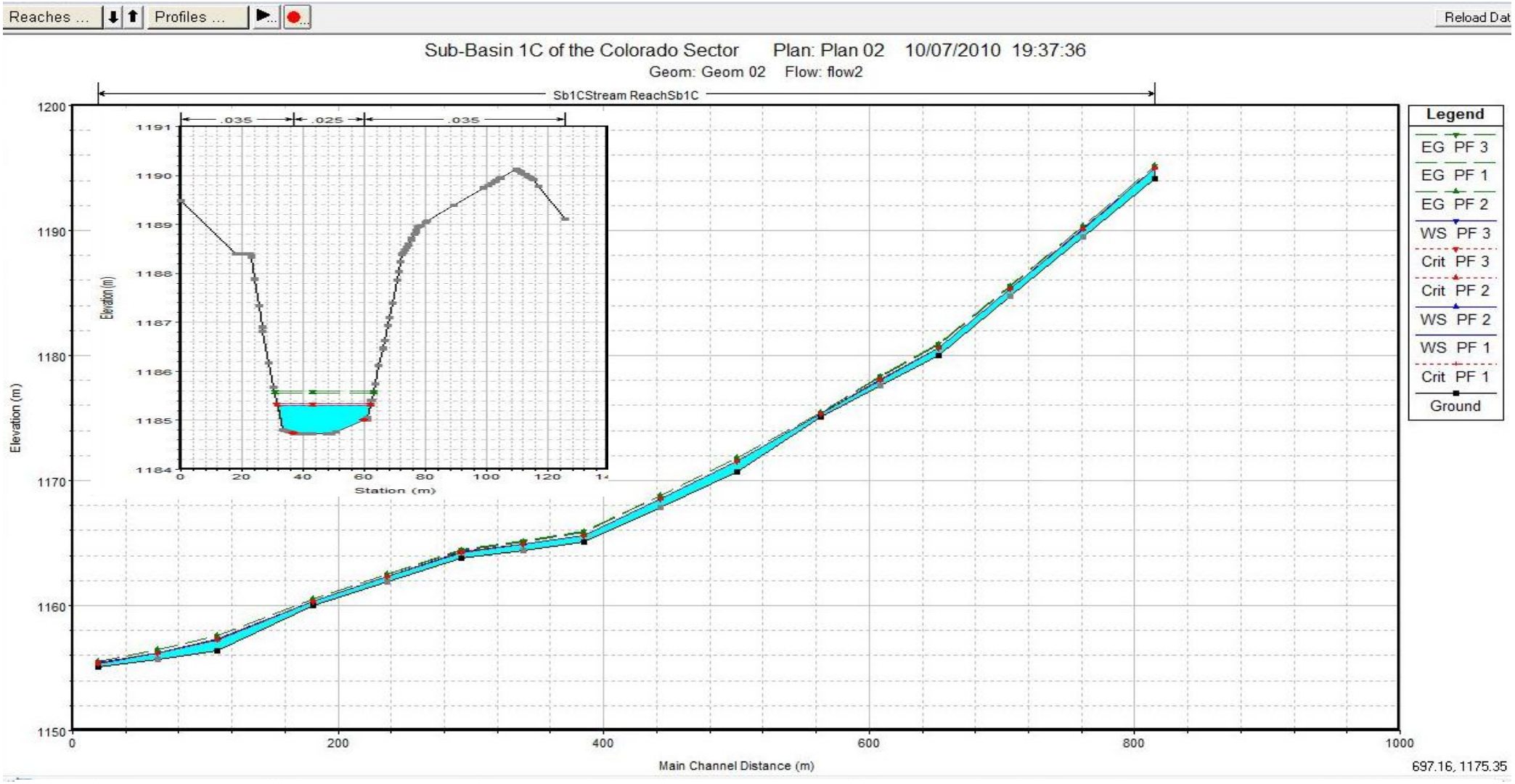

Figure 6B.10. Water surface elevation of stream Sb1C: 10 Yr. (PF1); 50 Yr. (PF2); and 100 Yr. (PF3); Shows profile and cross section of water surface level during flooding (See map location in figure 6A.4 Appendix 6A) . Source: Created by David Zúñiga (2012) using HEC-RAS (2002) version 3.13.

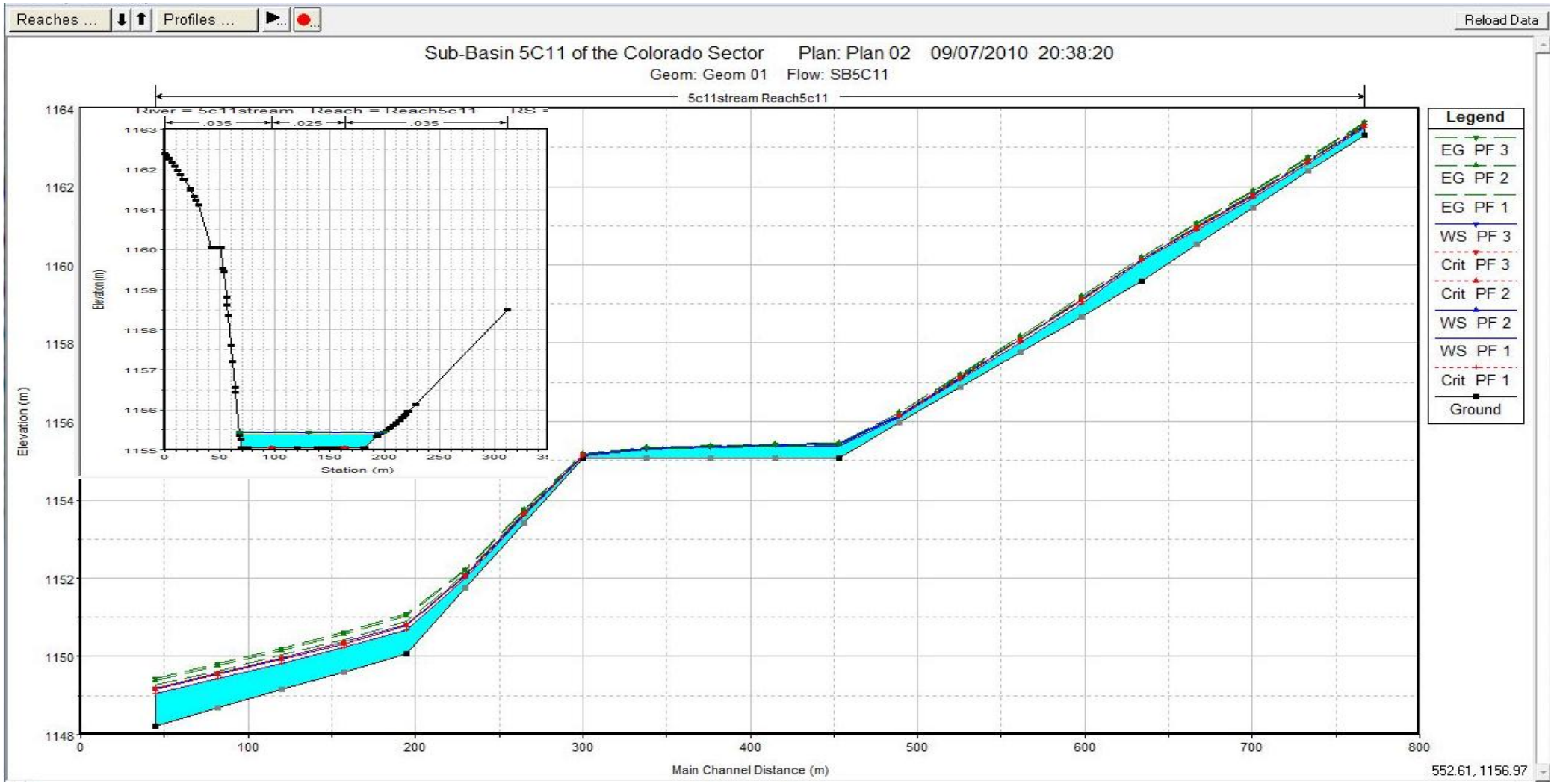

Figure 6B.11. Water surface elevation of stream 5C11: 10 Yr. (PF1); 50 Yr. (PF2); and 100 Yr. (PF3); Shows profile and cross section of water surface level during flooding (See map location in figure 6A.4 Appendix 6A). Source: Created by David Zúñiga (2012) using HEC-RAS (2002) version 3.13.

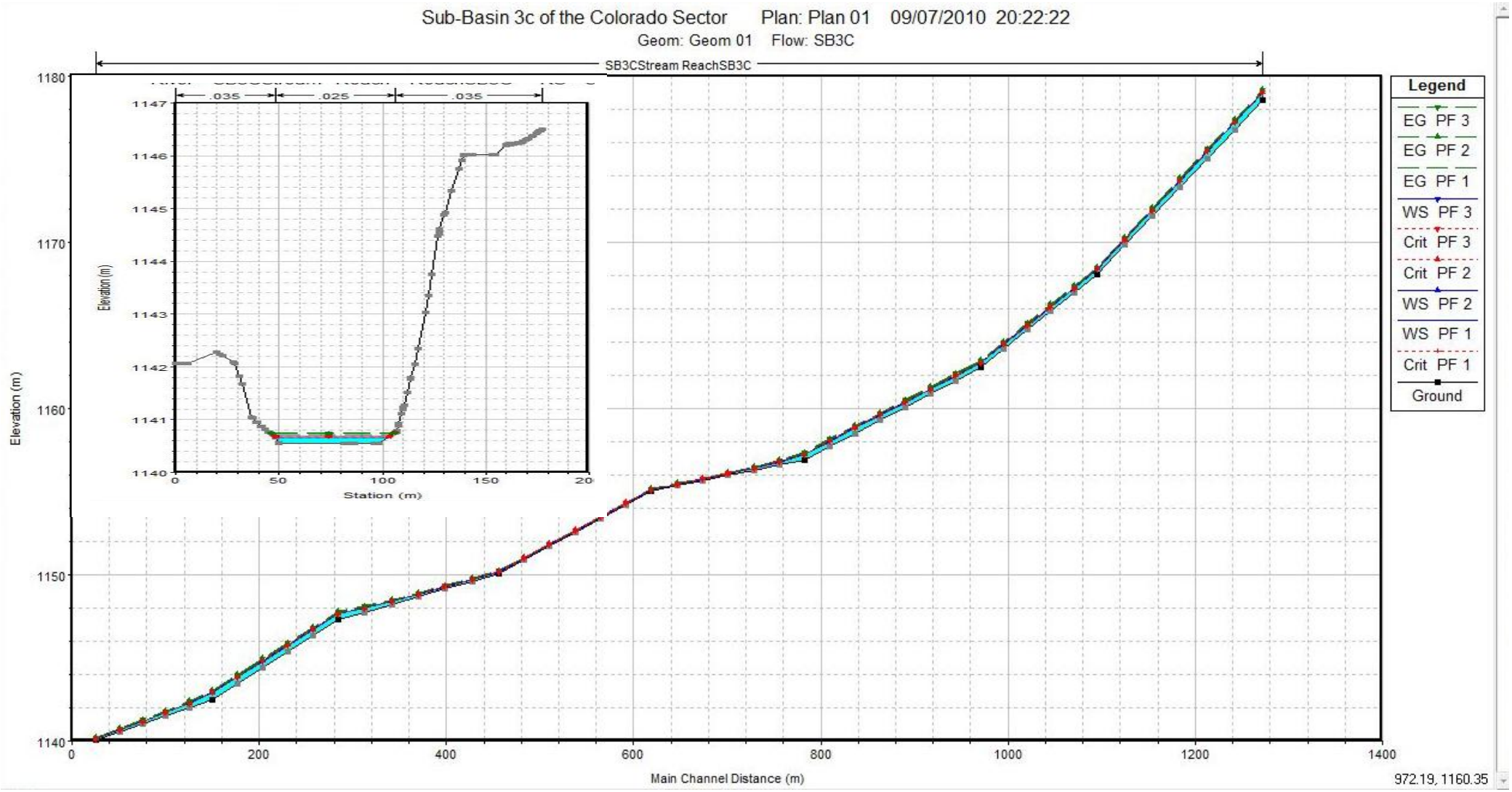

Figure 6B.12. Water surface elevation of stream Sb3C: 10 Yr. (PF1); 50 Yr. (PF2); and 100 Yr. (PF3); Shows profile and cross section of water surface level during flooding (See map location in figure 6A.4 Appendix 6A). Source: Created by David Zúñiga (2012) using HEC-RAS (2002) version 3.1.3.

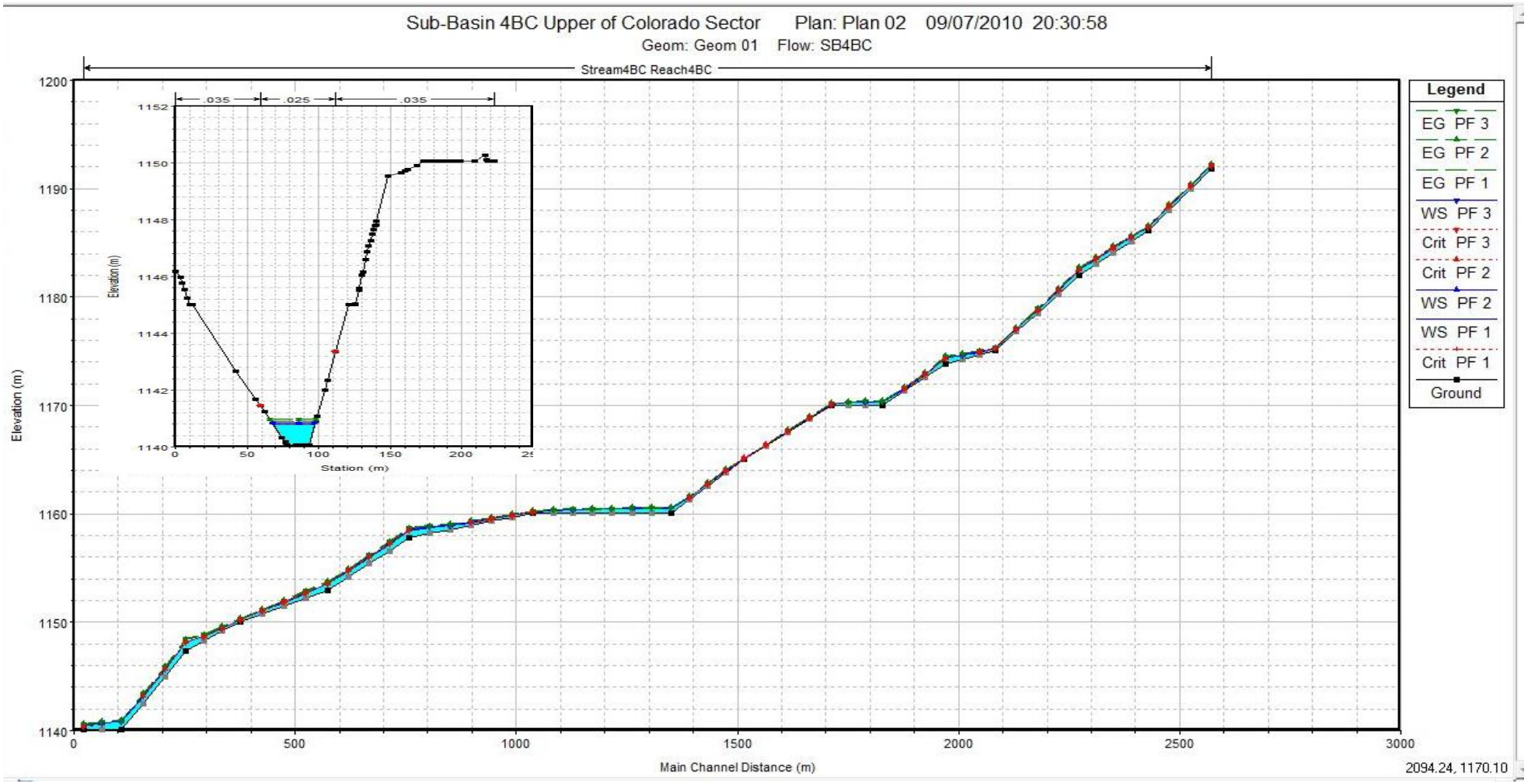

Figure 6B.13. Water surface elevation of stream Sb4BC: 10 Yr. (PF1); 50 Yr. (PF2); and 100 Yr. (PF3); Shows profile and cross section of water surface level during flooding (See map location in figure 6A.4 Appendix 6A). Source: Created by David Zúñiga (2012) using HEC-RAS (2002) version 3.1.3.

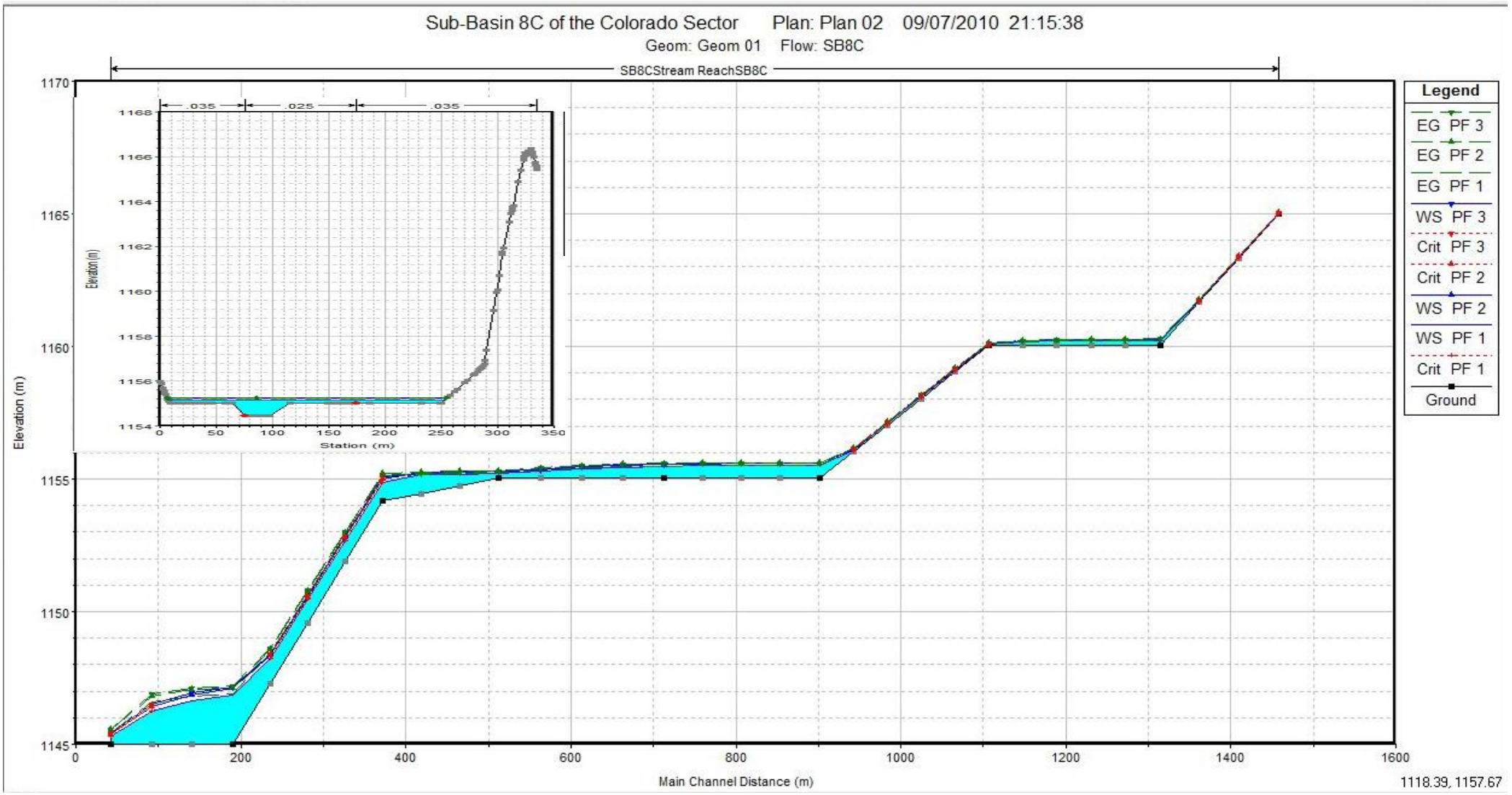

Figure 6B.14. Water surface elevation of stream Sb8C: 10 Yr. (PF1); 50 Yr. (PF2); and 100 Yr. (PF3); Shows profile and cross section of water surface level during flooding (See map location in figure 6A.4 Appendix 6A). Source:Created by David Zúñiga (2012) using HEC-RAS (2002) version 3.1.3.

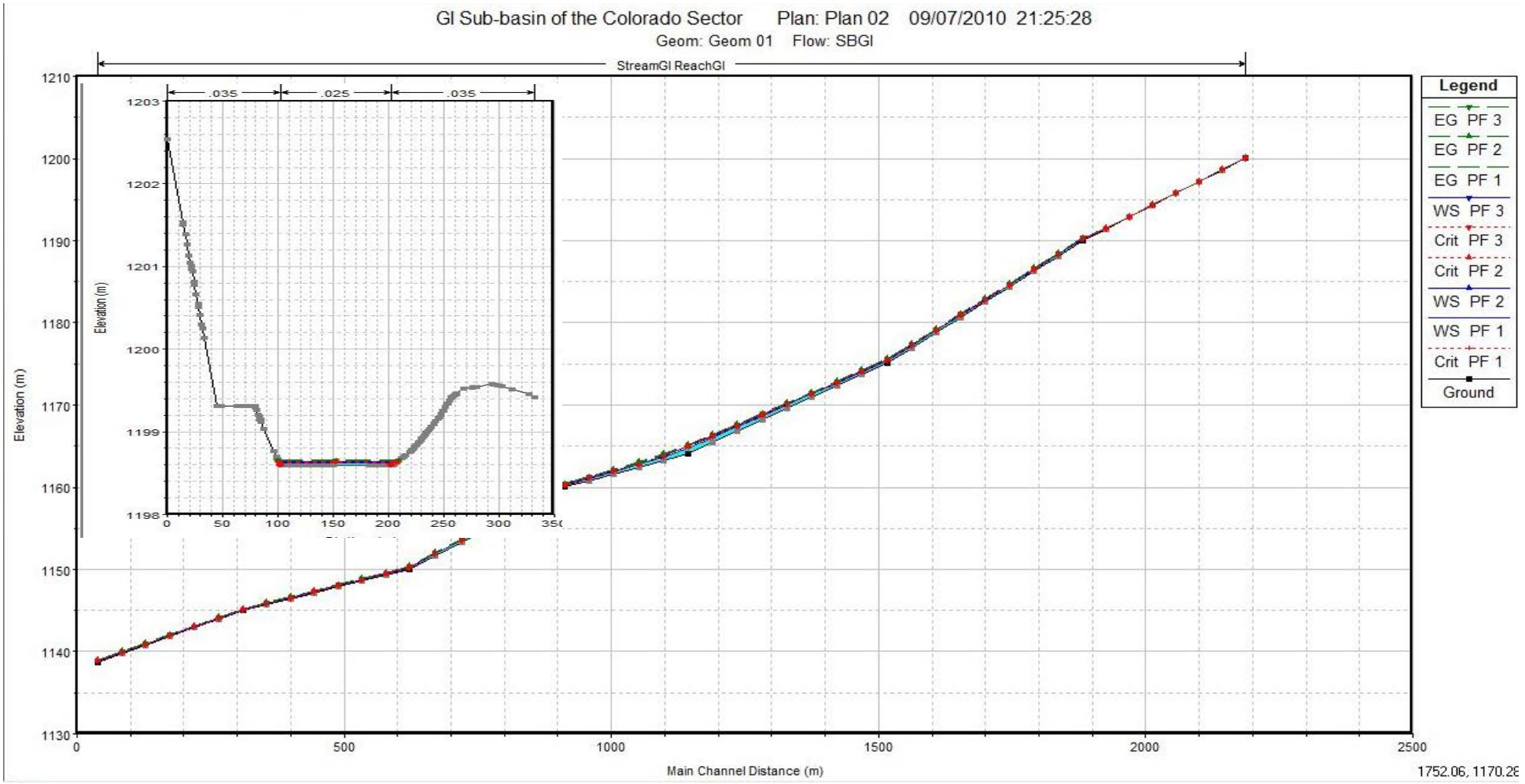

Figure 6B.15. Water surface elevation of stream SbGI: 10 Yr. (PF1); 50 Yr. (PF2); and 100 Yr. (PF3); Shows profile and cross section of water surface level during flooding (See map location in figure 6A.4 Appendix 6A). Source: Created by David Zúñiga (2012) using HEC-RAS (2002) version 3.1.3.

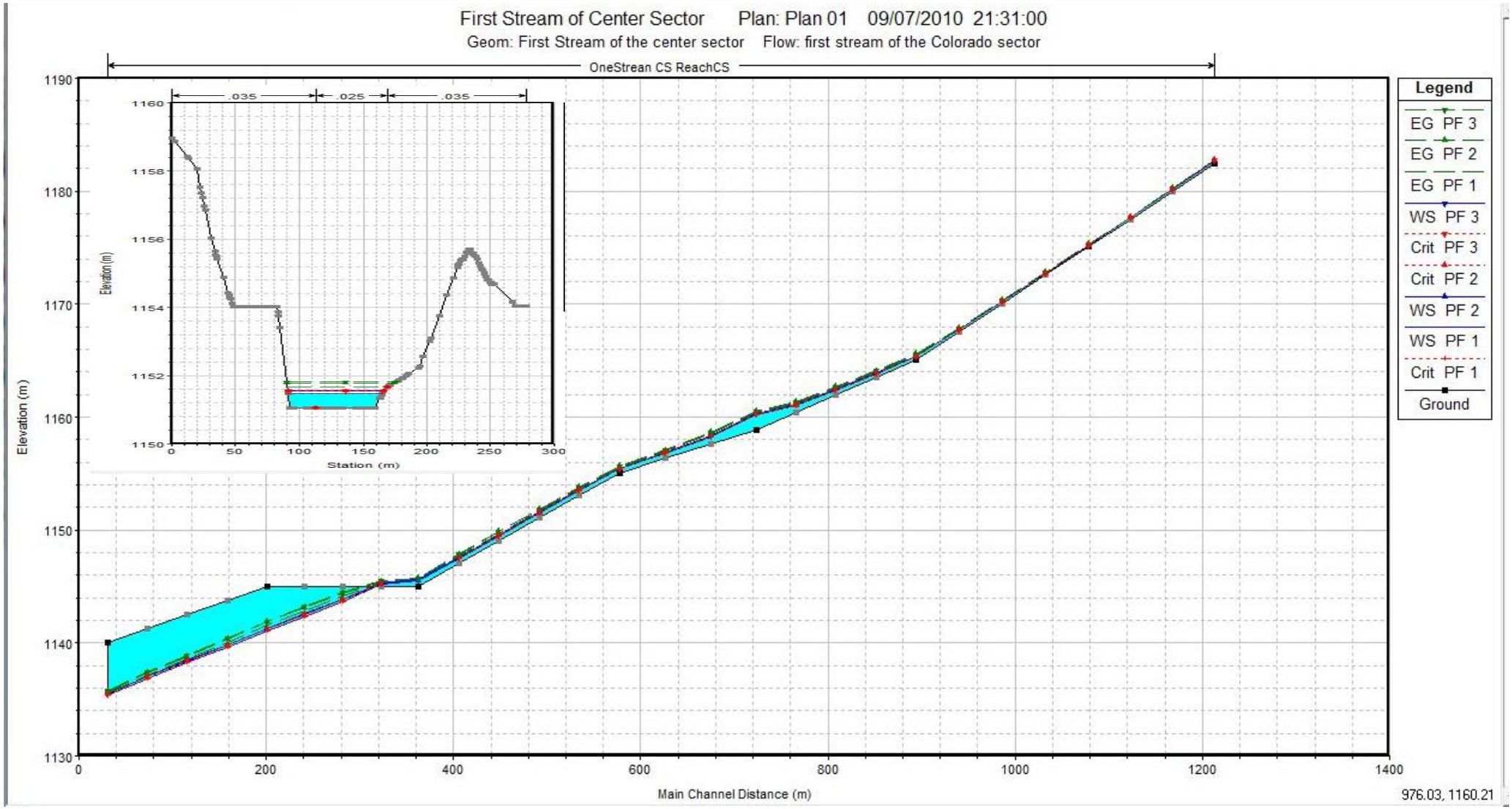

Figure 6B.16. Water surface elevation of stream FirstCS: 10 Yr. (PF1); 50 Yr. (PF2); and 100 Yr. (PF3); Shows profile and cross section of water surface level during flooding (See map location in figure 6A.15 Appendix 6A). Source: Created by David Zúñiga (2012) using HEC-RAS (2002) version 3.1.3.

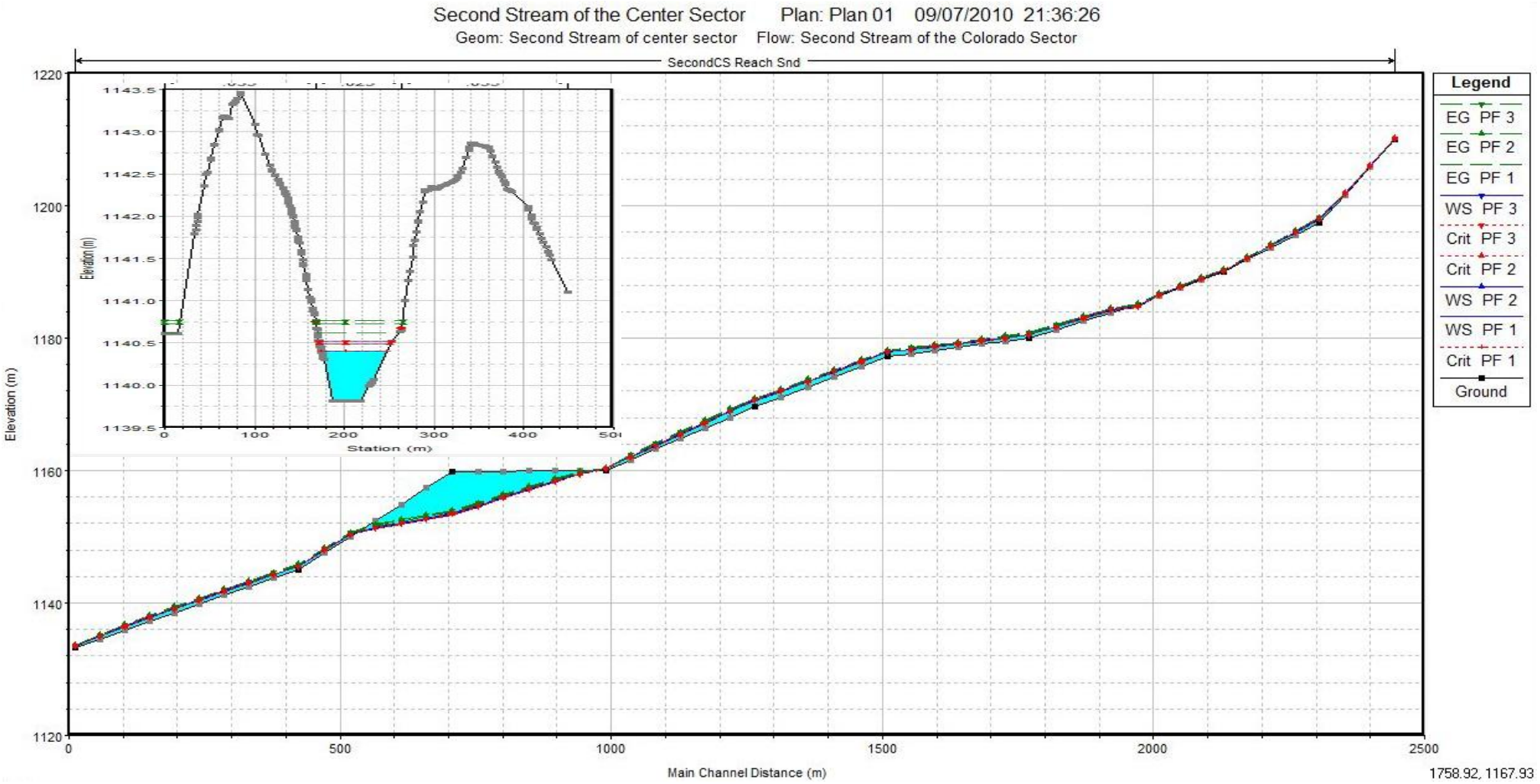

Figure 6B.17. Water surface elevation of stream S[nd]CS: 10 Yr. (PF1); 50 Yr. (PF2); and 100 Yr. (PF3); Shows profile and cross section of water surface level during flooding (See map location in figure 6A.15 Appendix 6A) . Source: Created by David Zúñiga (2012) using HEC-RAS (2002) version 3.1.3.

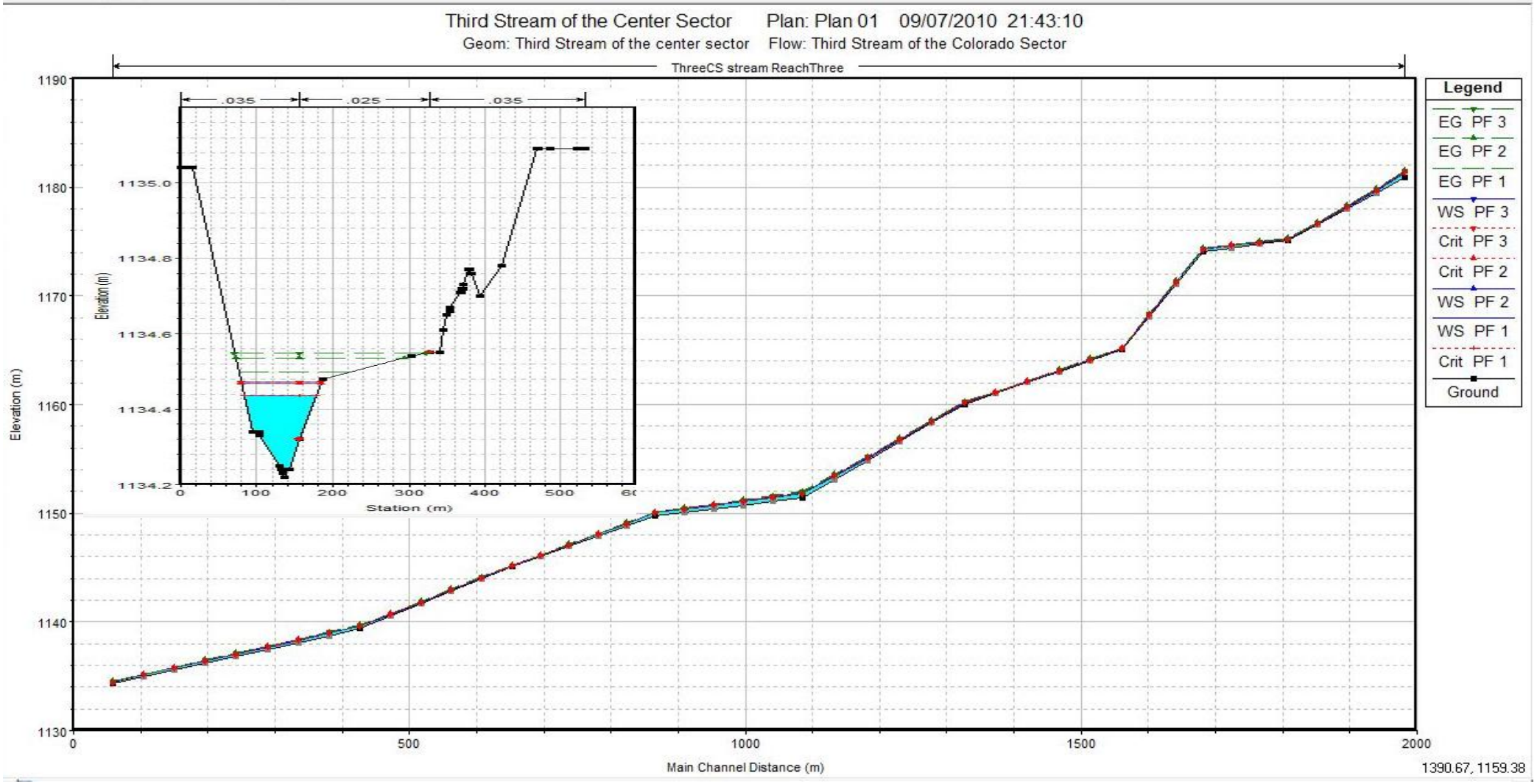

Figure 6B.18. Water surface elevation of stream ThirdCS: 10 Yr. (PF1); 50 Yr. (PF2); and 100 Yr. (PF3); Shows profile and cross section of water surface level during flooding (See map location in figure 6A.15 Appendix 6A). Source: Created by David Zúñiga (2012) using HEC-RAS (2002) version 3.1.3.

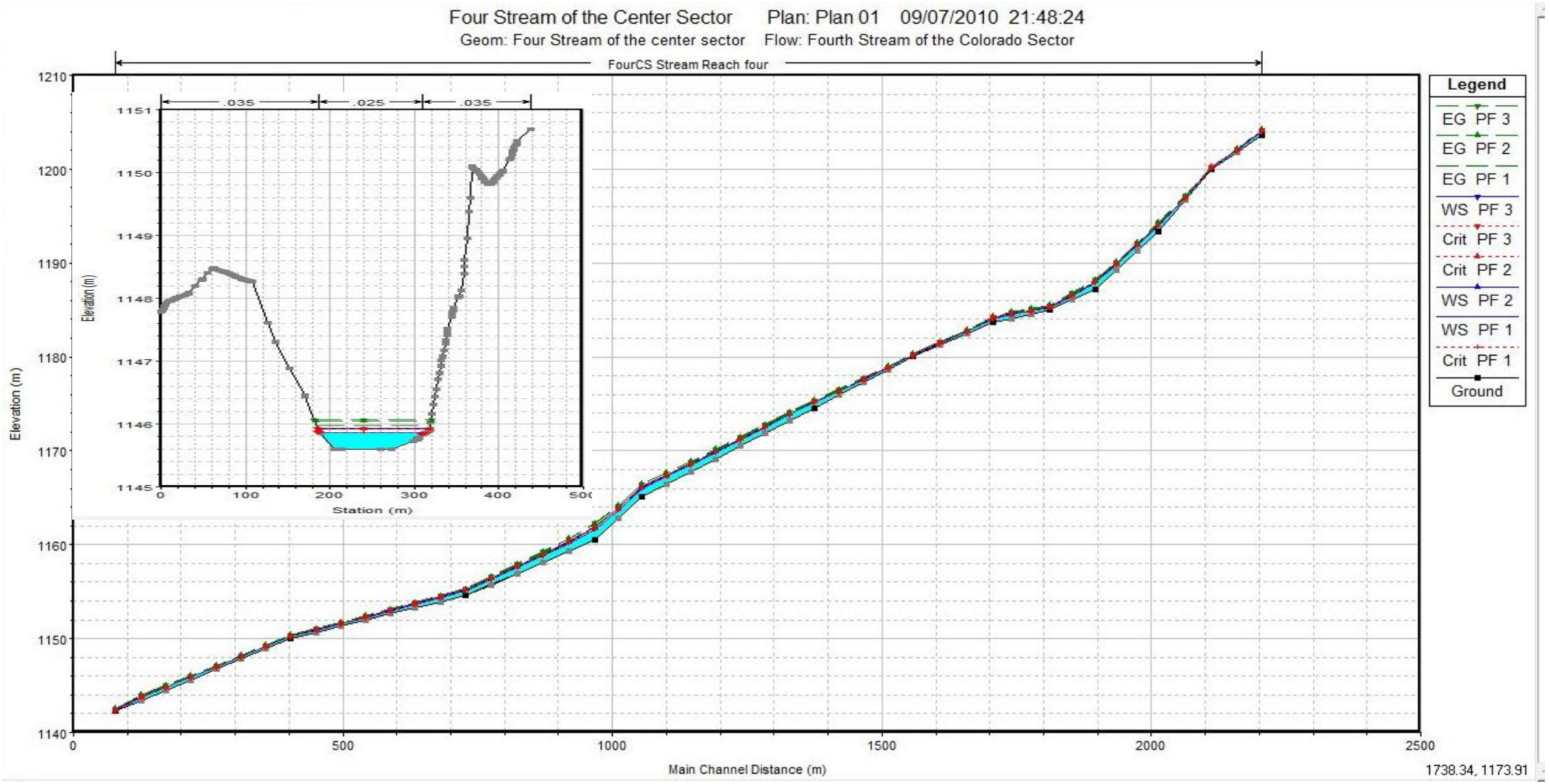

Figure 6B.19. Water surface elevation of stream FourCS: 10 Yr. (PF1); 50 Yr. (PF2); and 100 Yr. (PF3); Shows profile and cross section of water surface level during flooding (See map location in figure 6A.15 Appendix 6A). Source: Created by David Zúñiga (2012) using HEC-RAS (2002)

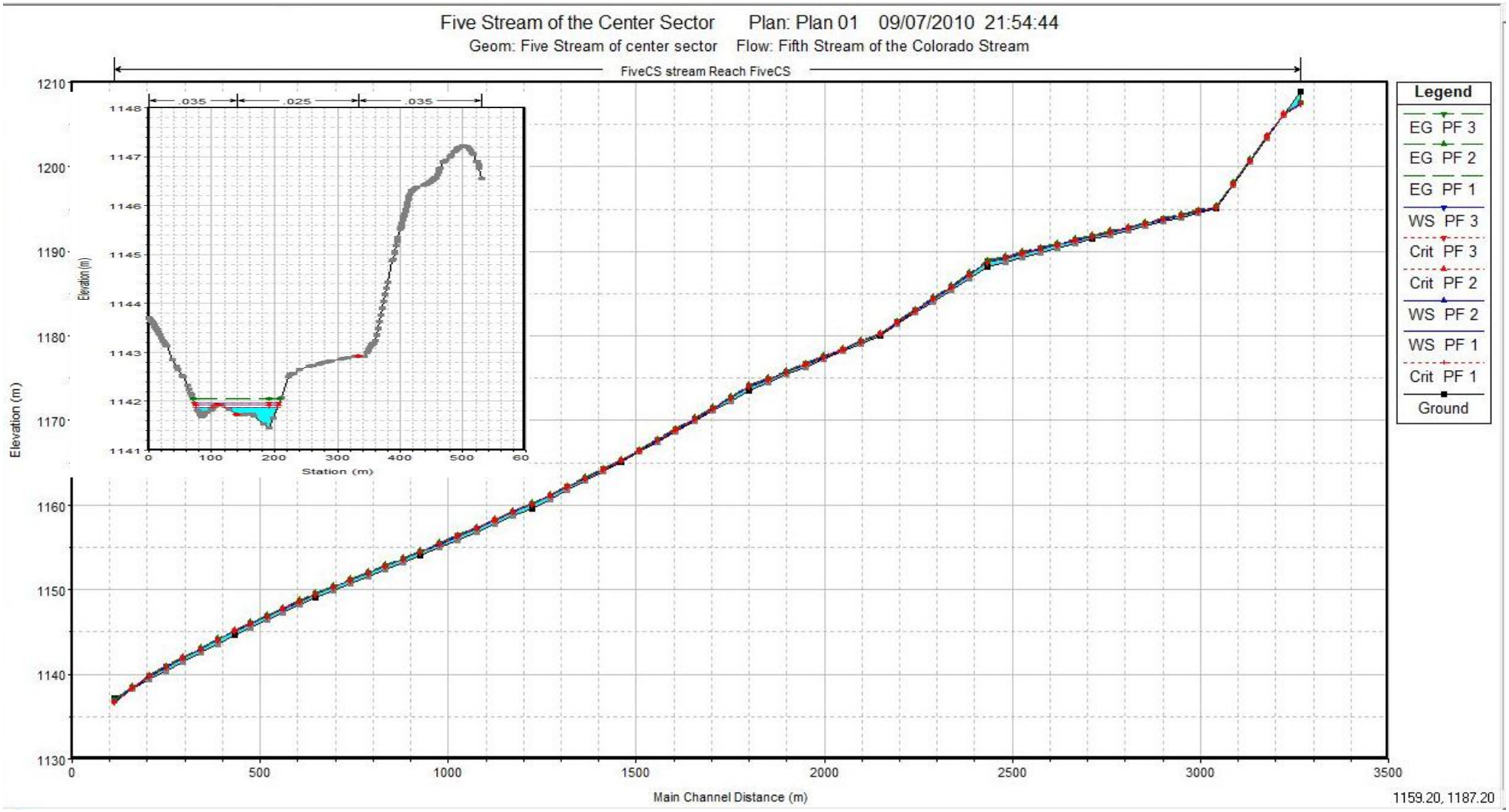

Figure 6B.20 Water surface elevation of stream FiveCS: 10 Yr. (PF1); 50 Yr. (PF2); and 100 Yr. (PF3); Shows profile and cross section of water surface level during flooding (See map location in figure 6A.15 Appendix 6A). Source: Created by David Zúñiga (2012) using HEC-RAS (2002) version 3.1.3.

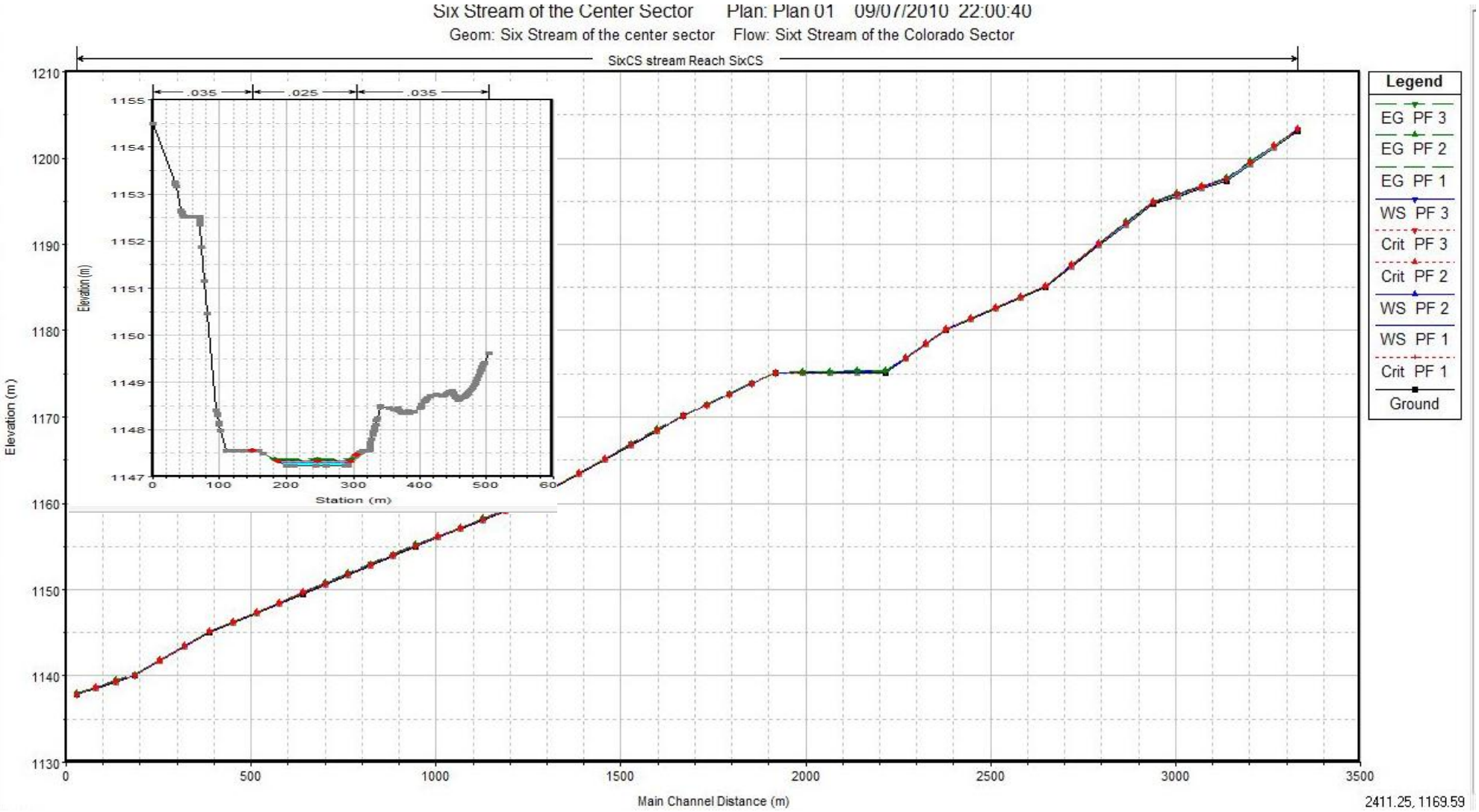

Figure 6B.21. Water surface elevation of stream SixCS: 10 Yr. (PF1); 50 Yr. (PF2); and 100 Yr. (PF3); Shows profile and cross section of water surface level during flooding (See map location in figure 6A.15 Appendix 6A). Source: Created by David Zúñiga (2012) using HEC-RAS (2002) version 3.1.3.

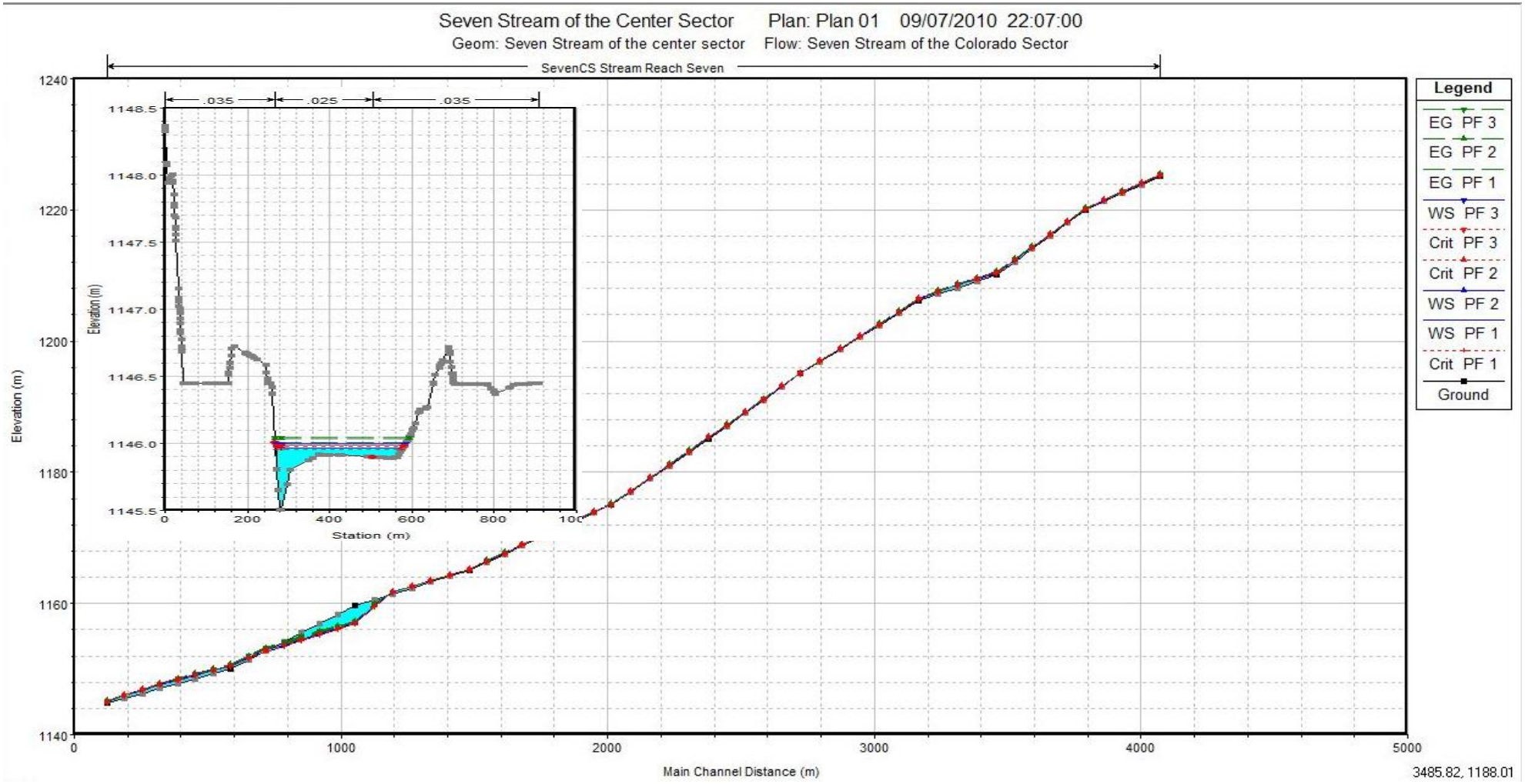

Figure 6B.22. Water surface elevation of stream SevenCS: 10 Yr. (PF1); 50 Yr. (PF2); and 100 Yr. (PF3); Shows profile and cross section of water surface level during flooding (See map location in figure 6A.15 Appendix 6A). Source: Created by David Zúñiga (2012) using HEC-RAS (2002) version 3.1.3.

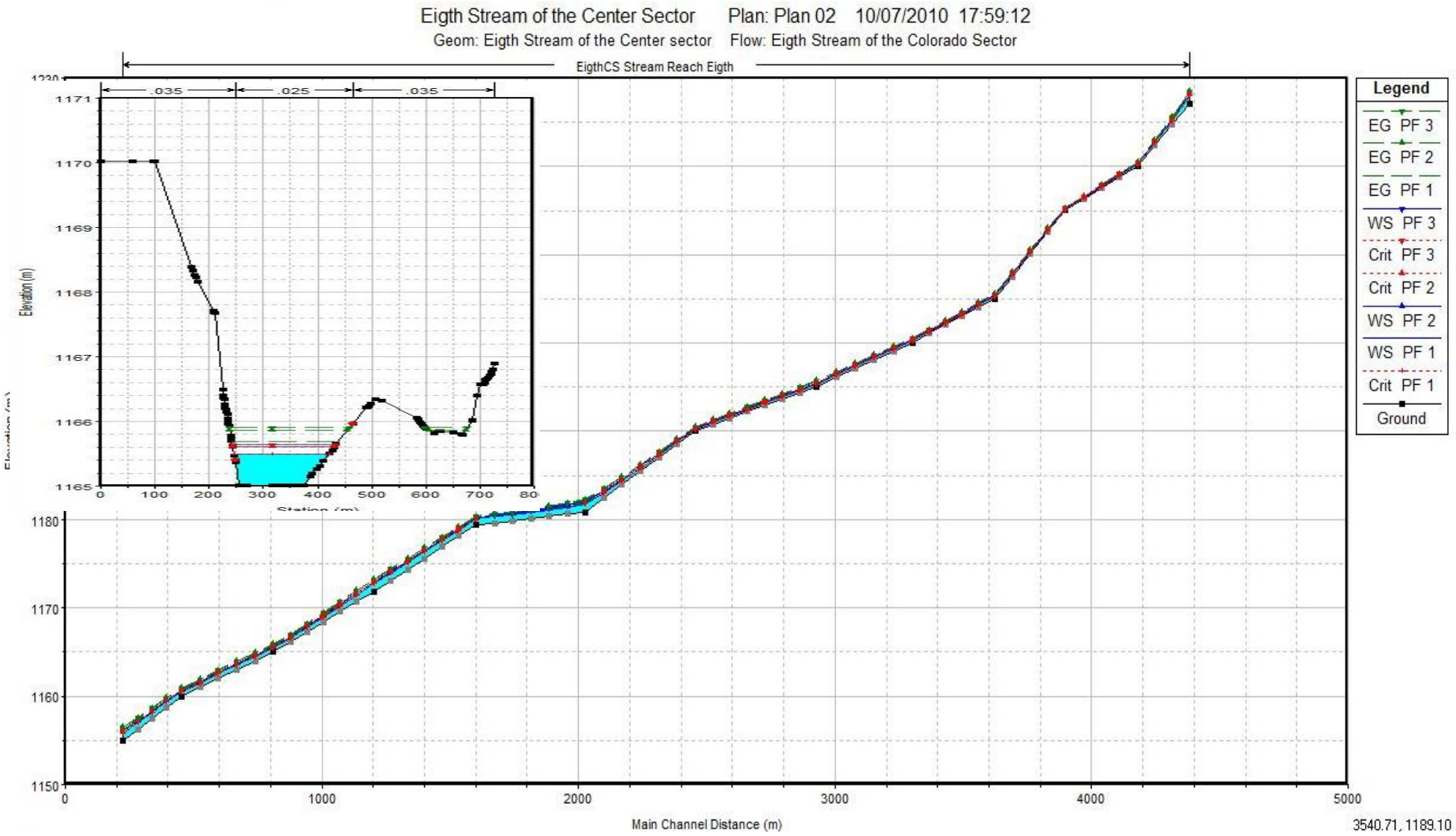

Figure 6B.23. Water surface elevation of stream EigthCS: 10 Yr. (PF1); 50 Yr. (PF2); and 100 Yr. (PF3); Shows profile and cross section of water surface level during flooding (See map location in figure 6A.15 Appendix 6A). Source: Created by David Zúñiga (2012) using HEC-RAS (2002) version 3.1.3.

APPENDIX 6C

The main components of the flooding risk were individually assessed. Firstly, the flooding hazard was derived using programs such as Arc-view 3.1 with the HEC-GeoRAS preprocessing and postprocessing extensions explained in Chapter 6.

Once the flooding hazard model was assessed, the vulnerability matrix model was obtained taking care to select the more appropiate parametres that affect Juárez city. Therefore, a detailed analysis of physiographic and demographic parametres is availlable in the "Juarezageb_2005_wgs84_Area" shape file census dataset. The more critical behaviour response observed during this analysis allowed examination of four vulnerability components as given in Figs. 6C.1 landuse (LU); 6C.2 population density (PD); 6C.3 scholarly degree or Educational level (SD) and 6C.4 medical service (MS) were acquired. These four vulnerability factors resulted from the census analysis were algebraically summed. However, in order to balance vulnerability degree the following factors were used: the landuse (PD) vulnerability component given the highest rank 40%, demographic features as: LU, MS and SD were assigned 20% each one. The previous factors were calibrated in a regional way analysing the census data and simulating them using geoprocessing model of Arc-GIS 10.1. Thus, the resulted total vulnerability matrix is derived from the addition of the four components mentioned above. At the final of this section is presented a simulation draft alternative model that include the actual Bravo River channel position as well its valley areas. The preliminary simulation was assessed using the Arc GIS 10.1 (2011) Program and selecting the file that contains demographic and physiographic information. After that, using the geoprocessing module of the Arc-GIS 10.1 (2011) was applied, the final Vulnerability matrix was obtained for five vulnerability levels (See Fig. 6C.5). Level 1 means low Vulnerability (LV), level 5 corresponds to Very High vulnerability (VH) whithin these levels medium, medium to high and high vulnerability is prevailing. This vulnerability model was built with weighted Population density as 40%, and the remaining components Land Use (LU), Scholarly Degree (SD) and Medical Services (MS) as 20% each one. Furthermore, the final flooding risk model was derived as the product between flooding hazard (Fig. 6C-6) and vulnerability (Fig. 6C-5) models. Thus, the final risk is presented in Fig. 6C-7. This Flooding risk model is the result of the transparent overlapping of Flooding hazard model over the vulnerability model.

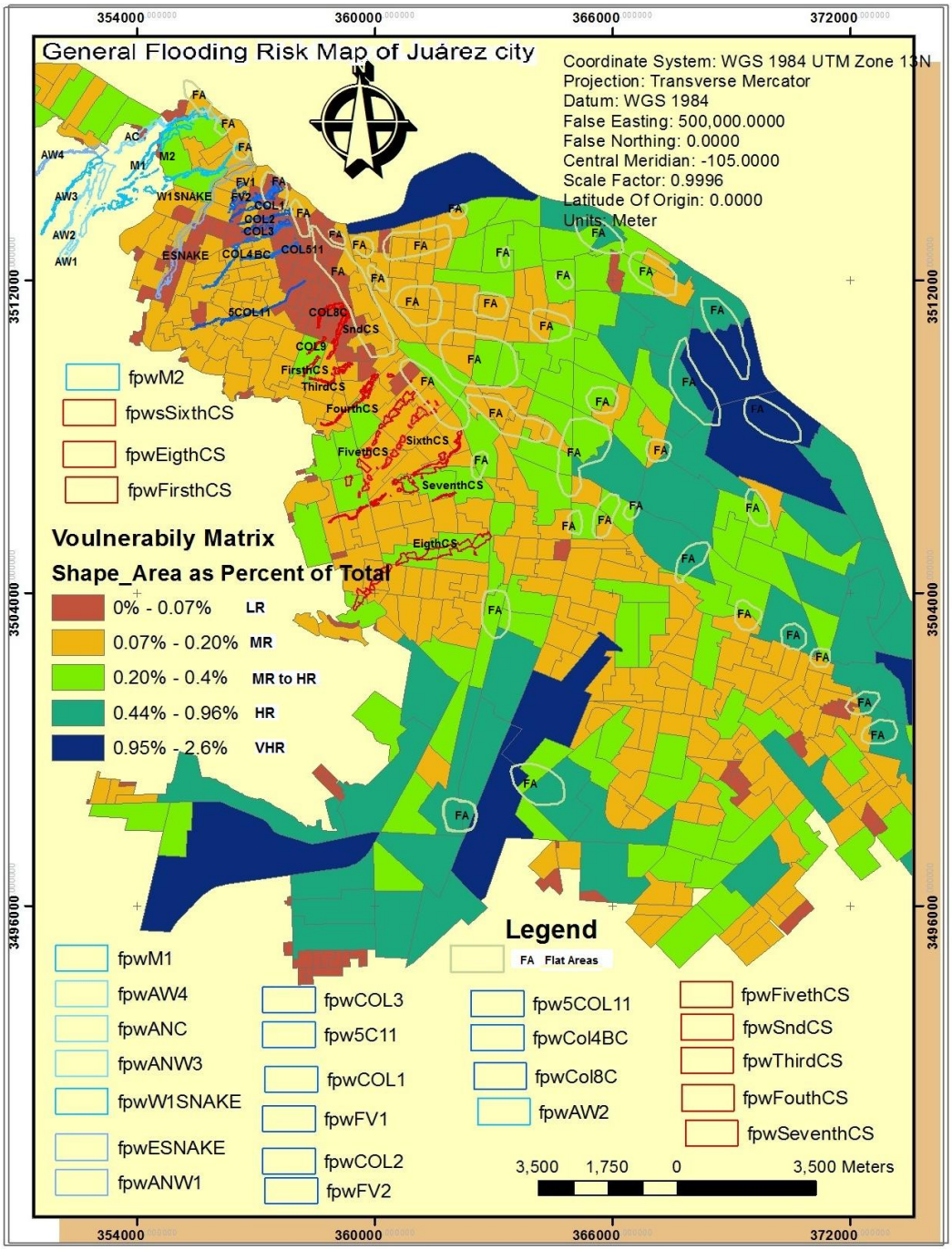

Fig. 6C.7 Juárez city Flooding Risk based on Vulnerability Matrix and Flooding Hazard map (See stream colour simbology). The legend shows five risk levels from (Low opaque red colour) to Very High (dark blue colour) derived from census demographic and physiographic datasets of Juárez city. Flood hazard level is colour coded. Created by David Zúñiga (2012) using INEGI (2007) juarezageb_2005_wgs84_Area shape file and geoprocessing tool application given on Arc-GIS 10.1 (2011)

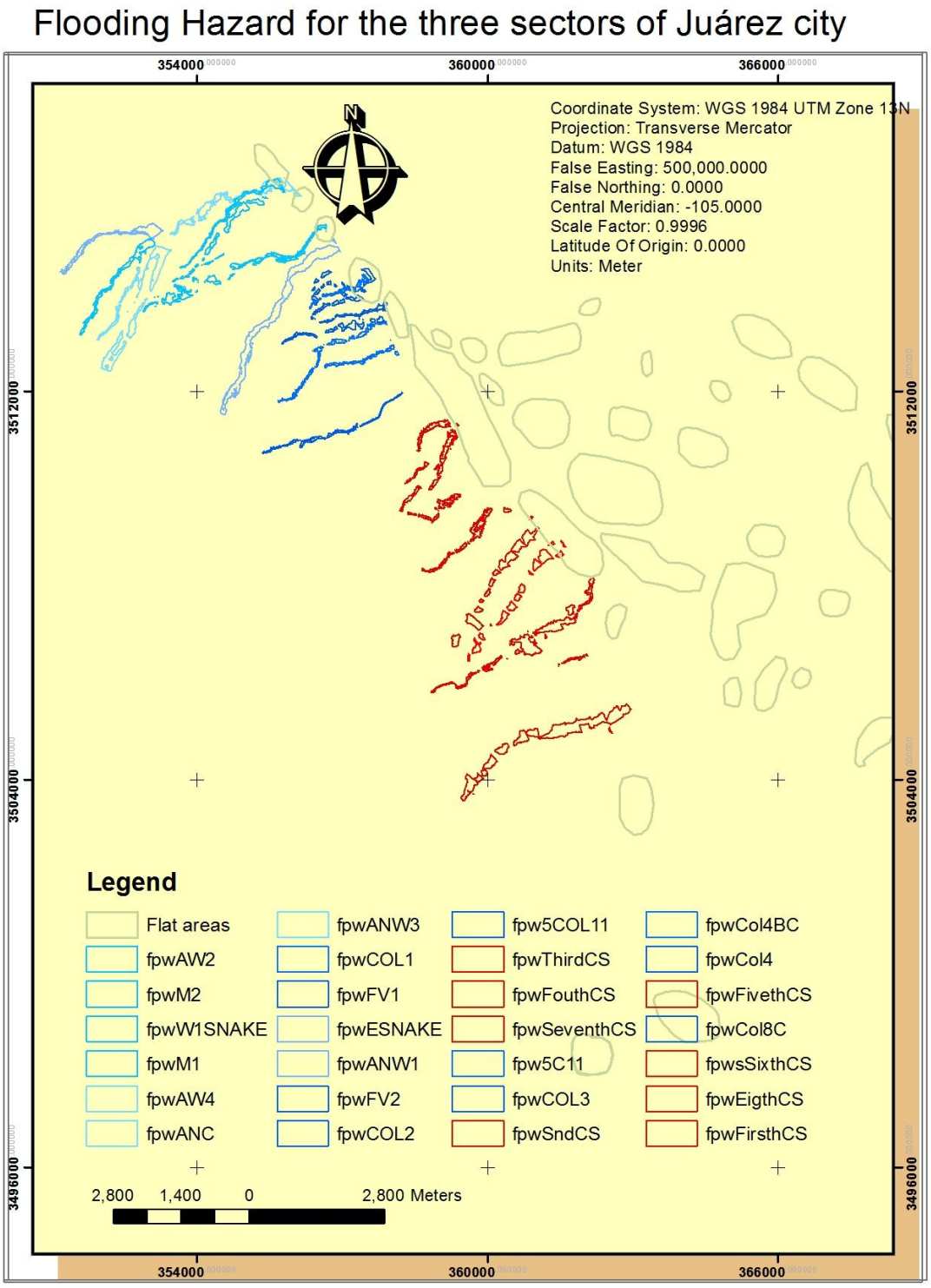

Fig. 6C.6 Juárez city Flooding Hazard map light blue colour corresponds to Sector 1 and 2 of Anapra basin, Blue colour to Centre basin and red colour to southeast basin and were derived from: Arc-View 3.1 and GeoHEC-RAS preprocessing and postprocessing extensions; HEC-RAS (2002) and Arc-GIS 10. Flat areas shapefile was collected from data in IMIP (2005)

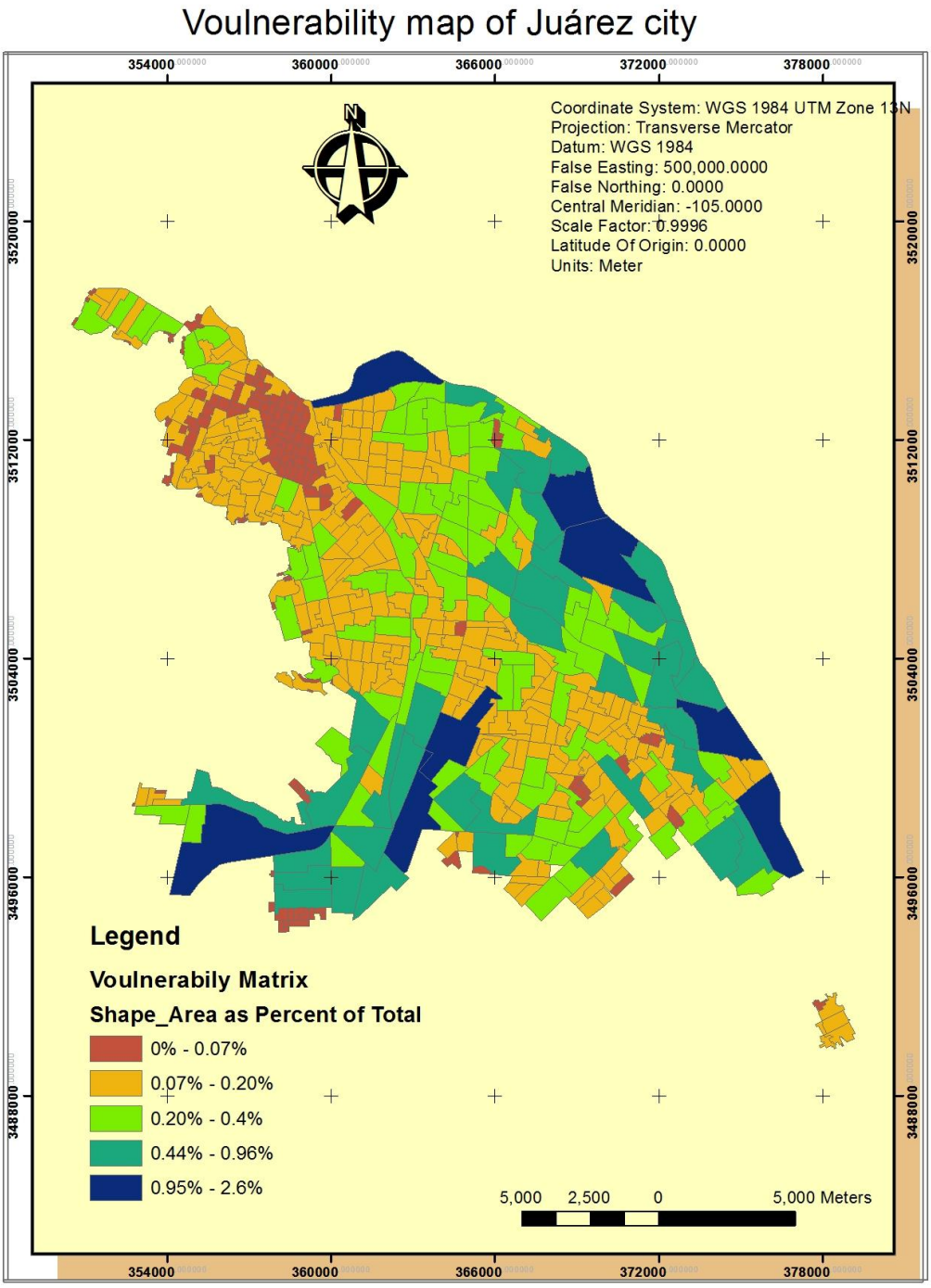

Fig. 6C.5 Juárez city Vulnerability Matrix based on: Population Density (PD); Land Use (LU); Medical Servises (MS) and Schoolarly Degree (SD). Legend shows five vulnerability levels from low opaque red colour to Very High (dark blue colour) derived from census demographic and physiographic datasets of Juárez city. Created by David Zúñiga (2012) using INEGI (2007) juarezageb_2005_wgs84_Area shape file and geoprocessing tool application given in Arc-GIS 10.1 (2011)

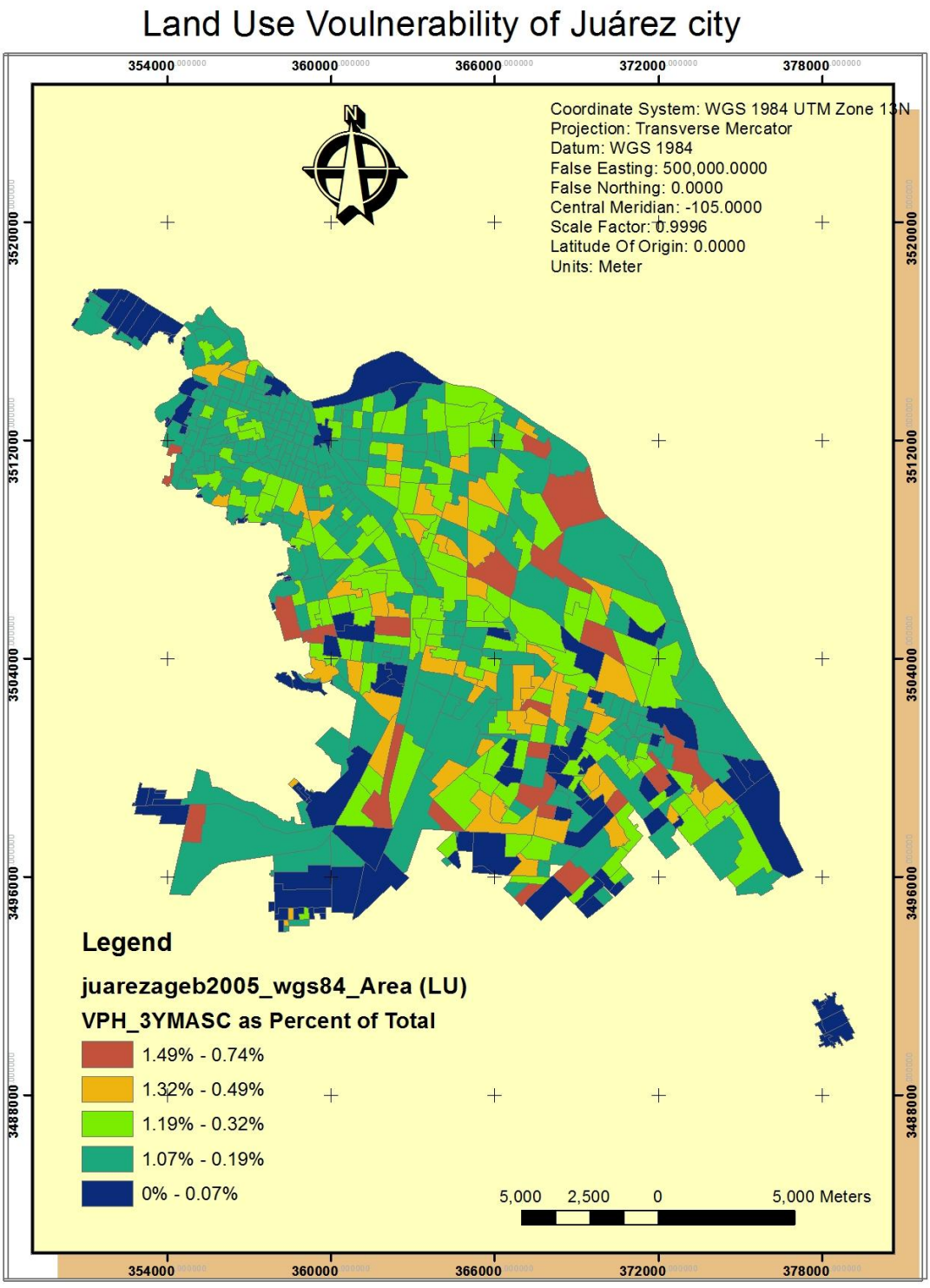

Fig. 6C.1 Juárez city Land Use vulnerability matrix (LU). Legend shows five vulnerability levels from Low (opaque red colour) to Very High (dark blue colour) derived from census demographic and physiographic datasets of Juárez city. Created by David Zúñiga (2012) using INEGI (2007) juarezageb_2005_wgs84_Area shape file and Arc-GIS 10.1 (2011)

Population Density Voulnerability of Juárez city

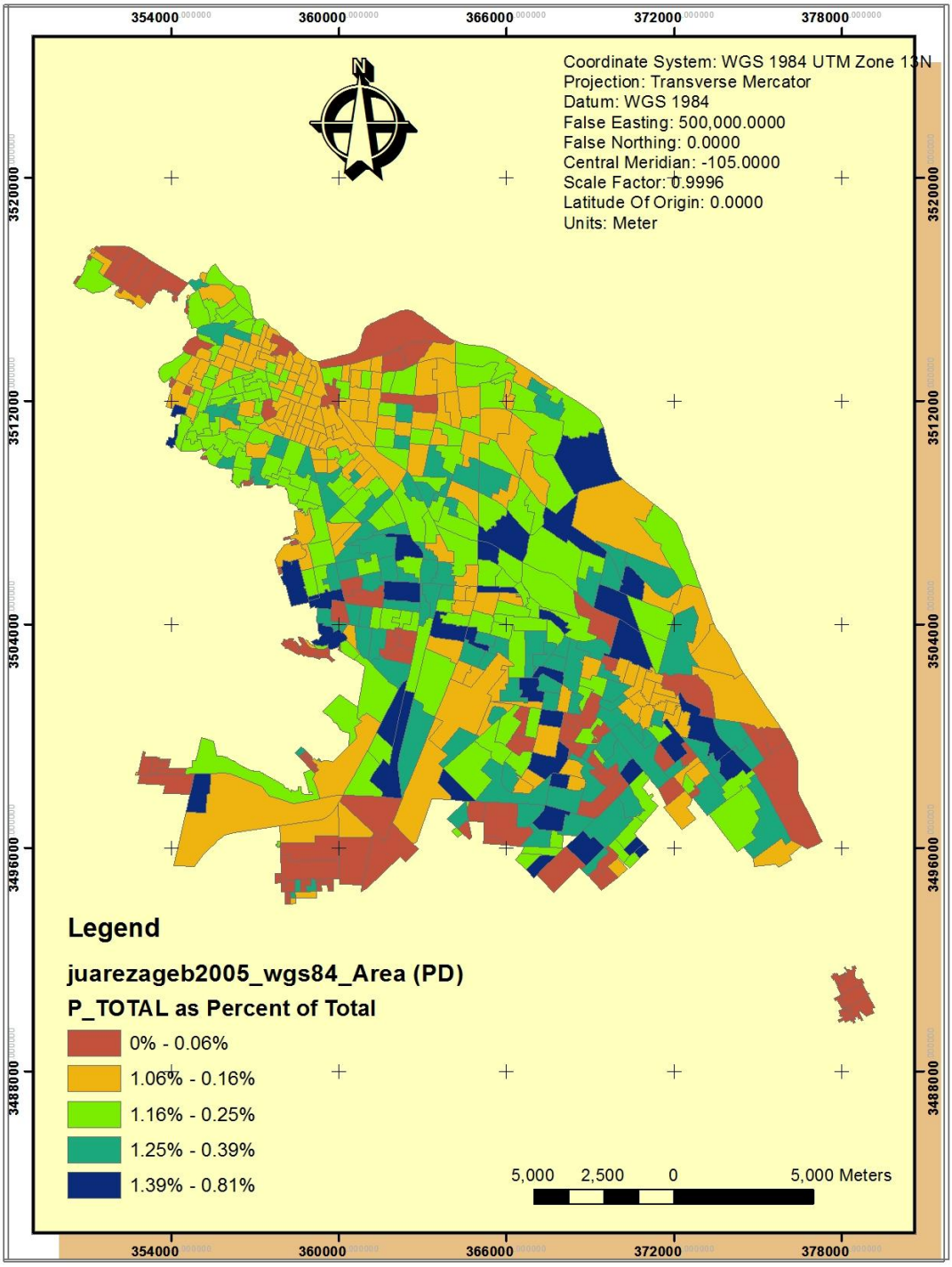

Fig. 6C.2 Juárez city Population Density (PD) vulnerability matrix based on: Legend shows five vulnerability levels from low (opaque red colour) to Very High (dark blue colour) derived from census demographic and physiographic datasets of Juárez city. Created by David Zúñiga (2012) using INEGI (2007) juarezageb_2005_wgs84_Area shape file Arc-GIS 10.1 (2011)

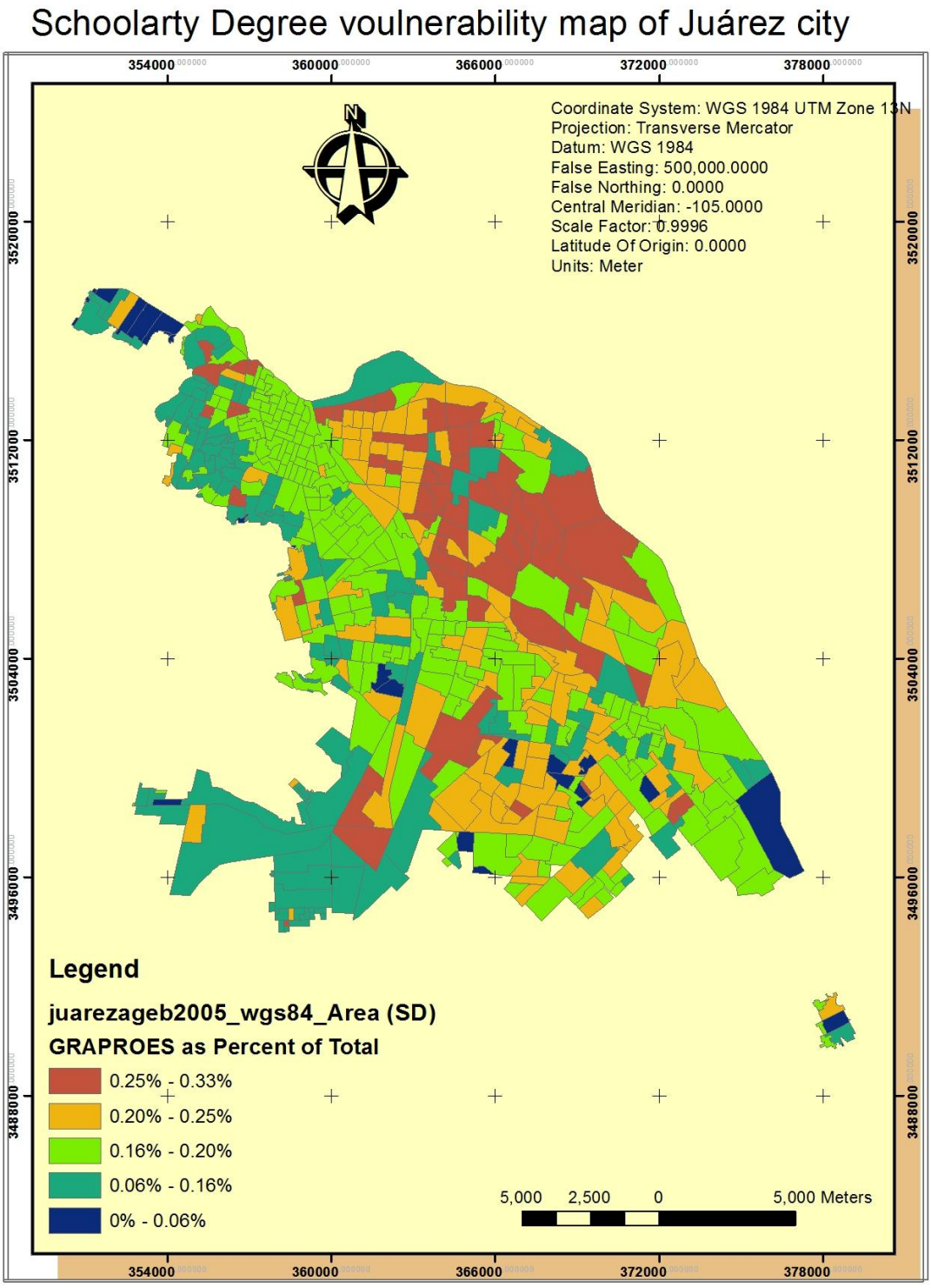

Fig. 6C.3 Juárez city Education Level Schooarly Degree (SD) vulnerability matrix: legend shows five voulnerability levels from low (opaque red colour) to Very High (dark blue colour) derived from census demographic and physiographic datasets of Juárez city. Created by David Zúñiga (2012) using INEGI (2007) juarezageb_2005_wgs84_Area shape file and Arc-GIS 10.1 (2011)

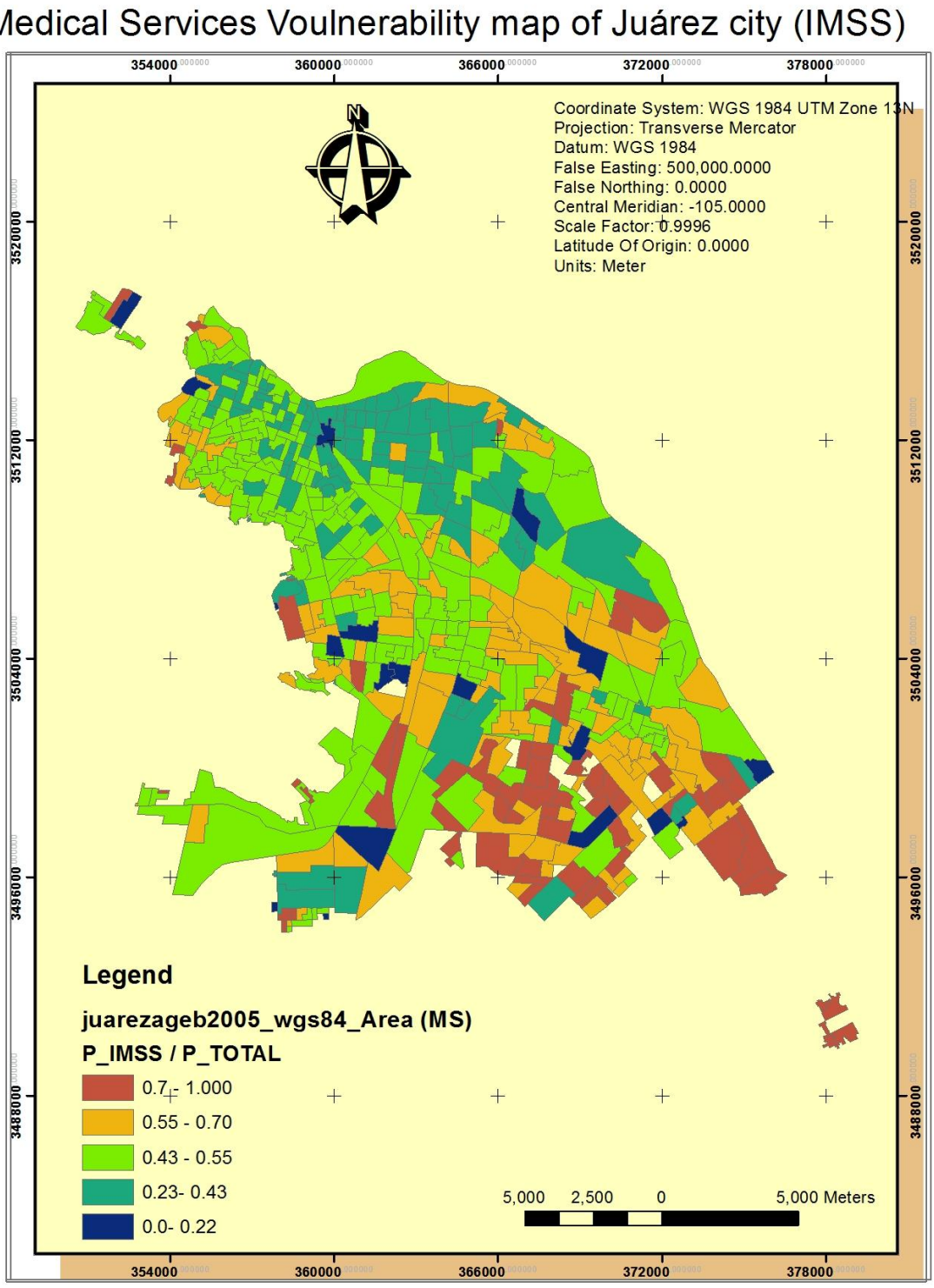

Fig. 6C.4 Juárez city Medical Services (MS) vulnerability matrix: Legend shows five voulnerability levels from low opaque red colour to Very High dark blue colour derived from census demographic and physiographic datasets of Juárez city. Created by David Zúñiga (2012) using INEGI (2007) juarezageb_2005_wgs84_Area shape file and Arc-GIS 10.1 (2011)

Appendix 6D;
Explanation of the vulnerability model

In order to explain the vulnerability model the following step by step description is presented.

1) Using the dataset " juarezageb_2005_wgs84_Area shape file" and Arc-GIS 10.1 program with geoprocessing module included, the dataset shape file is opened as many demographic and physiographic parametres of sectorized Juárez city. In this part a depth analysis of the census information is done. Then, the four vulnerability components for the study area emerge as: PD, SD, MS and LU. These independent vulnerability models are presented in Figs. 6.C1 to 6.C4 Appendix 6C.

2) Derived from previous simulation analysis and using the union (addition) tool of the geoprocessing module including in Arc-GIS 10.1 program. An idea of the more critical vulnerability combination parameters which impact the total vulnerability matrix of the study area is acquired. Therefore, in this particular examination the final model which fits the critical vulnerability model to the study area is presented in Figure 6.C5. This corresponds to 40% (PD); 20%(SD); 20% (MS) and 20% (LU). These percentages means the degree of vulnerability provided from the factors implicated, and the total matrix is formed by the addition (union) of the four vulnerability weighted components. The reason to assign these porcentages for the different components was because: Firstly, Population density of Juárez city with a 40 % represent the highest vulnerability factor and was assiged because the sectors more populated are located between the piedmont alluvial fans near to Juárez Mountains and the platform where these alluvial fan are connected with fluvial Bravo River deposits. Therefore, it is sensible to consider this factor in a practical sence. Secondly, the three remaining vulnerability factors as MS=20%, LU= 20% and SD=20% were assigned with the same factor (20%) because the less vulnerable people or rich people actually live in the flat areas distributed in sectors with less population density rather that in the mountains where more populated areas where identified once the Analysis of the dataset census was studied. In short, is difficult to assign the appropiate whole vulnerability matrix but in a practical sense the vulnerability matrix here presented is in a preliminary way correct. In the point 3

below an explanation is presented considering the probably influence of the Bravo River position in relation to the vulnerability matrix. 3) In order to obtain the vulnerability matrix, the union tool of the geoprocessing model is used. Once, obtained the four vulnerability components and their appropiate (%factor) then the total vulnerability matrix is assessed (See Fig. 6.C5 Appendix 6C). Note: I think these extensive examination is enough to assess in a practical sence this vulnerability matrix, even considering the proximity of the Bravo River but the problem maybe is not fully solved because a more complex spatial analysis is needed. The following Figs 6D.1 and 6D.2 were created in order to dilucidate the problem of proximity of Bravo River. In these figures a DEM derived from contour 5m levels was incorporated into the vulnerability matrix. In these DEM only five levels are considered: From 1115 to 1125 masl; 1125 to 1135 masl; 1135 to 1145 masl; 1145 to 1155 masl and 1155 to 1160 masl. Finally, overlapping the original vulnerability matrix model with the new DEM for proximity of the Bravo River The final vulnerability matrix model emerges and is shown in Figure 6D.1. On the other hand, using only (LU); (PD); (SD) and (MS) (See Figure 6D.2) is clear that is more practical the Vulnerability matrix considered on Chapter 6. Note: The reason for the incongruence of this draft is because a higher resolution DEM is needed.

General Flooding Risk Map of Juárez City (Including Bravo River influence)

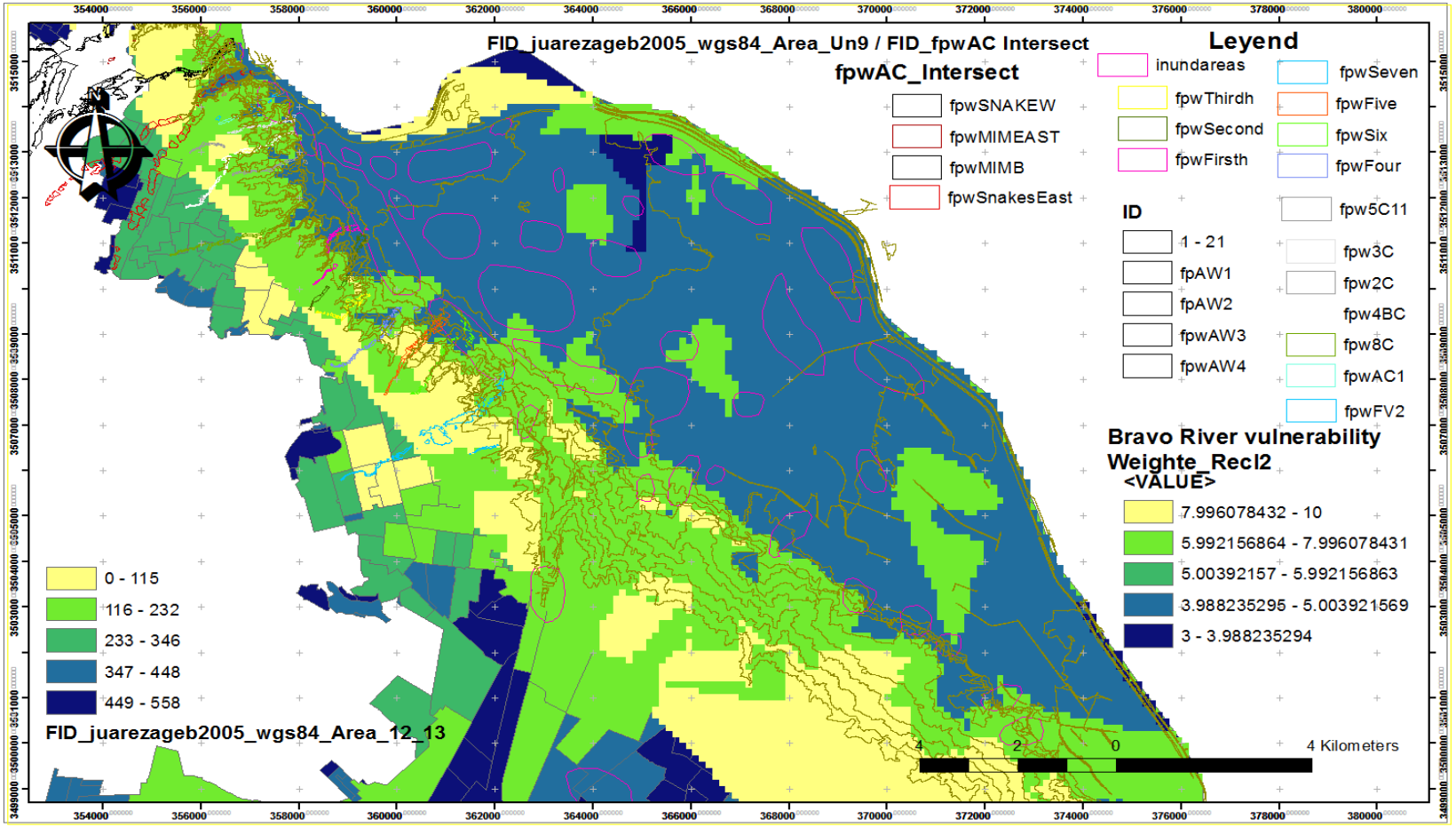

Fig. 6D.1 Juárez city draft vulnerability matrix: Legend shows five voulnerability levels Symbology named FID_ juarezageb_2005_wgs84_Area_12_13 means vulnerability matrix and Bravo River vulnerability Weighted_Rec12 means DEM of Bravo River level Created by David Zúñiga (2012) using INEGI (2007) juarezageb_2005_wgs84_Area shape file and Arc-GIS 10.1 (2011)

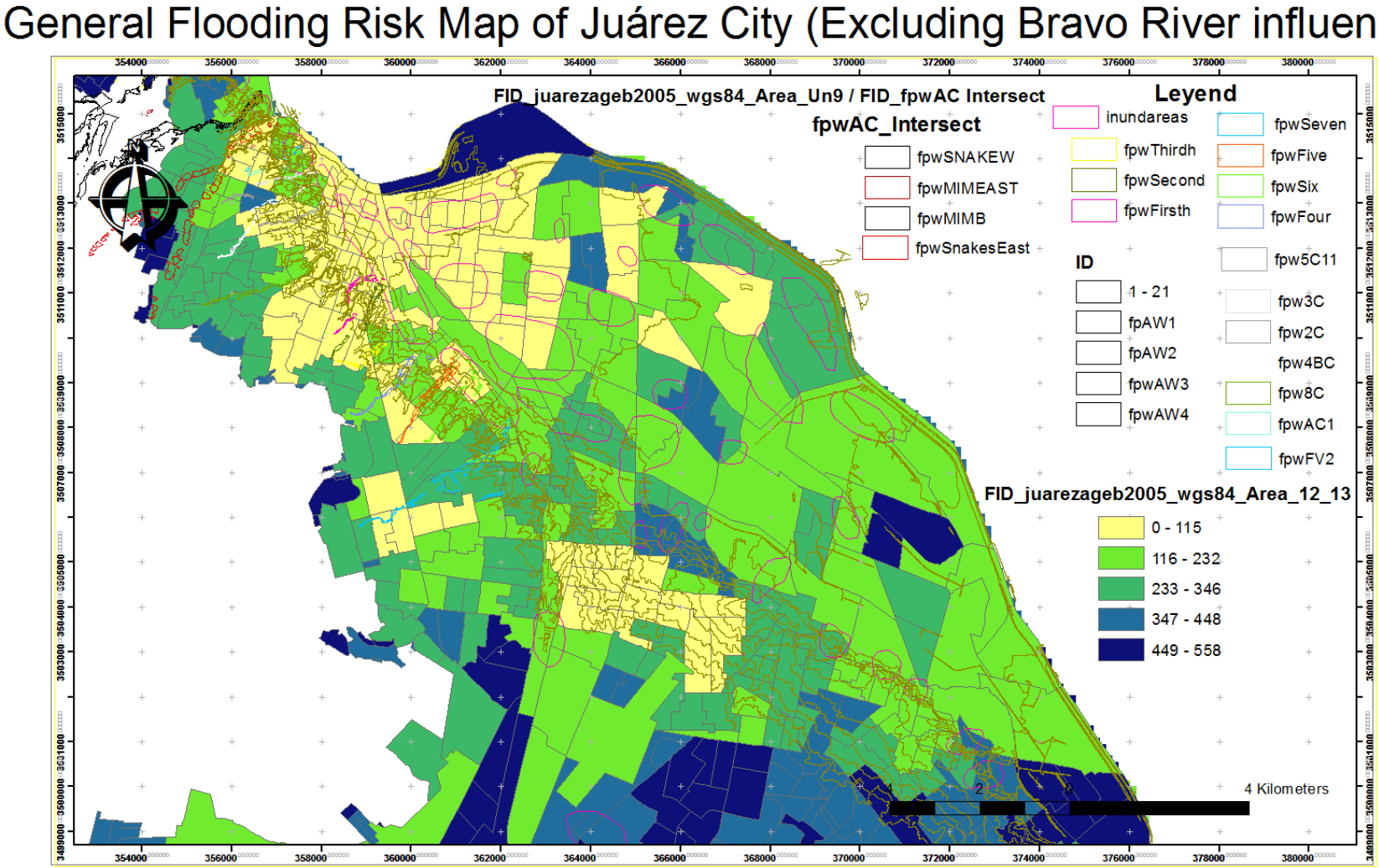

Fig. 6D.2 Juárez city draft vulnerability matrix: Legend shows five voulnerability levels Symbology named FID_ juarezageb_2005_wgs84_Area_12_13 means vulnerability matrix without the Bravo River influence Created by David Zúñiga (2012) using INEGI (2007) juarezageb_2005_wgs84_Area shape file and Arc-GIS 10.1 (2011)